HIGH PRESSURE SCIENCE AND TECHNOLOGY

PROCEEDINGS

XI AIRAPT International Conference

NAUKOVA DUMKA

HIGH PRESSURE SCIENCE AND TECHNOLOGY

PROCEEDINGS

XI AIRAPT International Conference

1

KIEV 1989

INTERNATIONAL ASSOCIATION FOR THE ADVANCEMENT OF
HIGH PRESSURE SCIENCE AND TECHNOLOGY

HIGH PRESSURE SCIENCE AND TECHNOLOGY

PROCEEDINGS

XIth AIRAPT International Conference

In 4 volumes

Volume 1

Kiev Naukova Dumka 1989

UDC 62-987:539.89

High Pressure Science and Technology: Proc. XI th AIRAPT Int. Conf.: In 4 vol / International Association for the Advancement of High Pressure Science and Technology. - Kiev : Naukova Dumka, 1988. - Vol. 1. - 452 p.

ISBN 5-12-000366-4(т.1). ISBN 5-12-001176-4.

The Proceedings composed of four volumes contain papers presented at the XIth AIRAPT International Conference "High Pressure Science and Technology" (Kiev, USSR, 12-17 July 1987).

Volume 1 of the Proceedings includes the papers on the following topics: state and properties of gases and liquids; structural and phase transformations in solids; synthesis and chemical kinetics.

The book is a direct reproduction of the camera-ready manuscripts submitted by the authors. No corrections have been made in the texts.

В сборник, состоящий из четырех томов, включены труды, представленные на XI Международную конференцию МАРИВД "Высокие давления в науке и технике (Киев, СССР, 12-17 июля 1987 г.)

В первый том вошли работы по следующим разделам: состояние и свойства газов и жидкостей; структурные и фазовые превращения в твердых телах, синтез и химическая кинетика.

Сборник отпечатан методом прямого репродуцирования с рукописей, предоставленных авторами. Авторские тексты не редактировались.

N.V.Novikov, Editor-in-chief,

Ye.M.Chistyakov, Scientific secretary

Н $\frac{1604090000-099}{M221(04)-89}$

ISBN 5-12-000366-4

ISBN 5-12-001176-4

The XIth AIRAPT International Conference "High Pressure Science and Technology"

organized and held by

AIRAPT

EHPRG

Academy of Sciences of the USSR

Academy of Sciences of the Ukrainian SSR

USSR State Committee on Science and Technology Scientific Council on Production and Machining Materials Using High Pressures

UkrSSR Academy of Sciences Scientific Council on High Pressur Materials Science

USSR Academy of Sciences Scientific Council on High Pressure Physics

Institute for Superhard Materials of the UkrSSR Academy of Sciences

Institute of High Pressure Physics of the USSR Academy of Sciences

PROGRAM COMMITTEE

A.M. Prokhorov	- chairman
P.S. Kisly	
Yu.A.Osipyan	
E.G. Ponyatovsky	- vice chairmen
V.E. Fortov	
V.E. Antonov	- secretary

LOCAL COMMITTEE

N.V. Novikov	- chairman
V.N. Dmitriev	
V.I. Trefilov	- vice chairmen
E.N. Yakovlev	
E.M. Chistyakov	- scientific secretary

INTERNATIONAL ADVISORY COMMITTEE

N. Ashcroft	USA	A. Onodera	Japan
B.I. Beresnev	USSR	Yu.A. Osipyan	USSR
C.B. Boyer	USA	E.G. Ponyatovsky	USSR
A.N. Dremin	USSR	S. Porowski	Poland
V.E. Fortov	USSR	A.M. Prokhorov	USSR
F.U. Franck	FRG	H.L.D. Pugh	UK
H.D. Hochheimer	FRG	G.A. Samara	USA
A. Jayaraman	USA	A. Sawaoka	Japan
G. Jenner	France	G.M. Schneider	FRG
R.N. Keeler	USA	J.W. Shaner	USA
D.D. Klug	Canada	R. Shashidhar	India
J. Kubat	Sweden	H. Stiller	GDR
A. Kusubov	USA	N.J. Trappeniers	the Netherlands
B. Le Neindre	France		
N.V. Novikov	USSA	W.A. Wakeham	UK
		E.N. Yakovlev	USSR

C O N T E N T S

SYNTHESIS AND CHEMICAL KINETICS

Supercritical Fluid Mixtures at High Pressures

E.U. Franck

Institute for Physical Chemistry, University of Karlsruhe,

12 Kaiserstraße, D7500 Karlsruhe, BRD

Abstract

With high pressures, supercritical fluids can be studied over a wide range of density. Extensive and continuous changes of physicochemical properties and phenomena are possible. New results are presented: Quantitative determinations of the solubility of a solid compound (caffeine as an example) in several polar and nonpolar supercritical gases and binary gas mixtures. The data could be useful in relation to "supercritical extraction" processes. Quantitative calculation of phase diagrams of binary and ternary systems to 2000 bar with a new equation of state is possible. The PVT-properties and the electrolyti conductance for the water-sodium hydroxide system in the whole composition range between the dilute solutions and the fused hydroxide were measured to 450 °C and - in part - to 4000 bar. The possibility of combustion in dense supercritical water-methane mixtures with injected oxygen is discussed and demonstrated with a "hydrothermal" flame in a supercritical phase at 2000 bar of pressure.

I. INTRODUCTION

Dense fluids at supercritical temperatures provide an excell field in which experimental and theoretical studies can be m of physicochemical properties and of their extensive and continuous variation with temperature, pressure and composit This is particularly true for fluid mixtures, because nonpol polar and even electrolytic fluids are miscible over wide ranges if the temperature is high enough. The critical phenoı of binary and ternary fluid systems have been predicted and discussed on the basis of thermodynamic considerations (1) a have been demonstrated experimentally (2) already a long tim ago. New possibilities have expanded the region of available data and systematic treatments on phase equilibria and thermophysical properties to include highly polar fluids and even supercritical electrolyte solutions (3),(4),(5).

The phase equilibria can be described by temperature-pressur mole fraction (T,P,x) diagrams. The "critical curve" between the two critical points of the pure components is usually interrupted, if the two partners differ considerably, for example in molecular polarity. The critical curve is a high temperature envelope of a two-phase region. Fig. 1, as an example, shows the TPx-diagram of the water-argon system to 3000 bar. The boundary surface of the two-phase region was calculated with a procedure mentioned below. The agreement with experiment is good. A few points along the critical cur are shown. This upper branch of the critical curve begins at the critical point of pure water and - passing through a shal

temperature minimum - extends to high pressures and temperatures. The minimum in temperature may be more pronounced or may disappear completely, as for water-helium (6), where the curve proceeds from the critical point of water directly to higher temperatures and pressures.

In the present contribution new results will be presented on very dilute supercritical solutions with some relevance for supercritical extraction. Subsequently, an equation of state to calculate critical curves and phase equilibria to very high temperatures and pressures will be demonstrated. A discussion of new PVT-data and of the electrolytic conductivity of water-sodium hydroxide mixtures over the whole range from fused hydroxide to dilute aqueous solutions above the critical temperature of water will follow - as an example for a comprehensive treatment of liquid salts and aqueous electrolyte solutions. First results on "hydrothermal combustion" with "supercritical flames" to 2000 bar shall finally be presented.

II. DILUTE MIXTURES - SUPERCRITICAL EXTRACTION

Processes to dissolve and extract solids or high boiling liquids with supercritical dense gases as solvents has received increased interest in the last decades. Although at present only a few of these processes are being used on an industrial scale, numerous suggestions for separation procedures have been made (7). Many recent publications concerning this subject are available (8)(9)(10)(11)(12) and experimental solubility results are given.

Quantitative solubility data, however, are rather difficult to obtain and relatively scarce. One possibility to obtain such data is, to use absorption spectra of the solute in the highly compressed supercritical solvent gas. Suitable high pressure optical cells equipped with sapphire windows have been constructed for such purposes. Series of measurements with anthracene in various gases and caffeine in some gases have been reported (13)(14). Some of these measurements were extended to 2000 bar. Technical applications at such high pressures may be rare, but the coverage of a wide density range sometimes facilitates the derivation of solubility equations. Very recently (15)(16) the solubility of caffeine as a test compound has been measured not only in pure gases but also in gas mixtures in order to study the combination of two solvent actions. Caffeine has a suitable absorption spectrum in the near UV-range with a band at 273 nm, the intensity of which was used for the concentration determination.

The influence of a gaseous solvent can be very clearly represented by the so-called enhancement factor, which is the ratio of the observed solute concentration c in the gas phase over the concentration c_o at the same temperature related to the vapour pressure of the pure solute compound with no solvent gas. Fig. 2 shows measured enhancement factors for caffeine at 373 K as functions of molar density for four gases. The solubility data were first obtained for different pressures, which in some cases extended to 2000 bar. With existing PVT-tables the data

were recalculated to obtain the density dependence of Fig. 2. The density data of methyl-trifluoride were derived by corresponding-state considerations from data for $CHClF_2$. It is impressive to see, that enhancement factors can increase with density by four orders of magnitude. It is plausible, that gases with molecules with high dipole or quadrupole moments are considerably better solvents. Methane and argon have been applied for comparison purposes. Analogous observations have been made earlier with anthracene (13). The curves indicate, that at very high densities they may become flat and reach a region of near density independence. From the increase of enhancement factors at low density, mixed virial coefficients B_{12} can be derived. The use of compressed helium to 2000 bar gives a negative logarithm of the enhancement factor, indicating a "negative" enhancement, a repulsion of the solute from the dense helium phase (15).

In technical processes of supercritical extraction the use of the addition of second gaseous components - "entrainers" - is occasionally mentioned. The desirable effects of such entrainers may have different causes. In the present investigation it was undertaken to study the combined action of two well-defined gaseous solvents as a function of their relative concentration. Fig. 3 gives some of the results. Binary mixtures of methane with trifluoro-methane and with carbon dioxide were used. Methane was applied as one of the components because of the higher contrast to the two other partners. Data of Fig. 3 were selected

for a constant volume density of 10 mol dm^{-3} and a constant temperature. It is clear, that the increase of the enhancement factor follows a relatively simple function of the mole fraction of the added polar compound. No drastic entrainer effects are observed in these cases, although the consequence of the addition of, for example, twenty mole percent of the polar methyl-trifluoride to methane is remarkable. The interaction energy between solute and solvent gas in dependence of density has also been derived from the temperature dependence of solubility. A simple relation can be found between these interaction energies and the "reduced", dimensionless dipole or quadrupole moments of the solvents (15)(16).

III. CALCULATION OF PHASE EQUILIBRIA AND CRITICAL CURVES

It is desirable to have the means to calculate the characteristic thermodynamic properties of binary fluid systems: The fluid-fluid phase equilibria in the TPx-space and the critical curve as well as the excess quantities of thermodynamic functions in the supercritical homogeneous region. For this purpose equations of state are needed, of which many exist. Recent surveys are available (17). Scott and van Konynenburg (18) have given a classification of critical curves for non-polar components. A systematic investigation of the influence of the polarity of one of the two partners on the shape of the critical curve was made by Gubbins and Twu (19). Successful procedures to calculate critical curves and three-dimensional phase boundary surfaces have been proposed - among others - by Mc Glashan (20), Deiters

(21), Kleintjens and Koningveld (22), Peter and Wenzel (23), and by Brunner (24) and Boublik (25). Not all of these methods are well suited for systems which include highly polar partners and not all are suited to cover wide ranges of high temperatures and very high pressures. In order to deal with aqueous, "hydrothermal", systems such possibilities are needed and it is also desirable, that coefficients in the equation are related to well-defined models of intermolecular interaction to be able to make predictions for systems not yet investigated experimentally. To meet these requirements an equation of state was designed (26) which is given in Fig. 4. This CF-equation contains only a limited number of parameters. It is of a modular type to permit later extensions and refinements. It is extensively discussed elsewhere (26). V_m denotes the molar volume. As in the van der Waals equation it has a repulsion and an added attraction term. The repulsion term is of the form derived by Carnahan and Starling from computer simulations (27). Only the particle diameter has been made slightly temperature dependent. For the attraction term a square well potential is used. Diameter σ and depth ε of which are derived from the critical constants of the pure partners. The relative width λ of the potential well can be set at values between 1.5 and 2.5 or can be derived from vapour pressure vurves. The mixing factors ξ and ζ are adjustable parameters. It should be emphasized that, because of the relative simplicity of the CF-equation its main field of application may be that of elevated temperatures.

One test of the equation was already shown in Fig. 1 for the system water-argon. The two phase boundary surface in the TPx-space, marked by isotherms, isobars and isopleths, is calculated with the CF-equation using $\xi = 0.67$, $\zeta = 1.0$ and $\lambda = 2.5$.

Only experimental points along the critical curve can be shown. Another example is presented in Fig. 5.

The critical curves have been determined experimentally for water-carbon dioxide (28) and for water-benzene (29) to 3000 and 2000 bar. These two curves are considerably different from the one in Fig. 1. The inflection to lower temperature is much more pronounced, which is a consequence of the attraction between the water-molecules and the carbon-dioxide and benzene molecules. In spite of this greater difficulty the agreement between experiment and calculation is still reasonable (30). The three-dimensional fluid-fluid equilibrium surface could also be calculated.

It turns out, that the application of the equation can be extended to include ternary systems, like water-carbon dioxide-benzene or water-nitrogen-hexane. The latter may be a simplified model system for fluid combinations which are encountered in connection with the exploitation of oil and gas deposits.
An improvement of the calculations can be obtained with a supplement to the CF-equation. The attraction term is enlarged

to include a term which takes into consideration three-body groups without new parameters with a so-called Padé-approximation. The result is an improved representation of the width of two-phase regions in the x-dimension. Critical surfaces for ternary systems could also be calculated quantitatively.

IV. THE WATER-SODIUM HYDROXIDE SYSTEM

For the comprehensive understanding of ionic fluids it is of basic interest to study binary electrolyte solutions over the whole range between the dilute solutions and the pure, fused ionic partner. Examples for such systems are difficult to find. One case, which has been investigated at 91 °C is tetra-n-butyl-ammonium picrate in n-Butanol (31). Another case is lithium chlorate in water at 132 °C (32). With both systems the electrolytic conductivity has been measured at atmospheric pressure. Variation of overall density was not possible. Both systems exhibit, at least at these moderate temperatures, special behaviour because of which they are not very good examples for the above stated variation.

The application of high pressures at high temperature can be of assistance in this situation. Aqueous systems are certainly of primary importance in this context for several reasons. With several kbar of pressure water can be obtained even at 400 or 500 °C at densities of 0.6 or 0.8 g cm^{-3} (33) and dielectric constants of 15 to 25 (34), where it is still an electrolytic solvent for suitable solutes. The alkali halides, however, have considerably higher melting points and cannot

easily be investigated togehter with dense aqueous solutions. Thus sodium hydroxide was chosen for a new study of this kind. Sodium hydroxide melts at 320 °C and is at this temperature or higher, completely miscible with water. A project was begun, to measure two basic physicochemical properties - molar volume and electrolytic conductivity - over the whole composition range from the dilute aqueous solution to the molten hydroxide and at temperatures to 450 °C and pressures up to 4000 bar. The molar volume is not only interesting by itself, but is also needed to convert the pressure dependence of other properties to density dependence. Aqueous supercritical sodium hydroxide solutions have some interest also in conncection with corrosion in electric power plant operation.

In Fig. 6 gives a selection of measured molar volume data at 400 °C in dependence of the mole fraction sodium hydroxide at three different pressures (35). The molar volume of water at 4000 bar is smaller than that of the hydroxide, but at 500 bar it is considerably higher. The deviation from ideal behaviour, that is from a linear composition dependence, is always negative. The molar volume around 40 mole percent of hydroxide is lower than that of the pure liquid hydroxide, indicating a considerable contribution caused by the water. The deviation from "ideal", linear behaviour is called the excess volume V^E. This quantity decreases markedly with increasing pressure from over eight $cm^3 mole^{-1}$ at 500 bar to nearly 2 cm^3 $mole^{-1}$ at 4000 bar. The fluid mixture tends to become more ideal as far as the volume

is concerned with increasing pressure. To what extent such a trend is general with aqueous electrolyte mixtures cannot yet be examined, since probably no similar systems have been investigated at such conditions.

The electric conductivity is particularly informative for ionic fluids. Thus the specific conductance has been measured for nine different hydroxide concentrations up to 450 °C and 2000 bar. Results are shown in Fig. 7 (36). The experimental difficulties to overcome in such measurements, mainly caused by the corrosive action of the fluids, are considerable. Thus, an accuracy as usual in conductance determinations can not be expected. The Fig. 7 shows that, beginning from the pure hydroxide, the addition of water at first produces only a modest increase of conductance. Decrease of effective charge carrier concentration and increase of ion mobility compensate each other. With further growing water content, an increase of conductance is observed, followed by a maximum and the necessary decrease to zero concentration. For comparison a few data for normal conditions are shown.

The molar conductance Λ in $cm^2 ohm^{-1} mol^{-1}$, as shown for 400 °C in Fig. 8 may, be more instructive. The conductance decrease from dilute solutions to moderate concentrations is very steep and at a mole fraction of 0.5 it is already approaching the fused salt magnitude. It is obvious, that a conventional

theoretical description, based on Debye-Hückel-theory will not suffice to represent this conductance behaviour over the whole concentration range. Functions which begin at the water-rich side do not adequately describe the conductance near the fused salt. A successful attempt has been made with a mixture concept, which combines several transport mechanisms. It is expected, that this procedure can serve for other systems as well.

V. COMBUSTION

The preceding thermodynamic investigations have shown, that dense supercritical water is completely miscible with second components of non-polar particles. This is true, for example, for water-methane and water-oxygen. Very probably also a mixture of both of the two gases can form a homogeneous phase with water. Thus one should assume, that "hydrothermal combustion" could be supported in such phases. An autoclave with sapphire windows was designed to hold and observe water-gas mixtures to 500 °C and 2000 bar. Through a narrow nozzle, injection of methane or oxygen into the pressurized aqueous mixture at slow flow rates of a few cubic millimeters per second is possible. If, for example, oxygen is slowly injected into a homogeneous mixture of water with 30 mole percent of methane, spontaneous ignition occurs already at temperatures as low as 700 K. Steadily burning flames are observed at 1000 bar and even at 2000 bar of pressure. A photograph of such a "supercritical" hydrothermal flame is shown in Fig. 9.* The formation of the flame is remarkable, since normally spontaneous ignition

*The Figure is given at the end of the book

temperatures for oxygen-methane mixtures are reported to be around 550 °C. The high pressure obviously reduces the ignition temperature markedly and the quenching effect of the dense water is not as pronounced as expected. The view of Fig. 9* is through sapphire windows of about 8 mm diameter. The medium in which this flame burns is a fluid of 70 mole percent water and 30 mole percent methane at 450 °C and 2000 bar. Phase seperations at these temperatures ($T_c(H_2O)$ = 374 °C) do not occur. Very recent supplementing experiments have been made with argon instead of water. The appearance of the flame is not very different. The burning velocity of these high pressure flames is very small: about 1 cm sec^{-1} or even less. High pressure flames described in the literature seem not to exceed about 70 bar of pressure.

VI. CONCLUSION

In conclusion it may be mentioned again, that the dense fluids at supercritical conditions are media which provide unique possibilities to explore the appearance and the variation of chemical and physical properties over very wide ranges of conditions. Unusual miscibility, high chemical reaction rates, continuous transition from molecular to ionic behaviour and other phenomena can be studied. Predictions for behaviour beyond the present experimental regions based on uncomplicated models and procedures appear to be feasible.

References

1. J.D. van der Waals, Ph. Kohnstamm: "Lehrbuch der Thermostatik", Vol. II, Verlag Barth, Leipzig 1906.
2. J.R. Krichevsky, D.S. Ciclis, Zhur.Fiz.Khim. 17, 126 (1943).
3. J.S. Rowlinson, F.L. Swinton: "Liquids and Liquid Mixtures", 3Ed. Butterworth, London 1982.
4. E.U. Franck, Physica, 139 + 140 B, 21 (1986).
5. E.U. Franck, J.Chem.Thermodynamics, 19, 225-242 (1987).
6. N.G. Sretenskaja, M.L. Japas, E.U. Franck, to be published in Ber.Bunsenges.Physikal.Chem.
7. L.C. Randall, Sep.Sci.Technol. 17, 1 (1982).
8. E.U. Franck, Ber.Bunsenges.Phys.Chem. 88, 862 (1984).
9. G.M. Schneider, E.Stahl, G. Wilke (Eds.), "Extraction with supercritical gases", Verlag Chemie, Weinheim 1980.
10. M.E. Paulaitis, J.M.L. Penninger, R.D. Gray, P. Davidson (Eds.), "Chemical Engineering at Supercritical Fluid Conditions", Am. Arbor Science Publishers, Am.Arbor Michigan 1982.
11. J.M.L. Penninger, M. Radosz, M.A. McHugh, V.L. Krukonis (Eds.), "Supercritical Fluids Technology", Process Technology Proceedings 3, Elsevier, Amsterdam 1985.
12. G. Brunner, S. Peter, Chem.Ing.Technik 53, 529 (1981).
13. G.L. Rössling, E.U. Franck, Ber.Bunsenges.Phys.Chem. 87, 882 (1983).

14. H. Ebeling, E.U. Franck, Ber.Bunsenges.Phys.Chem. 88, 862 (1984).

15. H. Ebeling: "Löslichkeit von Feststoffen in hochkomprimierten, überkritischen Gasen - untersucht am Beispiel des Coffeins", Thesis, Inst.f.Physikal.Chem., Univ. Karlsruhe 1987.

16. H. Ebeling, E.U. Franck, "Solubility of Caffeine in Compressed Supercritical Gases and Gas-Mixtures" to appear in Ber.Bunsenges.Phys.Chem. 1988.

17. S.M. Walas, "Phase Equilibria in Chemical Engineering", Butterworths, Boston, 1985.

18. R.L. Scott, P.H. van Konynenburg, Disc.Far.Soc. 49, 87 (1970). P.H. van Konynenburg, R.L. Scott, Phil.Trans. Roy.Soc. (London), A, 1980, 298, 495.

19. K.E. Gubbins, C.H. Twu, Chem.Eng.Sci. 33, 863, 879 (1978) G.H. Twu, K.E. Gubbins, C.G. Gray, J.Chem.Phys. 64, 5186 (1976).

20. M.L. McGlashan, J.Chem.Thermodynamics, 17, 301 (1985).

21. U. Deiters, Chem.Eng.Sci., 37, 855 (1982), Fluid Phase Equilibria 10, 173 (1983).

22. L.A. Kleintjens, Fluid Phase Equilibria 10, 183 (1983).

23. S. Peter, H. Wenzel: "Phase Equilibria and Fluid Properties in the Chemical Industry Symposium"EFCE Publ. Series, No. 11, (1980).

24. S. Peter, G. Brunner, R. Riha, Chem.Ing.Technik, 46, 623 (1979).

25. T. Boublik, J. Nezbeda, J.Chem.Phys.Letters 46, 315 (1977), 51, 1429 (1984).

26. M. Christoforakos, E.U. Franck, Ber.Bunsenges.Phys.Chem. 90, 780 (1986).

27. N.F. Carnahan, K.E. Starling, J.Chem.Phys. 51, 635 (1969).

28. K. Tödheide, E.U. Franck, Z.Phys.Chemie N.F. 37, 387 (1963).

29. Z.Alwani, G.M. Schneider, Ber.Bunsenges.Physikal.Chem. 71, 633 (1967).

30. E. Brandt: "Phasengleichgewichte ternärer, fluider wasserhaltiger Systeme bis zu hohen Drücken und Temperaturen", Thesis, Inst.f.Physical Chemistry, Karlsruhe, Univ. (1987).

31. R.P. Seward, J.Amer.Chem.Soc. 73, 515 (1951).

32. A.N. Campbell, W.G. Paterson, Can.J.Chem. 30, 1004 (1958).

33. R. Hilbert, K. Tödheide, E.U. Franck, Ber.Bunsenges.Phys. Chem. 85, 636 (1981).

34. M. Uematsu, E.U. Franck, J.Phys.Chem.Ref.Data 9, 1291 (1980).

35. S. Kerschbaum, "Die Dichte von H_2O-NaOH-Mischungen bis zu 400 °C und 4000 bar", Thesis, Institute for Physical Chemistry, Karlsruhe University (1987).

36. A. Eberz, "Elektrolytische Leitfähigkeit im System H_2O-NaOH im gesamten Mischungsbereich bis 450 °C und 3000 bar". Thesis, Institute for Physical Chemistry, Karlsruhe University (1987).

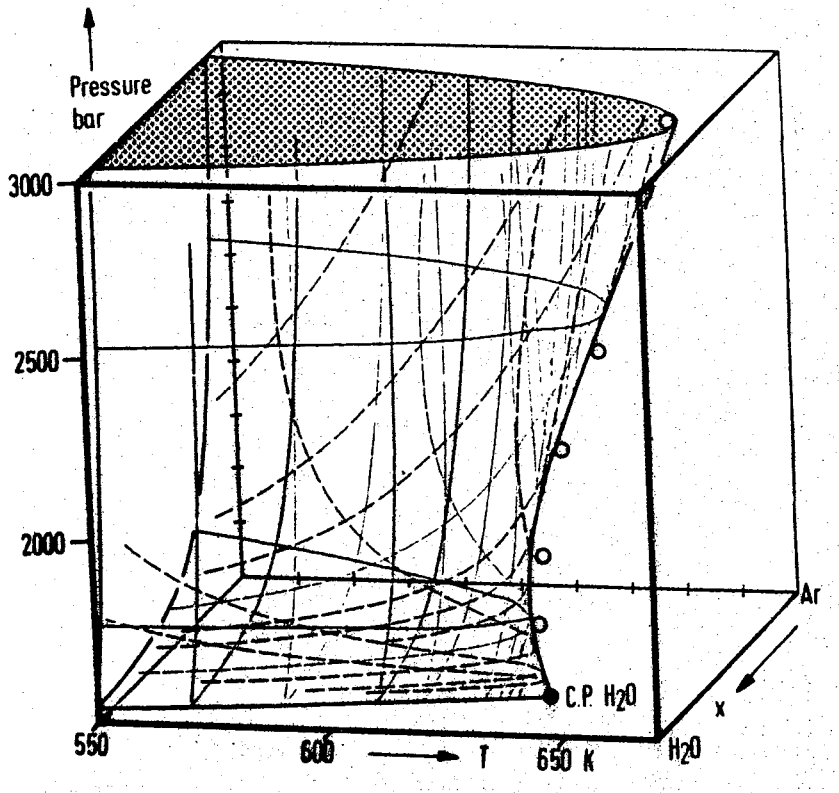

Fig. 1. Phase diagram of the water-argon system at high pressures and temperatures. o o o : Experimental points on the critical curve. x : Mole fraction of water.

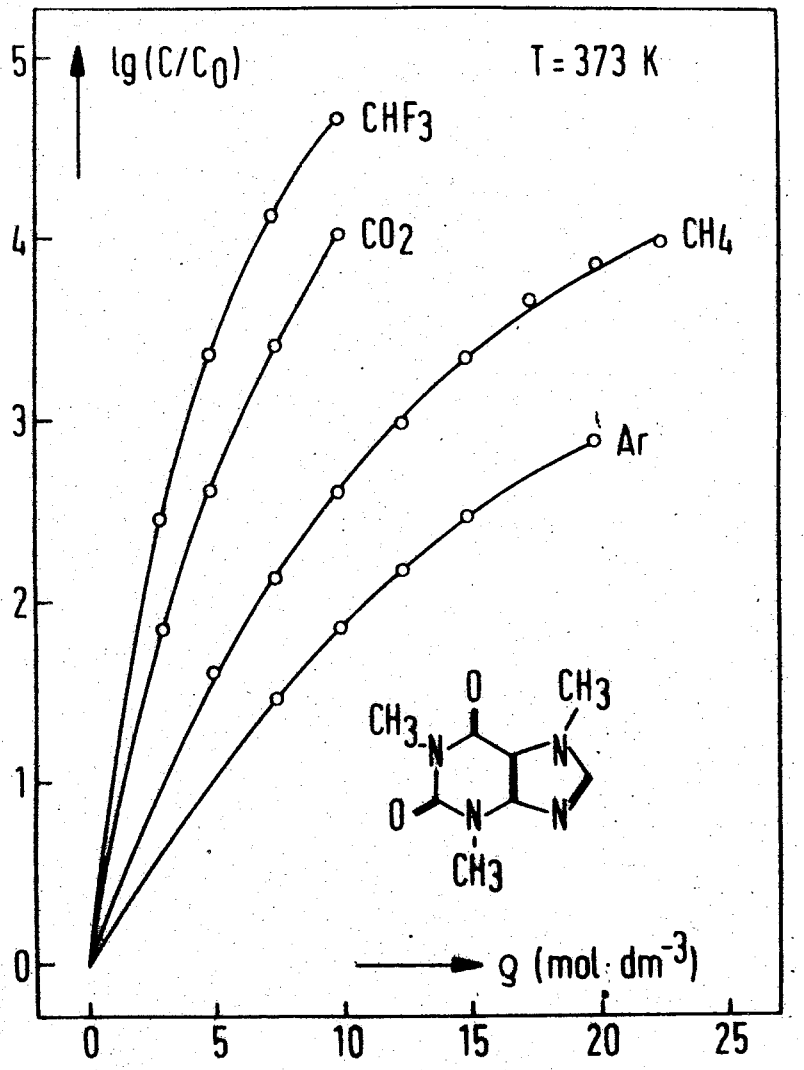

Fig. 2. Enhancement factors (c/c_o) of caffeine (see formula) in several gases as functions of gas density ϱ at 100 °C.

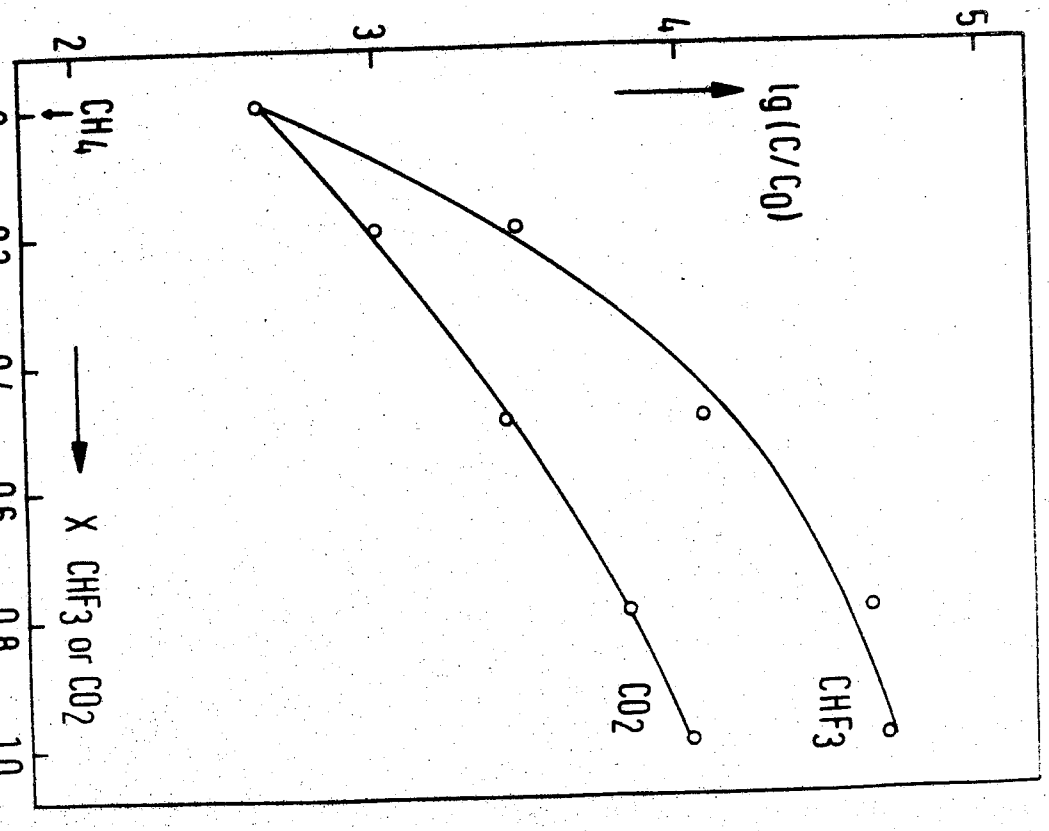

Fig. 3. Enhancement factors (c/c_0) of caffeine in CH_4-CHF_3 and CH_4-CO_2-mixtures as functions of mole fractions x of CHF_3 or CO_2. Temperature: 100 °C. Total gas density constant = 10 mol dm^{-3}.

28

$$p(T,V_m) = \frac{RT}{V_m} \cdot \frac{V_m^3 + V_m^2 \beta + V_m \beta^2 - \beta^3}{(V_m - \beta)^3} - \frac{4\beta RT}{V_m^2} (\lambda^3 - 1) \left[\exp\left(\frac{\varepsilon}{kT}\right) - 1\right]$$

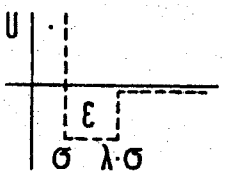

with $\beta(T) = \frac{\pi}{6} N_0 \sigma^3(T)$;

$$\beta(T) = \beta(T_c) \left(\frac{T_c}{T}\right)^{3/m}$$

$$\beta(T_c) = 0.04682 \frac{RT_c}{p_c} \; ; \; \frac{\varepsilon}{k} = T_c \cdot \ln\left[1 + \frac{2.6503}{(\lambda^3 - 1)}\right]$$

λ : preferably from 1.5 to 2.5 ; $m = 10$

For mixtures : $\varepsilon_{12} = \xi \sqrt{\varepsilon_1 \varepsilon_2}$; $\sigma_{12} = \zeta (\sigma_1 + \sigma_2)/2$.

29

Fig. 4. Equation of state to calculate phase diagrams, critical curves and supercritical homogeneous phases of binary fluid mixtures to high temperatures and pressures (26). The equation has a repulsion and an attraction term.

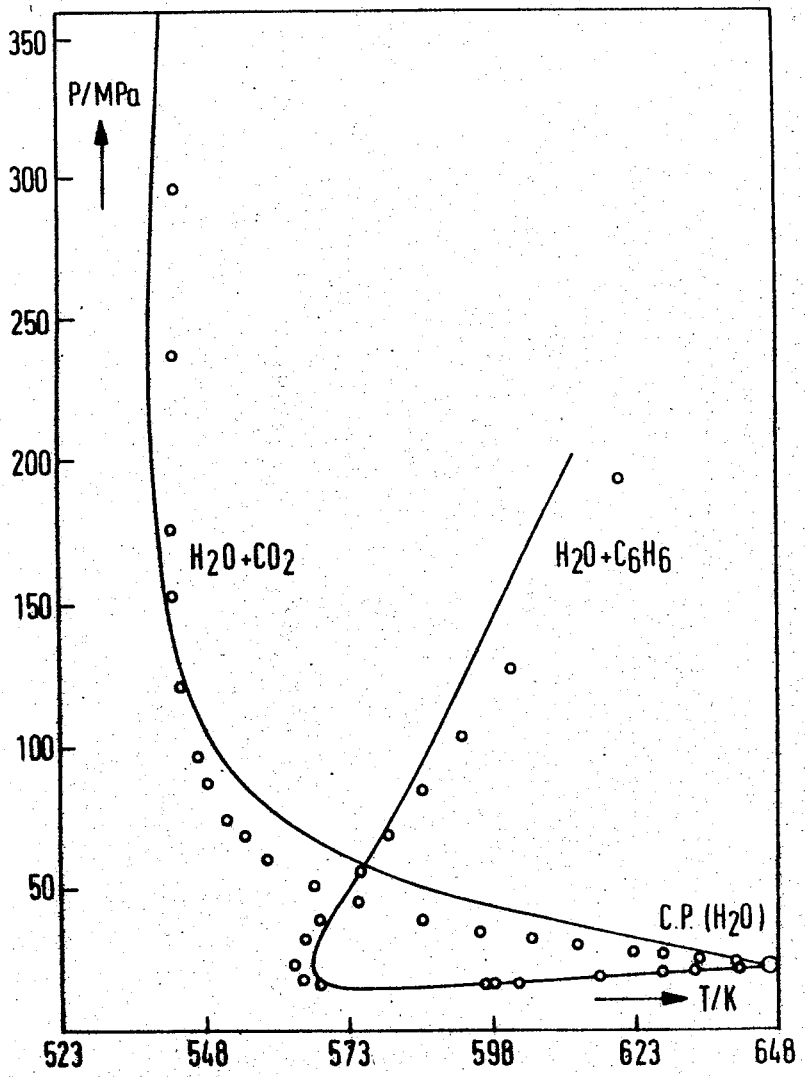

Fig. 5. Critical curves for the binary water-carbon dioxide and water-benzene systems, calculated with the equation of state (see Fig. 4). o o o : Experimental points.

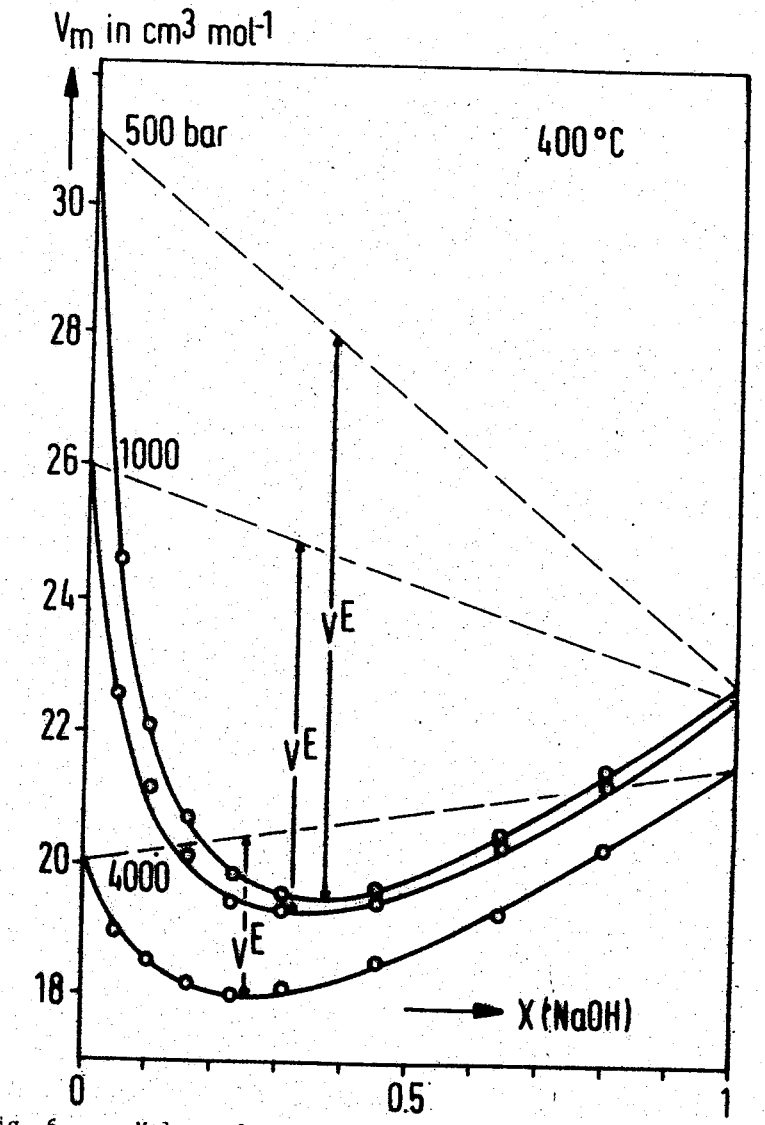

Fig. 6 Molar volumes of water-sodium hydroxide mixtures at 400 °C and three different pressures. V^E="Excess volume". x = mole fraction. o o o : Experimental points.

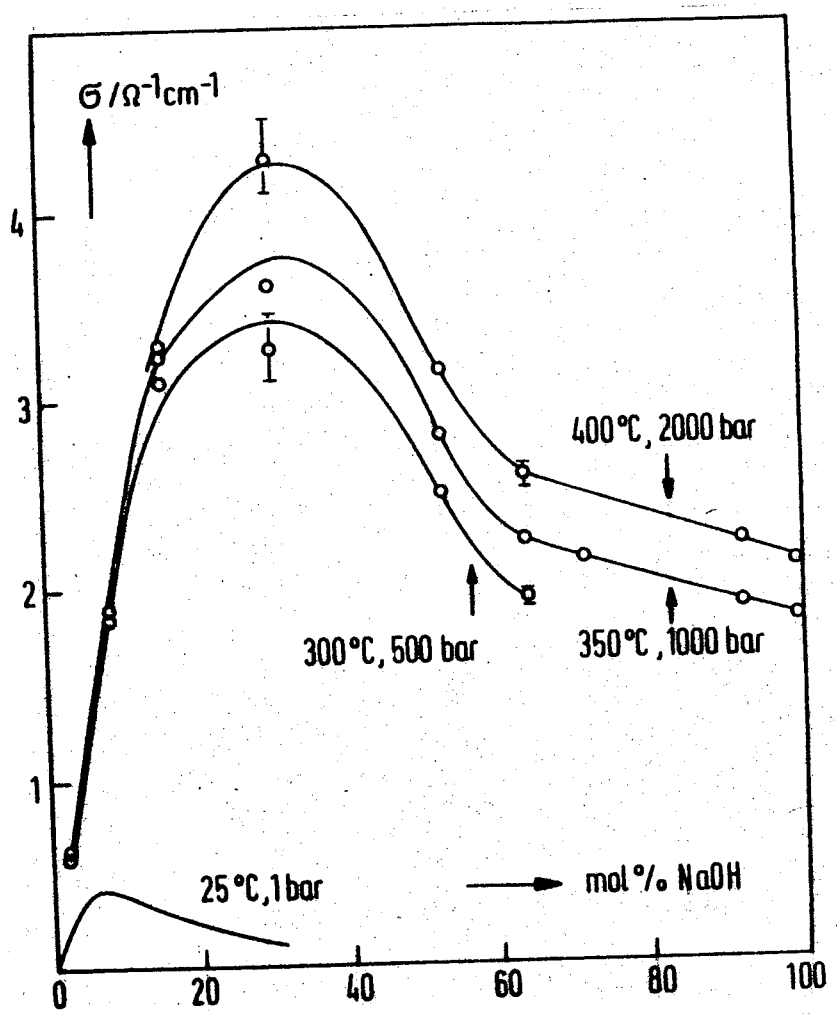

Fig. 7. Specific electrolytic conductance σ of water-sodium hydroxide mixtures at different temperatures and pressures. o o o : Experimental points.

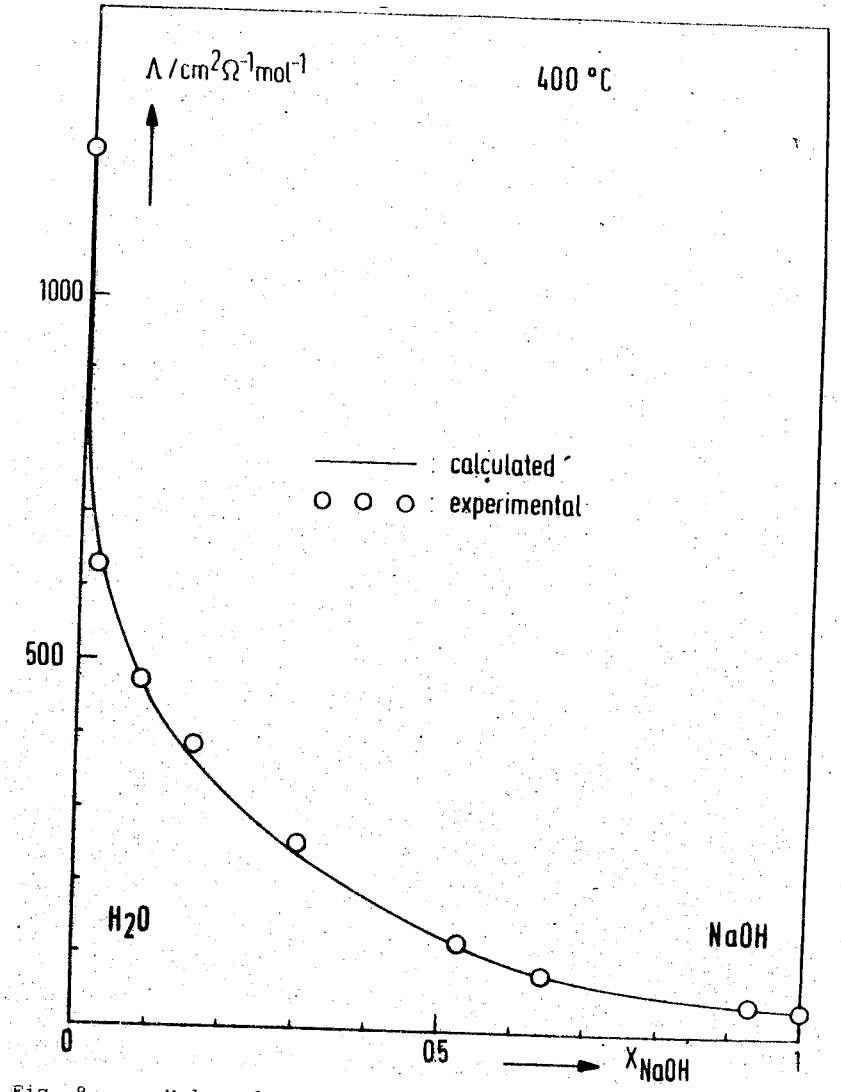

Fig. 8. Molar electrolytic conductance Λ of water-sodium hydroxide mixtures at 400 °C at a constant density of 50 mol dm^{-3}. The measurements were extended in part to 2000 bar.

THE STATISTICAL THEORY OF THE CONDENSED SYSTEM EQUATION OF STATE AT HIGH PRESSURES

V.M.Sysoev[I], A.V.Chaly[I], M.S.Labinov[2]
[I]Kiev Medical Institute, Kiev, USSR
[2]Institute of Technical Thermophysics, Kiev, USSR

One of the main problems in the statistical physics of condensed systems is the problem of the adequate equation of state to describe the thermodynamical properties of the substance in the wide range of pressure values. Here it is being solved by means of thermodynamic perturbation theory and the integral equations of the statistical theory of dense gases and liquids.

While investigating the dense matter in the wide range of pressure values, the question about the choosing of satisfactory small parameter takes place.

Considering the system behavior being far from stability boundaries (critical point, spinodal curve et al.), the relative volume difference $\Delta V=(V_o-V)/V_o$ may be used as the small parameter mentioned above. The $\Delta V \ll I$ condition is being realized in the wide pressure range only in case, when another dimensionless parameter

$$p_o \beta_{T_o} \ll I \qquad (I)$$

is also small. Here p_o, β_{T_o} - are the pressure value and isothermal compressibility corresponding to $V=V_o$. It is evident, that the accuracy of the condition (I) grows higher together with the pressure growth. In order to build the perturbation theory we use the scaling transformation of the statistical partition function

$$Q(N, T, V)=q^{3N} Q_V(N, T, V_o) \qquad (2)$$

Here $q^3 = V/V_o$,

$$Q_V(N, T, V_o)=(N!)^{-I} \int_{V_o} d\Gamma \exp\left[-U(\underline{r}_i/a)/k_\beta T\right] \qquad (3)$$

- the statistical partition function of the system, considering of N particles in V_o. The potential energy in (3) corresponds to the renormalized radius of the intermolecular forces action $a=a_o/q$.

Since ΔV value is taking place in the formula for the configurational part of the statistical partition function as the result of the above transformation, it gives us a possibility to build the perturbation theory row for the free energy. The application of the basic state on the (V_o, p_o) isotherm instead of basic system makes the main difference between our method and the standard methods of perturbation theory.

If we choose

$$\varphi_I(r) = \varepsilon (r/a_o)^{-m} \qquad (4)$$

or

$$\varphi_2(r) = \varepsilon \exp(-r/a_o) \qquad (5)$$

as the repulsive intermolecular potential, we obtain the equation of state being the modification of Tait equation

$$p-p_o=Nk_\beta T \Delta V/V + [\exp(\Delta V/A)-I]\,[B(T) + p_o]\,. \qquad (6)$$

Here $A=3/m$ for $\varphi_I(r) \sim r^{-m}$ and $A=3\,[\ln(\varepsilon/k_\beta T) + 2]^{-I}$ for $\varphi_2(r) \sim e^{-r/a_o}$ and

$$B(T) = - Nk_\beta T/V_o + p_k(T, V_o). \qquad (7)$$

Here $p_k(T, V_o)$ is the cohesive pressure of the basic state $V=V_o$, $p=p_o$, which is determined by the attractive intermolecular forces.

Since $V/V_o=\rho_o/\rho$ (ρ_o is the basic density) it is obvious, that the local scaling transformation $\underline{r}' = q(\underline{r})\underline{r}$ corresponds to the virtual changing of the density in the $\underline{r}$ point of the system under investigation. That is why it seems natural to choose the creative functional for the construction of the statistical theory integral equations as follows

$$\Phi = F_I(\underline{r}\,|\,\psi)\,\hat{\underline{M}}_{\underline{r}}\,(\psi/k_\beta T)=$$

$$=F_I(\underline{r}\,|\,\psi)\,[\exp(-\underline{r}\cdot\underline{\nabla}_{\underline{r}})-I]\,(\psi/k_\beta T). \qquad (8)$$

Here $F_I(\underline{r}\,|\,\psi)$ -one-particle distribution function in the external field ψ. The corresponding integral equation for the radial distribution function has the Ornstein-Zernike form with the direct correlative function such as

$$\hat{\underline{M}}_{\underline{r}}\, c(r) = -g(r)\hat{\underline{M}}_{\underline{r}}(\varphi/k_\beta T) \qquad (9)$$

The choosing (4) intermolecular potential together with the using

of virial theorem and compressibility formula gives us the opportunity to receive one of the modifications of the Tait equation from the equation (9) as follows:

$$\Delta V = \frac{\ln\left\{[p+B(T)] \,/\, [p_o+B(T)]\right\}}{A^{-I}+\ln\left\{[p+K(T)] \,/\, [p_o+K(T)]\right\}} \qquad (IO)$$

Here K is the adaptive parameter, having the sense of pressure value, under which the first coordinative number begins to change substantually. When $p \gg p_o$, $p \gg B(T)$, $p \gg K(T)$ the equation (IO) reaches simple form

$$p = p_o e^{\delta V_o/V}, \quad \delta = A^{-I}+\ln\left\{[p_o+B(T)] \,/\, [p_o+K(T)]\right\}. \qquad (II)$$

The one-parameter equation (II), being satisfactory for the supercritical pressures can be easily verified by means of experimental data. For water and steam it is beginning to fulfill at pressure values higher than $p=IO^4$ MPa. The processing of the experimental data for the water isotherms within the temperature range I75 °C to I000 °C and pressure range IO^4 MPa $\leq p \leq 2{,}5 \cdot IO^4$ MPa gives us the error value of the theoretical approximation of the specific volumes not higher than 0.2%.

The equations (6) and (IO) were verified for several liquids, such as water, n-propanol, ethylene, and n-hexane in the wide range of pressures and temperatures, where the condition (I) is correct. For some of these liquids within the pressure range IO^5-IO^9 Pa the good quantitative agreement between the calculated values and experimental data (with an accuracy of 0.0I% for the specific volumes and I% for isothermal compressibility) was reached.

Resuming the paper we must emphasize, that the conclusions, received by means of statistical physics method are not based on any model considerations, which makes it possible to apply the above equations of state for the investigation of dense gases, liquids and solids when the inequality (I) takes place.

DETERMINATION OF CONSTANTS FOR A GENERALISED TAIT EQUATION DIRECTLY FROM ULTRA SOUND MEASUREMENTS

W.G.Scaife, C.G. Lyons
Engineering School, Trinity College Dublin, Ireland

Introduction

The accurate determination of density of liquids at high pressures is a difficult experimental task. The demands made on precision are increased if the p, V, T data are to be used to de rive other thermodynamic quantities, which require estimates to made of derivatives from the equation of state f(p,V,T) = 0. Alt native methods of determining density are therefore of great val since they may help uncover unsuspected experimental flaws. Mea rements of the velocity of sound U(p,T) offer this possibility. One approach is to use an equation of state and data for the sp cific heat $C_p(T)$ at ambient pressure to predict the sonic veloc at elevated pressures, and compare this with direct measurement of U(p,T), /I/.

A more usual approach is to use measured sound velocities U(p,T), with densities $\rho(T)$ and specific heats $C_p(T)$ at ambie pressure to predict $\rho(p,T)$. A step by step, isothermal, proced has been described /2/, using

$$\rho(p) = \rho(0) + \int_I^p I/U^2(p,T)\, dp + T\int_I^p \alpha^2/C_p \, dp \qquad (I$$

Russian workers /3/ used an expression to calculate density,

$$\rho(p) - \rho(0) = 3/K_o \left| (U-U_o) + 2(Z_I + Z_2) \ln\left|\frac{U - Z_2}{U_o - Z_2}\right| - (Z_I + Z_2)\left[I/(U-Z_2) - I/(U_o - Z_2)\right]\right| \qquad (I$$

where K_o and Z_I come from isothermal fits of U(p,T), and Z_2 co from ambient pressure data. We propose a different approach, u non-linear least squares algorithms.

Sonic Tait Equation

We propose to obtain the parameters for the so called Tai equation by fitting all the values of U(p,T) in one operation.

call the equation with parameters so obtained the "sonic" Tait to distinguish it from the more usual form in which the parameters come from a fit of densities, the "density" Tait. Temperature can be incorporated into the Tait equation by writing /2/,

$$v(p,T) = V_o f_I(T) \left\{ I - A f_2(T) \ln \left[I + p/B f_3(T) \right] \right. \qquad (3)$$

in which f_I, f_2 and f_3 are polynomials in T of order three or higher. The parameters to be determined are A, B and Π_i (Π_i are the coefficients in f_2 etc). In the same way as other workers /2/ /3/, we assume values for density at ambient pressure i.e. V_o and coefficients for f_I. This equation can be readily manipulated to yield $(\delta v/\delta p)_T$, $(\delta v/\delta T)_p$, etc in terms of the parameters of the sonic Tait. Now,

$$U^2(p,T) = v(p,T)/K_s(p,T) \qquad (4)$$

$$K_s(p,T) = K_T(p,T) - T\alpha^2(p,T)v(p,T)/C_p(p,T) \qquad (5)$$

and

$$C_p(p,T) = C_p(p_o,T) - T \int_{p_o}^{p} (\delta^2 v/\delta T^2)_p \, dp \qquad (6)$$

Equations 3, 4 and 5 can be combined to give,

$$U_j(p,T) = \phi(p_j, T_j, C_{pj}, \ldots \Pi_i) \qquad (7)$$

The non-linear least squares program now fits U_j, p_j and T_j to (7) so as to minimize $\Sigma(U-\hat{U})^2$. The program requires initial guesses for the Π_i as well as expressions for e.g. $\delta\phi/\delta A$, $\delta\phi/\delta\Pi_2$ etc.

Once the parameters for (3) have been determined, it can be used to predict not only densities but K_T, K_s, γ etc for comparison with literature values.

Results (See Table)

Conclusions

The possibility of fitting a complete data set of U,p,T values to an equation of state in p,V,T like (3), using non-linear least squares, has been demonstrated. In the case of water at low pressures the results are satisfactory. At higher pressures, the

fit of U(p,T) is less satisfactory and the ability to predict density is quite poor. In the case of nonane the sonic Tait behaves less well. The discrepencies may in part be due to experimental deficiencies, or to inadequacy of equation (4) for the liquid involved. Finally the cause may lie in the form of the Tait equation, since much improved fits can be achieved by limiting the temperature span of the data used. It may be that inadequacies arising from the way that temperature is incorporated into (3), are magnified by this method of use.

Water

Range	A measured	B predicted	S	δ_{max}
0 - 100 C and 0.1 - 100 MPa	s-Tait /4/	ρ /6/ U /4/	.003 % I.4 m/S	.007 % 3.9 m/S
	d-Tait /5/	ρ /5/ U /4/	.001 % 2.8 m/S	.003 % 5.1 m/S
30 - 80 C and 0.1 MPa to 0.6 0.8 GPa	s-Tait /9/	ρ /10/ U /9/	.11 % 2.9 m/S	.40 % 13.5 m/S
	d-Tait /8/	ρ /8/ U /7/	.015 % 12.9 m/S	.12 % 30.0 m/S

n-Nonane

Range	A measured	B predicted	S	δ_{max}
0.1 MPa - 0.6 GPa	d-Tait /10/	ρ /10/ U /9/	.034 % 15.6 m/S	.11 % 53.0 m/S
30 - 100 C	s-Tait /9/	ρ /10/ U /9/	.28 % 7.4 m/S	.98 % 41.5 m/S
40 MPa - 200 MPa and 30 - 120 C	s-Tait /3/	ρ /10/ U /3/	.1 % 5.0 m/S	.23 % 15.6 m/S

Notes:
"s-Tait", equ.(3) with parameters from U data.
"d-Tait", equ.(3) with parameters from ρ data.
S is s.e.e. of δ, where δ=100 (A-B)/A for ρ and δ=A-B for U. / / source reference.

References

I. Lyons, C.G. and Scaife, W.G., A generalised Tait equation as a means of intercomparison of measured (pVT) data of hydrocarbon liquids. Physica (1986) 139 & 140B 113-115

2. Davis, L.A and Gordon, R.B. Compression of mercury at high pressure. J.Chem.Phys. (1967) 46 2650-60

3. Kir'yakov, B.C. and Kuzmin, V.N. Velocity of sound and thermodynamic properties of liquid n-nonane. Nauk Tr.Kursk State Ped.Inst. (1974) 40 216-221.

4. Chen, C.T. and Millero, F.J., Reevaluation of Wilson's sound speed measurements of pure water. J.Acoust.Soc.of Am.(1976) 60 1270-1273.

5. Fine, R.A. and Millero F.J., Compressibility of water as a function of temperature and pressure. J.Chem.Phys. (1973) 59 5529-5536.

6. Kell, G.S. and Whalley, E., Reanalysis of the density of liquid water in the range 0-150 degC and 0-1 kbar. J.Chem. Phys. (1975) 62 3496-3503.

7. Holton, G., Hagelberg, M.P., Kao, S. and Johnson, W.H.,Ultrasonic velocity measurements in water at pressures to 10,000 kg/cm2. J.Acoust.Soc.of Am. (1968) 43 102-107.

8. Grindley,T. and Lind, J.E., pVT properties of water and mercury, J.Chem.Phys. (1971) 54 3983-3989.

9. Melikhov, Y.F., Acoustical, thermal and calorific properties of n-nonane at high pressure (1981) Nauk Tr.Kursk Ped. Inst. 15 72-82.

10. Grindley, T. and Lind, J.E., The residual energy and entropy of hydrocarbon liquids and their relation to the liquid structure. J.Chem.Phys. (1978) 11 5046-5052.

SOME FEATURES OF PRESSURE INFLUENCE UP TO 1000 MPa ON INORGANIC SALT SOLUBILITY IN WATER

B.R.Churagulov
M.V.Lomonosov Moscow State University, Moscow, USSR

The thermodynamic analysis carried out in [1,2] has shown that the initial sign of the pressure coefficient of salt solubility in water (p.c.s. $-\partial m_s/\partial P$), where m_s is the molality of the saturated solution, should be opposite for the salts forming diluted (p.c.s >0) and high-concentrated (p.c.s. <0) saturated solutions. In the case of the latter (when the mole fraction of the salt $N_s \to 1$) prevails the contribution of the positive volumetric effect of the salt melting at the given T and P ($\Delta V^T_{melt.}$) to the partial molar volumetric effect of the salt phase dissolving into saturated solution ($\Delta \bar{V}_s$); in the case of the former, when $N_s \to 0$, prevails the contribution of the negative partial volumetric effect of mixing of the melted overcooled salt with saturated solution ($\Delta \bar{V}_{mix.s}$) resulting from ion hydration.

Consideration of the experimental and calculated values of p.c.s (for more than 70 solid phases) obtained by the author on the basis of both his own and literature data has confirmed the conclusions of the thermodynamic analysis. There were identified the limits of three concentration regions of saturated solutions of various pressure dependences of solubility [2,3,4].

The upper limit of the first concentration region where the solubility, as a rule, initially increases with increasing pressure (p.c.s. >0), can be determined from the concentration maximum on the dependence of the specific electric conductivity ($\varkappa$) of solution upon the concentration ($m_{\varkappa max}$) at 298 K and at the atmospheric pressure. For various types of electrolytes the value $m_{\varkappa max}$ is equal to the following (in mol/kg of water): 6-10 for 1,1 electrolytes; 2.5-4.0 for 1,2 electrolytes; 2-3 for 2,1 electrolytes; 1.7-2.0 for 2,2 electrolytes [5]. In 22 out of 28 solid phases ($m_s < m_{\varkappa max}$) p.c.s >0 for both anhydrous salts and water-rich crystal hydrates, for example, $Na_2SO_4 \cdot 10H_2O$ /4/. The only exception are 1,1 salts formed by weakly hydrated ions for which the negative $\Delta \bar{V}_{mix,s}$ is small with respect to the module: CsBr, CsJ, NH_4Cl, NH_4Br, NH_4ClO_4 (at 298 K) as well as CdJ_2, its aqueous solutions undergoing vigorous acidocomplexing followed by a considerable increase of the salt-water system volume [2,4].

In the case of salts with saturated solutions of very high concentration ($m_s > 12.0$, the third concentration region) solubility decreases with increasing pressure (p.c.s. < 0 for all the solid phases without any exception: 18 examples of anhydrous as well as crystal hydrates are available). This phenomenon manifests a qualitative analogy with the pressure dependence of non-polar solids solubility in non-polar solvents [4,6].

In the second (transition) concentration region ($m_{1\ max} < m_s < 12.0$) there are examples of both decreasing and increasing solubility with increasing pressure. Of more importance in this case becomes the amount of water of crystallization in the solid phase (the number "n"). In the case of water-rich crystal hydrates ($n \geq 4.0$) p.c.s. < 0 (there are 15 examples), which is the same as in the case of the salts in the third concentration region. For anhydrous salts and low-water crystal hydrates ($n < 2$), p.c.s > 0 (there are 12 examples), which is the same as for the salts in the first concentration region of saturated solutions.

There is a known case of the p.c.s inversion from plus to minus for one and the same solid phase ($CuSO_4 \cdot 5H_2O$) at the atmospheric pressure due to a great increase of the saturated solution concentration at the temperature rise from 298 to 348 K (from 1.43 to 3.18 mol/kg of water) and to a transition of the saturated solution from the first to the second concentration region (m_{max}-2.0 mol/kg of water) [4,7].

Isotherms m_s-P for 17 salt-water systems with the salts readily and moderately soluble in water were considered in the pressure range up to 1000 MPa [4]. In the case of all the salts with satured solutions belonging to the first concentration region (except cadmium iodide) as well as in the case of anhydrous salts and low-water crystal hydrates in the transition region one can observe: a) a monotonous increase of solubility with increasing pressure in the entire region of the solid phase presence ($CdCl_2 \cdot H_2O$, $CdSO_4 \cdot H_2O$, $ZnSO_4 \cdot H_2O$, $CdSO_4 \cdot 8/3H_2O_I$) up to 1000 MPa as in the case of potassium iodide; b) isotherms with the maximum (NH_4ClO_4 at 273 K, K_2SO_4, $CuSO_4 \cdot 5H_2O$, NaCl at 298 K, $CdBr_2$ at 348 K). For all solid phases in the third concentration region and for water-rich crystal hydrates in the second concentration region m_s decreases with increasing pressure to 1000 MPa at a decreasing rate: NH_4NO_3, $CdBr_2 \cdot 4H_2O$, $CdCl_2 \cdot 2.5H_2O$, $CdCl_2 \cdot 4H_2O$, $CdSO_4 \cdot 8/3H_2O_{II}$, $ZnSO_4 \cdot 6H_2O_{II}$, $CuSO_4 \cdot 5H_2O$ at 348 K, and all solid phases in the systems: $CaCl_2$-H_2O, $ZnCl_2$-H_2O, $ZnBr_2$-H_2O, ZnJ_2-H_2O, $Zn(NO_3)_2$-H_2O, $Cu(NO_3)_2$-H_2O,

$Cd(NO_3)_2$-H_2O. A similar picture is observed for CdJ_2. A single example of the isother with the minimum is given by water-rich crystal hydrate $ZnSO_4 \cdot H_2O$ which belongs to the transition concentration region. The presence of maxima and minimum is due to the sign inversion of $\Delta\bar{V}_s$ of different solid phases at increasing pressure to 1000 MPa. In general, the character of pressure dependence of solubility of the solid phases described above are determined by the sign and the value $\Delta\bar{V}_s$ and its variations depending on the increasing pressure, which is shown by the values $\Delta\bar{V}_s$ (for 22 solid phases) resulting from the experimental data. The breaks on the isotherms m_s-P correspond to the phase transformations, mainly, to the formation of water-rich crystal hydrates [4,8].

Within one salt-water system, upon the isothermal increase pressure, crystal hydrates with a great "n" are found to be, as a rule, in equilibrium with the saturated solution, and an increase of "n" makes p.c.s. increasingly negative. An increase of pressure to 1000 MPa finally results in p.c.s. becoming negative for 16 out of 17 salt-water systems studied.

Increasing pressure changes the temperature of incongruent melting and eutectics of crystal hydrates as well as the composition of the saturated solution $m_s(P,T)$ along the equilibrium lines of the phases 8. Consideration of the experimental data for 24 crystal hydrates (halides, sulphates, nitrates of cadmium, zinc and copper, chlorides of sodium and calcium, sodium sulphate) in accordance with the thermodynamic analysis has exhibited examples of both increase (16 examples) and decrease (8 examples) of $m_s(P,T)$ at the increasing pressure to 1000 MPa. In a number of cases a change of $m_s(P,T)$ with increasing pressure changes the type of crystal hydrate melting: a) from incongruent to congruent melting ($Na_2SO_4 \cdot 10H_2O$, $ZnBr_2 \cdot 3H_2O$, $ZnCl_2 \cdot 4H_2O$, $Cu(NO_3)_2 \cdot 6H_2O$, $CaCl_2 \cdot 6H_2O$); b) from congruent to incongruent melting ($ZnCl_2 \cdot 2.5H_2O$, $Zn(NO_3)_2 \cdot 6H_2O$). Accordingly, the type of crystalhydrate transformation changes from peritectic to eutectic, and vice versa.

The regularities described above were found to be the basis for qualitative prediction of the behaviour at high pressures to 1000 MPa and relatively low temperatures of water-salt systems which have not been studied experimentally.

References

1. B.R.Churagulov, Zh.fiz.khimii, 1987, v.61, No.1, p.236-239.
2. B.R.Churagulov. In: "Thermodynamics in Geology" (in Russian).

Materialy Vsesoyuznogo simpoziuma. Tezisy dokladov. Chernogolovka, 1985, p.170-171.

3. A.K.Lyashchenko, B.R.Churagulov. Zh.neorganich.khimii, 1983, v.28, No.2, p.456-465.

4. A.K.Lyashchenko, B.R.Churagulov. In: "Thermodynamic Properties of Solutions under Extreme Conditions" (in Russian). Mezhvuzovski sbornik nauchnykh trudov, Ivanovo, Ivanovo Institute of Chemical Technology Publishers, 1986, p.36-46.

5. A.K.Lyashchenko, A.A. Ivanov. Zh.strukturn.khimii, 1981, v.22, No.5, p.69-75.

6. E.P.Doane, H.G.J.Drickamer. Phys.Chem., 1955, v.59, No.5, p.454-457.

7. A.N.Yakushenko, B.R.Churagulov, Zh. fisich.khimii, 1984, v.58, No.6, p.1563-1564.

8. B.R.Churagulov. In: "Chemical Thermodynamics"(experimental studies) (in Russian), Moscow, Moscow State University Publishers, 1984, p.193-212.

PHYSICO-MATHEMATICAL SIMULATION OF METHANE AND ARGON REMOVAL ABSORBING PROCESS BY LIQUID AMMONIA FROM SYNTHESIS GAS OF AMMONIA PRODUCTION

A.I.Pyatnichko, V.L.Saprykin, V.S.Shevchuk
Institute of Gas of the Academy of Sciences
of the Ukrainian SSR, Kiev, USSR

The elaboration of the theoretical experimental model of the absorption process under the pressure of 30MPa and moderate temperatures included the experimental research of methane and argon absorption from the five-component mixture H_2-N_2-CH_4-Ar-NH_3 by liquid ammonia on a pilot plant and carrying out the computerized research of process statics.

Earlier theoretical [1] and experimental [2] research have not described clearly the methane and argon absorption by liquid ammonia.

Purge gas was fed under the pressure of nearly 28MPa for carrying out the experiments from the unit of ammonia synthesis after a water condenser, liquid ammonia of the secondary condensation being used as an absorbent. The waste absorbent was returned to the output line of liquid ammonia under the pressure from 3-4 MPa and the resulting gas streams being thrown out into the atmosphere. Liquid ammonia of the refregerator cycle under the pressure of evaporation of the order of 0.15-0.2 MPa was used for saturated absorbent cooling. The main part of the unit is an absorption column consisting of two sections: the upper one is an absorption section and the lower section is a stripping one. The absorber case is made of two pieces of the 180x28mm pipe connected by the threaded flanges with a lens-shaped seal. The column inside this case is composed of two parts made of slured connections of 15 thin-wall shells with 100mm internal diameter and 150mm high, with the bases of the mass-exchange arrangements being placed between them . Seven mass-exchanged plates were mounted in the absorption section of the column and 4 - in the stripping one.

Purged gas was fed into the absorber, under the lower plate of the absorption section through the separator and the heater. Liquid ammonia was fed to the upper portion of the column through the heater and the filter. In the process of the countercurrent heat-mass-exchange with feeding gas liquid ammonia passes through the

absorption section, absorbing inert gases to the stripping section where partial stripping of hydrogen and nitrogen from liquid by methane and argon takes place. From the column the saturated absorbent was fed first to the ammonia refregerators, then to the desorber. With the temperature falling the absorbed gases were isolated, a portion of them being returned from desorber to the absorber for the stripping.

Expenses, pressure, temperature in the representative points, level of the liquid in the desorber were controlled using the experimental unit.

The composition of gas samples which has been determined by the complex method, included reaction of the ammonia and chromatographic analysis of the gas samples at two chromatographs with argon and hydrogen as gas carriers.

The variable parameters during the experiment were under the pressure from 26 to 28 MPa: absorption temperatures from 325 to 353 K; desorption temperature from 253 to 268 K; the purge gas expenses from 20 to 100 nm^3/h; the liquid ammonia expenses from 0.15 to 0.77 m^3/h. The correctness of the test was evaluated by the material balance, the divergence of the balance being over 10%, the results were not taking into account.

The mathematical model of argon and methane absorptional removal included description of absorption-desorption statics and the ammonia syntheses stages. The mathematical description of the statics of the multicomponent absorption-desorption process is represented by the equations of the general and component material balances and also by the vapor-liquid equilibrium equations. The calculations of the absorption column have been conducted from plate-by-plate method of step-by-step approximation, beginning with the upper plate, gas solution heat in liquid ammonia having not been taken into account.

Fig.1 represents some results of the experimental (solid lines) and analytical (dotted lines) investigations of the argon and methane absorption degrees for different liquid/gas ratios: line 1 - experimental data (desorption temperature 253 K); line 2 - calculated data for the experiment conditions; line 3 - calculated data in optimum conditions (desorption temperature 248 K). The degree of absorption was calculated as:

$$E_x = (y_1 - y_2)/y_1 ,$$

where Y_1 and Y_2 - initial and final contents of inerts (Ar or CH_4) in the gas respectively.

The agreement of the experimental and calculated data is satisfactory, the root mean-square deviation being not more than 14%. Obtained experimentally degrees of the inerts absorption are not representative due to nonoptimal absorption and desorption conditions. The absorption degrees for the optimal process obtained using the mathematical model proved the possibility of the effective inert removal from the synthesis gas by liquid ammonia with feeding gas loading 17-21 mol/t NH_3 and L/V = 6.5-8 mol/mol ratio.

The technological process was developed as a result of this research which application for the synthesis unit with productivity of 1500 t NH_3/day will allow production of more than 15 thousand ton of extra ammonia in other words saving more than 15 mln nm^3 of natural gas per year [3].

References

1. Alesandrini, C.G., Sherman, A.D., Lynn, S., Ind. Eng. Chem. Process Des. Develop., 12, 217 (1973).
2. Jigirey, T.S., Maximuk, B.J., Pyatnichko, A.I., Shevchuk, V.S Chimicheskaia Technologia, 5, 10 (1980).
3. Pyatnichko, A.I., Saprykin, V.L., ibid., 4, 3 (1985).

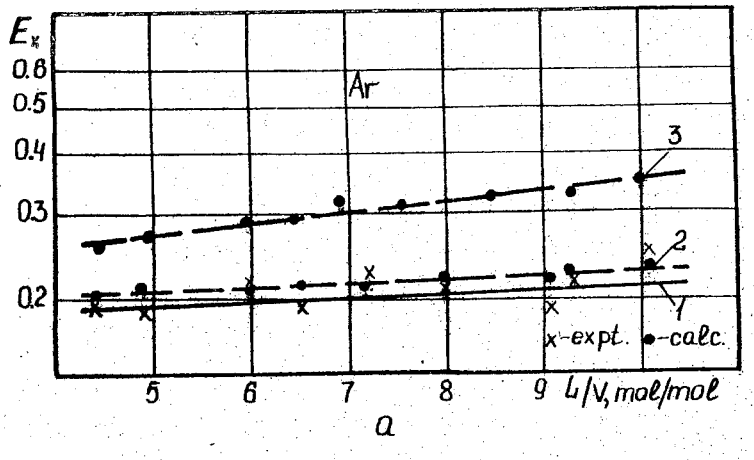

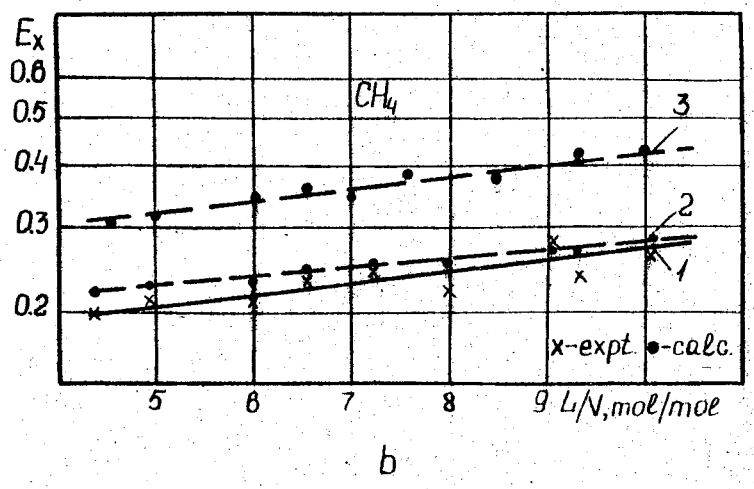

The degrees of inerts absorption dependent on the liquid/vapor ratio in the absorber under the absorption temperature 338 K: a- for argon; b- for methane.

SOUND VELOCITY IN PHASE SEPARATED BINARY GAS MIXTURES He-CO_2 AND He-Xe

L.L.Pitaevskaya
Institute for High-Pressure Physics, USSR Academy of Sciences, Troizk, USSR

The study of binary gas mixtures separating into two phases started long time ago and is actual now [1,2] we have investigated the mixture containing 7.7 mol.% Xe. In order to observe phase separation of gas mixture by an ultrasound method the chamber with 4 ultrasonic cells situated on different level in investigated gas was used [3]. The velocity of sound has been measured at 291-422 K and up to 300 MPa. The measurements conducted at the pressure decrease showed that sound velocity doesn't coincide with the one, taken at the increase and its value in the upper cell is greater than in the lower one. Having been increased to 350 K this discrepancy disappears. The results are presented in Fig.1 and the sound velocities values in pure gases are also given at 298 K /4, 5). The phenomena may by explain by fact that the pressure decreases quickly and so that the adiabatic cooling, which leads to the separation of the mixture takes place.

In order to measure sound velocity in the phase of system He-CO_2 we used the mixture containing 26.8 mol.% CO_2. Under separation two phases appear in the mixture: one phase is enriched with He, the other one is depleted.

The separation develops quickly and the equilibrium state remains for a long time under constant pressure and temperature. After sound velocity measurement we increase the pressure in the vessel again up to 10-12 MPa, add new portion of the initial mixture and automatic mixing of the former phase takes place. The separation into phases of other composition corresponding to the given pressure occurs. In Fig.2 the dependence of sound velocity on pressure is presented at a temperature of 298 K for the upper and lower cells in the He-CO_2 mixture and also for pure He [4] and CO_2 [5]. The sound velocity of the resulting phases is considerably lower in pure He within the entire investigated pressure range. The sound velocity in pure CO_2 is also higher than the one in both phases up to 180 MPa and then becomes higher than sound velocity in the liquid phase, but doesn't exceed the one in the lighter gas phase.

At pressures lower than 50 MPa the sound velocity in the liquid phase is higher than that of the gas one. However, the sound velocity in the gas phase grows faster than that of the liquid one, and at pressures higher than some "inversion pressure" exceeds the sound velocity in the coexisting liquid phase.

The theoretical calculations of the sound velocity in He-CO_2 coexisting phases were conducted by V.A.Abovskii on the basis of the disturbance theory for thermodynamic function of gas mixtures /6/. The results of his calculations are presented in Fig.2,3 by full lines. The sound velocity estimated by Abovskii for the data ref.I is shown by dashed lines.

It's obvious, that the measured and theoretical values of velocity are in good agreement.

At a temperature of 313 K (Fig.3) gas - gas equilibrium is observed. According to phase diagram /I/, at this temperature and the maximum achieved pressure (about 250 MPa) the system is near the bondary of the homogeneity region and phases are very close in concentrations. Therefore sound velocity values in phases don't vary much. In this case the sound velocity inversion is not observed.

Concluding, we would like to note that, as follows from the discussion given above, the values of sound velocity for different phase of the mixture strongly depend on the component concentrations in the phases. Therefore the sound velocity measurements may serve as a good method for phase equilibrium study of gas mixtures.

References

I. Tsiklis D.S. The separation of the gases mixtures //M.Chemistry, I969.

2. Hanayama Y. Velocity of Ultrasound Wave in Mixed Gases at High Pressure //Journ.Phys.Society Japan. -I979.-46, NI.-P.328-333.

3. Kanishchev B.E., Pitaevskaya L.L., Kurshin A.P. The apparatus for the investigation of gas separation on the phases by ultrasonic method //Pribory and tehnika exp. -I984.-N6.-P.I78-I80.

4. Pitaevskaya L.L., Bilevich A.V. Velocity of ultrasound in compressed helium //Russ.J.Phys.Chem.-I970.-44, N6.-P.I594-I595.

5. Pitaevskaya L.L., Bilevich A.V. Velocity of ultrasound in carbon dioxide under pressure up to 4.5 kbar //Russ.J.Phys.Chem.-I973.-47, NI.-P.227-229.

6. Abovskii V.A. The equilibrium mixtures of gases and liquids with anisotropic interaction of the particles //Dokl.Akad. Nauk SSSR.-I984.-279, N4.-P.900-904.

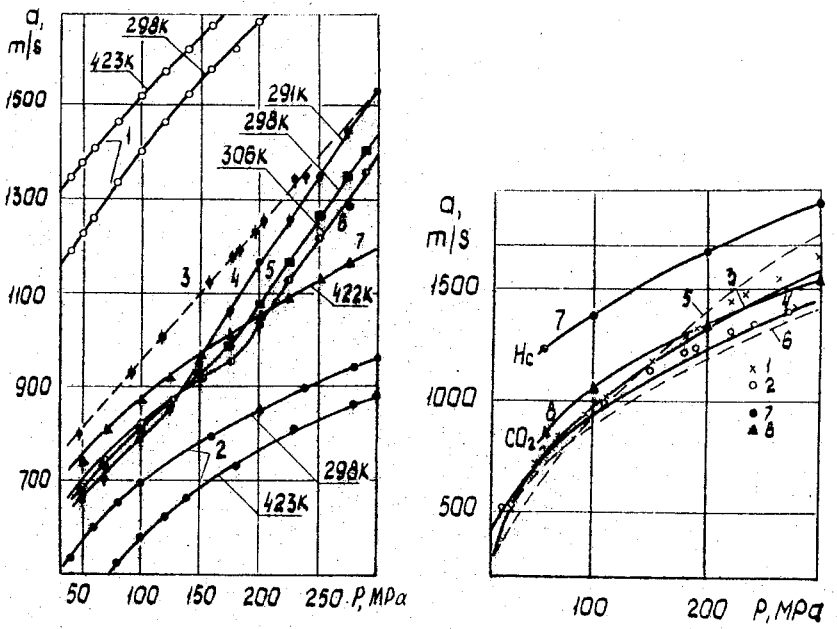

Fig.I. I,2 - sound velocity for He and CO_2; 3 - sound velocity for mixture He-Xe at 29I K under the pressure decrease; 4-7 - one under the pressure increase.

Fig.2. Sound velocity in two-phases mixture He-CO_2 at 298 K: I,2 - experimental data for the gas and liquid the phases; 3,4 - calculated for the gas and liquid phases; 5,6 - calculated data on basis phase diagram /I/ for the gas and liquid phases; 7,8 - data for He and CO_2.

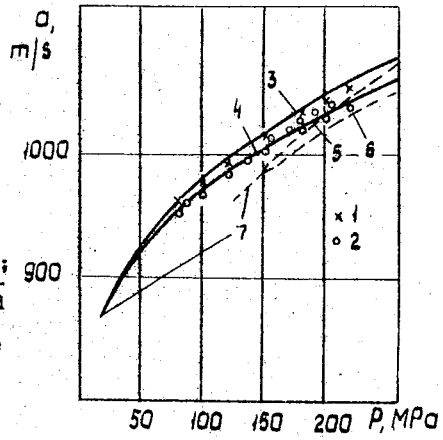

Fig.3. Sound velocity in two-phases mixture He-CO_2 at 313 K. The notations 1-6 same for the Fig.2; 7-dependence in the homogeneous region: solid line is the calculated data; dotted line is the calculated data on the basis phase diagram /I/.

SOLUBILITIES OF SOLIDS IN COMPRESSED GASES
A NEW ATTEMPT TO DISCRIBE AND TO CALCULATE

H. Lentz

Universität-Gesamthochschule Siegen

Fachbereich 8, Postfach 10 12 40

D-5900 Siegen

The solubility of solids or liquids in compressed gases is for thermodynamical reasons best to describe by the so called enhancement factor E. E is the quotient of the partial pessure of the solid component in the gas phase P . y (P: pressure, y: mol fraction) to the vapor pressure of the pure solid P_S. For high dilution is y = c . V (c: molar concentration, V: molar volume) and for ideal gases is

$$y \cdot P / P_S = c \cdot V \cdot P \cdot V_S^g / RT = c\, V_S^g = c / c_S.$$

Where T is the absolute temperature and V_S^g is the molar volume of the pure solid component in the gas phase. Hence in the literature $y \cdot P/P_S$ or c/c_S or mostly the logarithm of these quantities are plotted as functions of the molar density $d = V^{-1}$ or of the pressure. In all cases the graph of log E = f (d) is relatively simple (see e.g. [1] [2]). It starts at zero point with linear slope. The slope is decreasing with increasing density and here is a tendency for log E to reach a final plateau.

The suggested approach for the description of log E at constant temperature is:

$$(1)\quad \log E = \frac{m \cdot d}{1/b + d} = \frac{m \cdot b \cdot d}{1 + b \cdot d}$$

m and b are constants independent of the density but generally depending on the temperature. If the density is very small the slope of log E = f(d) will be m . b. At large densities log E will reach a hypothetic plateau m. The function of log E = f(d) appears here to be similiar to some well known other relations in physical chemistry e.g. to the so called Langmuir adsorption isotherm for gases.

Equation (1) can be linearised:

$$(2)\quad \frac{d}{\log E} = \frac{1}{m.b} + \frac{d}{m} \quad \text{or} \quad \frac{1}{V.\log E} = \frac{1}{m.b} + \frac{1}{m} \cdot \frac{1}{V}$$

Hence a plot of $(V \cdot \log E)^{-1}$ against the molar density will proof the validity of equation (1) and enable to determine the constants m.b as the inverse of the ordinate intersect and of the constant m as the inverse of the slope..

m has the hypothetical meaning of the final or of the maximum value of log E. However, m . b as the initial slope of log E = f(d) has the physical interpretation as the difference between the molar volume of the pure solid V_S and two times the value of the second cross virial coefficient B_{Sg}: $m \cdot b = V_S - 2\, B_{Sg}$.

The linearity suggested by equation (2) has been checked for anthracene dissolved in argon [2], carbon dioxide [2], methane [2], and ammonia [2], for caffeine in CO_2 [3], humid CO_2 [3] and ammonia [4] and for naphthalene in ammonia [5]. In all these cases the validity of the relation (2) and hence of equation (1) is convicingly demonstrated in the range of the

accuracy of the measurements. Therefore equation (1) can be used for the extrapolation of measurements to higher and to lower pressures. This is demonstrated for the extrapolation to higher pressures by the solubilities of naphthalene in ammonia [5]. The measurements up to 300 bar by a dynamic method have been used for calculations up to 2000 bar. The agreement of these calculations with measurements up to 1800 bar by a static method is very good. The extrapolation to lower pressures can be demontrated by the evaluation of the second cross virial coefficients from data measured in a moderate pressure range for anthracene-carbondioxide [2] and anthracene-methane [2]. For the first system at 373 K B_{Sg} = - 313 $cm^3\ mol^{-1}$ is reported [2]. From low pressure data [6] this coefficient should be -413 ±12 [6]. The extrapolation by equation (1) results in -450 ±20. For the antracene-methane [2] system at 350 K the cross virial coefficient is -250 [2], -316 [6] and -311 using equation (1) and at 390 K: -192 [2], -244 [6] and -220.

Equation 1 can be rearranged for usual applications to

$$(3)\quad \log y = \left(\frac{1}{m.b} + \frac{1}{m}\, d\right)^{-1} \cdot d + \log P_S - \log P$$

Thus for calculating the molfraction of the dissolved solid y at a given temperature and a given pressure we need the molar density of the gas, the vapor pressure of the pure solid and the two constants m . b and m. In the form of equation (3) the solubilities of caffeine in CO_2 [3] and ammonia [4] and of naphthalene in ammonia [5] have been described with good success.

In the equations 1 to 3 the quantities d and P_S and of course m . b or b and m or the inverse of these quantities are functions of the temperature. In the cases where equation 3 was applied the temperature-dependence of $(m.b)^{-1}$ was almost linear and m or m^{-1} was nearly independent of the

temperature in a temperature intervall of about 150 K and in the range of experimental accuracy.

Acknowledgement

The main part of this work has been done 1984 as a guest professor of the Kyungpook National University in Taegu. The hospitality of the Kyungpook National University and of the Minister of Education of the Republic of Korea (Basis science programm) and last not least the financial assistance of DAAD are gratefully acknowledged.

References

1. Braune H., Strassmann, F.
Über die Löslichkeit von Jod in gasförmiger Kohlensäure,
Z. physik.Chem. Abt. A, 1929, Bd 143, Heft 3/4, 225-243.

2. Rößling G.L., Franck E.U.
Solubility of Antracene in Dense Gases and Liquids to 200 °C and 2000 bar,
Ber. Bunsenges. Phys. Chem., 1983, 87, 882-890.

3. Lentz H., Gehrig M., Schulmeyer J.
Dynamic Solubility Measurements of Caffeine in Carbon Dioxide and in Carbon Dioxide Saturated with Water,
Physica, 1986, 139 & 140 B, 70-72.

4. Kim J.R., Lentz H.

Solubilities and Second Cross Virial Coefficients of Caffeine in Ammonia

submitted to: Fluid Phase Equilibria, 1987.

5. Kim J.R., Park T.K., Lentz H.

Solubility of Naphthalene in Liquid and Supercritical Ammonia

will be submitted to: J.Chem. Thermodynamics, 1988.

6. Nayour G.C., King Jr.A.D.

Solubility of Antracene in Compressed Methane, Ethylene, Ethane and Carbon Dioxide: The Correlation of Anthracene-Gas Second Cross Virial Coefficients Using Pseudocritical Parameters, 1970, 52, 10, 5206-5211.

EXPERIMENTAL STUDY OF CESIUM EQUATION OF STATE AT TEMPERATURES UP TO 2200K AND HIGH PRESSURES

N.B.Vargaftik[1], E.B.Gel'man[2], V.F.Kozhevnikov[1], S.P.Naurzakov[2]

[1]Moscow Aviation Institute, Moscow, USSR

[2]Kurchatov Institute of Atomic Energy, Moscow, USSR

The cesium critical parameters were measured in comparatively large number of works [1], but the precision of most of them is insufficient for interpretation of cesium PVT-properties in the critical region. The aim of this study is the measurement of cesium equation of state at lower density then our previous work [2]: not only in liquid phase, but in gas phase too, including coexistence curve. This is necessary for critical parameters determination and exclusion of errors of extrapolation of experimental isobars [2] to the saturation line.

The PVT data were measured by means of a two-zone dilatometer [3]. The stainless cylindric membrane [3] was replaced by soft bellow out of the same material. The bellow wall thickness was 0,08 mm, external diameter - 28 mm, internal diameter - 18 mm, the number of folds - 10. Cesium, that was in germetical dilatometer volume, was pressurized by argon medium through piston, mercury and bellow. The pressure difference ΔP on the dilatometer versus piston displacement Δh and corresponding dilatometer volume ΔV is shown in fig.1. When $\Delta V = 2,2$ cm^3 the pressure difference $\Delta P = 0,2$ at. This is less considerable then ΔP for cylindric membrane [3]. Hooke law is true for the bellow at these volume changes and so a reproduction of this plot is good. The volume of molibdenum and tangsten cells of this study was about 1,7 - 2,0 cm^3.

The experimental data are shown in fig.2. The measurements

were done along isobars at stationary conditions under increasing and decreasing temperature. The majority number of experimental points were obtained at excess pressures 9, 30, 70, 80, 90, 100, 108 and 120 kgf/cm^2 * (ate). The data obtained at higher pressures confirmed our data [2]. That is why the new data number at pressures $P > 150$ ate is not much. Isobar curves at 300 and 600 ate, shown in fig.2, are plotted by data [2].

The liquid-gas transition temperature on the isobars was measured by density jump both under heating and cooling of the sample. The error of these measurements was $\lesssim 1^\circ$ on thermometer scale, that was used. The temperature gradients along the cell were $\Delta T/T \lesssim 10^{-3}$. The measured values of gas-liquid transition temperature were in agreement with the values, calculated from empirical saturation pressure equation [4]. At pressures higher than 90 ate boiling was not observed. The points which correspond the saturated vapor density [5] are shown in fig.2 also. There is a good agreement at temperatures up to 1800K. This agreement is the most important at low pressure becouse at these coditions the literature data reliability is maximum and our experimental data error is maximum too.

The error of obtained density data changes from 0,2 % in dense liquid to 1 % in rarefied vapor.

The sample temperature was measured by three calibrated WRe5% - WRe20% thermocouples. The standard error of the thermocouples increases from 5° at 1300K up to 10° at 2100K. The pressure was measured by precision manometers with error ≈ 1 at for pressures $P > 100$ ate and 0,2 at for $P \lesssim 100$ ate.

* 1 kgf/cm^2 = 1 at $\approx$ 0,98 bar = $9{,}8 \cdot 10^4$ Pa.

The graphic estimate of cesium critical point parameters are $T_c = 1940 \pm 10$ K ; $P_c = 9{,}4 \pm 0{,}2$ MPa; $\rho_c = 0{,}39 \pm 0{,}01$ g/cm^3. These parameters disagree with earler data (see [1]) and agree with last Marburg group data [6].

As seen from fig.2 the coexistence curve is asymmetric. The reduced density $\varphi = |\rho^s - \rho_c|/\rho_c$ versus $\tau = (T_c - T)/T_c$ (ρ^s - density at saturation) for liquid (L) and vapor (V) coexistence curve branches are plotted in fig.3 (in logarithmic scale). As known [11] for dielectric substances both of them are proportional to τ^β at $\tau \ll 1$, where $\beta = \beta_V = \beta_L \simeq 1/3$. Practically it is true at $\tau \lesssim 10^{-1}$ [7]. As seen from fig.3, the situation for cesium is different: for vapor branch $\beta_V = 0{,}34$ but for liquid branch $\beta_L = 0{,}44$. The dashed lines are the extrapolation of them to $\tau \to 0$. In the nearest vicinity of the critical point both of these dependences must have $\beta \simeq 1/3$. In accord with our data it will be true for cesium at $\tau \lesssim 10^{-3}$. The observed shape of these plots may be explained by the fact that metal - isulator transition in cesium take place in nearest vicinity of critical point. That is in agreement with cesium electrical conductivity data [8].

As seen from fig.2, the cesium coexsistence curve diameter have a strong curvature. For the first time the breach of "rectiliner diameter law" for the simple substances was observed for mercury by I.K.Kikoin and A.P.Senchenkov [9] and then was supported by more precise mercury equation of state measurements [10]. Fig. reproduces the Guggenheim plot of coexistence curve of eight dielectric substances. The coexistence curves of mercury [10] and cesium with their diameters are shown in fig.4 too. As seen, the principle of corresponding states for mercury and cesium is not executed. It is concern mainly the liquid phase, where interaction between particles strongly depends on states of valence electrons.

One may assume that the opposition of diameters curvature $(\rho_1^S + \rho_v^S)/2 = f(T)$ for monovalent cesium and twovalent mercury is bound up with electron spectrum distingtion of these metals in liquid phase.

References

I. Ohse R.W., Babelot J.-F., Magill J., Tetenbaum M., Handbook of Thermodynamic and Transport Properties of Alkali Metals, Ed. R.W.Ohse, IUPAC Chem. Data N 30, Oxford, I985, p.329 - 347.

2. Vargaftik N.B., Kozhevnikov V.F., Ermilov P.N., High Temp.-High Pressures, I984, I6, 233 - 238.

3. Kozhevnikov V.F., Ermilov P.N., Prib. Tekh. Eksp., I982, N I, 209 - 2I2.

4. Pokrasin M.A., Roshchupkin V.V., Fokin L.R., Khandomirova N.B., in Teplofizicheskie Svoistva Veshchestv i Materialov, Issue N I9, p. 33 - 55, M., Izd.Standartov, I983.

5. Vargaftik N.B., Voljak L.D., Stepanov V.G., in Handbook of Thermodynamic and Transport Properties of Alkali Metals, Ed.R.W.Ohse, IUPAC Chem.Data N 30, Oxford, I985, p. 64I - 666.

6. Jungst S., Knuth B., Hensel F., Phys.Rev.Letters, I985, 55, N.20, p.p. 2I60 - 2I63.

7. Roach P.R., Phys. Rev., I968, I70, p. . 2I3 - 223.

8. Hensel F., Proc. 8-th Symposium on Thermophysical Properties, v.II, ASME, N.Y., I98I, p. I5I - I58.

9. Kikoin I.K., Senchenkov A.P., Fizika Metallov i Metallovedenie, I967, 24, N 5, p. 843 - 858.

I0. Kikoin I.K., Senchenkov A.P., Naursakov S.P., Gel'man E.B., Preprint IAE - 23I0, M., I973; V International Conference on High Pressure and Technology, Program and Abstracts, M., I975, p.I52.

II. Guggenheim E.A., J.Chem.Phys., I945, I3, N 7, 253 -26I.

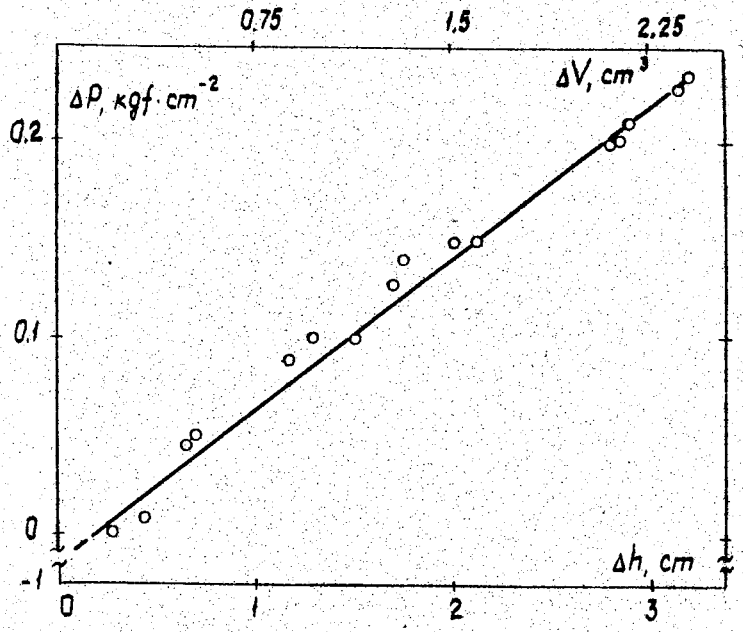

Fig.I. Pressure difference on the dilatometer.

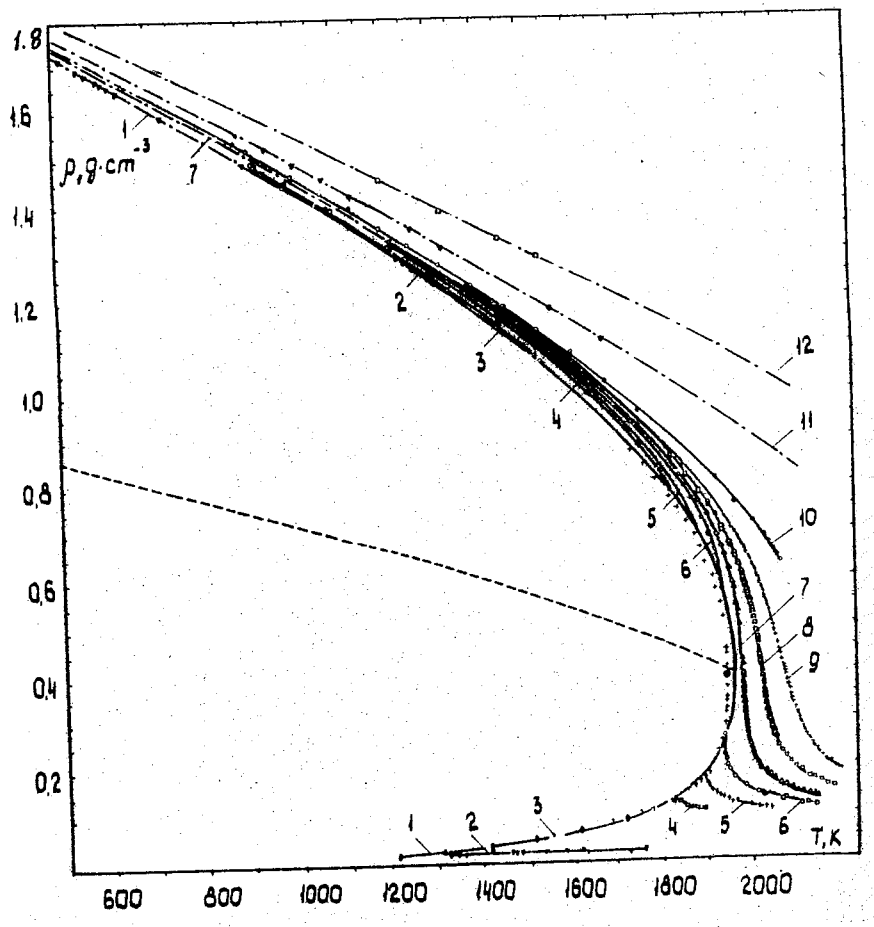

Fig.2. Cesium equation of state.

I - saturation curve. Isobars: 2 - 0,98 MPa; 3 - 3,04 MPa; 4 - 6,96 MPa; 5 - 7,94 MPa; 6 - 8,92 MPa; 7 - 9,90 MPa; 8 - I0,75MPa; 9 - II,9 MPa; I0 - I4,8 MPa; II - 29,5 MPa; I2 - 56,9 MPa. ◉ - critical point; ◖ - vapor density at saturation [5]; + - experimental data [6]; ◎ - critical point [6].

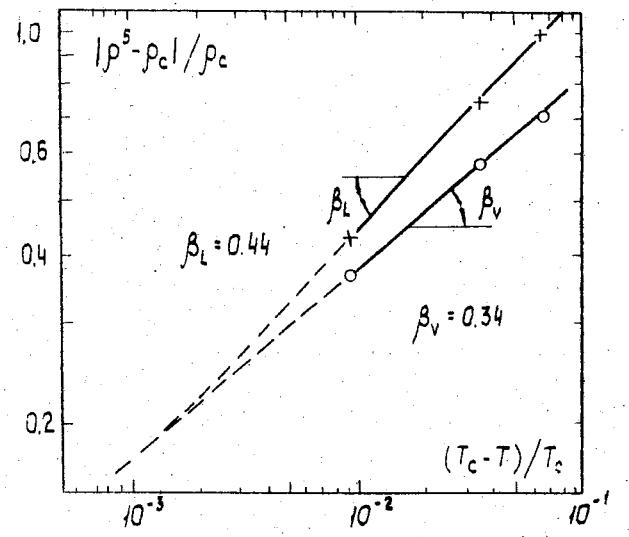

Fig.3. Liquid and vapor branches of cesium coexistence curve.

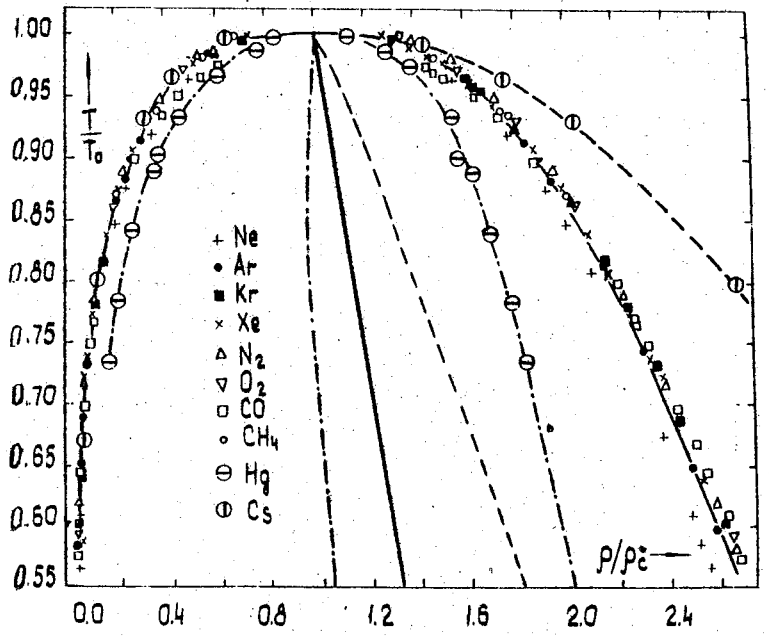

Fig.4. Coexistence curves and their diameters for dielectric fluids [II], mercury [I0] and cesium.

MULTINUCLEAR SPIN LATTICE RELAXATION TIME STUDIES OF SUPERCOOLED AQUEOUS SALT SOLUTIONS UNDER HIGH PRESSURE

E.W. Lang, H. Radkowitsch, W. Fink

Institut für Biophysik und Physikalische Biochemie
Universität Regensburg, D-8400 Regensburg, FRG

INTRODUCTION

Aqueous solutions under hydrostatic pressure ($p \sim 200$ MPa) can be undercooled to ~ 180 K and below (depending on the solute concentration) if the solution is emulgated in a cycloalkane/surfactant mixture (1). Thereby molecular motions are slowed down sufficiently and the measured relaxation rates become sensitive to the details of the molecular dynamics. A motional model is developed for water molecules hydrating the cations and a simple two-state model is sufficient to calculate the relaxation rate curve $1/T_1(T)$ for all concentrations of the solutes LiCl, $MgCl_2$ and the potassium halides. In this investigation we report spin-lattice relaxation times T_1 of ^2H-, ^1H-, ^{19}F-, ^6Li- and ^7Li-nuclei in the systems LiCl-($c \leq 11$ m), $MgCl_2$-($c \leq 5$ m), KCl-($c \leq 3{,}7$ m), KBr-($c \leq 4{,}6$ m), KJ-($c = 3$ m) and KF ($c \leq 12$ m)-water.

EXPERIMENTAL

Emulsions have been prepared by mixing 50 w-% salt/D_2O solution with 48 w-% cyclopentane/cyclohexane and 2 w-% sorbitan-tristearat. The mixing was done in a glove-bag under an argon-atmosphere by pressing the mixture through a stainless steel net within a syringe. Before mixing all components had to be degassed by at least five freeze-pump-thaw cycles to remove dissolved oxygen. All T_1 measurements have been obtained with the inversion recovery pulse sequence with alternating phases at 2.35 T and 7.0 T. They are considered reliable to ± 10 %. The temperatures have been measured with a miniature chromel-alumel thermocouple (Philips, Kassel) and are accurate to ± 1 K. The pressure has been measured with a precision Bourdon gauge (Heise, Connecticut) to ± 0.5 MPa.

RESULTS AND DISCUSSION

The motional model that will be applied considers water molecules adjacent to an ion to execute small-amplitude librations superimposed onto anisotropic orientational fluctuations about the local director (ion-oxygen direction). In addition the molecules diffuse around the ion and exchange occurs between hydration sites and bulk sites. Two correlation times enter the model, namely $\tau_i = \tau_{io} \exp(E_i/kT)$ to characterize the internal fluctuations and $\tau_o = (\tau_r^{-1} + \tau_{ex}^{-1})^{-1} = \tau_{oo} \exp(B/T-T_o)$ to account for overall tumbling and exchange processes. τ_{io} is considered to correspond to an attempt frequency for barrier crossing and is set equal to the inverse of the librational frequency. All other parameters have been estimated as explained elsewhere (2) except for the apparent activation energy which had to be adjusted as the only unknown quantity. Theoretical expressions for the relaxation rate have been worked out for electric quadrupole interactions (2), but may be obtained for magnetic dipole interactions in a straightforward manner. Instead of the librationally averaged quadrupole coupling constant $(\Gamma \cdot \chi_o)^2$ the averaged dipolar coupling factor $(\Gamma/\langle r_{IS}^3 \rangle)^2$ enters. The distance r_{IS} between the interacting nuclei may be obtained from scattering experiments or computer simulations. In the systems LiCl-, $MgCl_2$-, KCl-, KBr- and KJ the cations have been considered to be hydrated with the water molecules oriented with one lone-pair pointing towards the cation.

In the system KF the F^- anion interacts much stronger with water, hence has been considered the hydrated species with the water molecules pointing one OH-bond linearly towards the anion.

Table 1 collects the model parameters of all systems neccessary to describe the ^2H-$T_1(T)$ curves (2). Fig. 1 shows the T_o for the various solutions. Fig. 2 shows $T_1(T, p = 225\ MPa)$ for all concentrations in $MgCl_2/D_2O$ and Fig. 3 for KF-D_2O solutions. The decrease of the activation energy E_i from Mg^{2+} to K^+ may be understood in terms of a decreasing polarisation of the molecules and an increasing ionic radius which allows for less hindered internal fluctuations. Furthermore, the only significant influence of the anions is seen in their effect on the ideal glass transition temperature T_o (see Fig. 1).

To provide a further test to the model, ^1H- and ^6Li-T_1 have been obtained in an 11 molal $LiCl/D_2O$ solution. Both nuclei interact mainly via magnetic dipole interactions hence are sensitive to orientational and positional fluctuations. To the former the motional model has been applied whereby proper account has been taken of the known isotope effects on librations and Tg. Positional fluctuations have been modeled via a diffusion equation with reflecting boundary conditions (3). The relative diffusion coefficient $D_{rel} = D_{Li} + D_{H_2O}$ can be calculated easily, as D_{Li} and H_{H_2O} are known at ambient temperature in this system (4). The corresponding correlation time $\tau_d = a^2/D_{rel} = \tau_{do} \cdot \exp(B/(T-T_o))$ is assumed to follow a VTF-law also. The geometrical parameters entering the expression (distances of closest approach d) are known from neutron scattering work (5). Also the mass density is known at room temperature hence all parameters entering the expression for the positional fluctuations can be estimated from other experiments. Fig. 4 shows the experimental results together with the calculated relaxation time curve $T_1(T)$. $E_i(H_2O)$ is slightly smaller than $E_i(D_2O)$ which might be due to the weaker hydrogen-bonding ability of light water (see table 2).

Although a detailed discussion will not be given here the relaxation time curves $T_1(T)$ of the ^7Li isotope (Fig. 5) proove the dominance of electric quadrupole interactions of the ^7Li nucleus at this composition. This follows because both curves become congruent if plotted in a modified Arrhenius dia-

Table 1. Parameters of the motional model for ^2H-$T_1(T)$ in the solutions solute/D_2O under hydrostatic pressure ($p = 225$ MPa) (n_h - dynamic hydration number, $\chi_{eff}(^2H)$ - librationally averaged quadrupole coupling constant)

solute	τ_{oo} (ps)	τ_{io} (ps)	E_i (kJ/mol)	B (K)	$\chi_{eff}(^2H)$ (kHz)	n_h
$MgCl_2$	0.169	0.065	21.0 ($c^a \leq$ 4 m)	687.6	192 ($c \leq$ 4 m)	16 ($c \leq$ 3 m)
			21.4 (c = 5 m)		192 (c = 5 m)	12.5 (c = 4 m)
						10 (c = 5 m)
LiCl	0.169	0.065	20.2	687.6	192	6 ($c \leq$ 8 m)
						4.55 (c = 11 m)
KF	0.258	0.065	20.8 ($c \leq$ 8 m)	612.4	192 ($c \leq$ 8 m)	6 ($c \leq$ 8 m)
			21.6 (c = 12 m)		185 (c = 12 m)	4 (c = 12 m)
KCl	0.085	0.0498	16.7	687.6	201.2	6 ($c \leq$ 3.7 m)
KBr	0.085	0.0498	16.7	687.6	201.2	6 ($c \leq$ 4.6 m)
KJ	0.085	0.0498	16.7	687.6	201.2	6 (c = 3 m)

a) c (mol/kg)

Table 2. Parameters of the motional model for ^{6}Li-$T_1(T)$ and ^{1}H-$T_1(T)$ in 11 m $LiCl/H_2O$ solutions and of ^{19}F-$T_1(T)$ in 12 m KF/H_2O solutions.

solute	τ_{oo} (ps)	τ_{io} (ps)	E_i (kJ/mol)	τ_{do} (ps)
LiCl-H_2O c = 11 m	0.169	0.0471	18.7	0.979
	r_{HH} (nm)	r_{HLi} (nm)	d_{HH} (nm)	d_{LiH} (nm)
	0.159	0.257	0.225	0.300
	τ_{oo} (ps)	τ_{io} (ps)	E_i (kJ/mol)	τ_{do} (ps)
KF-H_2O c = 12 m	0.187			0.254
	r_{FH} (nm)	d_{FH} (nm)		
	0.177	0.177		

gram. Also only one broad minimum is seen with a T_{min} in rough agreement with the minima of the relaxation time curves for water nuclei. This suggests that ^{7}Li is relaxed mainly by the surrounding water molecules and that the same motions modulate the various interactions involved.

The system KF/H_2O has also been studied more thoroughly. In the 12 m solution all water is considered to belong to the hydration sphere of the anion. Because there are no diffusion coefficients available for this system under the given conditions D_{rel} had to be considered a free parameter (see table 2). It is important to note that for the linear configuration the internal mode does not contribute to the relaxation because of the large distance between F^- and the more distant proton of an adjacent water molecule. Fig. 3 shows the ^{19}F-T_1 in KF/D_2O and KF/H_2O. It is worth noting that the symmetric arrangement of a water molecule relative to the anion would reduce the calculated contribution of the orientational fluctuations to the total rate measured by nearly an order of magnitude. Hence it is concluded that the linear configuration seems to be in better accord with the data in a 12 molal solution.

ACKNOWLEDGEMENTS

We are indebted to Prof. Lüdemann for stimulating discussions. Financial support from the DFG and the Fonds der Chemie is gratefully acknowledged.

Ferences

1. E.W. Lang and H.-D. Lüdemann, Ber. Bunsenges. Phys. Chem., 89, 508 (1985).

2. E.W. Lang and L. Piculell, in Water and Aqueous Solutions (1986), p. 31, ed. G.W. Neilson and J.E. Enderby, Bristol, A. Hilger

3. L.-P. Hwang and J.H. Freed, J. Chem. Phys. 63, 4017 (1975).

4. E.J. Sutter and J.F. Harmon, J. Phys. Chem. 79, 1958 (1975).

5. J.E. Enderby, Ann. Rev. Phys. Chem. 34, 155 (1983).

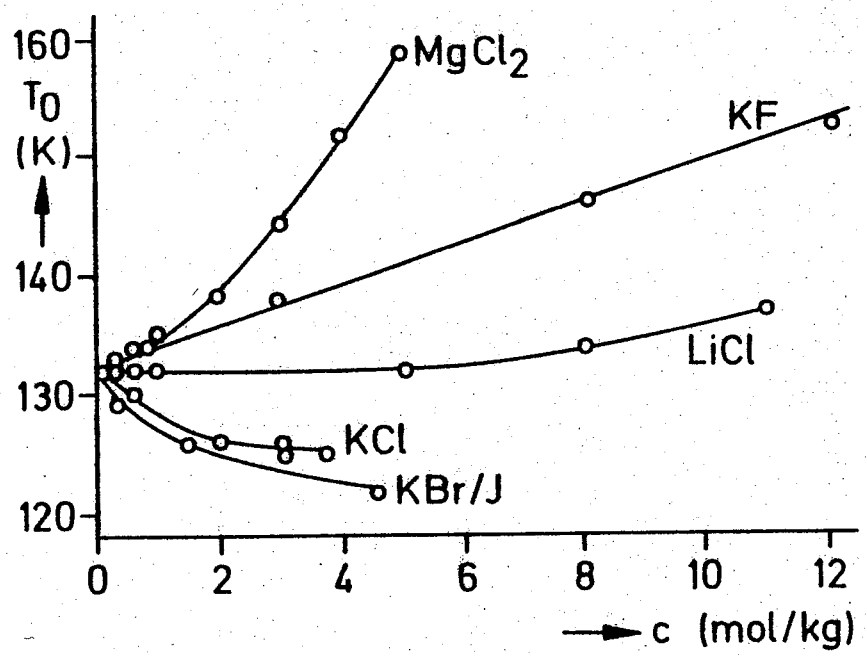

Fig. 1. Concentration dependence of the ideal glass temperature T_o of the various salts dissolved in D_2O.

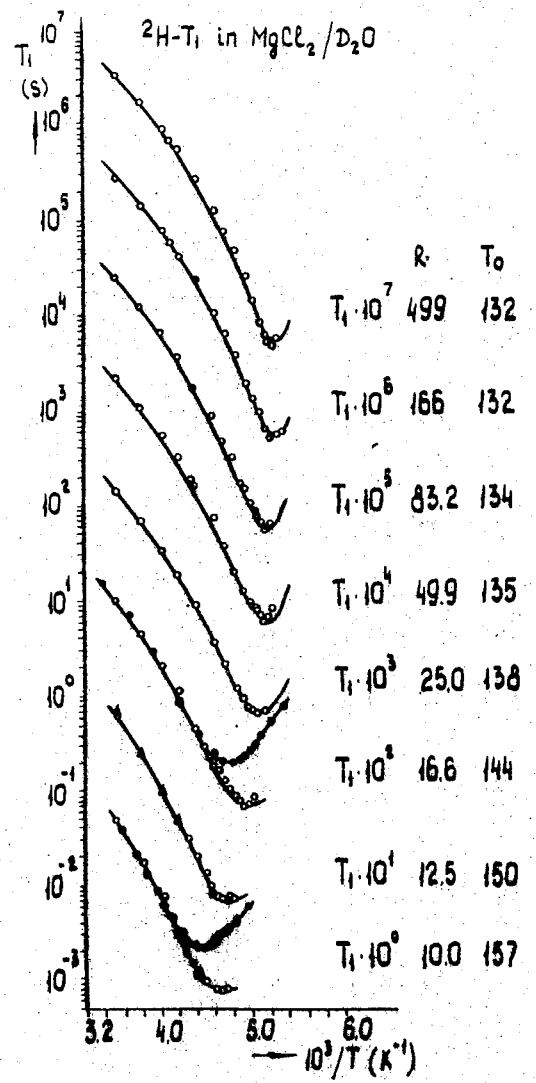

Fig. 2. ^2H-T_1 in $MgCl_2/D_2O$ solutions at various compositions. R(= mol D_2O/mol salt) versus inverse temperature at p = 225 MPa. Full curves correspond to calculated $T_1(T)$ according to motional model and two-state approximation (2).

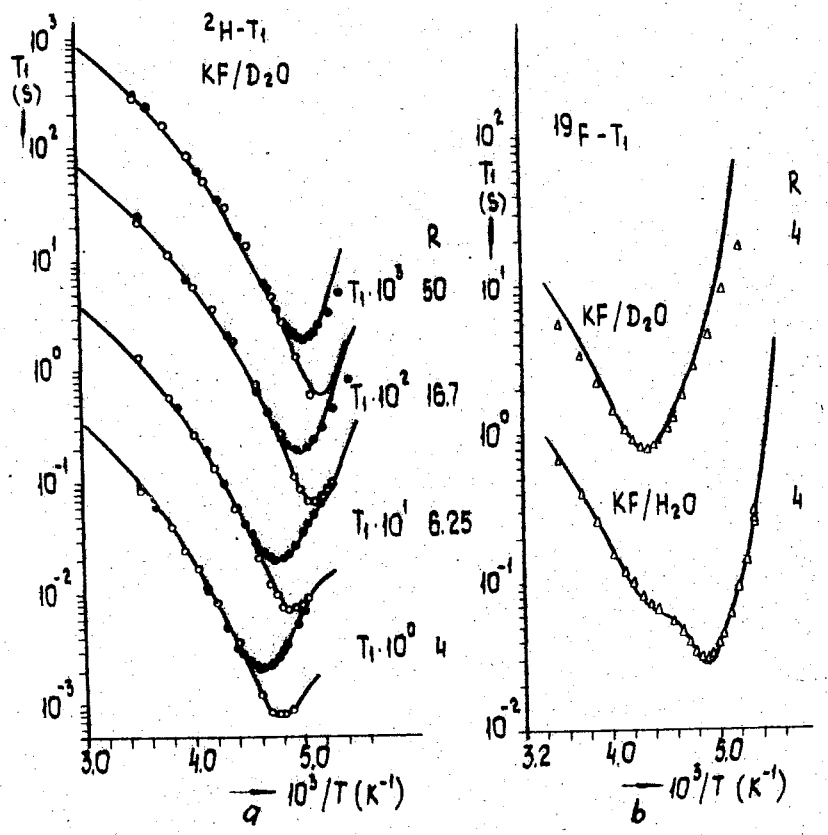

Fig. 3. a) ^{2}H-T$_1$ in KF/D$_2$O solutions at various compositions. R versus inverse temperature at p = 225 MPa. Full curve see Fig. 2.

b) ^{19}F-T$_1$ in 12 m KF/D$_2$O and KF (H$_2$O) versus inverse temperature at p = 225 MPa. Full curves correspond to calculated T$_1$(T) according to motional model.

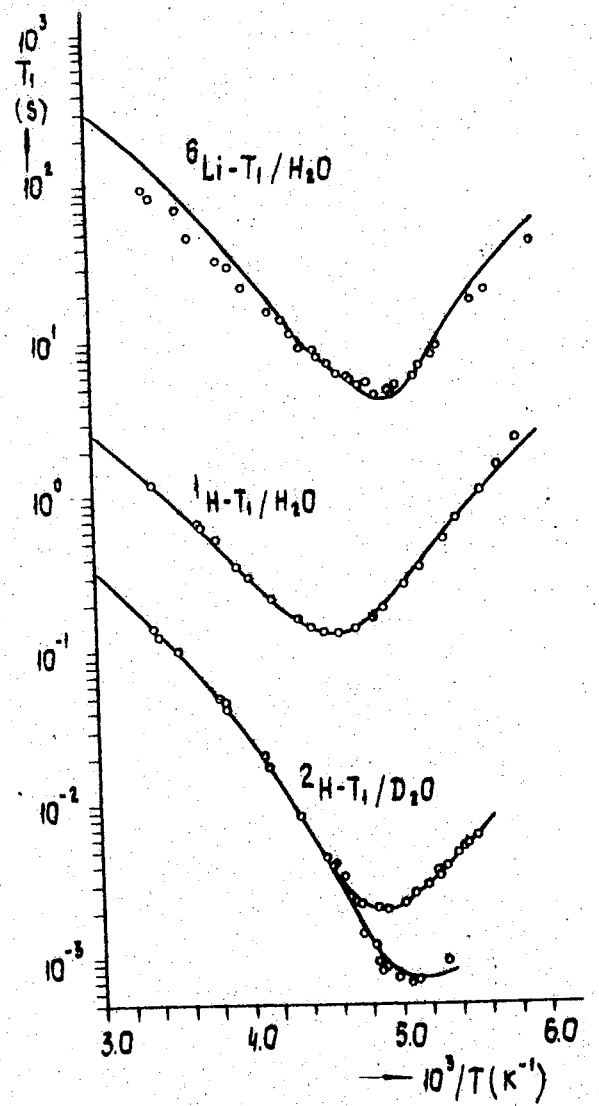

Fig. 4. ^{6}Li-T$_1$ and ^{1}H-T$_1$ in 11 m LiCl/H$_2$O solution and ^{2}H-T$_1$ in 11 m LiCl solution at 46.07 MHz and 15.35 MHz versus inverse temperature. F curves correspond to calculated T$_1$(T) according to motional model

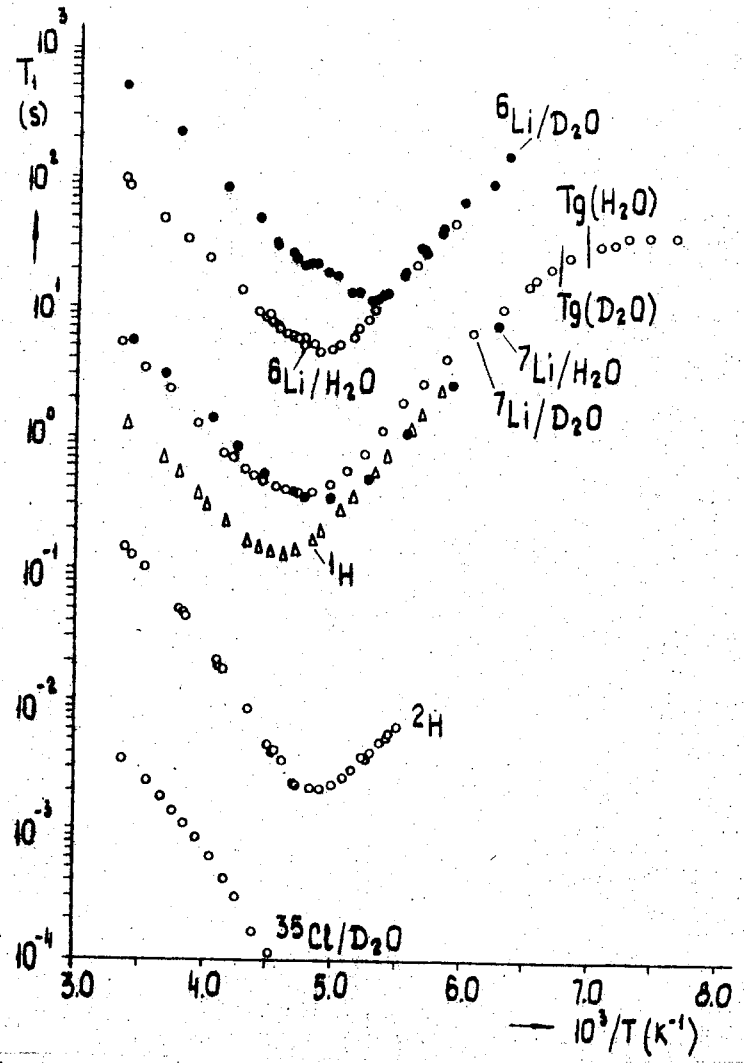

Fig. 5. Experimental relaxation times of various nuclei in 11 m LiCl/water solution versus inverse temperature.

HIGH PRESSURE NMR SELF DIFFUSION STUDIES ON SUPERCOOLED WATER

F.X.Prielmeier, R.J.Speedy*, H.-D. Lüdemann
Institut für Biophysik und Physikalische Biochemie
Universität Regensburg, D-8400 Regensburg, FRG
*Permanent Adress:
Dept. of Chemistry, Victoria University of Wellington,
Wellington, New Zealand

Liquid water reveals a number of unusual properties which occur only in a class of liquids like water and silicon dioxide showing an open network structure. This anomalous behaviour gets more pronounced at low temperatures, especially when water is studied in the supercooled range below its melting point. When pressure is applied on cold water the rates of tranlational [1] and rotational [2] diffusion increase. The rotational behaviour of the water molecules has been extensively studied at low temperatures and high pressures by NMR relaxation time studies [2,3]. However no work on the pressure dependence of the self diffusion coefficient or the viscosity in supercooled water has been reported so far. We now present measurements of the self diffusion coefficient of water at pressures up to 400 MPa and temperatures from 273 K down to 203.5 K at the highest pressures.

EXPERIMENTAL

The self diffusion coefficient was measured in bulk water contained in glass capillaries with an outer diameter of ≈ 800 µm and inner diameters between 70 and 200 µm. Details of the high pressure system have been published previously [4].

The measurements were done using the NMR pulsed gradient spin echo technique on a Bruker MSL 300 spectrometer with a superconducting 7T magnet. Figure 1 shows a cross section of the

probehead that was constructed for these measurements. The magnetic field gradient is produced by a pair of opposite Helmholtz coils wound on a glass dewar. The sample is cooled by a stream of cold nitrogen gas. The gradient coil is kept at room temperature in order to avoid any temperature effect on the gradient strength. The magnetic field gradient was calibrated using the self diffusion coefficient of water at room temperature given by Mills [5].

RESULTS AND DISCUSSION

The pressure dependence of the self diffusion coefficient at the various temperatures is shown in fig.2 together with literature values above 273 K [6] and extrapolated values at .1 MPa. These are about 10% higher than the values reported by Gillen et al.[7] at these temperatures, but Gillen's results are 5-10% lower than our values and literature values [6] from 252 to 298 K

At temperatures below 300 K the diffusion coefficient increases with initial compression . This behaviour gets more pronounced at lower temperatures. A similar pressure dependence has been found for the reorientational mobility $1/\tau_2$ which is obtained from ^{17}O longitudinal relaxation times [2]. However there is a remarkable difference in the effect of pressure on reorientational motion and translational motion at the lowest temperatures. At 243 K the diffusion coefficient is increased by ≈ 60% by an increase of pressure to 150 MPa and decreases at higher pressures ,whereas $1/\tau_2$ is increased by almost 150% at 250 MPa. The increase of mobility with pressure can be explained by a weakening of the hydrogen bond network and a distortion of the tetrahedral arrangement of the molecules. This causes a decrease of the strength of the directional forces on the molecules.

The isobaric temperature dependence of D can be described by a

power law equation as proposed by Speedy and Angell [8]:

$$D = D_0'T(T/T_s - 1)^{\gamma} \quad (1)$$

This equation implies that D extrapolates to zero at the singularity temperature T_s. $T_s(p)$ can be interpreted as a limit of stability for liquid water [8]. Our data together with high temperature literature values can be fitted to eqn. 1 for all pressures. The lower part of fig.3 shows the fit for p = 200 MPa. The agreement between the experimental data and the fitted curve is excellent. The T_s values obtained from the fits are shown in fig.4 together with the values obtained from T_1 data [2] and the homogeneous nucleation temperatures T_H. At low pressures the present results are in good agreement with the T_s values obtained from the T_1 data and are 5 to 10 K lower than T_H. At higher pressures however T_s falls above T_H, which is physically unrealistic.

At high pressures the temperature dependence of D is described better by the Vogel - Tammann - Fulcher (VTF) equation :

$$D = D_0'T\exp(-B/(T-T_0)) \quad (2)$$

This equation is known to describe the temperature dependence of the dynamic properties of many normal viscous liquids. Fitting the experimental data to this equation we obtain smaller standard deviatons at pressures above 150 MPa than with the fractional power law. The resulting fit for 200 MPa is shown in the upper part of fig. 3. The ideal glass transition temperatures T_0 obtained from the fits are in the range from 130 K to 160 K with a slight positive pressure dependence. These values are in good agreement with the T_0 values obtained from the T_1 data.

The change in the temperature dependence of D from eqn.1 to eqn.2 with increasing pressure indicates that with the application of pressure the anomalous behaviour of water is suppressed.

ACKNOWLEDGEMENTS

Financial support by the Deutsche Forschungsgemeinschaft and the Fonds der Chemie is gratefully acknowledged. R.J.S. thanks the DFG for a one year scholarship. F.K.P. acknowledges the support of his doctoral thesis by the Friedrich - Ebert - Stiftung.

References

1, Angell C.A., Finch E.D., Woolf L.A., Bach P.
J. Chem. Phys. 1976, 65, p. 3063.

2, Lang E.W., Lüdemann H.-D.
Ber. Bunsenges. Phys. Chem. 1981, 85, p. 603.

3, Lang E.W., Lüdemann H.-D.
J. Chem. Phys. 1977, 67, p. 718.

4, Gaarz U., Lüdemann H.-D.
Ber. Bunsenges. Phys. Chem. 1976, 80, p. 607.

5, Mills R.
J. Phys. Chem. 1973, 77, p. 685.

6, Weingärtner H.
Zeitschrift für Phys. Chem. 1982, Neue Folge 132, p. 129.

7, Gillen K.T., Douglass D.C., Hoch M.J.R.
J. Chem. Phys 1972, 57, p. 5117.

8, Speedy R.J., Angell C.A.
J. Chem. Phys. 1976, 65, p. 851.

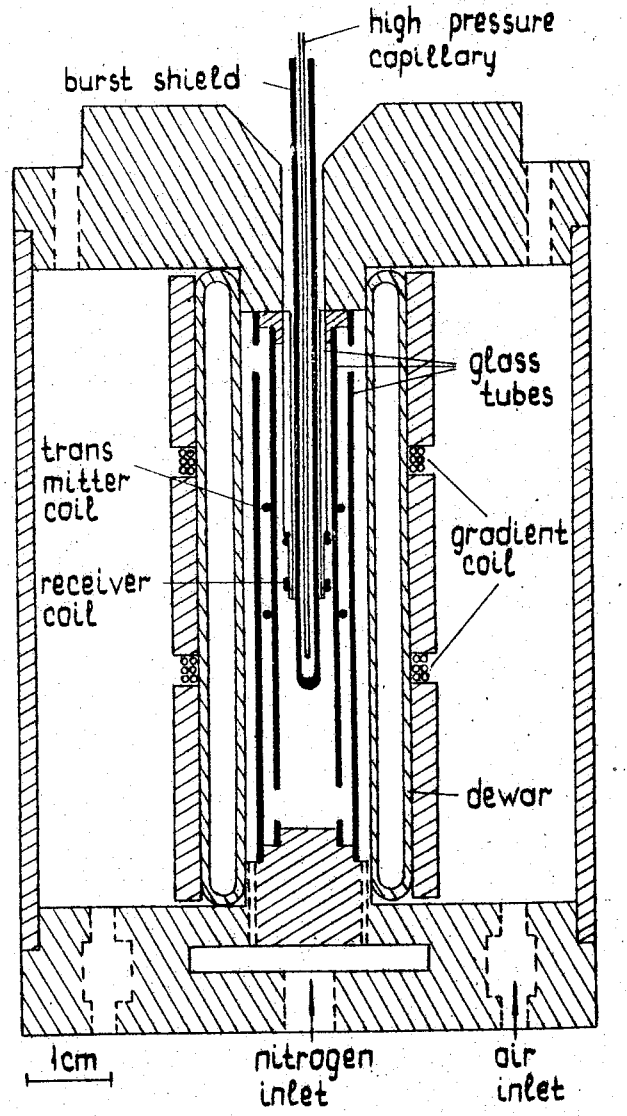

Fig. 1. NMR probehead for measurements of self diffusion coefficients. ν = 300 MHz.

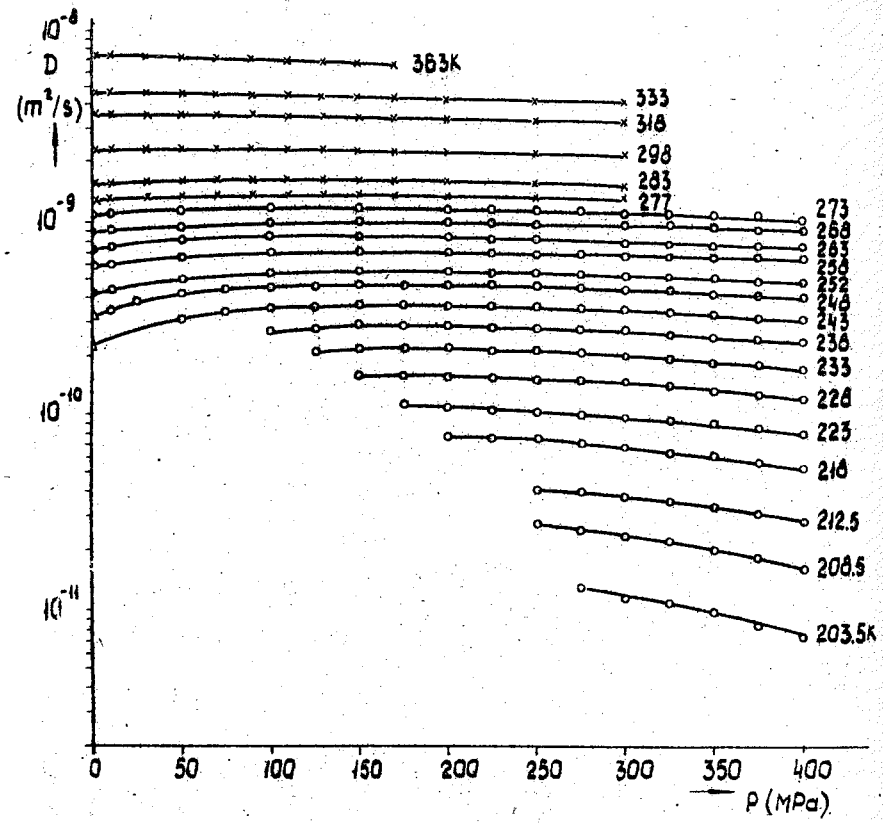

Fig. 2. Isotherms of the self diffusion coefficient D of water
o this work, × ref.6, Δ extrapolated.

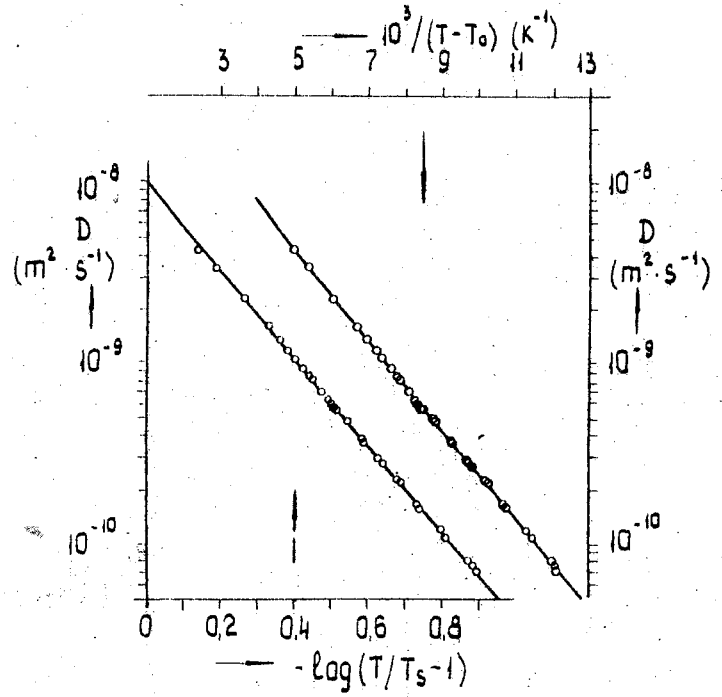

Fig. 3. Representation of the temperature dependence of D at P = 200 MPa:
lower part: eqn. (1), T_s = 193 K
upper part: eqn. (2), T_0 = 136 K.

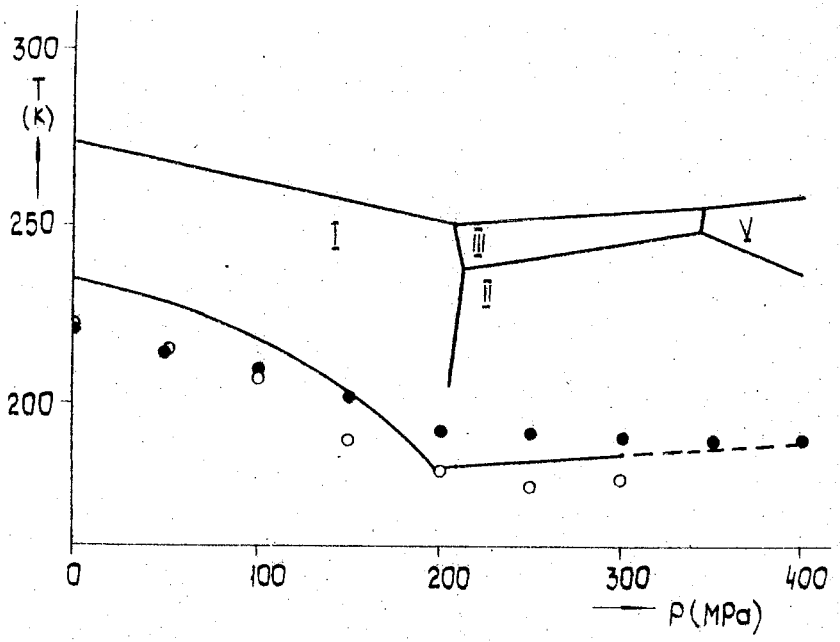

Fig. 4. Pressure dependence of T_s obtained from eqn. (1): • this work, o ref.2, T_H: homogeneous nucleation temperature.

METHODS OF PHASE EQUILIBRIA MIXTURE CALCULATIONS H_2-N_2-CH_4-Ar-NH_3 UNDER THE PRESSURE UP TO 40 MPa

V.L. Saprikin

Institute of Gas of the Academy of Sciences of the Ukrainian SSR, Kiev, USSR

The development of the absorption process of the argon and methane removal by liquid ammonia from the ammonia production synthesis-gas has required the creation of the calculation methods of the multicomponent vapor-liquid equilibrium for the gas mixtures being used in the ammonia synthesis process.

The author's [1] attempt to describe the phase equilibrium given mixture using modified equation BWR was of little success. In paper [2] a set of relations was described and the diagrams were plotted from which vapor-liquid compositions in equilibrium can be calculated at temperatures from 253 to 360 K and at pressures 5.07 MPa, 20.26 MPa and 40.53 MPa.

The purpose of given paper is to develop the calculation methods of vapor-liquid equilibrium for the five-component system at pressures 5-40 MPa and in the temperature range 243-373 K for typical set of ammonia synthesis circulating gases.

In equilibrium the fugacity of each the component in the vapor and liquid phases should be equal: $f_i^V = f_i^L$.

The vapor phase fugacity is related to the pressure P and to the vapor-phase molar fraction through the fugacity coefficient φ_i: $f_i^V = \varphi_i \, y_i \cdot P$.

Vapor-phase fugacities were calculated using a modified Redlich-Kwong equation of state (RK):Constant a and b of equation (RK) for all the components exept for ammonia were calculated as in the original of RK equation.

For the polar component of ammonia the following modification was applied

$$a, b = f(T). \qquad (1)$$

However, the results of the calculations showed little influence of temperature on b parameter in RK equation, a maximum variation being ±4% and, therefore, an ordinary equation was used for ammonia. The temperature influence on the parameter a was signi-

ficant and was described by the equation, obtained using the correlation regressive analysis:

$$\Omega_{a_{NH_3}} = -0.15275012 + 0.00288001 \cdot T - 0.00000387 \cdot T^2 \qquad (2)$$

Vapor-phase fugacity coefficients for all components ammonia included were calculated using the Prausnitz equation [3]:

$$\ln \varphi_i = \ln \frac{V_m}{V_m - B_m} + \frac{B_i}{V_m - B_m} - \frac{2\sum_i a_i y_i}{RT^{3/2} B_m} \ln \frac{V_m - B_m}{V_m} + \qquad (3)$$

$$+ \frac{a_m B_i}{RT^{3/2} B_m^2} \left(\ln \frac{V_m + B_m}{V_m} - \frac{B_m}{V_m + B_m} \right) - \ln \frac{P \cdot V_m}{R \cdot T},$$

where V_m - molar volume of mixture. The values of b_m and a_m were calculated as in the original of RK equation:

$$B_m = \sum_{i=1} y_i B_i; \qquad (4)$$

$$a_m = \sum_{i=1} \sum_{j=1} y_i y_j a_{ij} \qquad (5)$$

but the a_{ij} calculations were carried out in two ways: as mean geometrical and by Lorenz combination.

Then, the Lorenz combination was taken as the fundamental one as when calculating vapor phase of ammonia in a five-component mixture it has given the least error.

Let i=5 for the solute (ammonia), then liquid phase fugacity can be expressed as

$$f_5^L = \gamma_5 \cdot x_5 \cdot f_{pure5}^{P_5^S} \exp \int_{P_5^S}^{P} \frac{V_5 \, dP}{RT}, \qquad (6)$$

where γ_5 - liquid phase activity coefficient, V_5 - liquid phase molar volume, $f_{pure5}^{P_5^S}$ - saturated liquid fugacity, P_5^S - saturation pressure at temperature T. The molar volume of liquid in the Poynting correction term can be expressed through Wada's equation

$$V_5 = V_5^S \left[1 + 7\beta_5^S \left(P - P_5^S \right) \right]^{-\frac{1}{7}}, \qquad (7)$$

where V_5^S and β_5^S - the molar volume and saturated liquid compressibility respectively at temperature T and pressure P_5^S, the latter being calculated from Chueh's equation [4]. The pressure correction

term for the desolved components in liquid ammonia and partial fugacity of the components under infinite delution were calculated using the Alessandrini methods [2]. To calculate the activity coefficients the expanded Van Laar model was used. [5].

There are no experimental data on phase equilibrium of the mixture H_2-N_2-CH_4-Ar-NH_3 and data obtained using the diagrams of paper [2] lack accuracy due to graphical representation of the data. The comparison of calculated and experimental data for the ternary mixture H_2-N_2-NH_3 [6] and for the binary mixtures Ar-NH_3 and CH_4-NH_3 [7] showed satisfactory correspondence. The relative deviation at 18 test points was of the order of 3%.

Technique Ω_a correlation as a function of temperature introduces an insignificant accuracy loss as compared to experimental data while determining compressibility coefficients of H_2-NH_3 and CH_4-NH_3 mixtures and also out of the temperature and pressure ranges under consideration. This can be see from figure where data obtained are compared to the data [8].

References

1 Nohka, J., Sarashina, E., Arai, Y., and Shozaburo, S., Chem. Eng.Japan. 6 (1), 10 (1973).

2 Alessandrini, C.G., Prausnitz, J.M. Ind.Chem.Process Des.Develop., 11 (2), 253 (1972).

3 Prausnitz, J.M., "Molecular Thermodynamics of Fluid-Phase Equilibria", p.156, Prentice-Hall, Englewood Cliffs, N.Y. (1969).

4 Chueh, P.L., Prausnitz, J.M., AIChE J., 15 (3), 471 (1969)

5 Prausnitz, J.M., Chueh, P.L., "Computer Calculation for High--Pressure Vapor-Liquid Equilibria," p.82-90, Prentice-Hall, Englewood Cliffs, N.Y. (1968).

6 Michels, A., Skelton, G.F., Dumoulin, E., Physica, 14, 831 (1950).

7 Kaminisi, G., Toriumi, T., Bulletin of the Chemical Research Institute of Non-Aqueous Solutions, Tohoku University, 10, 51 (1961).

8 Nakamura, R., Breedveld, G.J.F., Prausnitz, J.M., Ind.Eng. Chem.Process Des.Develop., 15 (4), 11 (1976).

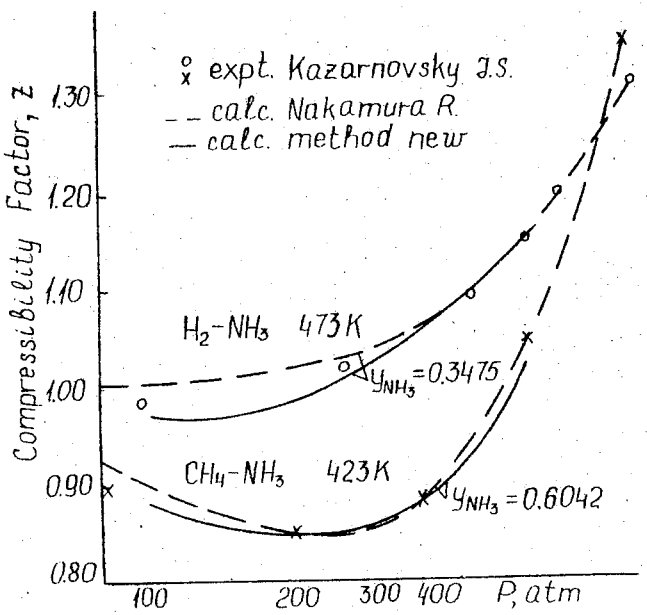

Compressibility factors for hydrogen-ammonia and methane-ammonia mixtures (the experimental data are taken from paper [2]).

STATE AND PROPERTIES OF INORGANIC AQUEOUS SOLUTIONS IN A WIDE TEMPERATURE, PRESSURE AND CONCENTRATION RANGE

V.M. Valyashko, K.G. Kravchuk
Kurnakov Institute of General and Inorganic Chemistry, USSR Academy of Sciences, Moscow, USSR

At normal pressure-temperature parameters the agregate state of substances in water-salt systems is easily defined as solid, liquid and gaseous. Such simple picture is lost at high temperatures because specific, "high temperature" properties of water-salt solutions arise and this is manifested in immiscibility and critical phenomena.

Immiscibility in water-salt solutions is quite usual at temperatures above 240-380 °C. Up to now, complete phase diagrams have been studied at least for 41 binary systems contained water and a salt which solves well at normal conditions [1]. There is no immiscibility only in 22 of these systems. This phenomenon is recorded in other 19 systems. Besides, according to experimental data the liquid immiscibility is a very usual property of the most water-silicate systems.

The critical phenomena in hydrothermal solutions make possible the continious transformation between liquid and gas without the phase reaction, by means of gradual alterations of phase properties on changing state parameters.

The critical phenomena between liquid and gas take place in the temperature range between the critical point of water and that of salt. At any temperatures the values of critical pressure are lower than pressures of critical isochore of pure water. The critical phenomena between two liquids may take place in higher temperature ranges, and the pressures concerned these phenomena may appear to be very high, which is of particular importance. At higher temperatures liquid immiscibility can be limited not only as a result of critical phenomena but by cristallisation of high temperature forms of ice, as well.

Now it is impossible to predict features of the phase equilibria for the individual water-salt system even if we know properties of both components. But there are some correlations which allow us to suggest the probable kind of phase diagram. For instance, the 2d (p-Q) type phase diagram which contains fluid region and critical phenomena in saturated solutions, is peculiar, as a rule, t

systems formed with water and high-melting-point salt [2,3]. The important information is given by salt solubility data at normal temperatures. If the concentration of a saturated solution exceeds the certain values called transition region concentration, then the system rather belongs to the 1st type diagram (without critical phenomena in saturated solutions. The location of the transition region - the concentration interval within the limits of which molecular interactions lose their water-like nature (characteristic features of diluted solutions) - is related to electrolyte charge. For (I-I) electrolytes the concentration is 10-20 mol %, for (I-2) and (2-I) - 5-12 mol %, for (2-2) - 2-5 mol % [2].

The development of the theory of complete phase diagrams makes it possible to systematize their types for binary and ternary systems [3, 4]. The comparison of phase diagrams constructions shows that the most distinctive features are placed around the critical parameters of pure water. So, in order to determine the type of diagram of the system under study it is necessary to have at least some experimental data of this region on phase equilibria at 350--400 °C. An information on the construction of and a complete diagram of the system under study which is contained in a topological scheme is very useful for design of an experiment and interpretation of its results [3, 4].

The behaviour of electrolytes solubility in aqueous systems is interesting not only for theory of phase diagrams, It is important for many processes where hydrothermal solutions are used especially for of single crystals growth. The progress in this method is obliged to the possibility of wide variation both of a magnitude of crystal solubility and a temperature coefficient of solubility in hydrothermal condition. Usually temperature and composition of solutes are changed to recieve an optimum condition of dissolution and crystallization. But in some cases, when the parameters of crystal growth are not far from immiscibility region or critical equilibria, the pressure influence becames comparable and even stronger than the temperature one.

An example of strong pressure influence on salt solubility at hydrothermal conditions is given in paper [5]. Results of experimental studying of $CaWO_4$ solubility in 32 wt.% K_2SO_4 aqueous solution at different pressures and temperatures are shown in Fig.1. Sharp jumps of $CaWO_4$ solubility can be understood only if the phase transformations of solvent are taken into account. 32 wt. % K_2SO_4

is a bulk composition of solvent but the real liquid solvent changes its concentration with a pressure as it is shown in Fig.1b.

The pressure dependence of salt solubility in supercritical regions is very similar to dependences found for gaseous, organic and mixed systems which are used in the processes of supercritical fluid extraction. The example with $CaWO_4$ shows that pressure variation can be used for extraction and deposition of the salt in the same way as it has been done for industrial processes of nicotine or caffeine extraction by CO_2-H_2O mixture. As a draft hypothesis we can say that sometimes the processes of extraction, transfer a deposition of low-soluble minerals in natural hydrothermal conditions depends to a larger degree on the pressure changes than on the temperature ones.

It is necessary to emphasize that all these conclusions are based on the fundamental principles of phase diagram construction general for any kind of systems with different volatility components.

References

1. V.M. Valyashko, K.G. Kravchuk, M.Yu. Korotaev. Phase equilibria of binary aqueous solutions of inorganic substances at high temperatures and pressures. In: Reviews on Thermophysical Properties of Substances, n.5(6), Moscow, IVTAN, pp.57-127, 1984.
2. V.M. Valyashko. Studies of water-salt systems at elevated temperatures and pressures. Ber.Buns.Ges.Phys.Chem. Bd.81, N4, pp.388-394, 1977.
3. V.M. Valyashko. Regularities of phase diagram construction for water-salt systems in wide interval of parameters. Zh. Neorgan. Khimii, v.26, pp.3044-3054, 1981.
4. V.M. Valyashko. Complete phase diagrams of binary systems. Z.Phys. Chim. (Leipzig), 267, N.3, pp.481-493, 1986.
5. M.I. Ravich. Water-salt Systems at Elevated Temperatures an Pressures, Moscow, Nauka, 150 p., 1974.

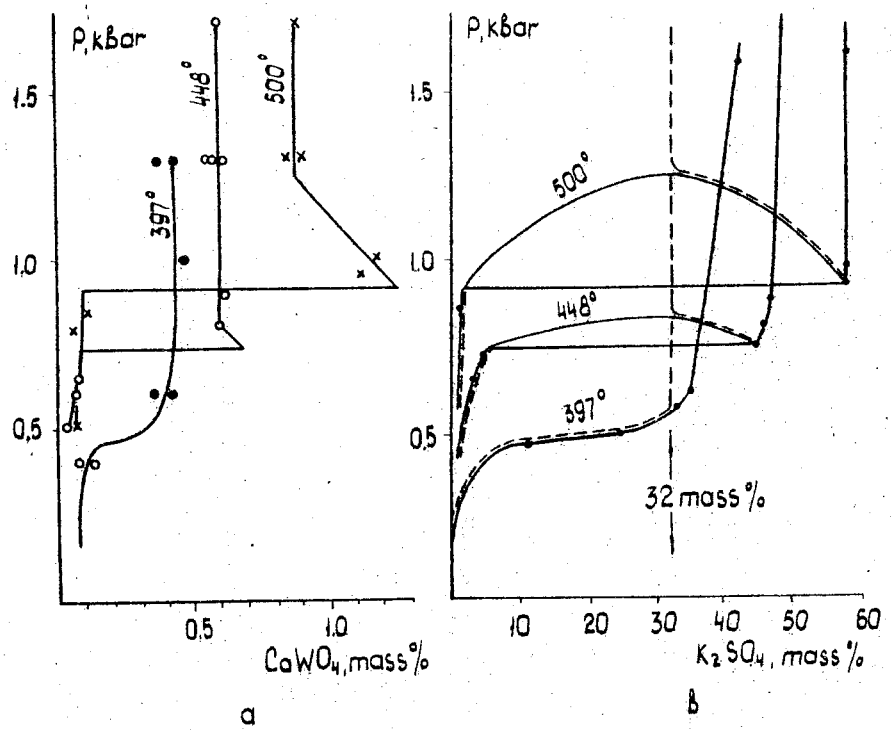

Solubility of $CaWO_4$ in 32 mass % K_2SO_4 aqueous at high temperatures and pressures (a) and real phase situation in K_2SO_4-H_2O system at the same parameters (b) Dashed lines shows the concentrations of K_2SO_4 in liquid phases at the parameters of $CaWO_4$ dissolution and constant bulk content of K_2SO_4 (32 mass %).

RAMAN SPECTRA OF SOME LIQUIDS WITHIN THE PRESSURE RANGE 0.1-800 MPa

A.K. Atakhodzhaev[1], F.S. Ganiev[1], A. Laisaar[2], F.Kh. Tukhvatullin[1], A. Shodiev[1]

[1]A.Navoi Samarkand State University, Samarkand, USSR
[2]Institute of Physics, Estonian SSR Acad. Sci., Tartu, USSR

Experiments have shown that the position, width and shape of the lines in the Raman spectrum of liquid substances are quite sensitive to the changes in external conditions.

In this work, the effect of high pressure on the frequency, width and shape of some polarized and depolarized Raman lines of toluene, acetonitrile, benzene, carbon disulfide, chloroform, aniline and cyclohexane was studied. The liquids were compressed in high-pressure cells equipped with quartz or sapphire windows. Raman spectra were recorded with a DES-12 or DFS-24 spectrometer by using a LG-38 or LG-62 gas laser. The spectral positions of Raman lines were determined against the neon reference lines. The half-width of the lines, determined as a full width at half maximum (FWHM), was not corrected for the apparatus function (instrumental contour) of the spectrometer, except for the last three liquids.

In total, 20 Raman lines of the above-mentioned liquids were examined within the pressure range 0.1-800 MPa at 20 °C. The highest pressures, P_{max}, used in each individual case, are listed in Table I. For toluene, acetonitrile, benzene and cyclohexane the P_{max} values are more or less close to the freezing pressure of these liquids at 20 °C as estimated from the experimental data for toluene [1] and as calculated from the Simon equation for the othe three liquids [2]. Besides, benzene was studied in the solid state as well, at pressures up to 130 MPa.

As is seen from Table I, in most cases the lines are shifted to higher frequencies with increasing pressure. For example, in the pressure range 0.1-750 MPa the frequency of the 217 cm^{-1} depolarized line of toluene increases by 11 cm^{-1} and that of the 521 cm^{-1} polarized line, by 3 cm^{-1}. Among all the substances studied, only for acetonitrile (the 2250 cm^{-1} line) and carbon disulfide (the 796.5 cm^{-1} line) the shifts to lower frequencies were observed. For benzene (the 606 and 992 cm^{-1} lines) the pressure

shifts in the liquid state were found to be greatly different from those in the solid state: in the liquid state the lines exhibited considerably larger shifts.

The pressure-induced shifts of the lines point to the change in the force constants of the respective vibrations due to the change of intermolecular interactions.

For the liquids studied, the increase in pressure causes, as a rule, a decrease of the half-width of the depolarized lines (except for the 217 cm^{-1} line of toluene) and an increase of that of the polarized lines. The narrowing of the depolarized lines with increasing pressure may partly be explained by the slow-down of molecular reorientations due to the increase in the viscosity of liquids [3].

For benzene the behaviour of the linewidths was determined also in the crystalline state. As pressure grows in the solid state, the half-width of the 606 cm^{-1} depolarized line decreases, whereas the half-width of the 992 cm^{-1} polarized line tends to increase, i.e. the character of the half-width changes for these lines is the same as in the liquid state. As an example, in Fig.1 the spectrograms of the 1586 cm^{-1} and 1606 cm^{-1} depolarized lines of benzene in the liquid and solid states are depicted.

The pressure-induced decrease of the half-width of depolarized lines for solid benzene gives reason to suppose that benzene preserves some freedom of molecular reorientation in the crystalline state, and this reorientation becomes slower with increasing pressure.

The results given above show that the assumption about the constancy of the linewidth, which is not connected with the rotational (reorientational) motion of molecules, is not valid in the case of high-pressure studies. The width of polarized lines and probably also the "residual" width of depolarized lines, caused mainly by vibrational relaxation, do change with pressure, and the rates of this change are rather considerable. In this respect, characteristic is an example of the 619 cm^{-1} depolarized line of aniline. According to the Rayleigh scattering data the reorientational relaxation time τ for aniline molecules is about 25 ps [4]. Hence, the contribution to the half-width of depolarized lines due to the rotational motion of molecules, as estimated from the relationship $\delta\nu=(2\pi c\tau)^{-1}$, where c is the velocity of light, should not exceed 0.2-0.3 cm^{-1}. However, in fact the half-width of the

Frequencies and half-widths of polarized (p) and depolarized (dp) Raman lines of some liquids at various pressures

Substance	Line frequency (literature data) (cm^{-1}) at P=0.1 MPa	Pressure P_{max} (MPa)	Frequency (cm^{-1}) at P=0.1 MPa	Frequency (cm^{-1}) at $P=P_{max}$	Half-width (cm^{-1}) at P=0.1 MPa	Half-width (cm^{-1}) at $P=P_{max}$	Pressure coefficient $(d\ /dP)\times10^2$ (cm^{-1}/MPa)
Toluene	217 (dp)	750	217	228	16.8	24.1	1.0
	521 (p)	750	520	523	4.2	6.7	0.3
	1004 (p)	796	1003	1005	12.9	14.3	0.2
	1031 (p)	796	1030	1033	13.1	17.9	0.6
Acetonitrile	375 (dp)	365	379	382	15.2	12.3	-0.8
	920 (p)	365	921	925	7.3	9.1	0.5
	2250 (p)	365	2253	2251	7.6	9.8	0.6
Benzene	606 (dp)	55	605	607	8.8	7.3	-2.7
	992 (p)	55	992	993	4.5	4.6	0.2
	1178 (dp)	55	1175	1177	15.0	13.2	-3.3
	1586 (dp)	55	1585	1586	13.9	12.6	-2.4
	1606 (dp)	55	1604	1606	14.0	11.7	-4.2
Carbon disulfide	655.7 (p)	440	655	656	3.8	4.2	0.1
	796.5 (p)	440	796	793	14.2	16.6	0.6
Chloroform	261 (dp)	120	-	-	8.0	6.6	-1.2
Aniline	619 (dp)	80	-	-	6.2	4.4	-2.3
Cyclohexane	1028 (dp)	25	-	-	13.1	12.4	-2.8

line mentioned decreases under pressure much more than this value, namely by 1.8 cm^{-1} at 80 MPa (see Table).

Thus, in the cases studied the pressure-induced changes in the molecular spectra of liquids are quite substantial and they reflect the changes in the structure and properties of liquids.

The authors would like to thank A.Ellervee and V.Shcherbakov for participation in experiments.

References

1. Weale K.E. Chemical Reactions at High Pressures. - London: E. & F.N. Spon, 1967. - XV, 349 p.-(P. 51, Table 3.7).
2. Babb S.E. Parameters in the Simon equation relating pressure and melting temperature // Rev. Mod. Phys. - 1963. - Vol.35, No.2. - P.400-413.
3. Sobelman I.I. Raman linewidth in vapour // Izv. Akad. Nauk SSSR. Ser. Fiz. - 1953. - Vol.17, No.5.- P.554-560. (In Russian).
4. Atakhodzhaev A.K. and Tukhvatullin F.Kh. Spectral Distribution of Intensity in the Wing of the Scattering Line of Liquids and Solutions. - Tashkent: Fan, 1981.- 123 p. (In Russian).

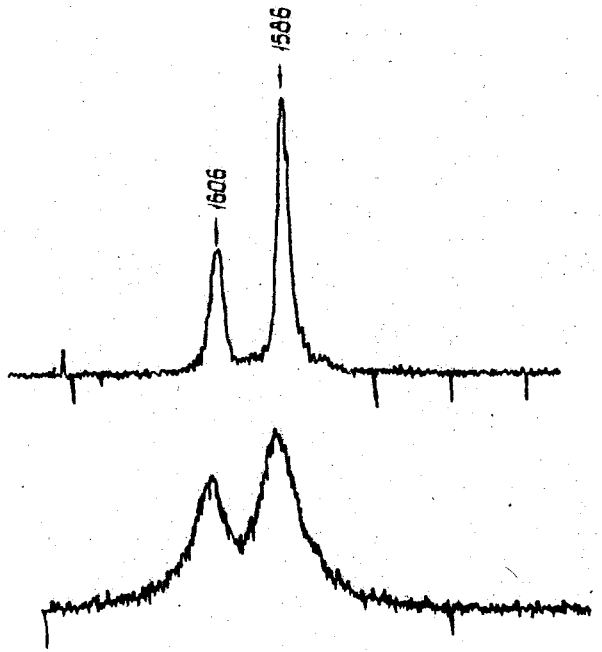

Spectrograms of the 1586 and 1606 cm^{-1} Raman lines of benzene in the liquid state at 0.1 MPa (lower spectrum) and in the solid state at 100 MPa (upper spectrum).

INFLUENCE OF PRESSURE ON THE ELASTIC AND VISCOUS PROPERTIES OF HYDROCARBON LIQUIDS

V.Moyseenko, I. Adamenko, L. Samoylenko, A. Tkachenko
The Kiev State University, Kiev, USSR

The purpose of the study was to find equation of state describing in the best way P-V-T data and giving the possibility to calculate the elastic, thermal and calorific properties, as well as to study the pressure dependence of elastic, viscous properties and the viscoelasticity for normal and cyclohydrocarbon liquids.

P-V-T data have been studied for n-alcanes (from n-hexane to n-hexadecane), aromatic hydrocarbons (from benzene to hehilbenzene) in the temperature range 313-473 K at pressure from 0.1-245 MPa by metallic bellows dilatometer using a linear differential transformer for measurement of displacement. The ultrasonic velocity has been measured in the same temperature and pressure range by the direct pulse-echo method of a fixed distance with frequency of 5 MHz. Preliminary we have satisfied ourselves that dispersion of ultrasonic velocity was absent in the frequency range 1.25-10 MHz within the indicated limits of the thermodynamic parameters change. The error of measurement of the density and the ultrasonic velocity was 0.3%. The isochoric viscosity of hydrocarbons was measured by the falling body method within the error 3-5%.

The isothermic and adiabatic bulk modulus, Puasson's coefficient, coefficient of thermal expansion, the increase in entalpy, in entropy and in isobaric-isothemic potential were calculated on the basis of the obtained experimental data.

We have analysed few parametric statistically founded equations of state, as well as those which more often than others are used in literature for describing the properties of molecular liquids:

equation of Tait-Tamman

$$\left(\frac{\partial V}{\partial P}\right)_T = -\frac{A'}{B+P}, \qquad (1)$$

equation of Marneghem

$$\left(\frac{\partial \ln V}{\partial P}\right)_T = -\frac{A^*}{B^*+P}, \qquad (2)$$

equation of Hudleston

$$\ln \frac{PV^{2/3}}{V_0^{1/3} - V^{1/3}} = A' + B'\left(V_0^{1/3} - V^{1/3}\right), \qquad (3)$$

equation of Golcobev-Guseinov

$$P = \frac{a}{V^3} + \frac{b}{V^7}, \qquad (4)$$

equation of Ahoondov-Mamedov

$$P = \frac{a^*}{V^2} + \frac{b^*}{V^9}. \qquad (5)$$

In order to solve which of these equations should be preferred we rearranged them to the form which contains the same experimental constants: P_o, V_o, K_{to}, $\left(\frac{\partial K_t}{\partial P}\right)_o$ [1,2]. The rearranged form of the analyzed equations of state was :

$$Z = \left[1 + \left(\frac{\partial K_t}{\partial P}\right)_o\right]^{-1} \cdot \left\{\exp\left[1 + \left(\frac{\partial K_t}{\partial P}\right)_o\right]\left[1 - \frac{V}{V_o}\right] - 1\right\}, \qquad (6)$$

$$Z = \left(\frac{\partial K_t}{\partial P}\right)_o^{-1} \cdot \left[\left(\frac{V_o}{V}\right)^{\left(\frac{\partial K_t}{\partial P}\right)_o} - 1\right], \qquad (7)$$

$$Z = \left[\frac{1}{3} + \left(\frac{\partial K_t}{\partial P}\right)_o\right]^{-1} \cdot \left\{\exp\left[1 + 3\left(\frac{\partial K_t}{\partial P}\right)_o\right] - \left[1 - \left(\frac{V}{V_o}\right)^{1/3}\right] - 1\right\}, \qquad (8)$$

$$Z = \frac{1}{28}\left[\left(\frac{\partial K_t}{\partial P}\right)_o - 3\right]\left[\left(\frac{V_o}{V}\right)^7 - 1\right] - \frac{1}{12}\left[\left(\frac{\partial K_t}{\partial P}\right)_o - 7\right]\left[\left(\frac{V_o}{V}\right)^3 - 1\right], \qquad (9)$$

$$Z = \frac{1}{63}\left[\left(\frac{\partial K_t}{\partial P}\right)_o - 2\right]\left[\left(\frac{V_o}{V}\right)^9 - 1\right] - \frac{1}{14}\left[\left(\frac{\partial K_t}{\partial P}\right)_o - 9\right]\left[\left(\frac{V_o}{V}\right)^2 - 1\right], \qquad (10)$$

where Z equals $(P-P_o)/K_{to}$. The comparison of the experimental and calculated (according to the formulas (6)-(10) [2, 3]) values shows that these equations are indistinguishable within the error 0.2--0.4% at low temperatures and at pressures up to 49 MPa. At higher pressures Tait-Tamman's and Ahoondov-Mamedov's equations are preferable. The further selection of equation of state was made by means of studying of pressure dependence of derivative $\left(\frac{\partial P}{\partial V}\right)_T$. Experimental dependence of $\left(\frac{\partial P}{\partial V}\right)_T$ on P has linear character in investigated interval of changes in P and T. Only Tait-Tamman's equation gives such a dependence. We have calculated parameters of this equation and have shown that it was suitable for the calculation of

bulk modulus, entalpy, entropy, Gibbs' potential [2]. Measurements were carried out of isochoric viscosity and ultrasonic velocity under conditions at which changes in temperature do not cause changes in packing of molecules [4]. In accordance with activation theories the molecular mechanism of viscous flow consists in uneven motion of molecules for distances equal to a mean value distance between molecules ($\bar{R}$), i.e. 0.1-1.0 nm; in addition, the dependence of viscosity on P and T may be described as:

$$\eta = \eta_0 \exp(E/kT), \qquad (11)$$

where E is the energy of activation equal to the height of potential barrier which must be overcome by molecules. In various theories E is identified with different energy characteristics of liquids: heat of evaporation, melt and etc.

In work /5/ for the case of high densities E has been identified with the energy of molecule vibration about equilibrium position with frequency ν which has been equal to

$$E = 2\pi^2 \cdot m \cdot \nu^2 \cdot q^2, \qquad (12)$$

here m is the mass of molecule, q is the amplitude of vibration which corresponds to the value of jump into the neighbouring vacant position. If ν is supposed to be equal to Debye's frequency ν_D:

$$\nu_D = \sqrt[3]{3N/4\pi V} \cdot C, \qquad (13)$$

where C is the ultrasonic velocity, V is the volume of mole of substance then we may calculate below-mentioned q-value for n-hexane using formulas (11)-(13).

The value of ultrasonic velocity ($C, \frac{m}{s}$) and (q, nm) for n-hexane on isochors

	ρ = 580 Kg/m^3			ρ = 757 Kg/m^3			
T,K	P,MPa	C, $\frac{m}{s}$	q, nm	T,K	P,MPa	C, $\frac{m}{s}$	q, nm
375.0	0.1	740	0.054	301.1	196.2	1900	0.026
412.1	19.8	820	0.046	328.1	245.0	1975	0.025

For other hydrocarbon liquids the value q is analogous to hexane and is about (0.1-0.01)$\bar{R}$. If the density is less than 2ρ of critic ones then the energy of activation is on the order of energy of thermal motion kT. All these show that the activation mechanism of viscous flow does not occur for hydrocarbons. It is possible to describe it as collisions, if the exchange by impulse is supposed to take place between 4-5 molecules.

We calculated the function $\tau = \eta / K_t$, that is the time of Maxwell's relaxation which is about 10^{-11}s. The dependence of τ on P passes across minimum as pressure increases. Such a dependence of function τ on P indicates that the influence of dissipation processes on viscoelastisitive behaviour of hydrocarbon liquids increases with the increase in pressure.

References

1. Mac Donald J.R., Rowell D.R. Discrimination between equation of state // J.Res.NBSA, 1971, 75, N5, p.441-443.
2. Адаменко И.И., Алтунин В.В. Уравнение состояния жидкой двуокиси углерода и пропилового спирта//Укр.физ.журн. 29,№12, 1984, с. 1791-1797.
3. Голик А.З., Адаменко И.И., Махно М.Г. Уравнение состояния, упругие, тепловые свойства алкилбензолов // Сб.Физика жидкого состояния 1982, №10, с.3-9.
4. Голик А.З., Адаменко И.И., Варецкий В.В. и др. Вязкость н-парафинов в интервале температур 20-140 °С и давлений до 2500 ат // Укр.физ.журн. 1976, 21, №2, с.177-180.
5. Waring C.E., Becher P. "Structure" in liquids and relation between the parameters of the Arrenius equation for reaction in the condensed phase // J.Chem.Phys. 1947, 15,N7, p.488--496.

DETERMINATION OF CRYSTAL STRUCTURE IN THE MULTIMEGABAR REGIME USING SYNCHROTRON RADIATION

Arthur L. Ruoff and Yogesh K. Vohra
Department of Materials Science and Engineering
Cornell University, Ithaca, NY 14853 USA

Excellent x-ray diffraction patterns can be obtained, even above 200 GPa (two megabars) using diamond anvil cells and synchrotron radiation from the Cornell High Energy Synchrotron Source (CHESS). We focus on the application of energy dispersive x-ray diffraction techniques. We also describe and illustrate the power of the wiggler source at CHESS. Comparisons are made in some cases with theoretical calculations.

INTRODUCTION

In energy dispersive x-ray diffraction (EDXD) a polychromatic x-ray beam is diffracted from a polycrystalline sample with the diffracted x-rays entering a slit at a fixed angle in front of a solid state detector. For EDXD studies, Bragg's law is

$$Ed = hc/2 \sin \theta \, . \qquad (1)$$

A spectrum consists of intensity versus energy obtained with the use of a solid state intrinsic germanium detector and a multichannel analyzer. The Cornell High Energy Synchrotron Source (CHESS) supplies the x-rays. Details of our use of EDXD with the diamond anvil cell (DAC) are described elsewhere [1,2].

RESULTS

Figure 1 shows an x-ray diffraction pattern of rhenium obtained using a 10 μm diameter collimated beam for 90 minutes at 216 GPa (2.16 Mbar) [3]. The sample volume is about 3×10^{-10} cm^3. The interplanar spacings for the twelve peaks are shown in Table 1. No phase transition was found and rhenium retains its hexagonal close packed structure (hcp) to 216 GPa. The c/a ratio for hcp

rhenium remains constant at 1.614. We have also used x-ray diffraction to obtain the pressure profile across the beveled diamond face as shown in Figure 2 [3]. In all cases the pressure was obtained from shock data of rhenium [4]. The unusual pressure profile in this case was due to the large bevel angle of 10° and the coefficient of friction between rhenium and diamond. In another experiment now underway using 5° bevels, the pressure profiles are smoothly varying without the step seen in Figure 2.

In another study on GaSb we found two new phase transitions to 110 GPa. Table 2 shows the comparison of calculated and experimental interplanar spacings and intensities of GaSb assuming a disordered simple hexagonal structure for this newly found phase [5].

In some cases approximate first principle theoretical calculations have been made and these are compared with experiment in Table 3. The agreement for InAs is excellent, for Ge good and for Si excellent (perhaps fortuitous) in two cases and only fair in the third case and for GaSb only fair. We were somewhat surprised by these last two comparisons which involved ab initio pseudopotential calculations.

In the past year a wiggler with white radiation became available on the A-1 line at CHESS. A wiggler is a magnetic system which forces the electron beam into a trajectory with a smaller radius of curvature than obtained in the dipole bending magnets by using a larger local magnetic field. The wiggler is of interest because it greatly increases the intensity of x-ray radiation at high energies. See Figure 3. We illustrate this in Figure 4 and Table 4 where we show results for primitive hexagonal silicon at comparable pressures and times using the same collimator [13]. We get twice as many well defined peaks with the beam from the wiggler as from the beam from the bending magnet. That could be very important in structural determinations.

Figure 5 shows diffraction patterns obtained for gold with the beam from the wiggler in 5 minutes and in 13 seconds (both at 112 GPa, same collimator, same spot on the sample). The 13 second pattern clearly suffices to show that gold is still fcc at this pressure and to determine the pressure. The gold

sample in this case was of 25 μm diameter in a spring steel gasket and the collimator diameter was 20 μm. There are no gasket peaks in the spectrum. This is an important result because it suggests that with the wiggler we can get to shorter times or use collimators with smaller holes. In fact this result and our earlier result on rhenium suggest that good diffraction patterns should be attainable for such materials using a 1 μm diameter collimator. Of course the sample will have to have grain sizes in the range 0.1-0.5 μm.

CONCLUSION

Finally as a review of the past we consider the maximum pressures at which good diffraction patterns were obtained at CHESS by our group versus the time at which papers were submitted. See Figure 6. A pattern is good if it has at least five good peaks and preferably six per lattice parameter. A sage once said, "Never make predictions, especially about the future." Ignoring such good advice we have extrapolated the curve to the end of this decade and shown the approximate times when very good x-ray diffraction patterns should be obtained at higher pressures (in parenthesis). If all goes well we should reach the maximum pressure attainable strength for diamond anvils calculated by Whitlock and Ruoff [14] approximately at the end of this decade. We expect to be working with diamond tips with flats of only 25 μm in diameter and with 1 μm collimators.

ACKNOWLEDGMENT

We wish to acknowledge the National Science Foundation for support of this work under Grant DMR 86-12289.

Table 1. Comparison of observed and calculated interplanar spacings for rhenium at 216 GPa ($V/V_o = 0.734$). The calculated interplanar spacings (d) are based on $a = 2.491 \pm 0.003$ Å, and $c = 4.020 \pm 0.005$ Å and $c/a = 1.614 \pm 0.004$. The excellent quality of diffraction data at this pressure is indicated by the small fractional deviation of the calculated line positions from the observed ones.

(hkl)	d_{obs} (Å)	$d_{calculated}$ (Å)	$\frac{d_{obs} - d_{cal}}{d_{obs}}$
100	2.154	2.157	-0.0014
002	2.004	2.010	0.0030
101	1.901	1.901	0
102	1.468	1.471	-0.0020
110	1.246	1.246	0
103	1.139	1.138	0.0009
200	1.078	1.079	-0.0009
112	1.056	1.059	-0.0028
201	1.043	1.042	-0.0010
202	0.9506	0.9504	0.0002
211	0.7996	0.7991	0.0006
114	0.7831	0.7821	0.0013

sample in this case was of 25 μm diameter in a spring steel gasket and the collimator diameter was 20 μm. There are no gasket peaks in the spectrum. This is an important result because it suggests that with the wiggler we can get to shorter times or use collimators with smaller holes. In fact this result and our earlier result on rhenium suggest that good diffraction patterns should be attainable for such materials using a 1 μm diameter collimator. Of course the sample will have to have grain sizes in the range 0.1-0.5 μm.

CONCLUSION

Finally as a review of the past we consider the maximum pressures at which good diffraction patterns were obtained at CHESS by our group versus the time at which papers were submitted. See Figure 6. A pattern is good if it has at least five good peaks and preferably six per lattice parameter. A sage once said, "Never make predictions, especially about the future." Ignoring such good advice we have extrapolated the curve to the end of this decade and shown the approximate times when very good x-ray diffraction patterns should be obtained at higher pressures (in parenthesis). If all goes well we should reach the maximum pressure attainable strength for diamond anvils calculated by Whitlock and Ruoff [14] approximately at the end of this decade. We expect to be working with diamond tips with flats of only 25 μm in diameter and with 1 μm collimators.

ACKNOWLEDGMENT

We wish to acknowledge the National Science Foundation for support of this work under Grant DMR 86-12289.

Table 1. Comparison of observed and calculated interplanar spacings for rhenium at 216 GPa ($V/V_o = 0.734$). The calculated interplanar spacings (d) are based on $a = 2.491 \pm 0.003$ Å, and $c = 4.020 \pm 0.005$ Å and $c/a = 1.614 \pm 0.004$. The excellent quality of diffraction data at this pressure is indicated by the small fractional deviation of the calculated line positions from the observed ones.

(hkl)	d_{obs} (Å)	$d_{calculated}$ (Å)	$\frac{d_{obs} - d_{cal}}{d_{obs}}$
100	2.154	2.157	-0.0014
002	2.004	2.010	0.0030
101	1.901	1.901	0
102	1.468	1.471	-0.0020
110	1.246	1.246	0
103	1.139	1.138	0.0009
200	1.078	1.079	-0.0009
112	1.056	1.059	-0.0028
201	1.043	1.042	-0.0010
202	0.9506	0.9504	0.0002
211	0.7996	0.7991	0.0006
114	0.7831	0.7821	0.0013

Table 2. Comparison of calculated and experimental interplanar spacings and intensities of GaSb in the (disordered) simple hexagonal type structure at 56.6 GPa. The lattice parameters used are a = 2.6981 Å and c = 2.4790 Å. The calculated relative intensities were obtained using the procedure described in Reference 1. A sample thickness of 20 μm was assumed.

hkl	d_{obs} (Å)	d_{cal} (Å)	Obs. Int.	Cal. Int.
001	2.468	2.479	33.2	18.0
100	2.336	2.336	64.7	57.9
101	1.702	1.700	100.0%	100.0%
110	1.348	1.349	30.5	27.9
002	1.240	1.240	4.9	6.8
111+200	1.185	1.185, 1.168	61.5	47.2

Table 3. Comparison of Some of our Experimental Transition Pressures with Calculated Phase transition Pressures

Material InAs	Experimental (GPa)	Calculated (GPa)	Reference for Calculations
InAs	7.0	7.8	28
		8.4	29
	17.0	19.5	27
GaSb	26.4±2.6	52.8	29
Si	78±3	80	30
		76	30
		116	31
Ge	74	84	12
	102	105 (a)	12

(a) The calculations show that the hcp phase has a lower free energy than the dhcp phase found experimentally.

Table 4. The comparison of the diffraction data for the high pressure primitive hexagonal phase of silicon obtained at the bending magnet and the wiggler station (Fig. 5). The E (observed) are the experimentally measured diffraction peak positions while the E (calc.) are the ones calculated based on the parameters indicated.

Bending Magnet P = 34.0 GPa a=2.4680Å, c=2.327Å (Ed=39.628)			Wiggler P = 35.5 GPa a=2.4624Å, c=2.3277Å (Ed=37.720)		
(hkl)	E_{hkl} (keV) (observed)	E_{hkl} (keV) (calc.)	(hkl)	E_{hkl} (keV) (observed)	E_{hkl} (keV) (calc.)
(001)	17.020	17.025	(001)	16.249	16.205
(100)	18.539	18.541	(100)	17.709	17.688
(101)	25.176	25.172	(101)	23.987	23.988
(110)	32.100	32.114	(110)	30.606	30.637
(002)	34.045	34.051	(002)	32.422	32.410
(111)	36.345	36.348	(111)	34.640	34.658
(200)	37.091	37.082	(200)	35.340	35.376
(102)	38.781	38.772	(102)	36.917	36.922
(201)	40.828	40.804	(201)	38.901	38.911
			(112)	44.629	44.598
			(210)	46.772	46.798
			(202)	47.893	48.615
			(003)	48.588	48.615
			(211)	49.482	49.525
			(103)	51.727	51.733
			(301)	55.427	55.484
			(212)	56.897	56.926
			(113)	57.463	57.464

References

1. Baublitz, Jr., M.A., Arnold, V. and Ruoff, A.L., "Energy Dispersive Diffraction from High Pressure Polycrystalline Specimens Using Synchrotron Radiation," Rev. Sci. Instrum. (1981), 52, 1616-1624.
2. Brister, K.E., Vohra, Y.K. and Ruoff, A.L., "New Micro-Collimated Energy-Dispersive X-ray Diffraction Apparatus for Studies at Megabar Pressures at the Cornell High Energy Synchrotron Source," Review of Sci. Instrum. 57, (1986), 2560-2563.
3. Vohra, Y.K., Duclos, S.J. and Ruoff, A.L., "High Pressure X-ray Diffraction Studies on Rhenium to 216 GPa (2.16 Mbar)," April (1987), Materials Science Center Report 6031, Cornell University, Ithaca, N.Y., 14853, USA., 1-15, Submitted for publication.
4. McQueen, R.G., Marsh, S.P., Taylor, J.W., Fritz, J.N. and Carter, W.J., in "High Velocity Impact Phenomena," Ed. Kinslow, R., New York: Academic Press (1970), 579 pp., p. 293.
5. Weir, S.T., Vohra, Y.K. and Ruoff, A.L., "Phase Transitions in GaSb to 110 GPa (1.1 Mbar)," June (1987), Materials Science Center Report 6143, Cornell University, Ithaca, N.Y., 14853, USA., 1-15. Submitted for publication.
6. Vohra, Y.K., Weir, S.T. and Ruoff, A.L., "High Pressure Phase Transitions and Equations of State of the III-V Compound InAs up to 27 GPa," Phys. Rev. (1985), B31, 7344-7348.
7. Christensen, N.E., "Calculated Equation of State of Indium Arsenide," Phys. Rev. (1986), B33, 5096-5102.
8. Zhang, S.B. and Cohen, M.L., "High-Pressure Phases of III-V Zinc-blende Semiconductors," Phys. Rev. (1987), B35, 7604-7610.
9. Duclos, S.J., Vohra, Y.K. and Ruoff, A.L., "hcp to fcc Transition in Silicon at 78 GPa and Studies to 100 GPa," Phys. Rev. Lett. (1987), 58, 775-777. In a subsequent experiment the pressure was extended to 110 GPa.

10. McMahan, A.K. and Moriarty, J.A., "Structural Phase Stability in Third-Period Simple Metals," Phys. Rev. (1983), B27, 3235-3251.
11. Chang, K.J. and Cohen, M.L., "Solid-Solid Phase Transistion and Soft Phonon Modes in Highly Condensed Si," Phys. Rev. (1985), B31, 7819-7826.
12. Vohra, Y.K., Brister, K.E., Desgreniers, S., Ruoff, A.L., Chang, K.J. and Cohen, M.L., "Phase Transition Studies of Germanium to 1.25 Mbar," Phys. Rev. Lett. (1986), 56, 1944-1947. Data was later obtained to 160 GPa on the same specimen in October 1986 after it had been held at 125 GPa for several months.
13. Vohra, Y.K., Duclos, S.J., Brister, K.E. and Ruoff, A.L., "The CHESS Wiggler White Beam: A New Dimension in X-ray Diffraction in the Megabar Regime," Materials Science Center Report #6030, Cornell University, Ithaca, New York, 14853, USA June (1987), 1-13. Submitted for publication.
14. Whitlock, J. and Ruoff, A.L., "The Failure Strengths of Perfect Diamond Crystals," Scripta Metallurgica, (1981), 15, 525-529.

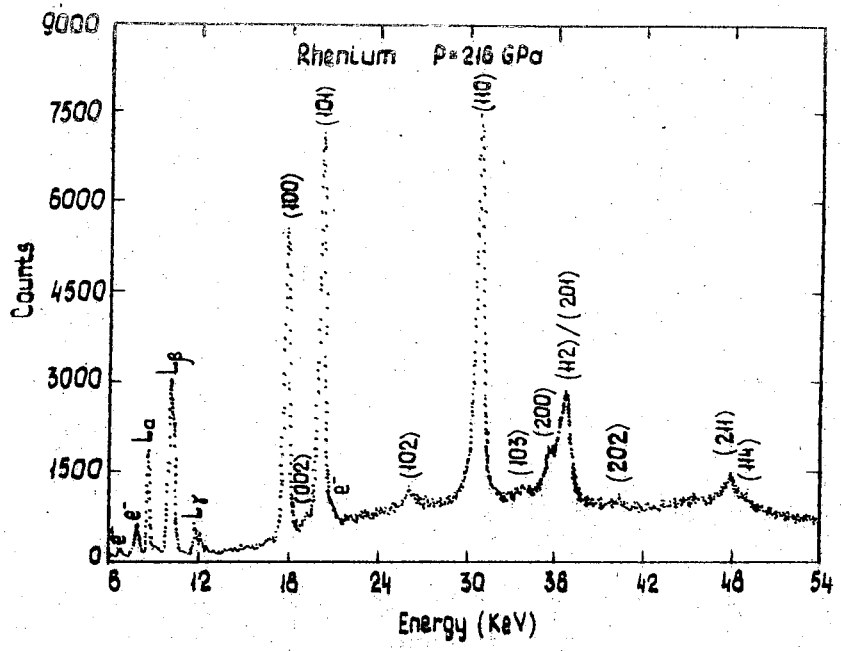

Fig. 1. The energy dispersive x-ray diffraction pattern of rhenium at 216 GPa. (Diffraction angle is 9.311°.) The twelve peaks in the spectrum are indexed according to a hexagonal close packed structure. The diffraction pattern was recorded with a 10 μm pinhole and the data collection time was 90 minutes. The spectrum shown is raw data.

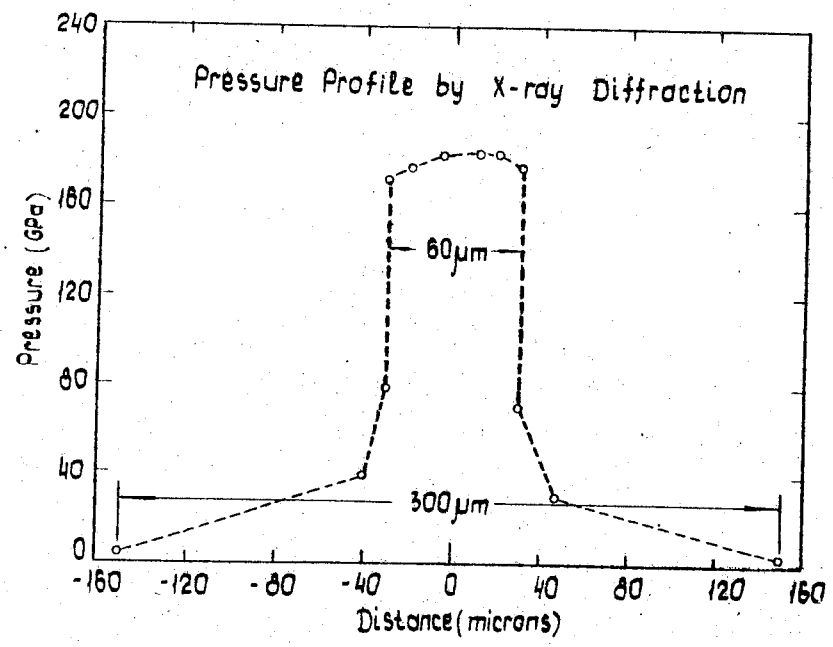

Fig. 2. The pressure profile on the rhenium gasket measured by x-ray diffraction techniques from the measured volume of rhenium at various locations. The distances shown are measured with respect to the center of the diamond or the highest pressure region in the cell. The diamond central flat of 60 μm diameter and the culet of 300 μm are also indicated. The maximum pressure in this profile was 183 GPa.

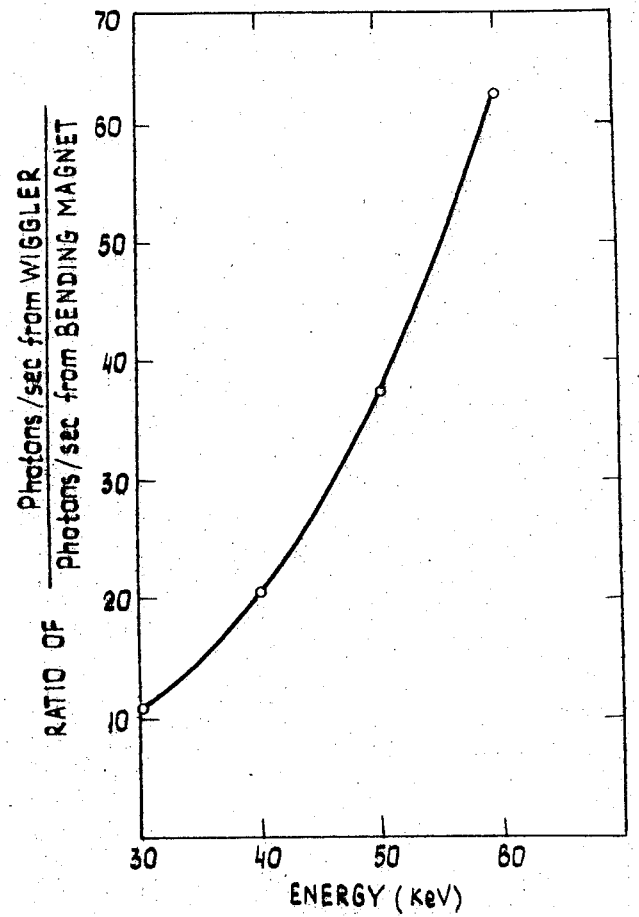

Fig. 3. The ratio of the photons/sec coming from the CHESS wiggler (A3 station) to the photons/sec from the bending magnet (B-station) as a function of the energy of the emitted x-rays.

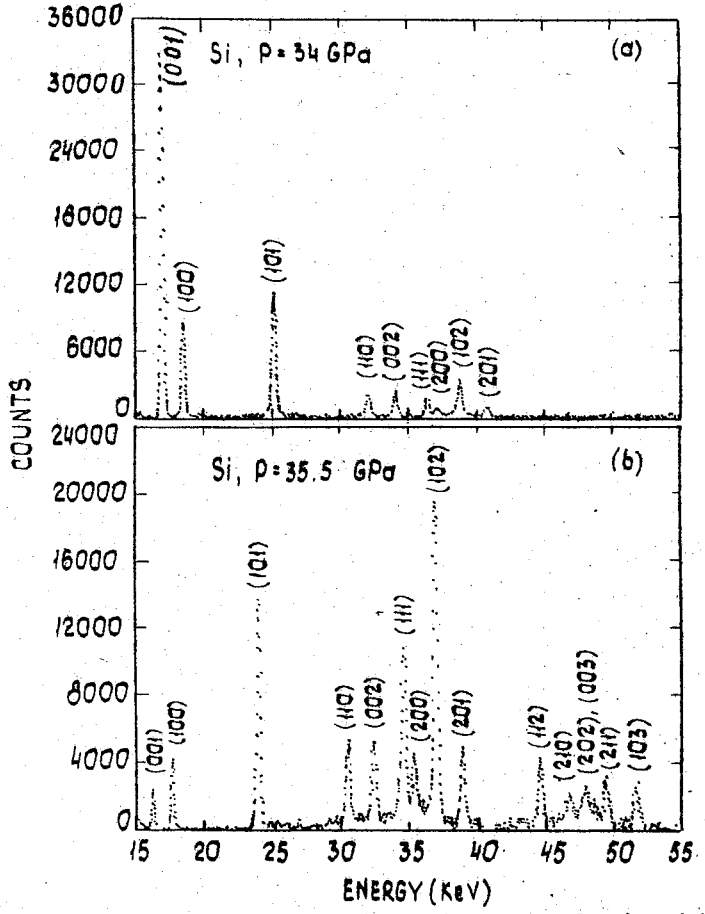

Fig. 4. The energy dispersive x-ray diffraction patterns for the primitive hexagonal phase of Si (a) at 34 GPa recorded at the bending magnet (Ed = 39.628), (b) at 35.5 GPa recorded at the wiggler station (Ed = 37.720). The storage ring energy is 5.3 GeV and the average electron current is 30 mA. The background has been subtracted from these spectra. The relative intensity of the diffraction peaks in the two cases are different because of the difference in the source spectrum and other factors. The wiggler spectrum shows distinct additional peaks in the high energy region.

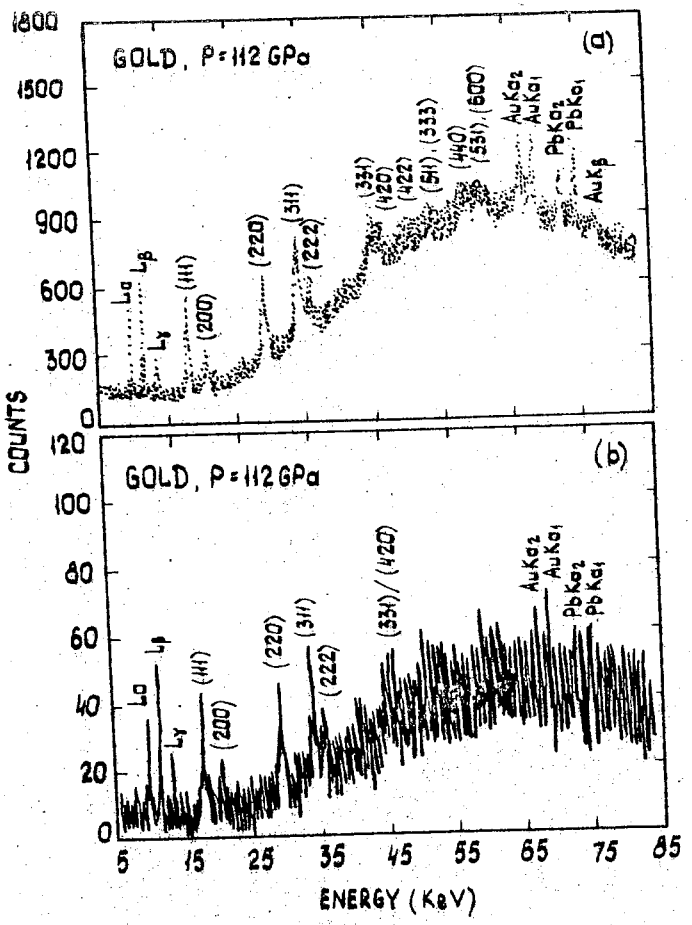

Fig. 5. The energy dispersive x-ray diffraction patterns of gold at 112 GPa taken with the wiggler white beam (a) in 5 minutes and (b) in 13 seconds. The diffraction angle is 9.406° (Ed = 37.932). The spectra shown are raw data without any background subtraction. The storage ring energy is 5.3 GeV and the average electron current is 30 mA.

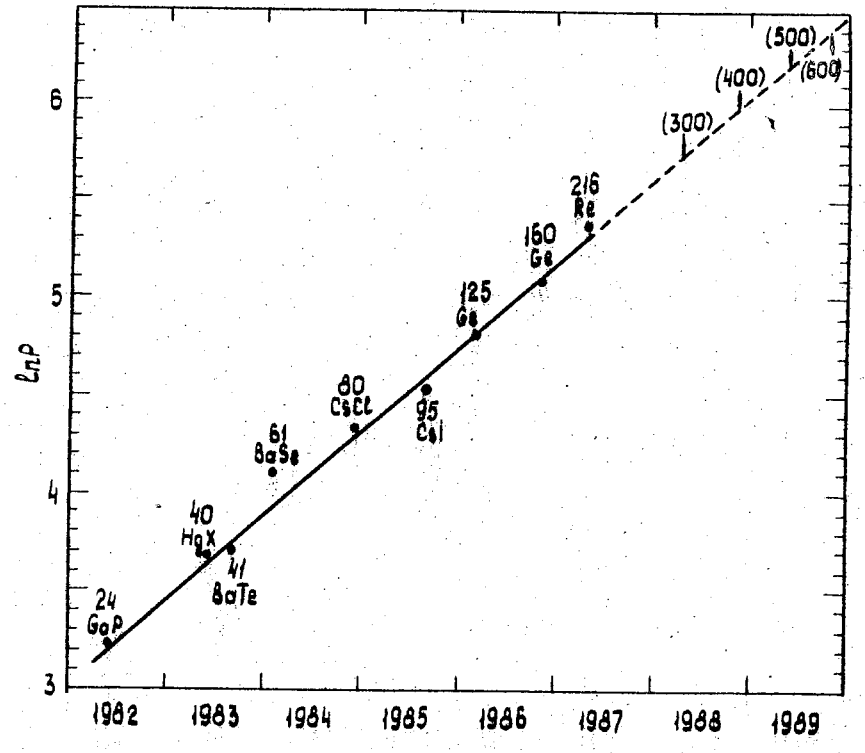

Fig. 6. Logarithm of the maximum pressure versus time at which very good diffraction patterns (5 or more peaks per lattice parameter) were obtained by our group at CHESS and time is the date when papers were submitted. Also shown are the materials and the corresponding pressure in GPa for each date. The quantities in parenthesis are extrapolated goals.

PRESSURE-INDUCED STRUCTURAL TRANSITIONS: A REVIEW OF RECENT PROGRESS

A.ONODERA, Y.FUJII
Department of Material Physics, Faculty of Engineering Science, Osaka University, Toyonaka, Osaka 560, Japan

Recent rapid progress in attaining very high static pressure has made it possible to undertake exploratory studies searching for pressure-induced phase transitions in solids. The transitions observed in simple systems, other than silicates, are in some cases of relevance to geophysical as well as planetary interiors implications. In this paper we review such transitions exemplified by two groups of materials ; NiAs-type compounds and iodine.

The hexagonal NiAs-type structure is formed primarily by chalcogenides or pnictides of transition metals. These compounds exhibit interesting magnetic and electrical properties arising from the incomplete d shells of the component transition metals [1]. It has been argued that the NiAs structure is likely to be formed in the lower mantle by simple oxides [2,3].

We have studied four different NiAs-type compounds with axial ratio, c/a, approximately equal to the ideal value (MnTe with c/a=1.62 and high-pressure phase of MnSe with c/a=1.63), very small (CrSb with c/a=1.32), and very large (TiS with c/a=1.95). Among the compounds studied, each NiAs phase of MnTe, MnSe, and CrSb undergoes structural transition into MnP-type structure at pressures 24, 31, and 17 GPa respectively. This transition is accompanied by a conspicuous decrease in the electrical resistivity in the case of MnTe [4,5] and MnSe. However, no discontinuity is observable in the resistivity of CrSb.

Table 1 summarizes the structural and electrical properties of TiS, MnSe, MnTe, and CrSb at high pressures. As the axial ratio becomes smaller in the NiAs structure, the pressure for the transition to the MnP structure becomes lower.

Figure 1 shows changes of the axial ratio with pressure for the NiAs phases of MnTe, MnSe, and CrSb. The axial ratios in Fig.1 deviate from the ideal value 1.63 as the pressure is increased toward the collapse of the NiAs lattice into the MnP lattice. Not shown in Fig.1 are data for TiS, in which the axial ratio first

increases from the ambient value of 1.95 to 2.02 up to 9 GPa and then decreases to 1.95 up to 22 GPa. No phase transition occurs in TiS below 22 GPa.

Table 1. Sequences of the pressure-induced phase transitions in the NiAs-type compounds

TiS	NiAs-type (c/a=1.95) semiconductive				
MnSe	NaCl-type semiconductive	: 10 GPa :	NiAs-type (c/a=1.63) semiconductive	: 31 GPa :	MnP-type? metallic
MnTe	NiAs-type (c/a=1.62) semiconductive	: 10 GPa :	Unknown semiconductive	: 24 GPa :	MnP-type metallic
CrSb	NiAs-type (c/a=1.32) metallic	: 17 GPa :	MnP-type metallic		

For simulative study of metallic hydrogen possibly existing in the Jupiter, iodine may be the best material because it is diatomic and it can readily be manipulated at room temperature. Optical [5,6], electrical resistance [6-8] as well as x-ray diffraction [9-15] studies have been carried out on this material under static high pressure. Also, Hugoniot has been measured under dynamic compression up to 180 GPa [16],

As given in Table 2, iodine has four phases under static pressure up to 65 GPa [10-15]. The three high-pressure phases are all monatomic. The structure at the highest pressure is face-centered cubic, being neither hexagonal close-packed nor body-centered cubic.

Figure 2 shows interatomic distances of iodine. While in the ambient molecular phase six different interatomic distances are observed, the number of the distances is decreased in the monatomic phase and it finally becomes single in the fcc phase.

Table 2. Sequence of the pressure-induced phase transitions of iodine

Phase	I	II	III	IV
Transition pressure	21 GPa	43 GPa	55 GPa	
Volume change	8.1%	0	1.8%	
Structure	base-centered ortho-rhombic	body-centered ortho-rhombic	body-centered tetragonal	face-cetered cubic
Space group	D_{2h}^{18}-Cmca	D_{2h}^{25}-Immm	D_{4h}^{17}-I4/mmm	O_h^5-Fm3m
Lattice parameter (A)	a=7.136 b=6.686 c=9.784 (0.1 MPa)	a=3.301 b=2.904 c=5.252 (30 GPa)	a=2.934 c=4.733 (49 GPa)	a=4.238 (64 GPa)

Recent experimental results shown above are expected to throw some insights into the interiors of earth and planets. On the other hand, theoretical approaches to the subjects are needed.

References

1. A. Kjekshus and W.B. Pearson, in "Progress in Solid State Chemistry" edited by H. Reiss, volume 1, pp.83-174, Pergamon, Oxford (1964).
2. C-Y. Wang, Phys. Earth Planet. Interiors, 3, 213-217 (1970).
3. A. Navrotsky and P.K. Davies, J. Geophys. Res., 86, 3689-3694, (1981).
4. M. Mimasaka, I. Sakamoto, K. Murata, Y. Fujii, and A. Onodera, J. Phys. C, in press.
5. H. L. Suchan, S. Wiederhorn, and H.G. Drickamer, J. Chem.Phys., 31, 355-357 (1959).
6. B.M. Riggleman and H.G. Drickamer, J. Chem. Phys., 38, 2721--2724 (1963).
7. L.F. Vereshchagin, A.A. Semerchan, N.N. Kuzin, and Yu.A. Sadkov, Sov. Phys. Dokl., 18, 249-250 (1973).
8. N. Sakai and T. Kajiwara, Rev. Sci. Instrum., 53, 499-502 (1982).

9. S.S. Kabalkina, T.N. Kolobyanina, and L.F. Vereshchagin, Sov.Phys.Dokl., 12, 50-54 (1967).
10. O. Shimomura, K. Takemura, Y. Fujii, S. Minomura, M. Mori, Y. Noda, and Y. Yamada, Phys. Rev., B18, 715-719 (1978).
11. K. Takemura, Y. Fujii, S.Minomura, and O. Shimomura, Solid State Commun., 30, 137-139 (1979).
12. K. Takemura, S. Minomura, O. Shimomura, and Y. Fujii, Phys.Rev.Lett., 45, 1881-1884 (1980).
13. K. Takemura, S. Minomura, O. Shimomura, Y. Fujii, and J.D. Axe, Phys. Rev., B26, 998-1004 (1982).
14. Y. Fujii, K. Hase, Y. Ohishi, N. Hamaya, and A. Onodera, Solid State commun., 59, 85-89 (1986).
15. Y.Fujii, K. Hase, N.Hamaya, Y. Ohishi, A. Onodera, O. Shimomura, and K. Takemura, Phys. Rev. Lett., 58, 796-799 (1987).
16. A.K. McMahan, B.L. Hord, and M.Ross, Phys.Rev., B15, 726--736 (1977).

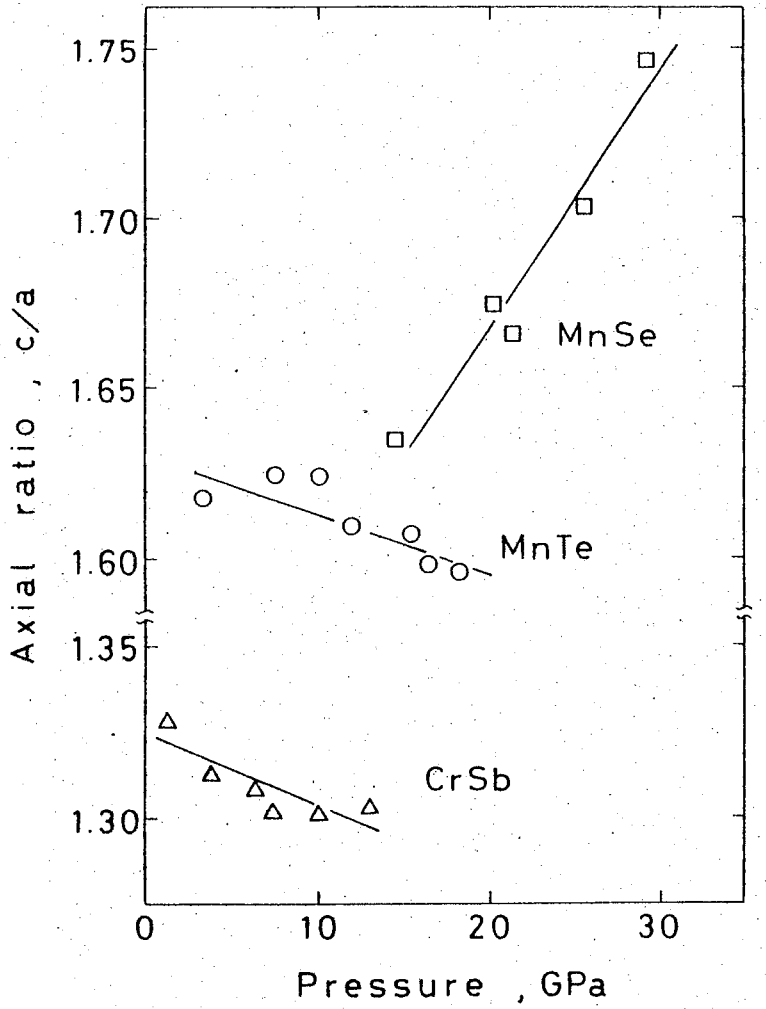

Fig. 1. Change of axial ratios for MnTe, MnSe, and CrSb.

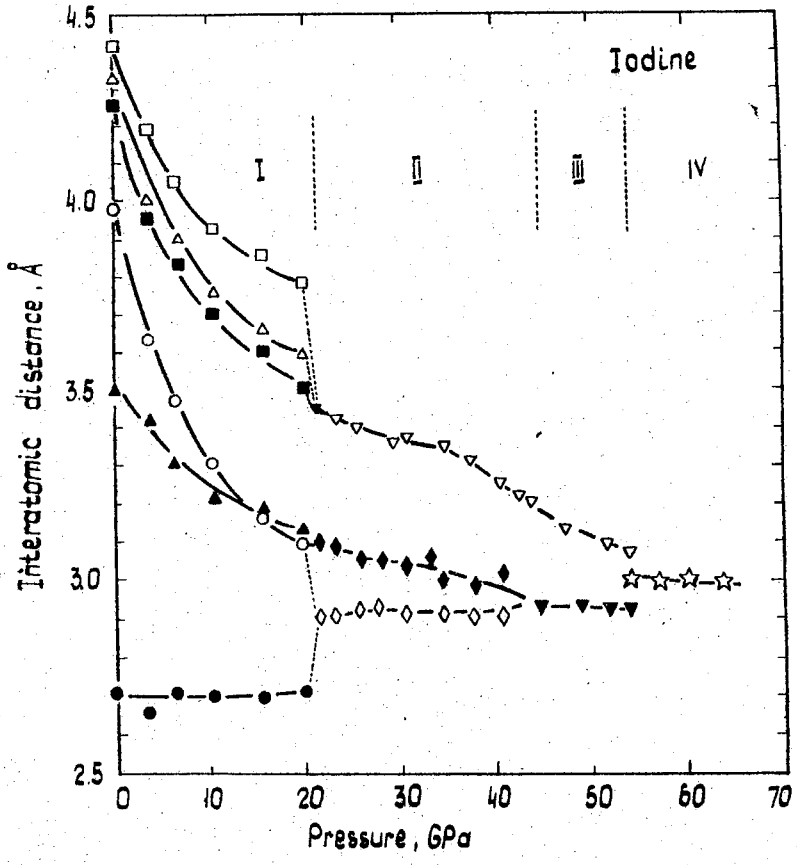

Fig. 2. Change of interatomic distances of iodine.

STRUCTURE AND DYNAMICS OF SIMPLE MOLECULAR SOLIDS UNDER PRESSURE

W. B. Holzapfel
Physics Department, University-GH-Paderborn
Paderborn, F.R. Germany

At first, high pressure data on structure and lattice dynamics are discussed just for the elements which form molecular solids. Whereas H_2, N_2, O_2 and F_2 show very particular behaviour, strong systematics are seen for Cl_2, Br_2 and I_2 under pressure. A comparison with the behaviour of IBr, HBr and HCl under pressure shows further systematics and contributes to a better understanding of H-bonding. The formation of symmetric H-bonds in HBr and DBr as well as in H_2O and D_2O is discussed on the basis of high pressure Raman, I.R. and X-ray data and simple model calculations. A look at some other diatomic molecular solids under pressure reveals that, in general, the transitions from molecular to ionic or covalent structures under pressure can be rather complex.

INTRODUCTION

The progress in high pressure technology in recent years has stimulated very strcngly experimental as well as theoretical studies on structures and dynamics of simple solids in the extended pressure range of up to 100 GPa and above.

First of all, structural phase transitions in simple metallic and covalent solids under pressure were considered as a test ground for various theoretical approaches (1,2,3) to the cal-

culation of structural energy differences, and in fact, not only know transitions pressures were reproduced with remarkable accuracy, but also new phase transitions were predicted for the first time rather precisely (4,5), as shown by later experimental observations (6). In some cases, however, the experimental studies found new and unexpected structures (7,8) and stimulated thereby further theoretical studies.

For molecular solids, on the other hand, the theoretical methods seem to be still less developed. Therefore, more support by experimental studies is still required in these case to establish extended pressure temperature phase diagrams and develop some deeper understandung of the observed phase transitions.

In fact, one can expect to gain a fundamental understanding of even the simpler molecular solids under pressure only if both more theoretical efforts and experimental studies are devoted to this subject where structural studies are just one starting point but more details may be revealed by lattice dynamical investigations.

In the present paper, I want to illustrate, therefore, the interplay of these different studies just on a few examples of simple molecular solids to reveal some of the many open questions in this field. However, before I discuss some of the results, I would like to review very shortly the techniques, which are presently used for these studies.

EXPERIMENTAL TECHNIQUES

The major progress in the experimental studies of molecular solids under pressure has been achieved by the various develop-

ments in diamond anvil high pressure techniques. Besides just visual observations, various techniques of optical spectrometry and X-ray diffraction were further developed for these studies.

In the case of high pressure powder X-ray diffraction, the use of synchrotron radiation with and without additional cryostats for the samples (9) led to significant progress. In high pressure single crystal X-ray diffraction, single crystals of new high pressure phases were grown under high pressure as for instance in the case of oxygen (10,11,12) and some delicate samples like I_2 were handled by the use of liquid nitrogen as pressure transmitting medium (13). A detailed discussion of some of these techniques has been given just recently (9,14). In the optical studies, progress has been made not only with Raman scattering (15) but also more recently with Brillouin scattering (16,17) and FTIR techniques (18).

EXPERIMENTAL RESULTS

In our experimental studies, we looked first of all for families of substances with similar behaviour. From this point of view, the heavier halogens chlorine, bromine and iodine form a family of molecular solids with first of all the same crystal structure at ambient pressure and at sufficiently low temperature, and there are other substances like the interhalogen IBr and some hydrogenhalogens with closely related structures (20). Therefore, I would like to review at first the high pressure results for these substances and than try to compare these results with some earlier data on the high pressure behaviour of ice.

THE HEAVIER HALOGENS

The ambient pressure crystal structure of the heavier halogens chlorine, bromine and iodine is illustrated in figure 1 (21). This structure (D_{2h}^{18}-Cmca) containes four molecules in the orthorhombic unit cell and can be considered as a layer type structure as long as the shortest intermolecular distances within the bc layers, r_2 and r_3, are much smaller than the shortest intermolecular distances between these layers, r_4 and r_5. Various attempts were made, to determine the variation of these distances in iodine under pressure by X-ray measurements using either powder (22,23) or single crystal diffraction techniques (13). The results of these studies are represented in figure 2. A comparison of these different sets of data shows that the earlier powder data (22) fit closely to the more precise single crystal data (13) and the discrepancy between the two sets of powder diffraction data may indicate that it is very difficult indeed to extract atom position parameters from high pressure powder X-ray data.

On the other hand, if one considers this structure in comparison with a cubic close packing of the individual atoms, one can notice that the distortions from a cubic close packing represented by $r_1 \neq r_2 \neq r_3 \neq r_4 \neq r_5 \neq r_6$ is continuously reduced within this structure under pressure up to the phase transition at about 20 GPa for iodine, where its "molecular" character is lost (24,25, 26). Very recent X-ray measurements on iodine in an extended pressure range show indeed (27,28) that the cubic close packing is finally achieved in metallic iodine through two more phase transitions at 45 and 55(2) GPa.

Bromine and chlorine at ambient pressure and low temperature are much further away from this "molecular dissociation" under pressure. However, a comparison with iodine may help to make some predictions about the high pressure behaviour also for these substances.

Since only polycrystalline samples of bromine and iodine were studied up to now by high pressure X-ray diffraction (29,30,31), it seems appropriate to apply some scaling rules in a comparison of these data with the more detailed data for iodine. The natural scale to be used thereby seems to be the bond length in the free molecules r_o. From the literature (21,32), we take r_o = 198,8(1) pm for chlorine, r_o = 228,1(1) pm for bromine and r_o = 266,6(1) pm for iodine to scale all the interatomic distances r_i presented in figure 2 for iodine together with the ambient pressure data for bromine and chlorine (21) from powder X-ray measurements. Finally, we plot the scaled interatomic distances $\bar{r}_i = r_i / r_o$ with respect to scaled atomic volumina $\bar{V} = V/r_o^3$ just in one common diagram as shown in figure 3, and we can notice that this scaling places the ambient pressure data for bromine and chlorine just on a smooth curve with the corresponding ambient and high pressure data of iodine. Encouraged by this observation, scaled lattice parameters $\bar{a} = a/r_o$, $\bar{b} = b/r_o$ and $\bar{c} = c/r_o$ are also included in this diagram as derived from the literature data for iodine (23) and from the data given in DÜsing's thesis (29) together with more recent data (31) for bromine and chlorine. Finally, the parameter $\bar{d}_2 = \sqrt{\bar{b}^2 + (\bar{c}/2)^2}/2$ is also included in figure 3 as a lower bound for $\bar{r}_2$. As one can see, the perfect scaling of all these structural parameters may give some strong support to the assumption that also the not directly determined variations of the interatomic distances $\bar{r}_i$ for bromine and chlorine under pressure may follow closely this same scaling.

Stimulated by the success of these scaling laws for the structural parameters, a similar scaling was also tested for the lattice dynamical data (19,33,34,35), however, there, the scaling showed only qualitative similarities but was not quantitatively perfect.

Therefore, it will be interesting to see in lattice dynamical models, which of the paramters may still be scaled and which do not follow a simple scaling.

In fact, an earlier preliminary lattice dynamical calculation showed variations of the effective bond charges (q_1,q_2,q_3) place on the bonds r_1, r_2, r_3 (36,37) which are reproduced here in one common diagram, figure 4, by the use of the scaled volumina $\bar{V}$ for the different elements. Appearently, this scaling works, however, the additional special "bond coupling parameter" which had been introduced before (38) to account for the special softness of the Ag stretching mode with respect to the B_{3g} stretching mode does not follow this scaling and a basic understanding of the physics behind this parameter is indeed still missing (39).

INTERHALOGENS

From point of view of structural systematics, also a close similarity was revealed for IBr with respect to I_2 and Br_2 under pressure (40). However, lattice dynamical studies (41) on IBr at intermediate pressures (0-15 GPa) as well as on ICl in a similar pressure range showed a rather complex behaviour and indicated, that also the structures have not yet been resolved in detail in this pressure range.

On the other hand, there are good reasons to assume that the structure of the high pressure phase of IBr (P > 1(GPa) is

closely related to the high pressure phase of HBr, and, therefore, a better understanding of IBr may also contribute to the understanding of the hydrogen bonds in HBr, HCl and similar substances under pressure.

HYDROGENHALIDES

HCl and HBr crystallize both at low temperatures and ambient pressure in the orthorhombic structure C_{2V}^{12} with proton ordering (42,43). This structure is isomorphic to the structure of IBr at low pressures and low temperatures and is also closely related to the normal structure of the heavier halogens. As show in figure 5, the usual assignment of the axis a, b and c differs from the usual assignment in the case of the halogens. For HCl and HBr, the differences in the values of a, b and c are small (42,43,44) and the hydrogen bonds seem to be nonlinear at ambient pressure (44).

As indicated in figure 5, this structure can be related also to a cubic close packing of the halogens which is slightly distorted by zig-zag chains of hydrogen bonds.

Raman studies on both HCl and HBr at low temperatures (100 K) and pressures up to 40 GPa (45) gave strong evidence for a first order phase transition in HBr at about 32 GPa and for no new phase in HCl up to 42 GPa. Preliminary powder X-ray measurements on HBr at 160 K and pressures up to 30 GPa confirm the orthorhombic structure for this phase III with $a \approx b < c$ and show that the unit cell volume is reduced at 160 K with respect to the volume at ambient pressure (phase I) by 50 % at 30 GPa (figure 6). With

these data (44), the results of the high pressure Raman study can be plotted also with respect to volume as shown in figure 7 (44). Two remarkable features can be seen in this diagram. First, a steep initial decrease in both the molecular stretching frequencies, which may be related to a straightening of the hydrogen bonds at low pressure, and second, the very strong decrease in the stretching frequencies just before the phase transition to phase IV, typical for the formation of symmetric hydrogen bonds (46,47). Detailed lattice dynamical calculations for these hydrogen halides under pressure are performed at the present time (48) and are supposed to result in new quantitative models for the hydrogen bonding.

ICES

For ices, the formation of symmetric hydrogen bonds had been predicted already long ago (49) and first experimental evidences for this effect were seen in Raman measurements on ice at low temperatures and high pressures (46,47) and have been discussed as indications for a first order phase transition between the phase ice VIII with nonsymmetric ordered hydrogen bonds and the new phase ice X with symmetric ordered hydrogen bonds corresponding to the cuprit structure (46). Additional evidence for the formation of symmetric hydrogen bonds in ices was found also in Brillouin measurements on ices VII at room temperature and pressures up to 67 GPa (17). In this case, the transition seems to be of second order. Both these studies just have touched an other range in the phase diagram of ice and have in fact already stimulated various theoretical considerations on the details of the phase diagram of ice in this extended pressure range (50,51).

CONCLUSIONS

The diamond anvil technique has opened up for experimental studies a wide new range in high pressure physics where interesting phenomena can be studied not only on metals and semiconductors but also on molecular solids with a rich variety of phase transitions and anomalous variations in the lattice dynamics.

ACKNOWLEDGEMENTS

This work was supported in parts by the Deutsche Forschungsgemeinschaft and in other parts by the Bundesministerium für Forschung und Technologie. Part of the work was performed with Synchrotron radiation in HASYLAB at DESY, Hamburg, F.R.G.

References

1. HAFNER, J., 1974, Phys. Rev. B 10, 4151.

2. YIN, M. T., and COHEN, M.L., 1982, Phys. Rev. B26, 5568.

3. SKRIVER, H.L., 1985, Phys. Rev. B 31, 1909.

4. MORIARTY, A., and McMAHAN, A.K., 1982, Phys. Rev. Lett. 48, 809.

5. McMAHAN, A.K., and MORIARTY, J.A., 1983, Phys. Rev. B 27, 3235.

6. OLIJNYK, H., and HOLZAPFEL, W.B., 1985, Phys. Rev. B 31, 4682.

7. OLIJNYK, H., and HOLZAPFEL, W.B., 1984, Phys. Lett. 103A, 137.

8. HU, J.Z., and SPAIN, I.L. 1984, Sol. St. Comm. 51, 263.

9. GROSSHANS, W.A., DÜSING, E.-F., and HOLZAPFEL, W.B., 1984, High Temp. High Press. 16, 489.

10. D'AMOUR, H., HOLZAPFEL, W.B., and NICOL, M., 1981, J. Phys. Chem. 85, 130.

11. SCHIFERL, D., CROMER, D.T., and MILLS, R.L., 1981, Acta Cryst. B 37, 1329.

12. SCHIFERL, D., CROMER, D.T., SCHWALBE, L.A., and MILLS, R.L., 1983 Acta Cryst. B 39, 153.

13. D'AMOUR-STURM, H., and HOLZAPFEL, W.B., 1986, Physica 139 + 140 B 328.

14. HOLZAPFEL, W.B., 1984, Rev. Phys. Appl. 19, 705.

15. HIRSCH, K.R., and HOLZAPFEL, W.B., 1981, Rev. Sci. Instrum. 52, 5

16. POLIAN, A., and GRIMSDITCH, M., 1983, Phys. Rev. B 27, 6409.

17. POLIAN, A., and GRIMSDITCH, M., 1984, Phys. Rev. Letters 52, 1311

18. HOLZAPFEL, W.B., SEILER, B., and NICOL, M. 1984, J. of Geophys. Res., 89, Suppl. B707.

19. JOHANNSEN, P.G., WEFRINGHAUS, C., and HOLZAPFEL W.B., 1987, J. Phys. C: Solid State Phys. 20, L151.

20. HOLZAPFEL, W.B., JOHANNSEN, P.G., and GROSSHANS, W.A., 1987, J. Lascombe (ed.) "Dynamics of molecular crystals" 1987, Elsevier Science Publ. Amsterdam.

21. DONOHUE, J., 1974, The Structures of the Elements, John Wiley, New York, p. 396.

22. SHIMOMURA, O., TAKEMURA, K., FUJII, Y., MINOMURA, S., MORI, M NODA, Y., and YAMADA, Y., 1978, Phys. Rev. B18, 715.

23. TAKEMURA, K., MINOMURA, S., SHIMOMURA, O., FUJII, Y., and AXE, J 1982, Phys. Rev. B26, 998.

24. TAKEMURA, K., FUJII, Y., MINOMURA, S., and SHIMOMURA, O., 1979, Solid State Commun. 30, 137.

25. TAKEMURA, K. MINOMURA, S., SHIMOMURA, O., and FUJII, Y., 1980, Phys. Rev. Lett. 45, 1881.

26. TAKEMURA, K., MINOMURA, S., SHIMOMURA, O., FUJII, Y., and AXE, J.D., 1982, Phys. Rev. B 26, 998.

27. FUJII, Y., HASE, K., OHISHI, Y., HAMAYA, N., and ONDERA, A., 1986, Solid State Commun. 59, 85.

28. FUJII, Y., HASE, K. HAMAYA, N., OHISHI, Y., and ONODERA, A., 1987, Phys. Rev. Lett. 58, 796.

29. DÜSING, E.-F., 1984, Diplomarbeit, Paderborn.

30. DÜSING, E.F., GROSSHANS, W.A., and HOLZAPFEL, W.B., 1984, Journal de Physique C8, 203.

31. GROSSHANS, W.A. (private communication).

32. DOWNS, A.J., ADAMS, C.J., 1975, in "Comprehensive Inorganic Chemistry" Vol. 2, ed. J.C. Bailar et al., Pergamon Press, Oxford, 1173.

33. SHIMOMURA, O., TAKEMURA, K., AOKI, K. in C.-M. Backman, T. Johanisson and L. Tegnêner (Eds.), Proc. 8th AIRAPT and 19th EHPRG Conf.: High Pressure in Research and Industry, Arkitektkopia, Uppsala, 1982, 272.

34. JOHANNSEN, P.G., and HOLZAPFEL, W.B., 1983, J. Phys. C16, 1961.

35. JOHANNSEN, P.G., and HOLZAPFEL, W.B., 1983, J. Phys. C16, L1177.

36. JOHANNSEN, P.G., and HOLZAPFEL, W.B., 1984, Journal de Physique C8, 191.

37. JOHANNSEN, P.G., DÜSING, E.F., and HOLZAPFEL, W.B., 1985, in S. Minomura (Ed.), Sol. State Phys. under Pressure: Recent Advances with Anvil Devices, KTK, Tokyo, 105.

38. KOBASHI, K., and ETTERS, D., 1983, J. Chem. Phys. 79, 3018.

39. JOHANNSEN, P.G., 1984, Dissertation, Paderborn.

40. FUJII, Y., OHISHI, Y., ONODERA, A., TAKEMURA, K., and REICHLIN 1985, Jap. J. Appl. Phys. 24, Suppl. 24-2, 606.

41. WAKOB, W., JOHANNSEN, P.G., and HOLZAPFEL, W.B., 1986, Physica 140 B, 523.

42. SIMON, V.A., 1971, J. Appl. Crystallogr. 4, 138.

43. ANDERSON, A., TORRIE, B.H., and TSE, W.S., 1981, J. of Raman Spectr. 10, 149.

44. HELLE, W., JOHANNSEN, P.G., DÜSING, E.F., GROSSHANS, W., and HOLZAPFEL, W.B., 1985, Europhys. Conf. Abstr. 9A, PFR-01-007.

45. JOHANNSEN, P.G., HELLE, W., and HOLZAPFEL, W.B., 1984, Journa de Physique C8, 199.

46. HIRSCH, K.R., and HOLZAPFEL, W.B., 1984, Phys. Lett. A101, 27

47. HIRSCH, K.R., and HOLZAPFEL, W.B., 1986, J. Chem. Phys. 84, 2

48. JOHANNSEN, P.G. (private communication).

49. HOLZAPFEL, W.B., 1976, J. Chem. Phys. 56, 712.

50. STILLINGER, F.H., and SCHWEIZER, K.S., 1983, J. Phys. Chem. 8

51. SCHWEIZER, K.S., and STILLINGER, F.H., 1984, J. Chem. Phys. 8

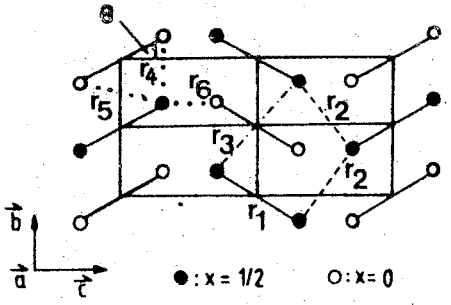

Fig. 1. Structure of solid chlorine, bromine and iodine (2).

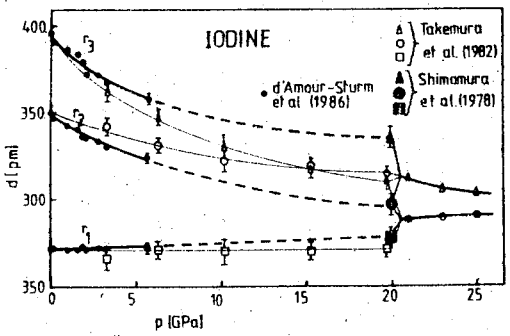

Fig. 2. Effect of pressure on interatomic distances for iodine (for references see text).

Fig. 3. Scaling rules for lattice parameters $\bar{a}$, $\bar{b}$, $\bar{c}$ and interatomic distances $\bar{r}_i$ of the heavier halogens (for references see text).

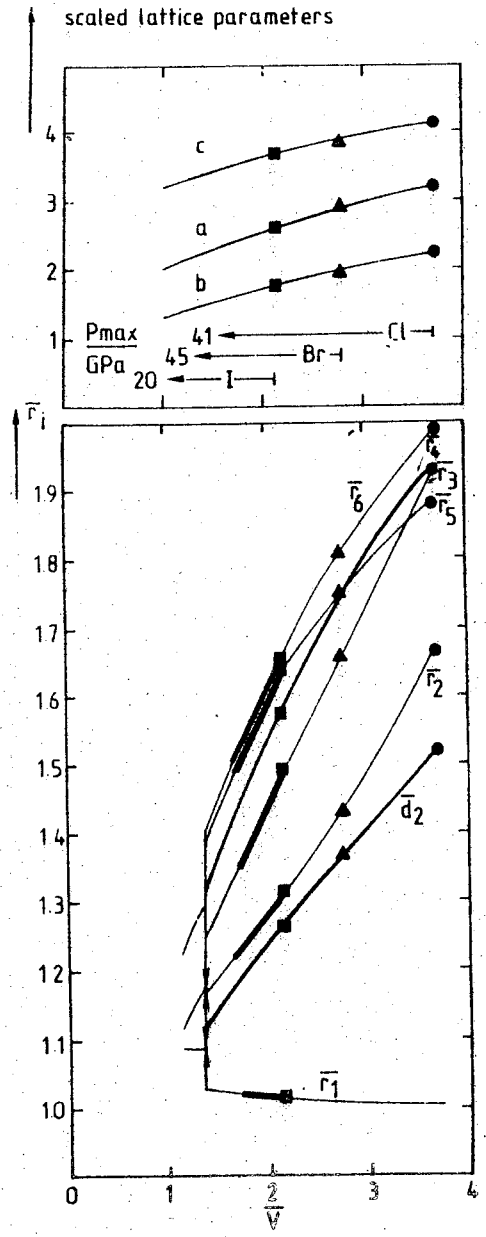

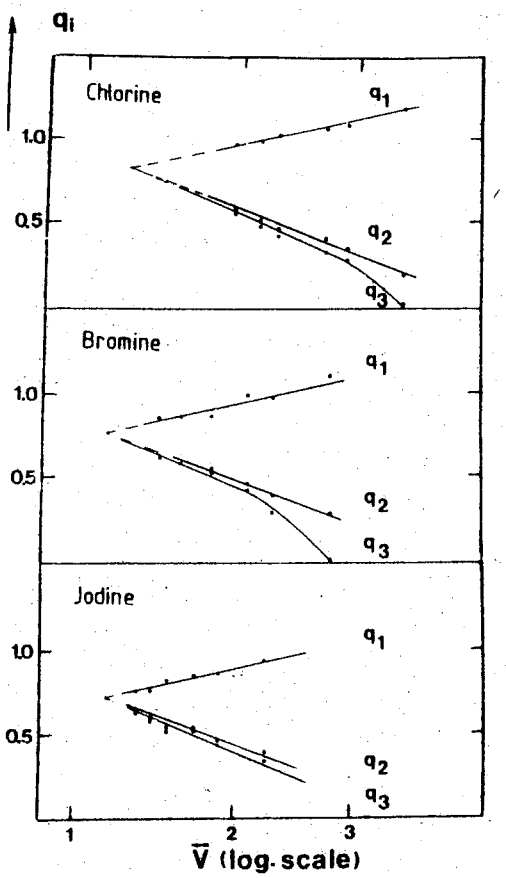

Fig. 4. Scaling rules for the bond charges of the heavier halogens (for references see text).

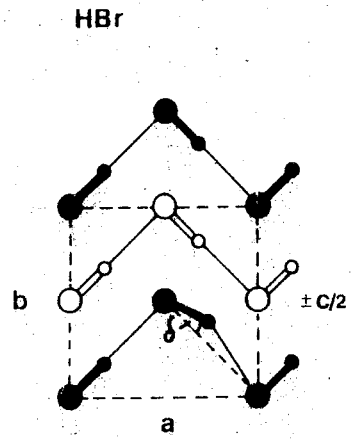

Fig. 5. Structure of solid HCl and HBr at low temperatures (42,44).

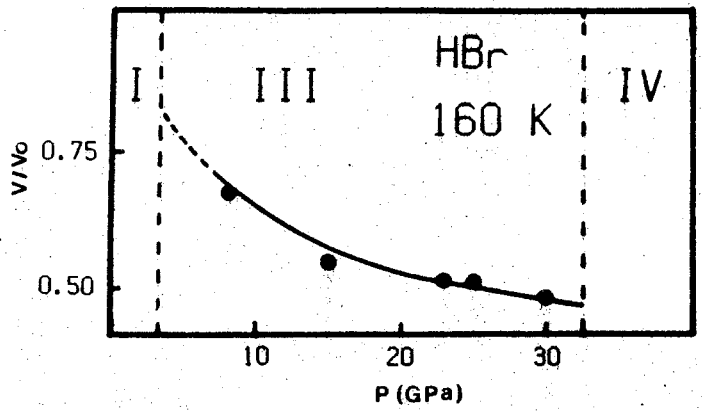

Fig. 6. Volume reduction of HBr at 160 K under pressure (44).

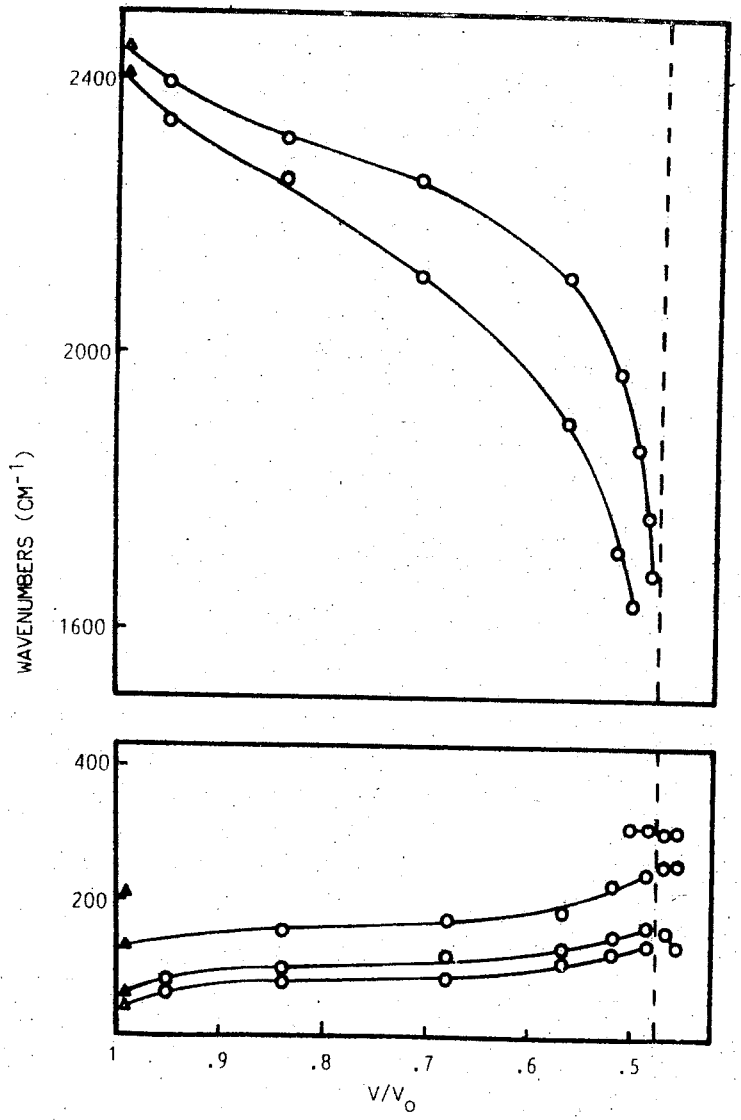

Fig. 7. Volume dependence of the Raman frequencies for HBr at 100 K (44).

X-RAY STUDIES OF THE SEMICONDUCTORS SnAs, InTe, TlS AND TlSe UP TO 43 GPa

G.B.Demishev, S.S.Kabalkina, T.N.Kolobyanina, T.I.Dyuzheva, V.G.Losev
Institute of High Pressure Physics of the USSR Academy of Sciences, Troitsk, Moscow region, USSR

The structures of the semiconductors SnAs, InTe, TlS and TlSe have been investigated using high-pressure (HP) diffraction technique - a gasketed diamond anvil cell (DAC) [1]. The pressure was measured by ruby fluorescence technique.

The first order reversible transition from NaCl to CsCl structure was found in SnAs with volume discontinuity 5%; the two phase area extends from 32 to 43 GPa. The volume change V/V_0 (P) of the SnAs is shown in Fig.1. In agreement with gomology rule [3], the same pressure effect has been found in Sn_xSb_{1-x} at P=9 GPa [2].

Two first order phase transitions were observed in InTe in a "hydrostatic" environment (ethanol-methanol mixture 1:4): type TlSe (InTe I) ⟶ type NaCl (InTe II) ⟶ distorted type CsCl (InTe III). The transition semiconductor-metal I ⟶ II is irreversible [4]; the volume discontinuity is 8% at P=0, it falls to zero as the pressure reaches 9 GPa; two phase area is 3.7-16 GPa. InTe II appeared at 3 GPa when the sample was in a nonhydrostatic environment.

Distorted CsCl type (InTe III) appeared at 17 GPa; the diffraction pattern corresponds to the superlattice of the simple tetragonal (ST) structure with c/a=0.97, that can be indexed on the basis of the orthorombic unit cell a=6.71 Å; b=6.95 Å; c=3.07 Å; Z=4, (P=36.9 GPa) on the contrary to the structure CsCl determined in [5].

The three first order transitions were found in TlS: type TlSe (TlS I)⟶ type α-$NaFeO_2$ (TlS II)⟶ distorted type α-$NaFeO_2$ (TlS III) ⟶ type CsCl (TlS IV). TlS II exists at 7-11 GPa and transforms to TlS III at P=11 GPa; phase I is retained up to 30 GPa. TlS II is metastable under ambient conditions. The lattice parameters are: TlS II - a=3.938 Å; c=21.74 Å; c/a=5.52; Z=6; $R\bar{3}m$ (P=0); TlS IV - a=3.202 A; (P=35.5 GPa). Band gap value for TlS II was estimated by the optical absorption spectroscopy $E_g=1.0\pm0.1$ eV at P=0.

The first order reversible transition to distorted CsCl type-ST was observed in TlSe at 19 GPa. Volume discontinuity is 2%. Volume change V/V_o with pressure for InTe, TlS and TlSe are shown in Figs.2-4. The volume data were fitted to Murnagan-Birch equation. The bulk modulus B_o and its pressure derivatives B'_o (P=0) are given in Table.

Bulk modulus B_o and its pressure derivatives B'_o of the phases of InTe, TlS and TlSe at P=0

Compound	Structure type	B_o,GPa	B'_o	P_k,GPa	r_k, Å
InTe I	TlSe	12	13	3.7	3.47
InTe II	NaCl	40	5.6		
TlS I	TlSe	29	6.7	6.0	3.30
TlS II	α-$NaFeO_2$	47.5	4.5		
TlSe I	TlSe	26.8	4.7	21.0	3.28

Instability of the type TlSe is related to the electrostatic repulsion of ions In^{+1} in InTe and Tl^{+1} in TlS and TlSe spaced along $\bar{c}$ [6]. The experimental results show that semiconductors of the TlSe type transform at pressure P_k, which corresponds to $r_k=c/2$ (Table). Phase of TlSe type retained up to 16 GPa in InTe and up to 25 GPa in TlS, when appeared the phase of CsCl type (TlS) or distorted CsCl type (InTe, TlSe) - the more dense phases of these compounds.

References

1. T.N.Kolobyanina, G.B.Demishev, T.I.Dyuzheva, V.G.Losev, S.S. Kabalkina. "Almaznaya kamera davleniya do 28 GPa dlya rentgenostrukturnyh issledovaniy", Prib.Tekh.Eksp., 1984,N.2,194-197
2. V.G.Losev, S.S.Kabalkina. "Rentgenograficheskoe issledovanie fazovyh prevrascheniy v sisteme olovo-surma pri davleniyah do 19 GPa", Fiz.Tverd.Tela, 1986, 28, 646-648
3. L.F.Vereschagin, S.S.Kabalkina."Rentgenostrukturnye issledovanya pri vysokom davlenii", Moskva,Nauka, 1979,174s.
4. L.Merrill,"Behavior of the AB-type compounds at high pressure and high temperatures",J.Phys.Chem. Ref.Data,1977,6,p.1248-1249
5. T.Chattopadhyay,R.P.Santandrea,H.G.von Schnering, "New high pressure phase of InTe",J.Phys.Chem.Solids,1985,46,p.351-356
6. Von D.Müller, H.Hahn. "Zur Struktur des $TlGaSe_2$", Z.anorg. allg.Chem., 1978, 438, S.258-272

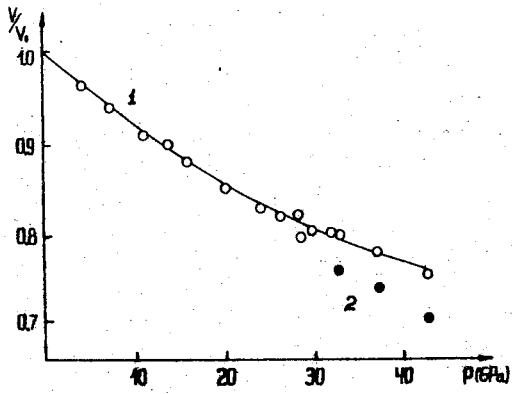

Fig.1. V/V_o versus pressure for SnAs: 1-type NaCl; 2-type CsCl.

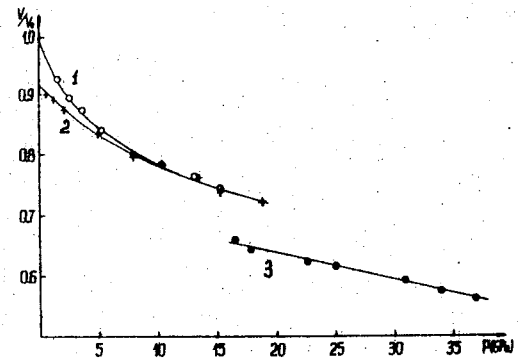

Fig.2.V/V_o versus pressure for InTe: 1-type TlSe; 2-type NaCl; 3-distorted type CsCl.

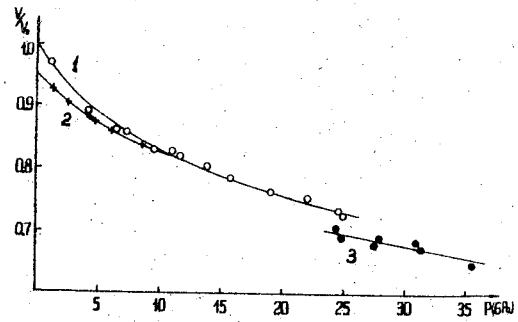

Fig.3. V/V_0 versus pressure for TlS:
1-type TlSe; 2-type α-$NaFeO_2$; 3-type CsCl.

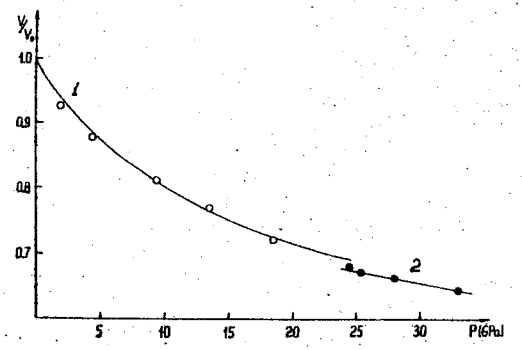

Fig.4. V/V_0 versus pressure for TlSe:
1-type TlSe; 2-type CsCl.

PHASE EQUILIBRIUM DIAGRAMS AND FORMATION OF DIAMONDS

Yu.A.Kocherzhinsky
Institute for Superhard Materials, Academy of Sciences
of the UkrSSR, Kiev, USSR

Artificial diamonds production started from phase equilibrium diagrams. R.J.Wedlake [1] indicates "... it was not until the work ([2] Yu.K.) of Leipunskii (1939) ... that people had any reasonable idea of the pressures required" (for diamond formation, Yu.K.). Later on diamond-graphite (D⇌G) diagram has been repeatedly refined [3-5].

In this work [2] O.I.Leipunskii has shown all the conceivable (permitted by the laws of nature) methods of diamond formation from graphite:

1. Direct G→D transformation in the P-T region of diamond thermodynamic stability under conditions far from D⇌G equilibrium.

2. Recrystallization through the liquid or gaseous phase in the region of diamond stability near D⇌G equilibrium.

3. Epitaxial growing of carbon on the diamond crystals surfaces in the region of graphite thermodynamic stability.

Recrystallization through the metal melt is the main industrial method of diamond production. The melting diagrams for carbon-metals systems proved to be the necessary tools in mastering the technological conditions of diamond production. The P-T region of diamond formation start in the presence of the given metal is found to be specified by the intersection (in P-T coordinates) of D⇌G equilibrium line with the line of carbon-containing eutectic in the given system (Fig.1). The diagram specifies not only the minimum P and T for possible formation of diamond from the given solvent, but also the temperature region (ΔT) in which diamond formation is possible (with the given solvent and pressure), the composition of the alloy in the given system (when the solvent comprises more than one metal) which provides minimum T and P for the start of diamond formation and maximum temperature region for diamond growth, the behaviour of carbon concentrations change in the melt at graphite and diamond boundaries with P and T, i.e. the concentration difference causing carbon diffusion through the melt from graphite to diamond (or vice versa). The diagrams of phase equilibrium at high pressures have

been constructed for a number of metals-carbon systems, binary (with Ni, Co, Fe, Mn, Ta) and ternary (C-Ni-Mn, C-Ni-Fe, C-Fe-Al, C-Fe-Si), these diagrams are shortly reviewed in the reference book [6].

There are statements, however, about "catalytic" effect of hard (crystalline) metals on diamond formation [7,8]. Actual experimental basis for such suppositions is the fact of diamond formation (e.g.[9,10]) in the presence of some carbide-forming metals (Cr, Nb, Ta, Fig.2) at temperatures lower than equilibrium solidus temperature for carbon phase (note that in this case carbides, metal-solvent and nontransformed graphite are always present together with diamond). For instance, in Ta-C system [9,10] TaC+D⇌liq. eutectic appears higher than 10 GPa, 3525K, but diamond is formed at 6.5 GPa, 2070K, i.e. by 1455K lower, this occurs only in the case when primarily graphite was in contact with tantalum metal and in the presence of TaC "insignificant quantity of diamonds identifiable only by X-ray diffraction has been obtained" ([9] p.37).

New interpretation of this fact is suggested in the work [11]. A metastable eutectic melt (eutectic of the starting phases) is primarily formed during the contact melting of materials capable to form intermediate compounds. If when increasing the content of the second component the liquidus line is sharply descended from both sides of the diagram, then the point of metastable eutectic is significantly lower than stable solidus. The presence of (metastable) liquid melt being in contact with graphite promotes diamond formation and growth on graphite surface.

Fig.3 shows the schematic diagram of Me-C system with an intermediate Me_xC compound. Extrapolation of liquidus lines (being the limits of components solubility in the melt) will give their intersection in the E_m point (metastable eutectic). At the temperature intermediate between E_m and E_1 (stable eutectic) the thermodynamic potential of the system in the state of the starting components mixture is maximum, while its stability is minimum. After formation of Me_xC compound the system has its minimum energy i.e. it is stable. The third state with an intermediate energy is, however, possible, the melt. When the starting components mixture is heated to the given temperature range (between E_m and E_1) the transformation to both states with the lower energy are energetically beneficial for the system and the part of the material transformed to each of them will be specified by the velocity ratio for the corresponding processes. The velocity of carbide formation on the contact surfaces of the starting phases is specified by carbon diffusion through the crystalline carbide, and the velocity of liquid eutectic melt formation is specified by carbon diffusion through the melt; diffusion velocity in liquid is higher than that in crystal and so in the first moment the melt formation is kinetically more beneficial. This melt metastability results in the process of immediate crystallization with formation of all phases stable under given P-T conditions including diamond in the case of contact melting under pressure ensuring diamond thermodynamic stability.

The possibility of metastable melting has been experimentally proved on chromium-carbon mixtures.

The four metastable eutectics can be constructed (in the order of melting temperatures increase) by extrapolation of liquidus lines for Cr-C stable diagram: Cr-C, Cr-Cr_3C_2, Cr-Cr_7C_3, Cr_7C_3-C. The first three melt lower than Cr-$Cr_{23}C_6$ equilibrium eutectic, the last one melts higher than $Cr_{23}C_6$ and lower than Cr_7C_3-Cr_3C_2 eutectic.

The tablets, 0.7 g each, compacted from powder mixture of chromium and graphite (14 to 42 atomic percent of the latter) have been investigated by differential thermal analysis while heated in argon at atmospheric pressure with the rate of 60 to 120K/min. One or more first heatings of mixtures with carbon content higher than 21 atomic percent surely reveal endothermic effects lower than the equilibrium solidus temperature for the given composition, and in many cases at the lower temperatures as compared with the most low-melting eutectic for the stable diagram (Cr-$Cr_{23}C_6$). Both phases included to the starting mixture are monomorphic at atmospheric pressure and so nothing but melting can induce the endoeffects. Fig.4 shows the DTA-curves for three heatings of mixture comprising 34 atomic percent of C, the rate of heating being 60K/min. The first one exhibits the following effects: that of Cr+$Cr_{23}C_6$ eutectic melting at 1810K (very slight) and that of incongruent melting for $Cr_{23}C_6$ at 1830K (very strong) and Cr_7C_3+Cr_3C_2 eutectic at 2020K. Besides, additional effects are observed at 1680K and 1725K unrelated to stable diagram. The further two curves exhibit no other effects but those usual for the given composition according to diagram, i.e. 2010K solidus and 2130K liquidus.

Metastable melting diagram constructed from experimental data for chromium-carbon system is presented in Fig.5.

The allowance for contact melting of metastable eutectics makes it possible to interpret the formation of diamonds in the presence of metals from common positions: in any case metal is a solvent and acceleration of diamond formation (a "catalytic" effect) is associated with recrystallization through the liquid phase.

References

1. Wedlake R.J. Technology of diamond growth //The properties of diamond/Ed.J.E.Field.-London-New York-San Francisco:Acad.Press, 1979.-P.501-535.
2. Лейпунский О.И. Об искусственных алмазах // Успехи химии. - 1939. - Т.8, вып.10.-С.1519-1534.
3. Berman R., Simon F. On the graphite-diamond equilibrium//Z. Elektrochem.-1955.-Vol.59,N.5.-P.333-338.
4. Diamond-graphite equilibrium line from growth and crystallization of diamond //F.P.Bundy,H.P.Bovenkerk,H.M.Strong,R.H.Wentorf//J.Chem.Phys.-1961.-Vol.35,N.2.-P.383-391.
5. Андреев В.Д., Малик В.Р.,Ефимович Л.П. Термодинамический расчет кривой равновесия графит-алмаз //Сверхтвердые материалы.-1984.-№2.-С.16-20.
6. Физические свойства алмаза: Справочник /Н.В.Новиков, Ю.А.Кочержинский,Л.А.Шульман и др.-Киев.Наук.думка, 1987.-С.8-24.
7. Фарафонтов В.И., Калашников Я.А. Механизм каталитического превращения графита в алмаз //Ж.физ.химии. - 1976.-Т.50,№4. - С.830-838.
8. Современные представления о каталитическом превращении углеродсодержащих веществ в алмаз//Н.Н.Шипков,Я.А.Калашников, В.П.Шевяков и др.//Цветные металлы.-1980.-№10.-С.68-71.
9. Каменецкая Д.С., Штеренберг Л.Е. T-P-N_c диаграмма состояния системы тантал-углерод//Диаграммы состояния тугоплавких систем.-Киев: ИПМ АН УССР, 1980.-С.32-38.
10. Каменецкая Д.С., Штеренберг Л.Е. Термодинамический расчет фазовых равновесий в области TaC-C при давлении до 10 ГПа // Сверхтвердые материалы -1982.-№3.-С.7-11.
11. Даниленко В.М., Кочержинский Ю.А., Кулик О.Г. Метастабильная диаграмма плавкости системы хром-углерод //Докл.АН СССР. - 1986.-Т.287, №4.-С.895-899.
12. Strong H.M.,Hanneman R.E. Crystallization of diamond and graphite//J.Chem.Phys.-1967.-Vol.46,N9.-P.3668-3676.
13. Бутыленко А.К., Игнатьева И.Ю. Влияние давления до 60 кбар на диаграмму плавкости системы Mn-Ni-C //Докл.АН УССР, сер.А, физ.-мат. и техн.науки. -1977.-№2.-С.161-165.

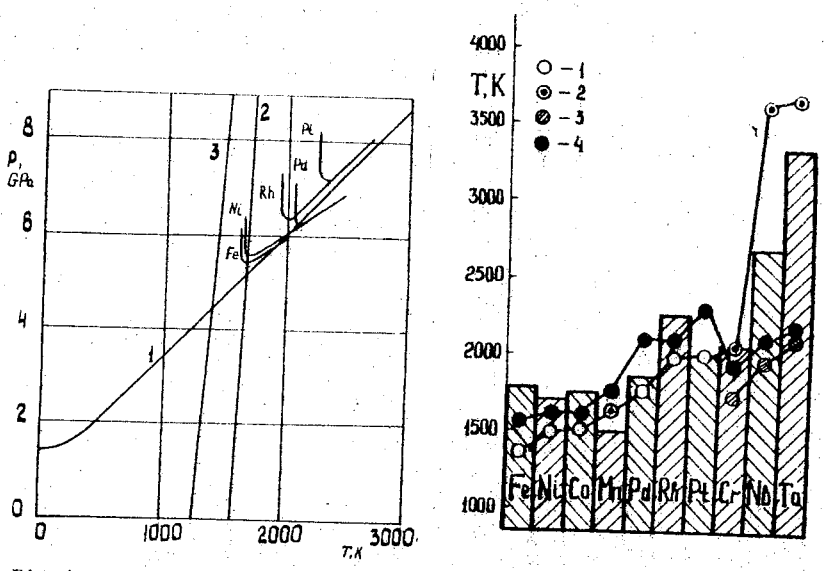

Fig.1. P-T regions of diamond formation in the presence of different metals (according to data of the work /4/ in comparison with D⇌G line (1) and eutectics melting temperature in carbon-nickel system (according to /12/) (2) and carbon-manganese-nickel system (according to /13/) (3).

Fig.2. Metals melting temperatures (columns), for equilibrium carbon-containing eutectics (1) of peritectics (2) in alloys of these metals with carbon, for metastable eutectics on the contact of the same metals with carbon (3) and minimum temperatures of diamond formation from graphite in the presence of the same metals (4).

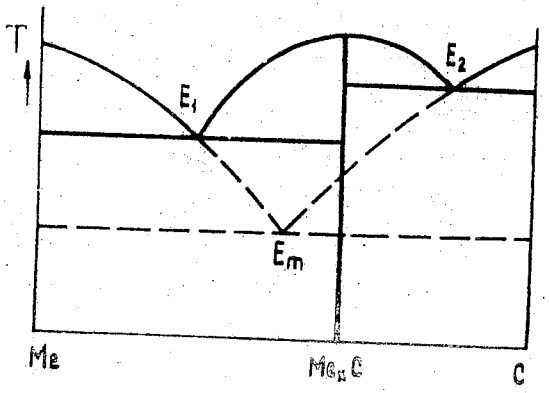

Fig.3. Schematic diagram for Me-C system with carbide formation.

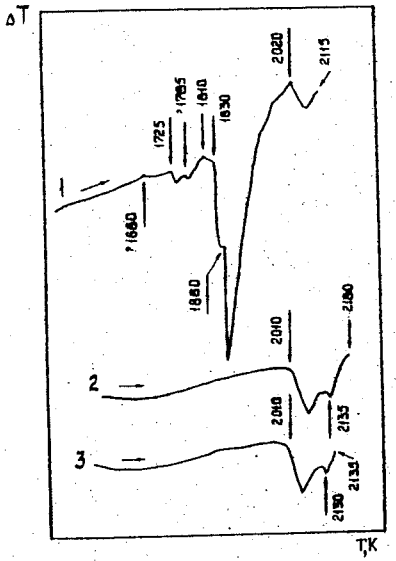

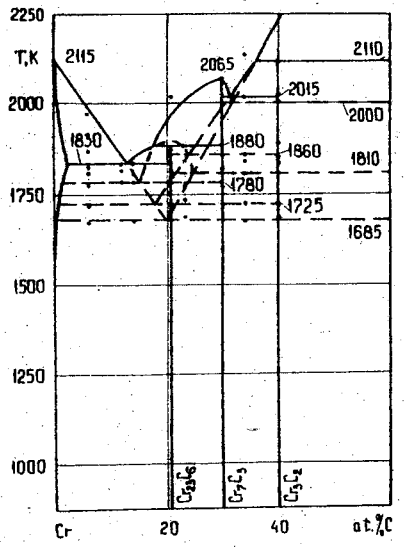

Fig.4. DTA-curves for chromium-graphite powder mixture heating /11/.

Fig.5. Metastable melting diagram for chromium-carbide system /11/.

THE INFLUENCE OF PRESSURE ON THE α - ω TRANSFORMATION IN Zr AND ITS ALLOYS

A.V.Dobromyslov, N.I.Taluts, K.M.Demchuk, A.N.Martemianov
Institute of Metal Physics, Academy of Sciences of the USSR, Sverdlovsk, USSR

As a result of high pressure application, in Zr and alloys based thereon with small content of β -stabilizers the ω -phase is formed. The ω -phase is retained in a metastable state after the pressure is removed due to the presence of hysteresis. The study of the formation mechanism of the ω -phase under pressure is of great importance in order to understand the nature of its appearance in Zr and Ti alloys in the presence of high β -stabilizer values. However, the structural features of the α - ω transformation are not fully studied. Our task has thus been to study the morphology and structural imperfection in the ω -phase formed under pressure and establish the atomic crystalline mechanism of the α - ω transformation.

Zr and Zr-2,5%Ti, Zr-2,5%Nb alloys were used for the investigation. The quenched specimens is the shape of disks, 4 mm diam and 0,1 and 2-3 mm thick, were subjected to volumetric quasihydrostatic compression in a toroidal container of lithographic stone.

The crystallography and morphology of the initial structure. Zr and Zr-2,5%Ti alloy in quenched state has the structure, containing the mixture of massive and lath martensite. The massive martensite is observed in the form of grains of different configuration. The lath martensite forms the packets of groups of parallel lath. The packets belong to different variants of Burgers orientation relations. The laths inside the packet are in close or twin orientation with one another. The plane between the laths coincides with $\{01\bar{1}1\}$ of the α -phase.

In Zr-2,5%Nb alloy after quenching the plate internally twinned martensite is formed. The structure of this alloy is not uniform, the sizes of primary and secondary martensitic plates differ substantially.

The morphology and imperfection of ω -phase formed under pressure. As a result of high pressure application, the noticeable change in the structure of quenched Zr and Zr-2,5%Ti alloy takes place. Part of the lath martensite packets is fully destructed and substituted by the large regions of ω -phase. The other part preserves its morphology, but the examination using microdiffraction shows that its internal structure is also that of the ω -phase (Fig. 1a, b*). The bright-field photographs show the specific stripe contrast. The analysis reveals that this is due to the great number of disordered stacking faults. The influence of pressure on Zr-2,5% Nb alloy does not lead to any particular changes in morphology of the quenched structure. The external forms of primary and secondary martensitic plates are fully preserved, however the plates have the ω -phase structure. After the action of pressure the transformation twins inside the martensitic planes disappear, and are substituted by the stripes (Fig. 1c*), similar to the case of pure Zr. Sometimes the stripes are "allowed", and the specific contrast due to the stacking faults is observed. The crystallographic analysis shows that the stacking faults lie in the planes $\{2\bar{1}\bar{1}0\}$ of the ω -phase.

The formation mechanism of the ω -phase. The analysis of the changes in structures of the quenched Zr and Zr-2,5%Ti and Zr-2,5%Nb alloys after the action of high pressure reveals that the difference in initial structures does not influence substantially the atomic crystalline mechanism of the $\alpha \rightarrow \omega$ transformation. The difference in the initial morphologic forms of the α -phase in Zr and Zr-2,5%Nb leads only to the fact, that the ω -phase formed under

*The Figure is given at the end of the book

pressure has the form of the massive or lath martensite in Zr, and the form of plate martensite in Zr-2,5%Nb.

The appearance of the diffuse scattering having the form of planes in the reciprocal space of the ω -phase (Fig.2), reveals the existence of a large number of linear defects, apart from plane defects in $\{2\bar{1}\bar{1}0\}_\omega$. The direction of the linear defects coincides with $[0001]$ of the ω -phase. The existence of such linear defects in the ω -phase lattice indicates that the formation of the high pressure phase in the α -phase lattice occurs by means of the displacement of the atomic rows, $[0001]$ rows in the ω -phase being the continuation of these rows. It may be shown, from the orientatio relations between β, α and ω phase, that this formation mechanism of ω -phase from α -phase is possible, if the lattice rearrangement takes place by the displacement of $\langle 11\bar{2}0\rangle$ atomic rows of the α -phase.

The process of $\alpha \rightarrow \omega$ transformation under pressure must be accompanied by the essential increase in the elastic energy of the metal or alloy. It follows from the fact, that the initial morphologic features of the structure of lath or plate martensite do not provide the minimum of the elastic energy of the $\alpha \rightarrow \omega$ transformation, because the appearance of these morphologic forms is due to the necessity to reduce the elastic energy in the process of $\beta \rightarrow \alpha$ transformation. Thus, the increase in the elastic energy in the Zr and its alloys after pressure treatment must lead to the additional structural features during the reverse $\omega \rightarrow \alpha$ transformation.

The reverse $\omega \rightarrow \alpha$ transformation. For the reverse $\omega \rightarrow \alpha$ transformation the specimens of Zr and Zr-2,5%Nb alloy were held at 300-500°C for different time. From X-ray diffraction it follows tha the stability of the ω -phase depends both on temperature and on

the time of heat treatment. The generalized data on the stability of the ω-phase are represented on Fig.3.

The morphologic peculiarities of the ω-phase formed under pressure reflect in the character of Zr structure at reverse $\omega \to \alpha$ transformation. Therefore the annealed α-phase rather often is observed taking form of packets, outwardly resembling those in Zr after quenching. However, in a number of cases the boundaries between the laths vanish and the grains of the α-phase with new orientations appear in the packet. At the same time, due to the elastic stresses in the specimens held under pressure, the relaxation twins are formed during the reverse $\omega \to \alpha$ transformation (Fig.1d*). In Zr-2,5%Nb alloy after the reverse $\omega \to \alpha$ transformation the restoration of the transformation twins inside the martensitic plates takes place. The elastic stresses in Zr-2,5%Nb alloy may apparently achieve considerable values, leading to somewhat unusual way of twinning at reverse $\omega \to \alpha$ transformation (Fig.1e*). In the case of Zr-2,5%Nb alloy the relaxation twins are formed in some equivalent systems. The crystallographic analysis shown, that the twinning plane coincides with $\{01\bar{1}1\}$ of the α-phase (Fig.1f*).

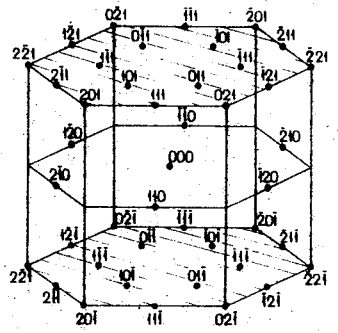

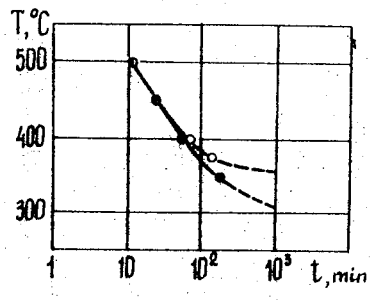

Fig.2.Reciprocal lattice of ω-phase with the diffuse scattering planes.

Fig.3.Temperature-time diagram of the $\omega \to \alpha$ transformation, • - Zr, o -Zr-2,5%Nb.

MECHANISM OF PRESSURE INDUCED BODY CENTRED TETRAGONAL TO HEXAGONAL CLOSE-PACKED TRANSITION IN Hg AND Hg_xCd_{1-x} ALLOYS

SURINDER M. SHARMA, HEMA SANKARAN, S.K. SIKKA,
R. CHIDAMBARAM

Neutron Physics Division, Bhabha Atomic Research Centre,
Trombay, Bombay, 400085, India

Our recent experimental studies have shown that the ambient pressure body centred tetragonal (bct) phase of $Cd_{1-x}Hg_x$ ($x > 0.25$) alloys transforms to a hexagonal close packed (hcp) structure under high pressure (for $x=0.35$, $P_t=2$ GPa and $x=0.5$, $P_t=6.4$ GPa) [1]. A natural extension is that elemental mercury also will transform from bct phase ($P > 3.5$ GPa) to hcp phase at a higher pressure. It was also pointed out that the bct and hcp structures are geometrically very close. Recently Lindgard and Mouritsen [2] have presented an analysis of bcc→hcp transformation in terms of Landau theory of two coupled strains ε_1 and ε_2. ε_1 represents the uniform strain required to take θ_c towards 120° and ε_2 the internal strain representing the shuffle of alternate (110) planes. Since the bct phase can be treated as special case of a more general bcc lattice, we provide a test of Lindgard and Mouritsen's analysis by evaluating the softening of W_N in Hg by a frozen phonon calculation.

Phonon frequencies are computed by a technique which uses Andersen's force theorem [3] and the linear muffin tin orbital method [4] to evaluate the electronic eigen values. The phonon distorted cell corresponding to 1/2 [110] <1$\bar{1}$0> mode is a four - atom simple tetragonal super cell, shown in fig.4 in ref.[1]. Sixty points in the irreducible wedge of the Brillouin zone were taken.

The changes of c/a of bct cell, caused by the strain ε_1, an input to our calculation, has been measured under pressure on a $Cd_{0.5}Hg_{0.5}$ alloy. A Syassen-Holzapfel type of high pressure diamond cell [5] with full cone energy dispersive x-ray diffraction system was employed (with a cone angle of 6°). For more details see ref.7. The results of the experiment are shown in Fig.1 along with alloy data [6].

The phonon frequency W_N was calculated under the following

conditions. (i) volume varied with c/a held fixed. (ii) both varied according to Fig.1. (iii) volume fixed and c/a varied. The frequencies are plotted in Fig.2.

It is at once evident that W_N does not soften completely under any of the above conditions. Curve 1 in Fig.2(a) shows that the system, in fact, stiffens under pure compression. On the other hand, as is shown in Fig.2(b) the variation of (c/a), at a fixed volume, brings about a significant change in W_N - a 10% increase in (c/a) results in 23% decrease in W_N. Curve 2 in Fig.2(a) represents an intermediate situation with c/a changing according to Fig.1. From the above, it is logical to conclude the absence of complete softening under any realizable state of this system. Therefore, this transformation should result from a large anharmonic coupling between the two strains as shown by Fig.2(b) confirming the suggestions of Lindgard and Mouritsen. It is also possible that in the defect strained regions, (eg. near dislocations) there is a favourable distortion of the bct cell (i.e. increase of c/a) giving rise to the realisation of a 'localised soft mode' [8]. This may lead to the formation of nuclei of hcp in the bct matrix and perhaps explain the time dependence of the resistance change after the transition point [1].

The authors are grateful to Prof. W.B.Holzapfel for details of diamond anvil cell.

References

1. V. Vijayakumar, Surinder M. Sharma, S.K. Sikka and R. Chidambaram. J. Phys. F : Met Phys. 16, 831, (1986).
2. P.A. Lindgard and O.G. Mouritsen.Phys. Rev. Lett 57, 2458, (1986).
3. A.R. Mackintosh and O.K. Andersen "Electrons at Fermi Surface", ed. M. Springford (University Press, Cambridge, p.149, (1989).
4. H.L. Skriver, The LMTO Method (Springer, Berlin, 1984)7.
5. G. Huber, K. Syassen and W.B. Holzapfel.Phys. Rev B15. 5123, (1977).
6. K. Schubert, V. Rosler, W. Mahler, E. Dorre and W. Schutt. Z. Metallk 45, 643, (1954).
7. Surinder M. Sharma, Vijayakumar, Hema Sankaran, B.K.Godwal, S.K. Sikka and R. Chidambaram. Solid State Physics, India (DAE) 29C, 267, (1986).
8. S. Mendelson, Journal De Physique Colloq C4, 139, (1982).

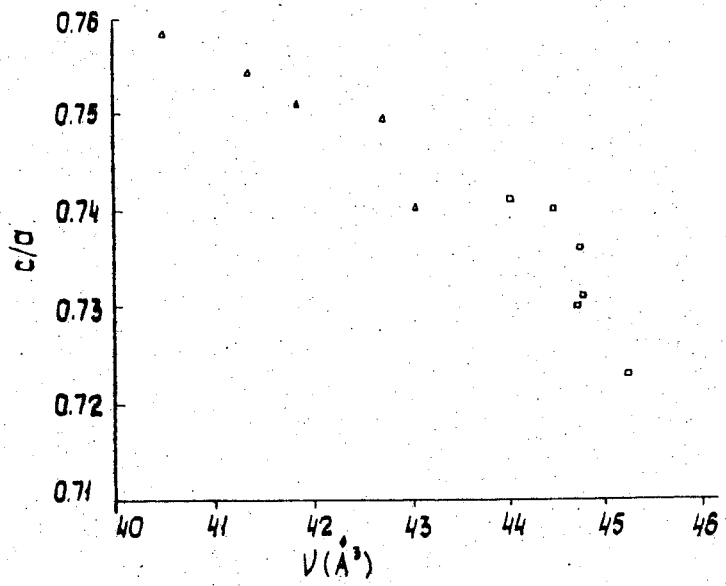

Fig.1. c/a as a function of volume, □ alloy data from Ref.6, Δ from our x-ray diffraction experiments.

Fig.2(a) Curve 1: Frequency W_N of the TA_1 1/2 [110] $\langle 1\bar{1}0 \rangle$ mode as a function of volume, c/a fixed at 0.72.
Curve 2: Frequency W_N of the TA_1 1/2 [110] $\langle 1\bar{1}0 \rangle$ mode as a function of volume, c/a varied according to Fig.1;
(b) Frequency W_N as a function of c/a. Volume kept fixed at 42.6Å³.

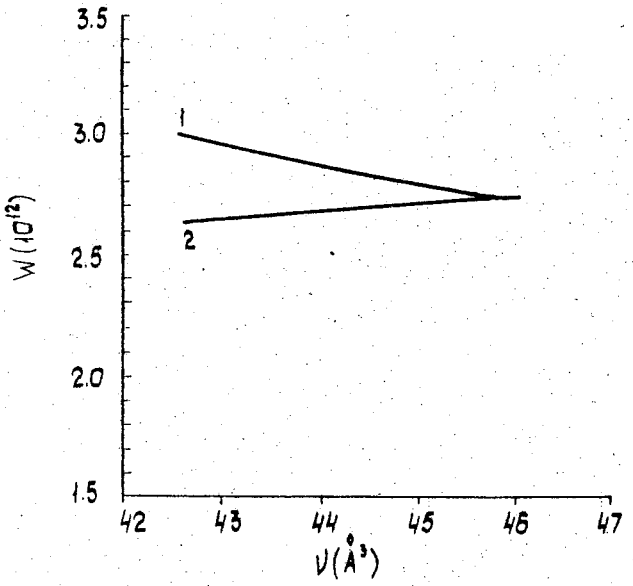

a

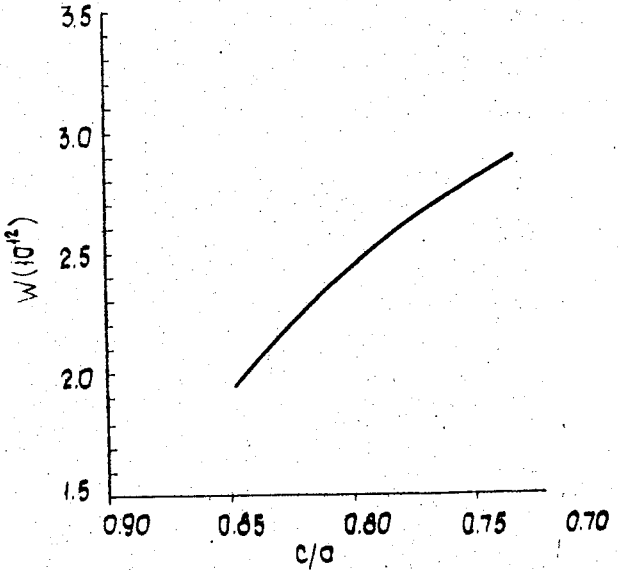

b

ON THE THEORY OF GERM FORMATION AT PHASE TRANSITIONS IN ELASTIC-PLASTIC BODIES

V.G.Baryakhtar, V.V.Tokii, D.A.Yablonskii
Donetsk Physico-Technical Institute, Academy of Sciences of the Ukrainian SSR, Donetsk, USSR

Non-uniform fluctuations of the order parameter (OP) in solids give rise to elastic shift deformations which considerably affect the OP fluctuation energy and the phase transition character itself. However in the vicinity of the second order phase transition line and also near the stability boundaries at the first order transition the OP fluctuations become abnormally big. So it becomes necessary to account not only elastic but plastic deformations as well. These aspects are considered in the present paper.

We shall consider only phase transitions which can be described within the Landau theory /1/. For simplicity we restrict ourselves to the case of the single-component OP and neglect the crystal anisotropy. Since at phase transitions the main contribution is made by the long wave fluctuations the plastic properties are most easily taken into account within the Genky medium /2/ with shift modulus μ_n depending on the shift deformation intensity $\Gamma=\sqrt{2(u_{ik}-1/3\,\delta_{ik}u_{ll})^2}$. Here u_{ik} is the deformation tensor. Then an expression for the thermodynamic potential density has a form of

$$\Phi=\Phi(\eta)+\lambda\eta^n u_{ll}+\frac{K}{2}u_{ll}^2+\int_0^\Gamma \mu_n(\Gamma)\Gamma\,d\Gamma, \qquad (I)$$

$$\Phi(\eta)=\Phi_0+\frac{a}{2}\eta^2+\frac{\beta}{4}\eta^4+\frac{\delta}{6}\eta^6+\dots,$$

where λ is the striction constant; n =I and 2 for linear and quadratic striction.

In a perfectly elastic body (particular case of the Genky medium) $\mu_n(\Gamma)=\mu$ and (I) at n =2 is transformed to the known relationship.

Similarly to /3/ we choose the model of an elastic-plastic body which passes from the elastic state $\mu_n(\Gamma)=\mu$ to the state of perfect plasticity $\mu_n(\Gamma)=\tau_s/\Gamma$ when the tangential stress intensity $\tau=\sqrt{1/2(\sigma_{ik}-1/3\,\delta_{ik}\sigma_{ll})^2}$ (σ_{ik} is the stress tensor) reaches the yield strength τ_s.

To consider the OP non-linear fluctuations $\eta=\eta(r)$ of an

arbitrary form is, quite naturally, impossible. In this paper an expression is obtained for the volume energy density of spherical and lamellar fluctuations.

Using an equilibrium equation $\frac{\partial\sigma_{ik}}{\partial x_k}=0$ one can determine deformation distribution $u_{ik}(r)$ in a body at the predetermined distribution $\eta(r)$ and then exclude $u_{ik}(r)$ from (I). And it should be mentioned that deformations caused by the OP fluctuations exist not only within the fluctuation region but outside it as well. Nevertheless it appears that the energy of deformations outside the fluctuation is proportional to its volume. Therefore total volume energy of the V fluctuation volume can be presented in the following form (for simplicity we give only the expression for the fluctuation in the symmetry phase)

$$F=\int\Phi\,dV=\left\{\Phi(\eta)-\frac{\lambda^2}{2K}\eta^{2n}+\frac{\delta}{4}\left[\eta^{2n}\theta(\eta_s-\eta)+f(\eta)\theta(\eta-\eta_s)\right]\right\}V \qquad (2)$$

where $\theta(\eta)$ is the Heavyside θ -function

$$\delta=2\lambda^2\frac{4}{3}\frac{\mu}{K}\left(K+\frac{4}{3}\mu\right)^{-1},\quad \eta_s^n=\frac{\sqrt{3}}{2}\frac{\tau_s}{\lambda}\frac{K+4/3\mu}{\mu},$$

$$f(\eta)=\begin{cases}2\eta_s^n\eta^n\ell_n\left(\eta/\eta_s\right)^h+\eta_s^{2n} & \text{— sphere}\\ 2\eta_s^n\eta^n-\eta_s^{2n} & \text{— plate}\end{cases} \qquad (3)$$

It should be mentioned that plastic properties of a body are manifested only if the OP fluctuation amplitude η is greater than some critical value η_s determined by the yield strength, elastic constants and striction bond value λ. Assuming $K\sim\mu$ we obtain

$$\eta_s^n\approx\tau_s/\lambda$$

Provided that $\lambda\sim T_c a_0^{-3}$ (T_c is the phase transition temperature, a_0 is the lattice constant) and τ_s can vary from substance to substance over the range of $(10^{-2}-10^{-9})\,\mu$ we obtain at $T_c\sim10^2$K.

$$\eta_s^n\sim\left(10^{-2}-10^{-9}\right)\frac{\mu a_0^3}{T_c}\sim 1-10^{-7}$$

The attention should be paid to the fact that in the lamellar fluctuation both elastic and plastic (at $\eta>\eta_s$) deformations are located only inside it. At the spherical fluctuation elastic deformations appear both inside and outside it. If, however, $\eta>\eta_s$

the fluctuation of radius R_φ is limited by the spherical shell of plastic deformations with external radius $R_\eta = R_\varphi (\eta/\eta_s)^{\frac{1}{3}}$ At $R < R_\varphi$ and $R > R_\eta$ deformations are of pure elastic nature.

Since there is a great interest for the investigation of the role of shift stresses (both of inner and external origin) and plastic deformations caused by them in the problem of germ formation at the first order phase transitions we shall illustrate the developed technique by an example of appearance of non-symmetrical phase germs. We restrict ourselves to the quadratic striction case ($n = 2$) and expansion of $\Phi(\eta)$ (I) with an accuracy to η^6. The condition of the first order phase transition is

$$B^* = B - 2\lambda^2/k < 0$$

Using (3) one can show that at $\eta > \eta_s$ the volume density of the lamellar germ energy is less than that of the spherical one. Therefore we shall consider only the lamellar germ.

The standard analysis show that at the germ-matrix equilibrium temperature($F = 0$; $F'_\eta = 0$; $F''_{\eta\eta} > 0$) depending on the relationship between the body constants both elastic germs with

$$\eta_T^2 = \frac{|B^*| - \delta}{d} \frac{3}{4} \qquad (4)$$

and plastically deformed ones with

$$\eta_n^2 = \frac{|B^*|}{4d} \left\{ 1 + 2\cos\left[\frac{1}{3} \arccos\left(1 - 24\eta_s^4 \frac{d^2\delta}{|B^*|^3} \right) \right] \right\} \qquad (5)$$

can appear. It is interesting to note that in the δ-τ_s phase diagram there is a line where energies of both equilibrium germs coincide.

As is seen from (4), (5) the OP value in the equilibrium germ coincides with its value in a uniformly distorted phase $\eta_0^2 = 3|B^*|/4d$ only in a plastically deformed germ and provided that $\tau_s = 0$.

Thus the analysis performed shows that the use of the undistorted phase parameters for the germ characteristics is strictly substantiated only for perfectly plastic bodies ($\tau_s = 0$).

References

I. Landau L.D., Lifshitz E.M.Statistical Physics.M:Nauka, I964.
2. Lourier A.I. Elasticity Theory. M.: Nauka, I970.
3. Lifshitz I.M., Gulida L.S. - DAN, I952, v.87, p.377.

HYDRODINAMIKAL ASPECTS OF DESINTEGRATION OF METASTABLE PHASES.

R.G.Arkhipov, Kh.Sh.Akhmetshackirova
High Pressue Physics Institute,
Troitzk, Moscow region, USSR

The complete phase transition can be achieved only if the experimental arrangement (the "thermostat") consumes the latent heat and the volume difference. In isolated system the transition terminates itself due to the Le-Shatelliet principle and the final concentration of a new phase is proportional to the initial oversaturation (the difference of thermodynamical potentials of initial and new phases $\Delta\Phi = \Phi_1(p_0, T_0) - \Phi_2(p_0, T_0)$). If the latent heat and the specific volume change are both small, it is easy to have a formula for the excess which ensure 100% instant transition on condition of thermoisolation and fixed volume:

$$\Delta\Phi = -\left(\frac{\partial p}{\partial V_1}\right)_{S_1} \Delta V^2 + \left(\frac{\partial T}{\partial S_1}\right)_{V_1} \Delta S^2 + 2\left(\frac{\partial T}{\partial V_1}\right)_{S_1} \Delta S \Delta V$$

This positively definite quadratic form may be rewritten in form

$$\Delta\Phi = -(V_1 - V_2)^2 \left(\frac{\partial p}{\partial V_2}\right)_T \left\{ \frac{C_{1p} - C_{1V}}{C_{1V}} \left[1 - \frac{dp}{dT} \Big/ \left(\frac{\partial p}{\partial T}\right)_{V_2} \right]^2 + 1 \right\}$$

Spontaneous transition from metastable states are of particular interest. In infinite resting media one has to deal with two discontinuities at least to connect initial and final states. In the case, when $\Delta\Phi$ is small, it can be proved, that number of possibilities, socalled "scenaria", is limited and one is able to do complete investigation. They are by no means to satisfy all hydrodynamical conservation law [1].

P-V diagram is the most convinient for consideration. We are inside the dashed region which corresponds to the mixture of initial and final phases not far from the phase equilibrim line. Starting from the point marked by asterisk * one can draw the isoentropy for initial media $V_1(p), S_1$ and the isoentropy for equi-

librium mixture $\tilde{V}(p)$, $\tilde{S}$, which are equivalent to shock wave curves. The mutual situation of both curves are determined by dimensionless parameters:

$$\sigma = \frac{c_{1p}^* - c_{1v}^*}{c_{1v}^*}, \quad \tau = 1 - \left(\frac{\partial T}{\partial p}\right)_{S_1}^* \Big/ \left(\frac{dT}{dp}\right)^*,$$

$$\Delta V = \frac{V_1^* - V_2^*}{V_1^*}, \quad \alpha_1 = \frac{1}{2}\left(\frac{\partial^2 V_1}{\partial p^2}\right)_{S_1}^* V_1^* \left(\frac{\partial p}{\partial V_1}\right)_{S_1}^{*2}$$

The whole necessary information about the new phase is included in the equation of state for the initial phase and $\left(\frac{dT}{dp}\right)^*$ and $\left(\frac{d^2T}{dp^2}\right)^*$ in the point $(*)$. The sound velocity in the mixture is always smaller then in the initial phase, but always real /2/ $\tilde{c}^{*2} = c_1^{*2}/(1+\sigma\tau^2)$.

The simplest is the case, when one can draw a tangent to the detonational curve from the initial point fixed on the isoentropy S_1 by $\varphi = \frac{\Delta\rho}{c_1^{*2}}$. When φ is small the case of two parallel discontinuities can be solved analytically. First goes the shock wave without transformation (fig.1) and then front of fusion, corresponding to the Jouguet point, after which occuers a mixture of initial and new phases with the concentration x of the new phase. When $0 \geq \sigma\tau^3\Delta V/\alpha(1-\tau)(1+\sigma\tau^2)^2$ the detonation regime is also possible. In this case first goes the detonation wave, corresponding to the Jouguet point, then after relaxation goes a weak discontinuity (fig.2). This type of transformation is considered more thoroughly in [4].

References

1. Landau L.D., Lifshic E.N. Mehanika sploshnyh sred, Gostehizdat, 1954.
2. Kuznetsov N.M. Dokl.AN SSSR-1964-155-№1-p.156.
3. Zeldovich Ia.B., Kompaneets A.S. Teoria detonatsii, Gostehizdat, 1955.
4. Arkhipov R.G., Akhmetshakirova Kh.Sh. Teplofiz. vysok. temp.-1986-24-№5-p.1003.

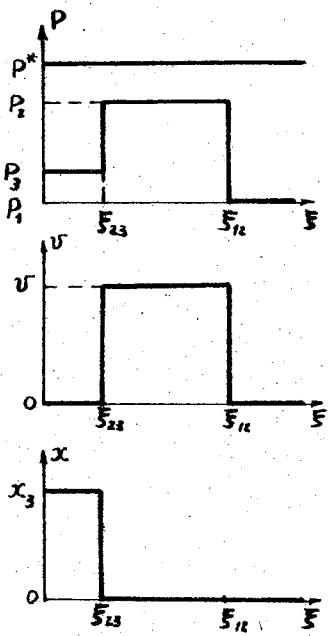

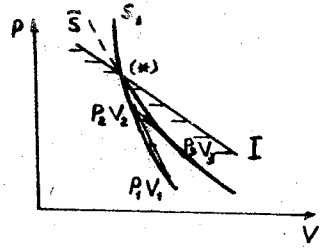

$$P_1 = \varphi\frac{(\tau-1)}{\tau}\frac{V_1^*}{V_1^* - V_2^*}$$

$$P_2 = -\frac{\alpha(1+\sigma\tau^2)}{\sigma\tau^2}P_1^2, \quad P_3 = \sqrt{\frac{1}{1+\sigma\tau^2}}P_1$$

$$\upsilon = -P_1$$

$$x_3 = \frac{\sigma\tau(\tau-1)}{\sqrt{1+\sigma\tau^2}}\frac{V_1^*}{V_1^* - V_2^*}P_1$$

$$\xi_{12} = 1 - P_1 + \frac{\alpha_1}{2}P_1$$

$$\xi_{23} = \frac{1}{\sqrt{1+\sigma\tau^2}} + (\alpha-1)P_1$$

Fig.1. The slow fusion regime. The pressure is measured from the point $(*)$ of crossing isoentropies with the phase equilibrium curve. ξ_{12}, ξ_{23} - velocities of discontinuities, υ - mass velocity.

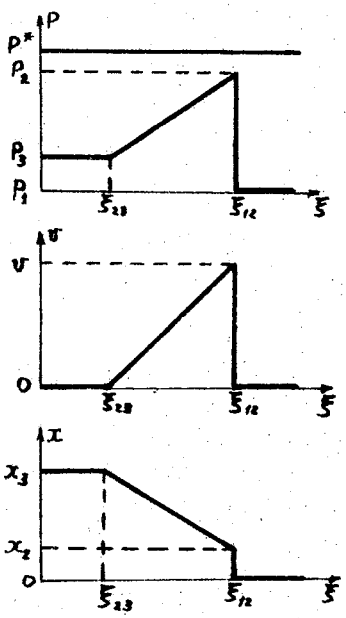

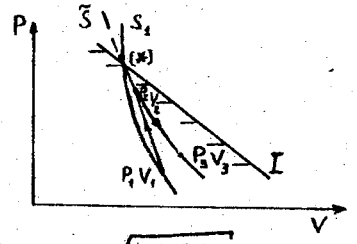

$$P_2 = P_1 + \sqrt{\frac{-G\tau^2 P_1}{\alpha(1+G\tau^2)^2}}$$

$$P_3 = \frac{1+0.5G\tau^2}{1+G\tau^2} P_1$$

$$v = \sqrt{\frac{-G\tau^2 P_1}{\alpha(1+G\tau^2)}} + \frac{G\tau^2 P_1}{\sqrt{1+G\tau^2}}$$

$$x_2 = G\tau(\tau-1)P_2\,,\quad x_3 = G\tau(\tau-1)P_3$$

$$\xi_{12} = \frac{1}{\sqrt{1+G\tau^2}} + \sqrt{\frac{-G\tau^2\alpha}{1+G\tau^2}} P_1 + \frac{\alpha(1+G\tau^2)-1}{\sqrt{1+G\tau^2}} P_1$$

$$\xi_{23} = \frac{1}{\sqrt{1+G\tau^2}} + \frac{\alpha-1}{\sqrt{1+G\tau^2}}(1+0.5G\tau^2)P_1$$

Fig.2. The detonation regime.

THE INFLUENCE OF HIGH PRESSURE ON THE RAPID SOLIDIFICATION OF THE SUPERCOOLED MELTS

V.V.Brashkin, S.V.Popova
Institute of High Pressure Physics
Troitsk, USSR

The influence of high pressure on the basic parameters of the rapid solidification is analysed in the framework of the homogeneous theory of crystallization using the well-known expression for the nucleation rate (I) and the growth rate (U) [1]:

$$I \sim \exp\left[-\frac{\alpha\sigma^3 V_s^2}{k\,T_m H_m^2}\,\tau^{-2}(1-\tau)^{-1}\right]\exp\left[\left(-\frac{\Delta G'}{k\,T_m}\right)(1-\tau)^{-1}\right], \quad (1)$$

$$U \sim \left\{1-\exp\left[-\frac{H_m}{RT_m}\,\tau\,(1-\tau)^{-1}\right]\right\}\exp\left[\left(-\frac{\Delta G''}{RT_m}\right)(1-\tau)^{-1}\right], \quad (2)$$

where α is a geometrical constant, σ is the surface tension, V_s - the volume of solid per mole, H_m - the latent heat of solidification, T_m - the melting temperature, $\Delta G'$ - the activation energy for nucleation, $\Delta G''$ - the activation energy for crystal growth, R - the gas constant,

$$\tau = \frac{T_m - T}{T_m} = \frac{\Delta T}{T_m}$$ - the relative supercooling.

The mean grain size (d) can be expressed from I and U like

$$d = \sqrt[4]{U/I} \sim \frac{\Delta T_c}{\dot{T}}\,U\,, \quad (3)$$

where T_c is the interval of crystallization, $\dot{T}$ - the cooling rate. To reach some fixed value of the supercooling it is necessary to have the cooling rate [2]:

$$\dot{T} \sim \Delta T_c \sqrt[4]{U^3 I}\,. \quad (4)$$

The temperature interval of crystallization can be approximately represented as:

$$\Delta T_c \sim \frac{H_m T^2 (T_m - T)^4}{\sigma^3 V_s^2 (4TT_m - 3T^2 - T_m^2) T_m^2} \cdot \qquad (5)$$

Let us suppose that $\Delta G'' \sim \Delta G' \sim \Delta G$ then from (I), (2), (3) and (5) it follows that

$$d \sim \frac{H_m^2 T^2 (T_m - T)^4}{\sigma^3 V_s^2 (4TT_m - 3T^2 - T_m^2) \dot{T} T_m^2} \exp\left(-\frac{\Delta G}{RT}\right)\left[I - \exp\left(-\frac{H_m \tau}{RT}\right)\right] \qquad (6)$$

and at the same time

$$d \sim \exp\left[\frac{\alpha \sigma^3 V_s^2}{4kTH_m^2} \tau - 2\right] \left[I - \exp\left(-\frac{H_m \tau}{RT}\right)\right]^{I/4} \cdot \qquad (7)$$

So using the expressions (7) and (6) we can find the dependence of the values $\Delta G(P)$ and $\sigma'(P)$ in case we define the d(P) and $\Delta T(P)$ dependences.

Some pure metals (Pb and In) are quenched from the melt at a pressure of 0.7 - 8 GPa with the cooling rate $\sim 10^3$ K/c and their average grain size, morphology and microhardness (H_μ) are investigated at room pressure. Also the supercooling (ΔT) of the melt is measured under the same pressures.

The supercooling was determined by chromel-alumel thermocouple located in the center of the sample.

The amplified signal of the thermocouple was stored by oscillograph C8-I2. All values (T_m, T, ΔT and $\dot{T}$) were measured in each experiment at the particular pressure.

The values of $H_m(P)$ for Pb were taken from [3] and for In H_m=3.47 kJ/mole at P=I GPa * (for higher pressures $H_m(P)$ was extrapolated). Other data necessary for the calculation were taken from [4].

It was found from the experimental results (see Table) using expressions (6) and (7)

$$\Delta G(P) \sim \Delta G(0) + \beta P, \qquad (8)$$

where $\beta = \frac{I}{3} V_a$ - atomic volume,

the values of σ' are in a good agreement with the model

$$\sigma'(P) \sim Y(P)\, V_a^{I/3}, \qquad (9)$$

* These data were given by L.N.DZHAVADOV before the publication [6]

where Y - the shear modulus, if we use the Y(P) data from the ref. [5].

The experimental (T_m, ΔT, d, H_μ) and the calculated (σ', ΔG) results for Pb and In

P (GPa)	T_m (K)	ΔT (K)	d (μm)	H_μ (MPa)	σ' in units of σ'_0	G (kJ/mol)
			Lead			
0	600±5	55±5	300	60±I0	σ'_0	8.6±0.I
2	735±I0	75±5	90±I0	I00±I0	(I.I5±0.02)	20±3
5	935±I0	I23±5	35±5	I20±I0	(I.37±0.03)	33±3
7.5	I085±I0	I60±5	I2±2	I90±I0	(I.77±0.04)	53±3
			Indium			
0	430±5	28±5	50	I8±5	σ'_c	6.6±0.I
I	470±I0	35±5	25±5	38±5	(I.I7±0.02)	I2±I
2	5I0±I0	40±5	I5±4	45±5	(I.25±0.03)	I7±2
5	625±I0	50±5	3±I	80±I0	(I.54±0.04)	33±3

It was found from expressions (4), (8), (9) that the value (T) from (4) for the "normal-melting" substances may either increase or decrease (to 10^I-10^3 times for $\tau = -\frac{I}{3}$) at P ≤ 5 GPa, but for P ~ I5 GPa it must decrease (to 10^3-10^7 times for $\tau = -\frac{I}{3}$).

For Cu it was found that at P > 6 GPa the morphology of grains changes from dendritic to cellular and the dimension of grains decrease from I4 μm (2 GPa) to 2.5 μm (8 GPa). These data allow to estimate the relative increasing of σ'(0.03 GPa^{-I}) and ΔG (0.I GPa^{-I}) at high pressure.

Under high pressure (up to 8 GPa) some binary copper-based alloys were rapidly quenched from the melts. It was found that at least for some compositions of these alloys the critical cooling rate decreased to about 10^3 times and more.

References

I. Turnbull D., Cohen M.H., in "Modern Aspects of the Vitrous State" Vol.I,ed.Mackenzie S.D.,Butterworths,London,I960,p.38-62.

2. Miroschnichenko I.C. Zakalka iz schidkogo sostojanija, M., Metallurgija, I982, I68 p.

3. Mirwald P.W., Determination of melting entropy by measurement of the volume change of melting at high pressure. - AIRAPT Conf., Boulder, Colo, New York-London, Plenum Press, 1979, vol.I, p.361-367.

4. Driz M.E., Svoistva elementov, M., Metallurgija, 1965, p.671.

5. Guiman M.W., Steinberg D.J., Pressure and temperature derivatives of the isotropic polycrystalline shear modulus for 65 elements, J.Phys.Chem.Sol., 1974, 35, NII, p.1501-1512.

6. Dzhavadov L.N., Krotov Yu.I., Determination of the thermodynamical properties under pressure; (the same Conference: XIth AIRAPT, July 12-17, 1987, Kiev, USSR).

THE STRUCTURE AND PROPERTIES OF THE BULK AMORPHOUS GALLIUM ANTIMONIDE OBTAINED BY QUENCHING FROM THE MELT

V.D. Gorbatenkov, V.I. Larchev, S.V. Popova, G.G. Skrotskaya
Institute of High Pressure Physics, Troitsk, USSR

The bulk amorphous samples GaSb were obtained at high pressure /7-9 GPa/ by rapid /$8 \cdot 10^2$ K/c / quenching from the melt. It was shown that Raman spectra of the amorphous high pressure phase a-GaSb very much resembled the corresponding data for thin amorphous films [1].

By changing the initial conditions of the synthesis /the external pressure and the temperature of the melt/ a different type of disordered samples can be obtained. The increase of the disordering results in the decrease of conductivity. So one can observe the metal-insulator transition that accompanies a large changing of conductivity, which decreases by a factor of 10^9 at T~10 K [2]. This phenomenon is well known for all tetrahedrally bonded compounds /for GaSb see ref. [3] /.

The temperature and the heat of crystallization of a-GaSb were investigated using scanning calorimetry method [4]. The heat of crystallization was found to be 8.7 ± 0.4 kJ/mol. The ratio of the heat of crystallization to the heat of melting is 0.35 and it is close to the corresponding values for a-Ge /0.34/ and a-Si /0.23/. The temperature interval of crystallization /440-500 K/ is close to the corresponding data for sputtered films of a-GaSb.

In this report we describe some preliminary experimental results on the short range order structure /SRO/ at room pressure and the stability of a-GaSb under high pressure.

A X-Ray diffraction was performed by transmission on a HZG-4 diffractometer with monochromated MoK_α radiation. After measuring the scattered X-Ray intensity, all corrections, normalization and Furier transformation were made in agreement with the rules described in [5].

The radial distribution functions /RDF/ are shown on Fig.1 in comparison with the RDF for amorphous thin films of GaSb [6]. The positions of the first and the second peaks /R_1=0.260 nm ; R_2= 0.438 nm/ and the numbers of the nearest neighbours /N_1=3.75, $N_2 \sim 12$/ are in a good agreement with the data for the thin films. But the appearance of the third peak with R_3=0.525 nm, $N_3 \sim 13$

obviously indicates the microcrystalline structure of the bulk samples.

In any case the bulk samples of a-GaSb have the diamond-like structure although the melt has the structure close to the primitive cube and the metallic type of conductivity.So the quenching from the melt at high pressure must lead to the preparation of metallic amorphous phase. This phase must transform to a semiconducting one at room temperature the pressure being released. It is known that sputtered amorphous films of GaSb undergo reversible transition from semiconducting to metallic state at a pressure of about 2.5 GPa [7]. But the pressure needed for synthesis of a-GaSb by rapid quenching from the melt is much higher. One of the assumptions is that the temperature of crystallization of the metallic and semiconducting states depends differently on pressure.

In connection with this we investigated the stability of a-GaSb in the wide range of /P,T/ conditions by isothermal annealing during 10 min. The crystallization of the samples was controlled by a X-Ray method after annealing. Also the electrical conductivity was measured as a function of pressure at room temperature. It was found that the temperature of crystallization decreases at low pressure and increases at high one. The sign changes at a pressure of $\sim$ 3.0 GPa. The drop of electrical resistivity occurs within the pressure range of 3.5-4.0 GPa (see Fig.2).

All these experimental data lead to the conclusion that by rapid quenching from the melt at high pressure the bulk samples of a-GaSb can be prepared. The electrical properties, temperature of crystallization, Raman spectra are very close to the corresponding properties of the sputtered amorphous films, but SRO is probably microcrystalline.

References

1. Larchev V.I., Melnik N.N., Popova S.V., Skrotskaya G.G., Talenskii O.N. Vlijanie visokogo davlenija na razuporjadochenie strukturi tetraedricheskich poluprovodnikov pri zakalke iz rasplava. Proc.Lebedev Physical Institute, 1985, N1, p.7-10.
2. Aleksandrova M.M., Demishev S.V., Kosichkin Yu.V., Larchev V.I., Skrotskaya G.G., Popova S.V. Metal-insulator transition in gallium antimonide caused by the disordering of the crystal structure. JETP Lett., 1986, 43, N4, p.230-233.
3. Naidu B.S., Sharma A.K., Sastry D.V.K., Syamalamba Y., Reddy P.J. Physical Investigations on amorphous films of some semiconducting compounds. J.Non-Cryst.Sol.,1980, 42, N2,p.637-652.

4. Aleksandrova M.M., Blank V.D., Larchev V.I., Popova S.V., Skrotskaya G.G., Transition temperature and heat of crystallization of amorphous bulk gallium antimonide obtained by rapid quenching from the melt. Phys.Stat.Sol., 1985,91, N1, p.-K8.
5. Wagner C.N.J., in "Liquid Metals", S.Z.Beer, ed.by M.Dekker, New York, 1972, p.257-329.
6. Shevchik N.J., Paul W., The structure of tetrahedrally coordinated amorphous semiconductors., J.Non-Cryst.Sol., 1973/19 13, N1, p.1-12.
7. Minomura S., Shimomura O., Asaumi K., Oyanagi H., Takemura K High-pressure modification of amorphous Si, Ge and some III-compounds. Proc. 7th Int.Conf. on Amorphous and Liquid Semiconductors. Ed. by W.E.Spear, Univ. of Dundee, 1977, p.53-57

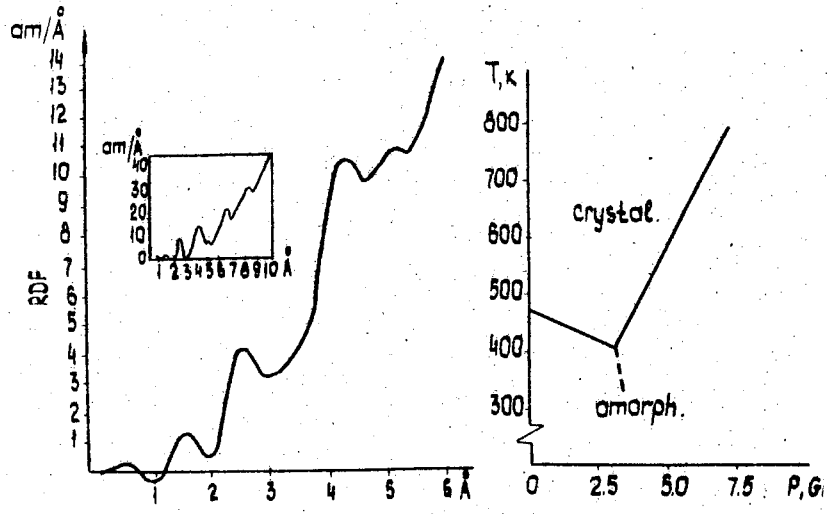

Fig.1. The radial distribution function (RDF) for amorphous GaS obtained at high pressure (in comparison with the RDF fo amorphous thin film of GaSb [6].

Fig.2. The dependence of the crystallisation temperature of a-G on pressure (in conditions of the isothermal annealing).

FORMATION OF AMORPHOUS ALLOYS BY SOLID-STATE REACTION AFTER HIGH PRESSURE ACTION

I.T.Belash, V.F.Degtyareva, E.G.Ponyatovsky
Institute of Solid State Physics,
USSR Academy of Sciences, USSR

The amorphous state of materials attract attention of both theorists and practical workers due to its specific physical and mechanical properties. An interest in the formation of amorphous alloy has traditionally centered on materials produced by rapid quenching from liquid state. It has been shown that a number of amorphous alloys may be formed via solid-state reaction, for example, by slow heating of thin films. In our investigation on the high pressure effect on the phase equilibria of binary alloy systems we have found a spontaneous amorphisation of some alloys under the normal condition after the high pressure action. This phenomenon was first observed in Cd and Zn alloys with Sb [1,2]. More recently the amorphous state was received in Al-Ge alloys.

The experimental data on amorphous alloys are summarized in Table 1, in which are given the alloy compositions contents, the pressure-temperature treatment parameters correspondent to the occurrence of new phases, their superconducting transition temperature (T_c), the conditions of alloy amorphization and the conditions of amorphous alloy crystallization.

The analysis of the experimental data shows a number of common factors favourable for the alloy amorphisation in the solid state after the high pressure action.

1. Initial alloy in the equilibrium state contains a semiconductor phase: compound (in alloys Zn-Sb and Cd-Sb) or element (in alloy Al-Ge).

2. A new intermediate phase is formed in the alloy at high pressure. The composition of the new phase is different from stoichiometric composition of the original semiconductor phase. As a rule, high pressure intermediate phases exhibit a metallic type of bonding and are superconductors (see the review [3]). The new phases Cd-Sb and Al-Ge alloys have a simple hexagonal structure (γ-phase), and new phase in Zn-Sb alloys has a γ-related distorted structure (δ-phase).

3. High-pressure phase is quenched after the pressure is removed at a low temperature (-190°C) and retain in the metastable state at normal pressure in liquid nitrogen.

4. Quenched high pressure phases are destabilized on heating to 20°C returning of the alloy to its ariginal state is inhibited due to a low atomic mobility and slow components redistribution, which hinder the attainment of the necessary stoichiometric composition for crystallization of semiconductor phase. All these reasons provide the existence of potential barrier for the equilibrium phases formation and lead to a spontaneous alloy amorphization (Fig.1,2).

5. Amorphous alloy are not found to decompose at low temperatures, while transform to crystal state by prolonged annealing at higher kinetically sufficient temperatures (see Table). The temperature and time of crystallization annealing depend on the alloy constituents.

All these factors being satisfied one can expect the solid state amorphization to occur in the other binary and multicomponent systems.

Phase content characteristic of alloys, amorphous after the high pressure action

Alloy composition, at.%	Equilibrium phases	Treatment parameters		Alloy state after quenching (1 bar, - 190° C)			Alloy state at 1 bar, 20° C	Crystallisation conditions
		P, kbar	T° C	Phase	Structure	T_c, K		
$Cd_{40}Sb_{60}$	CdSb+Sb	70	350	γ	simple hexagonal (c/a = =0.924)	4.9	amorphous (after 1-3 days)	20° C for 2-3 weeks
$Zn_{40}Sb_{60}$	ZnSb+Sb	85	300	δ	orthorhombic (distorted γ)	6.7	amorphous (after 1 hour)	150° C for 2 hours
$Al_{30}Ge_{70}$	Al+Ge	90	320	γ	simple hexagonal (c/a = =0.926)	8.2	amorphous (after 0.5 hour)	200°C for 3 hours

References

1. Belash I.T., Ponyatovsky E.G. Phase transformation in the Zn-Sb system at pressures up to 90 kbar. - High Temp. - High Press., 1975, v.7, N 5, pp.523-526.
2. Belash I.T., Ponyatovsky E.G. Phase transformation in alloys of cadmium and zinc with antimony at high pressures. 3. The CdSb-ZnSb system. Electric properties of amorphous $Cd_xZn_{1-x}Sb$ compounds after high-pressure treatment. - High Temp. - High Press., 1977, v.9, N 6, pp.651-655.
3. Degtyareva V.F., Ponyatovsky E.G. High pressure phases in alloys of B-elements - new electronic phases. - Fiz.Tverd. Tela, 24, N 9, 2672-2680.

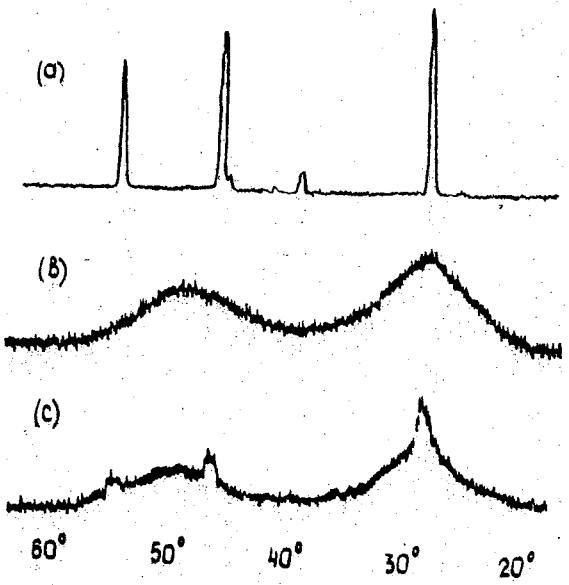

Fig.1. Diffraction patterns of alloy $Al_{30}Ge_{70}$ (CuK_α):
a) in equilibrium state
b) subjected to 90 kbar, 320°C; quenched to - 190° C, 1 bar and heated to 20°C at 1 bar;
c) annealed at 200°C for 1 hour.

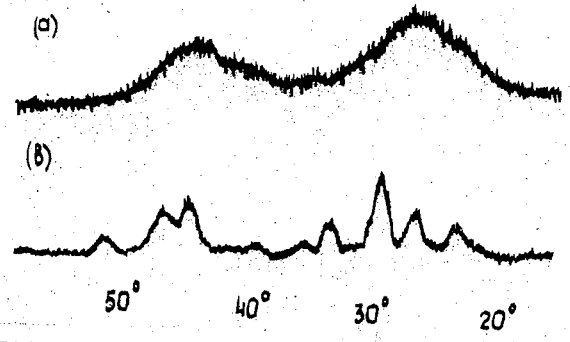

Fig.2. Diffraction patterns of alloy $Zn_{50}Sb_{50}$ (CuK_α):
a) subjected to 90 kbar, 350°C); quenched to - 190° C, 1 bar and heated to 20°C at 1 bar;
b) annealed at 150° C for 2 hours.

ELECTRONIC STRUCTURE AND HEAT OF FORMATION OF COBALT AND IRON HYDRIDES

C. Demangeat[1], C. Minot[2], N.I. Kulikov[3]

[1]LMSES (UA CNRS n° 306) Université L. Pasteur, 4, rue Blaise Pascal 67070 STRASBOURG, FRANCE.

[2]Chimie Théorique (UA CNRS n° 506) Université Paris Sud, Bât. 490, 91405 ORSAY, FRANCE

[3]L.F. Vereschagin Institute of High Pressure Physics, 142092 Troitsk, MOSCOU Region, USSR

ABSTRACT

Total energy local spin density energy band calculations are employed to study the heat of formation of the Co H system. Total energy of ferromagnetic fcc cobalt and of the hydride in the NaCl structure have been determined as a fonction of volume. The electronic structure of the iron-hydrogen system has been performed in terms of band structure calculation based on the Extended Hückel formalism. Allowing the iron lattice to relax, we minimize the energy of the system in terms of a variable lattice parameter. In the $(FeV)_2$ H system with hcp stacking the hydrogen atom located at tetrahedral interstitial site with 3V and 1Fe at nearest neighboring position appears to be the configuration with the lowest energy.

I. INTRODUCTION

The determination of the physical properties of solutions of hydrogen, even in such important and interesting transition metals as Fe, Co has remained scarce so far. This is related to the extremely low solubility of hydrogen at atmospheric pressure. The huge number of experimental data concerning the influence on the properties of these metals and their alloys was generally obtained for hydrogen concentrations comparable with those of various defects. In order to isolate the role of hydrogen as an alloying element we must be able to vary the hydrogen content over a wide interval of concentration. Hydrides can be synthe-

tized by placing the metal in an atmosphere of hydrogen whose thermodynamic potential is raised by compression to high pressures. The work with high pressure hydrogen, however, involves many experimental difficulties. This is related to its high compressibility, extremely low viscosity and chemical corrosiveness which greatly increases with temperature and pressure. Baranowski [1] was able to overcome this difficulty by designing a system in which a bronze bomb containing hydrogen was placed in a hydrostatic high pressure chamber up to 3GPA. He was therefore able to synthetize nickel and chromium hydrides under equilibrium conditions. To synthetize iron hydride a higher pressure was necessary and this was done under the guidance of Ponyatovsky [2]. The results of investigation of phase diagrams of metal-hydrogen systems, crystal structure, thermal stability, as well as magnetic and superconducting properties of recently obtained hydrides are reported in the book by Ponyatovsky et al [3].

The purpose of the present paper is to focuss on electronic structure and heat of formation of Co and Fe hydrides [4-7].

II. THE CoH SYSTEM

Switendick [8] has recently reported self-consistent electronic energy band structure of palladium and nickel hydrides, palladium and titanium dihydrides, in the soft core approximation.
The present paper reports on the heat of formation ΔE_{form} of the cobalt hydride, which is given by :

$$\Delta E_{form} = E_{CoH} - E_{Co} - \frac{1}{2} E_{H2} ,$$

whereas E_{CoH} and E_{Co} are respectively the total energy of the monohydride of Co and of the pure cobalt ; E_{H2} is the Hartree-Fock energy required to separate a hydrogen molecule into its constituent electrons ans protons.

Very few calculations have been devoted to CoH systems [10,11] ; unfortunatly these papers are restricted to the paramagnetic phase [10] or to the determination of the band structure [11]. Inthis work we study the ground-state poperties and the pressure induced magnetic properties of bulk CoH using

a total-energy approach : we have employed the LSDA and calculated the total energy as a function of volume by means of linear muffin-tin orbital (LMTO) method [12]. The Von Barth-Hedin exchange correlation [13], a scalar relativistic approximation for the valence electrons and a fully relativistic treatment of the core electrons, are utilized. Total energy for Co and CoH in the fcc and NaCl phases have been performed in terms of the lattice parameter [4]. Yet, the hcp phase of Co has the lowest energy and we have to include the difference between hcp and fcc phases [9]for a correct determination of the heat of formation. We obtain $\Delta E_{form} = 0.31$ eV, in good agreement with the experimental value 0.4 eV [14]. The magnetic moment, per Co atom, decrease from $1.58_{\mu B}$ to $1.4_{\mu B}$ in going from pure Cobalt to the mohydride of Co.

Calculations pertaining to other unstable hydrides will be reported in a forth coming publication [15].

III. THE FeH AND $(Fe_{1-x-x-y} V_x)_y$ H SYSTEMS

This is certainly a most difficult subject. Only a very few calculations concerning H on Fe [16,17] and references therein) or H in Fe ([5] and references therein) have appeared in the literature. The calculation of H in Fepresented here use a less sophisticated Extended Hückel method. With this rather simple approach it is possible to have an idea of the stable structure of the iron-hydrogen system by computing the total energy of the system in terms of a variable lattice parameter and with different hydrogen positions. We have performed calculations on the effect of hydrogen on the bcc and hcp phases of iron. Our results can be summarized as follows [5] :

a) We have shown that in both cases, the hydrogen atom is most probably located at the tetrahedral interstitial site.

b) The heat of formation of the hydride remains endothermic but, whereas the bcc phase of iron is more stable than the hcp phase is, the effect of hydrogen is to stabilize the hcp phase ; this is consistent with experimental findings [3].

c) Total energy of different types of geometrical arrangements of the

hydrogen lattice have been estimated. The most stable arrangement appears to be the one with hydrogen atom at 3rd nearest neighboring positions. These results are in agreement with a more general Switendick-Westlake criterion |18| which states that H-H distance is never less than 2.1 Å.

d) The H site is found to be slightly positively charged i.e., we have charge transter from H to the neighboring metallic atoms. To investigate in more details these charge transfers, we have performed calculations on various Fe_4 H clusters. Investigations of this small cluster consisting of four iron atoms in a tetrahedral symmetry and a hydrogen atom at top, bridge, hollow and insertion positions has been performed. This calculation mimics essentially surface adsorption vs. insertion in the bulk. The results obtained for the heat of formation are exothermic for top and bridge positions whereas hollow position and insertion are clearly endothermic. This trend is related to a change of charge transfer. When the charge transfer is from metal to hydrogen, the system is exothermic, whereas a charge transfer from hydrogen to metal leads to endothermic energy.

Point d) needs to be clarified through a systematic investigation of a complete series of transition metal hydrides. Up to now, we have results on vanadium hydride. In this case the system is exothermic with a charge transfer from hydrogen to the metal |6| which confirms our hypothesis. A complete report on a tentative correlation between the sign of the heat of formation and the sign of the charge transfer will be reported elsewhere |19|.

We have confirmed that hydrogen is exothermic against Vanadium whereas it is endothermic against iron. One interesting question to ask now is the following : how is the formation related to vanadium concentration in a $Fe_{1-x}\ V_x$ alloy.

Our calculations are restricted up to now to model periodic stacking of FeV, Fe_3V and FeV_3 structure with hcp and bcc stacking. Only results pertaining to the FeV alloy with model hcp stacking (one Fe layer followed by a layer of V...) have been completed. Parameters of the calculation are those of pure Fe and V systems |5,6|. Charge transfer is minimized by iter-

action. The FeV stoichiometric compound in the bcc phase appears to be more stable than the Fe and V isolated system.

In our hypothetical hcp system, build through a layer by layer representation, two different T sites (T_1 and T_2) are present. In site T_2, the hydrogen atom has 3Fe and 1V as neighbors ; In site T_1, the hydrogen has 3V and 1Fe as neighbors. The system with hydrogen in T_1 sites is more stable by 0.93 ev with respect to alloys with T_2 sites occupied. This result is consistent with the fact that hydrogen is endothermic against iron whereas it is exothermic against vanadium.

An hydrogen atom introduced in a lattice tends to dig its hole by pushing far away its metallic neighbors. The result is an increase of the volume of the metal. We have therefore computed the total energy of the system in terms of the dilatation of the interlayer containing the T_1 sites. We have found maximum stability of a distance of 2.17 Å whereas the Fe, V interlayer without hydrogen is separated by 2.14 Å (the c/a ratio is now equal to 1.57). We have also estimated the stability of the hydrogen atom along the C_3 axis which relies T_1, the center of the tetrahedron to the Fe atom. The lowest energy is not obtained when we increase the Fe-H distance as we would deduce at first sight through a correlation with the heat of formation, but is obtained when we move H towards Fe, along the C_3 axis. This seems to be a most interesting results which may probably related to the relative stabilities of the V-H and Fe-H molecules. More on this particular point is under present investigation.

References

1. Baranowski B., Ber. Bunsenges Phys. Chem. (1972) 76, 714.
2. Antonov V.E., Belash I.T., Degtyareva V.F., Poniatovsky E.G., Shiryav V.I., Dokl. Akad. Nauk. SSSR (1980) 252, 1384.
3. Poniatovsky E.G., Antonov V.E. and Belash I.T., Problems in Solid State Physics, eds Prokhorov A.M. and Prokhorov A.S., Mir Moscow (1984) 109.

4. Alouani M., Demangeat C. and Kulikov N.I.,
Phys. Lett. (1986) 119A, 234-236.

5. Minot Ch. and Demangeat C., J. Chem. Phys. (1987) 86, 2161-2167.

6. Minot Ch. and Demangeat C., J. Less Common Met. (1987) 130, 285-291.

7. Minot Ch. and Demangeat C., Physics of Materials, ed. M. Yussouff,
World Scien. Pub. Co., Singapore 1987.

8. Switendick A.C., J. Less. Common Met. (1987), 130 249-260.

9. Min B.I., Oguchi T. and Freeman A.J., Phys. Rev. (1986) B33, 7852.

10. Methfessel M. and Kübler J., J. Phys. F. (1982) 12, 141.

11. Alekseev E.S., Kulikov N.I. and Tatarchenko A.F.
J. Less. Common Met. (1987) 130, 261-266.

12. Andersen O.K., Phys. Rev. (1975) B12, 3060.

13. Von Barth U. and Hedin L., J. Phys. C (1972) 5, 1629.

14. McLellan R.B. and Oates W.A., Acta Met. (1973) 21, 181.

15. Kulikov N.I. and Demangeat C., Physics Reports, in preparation.

16. Fernando G.W. and Wilkins J.W., Phys. Rev. (1987) B35, 2995-2998.

17. Dreyssé H. and Riedinger R., Physics of Materials, ed. M. Yussouff,
World Scien. Pub. Co., Singapore (1987).

18. Switendick A.C., Z. Phys. Chem. N.F. (1979) 117, 89
Westlake D.G., J. less. Common Met. (1983) 93, 1.

19. Minot Ch. and Demangeat C., to be published.

PHASE TRANSFORMATIONS IN THE TITANIUM-HYDROGEN SYSTEM AT HIGH PRESSURES

I.O.Bashkin
Institute of Solid State Physics,
USSR Academy of Sciences, USSR

The well-known eutectoid T-x diagram [1] describes phase states of the Ti-H system at atmospheric pressure, i.e., solid solutions of hydrogen in the high-temperature b.c.c. β-Ti undergo the eutectoid reaction below 590 K and decompose forming the h.c.p. solid solution of hydrogen in α-Ti ($x=H/Ti \lesssim 0.1$) and the f.c.c. deficient γ-dihydride ($x \simeq 1.3$).

The α to ω transition occurs in pure titanium at high pressures [2]. So, one can suppose that this transition should result in some peculiarity in the T-P-x diagram of the Ti-H system.

In the present work we report some results concerning the T-P-x diagram of the Ti-H system and properties of the high-pressure phases in this system.

The effect of hydrostatic pressure to 27 kbar on the eutectoid temperature, $T_{eut.}$, was studied by DTA and resistance measurements on TiH_x in the composition range $0.33 \leq x \leq 0.85$ [3]. Experimental results are represented in Fig.1.

The eutectoid reaction had a hysteresis of 50 ± 20 K. There was observed a small difference in the values of $T_{eut.}$ measured using the two techniques. We explain this difference by the different character of the transformation at rapid and slow heating [3,4]. The eutectoid temperature slightly decreased when pressure was increased to 20 kbar, $dT_{eut.}/dP = -(0.4 \pm 0.4)$ K/kbar.

When pressure was increased over 20 kbar, two separate jumps of opposite signs appeared in R(T) curves instead of the anomaly

due to the eutectoid reaction. This is an evidence of a new phase region in the T-P-x diagram of the Ti-H system. The lower boundary of the discovered region has a slope of (-45 and -115)±10 K/kbar on heating and cooling, respectively. The slope of the upper boundary is 50±10 K/kbar both on heating and on cooling.

On decompression transition points in Fig.1 lay either at the line of transformation into the ($\alpha+\gamma$)-state ($T \leq 548$ K) or at the extension of the line of the high-temperature transformation on cooling (T=573 K). Hence, the equilibrium value of $T_{eut.}$ lies between 548 and 573 K.

In order to elucidate possible connection of the high-pressure phase (HPP) with a hydrogen-modified ω-phase, we performed a study of the effect of hydrogen on the α to ω transition pressure. The transition pressures were determined from the anomalies in the R(P) isotherms at quasi-hydrostatic pressures to 80 kbar and T=373 to 553 K [3].

The R(P) anomaly due to the α to ω transition at these temperatures had a form of a jump occuring in a pressure interval of 10 to 20 kbar width. Hydrogen content of x=0.13 lowered the α to ω transition pressure by 4 to 8 kbar (Fig.2). Further increase of hydrogen content resulted in a reduction of the resistance jump and a small additional decrease in the transition pressure (e.g., the maximum effect at 473 K amounted to 12 kbar).

Mutual position of lines in Fig.2 as well as shapes of the anomalies at the transition led to a conclusion that the phase region revealed at $P \gtrsim 20$ kbar is the existence region of some hydrogen-rich HPP [3,4].

Investigation of the structure and properties of the HPP was carried out on the $TiH(D)_x$ samples quenched from the region P=45 to 65 kbar and T=555 to 730 K to liquid-nitrogen temperature [6-9].

In the concentration range $x \lesssim 0.65$, quenched samples contained ω-phase which was not superconducting over 1.5 K and had the same lattice parameters as pure ω-Ti: a=4.625±0.005 Å, c=2.828±0.003Å. A small amount of the ω-phase could be discerned even at $x \simeq 0.70$.

A new phase coexisted with the ω-phase at hydrogen contents $0.13 \leq x \lesssim 0.7$. Quenched samples with $x \gtrsim 0.75$ did not contain the ω-phase. This new phase denoted as ε-phase [6,7] became superconducting at T_c=4.3±0.1 K. An orthorhombic structure with lattice parameters a=4.34, b=4.18, c=4.02 Å has been suggested for ε-$TiH_{0.71}$ [8]. Recent study [9] showed that superconducting phases of the Ti-H(D) system have an f.c.c. structure ($a \simeq 4.16$ Å) distorted to a different degree. An inverse isotope effect was displayed by the increase of superconducting temperature to T_c=5.0±0.1 K when hydrogen was substituted for deuterium. The enhancement of superconducting properties of the quenched samples is connected with the transition of interstitial H(D) atoms from tetra- to octasites of Ti sublattice [10].

The superconducting state in $TiH(D)_x$ is metastable at atmospheric pressure. A non-superconducting to 1.5 K f.c.t. δ-phase (a=4.208±0.005 Å, c=4.613±0.005 Å) was observed after heating of the quenched samples to room temperature. This phase decomposed on further heating of quenched samples to $T \gtrsim 430$ K, and the samples returned to the initial ($\alpha + \gamma$)-state.

References

1. W.M.Mueller, J.P.Blackledge, G.G.Libowitz (eds), Metal hydrides, Moscow, Atomizdat, 1973, 439 pp. - in Russian.
2. F.P.Bundy "Phase diagram of titanium under pressure", in New Materials and Methods of Research on Metals and Alloys", Moscow, Metalluggiya, 1966, 230-235 - in Russian.
3. E.G.Ponyatovsky, I.O.Bashkin, Yu.A.Aksenov "Investigation of the

phase diagram of the Ti-H system at pressures to 80 kbar and near-eutectoid temperatures" Fiz.Met.Metallovedeniye, in print.

4. E.G.Ponyatovsky, I.O.Bashkin, V.F.Degtyareva, Yu.A.Aksenov, V.I.Rashchupkin, D.N.Mogilyansky "Phase transitions in the Ti-H system at high pressures", J.Less-Common Metals, in print.
5. G.A.Lenning, C.M.Craighead, R.I.Jaffee "Constitution and mechanical properties of titanium-hydrogen alloys", Trans.Met.Soc. AIME, 1954, 200, N 1, 367-372.
6. E.G.Ponyatovsky, I.O.Bashkin, V.F.Degtyareva, V.I.Rashchupkin, O.I.Barkalov, Yu.A.Aksenov "Pressure-induced superconductivity in the titanium-hydrogen system", Fiz.Tverd.Tela, 1985, 27, N 11, 3446-3448.
7. E.G.Ponyatovsky, I.O.Bashkin "New phase transitions in hydrides of the I-A, III-A, and IV-A Groop Metals", Z.Phys.Chem.Neue Folge, 1985, 146, N 1, 137-157.
8. V.F.Degtyareva, I.O.Bashkin, D.N.Mogilyansky, E.G.Ponyatovsky "Phase transformations in $TiH_{0.71}$ and $TiH_{0.85}$", Fiz.Tverd.Tela, 1986, 28, N 6, 1698-1708.
9. I.O.Bashkin, V.Yu.Malyshev, V.I.Rashchupkin, E.G.Ponyatovsky "Composition and superconductivity of high-pressure phases in titanium hydrides", to appear in Fiz.Tverd.Tela.
10. A.I.Kolesnikov, V.K.Fedotov, I.Natkaniec, S.Habrylo, I.O.Bashkin, E.G.Ponyatovsky "Transition of hydrogen atoms into octahedral lattice sites in the superconducting phase of titanium hydride", Zh.Exp.Teor.Phys.-Pis'ma, 1986, 44, N 8, 396-398.

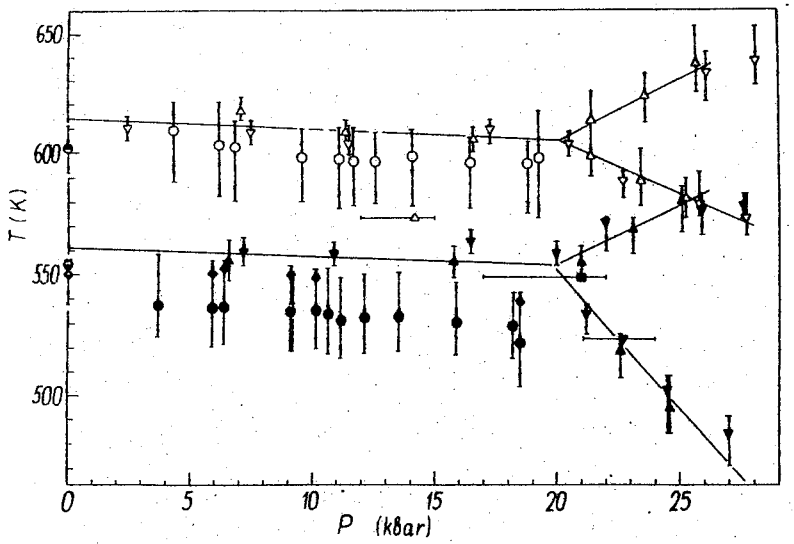

Fig.1. The T-P diagram of TiH_x hydrides in the composition range x=0.27 to 1.35.
DTA $TiH_{0.85}$: ○ , ● - the main peak and ◆ - a satellite peak. Shown are intervals of heat release. Resistance measurements: △ , ▲ - $TiH_{0.71}$; ▼ , ▽ - $TiH_{0.85}$; ■ - $TiH_{0.56}$; points at $P \gtrsim 20$ kbar correspond to the temperatures when R(T) deviated from a linear dependence. Cooling points are black. Points at atmospheric pressure correspond to DTA peaks in $TiH_{0.67}$ [5].

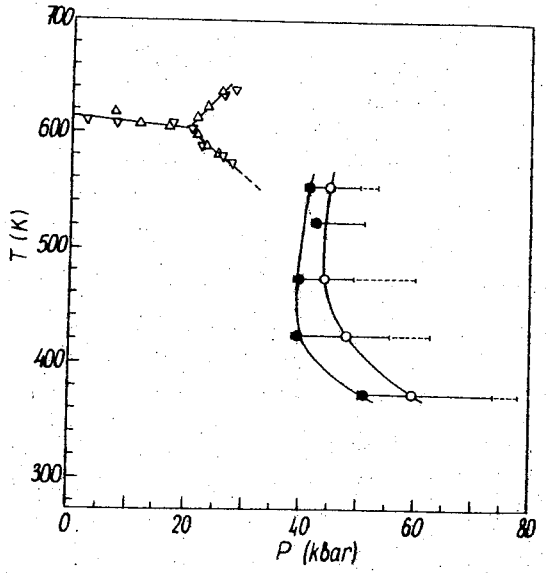

Fig.2. Some lines of the T-P-x diagram of the Ti-H system in the T-P projection.

α to ω transitions in Ti- ○ and in $TiH_{0.13}$- ●. Transition intervals are shown with solid (for $TiH_{0.13}$) an dashed (for Ti) bars. △ , ▽ - transformations in $TiH_{0.71}$ and $TiH_{0.85}$ on heating.

SOME PROBLEMS OF THE MODERN THEORY OF FREEZING

V.N. Ryzhov, E.E. Tareyeva
Institute for High Pressure Physics, Academy of Sciences, Troitsk, USSR

The first-principles description of the ordering in liquids is one of the most difficult problems of statistical mechanics. Now we present a version of the theory, recently proposed by Ramakrishnan and Yussouff [1] and the authors [2,3,4] and based on the exact nonlinear equation for the singlet distribution function (SDF) [2,3]:

$$\frac{\rho F(z_1|\Psi)}{z} = \exp\left\{-\beta\Psi(z_1) + \sum_{k\geq 1}\frac{\rho^k}{k!}\int S_{k+1}(z_1 \dots z_{k+1}) \times \right. \quad (1)$$

$$\left. \times F(z_2|\Psi)\dots F(z_{k+1}|\Psi)\,dz_2 \dots dz_{k+1}\right\},$$

where z is the activity, $S_{k+1}(z_1 \dots z_{k+1})$ is the irreducible cluster sum of Mayer functions, $\beta = 1/kT$, T -temperature, ρ - the mean number density in a volume V, $\Psi(z)$ - the external field. Using eq.(1) one can obtain pressure and activity as the functionals of SDF. For two phases to coexist in equilibrium, their temperatures, pressures and activities must be equal

$$T_1 = T_2\,, \quad P_1 = P_2\,, \quad z_1 = z_2\,. \quad (2)$$

The SDF $\rho(z) = \rho F(z)$ in the crystalline phase may be represented as follows:

$$\rho(z) = \rho_l + \Delta\rho(z)\,, \quad \frac{1}{V}\int \rho(z)\,dz = \rho_s\,.$$

Here ρ_l and ρ_s are the densities of the liquid and crystalline phases, respectively, and $\Delta\rho(z)$ has the symmetry of the lattice. Using eq.(2) we obtain the set of equations determining the ρ_l, ρ_s, $\Delta\rho(z)$. The properties of the liquid are included in thes

equations through the set of the direct correlation functions only Approximate solutions of these equations give the satisfactory agreement with experiment. $\Delta\rho(\vec{r})$ may be expanded in a Fourier series:

$$\Delta\rho(\vec{r}) = \rho_\ell \varphi_0 + \rho_\ell \sum_{K\neq 0} \varphi_K e^{iK\vec{r}},$$

where K is a vector of the reciprocal lattice. φ_0 determines the density change at the transition. From the equations it may be seen that if $\varphi_0 = 0$ then necessarily $\varphi_K = 0$. This means that for one-component classical systems there are not maxima on the curve of freezing at the P-T plane [3].

Two different broken symmetries distinguish crystalline solid from isotropic liquid: translational and rotational. These two symmetries are not independent. Rotating one patch of perfect crystal relative to another disrupts not only orientational correlations but translational correlations as well. But it is possible to imagine states of matter with long-range correlations of orientations of locally-defined crystallographic axes, having short-range translational order. The possibility of existence of such three-dimensional anisotropic states was examined in [5] by the computer simulation of Lehnard-Jones particles. In [5] it is shown that upon supercooling about 10% below the freezing temperature extended correlations between orientations of the vectors (bonds) connecting neighboring atoms appear with little or no increase of the translational correlation length. We propose the microscopic description of the transition of isotropic liquid into anisotropic phase based on eq.(1).

The long-range behaviour of the correlation function of the bond orientational order is determined by the four-particle distribution function $F_4(\vec{r}_1, \vec{r}_2, \vec{r}_3, \vec{r}_4)$ when $\vec{r}_1, \vec{r}_2$ and $\vec{r}_3, \vec{r}_4$ - two pairs of near neighbours and $|\vec{r}_1 - \vec{r}_3| = R \to \infty$.

The equation for $F_4(\vec{r}_1, \vec{r}_2, \vec{r}_3, \vec{r}_4)$ can be obtained from

eq.(1) with $\Psi(\vec{r})$ created by three particles at the points $\vec{r}_2, \vec{r}_3, \vec{r}_4$.

We shall write $F_4(\vec{r}_1, \vec{r}_2, \vec{r}_3, \vec{r}_4)$ in the following form:

$$F_4(\vec{r}_1, \vec{r}_2, \vec{r}_3, \vec{r}_4) = g(|\vec{r}_1 - \vec{r}_2|)\, g(|\vec{r}_3 - \vec{r}_4|)\,(1 + f(\vec{r}_1, \vec{r}_2, \vec{r}_3, \vec{r}_4)),$$

where $f(\vec{r}_1, \vec{r}_2, \vec{r}_3, \vec{r}_4) \to 0$ when $R \to \infty$, $g(|\vec{r}|)$ - radial distribution function. For $f(\vec{r}_1, \vec{r}_2, \vec{r}_3, \vec{r}_4)$ we have the expansion

$$f(\vec{r}_1, \vec{r}_2, \vec{r}_3, \vec{r}_4) = \sum_{mee'} B^m_{ee'}(\vec{r}, \vec{R}, \vec{\rho})\, Y_{em}(\Omega_1) Y_{e',-m}(\Omega_2),$$

where $\vec{r} = \vec{r}_1 - \vec{r}_2$, $\vec{\rho} = \vec{r}_3 - \vec{r}_4$, $\vec{R} = \vec{r}_1 - \vec{r}_3$, Ω_1 and Ω_2 are the angles of $\vec{r}$ and $\vec{\rho}$ with $\vec{R}$ respectively.

For $R \gg 1$ we have:

$$B^m_{ee'} \sim \exp(-R/R^m_e),$$

R^m_e is the correlation length. R^m_e tends to infinity when $e = 6$. The behaviour of R^m_e as a function of temperature at density $\rho = 0.973$ is shown in Figure. The instability occurs at $T = 0.54$. The computer simulation /5/ gives $T_c = 0.63$. This instability corresponds to the phase transition from isotropic to anisotropic liquid state. In this case the rotational symmetry of the pair distribution function is broken without changing the symmetry of SDF. The new phase contains some elements of icosahedral symmetry which correspond to m=5.

References

1. T.V. Ramakrishnan, M. Yussouff, First-principles-order-parameter theory of freezing. Phys.Rev.B., 1979, v.19, N5, p.2775--2794.
2. V.N. Ryzhov, E.E. Tareyeva. Towards a statistical theory of freezing. Phys. Lett., 1979, v.75A, N1,2 ; p.88-90.
3. V.N.Ryzhov. Some problems of the theory of phase transitions in molecular crystals. Thesis, Dubna, 1981, 150 p.
4. V.N. Ryzhov. Statistical theory of freezing of classical systems. Theor. Math. Phys. (USSR), 1983, v.55, N1, p.128-136.
5. P.J. Steinhardt, D.R. Nelson, M. Ronchetti. Bond-orientational order in liquids and glasses. Phys. Rev. B., 1983, v.28, N2, p.784-805.

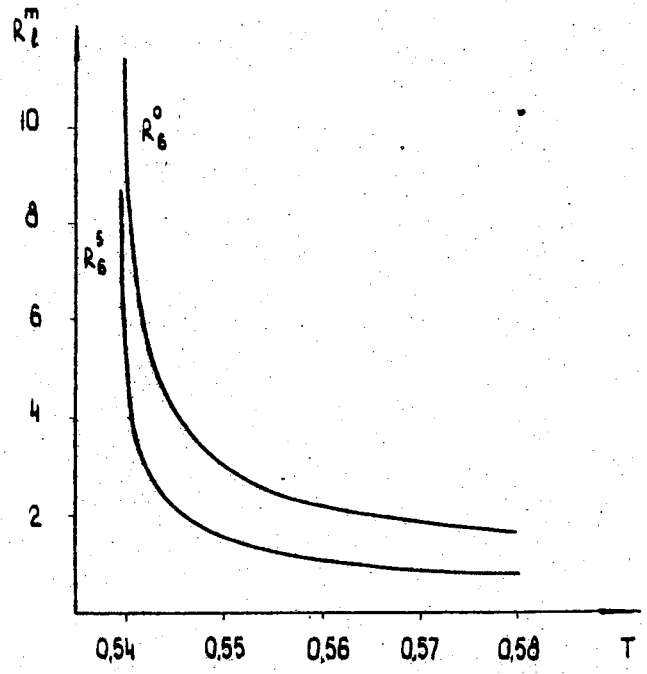

Temperature dependence of R_1^m.

Pressure induced phase transition in quasicrystalline Al-18 a/$_o$ Fe

Mohammad Yousuf*, V.S. Raghunathan*, N.V. Chandra Shekar*, S. Baranidharan† and E.S.R. Gopal+

*Indira Gandhi Centre for Atomic Research, Kalpakkam 603 102, India

+Physics Dept., Indian Institute of Science, Bangalore 560 012, India

Abstract. Electrical resistivity of quasicrystalline (qc) Al-18 a/$_o$ Fe indicates a reversible sharp drop at 57 ± 2 kbar. The pressure effect on the crystalline (c) state of the alloy is remarkably similar. That is, a sharp and reversible resistivity drop occurs at 65 kbar. We argue that the transition is electronic in origin.

QC phase is metastable and is having an aperiodic atomic arrangement, the effect of pressure on these system is expected to be interesting [1]. We report our high pressure electrical resistivity studies. Our principal results are: (1) The qc alloy undergoes a reversible transition at 57 kbar,(2) This phase exhibits a hierarehy of resistivity drops,(3) The The c phase exhibits remarkably similar behaviour, for instance, there is a large electrical resistivity drop at 65 kbar.

Fig. 1 indicats a continuous variation of electrical resistivity of qc Al-18 a/$_o$ Fe under pressure. Initially the resistivity decreases gradually. Above 20 kbar, the resistivity of the qc phase becomes almost insensitive to the pressure variation. However, above 57 kbar, the resistivity undergoes a steep drop. Moreover, it is observed that the resistivity drop is associated with a series of small steps causing a hierarehy of changes. The interesting past of the experimental result is its reversible nature associated with a hysteresis. The hierarchy of changes in resistivity is conspicuously absent during the unloading

cycle. When repressurized, the qc sample reproduces the steep decrease in resistivity alongwith the same hierarchy of changes. Experiments have also been performed on the c Al-18 a/$_o$ Fe to understand more about the observed pressure effect in the qc phase. Although the electrical resistivity of the c phase is smaller by a factor of 5, the reversible transition is indeed noticed at 65 $\pm$ 2 kbar as shown in Fig. 2. It is worth noting at this point that the hierarchy of transitions observed in the qc phase are absent in the c phase.

It has been argued that an appropriate candidate for yielding qc phase on rapid solidification is that alloy which has an inherent tendency to form icosahedral clusters in their crystalline state. As a consequence the local atomic arrangement and hence the local electronic structure in the qc phase must resemble those in the c phase. It then follows that the similarity of transitions in the two phases must be ascribed to the influence of pressure on the local atomic rearrangement and the ensuing changes in the electronic structure.

Comparing the high pressure behaviour of qc and c phases of Al-18 a/$_o$ Fe, it is noticed that the resistivity drop occurs in similar range of pressure (57-70 kbar). A well accepted model for qc Al-Mn is the one based on Mackay icosahedron following the atomic distribution in the c Al-Mn-Si phase. Similar attempts have been made to model the decagonal phase of Al-Fe. In the c $Al_{13}Fe_4$, the Fe atoms are surrounded by Al atoms, so that the d elctrons are localised on Fe atoms, consequently the d bands are extremely narrow and lie very close to the Fermi energy. This leads to a strong resonant scattering of the conduction electrons and results in a large contribution to the resistivity. This contribution will be similar in magnitude for both qc and c phases. The

high resistivity of the qc phase is therefore expected to be due to defects.

It is pertinent to consider Ce and other RE in which similar anomalies under pressure is found. The RE'S are endowed with extremely narrow f levels which delocalise under pressure. Recalling the fact that the d levels in the subject alloy are also extremely localise, explanation pertaining to RE's can automatically be aplied here. Finally, we point out that the efforts at developing structural models of qc phase based on the local atomic arrangements in the c phase is conclusively justified by the observed similarities of the electronic transitions in the two states.

One of us (MY) is grateful to Padmabhushan Shri C.V. Sundaram, Dr. P. Rodriguez and Dr. K. Govinda Rajan for their continuous encouragement.

References

1. Victor Jaya, Mohammad Yousuf, V.S. Raghunathan and S. Natarajan "High Pressure x-ray studies of quasicrystals Al-18 a/$_o$ Fe"
J. Phys. F. 1987, 17, L225-7.

2. Victor Jaya, Mohammad Yousuf, V.S. Raghunathan and S. Natarajan "Effect of pressure on the d spacings of the qc Al-18 a/$_o$ Fe"
Pramana: Rapid communication (To appear).

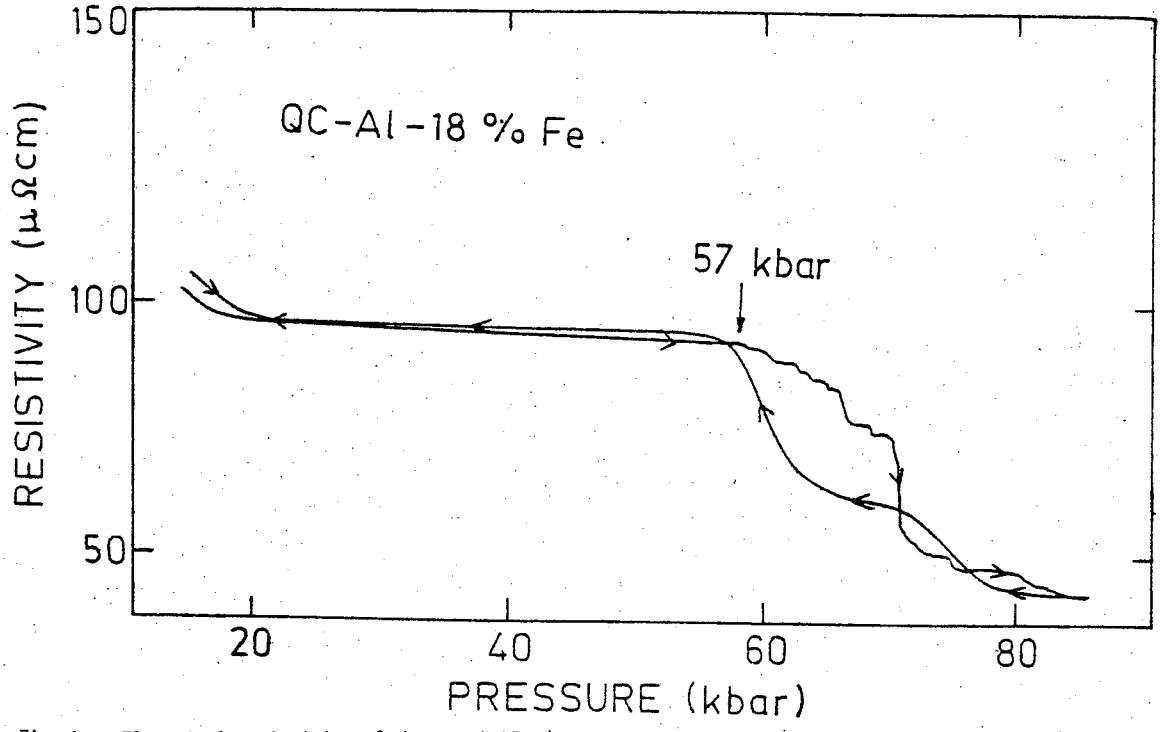

Fig. 1 . Electrical resistivity of the qc Al-18 a/$_o$ Fe vs pressure.

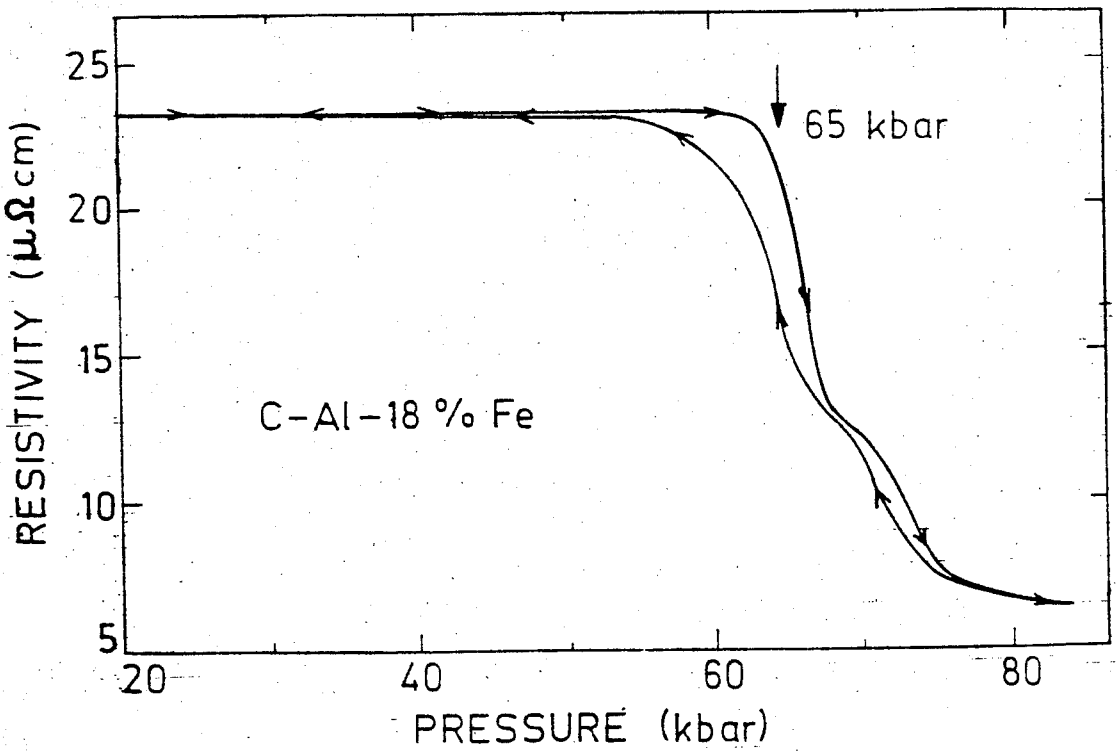

Fig. 2 . Electrical resistivity of the c Al-18 a/$_o$ Fe vs pressure.

NEUTRON STRUCTURE INVESTIGATIONS OF SOLID HYDROGEN UNDER PRESSURE

V.A. Sukhoparov[1], A.S. Telepnev[1], G.V. Kobelev[1], R.A.Sadykov[1], S.N. Ishmaev[2], I.P. Sadikov[2], A.A. Chernyshov[2], B.A.Vindriaevskiy[2]

[1]L.F.Vereshchagin Institute of High-Pressure Physics, Academy of Sciences of the USSR, Troitzk, USSR

[2]I.V.Kurchatov Institute of Atomic Energy, Moscow, USSR

Parahydrogen as well as orthodeuterium are the thermodynamically stable modifications of molecular hydrogen at low temperatures. These molecules are spherically symmetric and isotropic central intermolecular interaction predominates in cryocrystals formed from them. Being the simplest molecular crystals, these cryocrystals possess quantum properties: the amplitudes of zero-point vibrations constitute a noticeable fraction of the crystal lattice period. Therefore they seem to be expanded and have a high compressibility. The hydrogen isotopes are noticeably different in mass, so that the comparative study of their properties under pressure leads to better understanding of the role of zero-vibrations and of the interaction potential over rather wide range of intermolecular distances.

The possibility of polymorphous phase transitions was of great interest and was the topic of much discussions [1]. The direct structural investigations of solid hydrogen under pressure were carried out with the aim to solve this problem. The comparative analysis of results for light and heavy isotopes enables the prediction of the equations of state of solid deutero-hydrogen and tritium.

The investigations were carried out on two beams of pulsed neutron source from the LINAC "Fakel" (I.V.Kurchatov Institute of Atomic Energy). The experimental facility consists of: 1) the gas system for the sample preparation and its preliminary pressurization (the gas purification unit, the ortho-para-converter, the thermo- and the membrane compressor) ; 2) the hydraulic press ; 3) the special cryostat enabling the pressurization of hydrogen samples in piston-cylinder chamber at temperatures T=10 ÷ 300 K ; 4) the gas-type pressure cell (0÷600 bar) ; 5) various pressure cells (V =0.7÷15 ccm, P=0.4÷25 kbar) ; 6) the safety system for work with hydrogen under high pressure.

There is a set of neutron spectrometers on both beams. It is possible to measure the total interaction cross section, diffraction and inelastic neutron scattering on one sample simultaneously using the whole spectrum of neutrons and the time-of-flight technique. In detail the experimental technique has been described in [2-5].

The observation of structural phase transformations especially at low temperatures can be complicated by slow kinetics of processes. In order to remove this uncertainty we used various means of preparing the specimen, up to its melting under pressure and subsequent cooling at various rates. In the pressure range 0÷25 kbar and at T=4.2÷120 K, crystals of parahydrogen and orthodeuterium have the hexagonal close-packed structure. No o t h e r p h a s e was detected.

Up to 6 reflections could be resolved reliably. The relative widths of diffraction peaks didn't change with pressure. This significes the uniformity of its distribution throughout the specimen volume. The crystal lattice parameters of hydrogen isotopes as a function of pressure were determined ; and it can be concluded that c/a ratio is practically constant and is close to the ideal value [5,6].

The lattice parameters were determined at $T/T_m \leq 0.3$ where thermal expansion is negligible so that the experimental equations of state for parahydrogen and orthodeuterium correspond to T=0. The P(V)-dependence, obtained experimentally, was approximated by the Birch expression: $P(V)=\left(\frac{V_0}{V}\right)^{5/3}\sum_{n=1}^{3} A_n\left[\left(\frac{V_0}{V}\right)^{2/3}-1\right]^n$, where $A_1=\frac{3}{2}B_0$, $A_2=\frac{9}{8}B_0(B_0'-4)$ and V_0, B_0, B_0' -resp. molar volume, bulk modulus and its pressure derivative at P=0. They are

	V_0,cc/mole	B_0,kbar	B_0'	A_1,kbar	A_2,kbar
p-H_2	23.00±0.02	1.86±0.03	7.0±0.2	2.79±0.03	6.33±0.20
o-D_2	19.93±0.02	3.35±0.05	6.9±0.2	5.02±0.08	10.8±0.2

All the parameters were determined experimentally without additional data, as opposed to other equation of state measurements.

It should be noted that the values of $B_0'=7.0\pm0.2$ for classical cryocrystals of inert gases and for quantum cryocrystals (isotopic modifications of helium and hydrogen) are the same notwith-

standing different interaction potentials ; consequently the law of corresponding states is applicable. The information for contribution of zero vibtations may be obtained from comparison of equations of state of two isotopes, masses of molecules being different twice as much. Supposing that the interaction potential is identical for all isotopes and estimating the contribution of zero-point energy in harmonic approximation we get experimentally undetermined equations of state of other solid isotopes of hydrogen with parameters:

V_0=20.96 cc/mole, B_0=2.71 kbar, B'_0=6.9 - for deuterohydrogen ;

V_0=18.86 cc/mole, B_0=4.23 kbar, B'_0=6.8 - for tritium.

It follows from our results that the minimum of the lattice potential energy for hydrogen isotopes occurs at $V=V_S$=15.6 cc/mole, which is appreciably less than their equilibrium values at P=0. The value of the hydrogen bulk modulus at $V=V_S$ (B_S = 11.2 kbar) is comparable with typical values for the solid inert gases at P=0. The zero-point vibrations thus expand the lattice appreciably and determine the main differences in compressibility of the solid isotopes of molecular hydrogen.

References

1. Mills R.L. "The case of phantom phases in solid hydrogen". J.Low Temp.Phys., 1979, v.36, n.1, pp.231-245.
2. Vindryaevskiy B.A., Ishmaev S.N., Sadikov I.P. et al. "Facility at linac "Fakel" for neutron studies of solid hydrogen under high pressure". Preprint IAE-3122, Moscow, 1979, p.29.
3. Vindryaevskiy B.A., Ishmaev S.N., Podshibiakin V.D. et al.- "Cryostat for neutron studies under pressure at low temperatures" - Pribory i technika eksperimenta, 1980, n.4, pp.225--230.
4. Vindryaevskiy B.A. Ishmaev S.N., Sadikov I.P., Chernyshov A.A. "Neutron facility at linac "Fakel" for structure and dynamic studies in solids under high pressure". - Nucl.Instr. and Meth., 1981, v.180, n.1, pp.79-87.
5. Ishmaev S.N., Sadikov I.P., Chernyshov A.A. et al. "Neutron studies of solid hydrogen structure at pressure up to 24 kbar". -Zh.Exper. i Teor.Fiz., 1983, v.84, pp.394-403. Sov.Phys. JETP, 1983, v.57, p.228.
6. Ishmaev S.N., Sadikov I.P., Chernyshov A.A. et al. "Neutron diffraction on solid orthodeuterium at pressure up to 25 kbar". -Zh.Exper. i Teor.Fiz., 1985, v.89, n.4 (10), pp.1249-1257. Sov.Phys.JETP, 1985, v.62, n.4(10), pp.721-726.

HIGH PRESSURE EFFECT ON PHASE TRANSITIONS IN FERROMAGNETS AND FERROELECTRICS

E.A.Zavadskii
Physico-Technical Institute of the Ukrainian Academy of Sciences, Donetsk, USSR

The development of high pressure technology makes it possible to study such properties of substances which are not realized at atmospheric pressure. Though the high pressure region is very diverse it still covers only a part of possible states. Those states which were "hidden" in the region of negative pressures remained unaccessible to experimentators up to now. At present, however, there are undeniable proofs showing that the magnetic (electric) field can induce, at atmospheric pressure, those magnetic (electric) states which should spontaneously appear only in the negative pressure region. This became possible by changing the conditions of phase stability in external fields. The accumulated data on this matter are presented in monographs and review papers [I-6].

The magnetic (electric) field is known to shift the boundaries of the first order phase transition. It is easy to show that the temperature of the phase transition between states I and 2 is determined by a relationship

$$T = T_0 + \frac{P(V_2 - V_1)}{S_2 - S_1} - \frac{H(M_2 - M_1)}{S_2 - S_1},$$

where V_i, M_i and S_i denote the i-th phase volume, magnetization and entropy, respectively.

It is quite obvious that T_K changes in the field. But it is also obvious that at the fixed transition temperature the ap-

plication of a field is equivalent to the pressure change. In fact, the phase transition temperature does not change if condition

$$P = H(M_2 - M_1) / (V_2 - V_1)$$

is fulfilled.

Depending on the sign of the volume change at the transformation the transition boundary shifts towards either positive or negative pressures.

Let us assume that state I is a corresponding paramagnetic phase and state 2 is a ferromagnetic one. Then $V_2 - V_1$ determine spontaneous magnetostriction. Since in a ferromagnet with the positive spontaneous striction the Curie temperature decreases under the action of pressure, at $dT_K / dP < 0$ the magnetic field should shift the phase transition boundary towards the pressure increase and at $dT_K / dP > 0$ backwards.

It was shown [2,3] that in practice the phase boundaries can be shifted more than IO kbar. Within an intermediate region separating the initial and final states of the system the magnetic field can induce a ferromagnetic phase. Once appeared, this phase remains existing for an infinite period of time [3]. Induction fields are the functions of temperature and pressure and can be adjusted by changing the composition of specimens [2]. The most interesting are those substances in which the boundary of the spontaneous appearance of the ferromagnetic phase is located within the negative pressure region and the boundary of its disappearance is located within the positive pressure region. In this case even a short-time application of the magnetic field causes irreversible appearance of a new state of the substance which cannot be induced by any other means.

If in the high pressure magnetic phases $dT_K/dP>0$, in the high field the boundaries of these phases shift towards low-

er pressures therefore they can be induced even at the atmospheric pressure.

Classification of possible P-T diagrams, criteria and mechanisms of induction are described in the monograph [3].

In ferroelectrics the boundaries of the first-order phase transition are shifted by the electric field. Since transitions from the ferroelectric (FE) phase to the antiferroelectric (AFE) phase are also of the first order a possibility appears to draw an analogy between the induction of a magnetic phase by the magnetic field and the induction of a "hidden" FE phase by the electric field. In [4,5] an investigation was carried out of phase transitions in solid solutions of lead-lanthanum zirconate-titanate (LLZT) over a wide range of solid solution components under the action of strong electric fields and high hydrostatic pressures.

It was shown experimentally that substitution of lead by lanthanum results in broadening of AFE-states towards lead-titanate concentration increase. Between the FE- and AFE-states a region of FE induction has been found. From the analysis of experimental and calculated P-T-diagrams the metastable character of the FE-states in this region is proved.

Interaction of the regions with the FE and AFE-type of ordering coexisting below the Curie point and mechanical stresses inherent to systems with coexisting phases determine an abnormally big smearing of paraelectric phase transitions. The obtained results permit to explain, from one stand, all peculiarities of phase transitions in the LLZT system in terms of FE-AFE phase transitions.

Experimental revealing of the "hidden" phases stimulated an investigation of conditions at which these states become stable. Such investigations are carried out in two directions. The first

one is the study of the very process of induction of new states by the field, and the other one is connected with the analysis of probable mechanisms of the induced transformation.

The main conditions of inducing "hidden" phases are found. Methods of determination of lability boundaries of these states are developed. As for probable mechanisms of the induced transformations only the main ones have been outlined at present. But we hope that the revealed mechanisms will be further developed and the effect itself will be more completely described.

References

I. Kuzmin E.V., Petrakovskii G.A., Zavadskii E.A. Physics of magnetically ordered substances. - Novosibirsk: Nauka,1976.-222p.

2. Zavadskii E.A., Valkov V.I. In: High pressure physics. Kiev: Naukova dumka, 1979, - C.69-91.

3. Zavadskii E.A., Valkov V.I. Magnetic phase transitions. - Kiev : Naukova dumka, 1980. - 196 p.

4. Zavadskii E.A., Ishchuk V.M. Nature of metastable states in lead-lanthanum zirconate-titanate.-Donetsk,1984.-60p.(Preprint/Ukr.Acad.Sci.,Donetsk Physico-Technical Institute;N84-13(88)).

5. Zavadskii E.A., Ishchuk V.M. Metastable states in ferroelectrics.-Kiev: Naukova dumka,1987.-C.256.

6. Galkina E.G., Zavadskii E.A., Kamenev V.I., Yablonskii D.A. On the nature of the first order phase transition in manganese arsenide.-Donetsk,1983.-52p.(Preprint/Ukr.Acad.Sci., Donetsk Physico-Technical Institute; N83-8(63)).

DETERMINATION of the THERMODYNAMIC PROPERTIES under HIGH PRESSURE

L.N.Dzhavadov and Ju.I.Krotov
The Institute for High Pressure Physics of the USSR Academy of Science, Troitsk, USSR

The method of adiabatic compression (decompression) at small pressure change is attractive meaning the possibility to study the thermodynamic properties behaviour - the knowledge of $\left(\frac{\partial T}{\partial P}\right)_S$ as function of pressure and temperature allows to determine T - P dependences of C_p, S, $\left(\frac{\partial V}{\partial T}\right)_P$, θ [1,2]. The account may be carry out in general case and also using the corresponding states law approximation ($C_V = f(\frac{T}{Q})$).

General case. Let's assume the temperature dependence of heat capacity at normal pressure, $C_p(T,0)$, and values of $\left(\frac{\partial T}{\partial P}\right)_S$ in some T - P field adjacent to axis P=0 to be known. For calculation of C_p at given T and P the adiabat maintaning selected T and P is determined and then the change of heat capacity along this adiabat is calculated. In corresponding states law approximation C_V remains constant along the adiabat consequently in real case the task will be redused to calculation of small correction.

In experiment the measurement of ΔT is made under adiabatic conditions at finite value of ΔP. The derivative $\left(\frac{\partial T}{\partial P}\right)_S$ is determined as ratio $\frac{\Delta T}{\Delta P}$ and that is the average value in ΔT - ΔP field however the initial and final points on T - P diagram belong just the same adiabat. Consequently the adiabat covering the pressure interval exceeding ΔP may be constructed by simulation the experiment in which

the temperature and the preasure afer eacn pressure jump become initial for the next step. The values of $\left(\frac{\partial T}{\partial P}\right)_S$ for each atep at succesive construction of adiabat must be taken in the middle of the specified $\Delta T - \Delta P$ field. The dividing axis P by equal intervals of ΔP the adiabat begining from T_o (P=0) may be determined as follows:

$$T(P) = T_o + \Delta P \sum_{i=1}^{N} J_{si} ,$$

where J_{si} ($J_s=\left(\frac{\partial T}{\partial P}\right)_S$) is taken at $P=P_{i-1}+\frac{1}{2}\Delta P$ and T which is found from equation:

$$J_s\left(T, P_{i-1}+\tfrac{1}{2}\Delta P\right) = 2\,\frac{T - T_{i-1}}{\Delta P} .$$

The experimental data necessary to construct the family of adiabats are temperature dependences of J_s along isobars $P_{i-1}+\frac{1}{2}\Delta P$ where i=1,2,3...N.

The change of heat capacity along S=Const. line may be written as follows:

$$\left(\frac{\partial C_p}{\partial P}\right)_S = -T C_p \left(\frac{\partial j_s}{\partial T}\right)_P , \qquad (1)$$

where the designation $j_s=\frac{1}{T}J_s=\frac{1}{T}\left(\frac{\partial T}{\partial P}\right)_S$ is used. After integration one obtaines:

$$\ln \frac{C_p(T_1, P_1)}{C_p(T_o, 0)} = -\int_0^{P_1} T\left(\frac{\partial j_s}{\partial T}\right)_P dP .$$

Thus C_p (and consequently $\left(\frac{\partial V}{\partial T}\right)_P$) may be calculated at given T and P. If the volume is known as function of pressure at some fixed temperature T_r it is possible to calculate the full equation of states:

$$V(T, P) = V(T_r, P) + \int_{T_r}^{T} j_s(T, P) C_p(T, P)\, dT .$$

At presence of first order phase transition the change of entropy jump, ΔS_{tr}, along the equilibrium line is determined by equation:

$$\frac{d\Delta S_{tr}}{dP} = \frac{1}{T}\left\{\Delta C_p \frac{dT}{dP} - \Delta\left(J_s C_p\right)\right\} .$$

The accuracy of the calculate thermodynamic functions is determined mainly by values $\left(\frac{\partial j_s}{\partial T}\right)_P$ i.e. by difference $C_p(T_o,0)-C_p(T,P)$ where T_o, T, and P belong to the same adiabat. Thus for a "simple" object (C_v is function of $\frac{T}{\theta}$) the change of C_p along S=Const. line will be obviously smaller then C_p-C_v and at ~10% accuracy of $\left(\frac{\partial j_s}{\partial T}\right)_P$ the error of the ratio $C_p(T,P)/C_p(T_o,0)$ will not exceed ~0.5% as for majority solids the difference C_p-C_v does not exceed ~5% of C_v. The accuracy of adiabats constraction in first approximation will be:

$$\Delta T(P) \sim \left[T(P) - T_o\right] \frac{\Delta J_s}{J_s} ,$$

which for the error of J_s ~ 2 ÷ 3% gives 1 - 3 K at P~ 5.0 GPa. In this case the relative errors of computing C_p and $\left(\frac{\partial V}{\partial T}\right)_P$ will exceed the relative error of $C_p(T,0)$ by not more than ~ 0.5%(C_p) and ~ 3% ($\left(\frac{\partial V}{\partial T}\right)_P$).

The corresponding states law approximation. It can be shown that the ratio $\frac{T}{\theta}$ and consequently C_v are constant along adiabat if C_v is function of $\frac{T}{\theta}$ and characteristic temperature, θ , depends only upon volume. The characteristic temperature, in particular Debye temperature, alters at compression in the same extent as the temperature T along the adiabat does. Consequently if $j_s(P)$ is known one can calculate the pressure dependence of θ :

$$\ln \frac{\theta(P)}{\theta(0)} = \int_0^P \frac{C_p}{C_v} j_s dP .$$

To estimate thermodynamic properties in $C_p=C_v$ approximation following (1) the function $J_s(T,P)$ can be presented in form: $J_s(T,P)=T\varphi(P)$ i.e. in this case it is sufficient to known the presure dependence of J_s only at single temperature.

In present the experimental technique allowes to carry such experiments in pressure range up to 3.0 GPa and temperature range from 300 K to 700 K[3,4]. Fig.1 represents an example of the thermodynamic properties of Indium determined by this method.

The high pressure cell containes sample, heater, and temperature and pressure gauges. This assembly permits also to determine the phase transition lines both by thermal analysis (using the temperature dependense of heater resistance for temperature control and derivation of the registered signal with an operating amplifyer which provides sufficient sensitivity without any etalone and auxiliary thermocouple, Fig.2) and by "thermo-baric" analisis (registering the exess pressure in the cell during the heating which is a sensitive indicator of volume change at phase transition).

References

1. Dzhavadov L.N., "Pressure Dependence of Heat Capacity and Thermal Expansion of Stroncium", Fizika tverdogo tela, 1985, 27, II, pp.3310-3314.
2. Backstrem G., Ross R.G., "Specific Heat Capacity of Solids under Pressure from Measurement of $\left(\frac{\partial T}{\partial P}\right)_S$ ", International Journal of Thermophysics, 1985, 6, I, pp.101-105.
3. Boehler R., "Melting Temperature, Adiabats, and Gruneisen Parameter of Lithium, Sodium and Potassium versus Pressure", Phys. Rev. B: Condensed Matter, 1983, 27, II, pp.6754-6762.
4. Dzhavadov L.N., Krotov Ju.I., "Measurement of $\left(\frac{\partial T}{\partial P}\right)_S$ for Solids and Liquids under Pressure up to 3.0 GPa", Prib. i techn. exper., 1985, 3, pp.168-171.

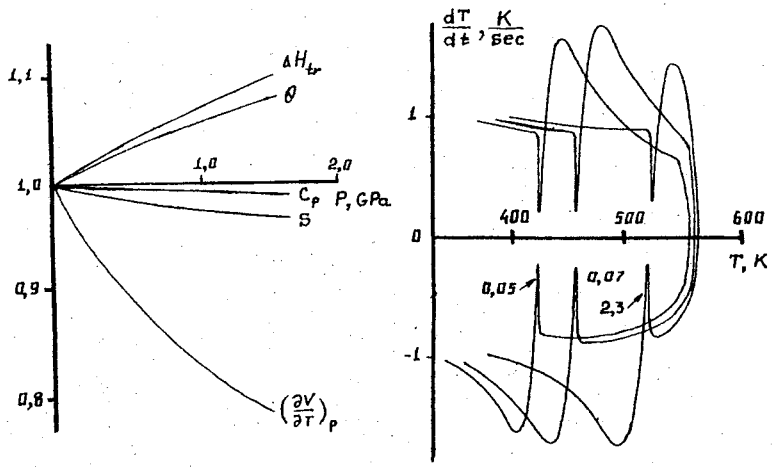

Fig.1. Relative cnanges of the thermodynamic properties of Indium at T=295 K. ΔH_{tr} - entalpy of melting as function of pressure along melting line.

Fig.2. Thermograms of melting and crystalization of Indium at pressures 0.05, 0.7 and 2.3 GPa.

A STUDY OF PHASE P-T DIAGRAM OF Rb_2ZnBr_4 BY NQR METHOD

I.P.Aleksandrova, E.V.Shemetov, V.L.Serebrennikov
L.V.Kirensky Institute of Physics, USSR Academy of Sciences, Siberian Branch, Krasnoyarsk, USSR

It is common knowledge that /I/ the temperature dependences of NQR, NMR, and ESR lineshapes within the high temperature region of incommensurate phase (I_c) of crystals K_2SeO_4, Rb_2ZnCl_4, Rb_2ZnBr_4 and $\{N(CH_3)_4\}_2ZnCl_4$ are well described by the model of reference phase lattice modulated by the plane wave (MPW). The spectra in the low temperature region of the I_c-phase are described within approximation of phase solutions lattice (PSL). In this region there are regularly alternating nearly commensurate domains of phase (F) to which the "lock-in" transition occurs at T_c, and solitons(walls), where the phase of the order parameter changes abruptly. MPW model predicts continuous variation of the modulation wave vector $q_\delta = (1-\delta)c^*/3$ when it approaches the "commensurate" value $q_s = c^*/3$ of the F-phase in T_c. This is confirmed by diffraction data /2-4/ on Rb_2ZnCl_4 and K_2SeO_4, as well as direct observation of the phase soliton lattice in Rb_2ZnCl_4 near T_c /5/. Meanwhile results of works on diffraction /6-8/ speak for q_δ to be equal to const in Rb_2ZnBr_4 up to 210 K, where the slope of the straight line changes and at T = 190 K δ rapidly falls to 0. The temperature dependence q_δ was assumed /7/ to be discrete and $\gamma = q_\delta/2\pi c^* = U/V$ (U and V are intergers) successively take values: 3/11; 5/17; 5/23; 9/29; 11/35 at $T \to T_c + 0$. This is consistent with the famous idea of the "devil staircase" /9/: instead of a single whole incommensurate phase there is a succession of narrow temperature regions of commensurate long periodical structures. Neutron-diffraction investigation of the modulated phase of Rb_2ZnBr_4 /8/ revealed coexistense of at least three modulations: 5/17 over the whole region from T_i to T_c, 11/37 and 7/23 near T_c. Besides, the odd-odd values of U and V were selected having in mind the maintenance of the F-phase point symmetry in the succession of the modulated phases, which by /10/ is not compulsory.

As the width of a single component of frequency distribution is finite, at V > 10 (V determines the cell multiplicity) the NQR spectrum of a long periodical commensurate structure is hardly distinguishable from the continuum distribution of frequencies limited by singularities, which is characteristic for the really incommensurate phase. As in the succession of long periodical structures pointed out in /7, 8/ V grows, in the NQR spectrum approaching $T_c + 0$ there should be smoother overlapping continuum distributions. The discrete spectrum is to be registered only below T_c for the structure with $\gamma = 1/3$ (F-phase).

In our first work /11/ the NQR spectra of ^{81}Br and ^{79}Br were recorded with the temperature pitch 5...10 K far from the phase transitions and ~2 K near the transitions. Obviously, Rb_2ZnBr_4 NQR spectra are to be thoroughly investigated especially at the temperatures $T < T_c + 30$ K. Applying pressure in the region of the expected "devil staircase" will probably expand the temperature interval of the existence of some phase at the others expense, thus making their observation easier.

The previous work /11/ recorded 12 lines of NQR of ^{81}Br and ^{79}Br in the vicinity of T_c. Under the conditions of this experiment in the NQR spectrum below 205 K at the background of continuum distribution there were selected 12 lines (F) with intensities increasing sharply in the vicinity of T_c, and a group of lines (H) with intensities reaching their maxima in the temperature range 192-190 K. Within the pressure range up to 250 MPa lines F and H coexist, and not only in the region of the modulated phase, but below T_c too. The intensities of the lines of group H grow continuously as the pressure increases, and over 250 MPa the spectrum consists of discrete lines H only (Fig.1). The lines of this group correspond to some high pressure phase (HPI). With the spectrum of about 500 MPa the NQR spectrum changes again: there are only four intensive singlet lines observed. The phase transition into the high pressure second phase (HPII) is the first order transition. Fig.2 shows phase P-T diagram of Rb_2ZnBr_4.

The assumption that in the range where q_δ = const the incommensurate phase of Rb_2ZnBr_4 is in fact a long periodical structure with $\gamma = 5/17$ does not contradict the data of NQR spectra /1/. Both high pressure phases are periodical structures having small values of V, as the observed spectrum is discrete. At atmospheric pressure it is possible to isolate a temperature range from T_c to T_H ($T_H > T_c$) where H lines are of the highest intensities. As the pressure rises T_H increases and there forms a line of phase diagram limiting HPI phase (Fig.2). The temperature difference between T_H and T_c at atmospheric pressure is comparable to the one cited in /12/ for two successive transitions.

In the vicinity of ~ 3 K over T_c main intensity of the spec-

trum is concentrated in the lines forming at $\delta \to 0$ of the ferroelectric structure, which is in accordance with our interpretation suggested in [1,11]. In the vicinity of T_c our data do not exclude formation of modulations I (5/17) and II (11/37) [8] which are to emerge in the spectra as continuum distributions. Modulation III, containing the "staircase": 7/23; 9/29 and 11/35 [8], corresponds, to our mind, to continuous diminishing of δ parameter of the wave vector $q_\delta = (1-\delta)c^*/3$ below $T=T_c+3$ K.

In Fig.2 the dash line indicates the lines of the phase diagram obtained from dielectric measurements [13]. An important feature of this diagram distinctive of our data is the existence on it of a triple point at P=60 MPa and T=190 K. Measurements at atmospheric pressure showed that the more imperfect is the sample, the wider is the interval between T_H and T_c. The possibility that some impurities can shift the triple point into the region of negative pressures can't be ruled out. In this case only the NQR lines of IV phase [13] (in our denotations - phase HPI) are observed in the spectrum.

References

1. I.P.Aleksandrova, chap.V, R.Blinc et al., chap.IV, in "Incommensurate phases in dielectrics", I.Fundamental, ed.by R.Blinc and A.P.Levanyuk, North-Holland, Amsterdam-Oxford-New York-Tokyo, 1986, p.143-308.
2. M.Iizumi, J.D.Axel, G.Shirane, K.Shimaoka, Phys.Rev., 1977, vol.B15, No.9, p.4392-4411
3. K.Gesi, M.Iizumi, J.Phys.Soc.Jap., 1979, vol.46, No.2,p.697-698
4. J.M.Perez-Mato, G.Madariuga, Solid State Commun., 1986,vol.58, No.2, p.105-109.
5. H.Bestgen, Solid State Commun., 1986, vol.58, No.3, p.197-201.
6. C.J. de Pater, J.D.Axel, R.Currat, Phys.Rev., 1979, vol.B19, No.9, p.4684-4689.
7. A.C.R.Hogevrost, P.M.de Wolff, Solid State Commun., 1982, vol.43, No.3, p.179-182.
8. M.Iizumi, K.Gesi, J.Phys.Soc.Jap., 1983, vol.52, No.7, p.2526-2533.
9. S.Aubry, in "Solitons and Condensed Matter", Solid State Sciences, vol.8, p.264, ed. by A.Bishop and T.Schneider, Springer, Berlin, Heidelberg, New York, 1978.
10. V.A.Golovko, A.P.Levanyuk, Physika Tverdogo Tela, 1981, vol.23, No.10, p.3170-3178.
11. I.A.Belobrova, I.P.Aleksandrova, A.K.Moskalev, Phys.Stat.Sol. (a), 1981, vol.66, No.1, p. K17-K20.
12. R.P.A.R.van Kleef, Th.Rasing, J.H.M.Stroelinga, P.Wyder, Solid State Commun., 1981, vol.39, No.3, p.433-437.
13. K.Gesi, Ferroelectrics, 1985, vol.63, p.413-421.

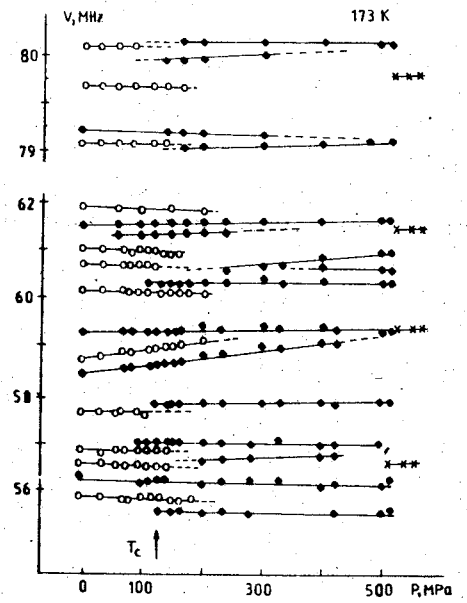

Fig. I. Isothermal dependence of frequencies of Br NQR spectrum lines in Rb_2ZnBr_4 at 173 K: O are spectrum lines recorded in work /II/; ◆ are the lines never observed before in the NQR spectrum.

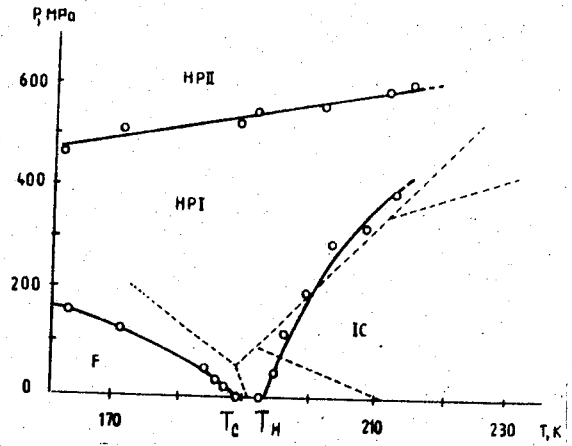

Fig.2. Phase P-T diagram of Rb_2ZnBr_4 in the region of temperatures and pressures under investigation.

PHASE DIAGRAMS AND PHYSICAL PROPERTIES PECULIARITIES OF $A_2^{IV}B_2^VC_6^{VI}$ GROUP CRYSTALS UNDER HIGH PRESSURES

E.I.Gerzanich, A.G.Slivka, P.P.Guranich, V.S.Shusta
Uzhgorod State University, Uzhgorod, USSR

$A_2^{IV}B_2^VC_6^{VI}$ crystals belong to ferroelectric-semiconductors family with displacive phase transition (PT) and $C_{2h}^5 \rightleftarrows C_S^2$ symmetry. They include $Sn_2P_2S_6$, $Sn_2P_2Se_6$ and $Sn_2P_2(Se_x\ S_{1-x})_6$, $(Pb_xSn_{1-x})_2P_2S_6$ and $(Pb_xSn_{1-x})_6P_2Se_6$ solid solutions. The isomorphous ions substitution results in Curie temperature drop T_c, which can be described by equations:

$$T_c \simeq 339-319\cdot x-372\cdot x^2 \qquad \text{for } (Pb_xSn_{1-x})_2P_2S_6$$

$$T_c \simeq 190-213\cdot x-611\cdot x^2 \qquad \text{for } (Pb_xSn_{1-x})_2P_2Se_6$$

$$T_c \simeq 343-255\cdot x-100\cdot x^2 \qquad \text{for } Sn_2P_2(Se_xS_{1-x})_6$$

It follows from the equations that for $(Pb_xSn_{1-x})_2P_2S_6$ near x=0.62, and for $(Pb_xSn_{1-x})_2P_2Se_6$ near x=0.41 the value of T_c=0K.

On x, T-diagram of $Sn_2P_2(Se_xS_{1-x})_6$ solid solutions at x=0.23 $\pm$ 0.02 the Lifshitz point (LP) is realized, splitting transitions onto commensurate and incommensurate phases (IP).

At x$>$ 0.23 the paraelectric-ferroelectric (FP) phase transition is realized through intermediate-incommensurate phase. In $Sn_2P_2Se_6$ two transitions take place under the atmospheric pressure: the second order PT - paraelectric IP at T_i=222 K and the first order PT - incommensurate-ferroelectrical phases (T_c=193 K). In $(Pb_xSn_{1-x})_2P_2Se_6$ crystals the $T_i(x)$ dependence is described by the equation $T_i \simeq 221-763x-269x^2$, which shows, that near x=0.66 the value of T_i=0K.

The aim of the present paper was to study p, T-phase diagrams of the group $A_2^{IV}B_2^VC_6^{VI}$ crystals and to compare experimental results of the different physical properties anomalies studies with theoretical conclusions.

To build p,T-phase diagrams the experimental study of the optical absorption edge and the temperature variation of light transmission with fixed wave-length, the temperature dependence of spontaneous polarization and of dielectric properties under high hydrostatic pressures was made. The experimental technique of physical properties study under the high hydrostatic pressures is described elsewhere /5/.

Fig.1 presents phase p,T-diagrams of $Sn_2P_2(Se_xS_{1-x})_6$ crystals with $0 \leqslant x \leqslant 0.20$. The dotted lines are the second order PT, the full lines are the first order PT. From the experimental results obtained it follows that in $Sn_2P_2(Se_xS_{1-x})_6$ crystals the hydrostatic pressure increase results in FPT temperature drop. Under the $p=p_1$ pressure the second order FTP (T_o) changes into the first order transition (T_c). A further pressure increase ($p > p_1$) results in the gain of the first order FPT character. This is evidenced by the magnification of jumps in the fixed wavelength light transmission, spontaneous polarization and energetical position of the optical absorption edge jump at T_c. Along with the phase order change, the FPT line splitting occurs recorded by the temperature dependence of light transmission, dielectric constant ε and the slope of dielectric loss angle tg δ. The dashed line in p,T-diagram in Fig.1 at $p > p_1$ is the second order DT line (T_i) from paraelectric into incommensurate phase.

In the $Sn_2P_2S_6$ crystal the LP occurs on p,T-diagram at $p = p_L = (0.18 \pm 0.02)$ GPa and $T = T_L = 295$ K. With Se content increasing in $Sn_2P_2(Se_xS_{1-x})_6$ the P_L-value is linearly decreasing and at x = 0.23 $\pm$ 0.02 the LP occurs under the atmospheric pressure. For crystals with x$>$ 0.23 LP is realized in the negative pres-

sure region. Table 1 lists some phase p,T-diagrams characteristics of the crystals studied.

In the presence of LP on the phase diagram between the values T_o, T_c and T_i the following relationship exists /6/

$$\frac{T_o - T_c}{T_i - T_o} \simeq 4.4 . \qquad (1)$$

By differentiating (1) with respect to p one obtains:

$$5.4 \cdot \frac{dT_o}{dP} - 4.4 \cdot \frac{dT_i}{dp} = \frac{dT_c}{dp} \qquad (2)$$

On the bases of the experimental constants $\frac{dT_o}{dp}$, dT_c/dp and dT_i/dp (see Table 1) one easily gets sure that equation (2) is satisfied for crystals $Sn_2P_2(Se_xS_{1-x})_6$ with $0 \leq x \leq 0.20$.

By pyroelectric effect studying in $Sn_2P_2(Se_xS_{1-x})_6$ ($o \leq x \leq 0.20$) crystals under high pressures, the spontaneous polarization P_s temperature dependence transformation is studied along p, T-phase diagram. Fig.2 shows temperature dependences P_s for $Sn_2P_2(Se_{0.04}S_{0.96})_6$ crystal under various pressures. At $p < p_1 = 0.14$ GPa the temperature change P_s in the vicinity of FPT has continuous nature. But at $p > p_1$ in the $P_s(T)$ dependence the ΔP_s jump occurs, which is an evidence of the phase transition character change. With a distance growing from LP($p > p_1$) the first order-character of FPT is increasing. This is evidenced by the pressure dependence behavior of the $\Delta P_s/P_s^H$ value (P_s^H - the P_s value from the saturation region of P_s (T) dependence $P_s(T)$), which is given on an insert of the fig.2. Taking into account that at $p_1 = 0.14$ GPa in the $Sn_2P_2 \sim (Se_{0.04}S_{0.96})_6$ crystal the phase transition is continuous in its nature and the temperature change P_s repeats the order parameter variation, one can evaluate the critical index β value and to follow its variation on approaching the LP on the second order PT line of the p,T phase diagram.

Table 1. Some characteristics of $Sn_2P_2(Se_xS_{1-x})_6$ and $(Pb_xSn_{1-x})_2P_2Se_6$ Fss p,T-diagrams

x, mol.%	p = Patm				-dT_o/dp, K/GPa	-dT_c/dp, K/GPa	-dT_i/dp, K/GPa	T_L, K	P_L, GPa
	T_o, K	T_c, K	T_i, K						
$Sn_2P_2(Se_xS_{1-x})_6$									
0	339.0	-	-		220	238	216	295	0.180
4	326.0	-	-		230	238	228.6	293	0.140
10	319.5	-	-		224.8	240	221.3	294	0.110
20	299.0	-	-		225.7	240.4	222.4	293	0.024
30	-	280.0	281.0		-	256.7	299.2	294	-0.055
60	-	222.0	225.5		-	302.5	263.8	292	-0.256
80	-	210.0	216.0		-	287.5	207.5	293	-0.371
100	-	193.0	222.0		-	245	163	293	-0.436
$(Pb_xSn_{1-x})_2P_2Se_6$									
20	-	125	167		-	170	140	293	-0.90
30	-	78	155		-	-	109	-	-

To find β we used the Domb's method, the essence of which is as follows /7/.

At $T < T_o$ temperature the temperature change of spontaneous polarization case be given as follows:

$$P_S = \text{const} \cdot (T_o - T)^{\beta} \qquad (3)$$

By differentiating and taking logs of the right and left hands of the equation one gets:

$$\lg\left|\frac{dP_S}{dT}\right| = \lg \gamma = \frac{\beta - 1}{\beta} \cdot \lg P_S + \text{const.} \qquad (4)$$

From the above one can see that the linear dependence slope $\lg \gamma = f(\lg P_S)$ defines the $\frac{\beta - 1}{\beta}$ value which permits, on the basis of experimental results, to find β-value. Table 2 lists the critical index values calculated by the above method. On approaching LP β-value drops and in close proximity to LP the β-value = 0.19 ± 0.03. The obtained β-value for $Sn_2P_2(Se_{0.04}S_{0.96})_6$ crystal near LP coincides with the theoretical one ($\beta = 0.19 \pm 0.02$) /8/ and the β-value got from temperature dependence of the optic axes plane rotation angles in the solid solutions of $Sn_2P_2(Se_xS_{1-x})_6$ near LP under atmospheric pressure /3/.

Table 2. A value of critical index β for $Sn_2P_2(Se_{0.04}S_{0.96})_6$ crystal under different pressures

p, GPa	β
0.0001	0.40 ± 0.03
0.0300	0.34
0.0760	0.30
0.0900	0.26
0.1149	0.24
0.1574	0.19

On the basis of the results got one can conclude that the Lifchitz point was included by the high pressure on the p,T-diagram of the group $A_2^{IV}B_2^{V}C_6^{VI}$ crystals and the critical index β, characterizing the order parameter behavior, is shown to coincide with its theoretical value.

References

1. Гомоннай А.В., Грабар А.А., Высочанский Ю.М. и др. Расщепление фазового перехода в сегнетоэлектрических твердых растворах. - ФТТ, 1981, 23, № 12, с. 3602-3606.
2. Парсамян Т.К., Хасанов С.С., Шехтман В.Ш. и др. Несоразмерная фаза в собственном сегнетоэлектрике $Sn_2P_2Se_6$. ФТТ, 1985, 27, № 11, с.3327-3331.
3. Высочанский Ю.М., Фурцев В.Г., Хома М.М. и др. Критическое поведение одноосных сегнетоэлектриков $Sn_2P_2(Se_xS_{1-x})_6$ в окрестности точки Лифшица. - ЖЭТФ, 1986, 91, №4(10), с. 1384-1390.
4. Сливка А.Г., Герзанич Е.И., Тягур Ю.И. и др. Фазовая p,T,x - - диаграмма сегнетоэлектрических твердых растворов $Sn_2P_2(Se_xS_{1-x})_6$. - УФЖ, 1986, 34, №9, с.1372-1374.
5. Герзанич Е.И., Фридкин В.М. Зависимость диэлектрических свойств $SbSJ$ от температуры и гидростатического давления. . - Кристаллография, 1969, 14, №2, с.298-302.
6. Michelson A. Phase diagrams near the Lifchitz point. I. Uniaxial magnetization. - Phys. Rev. B., 1977, v.16, No.1, p.577-584.
7. Chaves R., Amaral H., Levelut A. et al. Tricritical point induced by atomic substitution in $SbSe_xS_{1-x}$. -J.-Phys. Stat. Sol. (a), 1972, v.73., No.2, p.367-376.
8. Kaskil K., Selke W. Monte Carlo coarse graining for the three--dimentional axial next-nearest neighbor Ising model. - Phys. Rew.B., 1985, v.31, No.5, p.3128-3130.

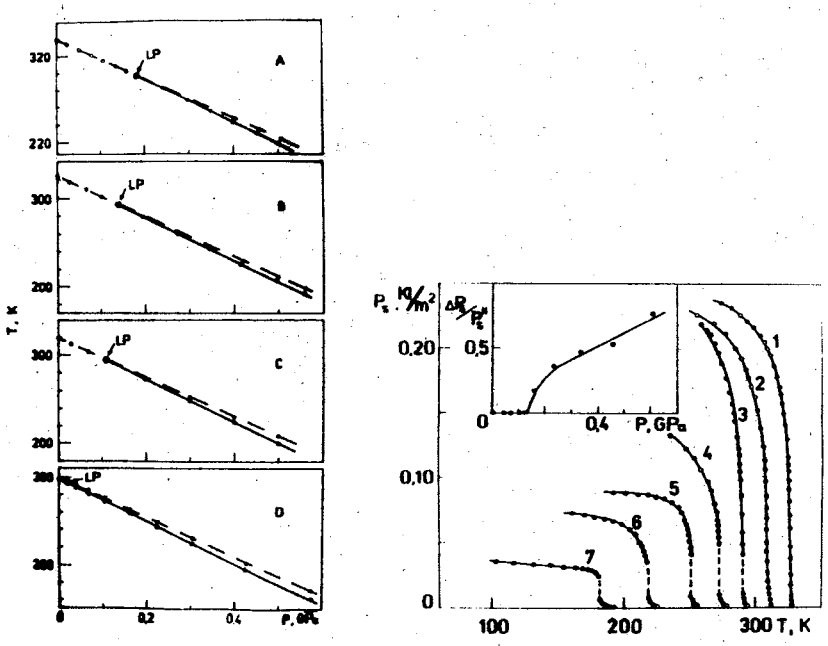

Fig.1. Phase p,T-diagrams of $Sn_2P_2(Se_xS_{1-x})_6$ solid solutions at x: A-0 ; B-0.04 ; C-0.10 ; D-0.20.

Fig.2. Temperature dependencies of spontaneous polarization P_s for $Sn_2P_2(Se_{0.04}S_{0.96})_6$ crystal under different hydrostatic pressures p, GPa: 1-0.0001 ; 2-0.0760 ; 3-0.1574 ; 4-0.2330 ; 5-3330 ; 6-0.4574 ; 7-6128 (inset - pressure dependence of $\Delta P_s/P_s^H$ value).

POLYMORPHISM OF $Pb_{1-x}Ce_xTe$ ALLOYS SYSTEM AT HIGH PRESSURES

N. Serebryanaya[1], Z. Malyushitskaya[1], M. Leszczynski[2], T. Suski[2]

[1]Institute of High Pressure Physics, USSR Academy of Sciences 142092, Troitsk, USSR

[2]UNIPRESS, Polish Academy of Sciences, Sokolowska 29, 01-142, Warsaw, Poland

The IV-VI compounds crystallize in three structures: rhombohedral As-type (α) in GeTe and its alloys, cubic rocksalt (β) in SnTe, PbS, PbSe, PbTe and their alloys, and orthorhombic GeS type (γ) in GeS, GeSe, SnS, SnSe and their alloys. Pressure induced transitions in SnTe, PbS, PbSe, PbTe have been revealed by volumetric, electrical resistance and X-ray diffraction methods [1,2] at 1.8, 2.2, 4.3 and 4.0 GPa respectively. The $\gamma \rightleftharpoons \delta$ phase transition into cubic structure CsCl type took place at 25.0, 21.5, 16.0, 13.0 GPa respectively [1]. $Pb_{1-x}Ge_xTe$ alloys system was chosen as the model to detect $\alpha-\beta-\gamma-\delta$ sequence of transitions at the same concentration and to compare with early studied $Sn_{1-x}Ge_xTe$ alloys system [2].

$Pb_{1-x}Ge_xTe$ alloys were obtained by annealing during four weeks at 873 K following by quench up to 300 K. They form continuous solid solutions with continuous $\alpha \rightleftharpoons \beta$ transition. This report seeks to investigate crystal structure and resistance anomaly R/R_0 (p) up to 12 GPa for two concentration of $Pb_{1-x}Ge_xTe$ alloys : x=0.25 (1) and x=0.375 (2). Both alloys are crystallized in α-GeTe type (α) with small angle distortion: $< 10'$ (1) and $32'$ (2), because of their diffraction data (MoK_α) were indexed on the base of pseudocubical facecentred structures: a_0=6.334±0.005 Å (1), a_0=6.303± 0.005 Å (2).

The anvil type apparatus was used for both experimental methods in loaded and unloaded cycles. Polyethylene-mixed (1:5) samples for X-ray diffraction (MoK_α) were put in a hole (ϕ 0.11 mm) in a boron annulus (ϕ 2 mm). Pressures were estimated from the equation state [3] data of NaCl used as the internal standard. The electrical resistance was measured in the apparatus with pyrophyllite and AgCl as pressure transmitting media.

Figure 1 shows the variation of the resistance as a function of pressure for alloys (1, 2). Two phase transitions were found in

alloy (1) at p≥1.5 GPa and p≥5.0 GPa. The latter transition is accompanied by twofold increase of resistance, but X-ray diffraction data revealed only one transition at 4.9 GPa. Diffraction data in the interval 0-6 GPa were interpreted as β -phase. In the interval 5-11 GPa the γ -phase structure was proposed to be orthorhombic GeS type, sp. gr.Pbnm, Z=4, parameters of cell: a =4.43 Å, b = 11.51 Å, c =4.32 Å at 6.8 GPa. Compressibility data $V/V_o(p)$ alloys (1,2) are plotted in Figure 2.

The strongest X-ray reflections of γ-phase and 4-5-fold increase of electrical resistance (Fig1) of alloy (2) were found at ~4.3 GPa. The X-ray diffraction data of alloy (2) γ-phase could correspond GeS structure or more symmetrical TlJ structure with just the same probability. Unlike alloy (1), reflections with h+k=2n+1 were absent at the pattern of alloy (2). However these reflections were weak and their absence might be caused by the large absorption of high pressure cell. The γ-phase structure of alloy (2) was proposed to correspond TlJ type due to supposed different changes of $R/R_o(p)$ and diffraction data. In the interval 0-6 GPa diffraction data were indexed as β-phase, and in the interval 4.3-12.0 GPa as TlJ structure, sp.gr. Cmcm, Z=4, cell parameters: a =4.21 Å, b =11.56 Å, c =4.37 Å at 6.5 GPa. Hysteresis of $\beta \rightleftarrows \gamma$ transition was absent at quasihydrostatical compression because of β-phase was found under unloading at 4.4 GPa. The volume decrease was ~ 3 per cent for $\beta \rightleftarrows \gamma$ phase transition of alloys (1,2).

The bulk modulus B_o and its pressure derivative B_o' at p=0 for β and γ phases of both alloys obtained by fitting Murnaghan-Birch equation to volume-pressure data were given in Table.

Bulk modulus B_o and its pressure derivative B_o' at p=0 for $Pb_{1-x}Ge_xTe$ alloys

x, %	phase	B_o, GPa	B_o'	references
0	β	38.9	5.4	/1/
	γ	36.8	5.4	"
25	β	42.7	3.4	This paper
	γ	76.7	4.1	"
37.5	β	40.7	4.4	"
	γ	46.9	3.9	"

On the basis of alloys (1,2) investigation we think that pressure induced phase transitions might take place as follows:

type NaCl (β) - type GeS (γ) - type CsCl (δ')
type α-GeTe(α)
type TlJ (γ) - type CsCl (δ)

This hypothesis is consisted with to generalized phase diagram of IV-VI compounds grounded on the quantum mechanical parameters [4]. According to this diagram rocksalt structure is stable for the ionic lead chalcogenides but α-GeTe, GeS and TlJ structures are formed with increasing of covalence. Pressure induced $\alpha \rightleftarrows \gamma$ phase transition of high Ge-atoms $Pb_{1-x}Ge_xTe$ alloys may take place without NaCl phase.

Thus depending on the α -phase angle distortion, the sequence of $\alpha \rightleftarrows \beta \rightleftarrows \gamma$ transitions (x=0.25) or $\alpha \rightleftarrows \gamma$ transition (x=0.375) may be found in $Pb_{1-x}Ge_xTe$ alloys.

We wish to thank Dr A.Szczerbakov from the Institute of Physics PAN for the crystal preparation.

References

1. Chattopadhyay T., Werner A., Schnering H.G. von Temperature and pressure induced phase transition in IV-VI compounds.// Res.Phys. Appl.-1984 - 19, N9. - p.807-813.
2. Kabalkina S.S., Serebryanaya N.R., Vereshchagin L.F. Phase transitions in compounds IV-VI at high pressures.// Sov.Phys. Solid State - 1968. - 10, -p.574-581.
3. Decker D.L. High pressure equation of state for NaCl, KCl and CsCl.// J.Appl.Phys. - 1971. - 42, N8. -p.3239-3242.
4. Littlewood P.B. The crystal structure of IV-VI compounds: I. Classification and description//J.Phys.C: Solid State Phys.- 1980. - 13, N26. - p.4855-4873.

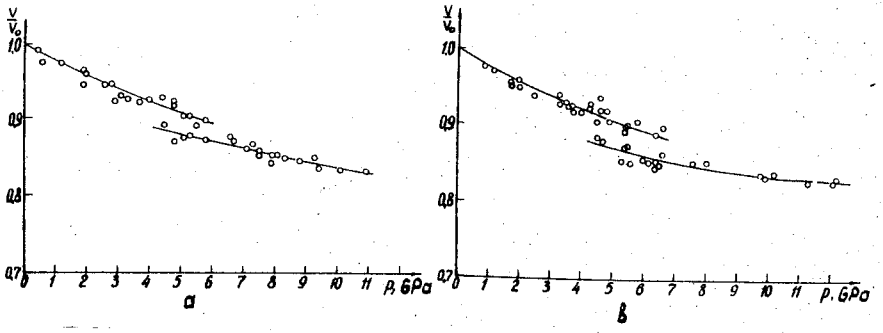

Fig. 1. Variation of the electrical resistance R/R_o of $Pb_{1-x}Ge_xTe$ alloys as a function of pressure: a)x=0.25, b) x=0.375.

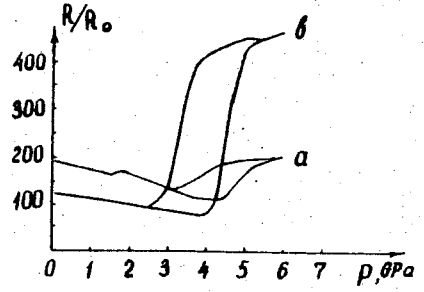

Fig. 2. Variation of the reduced volume V/V_o of $Pb_{1-x}Ge_xTe$ alloys as a function of pressure: a) x=0.25, b) x=0.375. Circles denote the experimental data, curves are obtained by fitting Murnaghan - Birch equation.

CONVERSION OF ELECTRONIC STRUCTURE IN CRYSTALS DURING IRREVERSIBLE POLYMORPHIC TRANSFORMATION UNDER HIGH PRESSURE

E.A.Shurakowskiy, Ja.W.Zaulitchny

Institute of Material Science Problems of the UkrSSR Academy of Sciences, Kiev, USSR

Introduction. The creation of high pressure metastable phases (HPMP) is caused by rebuilding of the electron energy spectra (EES) of crystals under compression. Due to the fact that HPMP in normal conditions preserve for a long time crystalline structure and properties acquired under pressure, the EES in them may have similarity to those in compressed crystals.

The aim of this paper therefore is to estimate by means of X-ray emission and photoelectron-spectroscopy the changes of EES in HPMP relative to initial crystals with metal (Zr, $MoGe_2$), metal-covalent (C,TaN), ionic-covalent (BN, SiO_2) and ionic (ScF_3) bonds.

The HPMP ω-Zr. The Zr valence band consist of hybridised s-, p- and d-states. As revealed from comparison of $L\beta_{2,15}$- and $M_{4,5}O_{2,3}$-X-ray spectra of α- and ω-Zr, the $\alpha \rightarrow \omega$-transformation results in the drift of delocalized pd-states to E_{Fermi} and appearanse of two-topes structure for these spectra. In this case the peaks of the density of localized d-states do not shift and coincide, though the energy of delocalized p-states increase by 2,0 eV. Being compressed, A- and B-atomic planes in α-Zr move nearer each other until they reach distances, which are comparable with B_1-B_1-distance in ω-Zr. Then the interaction between delocalized hybrid pd-orbitals, with the increasing energy [1], some new stronger localized bond B_1-B_1 appears.

The HPMP β-$MoGe_2$. The $\alpha \rightarrow \beta$-transformation in $MoGe_2$ shifts the peak of delocalized p-state of Ge, like those in the EES of ω-Zr, by 2,0 eV to E_{Fermi}, while the energy distributions of d-states of Mo in the both phases are similar. The diminishing of Mo-Ge-distances leads to increase of energy of delocalized p-states of Ge at valence band bottom and to overlapping of p-wave functions of Mo and Ge atoms resulting in rising of p-electron charge on Mo atoms. Therefore p-electrons which take part in Mo-Ge-bonds (these bonds in β-$MoGe_2$ grew in number and became more localized) are closer in Mo-atoms in respect α-$MoGe_2$. This leads to increasing (about 1,6 times) of the integral intensity Mo $M_{4,5}O_{2,3}$ X-ray emissions in its high-energy part and that of low-energy part of Ge$K\beta_5$-bands drops. The negativ charge redestribution in Mo-sites causes the shift of Mo$3d_{3/2}$ core level to E_{Fermi}-point too.

The HPMP ν-TaN and TaN_{cub}. The energy of delocalized pd-hybride states taking part in most prolonged Ta-N-bonds, which are oriented in basis planes (0001) of the crystals, may increase under compression of metal-like ε-TaN to such an extent that these bonds can collapse. By approaching the Ta atoms to each other the distance between them becam so short, that they create the shortest possible bonds Ta-Ta. In this case cohesion forces arise which will move the Ta-atoms situated between (0001) planes on these planes. Shifted from the above mentioted planes in the same directions N atoms are building new stronger localized bonds with Ta atoms (fig.1,a). The energy of electron states occupying these bonds must be stronger and so the position of $NK\alpha$-emission band in ν-TaN is by 1,8 eV higher than in ε-TaN. However, in valence band of ν-TaN in the accordance with the calculations there are still present delocalized pd-hybride states. The increase of pressure leads to further high energy shift of the above mentioted states [1]. As a result of it as soon as pressure reaches the level corresponding for a ν-TaN $\rightarrow$ TaN_{cub}-transformation the specified delocalized states rise over E_{Fermi}. In the whole the intensity of $NK\alpha$-emission band in TaN_{cub} decreases twice and their peaks begin to coincide with energy submaximum δ in ν-TaN. The comparison of the calculated zones for ν-TaN and TaN_{cub} [2] reveals that Np-states are concentrated predominantly in this region of EES TaN_{cub} while in ν-TaN there is present a great density of pd-hybridised states. As calculated there is considerable quantity of free Np-states in all points of the Brillouin zone in TaN_{cub} beyong the E_{Fermi}.

The HPMP lonsdaleite and diamond. We have studied the EES for three modification of carbon. It is evident that in the energy region occupied with delocalized p_z-states in graphite the intensity of $CK\alpha$ band is by 16 per cent lower than in lonsdaleite, because under compression the graphit atomic layers are moving closer to each other but energy of p_z-states increas and they are reformed to σ-orbitals. These transformation of carbon p_z-states are reflected in the form of $CK\alpha$ peak in lonsdaleite, which moves to high energy side by 2,4 eV. The shape and intensities of X-ray emission spectra do not change or change insignificantly in other regions of EES, corresponding to the localized $p_{x,y}$-orbitals of σ-character in graphite during graphyt-lonsdaleite-diamond transformation.

The HPMP cohesit and stishowit. In covalent α-quartz nonbonding p_y-orbitals are oriented along the most compressible C-O-direction [3] and correspond to the low energy maximum in $OK\alpha$-band spectra. After compression becomes enough to form cohesit these orbitals overlap and there appear a bonding orbital with the increased energy. It is reflected in the weakening of intensity of the above mentioned low energy maximum and, on the contrary, in strengthening of short energy slope of the $OK\alpha$-emission band in cohesit (fig. 1,b).

The action of increased pressure (~160 kbar) needed for the creation of a stishowit HPMP phase, leads to the energy increase of mixed pd-states, possessing a lesser delocaliztion extent. Moreover the p-states density in neighboorhood of Si atoms augments due to the increase of overlap of wave functions of Si and O and of cordination number, what is revealed in intensity growth of $SiK\alpha$ band by 1,8 times.

The HPMP BN_w and BN_{cub}. Graphyte-like modification BN_g with ionic-covalent bonding has a layer structure. The part of electron charge which is distributed between layers (0001) is mainly concentrated on the nitrogen atoms. Bp_z-states under compression transform into σ-bonding states and increase their energy ($\Delta E_{BK\alpha}$=1,2 eV) much more than Np_z-states due to their higher delocalization. Therfore the intensity of BK in BN_w in region of energy corresponding $BK\alpha$-peak in BN_g is by 12 per cent smaller, but the intensity of high-energy subpeak is greater by 28 per cent. Such increment of electron density in B-atomic sphere is connected with admixture of Np-states in newly created σ-bonds. Consequently that part of $BK\alpha$ band in BN_w reflects a new σ-bonding orbital generated during $BN_g \rightarrow BN_w$-transformation under compression. While newly created σ^*-antibonding orbital is reflected in the peak situated near the threshc of generation of the quantum X-ray yield spectrum in BN_w. Distribution of p_z-orbitals in the crystal grating of the BN_g points out the "Hofrieren" of layers during increasing overlap of Bp_z- and Np_z-orbitals is possible only due to the rise alternating σ-bonding and σ^*-antibonding orbitals in the atomic B-N-B-N chains directed along to C-axic.

The HPMP ScF_3 II. The ionic fluorides ScF_3I and ScF_3II have tightly localized around anions Fp-states which are reflected in X-ray $FK\alpha$-emissions. $FK\alpha$-emissions in ScF_3I and ScF_3II has the same energy position and half maximum width. The shift of density of p states in the direction to Sc-atom during $ScF_3I \rightarrow ScF_3II$ transformation results in double increase of intensity of the $ScK\beta_5$-band.

Conclusions. The influence of high pressure on electron structure and chemical bonding of crystals may by summarised as follows:

1. In process of creation of HPMP delocalized electron states are transforming to localized states and enhance their energy thereafter. In this case high-energy shift of peaks of the density of p-states is the greatest in metals and is diminishing during increasing of the ionicity (e.a. localisation of p-states). Decreasing the quantity of delocalized states (which is reflected in peaks of the X-ray emissions) in initial crystals results in smaller diminish there the intensity of spectra of HPMP (fig. 2). The energy of localized in chemical bonds d-states changes insignificantly.

2. During the creation of HPMP in the binary crystals the electron density grows owing to the increase of the overlap of p-wave function of metal and nonmetal atoms.

3. $\pi \rightarrow \sigma$ -transformation occurs by means of destruction of π-bonds during rise of σ-overlap along primary direction p-orbitals with resulting equalization of the lenght of bonds and the desribution of charge.

References

1. Kulikov N.I. Electronnaja structura perechodnych metallow pod dawleniem// Iswestija WUSOW, Physica, 1982. -24. -P. 50-63.
2. Popova S.W. Wlijanie wysokogo dawlenija na obrazowanie metastabilnych phas w dwoynych systemach (carbide, nytride, germanide y gallide perechodnych metallow // Diss. doc. phys.-mat. nauk, Moscou, 1982. -406 s.
3. Harrison W.A. Electronic structure and the properties of solides// ed.W.H. Freeman and company, San Francisco, 1980.- p.

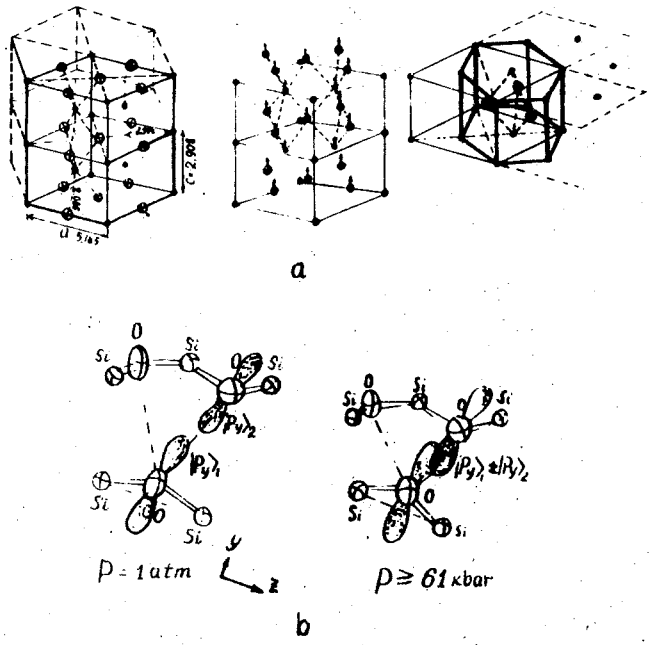

Fig. 1. The crystal chemistry mechanism of phase transformation ζ-TaN $\rightarrow$ γ-TaN (a); The main patterns of O-O-bonds building during polymorphic α-quartz $\rightarrow$ cohesit transformations (b).

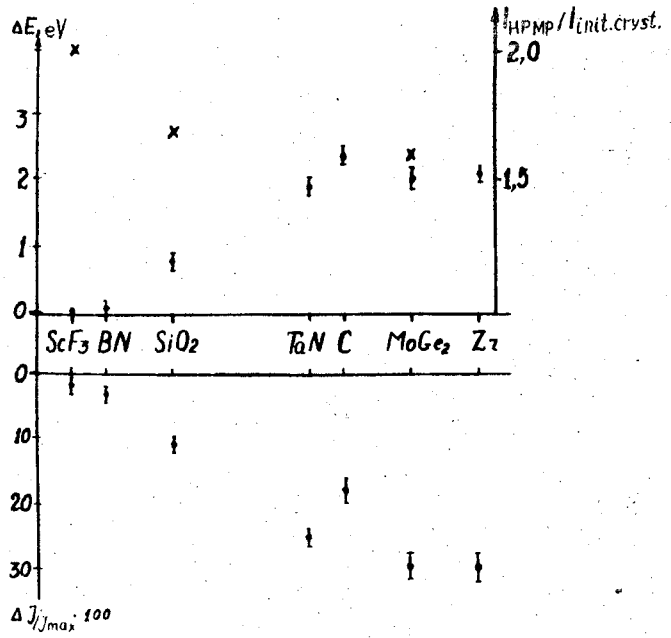

Fig. 2. The integral intensity drop in spectral region of p-density peaks and their high energy shifts plotted against the chemical bonds characteristics of the initial crystals HPMP (high pressure metastable phase) (I) The integral intensity increase of X-ray reflecting the p-states of cations after formation of binary HPMP - (X).

THE INFLUENCE OF ELECTRONIC BAND STRUCTURE ON THE PHASE STABILITY

E.S.Alekseev, R.G.Arkhipov, L.B.Litinsky, A.F.Tatarchenko
Institute of High Pressure Physics, USSR Academy of Sciences, Troitsk, USSR

Introduction

The nitrides of transition metals are existed usually in rock-salt structure, except the hexagonal nitrides of tantalum and niobium in which a violation of a stochiometric composition is present as well. We connect this violation with pecularities of electronic band structure.

We calculate the band structure of stochiometric hexagonal δ'-phase of TaN and details of band structure and Fermi surface by APV method in a small region of k-space for energies near the Fermi level. The band structure of stochiometric hexagonal NbN was calculated by LAPV method (the parameters of lattice for Nbn a = 5.5766 at.un., c = 5.2401 at.un.).

Main part

There are five valent electrons $3s^2 3p^3$ and $6s^2 5d^3$ for nitrogen and tantalum respectively. There are a great gibridisation of states of nitrogen atom $3s^2 p^2_{p+1}$ in the field of hexagonal symmetry, in which there are eight electrons. The states, which origin is d-zone of tantalum, are separated from the sp-zone may be filled by the last two electrons and that may lead to the dielectric state. But the weak intersection with the $d_{\pm 1}$ and $d_{\pm 2}$-zone leads to semimetalic state. The detailed calculations have been done near the G-A line and G_1A_4 level (not degenerated) and G_5A_6 level (twice degenerated) (see fig. 1). They intersect in the point of accidental degeneration close to the point, which is positioned near at 0.5 of the period G-A.

The twofold degeneration went out at the motion from the axis in any direction. As it is well seen from fig. 2 near point G (fig. 2a) the zones of heavy electrons G_5H and light holes are in contact and the zone of light electrons G_1H and G_1L is free near A point (fig. 2c). The heavy and light electrons zones are in contact and there is a gap between them and light holes. The heavy electros level is changing drastically at the motion through the point of accidental degeneration (fig. 2b). The maximum of curve is situated

at the hexagonal axis and the minimum is reached at a small distance from the hexagonal axis.

The weak overlap of zones (instead of contact) leads to filling by electrons, which are went away from the part of light holes zone near the A point to the region, which has a form of distorted toroid of minimum of electronic energy near the point of accidental degeneration. The surface of holes, which has a form of a spin, which is surrounding the A-point and elongated between the points of accidental degeneration in neibouring zone.

The volume of the region should be equal to volumes of two electronic toroids, which are surrounding the spin near the two ending points (the points of three-fold degeneration).

It is interesting to note that this kind of Fermi surface is very stable to changes of band structure. Only the value of small intersection near the A point is sensible to the ways of the calculation.

Conclusion

The estimation of concentrations $n^+ = n^-$ equals to $10^{-3} - 10^{-4}$ per one atom. This is anomalously small value. It showed lead to effective attraction of electrons and holes, exiton formation and instability to the transformation to the dielectric. But it is seen from experiment, that the instability is manifested as a violation of stochiomety by approximatly 10 % loss of nitrogen from the lattice.

The rigorous calculation of real defect structure is out of posibility now. It should be noted that the same results were obtained at the band structure calculation of hexagonal niobium-nitride. There are no such pecularities in the band structure of stochiometric ReC with the isomorphic structure.

References

1. A.V. Tsvyashchenko, S.V. Popova, E.S. Alekseev. Phys.st.sol.(b), 99, p. 899, 1980.

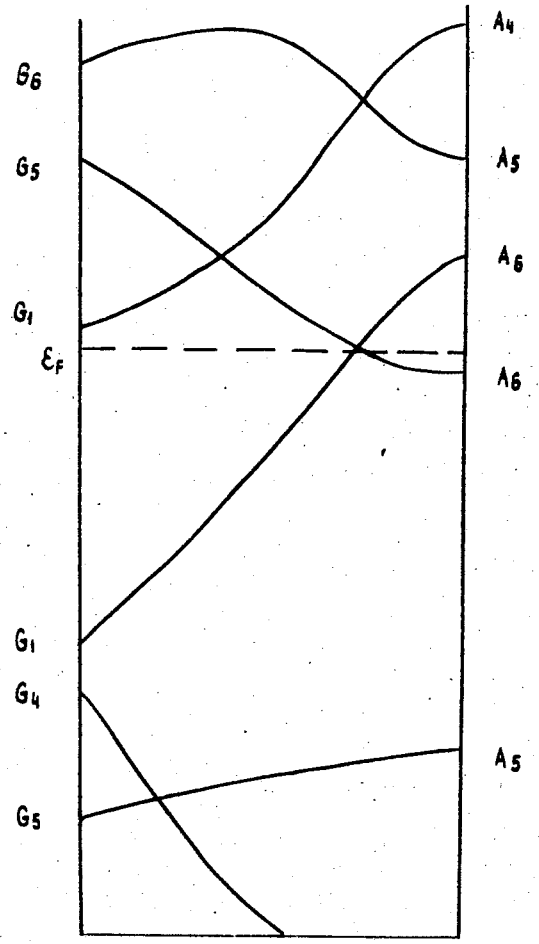

Fig. 1. Band structure of stochiometric NbN.

Fig. 2. The detail of NbN band structure in the direction H-A at different distance from A point.

SAMARIUM HEXABORIDE ISOSTRUCTURAL ELECTRON TRANSITION POSSIBILITIES UNDER HIGH PRESSURE

Ju. B. Paderno[1], E.S.Konovalova[1], T.N.Kolobjanina[2]

[1]Institute for Problems of Materials Science
UkrSSR Academy of Sciences, Kiev, USSR

[2]Institute of High Pressure Physics
USSR Academy of Sciences, Moscow, USSR

Rare earth hexaborides with cage boron lattice and consequently rigid structure have very small structure dimensions dependance to the vacancies and impurity atoms. Some publications related to rare earth hexaborides elastic characteristics obtaind by ultrasonic and X-ray methods under the high pressure. Shown that samarium hexaboride lattice with the mixed valency of samarium atoms is nearly 20% softer then that of other hexaborides with entire valency independently of its value +2 or +3. These earlier investigations were carried out up to the pressure 6 GPa [1,2]. The results of our electrical resistence and Hall-effect investigations at the pressures up to 10 GPa shown the change of electron structure and conduction electron concentration at low temperature [3,4] and didn't rule out the possibility of samarium valency change from mixed to entire value at pressures up 5,5 GPa in its hexaboride.

We have investigated the high pressure effect to the structure dimensions of mixed valency (SmB_6) and entire valency (CeB_6) compounds.

Lattice constant a(p) under pressure was determined from X-ray diffraction patterns indices up to (411) plane. Bulk modulus was calculated from the interplanar space changes of the (200),(210),(211) diffractions (see Figure).

Specimens were prepered by mixing CeB_6 or SmB_6 powders with sodium cloride powder as pressure sensor and pressing between two boron or diamond punches. One may pay attention the uniform spread in results for CeB_6 along whole region of pressures in contrast to SmB_6 that has the more spead in the middle of investigated range. It was used the linear approximation for the bulk modulus calculations. The bulk modulus values of some hexaborides obtaind in our experiment comparing with the literature data are presented in the table. The calculations were produced in two assumption. At first approximation for cerium and samarium hexaborides bulk modulus was performed in whole pressure range. The

Bulk modulus B_0 of some rare earth hexaborides

Material	B_0 GPa	Pressure GPa	Literary source
LaB_6	191	0 - 6	[1]
CeB_6	166	0 - 2	[2,5]
	166	0 -10	our data
SmB_6	139	0 - 6	[1]
	167	0 -10	our data
	145	0 - 6	our data
	190	0 - 10	our data
EuB_6	157	0 - 6	[1]
GdB_6	190	0 - 6	[1]

results have good agreement with literature data for cerium hexaboride[3], but the value for samarium hexaboride bulk modulus exceeds both literature at pressure up to 6 GPa and cerium hexaboride data in this approximation. Secondly the approximation was made in assumption of two linear regions p= 0-6 GPa and 6-10 GPa. The knee of 6 GPa was estimated by maximum dispertion a(p) and the energy band gap disappearing. In this case the bulk modulus at p= 0-6 GPa is in agreement with literature data and at p= 6-10 GPa value is larger and close to the others trivalent metal hexaborides. This anomalous is absent in cerium hexaboride.

On account of our experimental data it was calculated that thesamarium hexaboride bulk modulus change by pressure that is connected with the valency changes of samarium in its hexaboride.

References

1.H.E.King,S.G.La Placa, T.Penney,Z.Fisc // Effect of valence and intermediate valence on compressibility of the Rare Earth hexaborides/.Valence fluctuations in solids.-St.Barbara, North-Holland publishing company, 1981,p.333-336.

2.J.M.Leger,J.Rossat-Mignod , S.Kunii, T.Kasuya //High Pressure Compression of CeB_6 up to 20 GPa. /Solid State Commun.1985,,54, № 11,-p. 995-997.

3. N.V.Berman, N.N.Brandt,V.V.Moschalkov, et al.//Pressure influence on the correlation gap in mixed valency compound/ Pisma JETP, 1983, 38, №8, -p. 393-396.

4. M.M.Korsukova, N.N.Stepanov, E.V.Gontcharova, et al. //Electrical properties of single crystals of REM hexaborides at temperature and pressure variation / Borides and related compounds, 7-th Intern. Symp. on Boron, Abstracts, Uppsala, Sweden,1981, - p.31.

5. J.M.Leger // High pressure X-ray diffruction of cerium compounds in an improved diamond anvil cell / Rev.Phys.Appl.,- 1984, 19,№ 9 815-817.

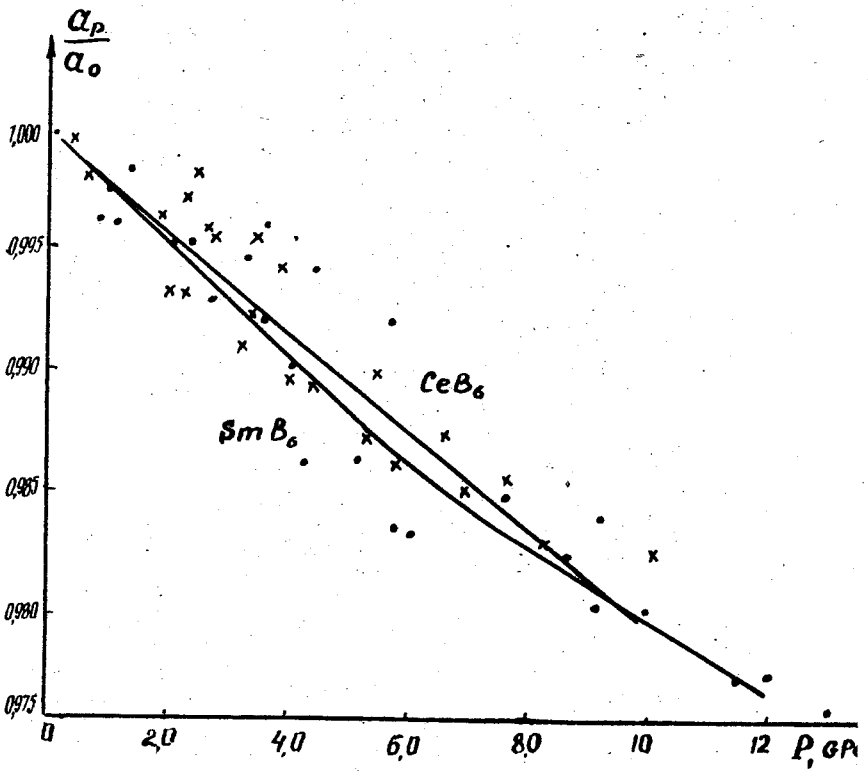

Pressure effect on changes in lattice constant for: (x) CeB_6 and (•) SmB_6

THE $2^{I}/_{2}$ PHASE TRANSITION INVESTIGATION UNDER PRESSURE IN BiSb ALLOY BY ACOUSTICAL METHODS

S.G.Buga[1], B.B.Voronov[2], L.K.Zarembo[2], A.I.Korobov[2]
[1]High Pressure Institute, Academy of Sciences, Troitsk, USSR
[2]Moscow State University, Moscow, USSR

The $2^{I}/_{2}$ phase transition (PT) phenomenon in metals, which is connected with the changing of a Fermi surface (FS) topology was predicted by I.M.Lifshitz [1]. As shown, the PT has to be accompanied with specific peculiarities in metal kinetic properties (electro- and thermal conductivity, thermoelectric power).

At the same time, there are anomalies in acoustical properties of metals near the PT point. The theory of the long wave sound absorption is considered in [2]. The nonlinear acoustical effects in the vicinity of PT were investigated in [3]. There was shown that the metals were the acoustical media with the essentially new type of nonlinearity. The exact solution of the elasticity equations in terms of simple Riemann waves as well as the acoustical wave (AW) profile changing during the propagation were considered. It is a rather difficult problem to investigate the profile of the propagating AW experimentally. The most convenient method for the experimental investigation of nonlinear acoustic properties of metals consists in the observation of harmonics of a monochromatic AW with the finite amplitude.

In the case $k\ell_0 \ll 1$ (k is a wave number, ℓ_0 is an electron free path) the expression for the linear $\tilde{C}^*$ and nonlinear $\tilde{C}^*_H$ elastic coefficients near the PT can be written in the form [4]:

$$\tilde{C}^* = \tilde{C} - \frac{3}{2}\gamma\left(U^{K}_{1x} - U^{C}_{1x}\right)^{1/2} = \tilde{C} - \Delta C, \qquad (1)$$

$$\tilde{C}^*_H = \tilde{C}_H + \frac{3}{4}\gamma\left(U^{K}_{1x} - U^{C}_{1x}\right)^{-1/2} = \tilde{C}_H + \Delta C_H, \qquad (2)$$

$\gamma \sim \Lambda^{5/2}$ (Λ is the deformation potential component, which is defined by the polarization and the direction of propagation of the AW), $U^{C}_{1x} = \frac{\partial U^{C}_{i}}{\partial x}$ is a static deformation of the sample, $U^{K}_{1x} = \frac{\partial U^{K}_{i}}{\partial x}$ is a static critical deformation corresponding to the PT point, $\tilde{C}$, $\tilde{C}_H$ are linear and nonlinear elastic coefficients correspondingly at the assumption of $U^{K}_{ik} = U^{C}_{ik}$.

Thus, both linear and nonlinear elastic coefficients obtain the certain corrections in the vicinity of PT. Moreover for $\tilde{C}_H$ coefficient which describes the cubic anharmonicity, the correction ΔC_H exceeds the coefficient itself as $|U^{K}_{1x} - U^{C}_{1x}| \ll 1$ in $(U^{K}_{1x} - U^{C}_{1x})^{-1/2}$.

In the present work we investigated the pressure dependencies $U_\omega(P), U_{2\omega}(P)$ of longitudinal and transversal bulk acoustical waves (BAW) at $\frac{\omega}{2\pi} = f_0 =$ 30 MHz at T = 4.2 K in Te doped $Bi_{0.926}Sb_{0.074}$ alloy. The method used is a new strong deformation (up to 0.3%) method based on an uniaxial compressing of bulk monocrystallic samples [5]. Different types of the phase transitions initiated by this kind of deformations were observed in Bi and BiSb alloys using Shubnikov - de Haas method [6]. Sound waves of different polarizations were propagating along the trigonal axis of the sample.

The U_ω and $U_{2\omega}$ amplitudes pressure dependencies of the transversal BAW polarized along byssectornal axis of the sample, pressure direction being along byssectornal axis, are shown at Fig.1 (two of three ellipsoids of an electron FS diminish during the PT and disappear at critical deformations). The analogous dependencies of the longitudinal BAW for the stress direction along the bynary axis are shown at Fig.2 (one ellipsoid disappears).

At the range of stress, corresponding to the PT point the experimental values change drastically. Decreasing of U_ω corresponds to the rising of the absorption coefficient $\alpha\omega$. Increasing of $U_{2\omega}$ signal shows considerable increasing of elastic nonlinearity because of the large value of the $\tilde{C}_H$ coefficient in the vicinity of PT.

The nonlinear parameters Γ for longitudinal and transversal BAW are:

$$\Gamma(P) = \frac{\tilde{C}^*_H}{\partial\tilde{C}} = \frac{1}{\partial\tilde{C}}\left(\tilde{C}_H + \Delta C_H\right) = \Gamma^0 + \Delta\Gamma. \qquad (3)$$

According to (I-3) the ratio of nonlinear parameters for transversal $\Delta\Gamma_{c\alpha\beta}/\Gamma^0_{c\alpha\beta}$ and longitudinal $\Delta\Gamma_{np}/\Gamma^0_{np}$ waves is [4]:

$$\frac{\Delta\Gamma_{c\alpha\beta}}{\Gamma^0_{c\alpha\beta}} \Big/ \frac{\Delta\Gamma_{np}}{\Gamma^0_{np}} = \frac{3C_{33} + C_{333}}{C_{44H}} \left|\frac{\Lambda_H}{\Lambda_3}\right|^2 \simeq 3,$$

where P is the pressure value. The experimental value for this ratio is 2.5 ± 0.5 which is a good agreement with theoretical data.

Using [2] we can estimate the electronic contribution to the absorption coefficients $\Delta\alpha^e_\omega$ ratio for longitudinal and transversal waves [4]:

$$\frac{\Delta\alpha^e_{\omega\,сдв}}{\Delta\alpha^e_{\omega\,пр}} = \frac{K^2_{сдв}\,|\Lambda_4|^2\,V_{пр}}{K^2_{пр}\,|\Lambda_3|^2\,V_{сдв}} = \left(\frac{C_{33}}{C_{44}}\right)^{3/2}\left(\frac{\Lambda_4}{\Lambda_3}\right)^2 \simeq 4,$$

where $V_{пр}$, $V_{сдв}$ the longitudinal and transversal sound velocities correspondingly. The $\Delta\alpha^e_{\omega\,сдв}/\Delta\alpha^e_{\omega\,пр}$ ratio obtained from the experimental results is 3 ± 1.

Thus the experimental data analysis shows that the observed anomalies in U_ω and $U_{2\omega}$ under uniaxial pressure in BiSb alloy samples are due to the 2½ phase transition which takes place at critical deformations. The vary fact of the PT was confirmed by direct observation using Shubnikov - de Haas method [5].

References

1. Лифшиц И.М. Об аномалиях электронных характеристик металлов в области больших давлений. ЖЭТФ, 1960, т.36, вып.5, с.1569-1576.
2. Давыдов В.Н., Каганов М.И. Особенности коэффициента поглощения длинноволнового звука при фазовом переходе 2,5 рода. ЖЭТФ, 1978, т.74, вып.2, с.697-701.
3. Лифшиц И.М., Ржевский В.В., Трибельский М.И. О нелинейных акустических эффектах в металлах вблизи точки ЭТН. ЖЭТФ, 1981, т.81, вып.4, с.1529-1541.
4. Буга С.Г., Воронов Б.Б., Зарембо Л.К., Коробов А.И. Особенности акустических свойств сплава BiSb в области электронно-топологического перехода. ФТТ, 1985, т.27, вып.8, с.2291-2298.
5. Брандт Н.Б., Кульбачинский В.А., Минина Н.Я., Широких В.Д. Способ создания сильных одноосных растяжений у монокристаллов. ПТЭ, 1979, вып.6, с.137-140.
6. Брандт Н.Б., Кульбачинский В.А., Минина Н.Я., Широких В.Д. Изменение зонной структуры и электронные фазовые переходы у Bi и сплавов BiSb при деформациях типа одноосного растяжения. ЖЭТФ, 1980, т.78, вып.3, с.1114-1131.

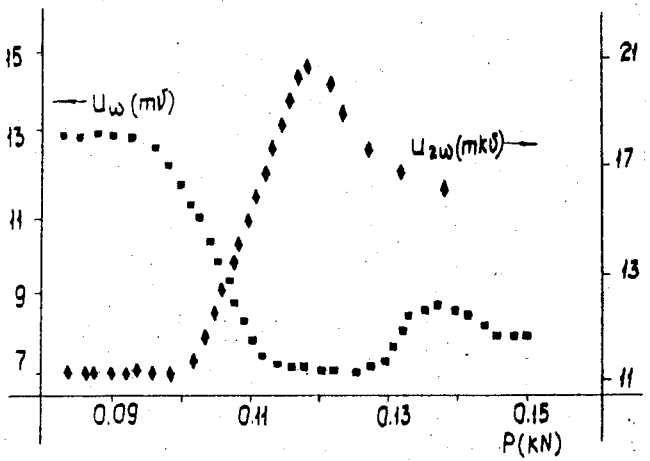

Fig.I. The pressure dependencies of U_ω and $U_{2\omega}$ amplitudes of transversal bulk acoustical waves in BiSb alloy. P is the pressure value.

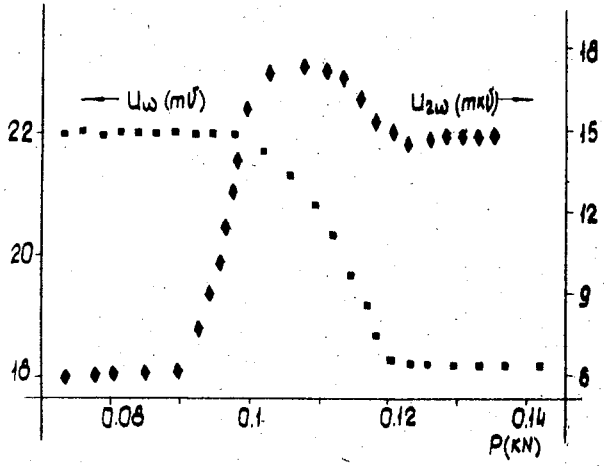

Fig.2. The pressure dependencies of U_ω and $U_{2\omega}$ amplitudes of longitudinal bulk acoustical waves in BiSb alloys. P is the pressure value.

ANOMALIES IN THE ELASTIC PROPERTIES AND SOME FEATURES OF THE ELECTRONIC TRANSITIONS IN LANTHANUM AND PRASEODYMIUM UNDER PRESSURES UP TO 84 KBAR

Yu.Ya.Boguslavskii, V.A.Goncharova, G.G.Il'ina
Institute of High Pressure Physics, Academy of Sciences
Troitsk, USSR

It is a point of view, that the structure sequence HCP-Sm-type-double-HCP-FCC realized in trivalent lanthanides under pressure is a measure of a occupancy of d-band [1]. Pressure enhances d-character of the conduction band of metals with unfilled or partially filled d-states: upon compression the relatively free 6s-states are overlapped more strongly than do the more localized 5d-states.

The experimental results obtained for some anomalous baric changes of the elastic properties of La and Pr in the dHCP- and FCC-phases as well as at known dHCP-FCC-transformation and phase transition with a distortion of the FCC-lattice are presented. One proposes an explanation of the observed features.

The measurements of the propagation for longitudinal $v_l(p)$ and transverse $v_t(p)$ elastic waves in polycrystalline samples of La and Pr were made by the pulsed-ultrasound method at pressures up to 84 kbar. The experimental procedure was described in [2].

Measured dependences of $v_l(p)$ and $v_t(p)$ (Fig.1) have permitted calculation of the pressure dependences of the bulk modulus $K_T(p)$, shear modulus $G(p)$, Debye temperature $\theta(p)$ (Fig.2) and reduced volume $V/V_0(p)$. The decrease of the transverse sound velocity in La and Pr at the pressures of 18-23 and 30-49 kbar, respectively, and a large hysteresis of $v_t(p)$ ($\sim$ 13

for La and $\sim$25 kbar for Pr) confirmed here the first-order phase transition and permitted the determination of its parameters. The obtained transition pressure was equal to 23±2 for La and 50±2 kbar for Pr. A considerable hysteresis of this transition in La and all the more in Pr is due to the small difference in the specific volumes of the coexisting phases. The pressure dependence of the longitudinal sound velocity $v_l(p)$ for both metals does not exhibit any hysteresis.

The softening both of longitudinal and transverse acoustic phonons with a concomitant ultrasound signal attenuation was observed at the pressures of 62-76 for La and 66-81 kbar for Pr. The lack of hysteresis in the $v_l(p)$ and $v_t(p)$ curves points to their features are not connected with the first-order phase transition. Decrease of $v_l(p)$ with pressure in the intervals of 62-76 and 66-81 kbar respectively for La and Pr leads to the continuous lowering of the bulk modulus $K_T(p)$ as 9 and 4% with the consequent its rising (Fig.2).

Decrease in transverse sound velocities for both metals at the pressure of 66-80 kbar in our experiment we connect with detected at $\sim$70 kbar continuous distortion of FCC-lattice, that was classified as a second-order phase transition [3]. However, in spite of high sensitivity of the ultrasound technique we were unable to detect any bulk modulus discontinuity.

Anomalies in elastic behavior of La and Pr in interval of 62-80 kbar can be explained within the framework of the pseudopotential method with allowance for 6s-5d-electron transitions. Physical cause of the anomalous increase of these metals compressibility under pressure is an increasing of d-character of the conductivity electrons, that in turn enhances their connec-

tion with the nucleus. It leads self-consistently to the less effective repulsion of valent and ion core electrons.

The analysis of our obtained expressions [4] for the equation of state and the bulk modulus within the framework of the pseudopotential model allowed to conclude that the observed decrease of the bulk modulus is due to the accelerated 6s-5d-electron transition process at 62-72 for La and 66-76 kbar for Pr. It is possible, that the decrease of compliance to contraction of the distorted FCC-lattice of La and Pr above 80 kbar is due to the Fermi-repulsion between electrons or due to the more thin effects connected with a permanently changed bottom curvature of the s- and d-bands in the process of the s-d-transitions.

Due to partially filled d-states of metals studied it was estimated the effect of the 6s-5d-electron transitions on the baric change of the compressibility within the framework of obvious Fridel's model. The estimation results showed that the compressibility anomalies observed are due to the accelerated 6s-5d-electron transition process also. Thus, two different models show the same cause of the anomalies.

Deviation from the experimentally observed equation of state and calculated one within the framework of the Fridel's model coincide satisfactorily.

Unlike the bulk modulus, the shear one G(p) is determined by the structure-dependent terms in energy. Band energy constitutes a considerable part of the polyvalent metals shear modulus. d-character enhancement of the conductivity electrons gives rise to increasing that in turn leads to decreasing shear modulus.

Let us note in conclusion that due to the same reasons it

should be expected the decrease in the shear and bulk moduli near the isomorphic electronic transition in FCC-Cs under pressure.

References

1. Duthie J.C., Pettifor D.G. Correlation between d-Band Occupancy and Crystal Structure in the Rare Earths. Phys.Rev. Lett., 1977, 38, N10, 564-567.
2. Goncharova V.A., Il'ina G.G. Anomalies in the Elastic Properties of Polycrystalline Lanthanum at Phase Transitions under Pressure up to 84 kbar. Zh. Eksp. Teor. Fiz., 1984, 86, N5, 1708-1714. /Sov.Phys. JETP, 1984, 59, N5, 995-998/.
3. Grosshans W.A., Vohra Y.K., Holzapfel W.B. Evidence for a Soft Phonon Mode and a New Structure in Rare-Earth Metals under Pressure. Phys.Rev.Lett., 1982, 49, N 21, 1572-1575.
4. Boguslavskii Yu.Ya., Goncharova V.A., Il'ina G.G. Anomalies in the Elastic Properties and Some Features of the Electronic Transitions in Lanthanum and Praseodymium under Pressure up to 84 kbar. Zh. Eksp.Teor. Fiz., 1986, 91, N 5, 1735-1743.

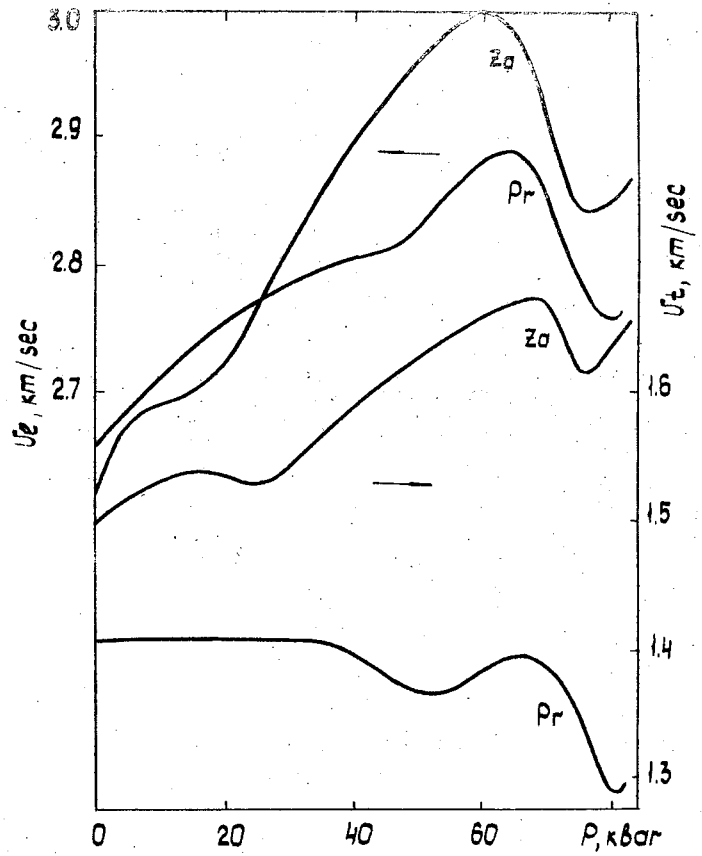

Fig. 1. Pressure dependence of the propagation velocities U_l and U_t of longitudinal and transverse ultrasonic waves, respectively, in polycrystalline lanthanum and praseodymium.

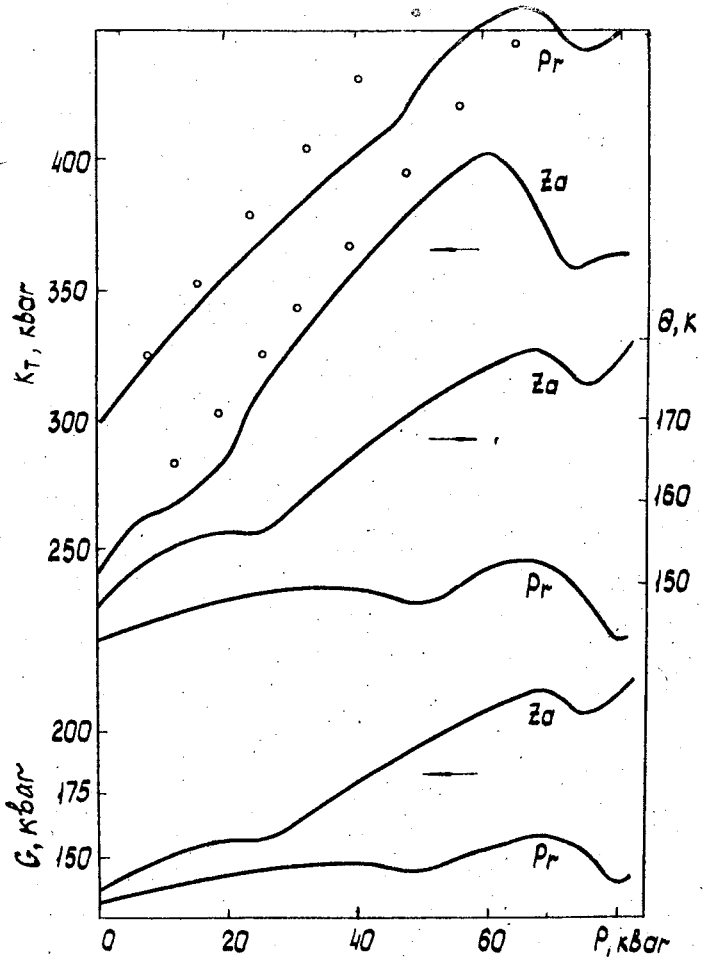

Fig. 2. Pressure dependence of the bulk modulus K_T, shear modulus G, and Debye temperature θ for polycrystalline lanthanum and praseodymium; o - calculation data for $K_T(p)$.

STRUCTURAL PHASE TRANSITIONS UNDER HIGH PRESSURE IN POROUS CRYSTALS

O.V.Kholdeev, I.A.Belitsky, B.A.Fursenko, S.V.Goryainov

Institute of Geology and Geophysics, Novosibirsk, 630090, USSR

The lacy frameworks of zeolites which form systems of through pore channels are ideal models for the investigation of structural phase transitions of the polyhedron rotation or pure displacement type in porous crystals under pressure.

Natrolite, $Na_2Al_2SiO_3O_{10}\cdot 2H_2O$, and paranatrolite, $Na_2Al_2SiO_3O_{10}\cdot 3H_2O$, with similar structure motives of the (Al,Si,O)-frameworks characterized by the order of Al and Si as well as by occupation of H_2O sites in channels were studied at hydrostatic pressures up to 50 kbar. The experiments were carried out in a diamond anvil cell using the methods of optical polarization microscopy, multichannel Raman microspectroscopy and X-ray diffraction.

Two structural phase transitions were found during natrolite compression in water: natrolite I → II at a pressure 7.5 kbar [1-3] and natrolite II → III at a pressure 13.0 kbar. The features of structural changes occurred are displayed in the Raman spectra (Figs 1,2) and X-ray diagrams obtained at a high pressure.

The investigation results allow the following conclusions to be made about the nature of structural phase transitions in narrow-pore crystals of the natrolite group.

1. A principal difference in the natrolite behaviour has been found depending on the molecule size of the pressure transmission medium. During compression in non-penetration media

such as ethanol, methanol, glycerine etc., a linear dependence of crystal compressibility on pressure is observed without phase transitions, single crystallinity being conserved. The compression in penetration medium (water) is followed by the structural phase transitions in natrolite I → II, II → III with the disturbance of the single crystallinity of the sample. The phase transitions are completely reversible and are not quenched by depressurization.

2. The structural phase transitions observed in natrolite are of the type of polyhedral tilting or displacement [4]. The phase transition of natrolite I → II is due to the introduction under pressure of H_2O molecules into the sites W_2 in the framework channels, which leads to the $[Al_2Si_3O_{10}]_\infty$ chain turn in the (001) plane with a correspondent increase in the parameters a and b as well in the unit cell volume, i.e. with an anisotropic "swelling" of the crystal, significant tensions being occurred which result in the destruction of the crystal into microblocks according to the cleavage planes (110), $(1\bar{1}0)$. The phase transition of natrolite II → III is followed by a decrease in unit cell volume with the general ordering of the phase III structure.

3. The Raman spectra and X-ray diagrams show that paranatrolite is different in structure from natrolite I and is close to natrolite II. A good coincidence of frequencies and relative intensities of the basebands of framework vibrations (140, 427, 530 cm^{-1}) as well as of the shape of stretching vibrations OH (3460 cm^{-1}) was shown by comparing Raman spectra of natrolite II and paranatrolite (Fig.1). The X-ray diagram of

natrolite II is close to that of paranatrolite. The unit cell parameters of both zeolites are similar: $a_o \cong b_o$ = 19.09(6), c_o = 6.47(2), V_o = 2360(14) for natrolite II at 7.5 kbar and a_o = 19.07, b_o = 19.13, c_o = 6.58, V_o = 2400 for paranatrolite under normal conditions [5].

4. The structural difference between natrolite I and paranatrolite is due to the fact that the arrangement of Al and Si in the former case is ordered and in the latter case it is disordered as well as to the presence of H_2O molecules in the W_2 sites under normal conditions in paranatrolite (in natrolite I these sites are vacant).

Under pressure in penetration medium the deformational disorder of the natrolite I structure occurs and it transforms into natrolite II where the statistically disordered occupation of the W_2 sites by the H_2O molecules incorporated under pressure leads to a deformation and displacement of the tetrahedrons TO_4 (T = Si, Al) with a disorder of valence angles O-T-O, T-O-T, the ordered spatial arrangement of Si and Al in the tetrahedrons being conserved. This type of structural transformation, which is due to a change of order in the filling of channels with rescpective changes in the framework order, can be widespread in porous framework silicates.

References

1. Kholdeev O.V., Belitsky I.A. High pressure effect on optical properties of fiber zeolites. In: IVth Bulgarian-Soviet symposium "Natural zeolites" Abstracts, Burgas 1985, p.9-10. (in Russian).

2. Kholdeev O.V., Belitsky I.A., Fursenko B.A. Optical properties of zeolites under high pressure in fluids. In: Proceedings of International Conference"Zeolite 85," Hungary, Budapest, 1987.

3. Belitsky I.A., Gabuda S.P., Moroz N.K. An increase in rate of molecular diffusion in zeolite at high hydrostatic pressures. DAN USSR, 1987, t.292, N 5, s.1191-1195 (in Russian).

4. Hazen R.M., Finger L.W. Polyhedral tilting: a common type of pure displacive phase transition and its relationship to analcite at high pressure. Phase Transitions, 1979, v.1, pp.1-22.

5. Chao G.Y. Paranatrolite, a new zeolite from Mont St.Hilaire, Quebec. Canadian Mineralogist, 1980, v.18, N 1, pp.85-88.

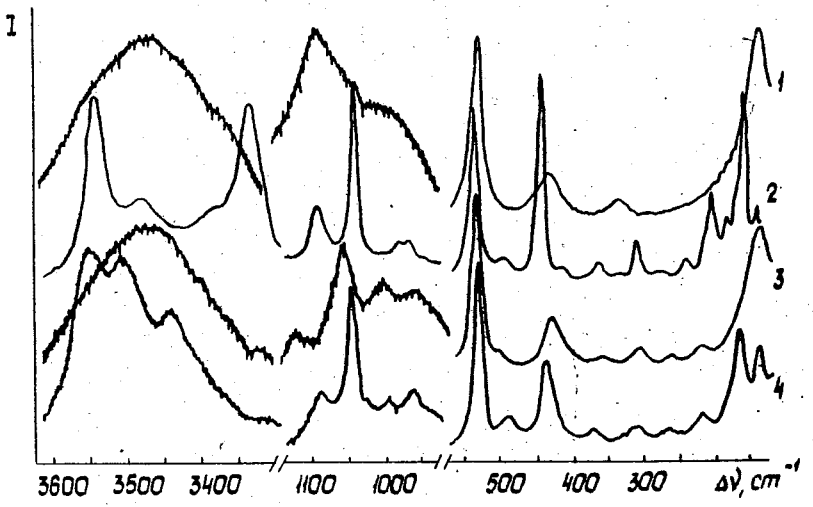

Fig.1. Raman spectra: 1 - paranatrolite (in water), 2 - natrolite I (P = 1 bar), 3 - natrolite II (7.5 kbar), 4 - natrolite III (13.0 kbar).

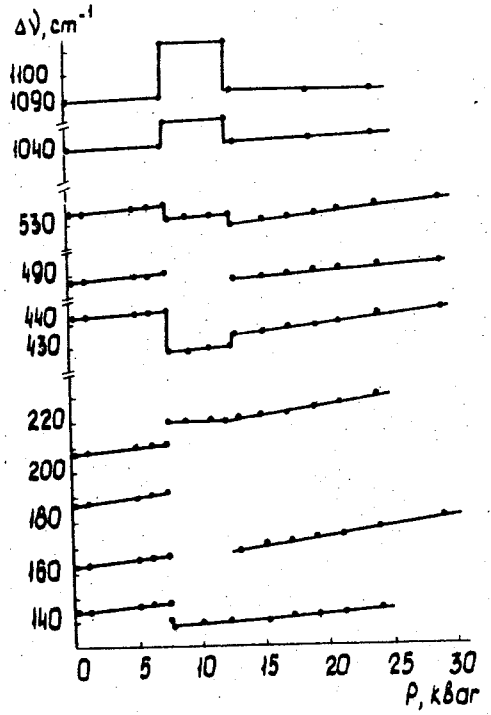

Fig.2. Frequencies of framework vibrations in Raman spectra of natrolite versus pressure in water.

THE STRUCTURAL VARIATIONS IN METALS DURING HIGH-PRESSURE DEFORMATION

L.N. Larikov, E.A. Maximenko, V.N. Dneprenko
Institute of Metal Physics, Academy of Sciences of the UkrSSR, Kiev, USSR

The deformation of metals under high hydrostatic pressure conditions, as compared with the traditional deformation methods, results in a change of both the strength and plasticity properties. It is due to the fact, that pressure effects on a behaviour of the crystalline structure defects specifying a metal structure formation. The structure formation is largely specified by an activity of the competitive processes of the localized and delocalized deformations. A comparative investigation of the local inhomogeneous structure being formed under applied high pressure conditions and without one was the aim of this work.

The deformation structure after drawing and hydrostatic extrusion was studied in Cu, Ni and Al metals. An axial texture having mainly ⟨100⟩+⟨III⟩ orientations is formed by both-kind deformations. As the X-ray microscopic investigation has shown after as little as 30% deformation each component of the texture corresponds to a definite kind of the dislocation structure [1,2]. A formation of the cellular dislocation structure is the result of a deformation localization. So, for example, for copper an average cell in the component ⟨100⟩ is twice as small and dislocation density is about three times higher than those in the ⟨III⟩ texture component. For each texture component the cell boundaries are regularly arranged respectively to a deformation axis in an axial section of the samples. For the ⟨100⟩ component the deformation is localized on the cell boundaries oriented along a texture axis and may be described by traces of the crystallographic slip planes ⟨100⟩ . As to the texture component ⟨III⟩ the cell boundaries are arranged along directions essentially different from a texture axis but parallel to the {III} plane traces.

According to the mechanism described in [3] the deformation is localized on the slip planes, the result of that the cell walls are formed parallel to the acting slip planes. In consequence of this, the ⟨100⟩ texture component is formed by nonoctahedral slipping but the ⟨III⟩ is formed by the octahedral slipping.

The difference in the deformation methods effects essentially a guantitative relation of the texture components. The X-ray data of Cu texture investigated by the reverse pole figures are given in Figure. The (III) : (I00) pole intensity relations for drawn (o) and hydroextrused (•) copper at various deformation degree ε were taken. For the hydroextrusion samples with the increase in deformation degree the number of the ⟨III⟩ component inerases more intensively than that of ⟨I00⟩ one. During drawing the texture component relation is constant approximately to 50% deformation but then a portion ⟨III⟩ increases sharply.

As two texture components are formed by acting of various slipping systems it may be concerned that the hydrostatic pressure promotes activation of the octahedric slipping during the early stages of the deformation. Later on a change occurs and the {100} plane slipping prevails.

A behaviour of the texture in Ni is the same. For aluminium in the early stages of hydrostatic extrusion the greater amount of the ⟨100⟩ component is formed than that during drawing and with the increase in deformation degree the texture component relations are altered only slightly. It is due to the fact, that the pressure leads to the increase in splitting of the dislocations, slipping along the {III} planes [4]. As copper, possesing greater stacking-fault energy, with increasing degree of the deformation and therefore the pressure during hydrostatic extrusion a splitting of the dislocations increases. As a result of this a cross slipping of the dislocations is inhibited and the less amount of the texture components ⟨III⟩ is formed. For aluminium the texture formation is effected earlier by the pressure, that is due to the lower magnitudes of the elastic constants.

With increasing deformation degree and the pressure a quantitative redistribution of the texture components is due to the partiale delocalization of the plastic deformation in the ⟨III⟩ texture component, and an increase in the localization of the deformation along the {I00} planes accompanied by formation of the large amount of ⟨I00⟩ texture.

For casting Al-based alloys the defects of pore type were healed by high pressure under quasihydrostatic conditions. In the most cases the pores have been healed completely, but an array of fine pores arranged along the grain boundaries was observed only in some places. Healing has a pure deformation character and is associated directly with the localized plastic deformation, as the

deformation is usually localized along shear bans between the pores [5]. As compared with a monolithic matrix of the samples a lowered microhardness near the residual pores was observed. The dynamic deformation softening seems to take place near the pores during high pressure treatment.

In Mo single crystals under high pressure a dynamic fragmentation process takes place. While treating the undeformed single crystals the dislocation pile-ups prevail in the structure, which represent the localized plastic deformation. While treating the predeformed single crystals rolled parallel to the {III} surface along the ⟨II2⟩ direction the dislocations are distributed more homogeneously owing to high pressure. The superimposed stress filds of the two-kinds seem to result in a stress relaxtion which initiates the plastic deformation delocalization. It is well-known that a decrease in the stability of some dislocations in bcc metals under the high pressure conditions results in the decrease in the fraction of the locking dislocations in the total density of the dislocations [6].

Therefore, the structure rearrangement in metals during deformation under the high pressure conditions is due to not only a changing magnitude of the extension of the dislocations but to a changing degree of the deformation localization as well.

References

1. Larikov L.N., Dneprenko V.N. Localnaya neodnorodnost' defektnosti kristallicheskoy reshetki v razlichnykh komponentakh tekstury pri otzhige hidroextrudirovannoy malolegirovannoy medi.- Metallofizika, 1975, 62, 19-24.
2. Larikov L.N., Dneprenko V.N. Evolyutsiya dislokatsionnoy struktury nikelya pri hidroextruzii. - Metallofizika, 1979, 76, 44-48.
3. Takeuchi T. Theory of high temperature type work-hardening of body-centred cubic metals.- J.Phys.Soc.Jap., 1970, N4, 995-964.
4. Dulin M.A., Tokiy V.V., Zaitsev V.I. O rascheplennykh dislocatsijakh v kristallakh, podvergnutykh vysokomu davleniyu. - Metallofizika, 1975, 62, 99-101.
5. Dodd B., Atkins A.G. Flow lokalisation in shear deformation of void-containing and void-free solids. - Acta Met., 31, NI, 1983,9-15.
6. Tokij V.V., Paniotov Yu.N. Vliyaniye napryazheniy na ustoichivost' krayevykh dislokatsiy I00 . - Fiz. tverd. tela, 1979, 21, N8, 2415-2422.

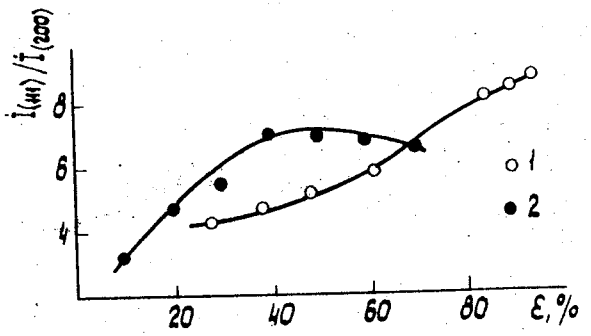

An intensity altered in copper texture with increasing deformation degree after drawing (I) and hydrostatic extrusion (2).

PHASE DIAGRAM OF DEUTERATED COPPER CHLORIDE IN VARIABLES: MAGNETIC FIELD, PRESSURE, TEMPERATURE

V.A. Galushko

Physico-Technical Institute of the Ukrainian Academy of Sciences, Donetsk, USSR

The paper presents results of experimental studies of high hydrostatic and axial pressure effect on the form and parameters of magnetic phase diagram (MPD) of antiferromagnetic single crystals of deuterated and hydrated copper chloride. These antiferromagnets (AFM) refer to rhombic class of bipyramidal crystals with two molecules in a primitive cell. Space group is D_{2h}. Magnetization easy axis coincides with crystallographic "a" axis. The equipment used for investigations made it possible to study the MPD of these antiferromagnets over a temperature range of (1.0-7.0)K in magnetic fields up to 7.0 T under the action of hydrostatic pressure up to 1.5 GPa or axial pressure up to 0.I GPa. The MPD parameters, namely T_N, Neel temperature, T_t, the triple point temperature , H_t, the triple point field , H_n, the spin-flop transition field of hydrated and deuterated copper chloride are given in the Table. It was found experimentally [1] that transition from antiferromagnetic (AF) and spin-flop (SF) phases to paramagnetic (PM) phase goes as the second-order phase transition (PT-II). Transition from the AF to the SF-phase at the external magnetic field H_n goes in the form of the first order phase transition (PT-I) with the formation of a intermediate state, i.e. thermodynamically stable domain structure of AF and SF phases over a temperature range from T=1.0 K to the triple point temperature. Parameters of the phase diagram of $CuCl_2 \cdot 2D_2O$ become 3% less as compared to the values of similar parameters of the phase diagram of the hydrated copper chloride which can be explained by the decrease of the exchange and anisotropy constants due to the increase of the crystal lattice constants at deuteration.

High hydrostatic pressure shifts the MPD of these AFM towards higher values of external magnetic field and temperature. And it should be mentioned that hydrostatic pressure up to I.5 GPa does not alter the order of phase transitions AF SF, AF PF, SF PF. Investigations showed linear dependence of the spin-flop transition field H_n on the pressure magnitude. For both AFMs dependences T_N, T_t, H_n are the linear functions of pressure.

Parameters of magnetic phase diagrams and their pressure derivatives, and magnetoelastic constants of antiferromagnet $CuCl_2 \cdot 2H_2O$ and $CuCl_2 \cdot 2D_2O$

		$CuCl_2 \cdot 2H_2O$	$CuCl_2 \cdot 2D_2O$
T_N, K		4.33	4.25
T_t, K		4.31	4.205
$H_t \times 10^{-1}$ T		8.5	8.3
$H_n \times 10^{-1}$ T		6.78	6.67
dT_N/dP K/GPa		1.8	1.72
dT_t/dP KGPa		1.53	1.54
dH_n/dP T/GPa		0.142	0.148
dH_n/dP T/GPa	"a"	0.21	
	"b"	0.07	
	"c"	0.05	
dT_N/dP K/GPa	"a"	3.04	
	"b"	0.65	
	"c"	-0.13	
$L^{(e)} \times 10^{23}$ T^2/J GPa	"a"	2.44	
	"b"	0.53	
	"c"	-0.11	
$L^{(e)}$	$\times 10^{23} T^2$/J.GPa	4.34	4.15
$L^{(e)}$		-4.56	-2.16
L_I		1.26	0.59
L_2		0.43	0.29

The study was made [2] of the effect of the axial compression of the specimen along the "a", "b" and "c" axes on the Neel temperature of $CuCl_2 \cdot 2H_2O$. The maximum change in T_N is observed in case of compression along the magnetization easy axis ("a" axis). This change is greater than in case of hydrostatic pressure. Values of dT_N/dP for "a", "b", "c" directions are given in the Table. Experimental results of the investigation of the spin-flop transition field at axial compression of the specimen along "a", "b", "c" directions are presented for T=I.75 K. With the axial compression increase value of H_n grows linearly for all directions studied. The most drastic change of H_n occurs in case of the crystal compression along the magnetization easy axis. Over the whole temperature range of the investigation of magnetically ordered state of $CuCl_2 \cdot 2H_2O$ at axial compression along the "a", "b" and "c" axes the spin-flop occurs as the first order phase transition. Coefficients dH_n/dP for "a", "b", "c" axes are given in the Table. These experimental results show that exchange and anisotropy determining the spin-flop transition field at the axial compression are anisotropic along the "a", "b", "c" axes and change linearly. The results obtained in our experiments made it possible to calculate, based on the theory [3], the values of magnetoelastic constants L which are presented in the Table.

The investigations performed yield the following conclusions:

I) Hydrostatic and axial compressions do not change the order of phase transitions in $CuCl_2 \cdot 2D_2O$ and $CuCl_2 \cdot 2H_2O$.

2) Hydrostatic and axial compressions linearly change exchange and anisotropy constants of these AFMs which is evidenced by the change of the parameters of magnetic phase diagram of these antiferromagnets.

3) Axial compression changes the values of parameters of magnetic phase diagram of AFMs more drastically than hydrostatic one does.

References

1. Galushko V.A., Ivanova S.V., Pashkevich Yu.G., Telepa V.T. Pressure effect on magnetic properties $CuCl_2 \cdot 2D_2O$ at low temperatures//Fiz.nizk.Temp.-1981.7, N7.-P.893-900
2. Galushko V.A., Kul'batskii V.P., Pashkevich Yu.G., Sobolev V.I Telepa V.T. Axial compression effect on Neel temperature of antiferromagnet $CuCl_2 \cdot 2H_2O$//Fiz.tverd.Tela.-1983.-25, N8.-P.915-917.
3. Baryakhtar V.G., Galkin A.A., Ivanova S.V., Kamenev V.I., Polyakov P.I. Magnetoelastic properties of copper chloride dihydrate under pressure//Fiz.tverd.Tela.- 1979.- 21.-N2. P. I5I5-I52I.

ISOBARIC ELECTRICAL RESISTANCE ALONG THE CRITICAL LINE IN NICKEL: AN EXPERIMENTAL TEST OF UNIVERSALITY

Mohammad Yousuf, P. Bhaskara Rao and Anil Kumar *
Indira Gandhi Centre for Atomic Research, Kalpakkam 603 102 India
* Physics Dept., Indian Institute of Science, Bangalore 560 012 India

Abstract. Analysis of the electrical resistance data along the critical line of nickel yields $\alpha = \alpha' = -0.114 \pm 0.008$, $A/A' = 1.256 \pm 0.007$ and $D/D' = 1.2 \pm 0.1$. These values are close to those predicted by the theory and are insensitive to pressure variation.

The concept of universality demands that if a field variable does not alter the symmetry of the ordered state, then all the quantities characterising the universality class should remain unchanged under the field variation [1]. Our motivation is to test this idea in nickel, a Heisenberg ferromagnet with d=3, n=3. Since, the magnetic energy is proportional to the electrical resistivity [2], in the range $T \to Tc$: $R = C_0 + C_1 t + C_2 t^2 + A t^{1-\alpha} \times (1 + D t^{0.57})$... (1). Similar expression with prime coefficient and exponents is used in the range $T \to Tc$. Characteristic to solids is the presence of imperfections and lattice strains leading to a distribution of Tc s [3]. In order to account for the above, the data points are fitted to $R^*(T, Tc, \sigma) = \int R(T, Tc-x) g_\sigma(x) dx$ ...(2). Here $g_\sigma(x)$ is a Gaussian in x of width σ. The integral is done numerically, using 15-point Hermite integration, and the width of the Gaussian is varied from 10^{-8} to 1 K to obtain minimun in the rms error. The values are reported in Table and Figure.

From the Figure and the Table, we notice that our investigation quantitatively verify the crucial assumption of the renormalisation group theory that a field variable, in the present case, pressure does not alter the values of α, α', A/A' and D/D'. This finding is a reflection of the smoothness of the critical line of nickel. An earlier investigation along the λ-line of He (d=3, n=2) led to similar conclusion, but our findings are the first ones in the magnetic systems. In case, the critical line has an extremum, the quantities which characterize a universality class shall be surely influenced by pressure or any other appropriate field variable in the neighbourhood of that extremum. Such a situation, indeed, occurs near a double critical point or even in antiferromagnets.

One of us (MY) is extremely grateful to Padmabhushan Shri C.V.Sundaram, Dr.P.Rodriguez and Dr.K.Govinda Rajan for constant encouragements.

Best fit values and the associated rms error m_r

P (kbar)	Tc	$\alpha = \alpha'$	A/A'	D/D'	m_r	From Eq.
10^{-3}	630.64	-0.115 ± 0.006	1.27 ± 0.002	1.2 ± 0.1	3.8×10^{-5}	(1)
	630.284	-0.115 ± 0.005	1.13 ± 0.007	1.2 ± 0.1	1.1×10^{-6}	(2)
20	638.26	-0.118 ± 0.008	1.23 ± 0.02	1.2 ± 0.1	6.3×10^{-4}	(1)
	638.369	-0.117 ± 0.007	1.17 ± 0.007	1.2 ± 0.1	9.7×10^{-5}	(2)
40	648.33	-0.114 ± 0.008	1.25 ± 0.002	1.2 ± 0.1	9.6×10^{-4}	(1)
	648.663	-0.117 ± 0.008	1.16 ± 0.002	1.2 ± 0.1	3×10^{-5}	(2)
50	652.14	-0.114 ± 0.008	1.23 ± 0.002	1.2 ± 0.1	1.1×10^{-3}	(1)
	652.146	-0.115 ± 0.006	1.16 ± 0.01	1.2 ± 0.1	9.6×10^{-5}	(2)

Symbols

Tc: Curie temperature
$t = |T-Tc|/Tc$
A: Critical amplitude
m_r: rms error
α: Critical exponent
D: Confluent singularity amplitude.

References

1. Kumar, A., Krishnamurthy, H.R. and Gopal, E.S.R., "Equilibrium critical phenomena is binary liquid mixtures". Phys.Rep., 1983, 98, 2, pp.57-143

2. Fisher, M.E. and Langer, J.S., "Resistive anomalies at magnetic critical points", Phys.Rev.Lett. 1968, 20, 13, pp.665-8

3. Kallback, O., Humble, S.G. and Malmström, G., "Critical parameters from electric resistance of nickel". Phys.Rev., 1981, B24, 9, pp.5214-20

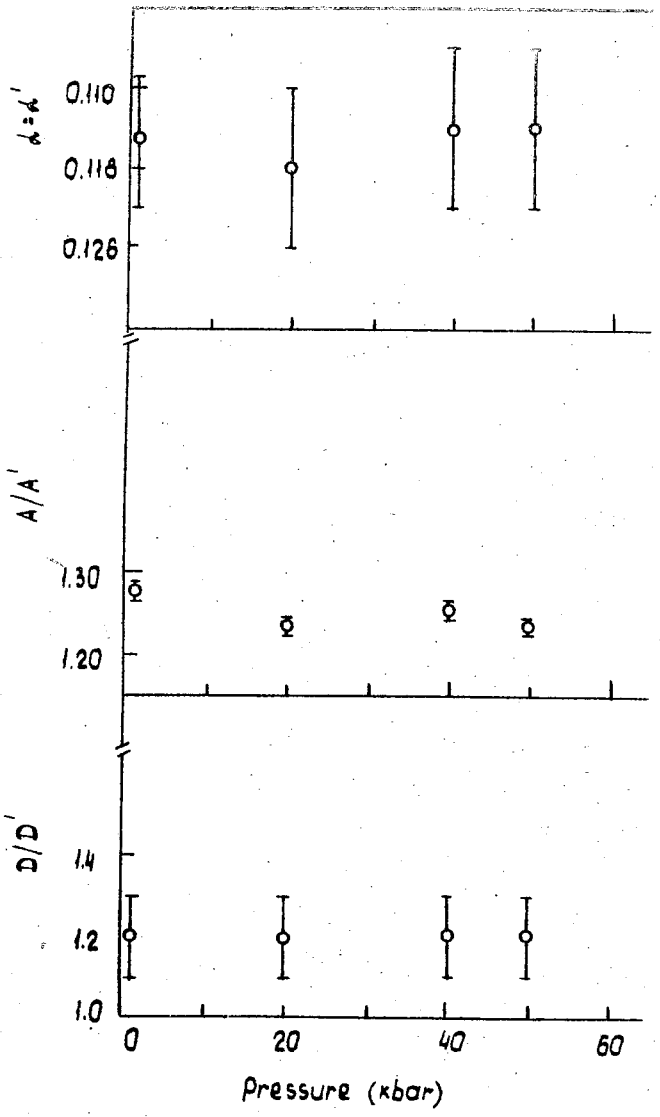

Critical exponents (α, α'), the critical amplitude ratio (A/A') and the ratio of the amplitudes of correction to singularity (D/D') as a function of pressure.

PHASE TRANSITIONS IN INTERCALATION COMPOUNDS OF GRAPHITE UNDER PRESSURE

N.B.Brandt, S.G.Ionov, V.A.Koulbachinskii, O.M.Nikitina
Moscow State University, Moscow, USSR

When acids, salts and alkali metals are intercalated into graphite the electronic density between the carbon atoms and the intercalating substance is redistributed. In the compounds formed by intercalation into graphite (GIC) the number of free carriers increases by several orders of magnetude - holes when the intercalate is a acceptor. The energy spectrum of current carriers in GIC is determined by the intercalation stage (number N of stage is equal to the number of carbon layers situated between the nearest layers of intercalating substance) and properties of intercalate. Fermi surface (FS) of GIC consists of several cylinders situated at the vertices of a hexagonal Brillouin zone. Their number is determined by the number of stage N and the value of Fermi energy (concentration of carriers) [1].

For second-stage compounds $C_{16}ICl$ in Shubnikov-de Haas oscillation (SdH) there is one frequency corresponding to cross-section of FS $S_2=290\ 10^{-42} g^2cm^2/s^{-2}$; for third-stage GIC $C_{24}ICl$ there are two frequencies corresponding to the cross-section $S_3^1=25\ 10^{-42} g^2 x$ x cm^2/s^{-2} and $S_3^2=530\ 10^{-42} g^2cm^2/s^{-2}$. At helium temperature positive magnetoresistance and Hall effect are observed. Hall effect doesn't depend upon the value of magnetic field. Concentration of holes are $2.6\ 10^{26}\ m^{-3}$ in $C_{16}ICl$ and $3.7\ 10^{26} m^{-3}$ in $C_{24}ICl$. Under pressure in GIC $C_{16}ICl$ decreasing of extremal cross-section are observed at a rate $\partial \ln S_2 / \partial P = -0.17\ GPa^{-1}$. When pressure $P \gtrsim 0.1$ GPa at helium temperature (this pressure corresponds to $P \gtrsim 0.4$ GPa at room temperature as fix pressure method was used in chamber with a kerosin-oil medium and the pressure at room temperature is $\simeq 0.3$ GPa higher then liquid helium temperature). Qualitative change of oscillations is occurred: in GIC $C_{16}ICl$ new frequency are observed which corresponds to internal cylinder cross-section of FS of $C_{24}ICl$ S_3^1.

When pressure goes up, the value S_3^1 increases at the rate $\partial \ln S_3^1 / \partial P = 0.27\ GPa^{-1}$; Fermi energy and concentration of holes decrease under pressure.

The structure of the specimen arising in the course of the phase transition can be explained on the basis of the domain model

of GIC. Since the penetration of the intercalate proceeds from the periphery of the specimen towards the center, domains of a particular stage, whose dimensions are smaller than the dimensions of crystallites, can form with the appearence of interfaces in the form of deformed graphite layers. Under the action of pressure at room temperature the iodine monochloride molecules diffuse in the basal plane, accompanied by a corresponding displacement of the domain walls, as shown in Fig.Ia.

In a framework influence of pressure on binary GIC of first stage $C_{I0}CuCl_2$ 0.6 ICl are investigated. In this compound the succession of layers are the next: graphite-$CuCl_2$-graphite-ICl-graphite and so on. Under atmospheric pressure there are two frequencies in SdH oscillations, corresponding to the cross-sections of the FS S_3=64 10^{-42} g^2cm^2/s^{-2} and S_I=1120 $10^{-42}g^2cm^2/s^{-2}$. When pressure rises, S_3 increases. Cross-section S_I increases at the rate $\partial \ln S_I / \partial P = -0.1$ GPa^{-1} but under pressure greater than $\simeq$0.2 GPa is not observed. Under hydrostatic pressure a new frequency appears in the SdH oscillations, corresponding to the cross-section of FS S_2=290 10^{-42} g^2cm^2/s^{-2} which is characteristic for the second-stage compound $C_{I6}ICl$ [2]. The data obtained confirm domain model of GIC. Iodine monochloride in $C_{I0}CuCl_2$ formes a first stage inside of domains of $C_{I0}CuCl_2$ during the process of intercalation of GIC $C_{I0}CuCl_2$ 0.6 ICl. Under the action of pressure at room temperature the iodine monochloride molecules diffuse in basal plane and form a GIC second stage $C_{I6}ICl$ near boundaries of domains $C_{I0}CuCl_2$ (Fig.Ib). So, under pressure we observed phase transition first stage - second stage. With an increase in pressure the amplitude of the SdH oscillations corresponding to the cross-sections S_I and S_3 decreases, while the amplitude of oscillations corresponding to the cross-section S_2 increases. This indicates an increase in the relative fraction of phase volume $C_{I6}ICl$ in the specimen. When pressure is removed, the initial structure is partially restored (Fig.2).

The change in holes concentration P depends upon change in cross-section of FS and height of Brillouin zone:

$$\frac{\partial \ln p}{\partial p} = \frac{\partial \ln S}{\partial p} - \frac{\partial \ln (d_0 + d_i)}{\partial p}$$

here d_0=3.35 Å, $d_i + d_0$ - repeat distance of the compounds. Compressibility of GIC is approximately two times grater than of

graphite, for graphite $\partial \ln d_0 / \partial P = -0.28$ 10^{-3} GPa^{-1} [3]. For our samples $|\partial \ln S / \partial P| > |\partial \ln (d_0 + d_i) / \partial P|$. It means that under pressure the hole concentration in GIC $C_{I6}ICl$ falls, because cross-section of FS S_2 decreases. In GIC $C_{I0}CuCl_2$ 0.6 ICl the both cross-sections S_3 and S_I increases under pressure, and hence concentration of holes increases.

References

1. Dresselhaus M.S., Dresselhaus G. Intercalation compound of graphite. Adv.in Phys., 1981, v.30, No.2, p.139-326
2. Brandt N.B., Kuvshinnikov S.V., Ionov C,G. Pressure induced change in the intercalation step in the graphite compound. Fiz.Tv.Tela, 1984, v.26, No.2, p.361-366
3. Clarke R., Uher C. High pressure properties of graphite and its intercalation compounds. Adv. in Phys., 1984, v.33, No.5, p.469-566

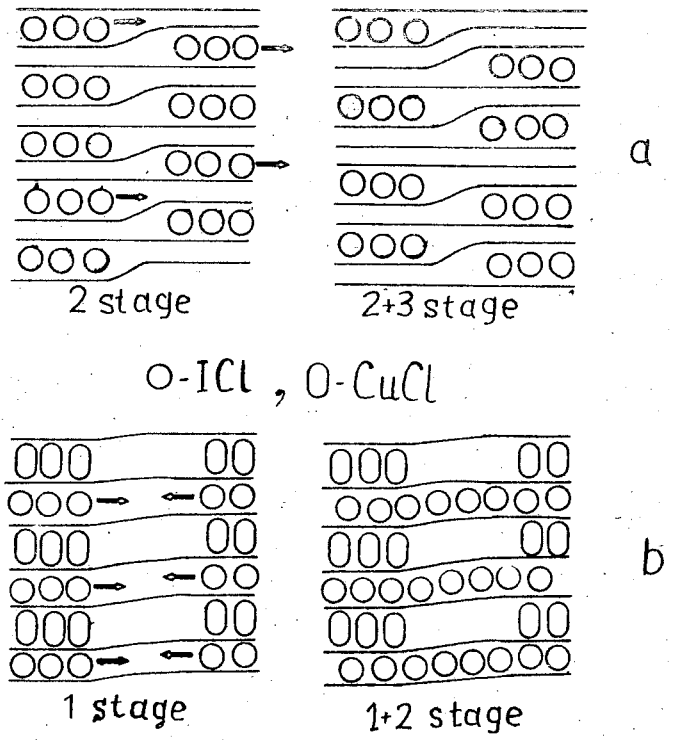

Fig.I. Model of pressure induced restructing of the domain structure of $C_{IO}ICl$ (a) and $C_{IO}CuCl_2$ 0.6 ICl (b).

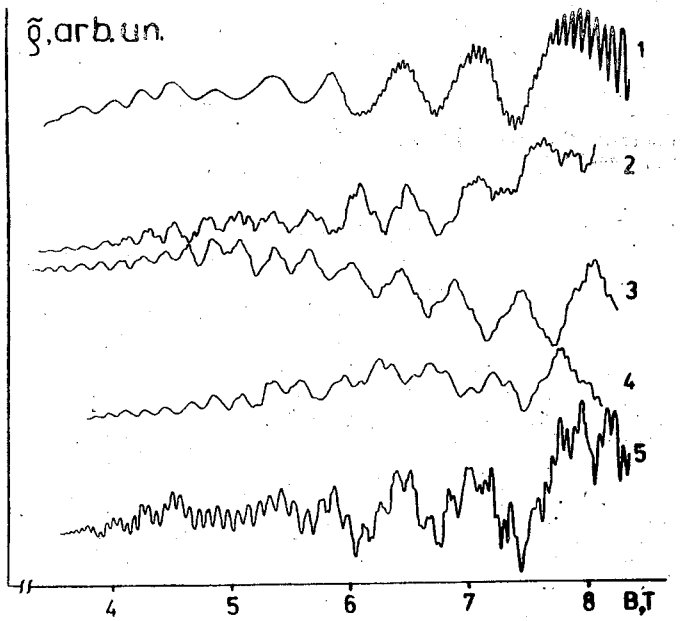

Fig.2. Dependence of the SdH oscillation on magnetic field in GIC $C_{IO}CuCl_2$ 0.6 ICl under different pressure P, GPa: I - IO^{-4} ; 2- 0.13; 3 - 0.26; 4 - 0.56; 5 - IO^{-4} after cycle of pressure.

THE INFLUENCE OF HYDROSTATIC PRESSURE TO THE GLASSY BEHAVIOR OF FERROELECTRIC (Ba,Sr)TiO_3 SOLID SOLUTIONS AND FERROELECTRICS OF RELAXOR-TYPE

P. Roth, E. Hegenbarth
Technical University Dresden, Section of Physics, German Demonratic Republic

The thermal and dielectric glasslike properties of relaxor ferroelectrics (single crystal and polycrystal) at low temperatures are well established [1], [2], [3]. The glasslike behavior at very low temperatures $T \leqq 1$ K can be described by quantum-mechanical tunneling of atoms or groups of atoms in a double-well potential (DWP). The dielectric behavior at higher temperatures $T \gtrsim 10$ K, which is marked by a large dielectric absorption peak found around nitrogen temperature in many glasses, is not well explained yet [4]. Pressure investigations allow conclusions about the volume dependence of the excitations responsible for the glassy properties.

Figure 1 shows the temperature dependence of the dielectric losses (ε'') of $(Sr_{0.61}Ba_{0.39})Nb_2O_6$ (SBN 39%) single crystal at different hydrostatic pressures. At ambient pressure ε'' has a maximum at the temperature T_M'=59 K. By hydrostatic pressure the loss maximum is shifted to lower temperatures, while the loss peak becomes higher and sharper. The increase of ε''(T) at temperatures T > 100 K is due to the dielectric losses which are connected with the diffuse ferroelectric phase transition (FPT) at T_o=350 K. At pressures $p \geqq 0.3$ GPa the loss maximum is shifted with $dT_M'/dp \approx -9$ K/GPa. In the vicinity of T_M' we have found anomalies of the dielectric constant (ε'). At pressures above 0.4 GPa ε'(T) has a small plateau at $T_M' \approx 70$ K, which is not essentially influenced by pressure. A similar behavior exhibit our pressure investigations at $Pb(Sc_{0.5}Nb_{0.5})O_3$ and $Pb_{0.915}La_{0.085}(Zr_{0.65}Ti_{0.35})O_3$ [5].

Contrary to the behavior of the ferroelectrics with diffuse FPT, our pressure investigations at polycrystalline $(Ba_xSR_{1-x})TiO_3$ (BST x), x = 3%, show an entire different behavior. Figure 2 indicates the temperature dependences ε'(T) and ε''(T) of BST 3%. At ambient pressure BST 3% has a sharp FPT paraelectric-ferroelectric (T_o=37 K) which is accompanied by a maximum of ε''. The

loss maximum at 75 K is due to the burning conditions of the polycrystalline specimen [6]. The glassy loss maximum at T_M'=11 K is not shifted by pressures $p < p_c$=0.23 GPa. At $p=p_c$ the position of the los maximum jumps to T_M'=30 K. Further application of pressure does not change T_M'. p_c is the critical pressure which is suppressing the FPT. At temperatures $T_M = T_M'$+2 K the dependence ε'(T) changes the slopes or shows weak plateaus. At increasing pressure the loss peak becomes broader and the height ε_M' (without the ferroelectric background) decreases exponentially, as it is shown in Figure 3. A similar behavior we have found at BST 6%, BST 20%, and KH_2PO_4 [5].

Under the simplified assumption of weak interacting electrical dipoles the Debye equations

$$\varepsilon'(T) = \frac{N\bar{p}^2}{\varepsilon_o k_B T} \cdot \frac{1}{1+\omega^2\tau^2} \qquad (1)$$

and

$$\varepsilon''(T) = \frac{N\bar{p}^2}{\varepsilon_o k_B T} \cdot \frac{\omega\tau}{1+\omega^2\tau^2} \qquad (2)$$

are valid, at which N is the number of dipoles per volume, $\bar{p}$ their average dipole moment, and $\omega/2\pi$ the measuring frequency. In the case of a thermal activated process the Arrhenius law is valid, and the relaxation time τ is described by

$$\tau = \tau_o \exp(E_a/k_BT) \qquad (3)$$

with the activation energy E_a. This process can be visualized by a particle moving in a DWP with barrier height E_a. First of all we consider for simplification no distribution of E_a and τ_o.
By evaluating the temperatures T_M' and T_M'', where ε'(T) and ε''(T) are maximally respectively, one gets by elimination of τ_o an equation for E_a:

$$k_BT_M'(E_a - k_BT_M'')\exp(2E_a/k_BT_M'') = \left[2E_a^2 - E_a(2k_BT_M' - k_BT_M'') - k_B^2T_M'T_M''\right] \times \exp(2E_a/k_BT_M'). \qquad (4)$$

With the experimental values of T_M' and T_M'' we have calculated E_a numerically according to Eq.(4). The results for SBN 39% indicating a linear decrease of E_a with increasing pressure. A linear extrapolation of the dependence $E_a(p)$ gives $E_a=0$ at a pressure of about.1.3 GPa. The increase of ε_M'' by pressure is a result of an increase of $N\bar{p}^2$. Hydrostatic compression lowers $\bar{p}$ if one assumes that the effective charges of the dipoles are not increased. Therefore the increase of $N\bar{p}^2$ by pressure is caused by an increase of the number of excited states.

An entire different behavior show our pressure experiments at BST 3%. At pressures $p < p_c$ we calculated $E_a \approx 10$ meV. At $p \approx p_c$ the value of E_a jumps to $E_a \approx 100$ meV. By further application of pressure E_a is not changed. The sudden change of E_a is connected with the change of the lattice structure. This behavior suggests the connection between FPT and glasslike excitations and is caused by a jumplike decrease of τ_0 and a jumplike increase of $N\bar{p}^2$ due to the change of the lattice structure.

References

1. W. Hässler and E. Hegenbarth, Glasslike behaviour of thermal conductivity at ferroelectric single crystals of relaxor-type, Ferroel, Lett. (1985) Vol. 4, pp.117-121
2. I. Henning, M. Mertig, R. Plath, G. Pompe and R. Schalge, Glasslike behaviour of $Sr_{1-x}Ba_xNb_2O_6$ (SBN) single crystals demonstrated by heat capacity measurements, phys. stat. sol. (a) (1982) Vol. 73, pp. K105-K109
3. E. Fischer, Dielectric and thermal properties of relaxation ferroelectrics at low temperatures, phys. stat. sol. (a) (1986) Vol. 97, pp.121-128
4. W.A. Phillips (Ed.), Amorphous Solids: Low Temperature Properties, Topics in Current Physics, Vol.24, Springer-Verlag, Berlin/Heidelberg/New York 1981, 167 pp.
5. E. Hegenbarth and P. Roth, to be published
6. E. Hegenbarth, Dielektrische und kalorische Untersuchungen an ferroelektrischen Keramiken bei tiefen Temperaturen, phys. stat.sol. (1962) Vol.2, pp.1544-1551

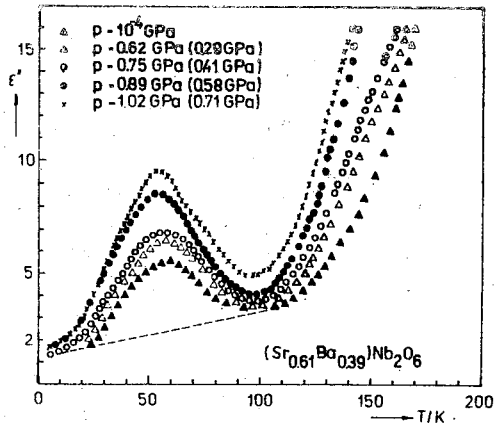

Fig. 1. Temperature dependence $\varepsilon''(T)$ of SBN 39% at different hydrostatic pressures. The values of pressure are indicated at room temperature and (in brackets) at the temperature T_M''.

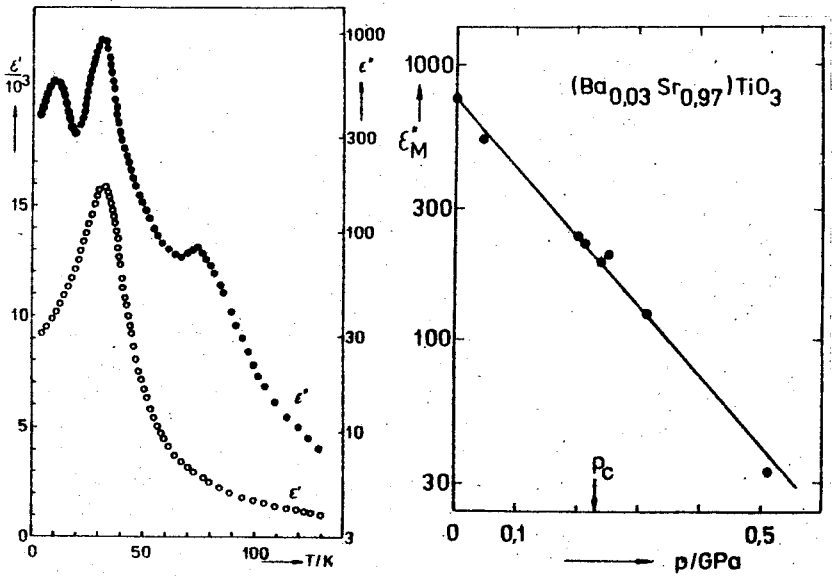

Fig. 2. Temperature dependences $\varepsilon'(T)$ and $\varepsilon''(T)$ of BST 3% at ambient pressure.

Fig. 3. Pressure dependence of the loss peak height of BST 3% at T_M''.

PHASE EQUILIBRIA UNDER HIGH PRESSURE IN Al-Si, Al-Ge SYSTEMS

O.I,Barkalov[I], G.V.Chipenko[2]
[I]Institute of Solid State Physics, Academy of Sciences of the USSR
[2]Institute for Superhard Materials, Academy of Sciences of the UkrSSR, Kiev, USSR

At atmospheric pressure Al-Si, Al-Ge alloys show simple eutectic T-C phase diagrams with limited solubility in solid state /I/.

Some binary alloys of B-elements, studied earlier /2/, displayed a monotonous increase of the superconducting transition temperature (T_c), as the electron concentration of the alloy (the quantity of valent electrons per atom) increased. The highest T_c values were observed for alloy with close-packed structures. So, one might expect that fcc Al-rich solid solutions of Si and Ge should have high critical temperatures, T_c.

The T-P-C phase diagrams of Al-Si, Al-Ge were investigated by means of differential thermal analysis (DTA) and by the "quenching-under-pressure" method. The superconducting transition temperature, T_c, was measured by the induction technique. The crystal structure of the samples was analysed by the X-ray powder technique at - I50 °C. For detail see paper /3/.

Solubility of Si and Ge in Al increases drastically under high pressure (up to I0 GPa). Solid solutions of 20 at.% of Si and I8 at.% of Ge were obtained. Rich solutions of silicon and germanium have high critical temperatures, T_c=II K and T_c=7 K, respectively, Figs.I,2 /4/.

We used the model of regular solutions with non-zero confusion volume to calculate Al-Si, Al-Ge T-P-C diagrams at pressures up to I0.3 GPa and 7.5 GPa, respectively. In calculation we took account to thermal phase expansion, the compressibility of all the phases being assumed equal. Eutectic temperature vs pressure calculated and experimental (DTA) curves are presented in Fig.3. Isobaric cross-sections of both of diagrams are given in Figs.4,5. In the melting curve of eutectic in the Al-Ge system Fig.3, one can see a break line at the pressure of 7.3 GPa due to the formation of new intermediate phases. These phases were obtained by the "quenching-under-pressure" method after treatment at 9 GPa and 3000°C. The first phase γ of 70 at.% of Ge content has a simple hexagonal structure with a=2.830 Å, c=2.622 Å (±0.005 Å), c/a=0.927

and T_c=8.2 K. The other one has a low-symmetry structure, and is denoted as X-phase, its composition being 45+50 at.% of Ge and T_c=5.2 K.

At room temperature the samples with γ -phase undergo a crystal-to-amorphous state transition. Crystallization of amorphous alloys takes place when sample are annealed at 200 °C for 3 hours.

So, at high pressures the region of solid Al(Si), Al(Ge) solutions is extended and two new-intermediate superconductive phases are formed.

References

I. Hansen M., Anderko K., Constitution of Binary Alloys. McGraw Hill Publ.Co., New York/Toronto/London I958.

2. Ponyatovskii E.G., Degtyareva V.F. New electron phases of B-element alloys-obtained by high pressure. -Fizika i teknika visokikh davlenii. - I98I, 6, 3-24.

3. Degtyareva V.F., Ivakhnenko, Ponyatovskii E.G., Rashupkin V.I. Crystalline Structure and Superconductivity of Pb-Sb Alloys after Action of High Pressure. - Fizika Tv.Tela (Sov.), I978, v.20, No.2, 412-417.

4. Degtyareva V.F., Chipenko G.V., Belash I.T., Barkalov O.I., Ponyatovskii E.G. F.C.C. Solid Solutions in Al-Ge, Al-Si Alloys under High Pressure.- Phys.State Sol.(a), I985, 89, KI27-KI3I.

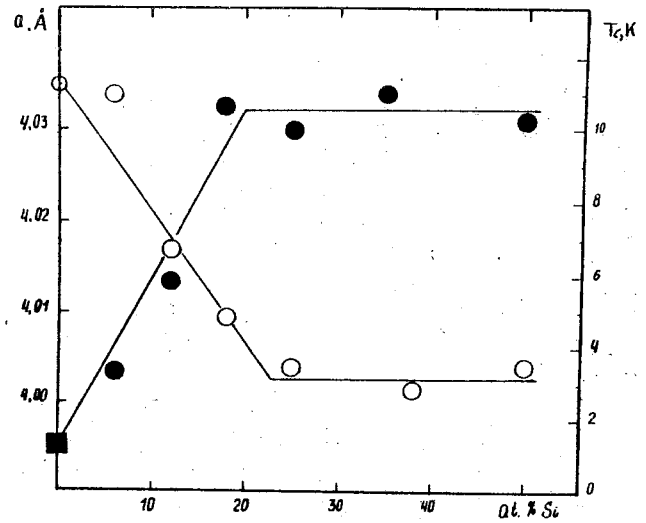

Fig. I. Dependence of lattice parameter a and T_c on the composition of the Al-Si alloy:
o - lattice parameter a of fcc solid solution; • - superconducting transition temperature T_c; ■ - T_c of pure Al.

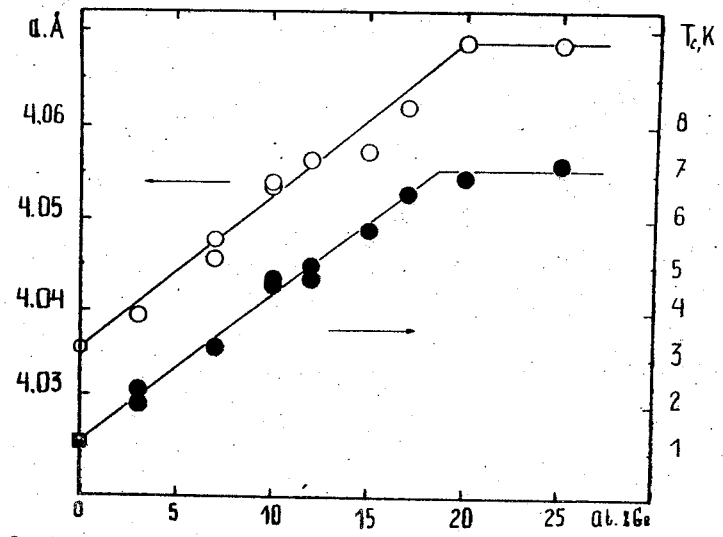

Fig.2. Dependence of lattice parameter a and T_c on the composition of the Al-Ge alloys:
o - lattice parameter a of fcc solid solution; ○ - superconducting transition temperature T_c; ■ - T_c of pure Al.

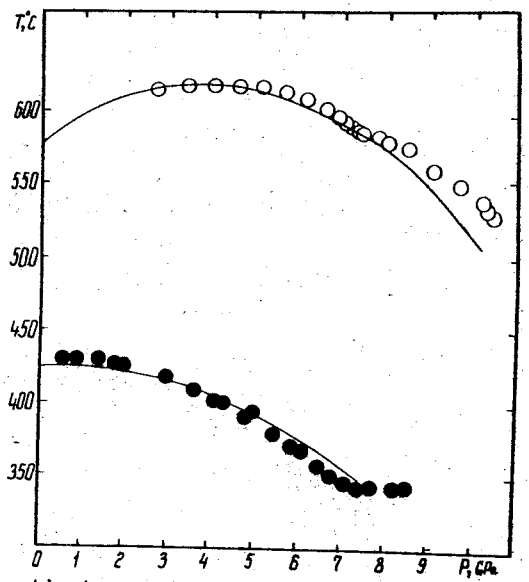

Fig.3. Eutectic temperature versus pressure:
o - experimental curve (DTA), Al-Si; — - - calculation, Al-Si;
• - experimental curve (DTA), Al-Ge; — - calculation, Al-Ge.

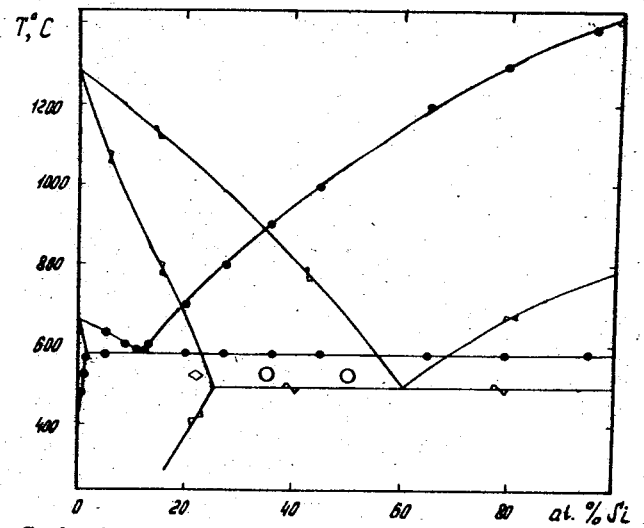

Fig.4. Isobaric sections of T-P-C phase diagram Al-Si:
• - experiment, P=0 GPa /I/; — - calculation, P=0 GPa; -∿- - calculation, P=10.3 GPa; o - experiment (DTA), P=10.3 GPa;
◊ - experiment, P=10.3 GPa fcc solid solution Al(Si).

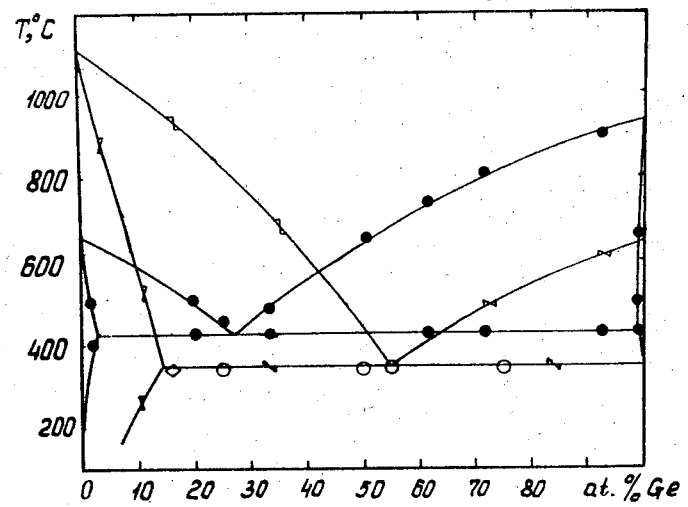

Fig.5. Isobaric sections of T-P-C phase diagram Al-Ge: ● - experiment, P=0 GPa /I/; — - calculation, P=0 GPa; ⌒ - calculation, P=7.4 GPa; o - experiment (DTA) P=7.4 GPa; ◊ - experiment, P=7.4 GPa, fcc solid solution Al(Ge).

EFFECT OF HIGH PRESSURE ON PROPERTIES OF ZINC-CONTAINING GLASSES

A.S.Smolyar, E.B.Vishnevskiy, N.N.Nekoval',
A.R.Kryuchkova, V.G.Malogolovets
Institute for Superhard Materials, Academy of Sciences of the UkrSSR, Kiev, USSR

High pressure beginning from a certain value (so called "threshold" pressure) changes a number of glass properties [1], among which the changes in their density have been studied most of all [1, 2].

The present paper studies changes in some properties of crystallizable zinc-borosilicate glasses and in their structure due to the exposure to high pressure with and without heating. The glasses under study exhibit a high zinc oxide content (Table).

It is seen from Table that high pressure processing increases microhardness of glasses by 5.4 to 20.7%. It follows from the figure that most microhardness measurements (75%) made on the glass N7 fall at the same value. Scattering of microhardness values is considerably lower than that for initial glasses. It shows that the high-pressure processing of glass results in its higher homogeneity as well as in its high strength (judging by an average microhardness value) [3].

Under pressure of 10 GPa the glass density increases by 3.12 to 14.29% and approaches that of glass ceramics in this system (4000-4190 kg/m^3), and refractive index increases by 2.42 to 4.59% The effect of high-pressure dependence of glass density decreases with increase of silicon dioxide content in glasses [4].

In IR-spectra from starting glasses the absorption at 950 and 570 cm^{-1} related to the vibration of [SiO_4] groups increases on passing from the composition 1 to the composition 5 and from the composition 6 to the composition 11 [5] and the intesity of bands

Final composition and properties of glasses before and after loading

Number of glass	Oxide content, mass %			Pressure 4.3 GPa				Pressure 10 GPa				
				microhardness			H.10^{-7} Pa	density ρ/1000 kg/m^3			refractive index	
	ZnO	B_2O_3	SiO_2	H_0	H	$\frac{\Delta H}{H_0}$, %	ρ_0	ρ	$\frac{\Delta\rho}{\rho_0}$, %	n_{e_0}	n_e	$\frac{\Delta n_e}{n_{e_0}}$, %
1	65	35	-	515	543	5.43	3.72	3.95	6.18	1.661	1.725	3.85
2	65	30	5	552	631	14.31	3.66	3.90	6.55	1.656	1.715	3.56
3	65	25	10	550	598	8.72	3.78	3.96	4.76	1.665	1.718	3.18
4	65	20	15	567	620	9.34	3.72	3.84	3.23	1.647	1.708	3.70
5	65	15	20	569	630	10.72	3.85	3.97	3.12	1.644	1.702	3.52
6	60	40	-	506	535	5.73	3.36	3.84	14.29	1.633	1.708	4.59
7	60	35	5	512	618	20.70	3.55	3.79	6.76	1.642	1.706	3.90
8	60	30	10	517	619	19.72	3.61	3.88	7.48	1.647	1.710	3.83
9	60	25	15	546	619	13.37	3.59	3.94	9.75	1.658	1.705	2.83
10	60	20	20	548	614	12.04	3.81	3.99	4.72	1.660	1.715	3.31
11	60	15	25	573	627	9.42	3.75	3.87	3.20	1.656	1.696	2.42

related with $[BO_3]$ groups decreases (1300, 700 cm^{-1}). All IR-spectra contain a 1050 cm^{-1} band, which characterizes the vibration of $[BO_4]$ groups.

High pressure effect results in smoothing the bands attributed to the vibration of $[SiO_4]$ and $[BO_3]$ groups (950 and 1300 cm^{-1}), which is due to the lowering of local symmetry of the structure groups of silicon and boron.

Zinc-borate glass 6 was subjected to pressure of 5.2 GPa and temperature of 1300 °C. Due to crystallization under pressure the density of the glass increases by 26.8%, its microhardness triples and attains that of topaz. Coordination of zinc concerning oxygen does not change, and under these conditions, unlike normal ones, the tolal boron transition from ternary coordination (concerning oxygen) to quarternary one is observed. Metastable crystal phases do not precipitate and the high temperature zinc metaborate β-ZnO-B_2O_3 is the only phase in it, the interval of its occurrence in glass ceramics under high pressure extends by more than 200 °C [5].

Zinc metaborate is found to be far harder (the hardness is 8 Mohs) than any other known borate, moreover it crystallizes both at high pressure and at atmospheric pressure. Using IR-spectroscopy the structure is shown to exhibit B-O tetrahedra $[BO_4]$ in combination with Zn-O octahedra $[ZnO_6]$.

References

I.Мазурин О.В., Стрельцина М.В., Швайко-Швайковская Т.П. Свойства стекол и стеклообразующих расплавов. Справочник. т.I. -Л: Наука, I973. - 444с; т.2, I975, -632с; т.3, I977. -588с.

2. Прянишников В.П. Система кремнезема. -Л.:Стройиздат. I97I. - 240 с.

3. Смоляр А.С., Малоголовец В.Г., Нековаль Н.Н. и др. Влияние высокого давления на цинк-боросиликатные стекла. // Физика и техника высоких давлений. - Киев: Наукова думка, 1980. - №2. С.79_82.

4. Смоляр А.С., Нековаль Н.Н., Малоголовец В.Г. и др. Изменение свойств боратных стекол под действием давления 10 ГПа. //Влияние высокого давления на структуру и свойства материалов. - Киев: ИСМ АН УССР, 1983. - С.87-90.

5. Смоляр А.С., Вальтер А.А., Вишневский Э.Б. и др. Влияние высокого давления и нагрева на цинкоборатное стекло. // Физика и техника высоких давлений. - Киев: Наукова думка, 1980. -№12.С.82-85.

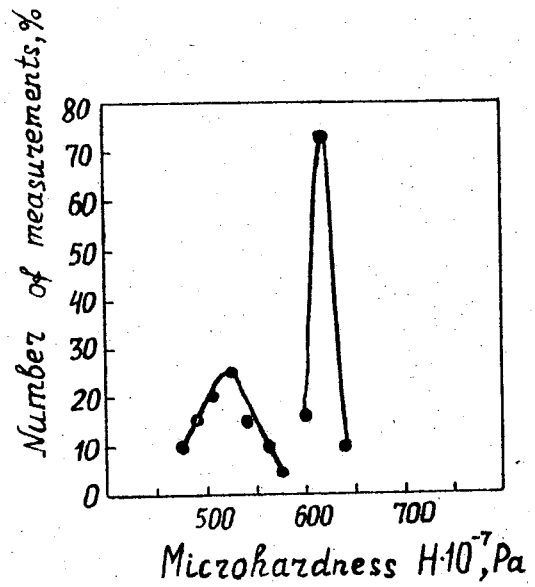

Distribution of glass (N7) microhardness:
1-before loading; 2-after being subjected to 4.3 GPa

HIGH PRESSURE PHASES OF B-METAL ALLOYS - NEW ELECTRONIC PHASES

V.F.Degtyareva
Institute of Solid State Physics, USSR Academy of Sciences, USSR

Elements of B-subgroups of the periodic table are inclined to polymorphism under pressure. The main trend in the structural change of B-elements is transition with a pressure increase into a denser, metallic state. This trend can be extended to alloy systems and it has been supported by the experimental investigations of several binary B-metal alloys under high pressure [1]. The newly found high pressure intermediate phases have a metallic type of bonding, and their structure is determined primarily by an average valence electron concentration (VEC). In this sense a new family of B-B phases can be considered as Hume-Rothery phases, if one wants to extend the definition beyond the VEC range of the original, noble-metal based Hume-Rothery phases.

With an increase in n_e there occurs a transformation to less compact structures with decreasing the coordination number, N, and packing density, η . A series of the electron B-B phases begins with the Hume-Rothery phases of 1÷2 el/atom VEC range (N=12÷8 and η =0.74÷0.68). The chain of the electronic phases can be continued by high-pressure phases [1] and splat cooling phases [2-4] in the range of higher n_e. The B-B-phase of n_e=3÷5 el/atom can be grouped according to their structures into simple hexagonal γ and simple cubic λ phases with N=8÷6 and η =0.62÷0.52. These structures are arranged by stacking of atomic nets, hexagonal or square, in sequence AAA... Simple hexagonal and simple cubic structures produce a whole family of related structures by slight lattice

Characteristic of intermediate phases in In-Sb alloys

Phase	Structure	Number of atom per unit cell	Lattice parameters, Å: a	Lattice parameters, Å: c	Atomic volume $V, Å^3$	Alloy content, at.%Sb	Number of electrons per atom n_e	Electron concentration n_e/V	Fermi-Sphere radius $k_F, Å^{-1}$	Brillouin plane parameter, $Å^{-1}$
γ	hexagonal	1	3.205	2.981	26.51	35	3.7	0.140	1.606	$\frac{\pi}{d_{101}} = 1.547$
β-Sn	tetragonal	4	5.842	3.184	27.18	55	4.1	0.151	1.647	$\frac{\pi}{d_{220}} = 1.521$;
$\mathcal{H}$	cubic	1	3.047		28.29	70	4.4	0.166	1.700	$\frac{\pi}{d_{211}} = 1.555$ $\frac{\pi}{a}\sqrt{2} = 1.457$; $\frac{\pi}{a}\sqrt{3} = 1.786$

distortion. The transformation of one to the other structure is attainable by small atomic displacements in close packed planes (Fig.1). The examples of the phases discussed can be found in the papers dealing with the effect of pressure on the alloys In-Sb [5], Ge-Sb [6], Ag-Ge, Au-Ge [7], Pb-Sn [8], Zn-Sb, Cd-Sb [9].

The phase existence ranges are determined by the electron concentration related to an average atomic volume $n_e/V \approx$ const. [1]. This condition corresponds to the constant value of the Fermi-sphere radius for free electrons $k_F=(3\pi^2 n_e/V)^{1/3}$ in the phase existence range. A successful explanation of the stability of the Hume-Rothery phases within certain values of electron concentration has been given proceeding from the concept on the interaction between the Fermi surface of the valence electrons and the Brillouin zones planes of the given structure [10]. Similar reasons should also determine the structure stability of the B-B phases under consideration. Figure 2 represents Brillouin-Jones zones for simple structures γ, β-Sn and $\mathcal{H}$ in extended k-space. Table lists the values of the Fermi-sphere radii and Brillouin-plane parameters, calculated from the experimental data on γ, β-Sn and $\mathcal{H}$ phases in In-Sb alloys [4,5].

References

1. Degtyareva V.F., Fouyatovskii F.G. High-Pressure Phases in the Alloys of B-Elements- a New Tyoe of Electron Phases. - Fiz. Tverd.Tela (Leningrad), 1992, 24, No 9, 2672-2680 (in Russian).
2. Srivastava P.K., Giessen B.C., Grant N.J. New metastable electron phases in binary B-metal alloys. - Acta Met., 1968, 16, 10, 1199-1206.
3. Kane R.H., Giessen B.C. and Grant N.J. New metastable phases in binary tin alloy systems. Acta met., 1966, 14, N 5, 605-608.

4. Giessen B.C., Kane R.H., Grant N.C. A Metastable intermediate phase in the system indium-indium antimony. - Nature, 1965, 207, 854-855.

5. Degtyareva V.F., Belash I.T., Chipenko G.V., Ponyatovskii E.G., Rashupkin V.I. Intermediate Phases in the In-Sb System Obtained by the Action of High Pressures. - Fiz.Tverd.Tela (Leningrad), 1983, 25, No 10, 2968-2974 (in Russian).

6. Chipenko G.V., Degtyareva V.F., Ponyatovskii E.G. High Pressure Phase in Ge-Sb Alloys. - Fiz.Tverd.Tela (Leningrad), 1983, 25, 4, 1228-1231 (in Russian).

7. Chipenko G.V., Degtyareva V.F. The Formation of Hume-Rothery Phases in the Ag-Ge and Au-Ge Alloys Under High Pressures. - Fiz.Tverd.Tela (Leningrad), 1934, 26, No 4, 1210-1212 (in Russian)

8. Degtyareva V.F., Ivakhnenko S.A., Rashupkin V.I. New Intermediate Phases in the Pb-Sn System Induced by High Pressure. - Fiz. Tverd.Tela (Leningrad), 1981, 23, No 4, 1177-1178 (in Russian).

9. Belash I.T., Degtyareva V.F., Ponyatovskii E.G., Rachupkin V.I. New Intermediate phases and amorphous state in Cd-Sb and Zn-Sb alloys Produced by the High Pressure Action. - Fiz.Tverd.Tela, 1987, v.29, No 6, 1788-1792.

10. H. Jones. The theory of Brillouin zones and electronic states in crystals. - North Holland Publishing, Amsterdam, 1962, p.268.

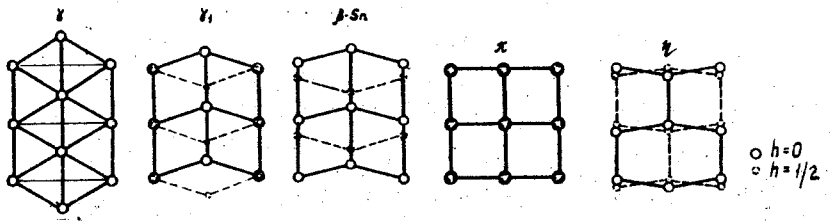

Fig. 1. Crystal structures of the related B-B-phases (a projection on the close packed planes is given).

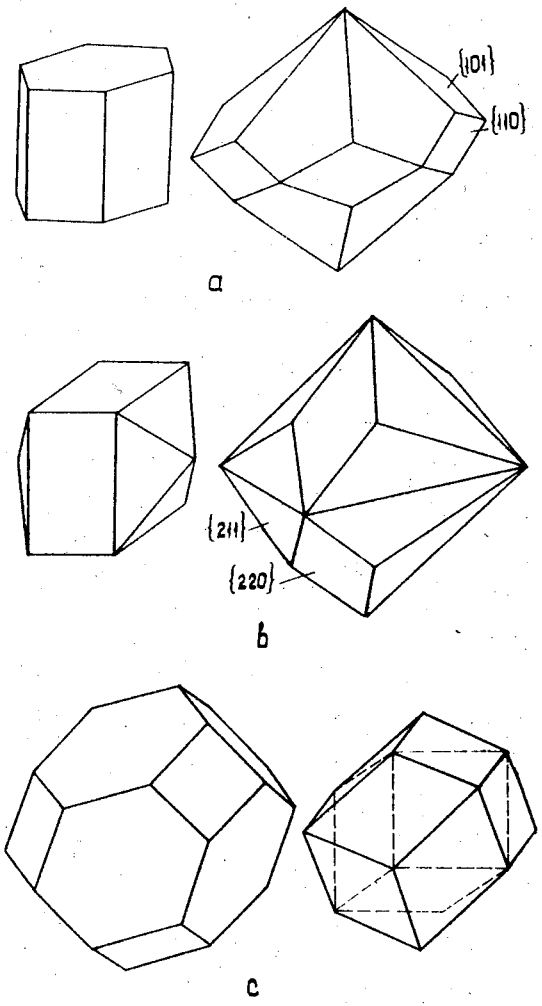

Fig. 2. Brillouin-Jones zones for simple hexagonal (a), white-tin (b) and simple cubic (c) structures.

TO THE QUESTION OF BAROCRYSTALLIZATION OF METALS AND ALLOYS

G.P.Borisov

Institute for Casting Problems, UkrSSR Academy of Sciences, Kiev USSR

Pressure as well as temperature is an independent thermodynamic parameter which defines both the state of metals and alloys, and the conditions of phase transformations being encountered in them. Moreover, the pressure action on the phase transformations, in some cases, may essentially top the temperature effect. On the ground of distinctions in principle to the point of view of atoms oscillation between the states of material of the given volume and in the case of the attainment of this volume due to the temperature variations or due to the uniform compression, the pressure reveals, in essence, the new potentialities inherent in an action on the condensed state of materials /I/.

Nevertheless, the main parameter in the control of the processes of phase transformations in metallic systems (MS) until now is temperature, and the principal method for the intensification of the crystallization processes is inherent in the cooling rate of MS.

An essential progress has been achieved in this direction associated with the development of high-speed processes of crystallization through liquid-state hardening, sedimentation onto the substrata being cooled, in ion-plasma and thermal spraying, and also by laser treatment, providing for the attainment of cooling rate values, V_t, up to 10^8 - 10^{10} K/s. However, the amorphous layer thickness, with $V_t = 10^{10}$ K/s, according to /2/, does not exceed 10 nm, and when $V_t = 10^6$ K/s, it cannot top 10 /um since the intensity of heat-removal is then limited by heat and physical properties of that metal. Thus, the further rise of MS cooling rates through the intensification of only heat-removal seems to have achieved a certain limit even in thin films.

The way out of an established situation can be found via the high pressure. As is shown in work /3/, the applying to MS of the 2-5 GPa pressure permits receiving some amorphous materials with thickness I mm and the reduction in cooling rates by I.5-2 times, as compared to the rates required in air pressure (10^3-10^4 K/s and 10^6 K/s, respectively).

The realization of the process of barocrystallization providing for the progress of a required (for the volume crystallization of the melt) supercooling of MS through a proper increase of liquid-solid phase transition temperature, under the action of pressure, reveals the prospects as to achieving the high rates of crystallization (commensurable with the rate of pressure-arise, V_p) in by far large volumes of MS, than it was in the case of high-speed cooling. The last circumstance gains a special significance for casting technologies when solving the problem to achieve high degrees of chemical and physical homogeneities of cast materials in sections of shaped castings and ingots and the further upgrading of their quality.

Of an importance is the fact that in contrast to the crystallization processes being carried out under conditions of outward heat-removal which can be accompanied by the arise of a certain temperature gradient within a section of the casting being solidified, via the pressure it is possible to achieve the required for the process of crystallization supercooling, in practice, simultaneously, at the whole of the volume of MS, with the rate of the achievement of the barocrystallization pressure.

Hence the barocrystallization pressure value can be estimated so that the crystallization temperature increment, MC ΔT_p, being achieved under the action of pressure, could meet condition

$$\Delta T_p \geqslant \Delta T_t + \Delta T_H, \qquad (I)$$

where ΔT_t is the value of the melt superheat over the melting temperature at atmospheric conditions; $\Delta T_H = H/C_p$ - temperature of an additional heating-up of MS due to crystallization heat liberation, H; C_p - molten metal specific heat.

So, for example, for the molten aluminium superheated by $\Delta T_t \approx 15$ K, with regard for the compensation of ΔT_H according to (I), value T_p constitutes ~ 370 K. To achieve the rise of the melting temperature of Al by this value an additional effect of the pressure of order of 6 GPa, will be wanted. Under conditions of crystallization with the action of high-speed pressure value ΔT_p (I) must be estimated with regard for a correction for the compensation of the temperature growth of MS, due to adiabatic compression of ΔT_a /4/.

An analysis of numerous experimental data (see Figure) indicates that in the absence of high superheats of molten MS the ro-

le of pressure as an intensifier for the process of casting solidification proves to be now at its very low values, coming to hundredth fractions of MPa (I dots). The observed effect can be achieved through the intensification of the heat exchange process, under the action of pressure, between the casting and the mold.

The subsequent growth of pressure along with the heat exchange intensification has all the more a direct effect on the crystallization process (2-7 dots). The extrapolation of the experimental curve shown in Figure corroborates the reality of the realization of the MS barocrystallization process in the field of pressures measured in GPa, where the duration of the casting solidification goes to zero.

The influence of pressure on crystallizatcn processes is especially noticeable when it is applied to MS where the superheat corresponding to the development of nuclei of crystallization has already been achieved via the heat removal. In the given conditions even the highly negligible additional supercooling yet, being achieved via the superposition of pressure, essentially causes growth of nuclei of crystallization. So, for instance, when increasing the additional supercooling of mercury only by a degree (from I8 to I9 K), under the action of some 20 MPa pressure, the number of nuclei of crystallization increases by 20 times /5/.

From the said here findings it is obvious and advisable to furtherly carry out the investigations as to determining the optimum values of the reference temperature of MS as well as of the pressure imposed on that temperature, which both provide for the production of cast materials with the structures and properties assigned in advance.

References

I. Гоникберг М.Г. Химическое равновесие и скорость реакции при высоких давлениях. -М.: Химия. I969 -

2. Золотухин И.В. Физические свойства аморфных металлических материалов. - М: Металлургия. I986 - I76 с.

3. High-pressure rapid solidification technology for amorphous materials of Cu-Sn alloys within the range of thickness of I mm / Grosse G., Kleinschmidt U.Mattern N.,etc.// 6 Int.Symp.High-Purity Mater.Sci.and Technol.Dresden, May 6-I0, I985. Poster abstr.-Oberlungw; -I985.-Pt.I-P.I4I-I42.

4. Sekhar J.A.Solidification by pressure application// Scripta Metallurgica,-I985 -Vol.I9.-P.I429-I433.

5. Аптекарь И.А.,Каменецкая Д.С. О влиянии давления на зарождение центров новой фазы//Физика металлов и металловедение. - I962. - I4, вып.2, -с.3I6-3I8.

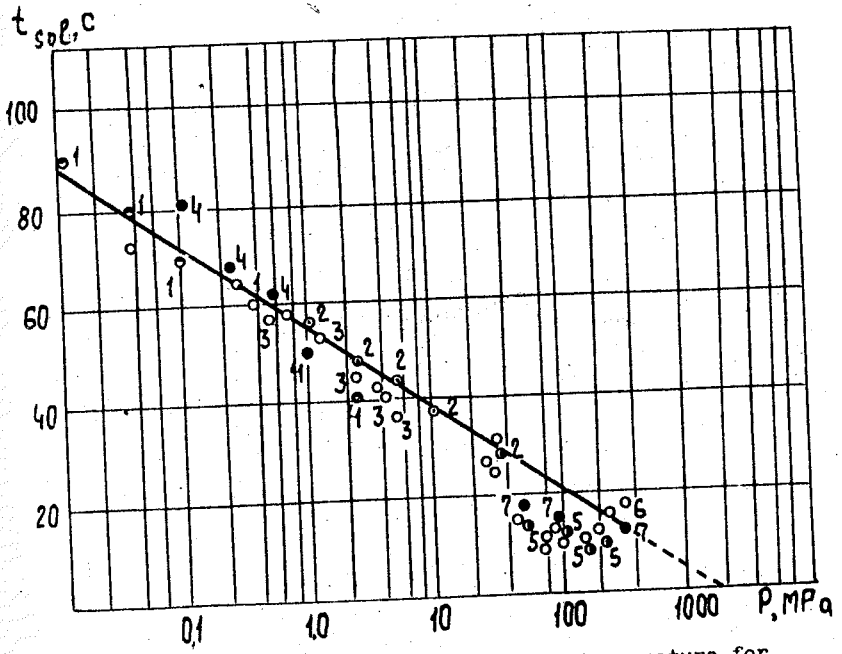

Pressure dependence of solidification temperature for liquid aluminium.

CHEMICAL INTERACTION AND POLYMORPHISM OF BORON NITRIDE IN RHF_2-BN(R-Li, Na,K,NH_4) SYSTEMS

K.P.Burdina[1], Ya.A.Kalashnikov[1], O.A.Zanevsky[2]

1 Moscow State University, Moscow, USSR

2 Institute for Superhard Materials, Academy of Sciences of the UkrSSR, Kiev, USSR

At present, great attention is paid to the development of new technological conditions for cBN synthesis. In this connection studies are carried out in our country and abroad to search for novel efficient activators of hBN ⟶ cBN transformation.

In this work a generalization is performed of experimental data on the mechanism of cubic boron nitride formation in the presence of hydrofluorides.

X-ray phase analysis has shown that even at temperatures and pressures well below the region of cBN formation the hydrofluoride is decomposed to medium fluoride and hydrogen fluoride. The process of ammonium hydrofluoride dissociation differs from those for alkali hydrofluorides, because in this case a gase phase contains not only hydrogen fluoride, but ammonia too:

$$MeHF_2 \rightarrow MeF + HF,$$
$$NH_4HF_2 \rightarrow NH_4F + HF,$$
$$NH_4F \rightarrow NH_3 + HF,$$

where Me is Li, Na, K.

Besides, together with hBN and cBN one more phase has been identified in the reaction products. X-ray phase analysis has allowed to suppose that this phase is ammonium tetrafluoroborate (NH_4BF_4) formed by the reaction:

$$4HF + BN \rightarrow NH_4BF_4.$$

The presence of NH_4BF_4 in the reaction products has been also confirmed by the method of IR-spectroscopy. Formation of this compound according to diagram indicated has been also identified by experiments conducted at atmospheric pressure in the sealed ampule.

The reactions indicated run during the short initial period of time (10 to 15 seconds)[*]. And only then immediately follows the process of cBN synthesis.That is hBN ⟶ cBN transformation starts now in a three-phase system:

$$hBN \xrightarrow{MeF,\ NH_4BF_4} cBN,$$
$$hBN \xrightarrow{NH_4BF_4,\ NH_3} cBN.$$

Therefore ammonium tetrafluoroborate in its pure form has been logically expected to be also the initiator of hBN ⟶ cBN transformation. Experiments with pure NH_4BF_4 obtained under atmospheric pressure which was added to initial hBN confirmed the point.[*]

P-T phase diagrams for RHF_2-BN systems, presented in Figure, have been drawn from experimental data. The regions of cBN in the presence of other matters have been also shown here.

An attempt has been made of formal kinetic description of hBN ⟶ cBN transformation process in $MeHF_2$-BN(Me is Na, K) and NH_4BF_4 systems.

The initial stage of transformation (with transformation degree values $W \leq 0.15$ to 0.20) corresponding to the period of cubic boron nitride nucleation has been found to run under kinetic conditions.

To find out the quantitational laws for cBH formation in tim in the given systems with $W \geq 0.15$ to 0.20 an experimental evaluatio has been performed of the degree of hBN ⟶ cBN transformation versus conditions of this reaction realization. An immediate result of experiments conducted under isothermal conditions was obtaining of

[*] Особенности синтеза β-BN в присутствии гидрофторидов щелочных металлов/О.А.Заневский, К.П.Бурдина, Л.Г.Севастьянова, Я.А.Калашников//Сверхтвердые материалы. - 1986. - №4. - С.3-6.

kinetic curves in "transformation degree" - "time" coordinates, $w=f(\tau)$, represented as diagrams.

To reveal the limiting stage for the process a formal kinetic treatment of experimental relations $w=f(\tau)$ in the range of $0.15 \leq W \leq 0.85$ has been performed using kinetic equation based on definite models of solids interaction:

$$f_1(w) = \ln\ln\frac{1}{1-W} = \ln K_1 + m\ln\tau,$$

$$f_2(w) = 1-\sqrt[3]{1-W} = K_2\tau,$$

$$f_3(w) = \left(1-\sqrt[3]{1-W}\right)^2 = K_3\tau,$$

where K_1, K_2, K_3 are the transformation rate constants and m is the parameter depending on reaction mechanism, nucleation rate and nuclei geometry. The starting reagents (hBN) diffusion through the layer of MeF and NH_4BF_4 which appears to run in condensed phase has been identified as formal limiting stage of the process.

$NaHF_2$-BN and KHF_2-BN systems have been analyzed by DTA method at pressures of 4.0 to 5.0 GPa and temperatures up to 1000 °C. Thermograms analyzed give a reason to state that in the given systems some phases contained in the mixture are melted under proper conditions. The nature of reactions running in the two systems is somewhat different.

A complicated process runs in KHF_2-BN system including KHF_2 melting and decomposition with further formation of NH_4BF_4 and its subsequent melting. Melting of $NaHF_2$ was not observed in $NaHF_2$--BN system. Its immediate decomposition with practically simultaneous formation of ammonium tetrafluoroborate, is followed by transition to its liquid phase.

Thus DTA data have confirmed the results of kinetic studies and suggest that cBN is synthesized from the solution of phases indicated.

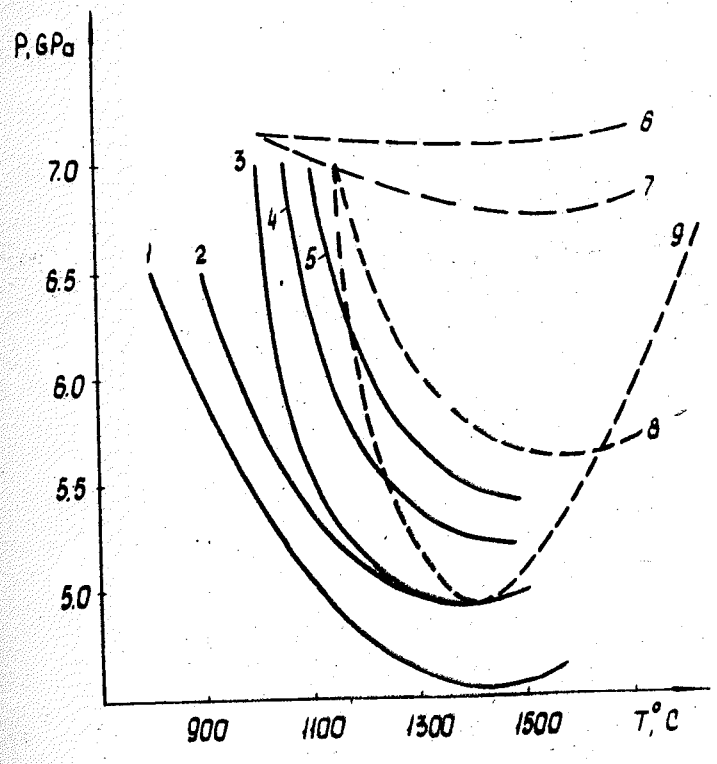

P-T phase diagrams for boron nitride in the presence of: 1-KHF_2; 2-NH_4BF_4; 3-$NaHF_2$; 4 -$LiHF_2$; 5-NH_4BF_4; 6 -KF; 7 -NaF; 8-LiF; 9-Mg_3N_2.

THE PHASE ORDER-ORDER TRANSITIONS UNDER PRESSURE

A.I. Nosar', V.I. Ryzhkov, A.A. Smirnov
Institute of Metal Physics, Academy of Sciences the UkrSSR, Kiev, USSR

The statistics-thermodynamic theory of the equilibrium phase order-order transitions in binary alloys taking account of available nonequivalent atomic positions in an alloy crystalline-lattice is recently developed [1]. There are same examples of such transitions, e.g., varying arrangment of the interstitial atoms on nonequivalent interstices, the atomic transitions between both the bulk and subsurface nodes [2], etc.

Let us consider the problem conserning the order-order transitions under pressure in the framework of the isotropic pair atom-interaction model on the configuration approximation, neglecting the correlation effects. We shall neglect geometric crystalline lattice distortions of alloy, restricting ourselves by the single-phase interstitial alloys, in which the atoms distributed along two-type nonequivalent positions may be described by one single-component long-range-order parameter x.

The equilibrium distribution N_H of the H-kind atoms along the positions N (which consist of one-kind $N_1 = \nu^{(1)} N$ positions (interstices) and the second-kind $N_2 = N - N_1$ nonequivalent positions (interstices) in the A-H binary-alloy lattice may be obtained on condition, that the thermodynamic potential Φ in the self-consistent-field approximation and in the framework of a variable-volume model is minimal.

The configuration part of the potential Φ may be represented as follows

$$\Phi = E(P,x) + PV(x,P) + kTN \sum_{i=1}^{2} \nu(i) \left[P_H^{(i)}(x) \ln P_H^{(i)}(x) + (1 - P_H^{(i)}(x)) \ln (1 - P_H^{(i)}(x)) \right], \quad (1)$$

Here, $P_H^{(i)}(x)$ is the prior probability for finding the H-kind atom in the i-th position, $\nu(i)$ is the i-th location concentration. The probabilities $P_H^{(i)}(x)$ are lineary coupled with the order parameter x.

$$P_H^{(i)}(x) = c + \gamma_i x, \quad (2)$$

where $c = \frac{N_H}{N}$, but the coefficients γ_i satisfy a simple relation $\sum_i \nu^{(i)} \gamma_i = 0$ ($\sum_i \nu^{(i)} = 1$). k is the Boltzman constant, T is the absolute temperature, P is the external pressure, E(P,x) is the configurational part of the crystal energy. In an assumed approximation we may write

$$E(P,x) = N \sum_i \nu(i) P_H^{(i)}(x) \Big[\sum_{i1} U_{HA}(\rho_{i1}(P)) Z_{HA}(\rho_{i1}) + 1/2 \sum_j \sum_{\rho i1} U_{HH}(\rho_{i1}(P)) Z_{HH}^{ij}(\rho_{i1}) P_H^{(j)}(x) \Big], \quad (3)$$

where, $U_{HA}(\rho_{i1}(P))$ and $U_{HH}(\rho_{i1}(P))$ are the values of the interaction energies of atomic pairs A-H and H-H, respectively, spaced $\rho_{i1}(P)$ to be the radius of the 1-st coordination sphere, being drawn around the i-th interstice under pressure P.

The crystal volume V(x,P) for the assumed model is determined by the following expression

$$V(x,P) = V_o(1 - \varkappa P) + N \sum_i \nu(i) \omega_i P_H^{(i)}(x) = V_o (1 + Q(P) x), \quad Q < 1, \quad (4)$$

where, ω_i is the varying crystal volume with the H atom addition in the i-th-kind position, $\varkappa$ is the compressibility, V_o is the crystalline-matrix volume at $N_H = 0$, $P = 0$.

Available external hydrostatic pressure in cubic crystals results in an isotropic variation of both the interatomic distances and radii of the corresponding coordination spheres. Thus it may be written

$$U_{HA}(\rho_{i1}(P)) = U_{HA}(\rho_{i1}^{o}) + \Delta U_{HA}^{i1} Q(P,c), \quad (5)$$

$$U_{HH}(\rho_{i1}(P)) = U_{HH}(\rho_{i1}^{o}) + \Delta U_{HH}^{i1} Q(P,c),$$

where, $\Delta U_{HA}^{i1} = \frac{\rho_{i1}^{o}}{3} \left(\frac{dU_{HA}}{d\rho_{i1}}\right)_{\rho_{i1}^{o}}$, ρ_{i1}^{o} is the value of $\rho_{i1}(P)$ at $P=0$, $N_H=0$.

The pressure value P_o, at which the phase order-order transitions takes place in crystal, is determined by the equation system

$$\dot{\Phi}(x,P,T) = 0, \quad \ddot{\Phi}(x,P,T) \gtrless 0,$$
$$\Phi(x_I,P_o,T) = \Phi(x_2,P_o,T) \qquad (6)$$

Under pressure P_o a stepwise variation of the order parameter x by the value $|\Delta x| = |x_I - x_2|$ takes place, which may be fixed experimentally according to the corresponding abrupt variation of the crystal volume by the value

$$\Delta V(P_o) = N \sum_i \nu^{(i)} \omega_i \gamma_i \Delta x. \qquad (7)$$

In the framework of the assumed approximations by using Eqs. (I), (3), (4) the system (6) may be represented as follows

$$P = P^* \left[\frac{(\alpha_o + x) - (\frac{T}{T_o}) L(x)}{\alpha_I + x} \right], \qquad (8)$$

$$\frac{P}{P^*} \gtrless \frac{\left[(\alpha_o + x) - \frac{L(x)}{\dot{L}(x)} \right]}{\left[\frac{L(x)}{\dot{L}(x)} - (\alpha_I + x) \right]} \qquad (8')$$

$$\left(\frac{T}{T_o}\right) \sum_i \frac{2}{(1 - \nu^{(i)})} \left[(1 - c) \ln \frac{1 - P_H^{(i)}(x_2)}{1 - P_H^{(i)}(x_1)} - c \ln \frac{P_H^{(i)}(x_1)}{P_H^{(i)}(x_2)} \right] = \left(1 - \frac{P}{P^*}\right)(x_1^2 - x_2^2), \qquad (8'')$$

Here, $L(x) = \sum_i \frac{\gamma_i}{(1 - \nu^{(i)})} \ln \left[\frac{P_H^{(i)}(x)}{1 - P_H^{(i)}(x)} \right]$,

$$\dot{L}(x) = \frac{\partial L(x)}{\partial x}.$$

α_o, α_I, T_o, P^* are the parameters, not depending on P,T,x.

The order of the value of these parameters is $|\alpha_o| < 1$, $|\alpha_I| \leq 1$, $P^* \sim 10^5$ bar, $kT_o \sim 2 \cdot 10^{-2}$ eV. A specific view of the parameters α_o, α_I, T_c, P^* may be found as algebraic relations from both the values $U_{H\beta}(\rho^o_{il})$ and $\Delta U^{il}_{H\beta}$ (β = H, A).

As seen from Eq.(8), at T = const there is such a pressure $P_{oo} = P^* \frac{\alpha_o}{\alpha_I}$ at which the system has an equilibrium solution x = 0, i.e., there is no initial nonequivalence as to location of the H atomes in the matrix.

By removing the pressure (P = 0), Eq.(7) is transformed into the known equilibrium equation

$$kT\, L(x) = R_1^o x + R_2^o \qquad (9)$$

to be investigated in detail in [I]. It is seen, that at $P \neq 0$ Eq.(8) may be rewritten in the form of Eq.(9) by introducing $R_I(P) = R_I^o - \Delta R_I^o P$, $R_2(P) = R_2^o - \Delta R_2^o P$.

In this case

$$kT_o = -\frac{R_I^o}{\nu^{(i)}(I - \nu^{(i)})}, \quad P^* = \frac{R_I^o}{\Delta R_I^o}, \quad \alpha_o = \frac{R^o_2}{R_I^o}, \quad \alpha_I = \frac{\Delta R_2^o}{\Delta R_I^o}.$$

A form of the values R_I^o, R_2^o is gi in [I].

The investigation of the equilibrium equation (8), (8'') sh that for the system with $T_o > 0$ under pressue the order-order tra sition with changing sign of the order parameter is only availat but for the system with $T_o < 0$ the same transitions are also ava lable without any change. The parameter α_I determines the equi brium value $\tilde{x}$ at sufficiently large $P(\tilde{x} \leq \alpha_I)$.

Let us consider particularly the H atomic distribution alo both the octahedral (O) and tetrahedral (T) interstices in fcc tice metal A ($\nu^{(I)} = I/3$, $\nu^{(2)} = 2/3$, $\gamma_I = 2/3$, $\gamma_2 = -I/3$, $c = I/3$, $P^* > 0$, $T_o > 0$). In this case, when $x > 0$, $P_H^{(I)} > P_H^{(2)}$, the interstitial atoms occupy the interstices (O) mainly, but $x < 0$ ones do the interstices (T).

For such systems and at P=0 with changing temperature the der-order transitions are available. In this case for alloys

$\alpha_o > 0$ and with increasing temperature the atom transition from the (T) interstices into (O) ones takes place, but for alloys with $\alpha_o < 0$ the contrary one does. With increasing value of $|\alpha_o|$ a magnitude of the order-order transition temperature is lowered. The external pressure P does not only shift this temperature but may change the transition direction as well. If at $\alpha_o > 0$ and $\alpha_I < 0$ the transitions (T)→(O) are also remained at $P \neq 0$, then for the systems with $\alpha_o > 0$ and $\alpha_I > 0$ at $P \neq 0$ with increasing temperature the transitions (O)→(T) are already realized. The same variation of migration direction of the interstitial atoms with increasing temperature for pressured alloys is available for alloys with $\alpha_o < 0$ and $\alpha_I < 0$ as well.

The order-order transitions are also available at T = const owing to changing pressure only. For the alloys with $\alpha_o > 0$, $\alpha_I < 0$ and with increasing P the transitions (T)→(O) are realized, but for alloys with $\alpha_o < 0$, $\alpha_I > 0$ the transitions (O)→(T) take place, at the same time for the systems with $|\alpha_I| \ll 1$ a nonequivalence of the H-atom-filled sites is vanished.

A sign of the parameter α_I, when $|\alpha_I| \lesssim c$, determines a type of the H-atom-occupied-interstices at high pressure P, as a corresponding transition direction of the interstitial atoms during the order-order transitions.

Figs I, 2 show the equilibrium dependences x(T), x(P), plotted by formulae (8), (8'), (8''), having various α_o and α_I. As seen from the figures, the transitions occur at pressures $P_o \sim 0.7P^*$ (at a temperature of 0.05 T_o). With increasing temperature the value of P_o is lowered, as the order-order transition temperature decreases with increasing applied P.

We shall note in conclusion, that the pressured order-order transitions were observed in transition-metal hydrides /3/, when the (T)→(O) transition took place with increasing P.

References

1. Smirnov A.A. Obobshchennaya teoriya uporyadocheniya splavov.- Kiev: Naukova dumka, 1986. - 165 s.
2. Bobyr' A.M., Ryzhkov V.I. K teorii izostrukturnykh fazovykh perekhodov v pripoverkhnostnom sloye binarnykh splavov. Ukr. Fiz. Jhurnal. - 1985. - 30, N2 - s. 245-248.
3. Somenkov V.A., Irodova A.V., Shil'shtein S.Sh. O fazovykh perekhodakh v hidridakh perekhodnykh metallov pri vysokikh davleniyakh. Fiz.Tverd. Tela.- 1985.- 28, N10.-s.3200-3203.

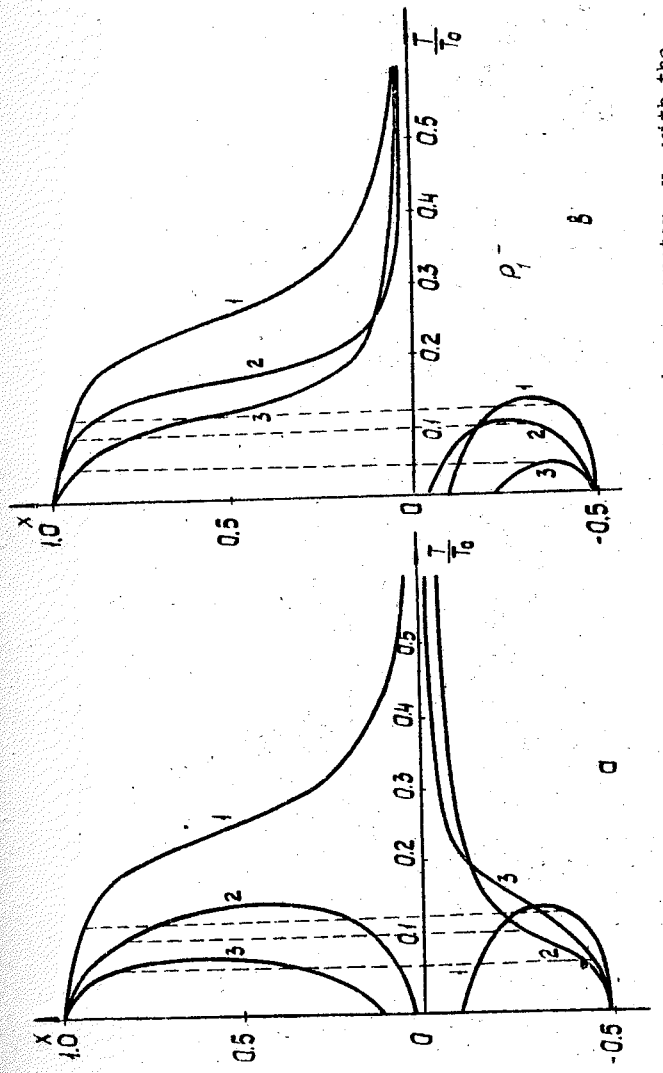

Fig. I. An equilibrium isobaric variations of the order parameter x with the temperature:
a) α_o=0.0I; α_I=0.I; I-P=0; 2-P=0.3P*; 3-P=0.6P*;
b) α_o=0.0I; α_I=-0.I; I-P=0; 2-P=0.3P*; 3-P=0.6P*.

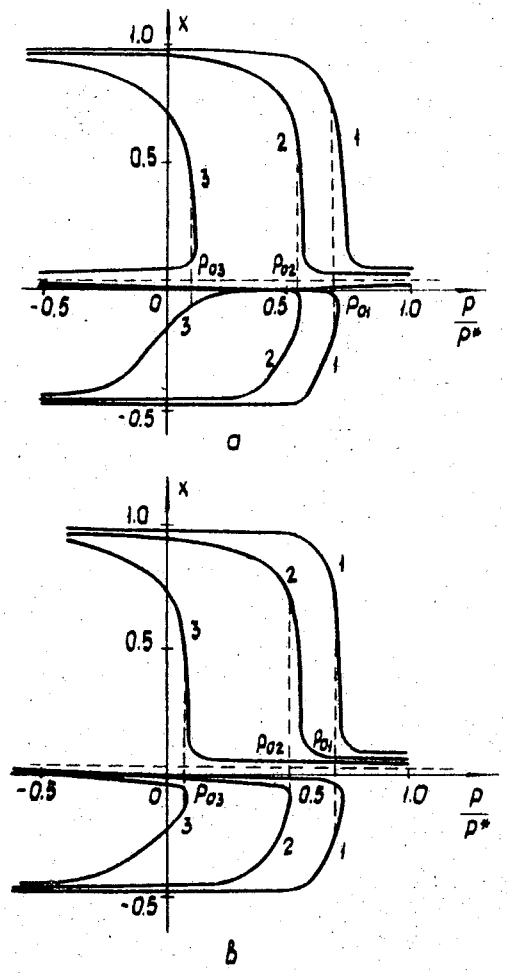

Fig. 2. An equilibrium isothermal variations of the order parameter x with pressure :

a) α_o=-0.001 ; α_I= -0.002 ; b) α_o=0.001 ; α_I=-0.002;

$I - t = \frac{T}{T_o} = 0.05$; 2- t = 0.1 ; 3 - t = 0.2.

EVIDENCE OF PRESSURE INDUCED SHORT RANGE ORDER IN FeNi INVAR ALLOYS

M.R.Gallas, L.Amaral, A.Vasquez and J.A.H. da Jornada
Instituto de Física, UFRGS
90049 Porto Alegre, RS, Brasil

INTRODUCTION

Iron-nickel alloys in the Invar region, have been the subject of considerable investigations [1-5]. The peculiar behaviour of the magnetic properties is usually related to a positive exchange interaction between Fe-Ni and Ni-Ni pairs that favours ferromagnetism, and a negative interaction between Fe-Fe pairs favouring antiferromagnetism. As a result, there are drastic changes in the magnetic properties with concentration that should depend strongly on the degree of atomic order.

In fact, from the existing neutron diffraction and Mössbauer spectroscopy studies, it is possible to see a correlation between the degree of short range order (s.r.o) with hyperfine fields [1,3].

In this work we present a study of the effects of high pressure annealings on the Mössbauer spectra in FeNi Invars.

EXPERIMENTAL

Iron-nickel samples with compositions of 30, 32.5 and 35 at% Ni have been prepared by arc melting under argon and then homogeneized at 1273 K in vacuum for four hours. Nominal purities are 99.99 at.% for Ni and 99.+ at.% for Fe. The high pressure annealings were done at a pressure of 6 GPa in a Gilder type apparatus, with internal heating. The thermal treatments under pressure consisted in a stepwise cooling from about 1200 K to 473 K, over a period of one week.

For comparison, thermal annealings under vacuum have been done. The starting temperature was set at 1080 K, because according to high pressure diffusion experiment in FeNi system

[2], a pressure of 6 GPa would reduce the rate of diffusion for about 10%. This procedure is important to keep the same kinetics for comparing the treatments at zero and 6 GPa pressure.

The Mössbauer measurements have been done in a conventional transmission geometry with a $^{57}Co/Rh$ source operated in the constant acceleration mode.

RESULTS AND DISCUSSION

The samples with 30 at % Ni annealed at zero pressure gave single Mössbauer absorption peaks, which were fitted with a Lorentzian function, yielding a linewidth (Γ) of 1.3 mm/s, in agreement with previous works [3,5]. Annealing at high pressure produced an increase of Γ, to a value of 2.6 mm/s. The reason for this increase seems to be an increase in s.r.o., since studies of Mössbauer spectroscopy [3] and neutron diffraction [1] of FeNi Invar subjected to different thermal treatments, indicate an increase in linewidth with s.r.o. for this composition. However, the observed increase in Γ could be explained also by a small change in composition or strains, induced by the high pressure treatment. In order to clarify the effect of strains we measured the sample after a cold rolling, and observed a considerable reduction in Γ, to a value of 0.7 mm/s. To check if some chemical changes occur, we subjected the already pressure annealed samples to a similar annealing under vacuum, and observed that Γ returned to the value of 1.3 mm/s. Figure 1 displays the Mössbauer spectra of 30 at.% Ni samples, submitted to different treatments.

Those results, together with the above mentioned results of neutron diffraction, strongly support the idea that pressure induces an increase in s.r.o.

A rough estimate of the change of the s.r.o. parameter α was made as described in ref.4. Assuming that the hyperfine field on Fe sites is governed solely by its nearest neighbors, a change in s.r.o. can be related to a change in Ni concentration. Taking the results of ref.5 for the dependence of Γ with concentration, then our results yields $\partial\alpha/\partial P \approx 0.001\ GPa^{-1}$.

For the 32.5 and 35 at % Ni samples, good fitting were achieved only by a distribution of magnetic fields. The spectra contains one major contribution at 255 kGauss, for the 32.5 at% Ni sample and two major contributions at 235 and 275 kGauss, for the 35 at.% Ni sample. These magnetic fields increase slightly for the pressure annealed samples.

For the 30 at.% Ni sample, we made also a search for evidence of long range order by means of a step scanning X-ray diffraction using CoK_α radiation, with negative results. However it is interesting to point out that an ordered phase in this composition range, related to $L1_2$ structure (Cu_3Au) has been proposed and searched for a long time, but no secure indication of success has been reported till now. As our results shows evidence of increase in s.r.o. with pressure, probably it would be possible to get the ordered Fe_3Ni phase at sufficiently high pressure annealings.

The authors thank Prof. J.Danon, for helpful discussion.

This work was supported in part by CNPq, CAPES and FINEP.

References

1. Men'shikov A.Z., Arkhipov V. Ye., Zakharov A.I. and Sidorov S.K., Atomic Correlation in Iron-Nickel Invars, Fiz. metal. metalloved., 1972, 34, 2, 309-315.
2. Schmidtmann V.E. und Dorner K.H., Beeinflussung der Diffusion bei den System Kobalt-Nickel und Eisen-Nickel durch allseitigen Druck bis 34 kbar, Archiv für das Eisenhuttenwesen, 1968, 39, 6, 469-476.
3. Makarov V.A. and Puzey I.M., Investigation of the Atomic Correlation in Iron-Nickel Invars by Means of the Mössbauer Effect, Fiz.metal. metalloved., 1974, 38, 1, 161-168.
4. Rodionov Yu.L., Isfandiyarov G.G. and Sarsenbin O.S., Ordering of Iron-Nickel Alloys, Fiz. metal. metalloved., 1979, 48, 5, 979-985.
5. Scorzelli R.B., Etude de Alliages Fe-Ni de la Meteorite Santa-Catharina par Spectrometrie Mössbauer et Diffraction de Rayons X, These de Doctorat D'Etat, Paris, 1982.

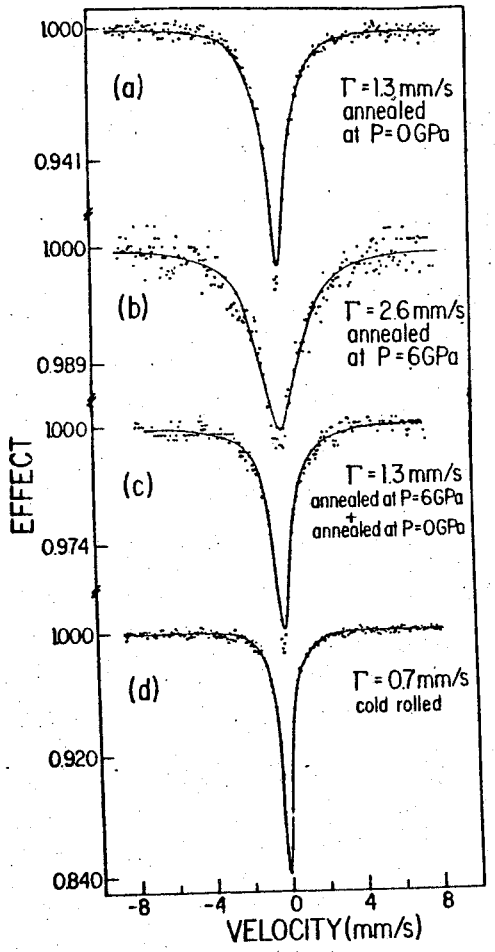

Mössbauer spectra of $Fe_{0.7}Ni_{0.3}$, measured at room temperature, for samples prepared by different treatments, as described in the text.

THE STRUCTURAL TRANSFORMATION SEQUENCE DURING THE SYNTHESIS PROCESS UNDER HIGH PRESSURE AND TEMPERATURE FOR THE Eu_2O_3-Tb_4O_7 SYSTEM

Su Wenhui and Zhou Jianshi
Group of Solid State Physics, Physics Department,
Jilin University, Changchun, P.R.China

Abstract

This work includes the studies of $EuTbO_3$ production quenched under high pressure and the structural changes during the synthetic process, using X-ray powder diffraction (XRD). A new phase of solid solution $(Eu^{3+}Tb^{3+})O_3$ which has not been reported before and the sequence of structural transformation at high temperature and high pressure were studied. The magnetic susceptibility of $(EuTb)O_3$ at room temperature was measured with vibrating-reed magnetometer.

Introduction

Eu shows vibrant-valence phenomena and Tb possesses complex electron configuration. They are striking elements in the rare earth family. Up to now the ABO_3-type compound or solid solution composed by the elements of Eu and Tb has not been obtained. According to empirical ionic radii in the system of SP-76 (Shannon, 1976) we have calculated the tolerant factor t which is related to the stability of perovskite-like structure. For the compounds of $Eu^{3+}Tb^{3+}O_3$ and $Eu^{2+}Tb^{4+}O_3$, the factor t is 0.761 and 0.900, respectively. The latter falls into the stable area of P-type structure. The factor t of $Eu^{3+}Tb^{3+}O_3$ is too little to stabilize it in P-type structure. But because of the formula $\bar{r}=(r_{Eu^{3+}} + r_{Tb^{3+}})/2=1.09A$, $Eu^{3+}Tb^{3+}O_3$ satisfies the stability condition of B-type (rare earth oxide) solid solution. From two reference criteria t and $\bar{r}$ it is possible to synthesize $EuTbO_3$ compound (2^+-4^+) and solid solution (3^+-3^+) respectively.

High pressure plays an important role for the synthesis of ABO_3-type compound (Su Wenhui, Wu Daiming, Ma Xianfeng et al, 1985). High pressure can stabilize the material which possesses some little factor t in perovskite-like structure or its distorted type (Su Wenhui, Wu Daiming, Li Xiaoyuan et al, 1985). Fur-

thermore, some new materials that can not be made by normal chemical reaction could be synthesized under high pressure and high temperature, such as $PrTmO_3$ (ibid, 1985; 1986). It is expected to synthesize $EuTbO_3$ under high pressure.

The synthetic work was done with starting material of Eu_2O_3 (C-type rare earth oxide structure) and Tb_4O_7 (flurite type structure). Up to now, the studies of reaction mechanism for solid state material at high temperature and high pressure, which is a very interesting frontier problem,is rather scarce. If the transformation of starting materials during the high temperature and high pressure synthesis could be identified, it would help to understand this problem.

The aim of this work is to study the structural transformation of the products quenched under high pressure for Eu_2O_3 + Tb_4O_7 system by X-ray powder diffraction, to synthesize $EuTbO_3$ and to measure its magnetic susceptibility.

Experiment

The starting material is Eu_2O_3+Tb_4O_7 with purity of 99.95%. Starting material weighed in ratio 2:1 was mixed and ground for 40-50 min, to make homogeneous mixture. Before the weighing and synthesizing, the material was heated at 950 ^{o}C for two hours and sintered at 1000 ^{o}C for 1-2 hours in air, to eliminate the moisture and absorbed gas. The samples were pressed into 4 mm pellets with steel pill and then put into high pressure cell.

We used improved Girdle-type high pressure apparatus. The force source is 500 ton two-anvil machine. The schematic diagram of chamber assembly is shown in Fig.1. The pressure calibration is decided by the transition points of Bi, Tl and Ba. The temperature in each synthetic process was measured and controlled with Pt-6%Rh---Pt-30%Rh (Ø 0.18 mm) thermal couple. The samples were subjected to pressure before temperature was raised. After holding at anticipated temperature for 30-60 min, the samples were quenched under pressure. The cooling rate is about 80-120 ^{o}C/s. The pressure was then released.

X-ray powder diffraction was performed with a Rigaku 12KW diffractometer, using graphite monochromator, Cu-K_α radiation (=1.5418A), high-purity silicon as internal standard, at a scanning rate of $2^{o}(2\theta)$/min. The diffraction patterns were indexed

with a computer and unit cell parameter were calculated and refined by least-square method.

The errors in temperature and pressure during the process are $\pm$20 ^{o}C, $\pm$1$_{\delta}$5 Kb, respectively. The errors in crystal parameter is $\pm$0.004 A.

The magnetic susceptibility of some products was measured with a home-made sensitive vibrating-reed magnetometer (Li Xiaobing, Zhang Yupu et al, 1985).

The curve of TG-DTA in oxygen for the products was obtained with Rigaku 8076E.Thermal analyzer to identify the valence of products. The result is shown in Fig.2.

Results and Discussion

The cell parameters and structures of products $EuTbO_3$ under different pressures and temperatures are listed in Table 1.

1) It can be seen in Table 1 that all the products under 26 Kb and 1200-1410 ^{o}C are single phase with B-type rare earth oxide structure. No trace of P-type structure has been found. The crystalline quality of the products is fine. The product of 26 Kb, 1290 ^{o}C,60 min holding is the best one (shown in Fig.3(a)), being light yellow in color.

By calculating the weight gain due to oxidation, it was determined that almost all of Tb ion is in positive trivalence state, so Eu ion is also in the same valence state. This result corresponds with the same conclusion made by the Mössbauer study (Liu Xiaoxiang, Su Wenhui, Jin Mingzhi et al, 1986). From this point, it is believed that the product's formula is $Eu^{3+}Tb^{3+}O_3$, instead of $Eu^{2+}Tb^{4+}O_3$.

In order to distinguish the product $EuTbO_3$ between compound and solid solution, the relative ratio between Eu atom and Tb atom was changed to +10%, namely $Eu_{4/5}Tb_{6/5}O_3$ and $Eu_{6/5}Tb_{4/5}O_3$, then the synthesis was carried out. From X-ray powder diffraction pattern, it is obvious that the product's structure is still of B-type, and its cell parameter changes continuously (see Table 1). This result means that $EuTbO_3$ is a kind of solid solution $(EuTb)O_3$, which is also consistent with the result obtained from Mössbauer studies. The result of Mössbauer absorption study shows that there is a disorder of distribution between Tb and Eu atoms (Liu Xiaoxiang, Su Wenhui, Jin Mingzhi et al, 1986).

Table 1. Synthetic conditions and results

Formula	Synthetic conditions	Structure	a(Å)	b(Å)	c(Å)	(°)
$(EuTb)O_3$	1200±7 °C 26Kb, 45M	B	6.840 14.120	3.578 3.582	5.961 8.775	93.68 100.13
$(EuTb)O_3$	1250±10 °C 26Kb, 40M	B	6.826 14.093	3.573 3.574	5.953 8.766	93.64 100.17
$(EuTb)O_3$	1240±10 °C 26Kb, 30M	B	6.821 14.084	3.571 3.574	5.950 8.759	93.62 100.17
$(Eu_{4/5}Tb_{6/5})O_3$	1250±15 °C 26Kb, 30M	B	6.824 14.10	3.576 3.577	5.954 8.766	93.66 100.15
$(Eu_{6/5}Tb_{4/5})O_3$	1270±15 °C 26Kb, 30M	B	6.836 14.113	3.581 3.584	5.960 8.779	93.65 100.14
$(EuTb)O_3$	1270 °C 26Kb, 30M	B	6.822 14.090	3.573 3.575	5.951 8.762	93.66 100.14
$(EuTb)O_3$	1290±10 °C 26Kb, 60M	B	6.819 14.077	3.573 3.586	5.948 8.744	93.62 100.34
$(EuTb)O_3$	1310 °C 26Kb, 50M	B	6.822 14.086	3.571 3.573	5.949 8.757	93.65 100.13
$(EuTb)O_3$	1330±10 °C 26Kb, 30M	B	6.834 14.102	3.573 3.576	5.956 8.769	93.65 100.16
$(EuTb)O_3$	1410±5 °C 26Kb, 10M	B	6.830 14.091	3.574 3.577	5.952 8.768	93.66 100.18
$(EuTb)O_3$	1000 °C 26Kb, 30M	B	6.822 14.09	3.572 3.570	5.947 8.762	93.71 100.08
$(EuTb)O_3$	710±20 °C 26Kb, 30M	B-EuTbO$_3$ B-Eu$_2$O$_3$	13.991 14.079	3.664 3.608	8.764 8.749	100.42 100.08
$(EuTb)O_3$	540±20 °C 26Kb, 30M	B-Eu$_2$O$_3$ B-Tb$_2$O$_3$ F-Tb$_4$O$_7$	13.974	3.625	8.811	100.15
$(EuTb)O_3$	1115 °C 33Kb, 15M	B-Tb$_2$O$_3$ B-Eu$_2$O$_3$				

The solid solution B-$(EuTb)O_3$ with single phase synthesized under high pressure and high temperature is a new material which has not been reported before.

2) The X-ray powder diffraction patterns of the products listed in Table 1 were indexed to two kinds of cell. The second one is the same as traditional B-Sm_2O_3 type cell with C2/m space group and six molecules of R_2O_3. The first one also with C2/m space group is analysed by the four-circle-diffractometer during the structural determination of single crystal $EuTbO_3$ also grown

under high pressure (Zhou Jianshi, Su Wenhui and Yang Guangdi, 1985), which includes two molecules of R_2O_3. In general, small cell is more believable than large one, but the results of indexing for the products listed in Table 1 demonstrate that under given pressure, the performance is better for the sample synthesized at higher temperature with the second cell and also for that synthesized at lower temperature with the first cell. The number of diffraction lines for the product synthesized at higher temperature is less than that synthesized at lower temperature. This would imply that structural symmetry is increasing with the temperature.

3) From X-ray diffraction pattern, it can be seen that there is coexistence region of four phase B-Tb_2O_3, F-Tb_4O_7, B-$EuTbO_3$ and B-Eu_2O_3 for the sample synthesized under given pressure and at less than 1000 °C. For the products synthesized above 700 °C, the intensity of diffraction from B-$EuTbO_3$ phase increases obviously (see Fig.3 c.d.e). The transformation of Eu_2O_3 from C-type to B-type is easy in the condition of high temperature and high pressure, but the behavior of F-Tb_4O_7 in the similar condition is unknown yet. From the data obtained before, the fluorite structure MO_2 with unique M^{4+} cations is stable at high temperature and even high pressure, but the condition is different for Tb_4O_7 which crystallizes in the fluorite structure with a lot of oxygen vacancies. There are 50 percent Tb^{3+} cations in F-Tb_4O_7. It was believed that there are two tendencies under high pressure. The first is to increase coordinate number and the second is to increase density. It is helpful to compare the density and coordinate number among several derivatives of TbO_{2-x}. The sequences of coordinate number and density are C(6) B(6.7) A(7) F(8) and C F B A, respectively. The coordinate number of F-Tb_4O_7 is less than 8 in average. Under high pressure, the transformation occurs from F-Tb_4O_7 to B-Tb_2O_3 with similar coordinate number and greater density. In this process, Tb cation changes its valence from Tb^{4+} to Tb^{3+}, meanwhile the oxygen anions remove from the lattice for neutrality. At this point, there is a reductive effect in the process of high pressure synthesis.

The sequence of the structure in the synthetic process is as follows: C-Eu_2O_3+F-Tb_4O_7 $\longrightarrow$ B-Eu_2O_3+B-Tb_2O_3 $\longrightarrow$ B-$(EuTb)O_3$. Because of the similar crystal parameters of B-Eu_2O_3 and B-Tb_2O_3 it is possible there is a diffusion of Tb cation in B-Eu_2O_3 structure and Eu cation in B-Tb_2O_3 as well.

4) The method of coprecipitation was used in making the starting material. The synthetic result is also listed in Table 1. The XRD pattern shows that compared with powder mixtures, the time and temperature for the synthetic process were decreased. For example, under 2.6 GPa, the crystalline quality of the product at 1240 °C, 30 min, using coprecipitated material, is similar to that at 1290 °C, 60 min, using powder mixtures.

5) The magnetic susceptibility of some products was measured. The molar magnetic susceptibility of Eu_2O_3 was taken as calibration in the measurement. The results are listed in Table 2. The symbol * indicates theoretical calculated results according to the ratio of components and their individual magnetic susceptibilities.

Table 2

Eu_2O_3	Tb_4O_7	$(Eu_{6/5}Tb_{4/5})O_3$		$(EuTb)O_3$		$(Eu_{4/5}Tb_{6/5})O_3$	
calibration		synth.	star.	synth.	star.	synth.	star.
7.08	80.5	20.0	20.3*	26.0	23.6*	26.5	23.4*

The susceptibility of synthesized materials is somewhat higher than that of starting materials, but the former still belongs to paramagnetic material.

Acknowledgement

This work was sponsored by the Science Fundation of Chinese Academy of Sciences.

References

1. Du Youru, et al.(1984). Rare Earth, 1, 4-7 (China).
2. Hoekstra, H.R. (1966), Inorg.Chem. 5, 754-757.
3. Li Xiaobing, (1985). M.D.Thesis. Jilin University. P.R.C.
4. Liu Xiaoxiang, Su Wenhui, Jin Mingzhi et al. (1986). To be published.
5. Shannon, R.D. (1976). Acta Cryst. Sect.A.32, 751.
6. Su Wenhui, Wu Daiming, Li Xiaoyuan, et al.(1985) New Frontiers in Rare Earth Science and Applications, edited by Xu Guangxian and Xiao Jimei.Vol.1,pp.342-345.Science Press.Beijing. China.
7. Su Wenhui, Wu Daiming, Li Xiaoyuan, et al.(1986) Physica.
8. Su Wenhui, Wu Daiming, Ma Xianfeng, et al.(1986) Physica.
9. Zhou Jianshi,Su Wenhui and Yang Guangdi.(1985) To be published.

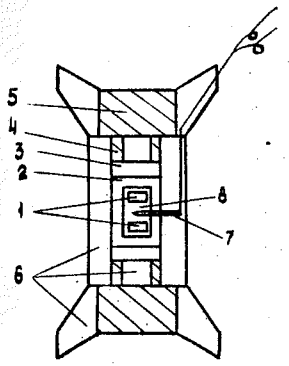

Fig.1. Diagram of chamber assembly: 1-sample; 2-carbon heater; 3-steel pellet; 4-steel cylinder; 5-steel tip; 6-pyrophyllite; 7-thermal couple; 8-BN capsule.

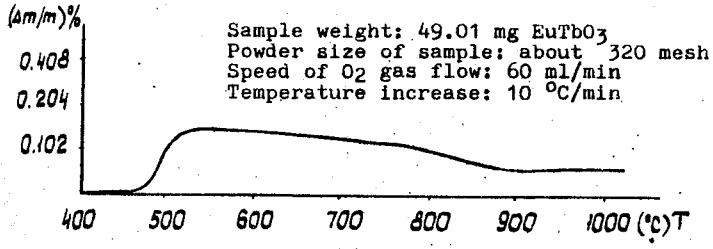

Fig.2. Thermolysis curves. Weight as function of temperature.

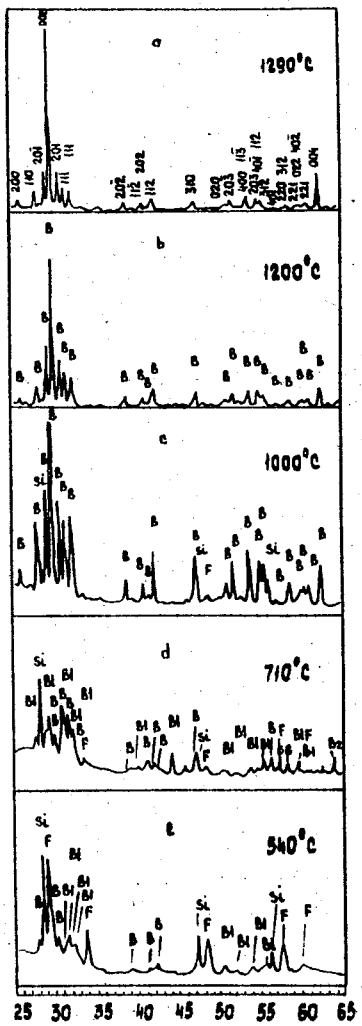

Fig.3. XRD pattern.

High Pressure Studies of the Tantalum/Hydrogen System

A.W.Szafranski and M.Tkacz

Institute of Physical Chemistry, Polish Academy of Sciences

ul.Kasprzaka 44/52, 01-224 Warszawa

1. Introduction

In the previous paper [1] we presented results of our resistometric studies of the Ta/H system. It was found that the R(T)-relationship is monotonic in the whole temperature range (1.5 - 400 K) but the dR/dT derivative goes through sharp two or three maxima. We assumed that they indicated phase transitions. One or two transitions were observed at elevated pressures and temperatures and one more at low temperatures (LT). X-ray analysis indicated that the LT resistive transition corresponds to the change of the crystal structure from f.c. orthorhombic to the b.c. tetragonal lattice (for H/Ta > 0.8). The two high-pressure high-temperature transitions was interpreted as an evidence of the existence of a new hydride phase.

In this work the maximum pressure limit was increased to 28 kbar and thus the temperature and pressure range of existence of this new hydride phase could be estimated.

2. Experimental

The measurements at pressures exceeding 10 and 20 kbar have been performed with use of the pressure devices described in [2] and [3], respectively. The tantalum sheet, 0.3 mm thick,

was coated with palladium layer [4] in order to make hydrogen absorption possible at relatively low temperatures. The samples were heated with use of small cylindrical electrical heater placed inside the pressure device. Small dimensions of the samples and their horizontal location, perpendicular to the axis of the heater resulted in small temperature gradient. The temperature was determined from the resistance of the reference platinum samples located in close neighbourhood of the Ta samples. These platinum sensors were calibrated at normal pressure. The calculated temperature was corrected due to pressure dependence of resistance of platinum.

The rest of experimental details can be found in [1].

3. Results

In fig. 1 is shown a typical for the hydrogen pressures exceeding 30 bar temperature dependence of the electrical resistance of tantalum/hydrogen system measured in the pressure chamber and thereafter in the cryostat at normal pressure (with the samples displaced in the cooled down state). No marked hysteresis (i.e. not greater than 2 K) was observed in the high pressure range contrary to the LT region. The corresponding temperature dependence of the temperature derivative is also given in this figure showing a relative sharpness of the resistive transitions at the phase boundaries. The pressure dependence of the derivative related to the peak values is given in Fig. 2. It is worth noting a steep increase of the derivatives corresponding to both high-pressure transitions above ca 10 kbar. The

measured transition temperatures (i.e. the temperatures related to the maxima of the derivative) of the Ta/H system up to 28 kbar are given in Fig. 3. The δ-, α-, and φ-regions correspond to f.c. orthorhombic hydride phase, solid solution of hydrogen in tantalum and the new high pressure phase, respectively. The temperature range of existence of the latter depends on the hydrogen pressure. This phase appears first at 30 bar but tends to disappear at high hydrogen pressures. Above ca. 5 kbar the temperatures, T_{tr}, of the δ-φ and φ-α transitions depend approximately linearly on hydrogen pressure and a simple extrapolation gives the following high-temperature, high-pressure limit for the existence of this phase: T_{tr}=379± 2 K and p_{H_2}=32.5± 2 kbar.

An unexpected dependence of resistance of tantalum on H_2-pressure was found at elevated temperatures. A typical picture corresponding to a single experiment is given on Fig. 4. A marked minimum in the $R(p_{H_2})$-relationship is observed in the region of α-phase. At a temperature of 335 K, i.e. in the region of δ-phase the curve flattens above 1 kbar. At the intermediate temperatures the $R(p_{H_2})$-isotherms intersect the phase boundaries. No anomalies can be seen at the α-φ or δ-φ transitions, but a rather sharp decrease of resistance occurs when going from the φ to δ phase. This suggests a marked difference of hydrogen content of both phases in equillibrium.

The resistance minimum which is present in the α- phase is also observed in the φ-phase region. The origin of the minima remains unclear. It is rather not due to the stoichiometric order of the hydrogen sublattice since this can be first expected for hydrogen content H/Ta=2 while the

highest hydrogen contents in Ta determined after removing the samples from the pressure device cooled down to 220 K did not exceed the value of H/Ta=0.86.

Acknowledgments

The authors are mostly grateful to Prof. H.Zuechner for supplying the Pd-coated tantalum.

References

1. A.W.Szafranski, M.Tkacz, S.Majchrzak and H.Zuechner; J.Less-Common Met. 101, 523 (1984).
2. B.Baranowski and W.Bujnowski; Roczniki Chemii 44, 2271 (1970).
3. B.Baranowski; Ber.Bunsenges. phys. Chem. 76, 714 (1972).
4. N.Boes and H.Zuechner; Z. Naturforsch. 31a, 754 (1976).
5. U.Koebler and J.M.Welter; J.Less-Common Met. 84, 225 (1982).

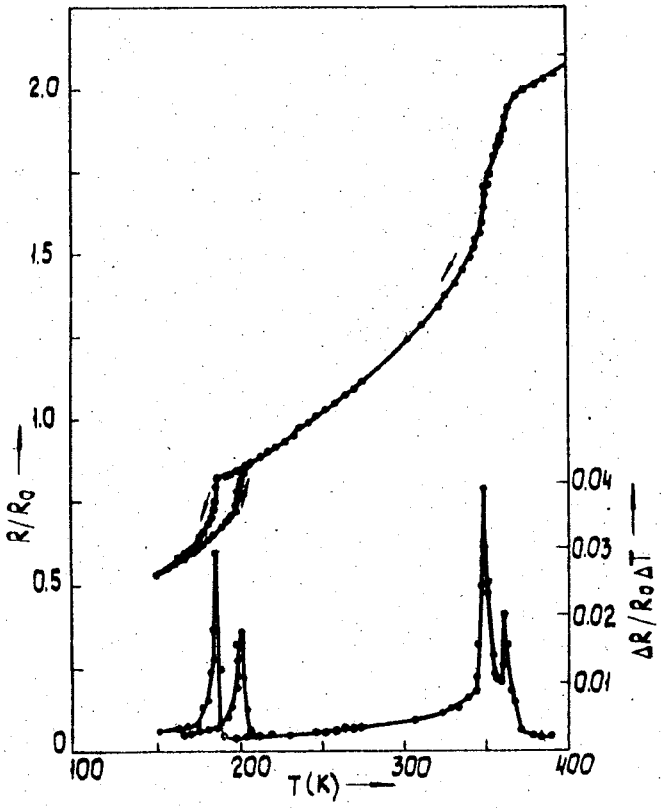

Fig. 1. Typical R(T)-dependence measured in the pressure chamber (15 kbar, 230 K<T<400 K) and in the cryostat (normal pressure, T<230 K).

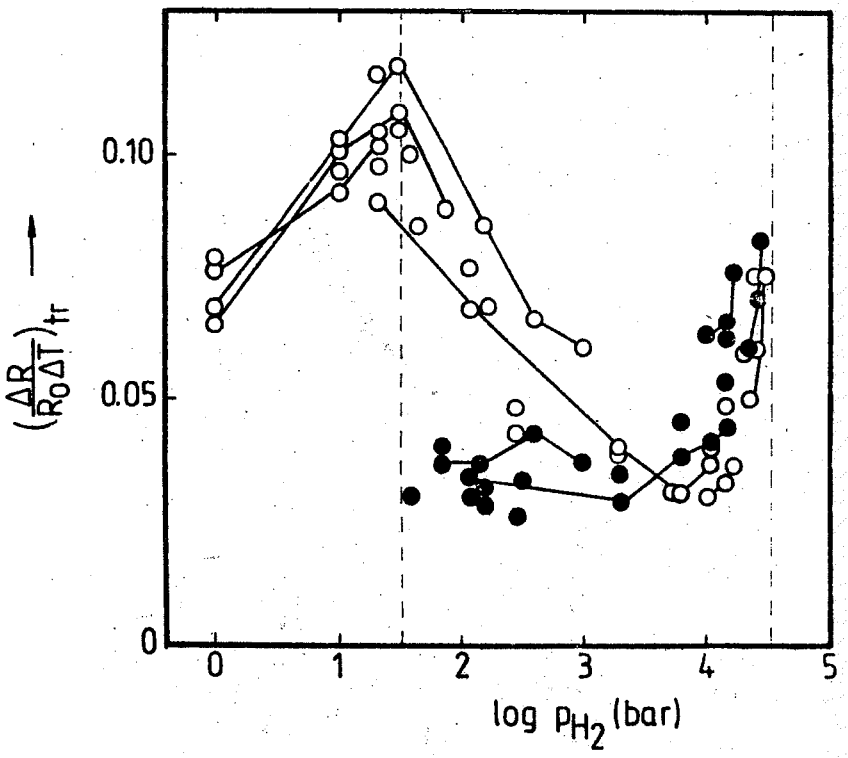

Fig. 2. Temperature derivative of resistance related to the transition temperatures as a function of hydrogen pressure. The points corresponding to a single experiment are connected with a solid line. The dotted vertical lines indicate the pressure range of existence of the φ-phase.

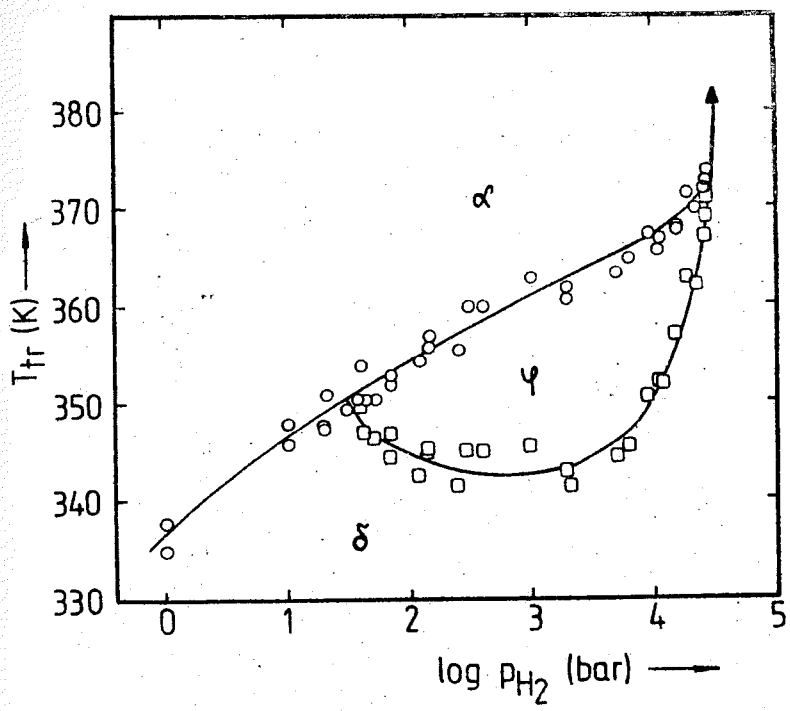

Fig. 3. Transition temperatures of the Ta-H system at elevated temperatures and pressures.

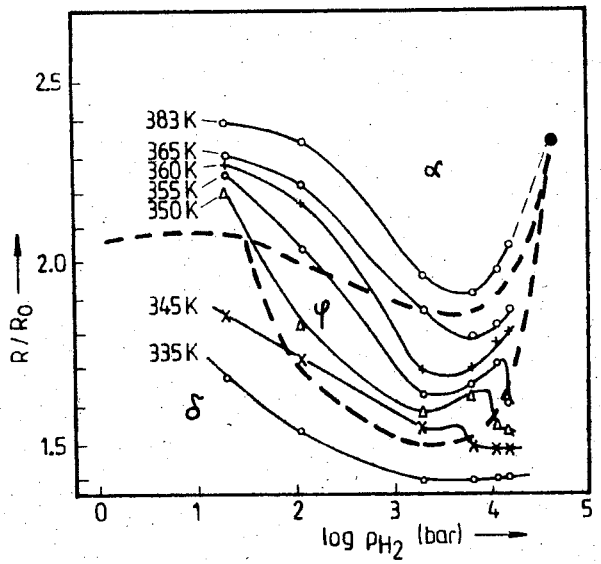

Fig. 4. Resistance vs. hydrogen pressure isotherms (single experiment). The dashed lines indicate roughly phase boundaries.

THE INFLUENCE OF HYDROGEN INTRODUCED BY THE HIGH PRESSURE TECHNIQUE ON SELECTED PROPERTIES OF THE fcc Ni-V ALLOYS

S.M.Filipek, A.W.Szafranski and S.Majchrzak
Institute of Physical Chemistry, Polish Academy of Sciences
01-224 Warsaw, Poland

Introduction

Since the high pressure technique was successfully used for the synthesis of the nickel hydride from the elements [1], the influence of the hydrogen, compressed to very high pressures, on the properties of nickel alloys was intensively investigated [2-4]. Among the nickel 3d-3d alloys a considerable interest attract Ni-Cr and Ni-V alloys because of their electronic properties responsible for non typical magnetic behavior [5], electrical resistivity [6] and thermoelectric power [7]. The interpretation of these properties is based on the concept of the virtual bound state proposed by Friedel [8]. In this aspect one can expect that the influence of hydrogen on the properties of both these alloys would be also an interesting task of experimental research. However in contrast to the Ni-Cr-H [3,9] there are almost no reports concerning the Ni-V-H system.

In this paper the influence of hydrogen on the electrical resistance of the fcc Ni-V alloys is described up to about 2.5 GPa of the hydrogen pressure. Low temperature behavior of the electrical resistance of these alloys in the hydrogen free and hydrogenated states is compared. The structural data for the hydrogenated alloys as well as their H/Me atomic ratios in equilibrium conditions at the several hydrogen pressures are also given.

Experimental

All samples ($Ni_{0.97}V_{0.03}$, $Ni_{0.94}V_{0.06}$, $Ni_{0.91}V_{0.09}$, $Ni_{0.88}V_{0.12}$, $Ni_{0.85}V_{0.15}$) used in this work were generously provided by professor Y.Sakamoto from Nagasaki University. The hydrogenation was realized by use of the high pressure piston-cylinder apparatuses described elsewhere [10,11]. The hydrogenated samples destined for low temperature measurements or for X-ray and masspectrometric analysis (to determine the hydrogen to metal atomic ratio) were taken from high pressure apparatus cooled down to

-80 °C. The X-ray measurements were carried out at temperature of liquid nitrogen.

Results and discussion

The results of measurements of the relative electrical resistance of fcc Ni-V alloys are shown in Fig.Ia and Fig.Ib. As can be seen, the vanadium addition (even as small as 3 at.%) into the nickel matrix caused drastic change of the electrical resistivity of the resulting β hydride. In spite of nearly the same hydrogen concentrations and lattice expansion effects the electrical resistivity of pure nickel decreases about 30 % during β hydride formation [12] while in the case of $Ni_{0.97}V_{0.03}$ alloy almost 100 % increase is observed. Results of low temperature measurements presented in Fig.2a show that this increase is due mainly to the large increase of residual resistivity of hydride phase caused by the introduction of vanadium into the nickel matrix. Similar effect was observed for hydride phases of nickel doped with iron [12] or cobalt [13].

A rather surprising fact is that hydrogen pressure corresponding to the hydride phase formation (directly related to the hydrogen activity needed to form the hydride) increases as a function of vanadium content in the alloy. Moreover, as can be seen from Table, the hydrogen uptake remarkably decreases with vanadium concentration in the alloy. In the same time the hysteresis loop observed on $R_p/R_0 = f(p_{H_2})$ curves (Fig.Ia and Fig.Ib) become narrower and disappears completely near $Ni_{0.91}V_{0.09}$. It means that the miscibility gap in the hydrogen-alloy system should extend only to this composition what is confirmed also by X-ray data plotted on Fig.3. Similar behavior was observed by Sakamoto [14,15] also for Pd-V system in which the miscibility gap was closed near 7 at.% of vanadium.

The low temperature measurements of the electrical resistance (Fig.2a and Fig.2b) indicate that residual resistivity of the Ni-V alloys increases upon the hydrogen absorption. An anomalous temperature dependence (change of the slope of the R/T) curves and hysteresis of the electrical resistance in $Ni_{0.97}V_{0.03}$ (not presented here) and $Ni_{0.94}V_{0.06}$ is observed below 150 K, suggesting possibility of the phase transition in the hydrogenated alloys. However the X-ray data, received for these hydride phases, carried out in liquid nitrogen temperature and in ~ 200 K are not different.

Hydrogen concentration in Ni-V alloys as function of hydrogen pressure at 298 K

Alloy	Hydrogen concentration H/Me for the following pressure		
	0.75 GPa	1.05 GPa	1.4 GPa
pure Ni	0.99		
$Ni_{0.97}V_{0.03}$	0.73	0.95	0.98
$Ni_{0.94}V_{0.06}$	0.17	0.94	0.96
$Ni_{0.91}V_{0.09}$	0.03	0.63	
$Ni_{0.88}V_{0.12}$	0.03	0.12	0.27
$Ni_{0.85}V_{0.15}$	0.02	0.09	0.15

Conclusions

On the basis of measurements performed the following conclusions can be formulated:

1. The vanadium present in the nickel lattice increases the hydrogen pressure needed for hydride formation and has negative effect on the hydrogen absorption in the alloy.

2. The miscibility gap in (fcc Ni-V alloy)-hydrogen system disappears near 9 at.% of vanadium.

3. The low temperature measurements indicate possibility of phase transition in hydrogenated $Ni_{0.97}V_{0.03}$ and $Ni_{0.94}V_{0.06}$ alloys.

Acknowledgements

The authors are grateful to professor Y.Sakamoto for providing the nickel-vanadium alloys used in this work.

References

1. Baranowski B., Wisniewski R.:Bull.Acad.Polon.Sci. (1966) 14,273.
2. Baranowski B.: Metal-Hydrogen Systems at High Hydrogen Pressures, in Hydrogen in Metals II; ed. by G.Alefeld and Y.Völkl Berlin - Heidelberg - New York 1978 pp.157-199.
3. Ponyatovsky E.G., Antonov V.E. and Belash I.T.: High Hydrogen Pressures. Synthesis and Properties of New Hydrides, in Problems in Solid-State Physics; ed. A.M.Prokhorov, Mir Publishers Moscow 1984.
4. Filipek S.M.,Baranowski B.:Preparation of Metallic Hydrides by High Pressure Technique,in Proc.6th Intern.Symp.High Purity Materials in Science and Technology.May 6-10,1985 Dresden, GDR p.90-106.

5. Collins M.F. and Low G.G.: Proc.Phys.Soc. (1965) 86, 535.
6. Ikeda K.: J.Magn.Magn.Mat. (1985) 49, 161-171.
7. Wang T.P., Starr C.D. and Brown N.: Acta Met.; (1966) 14, 649.
8. Friedel J.: Adv.Phys. (1954) 3, 446, Nuovo Cimento Suppl. (1958) 2, 287
9. For example: Bauer H.J. and Kohler K.A.; Phys.Lett. (1972) 41 (4), 291.
Martin W.E., Bauer H.J., Filipek S.M. and Baranowski B: J. Less-Common Met. (1984) 103, (2), 259.
10. Baranowski B., Bujnowski W.: Roczniki Chem. (1972) 76, 714.
11. Filipek S., Baranowski B. and Klukowski M.: in J.Schilling and R. N.Shelton (eds.), Physics of Solids under High Pressure, North-Holland, Amsterdam, 1981, p.231.
12. Baranowski B. and Filipek S.: Roczniki Chem.: (1973) 47, 2165.
13. Filipek S.M., Baranowski B. and Yoneda M.: Roczniki Chem.: (1977) 51, 2243.
14. Sakamoto Y., Yuwasa K and Hirayama K.: J.Less-Common Met. (1968) 26, 522.
15. Sakamoto Y.: Private communication.

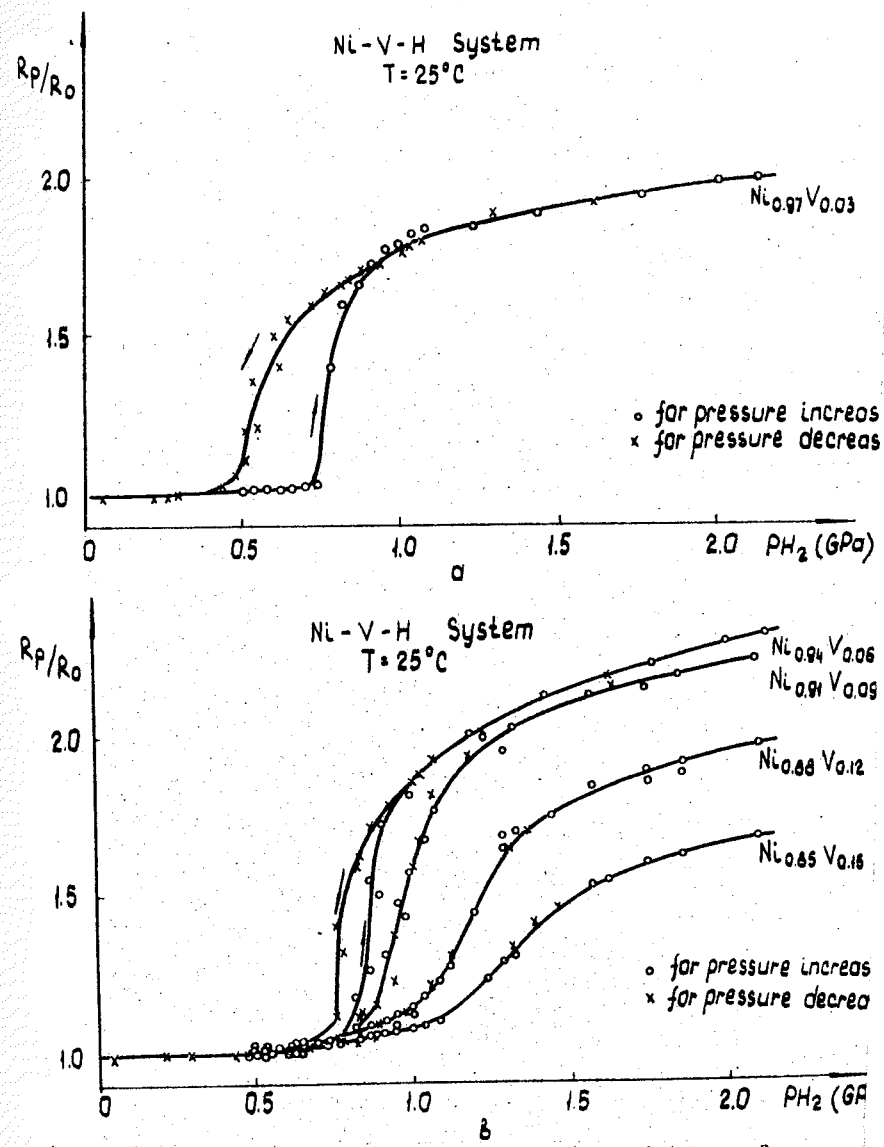

Fig.1a, b. The stationary relative electric resistance of Ni-V alloys as function of hydrogen pressure at 25 °C (R_p - resistance at hydrogen pressure p; R_o - resistance at normal pressure of an inert gas).

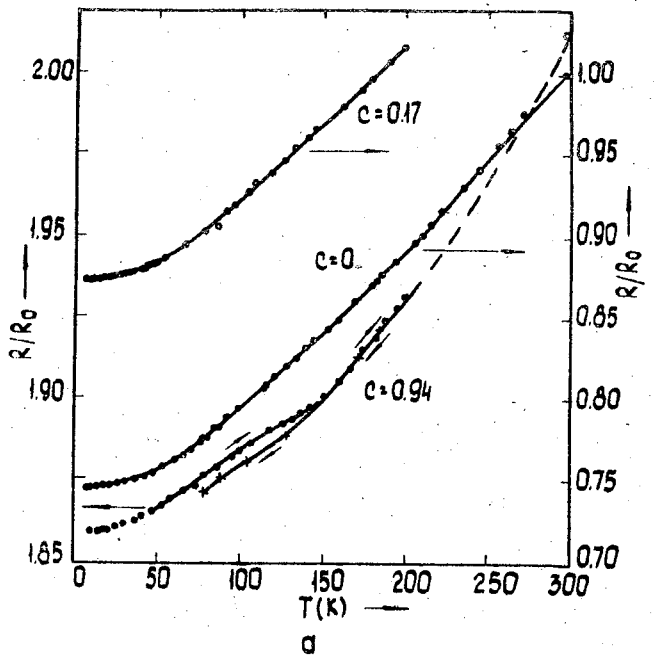

a

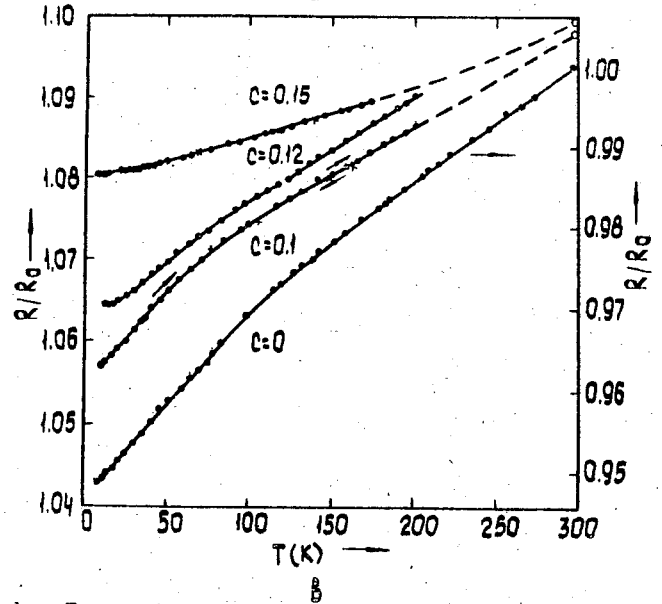

b

Fig.2a,b. Temperature dependence of electrical resistance of the $(Ni_{0.94}V_{0.06})_IH_c$ and $(Ni_{0.85}V_{0.15})_IH_c$ alloys

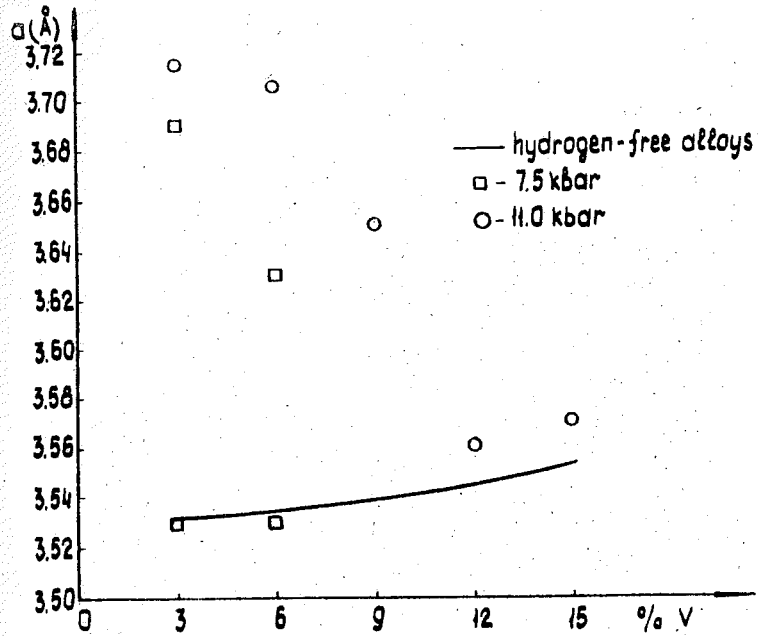

Fig.3. Lattice parameters of Ni-V-H alloys as function of C concentration.

BEHAVIOR OF ELEMENTAL CARBON UP TO VERY HIGH TEMPERATURES AND PRESSURES

F.P. Bundy, retired from General Electric Research
and Development Center. Home address: PO Box 29,
Alplaus, New York 12008, USA

BRIEF REVIEW

The pressure-temperature phase diagram for elementary carbon has a long and interesting history which is covered fairly comprehensively in [1] and will not be repeated here. Figure 1 summarizes the "older" P, T phase diagram, up to about 40 GPa, and 5000 K. The background for the graphite/diamond equilibrium line is given in [2], [3], [4], and that for the melting line of graphite by [5] and [6]. The positions and slopes of the melting lines for metastable graphite and metastable diamond are discussed in [3] and [5]. Recent experimental results suggest that the slope of the diamond melting line may be positive, and this will be discussed later in this paper. The solid-to-solid, martensitic transformation of hex graphite to hex diamond is discussed in detail in [7].

STABILITY OF DIAMOND

In the 1960's and 1970's it was generally believed that the diamond form of carbon would respond to the application of higher pressures and temperatures in much the same way as its sister elements Si and Ge. Forecasts based on ionicity theory indicated that diamond would collapse to a metallic form at a pressure in the range of 170 GPa [8]. This was proved wrong when Mao and Bell attained measured pressures of over 170 GPa in opposed diamond anvil apparatus [9] in 1978, and later when over 250 GPa was attained without any indication of collapse of the pressure faces of the diamond anvils [10]. This behavior of diamond, which is so different from that of Si and Ge, had already been predicted by Yin and Cohen [11], and by Biswas, et al. [12], using improved theory which indicated that diamond should be stable relative to competing metallic structures (fcc, bcc, hcp, simple cubic, β-tin, or BC8) up to pressures around 1200 to 2300 GPa.

PHASE DIAGRAM AT HIGHER P, T's

About 1962, application of transient electrical resistance heating techniques to specimens in static pressure apparatus made possible temperature excursions up to about 5000 K for time periods of milliseconds. Specimens subjected to shock compression conditions (microseconds) had been studied for many years. In the pressure-volume Hugoniot data curves from shock compression experiments the transformation of graphite to

diamond could be seen. For higher pressures and temperatures the shock data did not reveal clearly any additional abrupt specific volume changes that might be interpreted as a phase change in the solid state, - or to melting.

In 1979, Grover [13] on the basis of an "equation of state" model for a metallic form of carbon which would be consistent with data from shock compression experiments on diamond reported by Pavlovskii [14], suggested a solid phase of metallic carbon above 11.5 GPa and 3700 K. Neither of the models of [8] or [13] agrees very well with the older experimental observations by Bundy, [3], [5], or with the recent observations of Bassett, et al., [15], and of Shaner, et al. [16], [17].

In Bassett's and Weather's [15] experiments small particles of diamond in some experiments, or of graphite in others, were embedded in NaCl and were melted at pressures of 5.0 and 30 GPa in a diamond anvil cell using a pulsed YAG laser. After such treatment the samples were removed from the cell and the structures of the quenched phases were studied by transmission electron microscopy. The melted regions of the sample were found to consist of nearly perfect spheres of carbon ranging in size from about 1μm to less than a few nanometers. In the diamond sample melted at 30 GPa the larger spherules (>0.2μm) were polycrystalline diamond with either a granular or radial texture, while the smaller spherules gave diffraction patterns with four diffuse rings that correspond to the 002, 100, 004 and 110 spacings of graphite. Detailed study of the diffraction rings indicated a radial orientation of the c-axis of the disordered graphite. The spacing between the 002 layers depended upon the pressure at the time of solidification, ranging from 3.4Å for melts at less than 10 GPa to about 2.8Å for melts at 30 GPa. These observations are interpreted to suggest that in liquid carbon both sp^2-type (graphitic) and sp^3-type (diamond) bondings exist, and the amount of sp^3-type increases with pressure. Upon quenching, the smaller spherules retain enough of the crosslayer sp^3 "stitching bonds" to hold the average 002 layer spacing to less than that in simple graphite. The fact that the larger spherules go to polycrystalline diamond suggests that a longer quenching time may allow recrystallization to the thermodynamically stable diamond.

In the Bassett and Weathers laser-melting experiments one branch of the optical system monitored the intensity vs wavelength of the thermal radiation emitted by the specimen region of the sample. By fitting the I (λ) curve obtained to I (λ) curves for different black body temperatures the temperature of the specimen was obtained with an accuracy of about 300 degrees at about 5000 K. In most of the experiments temperatures between 5000 and 6000 K were indicated. The experiments that have been done to date indicate roughly that the melting point of diamond increases somewhat with pressure.

The relatively recent experiments by Shaner and colleagues [16], [17], using shock compression techniques have provided some information on the stability of diamond and the magnitude of its melting temperature at higher pressures. In the experiments of [16] a special technique was used to measure the velocity of sound in the specimen material while in the hot shock-compressed state. In their experiments with carbon the results were consistent with the specimen remaining as solid diamond in the range of 80 GPa, 1500 K to 140 GPa, 5500 K, indicating that the melting temperature of diamond at 150 GPa must be at least 6000 K.

In the work reported in [17] in which the electrical resistivity of the carbon specimen was measured at various pressures and temperatures along the shock Hugoniot up to 50 GPa, 3000 K, no drop in resistance was observed that would indicate transformation to metallic solid or liquid.

Taking into account these new experimental results, and an excellent review of the thermodynamic properties of carbon by Gustafson [18], Fig. 2 portrays the author's present concept of the most probable P, T phase diagram for elemental carbon. The diamond phase occupies a remarkably large part of it.

LIQUID CARBON

In [1] the anomaly was pointed out that liquid carbon had been found by early experimenters to be an insulator at low pressures (<.02 GPa), but metallic at pressures above 1 GPa. Ferraz and March [19] made a theoretical study of this problem and came up with the possibility that there might be two liquid phases, insulating and conducting, with the metallic liquid phase existing at pressures above about 0.1 GPa.

Shaner [20] very recently reported on experiments using electrical pulse heating of glassy carbon rods of initial density of 1.8 gm/cc in inert gas atmospheres at pressures up to 0.4 GPa to temperatures around 6000 K. The heating was slow enough to assure constant pressure expansion but fast enough to avoid hydrodynamic instabilities in the molten carbon. Electric resistance and density were monitored. The rods compacted to graphite density at about 3000 K and then showed a continuous increase in specific volume and a rough constancy in electrical resistivity of about 1mΩ-cm, up to 6000 K.

Very recently some very precise and complete experiments on the transient electrical resistance heating of pyrolytically grown fine whiskers of graphite were reported by Heremans, et al., [21], which show definitely that liquid carbon is metallic with a resistivity of about 30$\mu\Omega$cm and nearly temperature independent. Also their results quantitatively verify the 1963 results of Bundy [5] from experiments at about 4.8 GPa in regard to the temperature coefficient of resistivity of graphites of various degrees of crystal perfection, the enthalpy of solid graphite at the melting point, and the heat of fusion (~25 kcal/mole).

During the last few years some very detailed experiments have been carried out by various groups using laser pulse heating of highly ordered pyrolytic graphite (HOPG), and of amorphous vapor-deposited carbon films, to produce transient melting. The reflectivity of the irradiated areas were monitored by an optical probe beam of different frequency. Experimenters using 248 nm, 30 nsec laser pulses, [22,23,24] observed very definite and quantitative evidence of melting, but found that ejected material from the irradiated area fouled the monitoring beam and made the reflectivity measurements unreliable. However the melt dynamics analysis indicated that the liquid phase had to have a thermal conductivity of a metallic liquid to explain the observed results [23]. By contrast, other experimenters [25] tried using laser pulses of about .001 the duration (532 nm, 20 psec) of the other group, with the intent of getting the energy insertion accomplished and the reflectivity measured before there was time for ejected material to interfere. Their results indicated that an ultra-fast phase transformation takes place during the pulse when the fluence reaches 0.14 mJ/cm^2 and that the reflectivity of that phase is lower than that of the HOPG specimen. This was opposite to that observed using the same system with specimens of semiconductors like Si, and also opposite to that expected for a metallic liquid carbon.

For such short energy insertion times there are some questions about the transfer time of the energy of the electron system to the crystal lattice, and about the induced pressure within the energized zone. Rough calculation indicates that the transit time of a pressure shock wave through the thickness of the energized region of the specimen is much larger than the duration of the laser pulse. In this case the heating would occur at approximately constant volume because there would not be time for the region to expand. Using the data from Gustafson [18] on the molar volume of graphite vs pressure, and vs temperature, - shown here in Fig. 3, - one can determine the "thermal pressure" generated in the specimen for various allowed (by acceleration time) amounts of thermal bulk expansion, ΔV. For example, from Fig. 3 one can see that the thermal expansion produced by heating from 300 to 4500 K could be cancelled by the compression of about 24 GPa pressure, which would be the case of $\Delta V=0$, - that is heating at constant volume. Thus, one can work out P, T paths that correspond to $\Delta V=0$, $\Delta V=1/2$, etc. Figure 4 is the P, T phase diagram of Fig. 2 with a logarithmic P axis, and on it are dubbed in the P, T paths during fast energy insertion (as in laser pulsing) corresponding to conditions giving ΔV's ranging from 0 to 0.9. For picosec pulse heating, which corresponds to near $\Delta V=0$ circumstances, the P, T conditions track through the *fast* graphite-to-diamond reaction region where transformation to diamond could cause the drop in reflectivity and major increase in resistance reported in [25]. If the temperature rise time is such that about 0.9 of the possible thermal expansion can occur then the P, T path would be about as shown by the $0.9\Delta V$ curve. This crosses the melt line of graphite to the "metallic" liquid, and could account for

the results given in [23]. The constant pressure "slow" experiments of Shaner [20] would track, as shown, across the diagram at about 0.25 GPa to meet the graphite melting line near the Ferraz/March proposed boundary between non-metallic and metallic liquid carbon. A positive slope of the diamond melting line would account for the 1963 result of Bundy [3] where the freezing of carbon within a shell of solid diamond at initial pressures above the graphite/diamond/liquid triple point always resulted in a mixture of diamond and graphite crystals. With the liquid less dense than diamond freezing would cause lowering of the local pressure into the graphite stable region and graphite crystals would grow.

APPROPRIATE NEW EXPERIMENTAL WORK

In the author's view the areas of high temperature behavior of carbon that need particular attention are: (i) the slope of the diamond melting line, and (ii) the nature and character of liquid carbon. Are there two liquid phases, one metallic and the other non-metallic?

Determination of the melting line of diamond can probably best be accomplished by refining experiments of the type referred to in [14], [15] and [16]. Determination of the character of liquid carbon will require great refinement of experiments of the type referred to in [16] and [19]. These goals are now within sight, and it is hoped that they will be reached.

References

1. Bundy, F.P., "Behavior of Carbon at Very High Pressures and Temperatures", Koninkl.Nederl. Akademie van Wetenschappen-Amsterdam, Proceedings, Series B, 72, No. 5 (1969), pp 302-316.
2. Bundy, F.P., Bovenkerk, H.P., Strong, H.M., Wentorf, R.H. Jr., "Diamond-Graphite Equilibrium Line for Growth and Graphitization of Diamond", J. Chem. Phys. (1961), *35*, No. 2, 383-391.
3. Bundy, F.P., "Direct Conversion of Graphite to Diamond in Static Pressure Apparatus", J. Chem. Phys. (1963), *38*, No. 3, 631-643.
4. Kennedy, C.S. and Kennedy, G.C., "The Equilibrium Boundary Between Graphite and Diamond", J. Geophys. Res. (1976), *81*, 2467-2470.
5. Bundy, F.P., "Melting of Graphite at Very High pressure", J. Chem. Phys. (1963), *38*, No. 3, 618-630.
6. Fateeva, N.S. and Vereshchagin, L.F., "The Melting Line of Graphite at High Pressure", Pisma Zh. Eksp. Teor. Fiz. (1971), *13*, 157-159.

7. Bundy, F.P., Kasper, J.S., "Hexagonal Diamond - A New Form of Carbon", J. Chem. Phys. (1967), *46*, No. 9, 3437-3446.
8. Van Vechten, J.A., "Quantum Dielectric Theory of Electronegativity in Covalent Systems. III. Pressure-Temperature Phase Diagrams, Heats of Mixing, and Distribution Coefficients", Phys. Rev. (1973), *B7*, 1479-1507.
9. Mao, H.K. and Bell, P.M., "High-Pressure Physics: Sustained Static Generation of 1.36 to 1.72 Megabars", SCIENCE (1978), *200*, 1145-1147.
10. Goettel, K.A., Mao, H.K., and Bell, P.W., "Generation of Static Pressures above 2.5 Megabars in a Diamond Anvil Pressure Cell", Rev. Sci. Instr. (1985), *56*(7), 1420-1427.
11. Yin, M.T. and Cohen, M.L., "Will Diamond Transform Under Megabar Pressures?", Phys. Rev. Ltrs. (1983), *50*, 2006-2009.
12. Biswas, R., Martin, R.M., Needs, R.J., and Nielson, O.H., "Complex Tetrahedral Structures of Silicon and Carbon Under Pressure", Phys. Rev. B (1984) *30*(6), 3210-3213.
13. Grover, R., "Does Diamond Melt?", J. Chem. Phys. (1979), *71*, 3824-3829.
14. Pavlovskii, M.N., "Shock Compression of Diamond", Sov. Phys. Solid State (1971), *13*, 741-742.
15. Bassett, W.A. and Weathers, M.S., "Melting of Diamond at 30 GPa", Bull. Amer. Phys. Soc., (1987), *32*, No. 3, p. 608, Abs. of Paper GS6.

    Weathers, M.S. and Bassett, W.A., "Melting of Carbon at 50 to 300 kbar", accepted for publication in Phys. and Chem. Minerals (1987).
16. Shaner, J.W., Brown, J.M., Swenson, C.A., and McQueen, R.G., "Sound Velocity of Carbon at High Pressures", J. de Physique, (1984), *45*, C8, 235-237.
17. Mitchell, A.C., Shaner, J.W. and Keeler, R.N., "The Use of Electrical Conductivity Experiments to Study the Phase Diagram of Carbon", Physica (1986), *140B*, 386-389.
18. Gustafson, P., "An Evaluation of the Thermodynamic Properties and the P, T Phase Diagram of Carbon", Carbon, (1986), *24*, No. 2, 169-176.
19. Ferraz, A. and March, N.H., "Liquid Phase Metal-Non Metal Transition in Carbon", Phys. Chem. Liq. (1979), *8*, 289-298.

20. Shaner, J.W., "Equation of State and Electrical Conductivity of Carbon Pulse Heated to 6000K", Bull. Amer. Phys. Soc., (1987), *32*, No. 3, 607-608, Abs. of Paper GS4.

21. Heremans, J., Olk, C.H., Eesly, G.L., Steinbeck, J. and Dresselhaus, G., "Observation of Metallic Conductivity in Liquid Carbon", submitted to Phys. Rev. Lett. (1987).

22. Venkatesan, T., Jacobson, D.C., Gibson, J.M., Elman, B.S., Braunstein, G., Dresselhaus, M.S., and Dresselhaus, G., "Measurement of Thermodynamic Parameters of Graphite by Pulsed-Laser Melting and Ion Channeling ", Phys. Rev. Lett. (1984), *53*, 360-363.

23. Steinbeck, J., Braunstein, G., Dresselhaus, M.S., Venkatesan, T., Jacobson, D.C., "A Model for Pulsed Laser Melting of Graphite", J. Appl. Phys. (1985), *58*, 4374-4382.

24. Dijkkamp, D., Venkatesan, T., Wu, X.D., Steinbeck, J., Dresselhaus, M.S., and Dresselhaus, G., "Time-Resolved Reflectivity and Transmission Study of Pulsed Laser Induced Evaporation Dynamics of HOPG and Carbon Films", Bull. Amer. Phys. Soc., (1987), *32*, 608-609, Papers GS10, GS11, GS12.

25. Malvezzi, A.M., Bloembergen, N., Huang, C.Y., "Time-Resolved Picosecond Optical Measurements of Laser-Excited Graphite", Phys. Rev. Lett. (1986), *57*, 146-149.

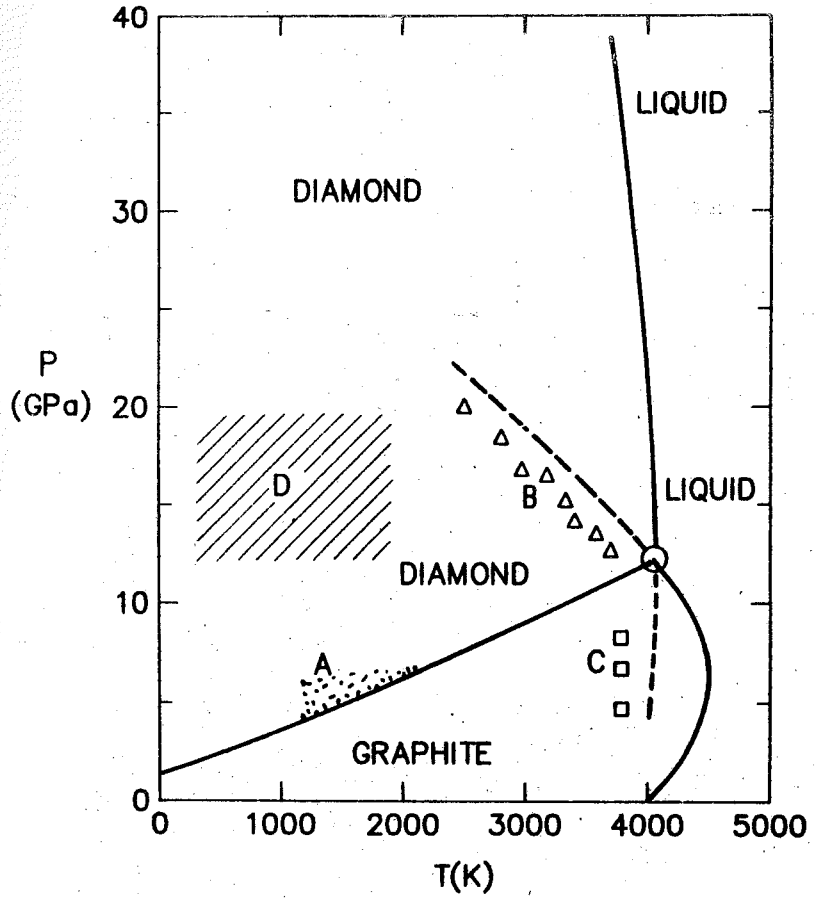

Fig. 1. "Old" P, T phase diagram for elemental carbon showing: (A) region for catalytic transformation of graphite to diamond; (B) region of spontaneous fast graphite-to-diamond; (C) region of spontaneous fast diamond-to-graphite; and (D) region of spontaneous slow martensitic transformation of hex graphite to hex diamond.

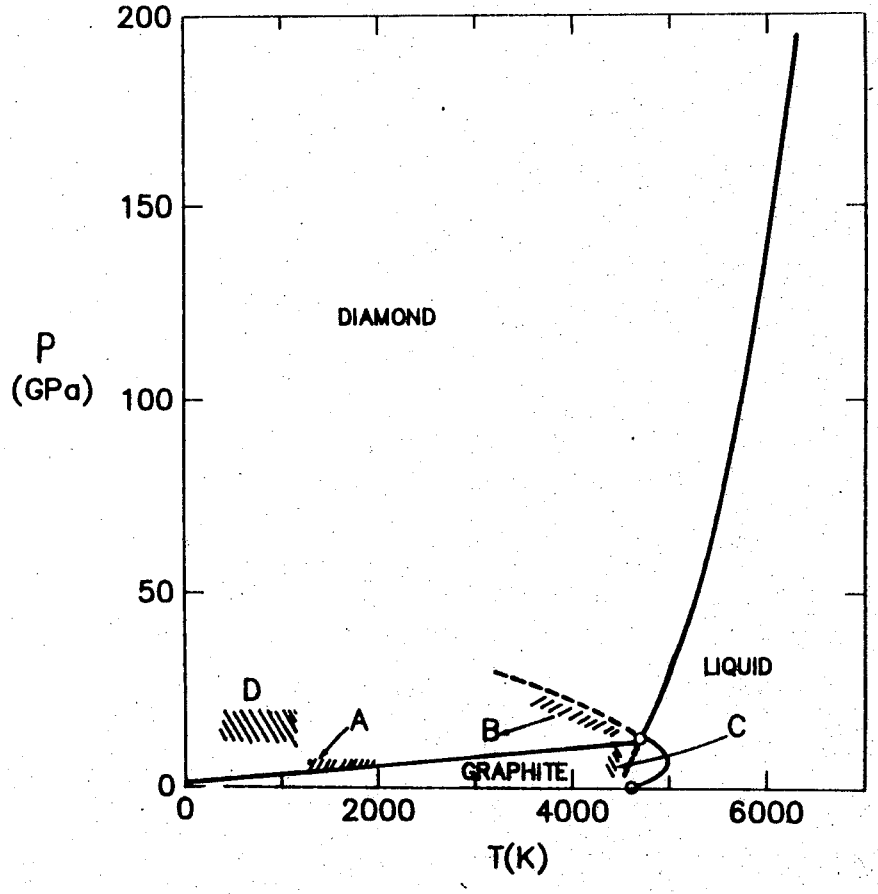

Fig. 2. Most probable P, T phase and reaction diagram for elemental carbon as of May 1987. (A) Region of catalyst/solvent diamond synthesis from graphite. (B) Region of fast spontaneous graphite-to-diamond transformation. (C) Region of fast spontaneous diamond-to-graphite transformation. (D) Region of martensitic transformation of hex graphite to hex diamond.

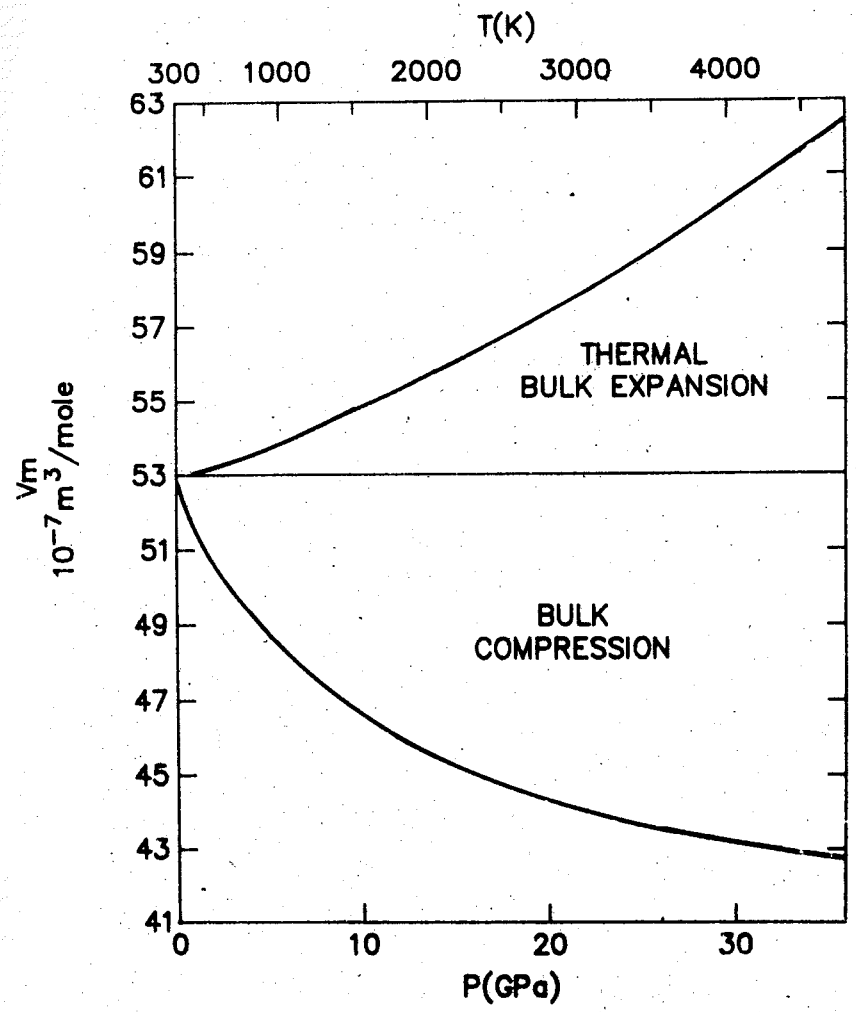

Fig. 3. Bulk thermal expansion and pressure compression for graphite from Gustafson [17].

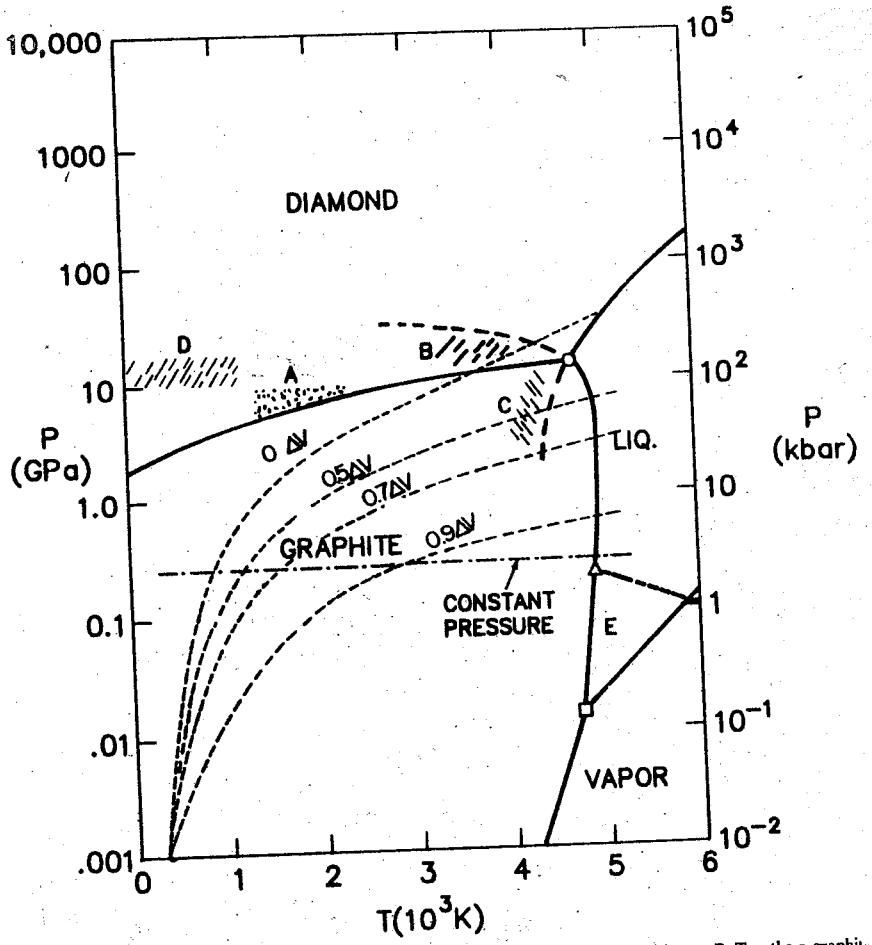

Fig. 4. New P, T phase diagram of Fig. 2 with logarithmic pressure axis. Dubbed in are P, T paths a graphite specimen would take during fast energy insertion with various constraints on bulk expansion. 0 ΔV means heating at constant volume.

DIAMOND FORMED OF ORGANIC COMPOUNDS

E.N.Yakovlev
The L.F.Vereshchagin High Pressure Physics Institute
Academy of Sciences of the USSR, Troitsk, Moscow Region,
USSR

Today the main part of diamonds used in industry is manufactured synthetic diamond, made from graphite by the solvent-catalyst process at high pressure. Not only graphite but several different carbonaceous materials can be used to supply the carbon for diamond synthesis in the solvent-catalyst process: wood, coal, butter ... etc [1].

Method of producing diamond by converting substances into diamond had been proposed one hundred years ago in 1880 by Hennay J.B. [2]. But only in 1965 R.H.Wentorf [3] had found that organic compounds transform to diamond. In his high-pressure (up to 150 kb), high-temperature (up to 3000 °C) experiments Wentorf studied the pyrolysis of hydrocarbons and carbonaceous materials: naphtalene, anthracene, polyethylene. Most of these yielded diamond some of these yielded graphite.

The diamond formed by pyrolysis of organic compounds [3] was white, resembling paraffin wax in appearence and mechanical properties.

In our experiments under high pressure and high temperature [4-6] we investigated hydrocarbons (C_nH_m) and carbohydrates ($C_nH_mO_p$) including substances mentioned in [2].

Figure shows typical diamonds from these substances. The crystals are 1-200 μm in size, mainly 5-20 μm in size.

Most of the diamonds obtained in the above mentioned experiments were the polycrystalline aggregates (druses). The separate monocrystals of the druse were often in the form of octahedron and plate (see Figure*). Usually the diamonds were transparent colourless, bluish, yellowish, greenish crystals depending on the starting material. The small crystals of diamond incorporeded into diamond during the growth were the only type of inclusions into the diamond. The main part of the crystals were twins. The isometric shape of the crystals appeared very seldom. The dark and skeletal crystals were absent but such type of crystals was often generate in the solvent-catalyst process from graphite [7].

*The Figure is given at the end of the book.

X-ray data indicated that the products of reaction were diamond, diffraction lines were narrow [4-6]. The graphite appeared in the products too and was detected by its X-ray diffraction pattern.

The yield of graphite increases with the decrease of P-T parameters. Under low pressure and temperatures the organic substances whatever its nature was formed diamond. It is necessary to note that this result is different from the results by Wentorf [3]. In his experiments the compounds such as naphtalene, antracene... which contain aromatic ringe favour the formation of graphite. On the basis of these results Wentorf [3] made the conclusion that the amount of diamond in the synthesis strongly depends on the structure of starting materials.

With general point of view the structure of the starting material is very important for the parameters of diamond forming but in our experiments we didn't establish the connection between the type of the chemical bond of the hydrocarbon and the yield of diamond.

The diamond synthesized from hydrocarbons (without catalyst metals) were investigated by ESR method [8]. The paramagnetic nitrogen content is relatively low (10^{18} cm^{-3}). The ESR signal were only from the nitrogen atoms. The ESR characteristics of the diamonds formed from hydrocarbons were closer to the natural diamonds than to the diamonds generated in the solvent-catalyst process from graphite. The ESR line of the nitrogen with $\Delta H=3-4$ had been found only in the natural diamonds and in the diamonds formed from hydrocarbons.

On the basis of these experiments the authors of [8] had proposed that the diamond forming from hydrocarbons is similar to the natural diamond.

The multiformity of hydrocarbons and carbohydrates allows us to hope for the obtaining of diamond with a wide spectrum of physical properties. We are at initial stage of the study of the forming process and properties of such diamonds. By now was established, that the electrical resistivity of these diamond is more than 10^{10} Ohm-cm, that after heating to about 1200 ^{o}C in inert atmosphere these diamonds didn't change the mechanical properties but the diamonds obtained in catalyst process after the same heating were too weak.

The obtaining of diamond from organic substances without catalyst metals is very important for the better understanding of diamond-growth mechanism particularly in the nature and for the practical applications in future.

References

1. Bundy F.P., Strong H.M., Wentorf R.H. Methods and mechanisms of synthetic diamond growth. Chemistry and Physics of Carbon, 1973, 10, No.4, p.213-263.
2. Hannay F.R.S.E. On the Artificial Formation of the Diamond. Proc. Royal Soc. 1880, p.188-189, p.450-461.
3. Wentorf R.N. The behaviour of some carbonaceous materials at very high pressure and high temperature.J.of Phys.Chem., 1965, 69, No.9, p.3063-3069.
4. Yakovlev E.N., Voronov O.A. Almasy is uglevodorodov. Almasy i sverhtverdie materialy, 1982, vip.7, s.1-2.
5. Yakovlev E.N., Voronov O.A., Rahmanina A.V. Sintes almasov is uglevodorodov. Sverhtverdie materialy, 1984, No.4, s.8-11.
6. Yakovlev E.N., Shalimov M.D., Kulikova L.F., Slesarev V.N. Sintes almasov is uglevodorodov.Schurn.fis.chim.,1985,59,No.6, 1517-1518.
7. Serebryanaya N.R., Losev V.G., Voronov O.A., Rahmanina A.V., Yakovlev E.N. Morphologiya cristallov almasov, sintesirovannih is uglevodorodov. Kristallographiya, 1985, 30, No.5, 1026-1027.
8. Nachalnaya T.A., Podsyarei G.A., Shulman L.A., Voronov O.A., Rahmanina A.V., Yakovlev E.N. Nekotorie osobennosti spectrov EPR almasov, sintesirovannih is uglevodorodov. Fisika i technika visokich davlenii, 1986, vip.21, s.40-42.

KINETICS OF THE GROWTH OF DIAMOND CRYSTALS UNDER HIGH PRESSURES

D.V.Fedoseev, B.V.Derjaguin
The Institute of Physical Chemistry of the USSR Academy of Sciences, Moscow, USSR

Two steps may be identified in the diamond synthesis; namely, - nucleation (the formation of nuclei), and the growth of crystals proper. In accordance with the colloid theory of diamond nucleation in the range of its thermodynamic stability [1,2], the diamond nuclei are formed through a solid-phase transformation of graphite crystallites that convert into a metal melt, when a starting carbon material is dissolved (under dissolution).

The amount of work required for such a transformation may be represented as follows:

$$U = U_{hom} \cdot F \qquad (1)$$

where F is a function dependent on the surface energies of diamond and graphite, the value of F decreasing as the contribution of the prismatic faces of a graphite crystallite to its total surface increases; and U_{hom} is the amount of work, required for the formation of a critical nucleus.

We note that no suppositions on the saturation of a metal melt by carbon has been made in deriving formula (1).

A difference in chemical potentials, $\Delta\mu$, between diamond and graphite may be represented in the following form:

$$\Delta\mu = \int_{P_e}^{P} (V_\alpha - V_\beta)\, dP \qquad (2)$$

where P_e is an equilibrium pressure at a given temperature; P is a synthesis pressure; V_α and V_β are the atomic volumes of diamond and graphite, depending on a pressure applied. Hence, the metastability of graphite with regard to diamond at $P > P_e$ is determined by the fact that graphite is compressed by a pressure applied. The presence of a metal melt facilitates the initial step, formation of nuclei. Note that the diamond nuclei formed may be found in a nonsaturated carbon solution, these nuclei undergoing gradual dissolution.

Moreover, the solid-phase transformation of a graphite crystallite into a diamond nucleus is most likely to take place just in a nonsaturated solution.

In Yu.V.Naidich et al.'s works,it has been shown that the contact angles of wetting graphite and diamond by molten metals to be used during synthesis of diamond, increase as the molten metals are saturated by carbon [3]. Now, for example, at a temperature of 1550 °C the contact angle of pure iron with graphite is equal to about 17°; yet the contact angle becomes equal to about 98°, when it is saturated by carbon up to about 21 at.% - that is, a substantial increase in the interphase energy occurs. The ratio of the surface energies of diamond and graphite remains practically invariable when a solution is saturated. Therefore, in formula (1) the value of F does not change. However, since the work involved into the homogeneous formation of a critical nucleus (the first cofactor in formula (1)) is proportional to cube of the surface energy, the value of U_{hom} may vary by an order of magnitude.

Therefore, graphite crystallites will most likely transform into a diamond nucleus at the initial step of synthesis process, when the metal melt is not yet saturated by carbon, with regard to graphite (and is not supersaturated with regard to diamond). The number of crystallization sites formed in the system will be determined just by that step, while the nucleation rate will further decrease drastically. This has been corroborated by many works on synthesis of diamond and cubic boron nitride [4,5].

The number of crystallization sites depends on the graphite--metal contact surface, on the structure of the starting coal--graphite material, and on the preliminary saturation of metal by carbon [7]. Thus, the nucleation step may be controlled, not only by varying the preset values of temperature and pressure, but also by changing the dispersity and properties of the starting coal-graphite material and metals.

The undissolved diamond nuclei will further grow from a solution of carbon in molten metal, which is supersaturated with regard to diamond. In a general case, the crystals growth process comprises the steps of dissolution of graphite, diffusion of carbon toward diamond, and the growth of its faces.

Owing to transition of graphite into a denser phase, diamond, the pressure in the synthesis chamber decreases, since the volume of the reaction space remains invariable. Therefore

$$M_{\beta o} = M_\beta + M_\alpha,$$

$$\frac{M_{\beta o}}{\rho_{\beta o}} = \frac{M_\beta}{\rho_\beta} + \frac{M_\alpha}{\rho_\alpha},$$

where $M_{\beta o}$ is the initial mass of graphite having a density of $\rho_{\beta o}$, M_β is the mass of graphite having a density of ρ_β, which has remained on the formation of M_α diamond; ρ_α is the diamond density. From these relationships, it follows that

$$M_\alpha = M_{\beta o}\frac{\rho_{\beta o}-\rho_\beta}{\rho_\alpha-\rho_\beta}\cdot\frac{\rho_\alpha}{\rho_\beta}. \qquad (3)$$

The maximum value of M_α is attained, when, owing to a change in pressure, the density of graphite becomes equal to $\rho_{\beta e}$, i.e., the density under a pressure P_e. Since

$$M_{\alpha m} = \frac{4}{3}\pi r_m^3 \rho_\alpha N,$$

where r_m is the maximum size of a diamond crystal (in the assumption of monodispersity of crystals that are assumed to be spherical in shape), N is the number of crystallization sites, then

$$r_m^3 = \frac{M_{\beta o}}{\frac{4}{3}\pi\rho_{\beta o}N}\cdot\frac{\rho_{\beta o}-\rho_{\beta e}}{\rho_\alpha-\rho_{\beta e}}. \qquad (4)$$

The ratio

$$\frac{r^3}{r_m^3} = \frac{(\rho_{\beta o}-\rho_\beta)(\rho_\alpha-\rho_\beta)}{(\rho_{\beta o}-\rho_{\beta e})(\rho_\alpha-\rho_{\beta e})}, \quad \frac{\rho_\alpha-\rho_\beta}{\rho_\alpha-\rho_{\beta e}} \approx 1$$

since the ratio may be written in the following form

$$\frac{r^3}{r_m^3} = 1-\frac{\rho_\beta-\rho_{\beta e}}{\rho_{\beta o}-\rho_{\beta e}}. \qquad (5)$$

Since the graphite density depends practically linearly on pressure within a narrow pressure range, $\rho-\rho_e$, then

$$\rho-\rho_e = (\rho_o-\rho_e)\left(1-\frac{r^3}{r_m^3}\right). \qquad (6)$$

Here ρ_o is the initial pressure of synthesis.

The formula for diamond crystals growth kinetics always includes a difference in the equilibrium concentrations of carbon over graphite and diamond, ΔC. Since the pressure in the system varies, then, while taking into account Eq.(7), we have

$$\Delta C = \Delta C_o\left(1-\frac{r^3}{r_m^3}\right), \qquad (7)$$

where ΔC_o corresponds to the initial pressure.

At $\rho \to \rho_e$, the ratio $\frac{r}{r_m} \to 1$, and a difference in equilibrium solubilities $\Delta C \to 0$.

Generally, when carrying out investigation of the diamond growth kinetics, the dependence of the following form is obtained:

$$\frac{dr}{dt} = f(K_i, r)\Delta C, \qquad (8)$$

where K_i are the kinetic constants of diamond growth, graphite dissolution, and carbon diffusion in molten metal.

If Eq.(7) is taken into account, the crystals growth kinetics is determined by the following relationship:

$$\int_0^r \frac{dr}{f(K_i, r)\left(1-\frac{r^3}{r_m^3}\right)} = \Delta C_o t. \qquad (9)$$

The limiting stage of synthesis process will determine a specific form of dependence of a crystal size on the synthesis time.

References

1. Fedoseev D.V., Derjaguin B.V. Kolloidny zhurnal, 1979, v.41, N4, p.750.
2. Fedoseev D.V., Derjaguin B.V. DAN SSSR, 1986, v.286, N1, p.113.
3. Naidich Yu.V., Kolesnichenko G.A. Interaction of Metal Melts with the Diamond and Graphite Surface. Kiev. Published in Russian by "Naukova Dumka", 1967, p.87.
4. Bezrukov G.N., Polyakov V.P., Mukhanstkulova M.M., Loladze N.G. Superhard Materials (in Russian), 1982, N2, p.7.
5. Shapilo V.B., Sergeev V.V. Powder Metallurgy (in Russian), 1985, N4, p.48.
6. Fedoseev D.V., Derjaguin B.V., Varshavskaya I.G., Semenova-Tyan-Shanskaya A.S. Crystallization of Diamond. Moscow. Published in Russian by "Nauka", 1984, p.135.

MARTENSITIC TRANSFORMATIONS IN CARBON AT HIGH PRESSURES

A.V.Kurdyumov
Institute for Materials Science Problems
Academy of Sciences of Ukrainian SSR
Kiev, USSR

At high pressures direct graphite-to-diamond transformations can have either martensitic or diffusion nature. Martensitic mechanism is characteristic at relatively low temperatures (to ~2000 K), diffusion mechanism is typical for higher temperatures and also for low-crystalline original structures [1,2].

It is found [2,4] that the first stage of martensitic diamond formation is the transformation of graphite into lonsdaleite. Being a metastable high pressure phase, lonsdaleite transforms into the stable phase - diamond. The succession of martensitic transformations graphite → lonsdaleite→ diamond takes place as in static compression so in shock compression.

The regular mutual orientation of lonsdaleite and graphite

$$(100)_l \parallel (001)_g, \quad [10\bar{1}0]_l \parallel [0001]_g \qquad (1)$$

was firstly observed by means X-ray study of samples prepared by high static pressures [5]. We observed the orientation (1) when studying the shock compression products of graphite using transmission electron microscopy methods (Fig.1*). Therefore, crystallography of graphite → lonsdaleite martensitic transformation in static and shock compression conditions is the same. From relationship (1) it follows that during graphite → lonsdaleite transformation the $(001)_g$ planes are changed into the $(100)_l$ planes. For the first time it was noticed by Lonsdale [6].

The graphite → lonsdaleite transformation pattern allowing for relationship (1) was suggested in [7]. This pattern provides for the formation of an intermediate graphitelike structure with layer sequence ADAD (Fig.2), compression structure ADAD along c axis and splitting or flat $(001)_g$ layers into two planes $(100)_l$. The formation of the intermediate ADAD structure as shown in Fig.2, results from homogeneous shear of rhombohedral graphite lattice with ABCA layer sequence through an angle of 12°.

The study of samples prepared using shock [3] and static [4]

*The Figure is given at the end of the book

compression methods showed the lonsdaleite - diamond transformation to be of martensitic nature also. Between these phases the orientational relationship takes place

$$(111)_d \parallel (001)_l, \quad [112]_d \parallel [10\bar{1}0]_l \qquad (2)$$

Electron diffraction pattern with $[1120]_l \parallel [110]_d$ zones axes (Fig.3*) allows to observe some important features of both phases. Using the dark-field images we determined the crystal blocks dimensions being 4-5 nm for lonsdaleite and 10-15 nm for diamond. The lonsdaleite hol reflections are broaded into diffuse hol streaks, which are caused by one-dimensional disorder of its structure.

The formation of new diamond portions with the increase in compression temperature is accompanied by relaxation processes of polygonization, recrystallization and one-dimensional ordering of diamond structure. While this long-period polytypes are formed.

So martensitic graphite → lonsdaleite → diamond transformations are realized by formation of the intermediate ADAD structure and long-period tetrahedral polytypes. The ADAD structure was observed while studying martensitic transformations in boron nitride [8].

References

1. Курдюмов А.В., Пилянкевич А.Н. Фазовые превращения в углероде и нитриде бора. - Киев: Наук.думка.- 1979.- 188 с.
2. Курдюмов А.В., Островская Н.Ф., Голубев А.С. Механизм образования, стабильность и реальная структура лонсдейлита //Сверхтвердые материалы.- 1984. - №4.- С.17-25.
3. Структурное исследование продуктов ударного сжатия графита / Балан Т.Р., Боримчук Н.И., Бочко А.В. и др.//Сверхтвердые материалы.- 1983. - №3. - С.19-23.
4. Особенности структуры и механизм образования лонсдейлита / Курдюмов А.В., Слесарев В.Н., Островская Н.Ф. и др. //Докл. АН СССР. - 1980. - Т.255, №6. - С.1382-1385.
5. Bundy F.P.,Kasper J.S.Hexagonal diamond - a new form of carbon //J.Chem.Phys.-1967.-V.46,No.9.-P.3437-3446.
6. Lonsdale K.Formation of lonsdaleite from single-crystal graphite //Amer.Miner.-1971.-Vol.56,No.1-2.-P.333-336.
7. Курдюмов А.В. О механизме прямых фазовых превращений в углероде и нитриде бора //Докл.АН СССР.-1975.-Т.221,№2.-С.322-324.
8. Курдюмов А.В., Олейник Г.С. О метастабильных структурах графитоподобного нитрида бора // Кристаллография.-1984. Т.29, №4, С.792-793.

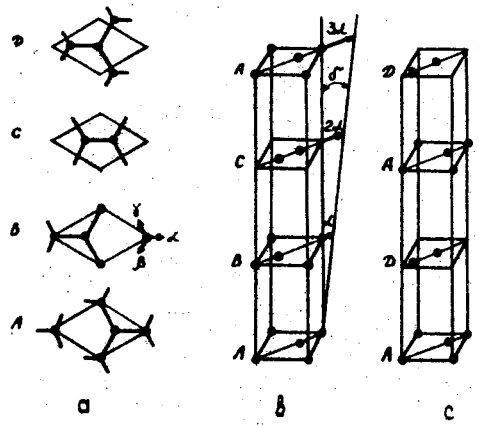

Fig.2. Homogeneous shear of rhombohedral graphite ABCA lattice at martensitic transformation: a - layer stackings in graphite-like structures; b - ABCA lattice before the shear; c - ADAD lattice as a result of the shear.

THE THERMODYNAMIC FUNCTIONS AND THE REGIONS OF P-T STATES OF DENSE CARBON AND BORON NITRIDE MODIFICATIONS

V.D.Andreev[I], A.B.Bochko[2], V.R.Malik[I]
[I]Institute for Superhard Materials, Academy of Sciences of the UkrSSR, Kiev, USSR
[2]Institute of Materials Science, Academy of Sciences of the UkrSSR, Kiev, USSR

For the first time the thermodynamic functions for boron nitride and carbon were defined in the temperature interval of 300 to 4000 K by a computational procedure which was impossible in the previous empirical approach. This involved the application of the theoretical functions from [1,2,3]. There the temperature dependence of the heat capacity is characterized by a sum of two Debye functions that reflect the contribution of vibration modes of different characteristic temperature into the heat capacity. The above-mentioned theoretical functions make it possible to calculate the thermodynamic function without allowing for the anharmonic effect in the temperature range rather wider one than that wherein the initial experiments were conducted. It is sufficient for their computation to define Debye characteristic temperatures. One of the procedures of their calculation using experimental enthalpy data is described in [4]. Besides, this work contains the majority of known experimental and theoretical data which enables to compare various methods of the thermodynamic functions characterization for carbon and boron nitride.

The specific heat capacity of graphite and graphite-like boron nitride was calculated by the equation [2]:

$$C_V = \frac{2}{3} RD\left(\frac{\theta^a}{T}\right) + \frac{1}{3} RD\left(\frac{\theta^c}{T}\right), \qquad (I)$$

where θ^a, θ^c are the Debye temperatures that correspond to vibrations parallel (axis a) and perpendicular (axis c) to base planes of graphite and g-BN lattices: R is the gas constant; T is the absolute temperature.

For diamond and sphalerite (wurtzite) - like BN:

$$C_V = 3RD\left(\frac{\theta}{T}\right) \qquad (2)$$

In the calculations the following magnitudes of the Debye temperatures were used: θ^{a}_{g}=2300 K, θ^{c}_{g}=800 K, θ_{d}=I850 K, θ^{a}_{gBN}=2I00 K, θ^{c}_{gBN}=730 K, θ_{sBN}=I608 K, θ_{wBN}=I580 K.

According to /3/ the Debye function:

$$D(\theta/T)=\frac{3T^3}{\theta^3}\int_0^{\theta/T}\frac{y^3dy}{e^y-1} \qquad (3)$$

was calculated by two equations:

for up to I500 K

$$D(\theta/T)=\frac{3\pi^4}{15}\left(\frac{\theta}{T}\right)^3-3\sum_{k=1}^{\infty}\frac{1}{k}\left[1+\frac{3}{k}\left(\frac{T}{\theta}\right)+\frac{6}{k^2}\left(\frac{T}{\theta}\right)^2+\frac{6}{k^3}\left(\frac{T}{\theta}\right)^3\right]e^{-\frac{k\theta}{T}}, \qquad (4)$$

for above I500 K

$$D(\theta/T)=-\frac{3}{8}\frac{\theta}{T}+3\sum_{k=0}^{\infty}\frac{B_{2k}}{(2k+3)(2k)!}\left(\frac{\theta}{T}\right)^{2k}, \qquad (5)$$

where B_{2K} are the Bernoulli's numbers.

The specific heat capacity, C_p, was calculated by the semi-empirical formula deduced by Nernst and Lindemann /I/ and taking into account the equations (I) to (5).

It was the first case of applying the temperature functions of the linear expansion coefficient and that of volume compressibility in the calculations.

The graphite-diamond, g-BN-sBN and g-BN-w-BN equilibrium lines were defined on the M-4030 computer. The results obtained that conform well with the experimental data are given in Fig.I.

The problem of the isothermal carbon compression within the entire temperature range of graphite and diamond existence (T=0... ...4000 K) was solved by the method of potentials of interatomic interactions for covalent and Van der Waals forces /5/. The following expressions were used for the potentials:

of covalent forces:

$$U^{6}(z)=U^{6}_{0}\frac{n\cdot m}{n-m}\left[-\frac{1}{m}\left(\frac{z_0}{z}\right)^m+\frac{1}{n}\left(\frac{z_0}{z}\right)^n\right]$$

of Van der Waals forces:

$$U^{\pi}(z)=-Az^{-6}+C\exp(-\beta z)$$

The theoretical compression isotherms exhibit the minimax character similar to that of Van der Waals ones for the gas-liquid system (Fig.2). The points of intersection of the graphite isotherm with that of diamond when superimposed on the (P,T)-diagram are located on the graphite-diamond equilibrium line defined by the thermodynamic calculations and the points of maxima form a line of barrier for the direct transformation which conforms well with the experimental data.

The established force barrier line of transformation has a corresponding energy barrier equal to I34.7 kJ·mol^{-I} at T=0 and lowering to 50.8 kJ·mol^{-I} at the triple point. Considering then the presence of the thermal energy $Q=\int_0^T C_v dT$ in the system one can conclude that the numeric data obtained satisfy the energy condition of the graphite-diamond transformation ($E_{g\to d}\geq E_{sp^2\to sp^3}$= =62.8-7I.2 kJ·mol^{-I}) related to the necessity to translate carbon atoms from sp^2 to sp^3 excitation state.

References

I. Мейер К. Физико-химическая кристаллография: Пер.с нем..-М.: Металлургия, I972. - 480 с.

2. Morgan W.C. Thermal expansion coefficients of graphite crystals //Carbon. - I972. - Vol.IO, NI. - P.73-79.

3. Жарков В.Н., Калинин В.А. Уравнение состояния твердых тел при высоких давлениях и температурах. - М.: Наука, I968. - 3I2 с.

4. К методике расчета характеристических температур углеродных материалов из экспериментальных данных энтальпии с помощью ЭВМ//Л.М.Бучнев, Маркелов Н.В., Смыслов А.И., Волга В.И.// Заводская лаборатория. I980. - №8. - С.73I-733.

5. Современная кристаллография. - М.: Наука, I979. - Т.2, 360 с.

6. Alder B.J., Christian R.H. Behavior of strongly shocked carbon //Phys.Rev.Let. - I96I. - Vol.7, NIO. - P.367-369.

7. De Carli P.S., Jamison J.C. Formation of diamond by explosive shock// Science.-I964. - Vol.I33, N3467. - P.I82I-I822.

8. Wentorf R.H. The behavior of some carbonaceous materials at very high pressures and high temperatures//J.Phys.Chem. - I965. - Vol.69, N9. - P.3063-3069.

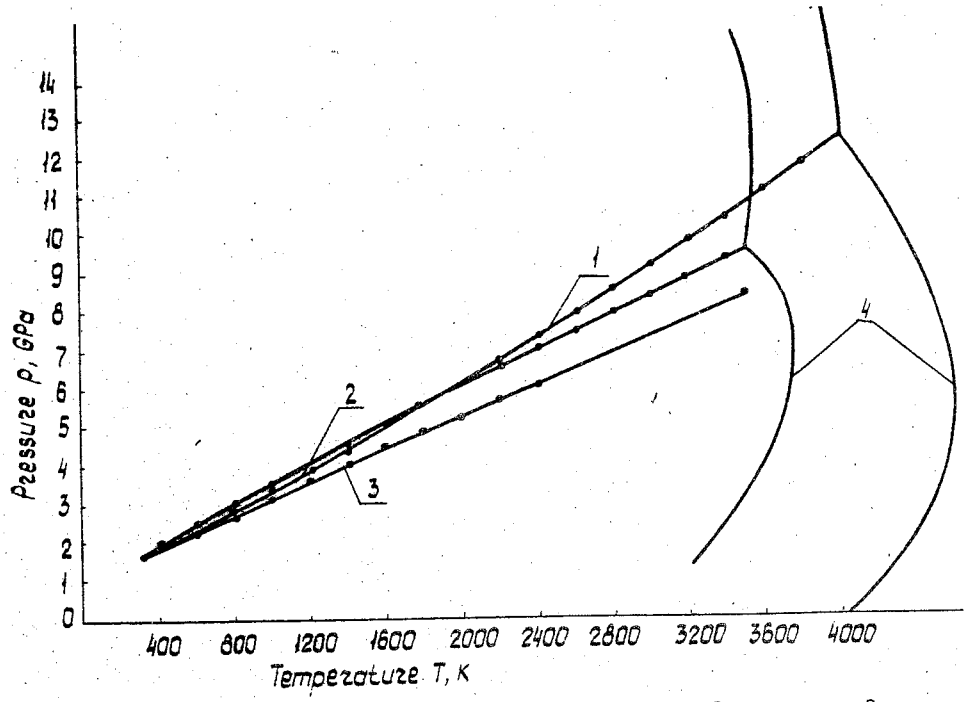

Fig.I. The equilibrium lines: I - graphite-diamond (Θ_g^a =2300 K, Θ_g^c =800 K, Θ_a=1850 K, ΔH_{300K}=158 kJ·kg^{-1}) ; 2 - g·BN - s·BN ($\Theta_{s\cdot BN}$ =1608 K, $\Theta^a_{g\cdot BN}$=2100K, $\Theta^c_{g\cdot BN}$=730 K, ΔH_{300K}=135.0 kJ·kg^{-1}) ; 3- g-BN-w-BN ($\Theta_{w\cdot BN}$=1580 K, ΔH_{300K}= =135.0 kJ·kg^{-1}) ; 4- lines of carbon and BN melting

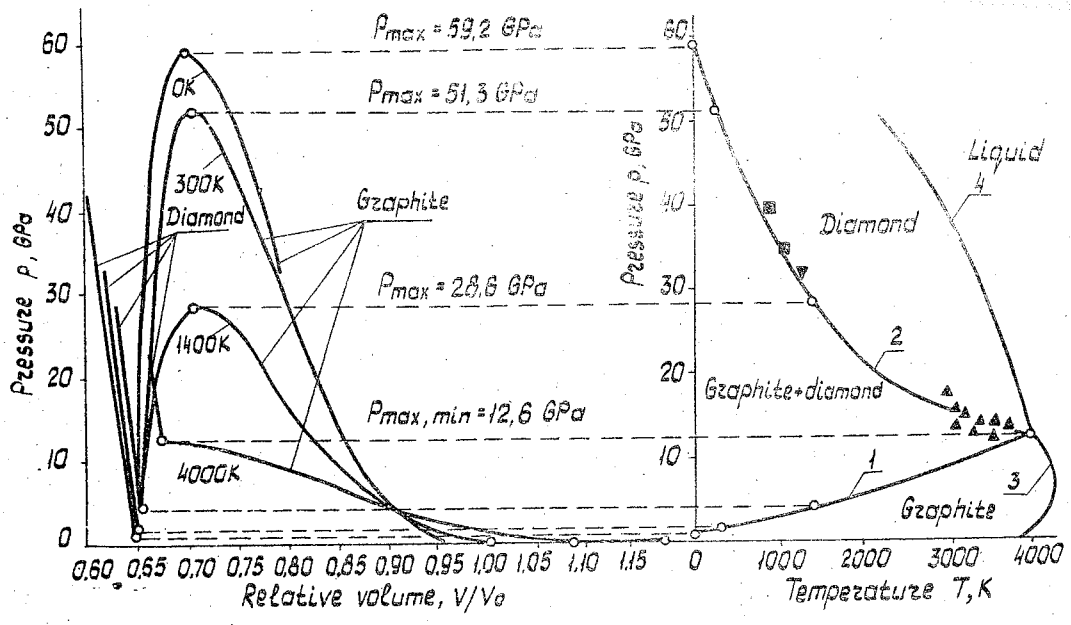

Fig.2. The compression isotherms of the p(V) and (P,T)-diagrams for C in the graphite-diamond system: I-the theoretical line of barrier for the direct graphite-diamond transformation ; 2-graphite-diamond equilibrium line ; 3-line of graphite melting ; 4-line of diamond melting ; the experimental data: ▣-/6/ ; ▼-/7/ ; ▲ -/8/.

EFFECT OF PRESSURE ON PERICYCLIC REACTIONS WITH SPECIAL EMPHASIS ON ENE REACTIONS

G. Jenner
Université Louis Pasteur, EHICS, Strasbourg, France

Introduction

The mechanism of bond forming and bond breaking has fascinated generation of chemists. Pressure was found to exert a deep influence on both processes. Pericyclic reactions were particularly considered. These reactions involve transition states wherein all bonding changes occur on a closed curve.

The kinetic pressure effect in these reactions is usually strong provided full concertedness (e.g. simultaneity of all bond events). The most outstanding example is represented by the Diels-Alder reaction which has been extensively studied by means of high pressure kinetics either from the mechanistic standpoint [1] or via a synthetic approach [2].

A less studied class includes the ene reaction which presents some analogy with the Diels-Alder addition, except that it cannot have elements of symmetry like [4 + 2] cycloadditions. The reaction consists in a multicenter addition with migration of the ene double bond, allylic hydrogen abstraction from the ene component with transfer to the enophile and creation of a new bond at the unsaturated termini :

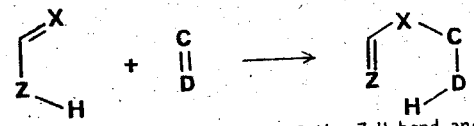

The process understands breaking of the Z-H bond and formation of two new bonds X-C and D-H.

I. Mechanistic considerations

The mechanism of the ene reaction is of considerable importance. Does the reaction proceed via a pericyclic transition state ? Does it involve intermediates and if so, what are the intermediates ? One way to approach the problem is now well assessed. Numerous studies have showed

that high pressure kinetics yielding the volume of activation can help to locate the transition state along the reaction axis [3]. Actually, the volume of activation $\Delta V^{\neq}$ must be compared to the reaction volume ΔV.

As shown on the above chemical equation, the ene reaction involves hydrogen transfer from the atom Z to the atom D, the migration is thus termed as a Z--H--D transfer.

a) C--H--O hydrogen transfer

A typical reaction is the addition of an activated carbonyl bond (enophile) to C=C double bonds. It is evident that these reactions occur readily when the enophile is substituted by electron-demanding groups and the ene component by electron-releasing groups (E = CO_2R) :

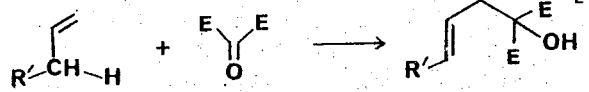

The pressure study yielded the data listed in Table 1 [4]. The comparison of $\Delta V^{\neq}$ with ΔV (e.g. the θ -value) is self-evident. The θ-values are consistent only with a concerted mechanism : the transition state is structurally similar to the product. If an intermediate were involved, the θ-value would experience much lower values. Interesting additional information can be deduced from the activation volume data. $|\Delta V^{\neq}|$ is higher than $|\Delta V|$ in most cases. Such a situation would mean that the transition state is more compact than the final state and, in fact, was also found in some Diels-Alder reactions involving transition states stabilized by secondary orbital effects. The present ene reactions are undoubtedly related with a tight transition state involving angular hydrogen transfer.

b) O--H--O hydrogen transfer

A representative example is the addition of mesoxalates to a carbonyl bond (E = $CO_2C_2H_5$)

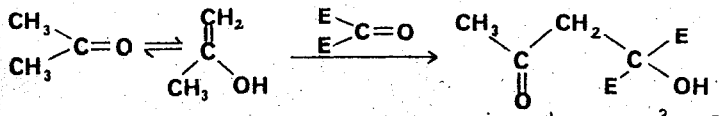

The pressure study yielded following data [5] : $\Delta V^{\neq} = -30\ cm^3.mol^{-1}$ and $\theta = 0.88$. In this reaction, θ is slightly smaller than unity, however, the transition state is still close to the product. As a conse-

quence, the breaking of the first O-H bond and the formation of the second H-O bond should occur in a nearly concomitant way.

c) C--H--N hydrogen transfer

Diazene esters are strong enophiles reacting readily with any olefin. Pressure kinetic analyses were effected with cyclic olefins [6] (Table 2)

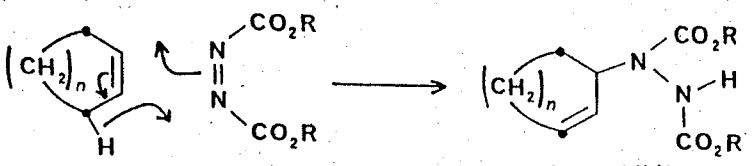

As immediately observable, these (C--H--N) ene reactions exhibit a different pressure-behavior. The θ-values stand back from unity, meaning that the reactions are less sensitive to pressure. The most economical explanation would consider a sequential mechanism, for example the diradical pathway which would nicely accommodate the volume data. This mechanism would certainly apply to the cyclopentene and cyclohexene reactions (θ is 0.68 and 0.58 respectively), whereas higher cycloalkenes would react according to pathways in the borderline region of competing concerted and two-step mechanisms.

As a conclusion, a concerted transition state is normally preferred for ene reactions. However, as inferred from the activation volume data, the mechanism can range from a rate-limiting hydrogen abstraction through a spectrum of concerted reaction to rate-limiting biradical formation.

II. Synthetic considerations

The energy requirements for the ene reaction make the thermal uncatalyzed reaction a poor-yielding preparative procedure, unless temperature is raised over 150-200°C. The reaction, however, leads in these conditions to unwanted side products.

As examplified in the first part of this paper, concerted ene reactions are characterized by high negative values for the activation volume. Consequently, high pressure may direct the ene reaction toward the desired path. An early pressure application was made by Gladysz [7] demonstrating the beneficial effect of pressure on β-pinene ene

reactions : excellent yields of the ene product were obtained (75-100 %) with full selectivity. The scope of the reaction was extended by application of both pressure and temperature in a flow apparatus : toluene reacts with the unactivated cyclohexene to yield the ene product [8].

Cycloheptatriene enters several types of reactions depending on the second addend. With homonuclear bonds, it reacts mainly according to a [4 + 2] cycloaddition (norcaradiene adducts). With heteronuclear bonds, the ene reaction competes with the cycloaddition. Since the volumes of activation for both processes are of the same order of magnitude, high pressure cannot differentiate the reactions. Nonetheless, it was found that pressure has a considerable effect on the reaction sequence as illustrayed below [9] (E = CO_2CH_3) :

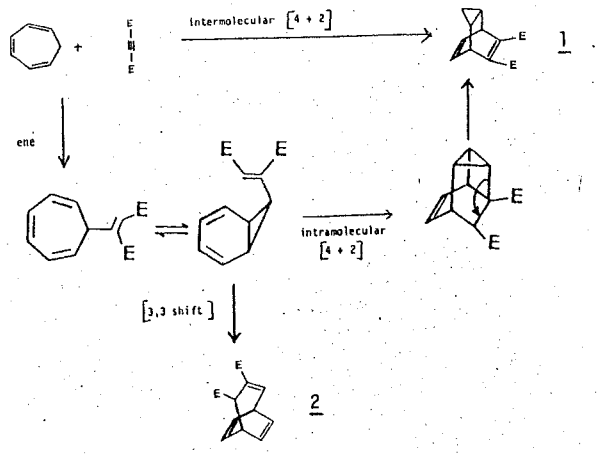

Under high pressure, only the norcaradiene adduct 1 is obtained via inter- and intramolecular [4 + 2] cycloaddition, while at atmospheric pressure, 1 and 2 are produced in a 2:1 ratio.

With the carbonyl bond activated by ester groups (mesoxalates), cycloheptatriene reacts only under high pressure to yield the ene product in 72 % yield [9].

Reactions of 2,5-dimethylfuran or -thiophene with activated carbonyl compounds at 800-1000 MPa give adducts 3 presumably via an ene mechanism [10].

Table 1.

Pressure effect on (C--H--O) ene reactions (volume data calculated for 25°C)

Alkene	R	$\Delta V^{\neq}$ [a]	ΔV [a]	θ [b]
1-Hexene	CH_3	- 28.4	- 27.0	1.05
2-Methyl-1-pentene	CH_3	- 26.2	- 26.5	0.99
2,4,4-Trimethyl-1-pentene	CH_3	- 32.0	- 30.9	1.04
2-Ethyl-1-butene	CH_3	- 34.9	- 31.3	1.12
2,3-Dimethyl-1-butene	CH_3	- 33.5	- 31.9	1.05
β-pinene	C_2H_5	- 29.2	- 28.0	1.04

[a] The volumes are given in $cm^3.mol^{-1}$

[b] θ is the ratio $\Delta V^{\neq} : \Delta V$

Table 2.

Pressure effect on (C--H--N) ene reactions (volume data calculated for 25°C)

Cycloalkene	$\Delta V^{\neq}$ $cm^3.mol^{-1}$	ΔV $cm^3.mol^{-1}$	θ
cyclopentene	- 23.1	- 33.9	0.68
cyclohexene	- 19.7	- 34	0.58
cycloheptene	- 25.8	- 34	0.76
cyclooctene	- 26.9	- 34	0.79
cyclodecene	- 26.4	- 34	0.78

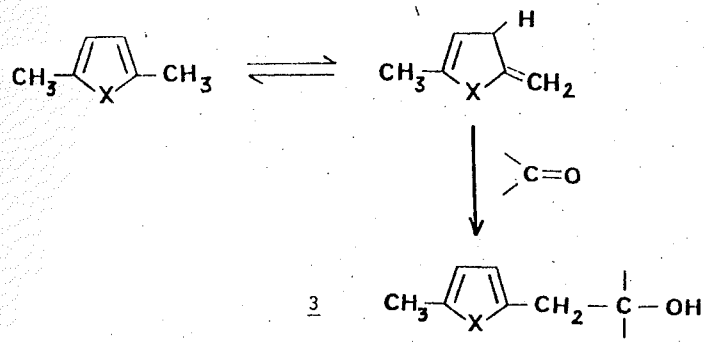

3

References

1. Grieger R.A. and Eckert C.A., Mechanistic evidence for the Diels-Alder reaction from high pressure kinetics, J. Amer. Chem. Soc., 1970, 92, 7149-7153.
2. Dauben G.W., Gerdes J.M. and Smith D.B., Organic reactions at high pressure, J. Org. Chem., 1985, 50, 2576-2578.
3. Jenner G., Analyse du profil volumique des réactions péricycliques à l'aide de la piézochimie, Bull. Soc. Chim. France, 1984, 275-284.
4. Jenner G. and Papadopoulos M., Concertedness in thermal intermolecular ene reactions, J. Org. Chem., 1982, 47, 4201-4204.
5. Ben Salem R. and Jenner G., Mechanism of the (O--H--O) hydrogen transfer, Tetrahedron Lett., 1986, 27, 1575-1576.
6. Jenner G. and Ben Salem R., Influence de la pression sur le transfert (C--H--N), Nouv. J. Chim., submitted.
7. Gladysz J.A. and Yu Y.S., Ene reactions of β-pinene at 40 kbar pressure, J. Chem. Soc., Chem. Comm., 1978, 599-600.
8. Metzger J. and Köll P., Intermolecular ene reactions in a HP/HT flow apparatus, Angew. Chem. int. ed., 1979, 18, 70-71.
9. Jenner G; and Papadopoulos M. High pressure addition reactions involving cycloheptatriene, J. Org. Chem., 1986, 51, 585-589.
10. Jenner G., Papadopoulos M., Jurczak J. and Kożluk T., Reactions of furans and thiophenes with activated carbonyl compounds, Tetrahedron Lett., 1984, 25, 5747-5750.

THE CAPILLARY PHENOMENA AND THE GRAPHITE-TO-DIAMOND PHASE TRANSFORMATION IN THE PRESENCE OF METAL MELTS

Yu.V. Naidich[1], A.A. Shul'zhenko[2], A.V. Andreyev[2], O.B. Loginova[1], V.M. Perevertailo[1]

[1]Institute of Materials Science Problems, Academy of Sciences of the UkrSSR, Kiev, USSR

[2]Institute for Superhard Materials, Academy of Sciences of the UkrSSR, Kiev, USSR

To study surface and contact properties in the interface between multicomponent metal melts and diamond (graphite) is important both from the point of view of a further development of the physicochemistry of surface and capillary phenomena and for gaining a more deep insight into the mechanism of graphite-to-diamond conversion in the presence of metal melts.

The surface and adhesion properties were defined in this work by the "sessile drop" method in a vacuum of 10^{-13}Pa. For the Cu-Mn-graphite system the wetting angles were defined under high pressure conditions by a purpose-devised technique based on the fact that an equilibrium shape of a melt drop lying on a graphite substrate placed into a high pressure cell had been formed in an inert liquid medium (flux melts) under uniform pressure. As a solid phase the МПГ-6 graphite and single crystals of natural diamond ((III) face) were used.

The concentration dependencies for the wetting angle observed when graphite and diamond interact with binary alloys Cu-Mn and Ge-Mn are shown in Fig.1. The analysis of the curves obtained shows that manganese in an alloy with copper is an adhesion-active component in respect to graphite both under vacuum and under high pressure. The adhesion activity of manganese grows with pressure (the wettability improves).

The results of studying the capillary properties of the melts under investigation in respect to graphite and diamond were compared with the degrees of graphite-to-diamond conversion in the presence of the same metal melts. Fig.2 shows curves for the concentration dependency of the adhesion tension and the degree of graphite-to-diamond conversion in the process of diamond synthesis using Cu-Mn and Ge-Mn alloys.

In the Cu-Mn system a rather high degree of the graphite wetting is attained at Mn content of 20 to 30 mol %. At the same

time the degree of graphite-to-diamond conversion in the process of synthesis is substantial and amounts to 33 to 36%.

In Ge alloyed with Mn a high degree of graphite and diamond wetting is achieved by an increase of Mn concentration in the alloy up to 70-80 mol %. It is these contents of manganese in germanium that lead to the degrees of graphite-to-diamond conversions in the presence of these alloys which are closer to those defined for the Cu-Mn alloys containing 20 to 30 mol % Mn.

As is seen from Fig.2, various alloys (Cu-Mn and Ge-Mn) containing inequal amounts of Mn but having equal adhesion tension given synthesis parameters provide close values of the conversio degree. One should also note a sharp rise in the degree of graph te-to-diamond conversion in the presence of the Ge-Mn alloys at 60 to 70 mol % concentration of Mn, i.e. in the region of a shar increase in the wettability of graphite and diamond by these all ys. The degree of conversion rises approximately by a factor of despite the fact that the melting temperature of these alloys higher in this concentration range by almost 200 °C.

The adhesion properties and the diamond synthesis process re also studied using germanium melts containing nickel, mangane chrome, vanadium and titanium as additives. Being inactive in re pect to carbon germanium acted as a solvent for refractory trans tion metals and allowed to produce alloys of different wetting lities and energies at the interface with diamond and graphite.

Thus, it became possible to use for the diamond synthesis se melts which equally wet graphite and diamond but due to the troduction of various transition metals into the melt are chara terized by different Gibbs energy values for the metal- carbon action (by a different-forming ability). The magnitude of this e gy for metals used in this work increases from nickel to titani

The concentration dependencies of wetting angles found in interaction of graphite with germanium alloys, containing various adhesion-active metals are shown in Fig.3. Pure germanium is in tive in respect to graphite and diamond surfaces (the wetting a les are 147° and 145° respectively), which is defined by weak sical forces of interaction between these phases. The affinity metals to carbon increases in a row from nickel to titanium. Th wetting of graphite by the melts under investigation improves the same consequency,

Fig.4 shows the dependencies of the degrees of graphite--diamond conversion in the process of synthesis and those of

change in the adhesion tension of melts interfaced with diamond whose wetting ability is the same when interacting with graphite (wetting angle is 50°) on the magnitude of Gibbs energy in the reaction of metal with carbon. With the increase of the carbide-forming rate (the values of Gibbs energy are more negative) the degree of graphite-to-diamond conversion in the system drops sharply.

In the presence of germanium alloys containing titanium and vanadium the degree of conversion will be practically zero (in spite of the fact that these melts wet graphite and diamond rather well) which cannot be explained just by a certain increase in the magnitude of interphase energy at the interface diamond - metal melt.

Such a sharp drop in the degree of graphite-to-diamond conversion in the presence of germanium alloy containing vanadium and titanium is probably brought about by an intensive carbide forming process in the system what leads to a sharp decrease in the content of free carbon in the melt and prevents the transportation of carbon to the surface of a growing crystal.

It follows that the major requirement to the metal melts which are planned to be used as a solvent-catalyst in the diamond synthesis process must be their high capillary activity in respect to diamond and graphite stipulated by the process of carbon solving in a metal, and not by the carbide formation in the region of contact.

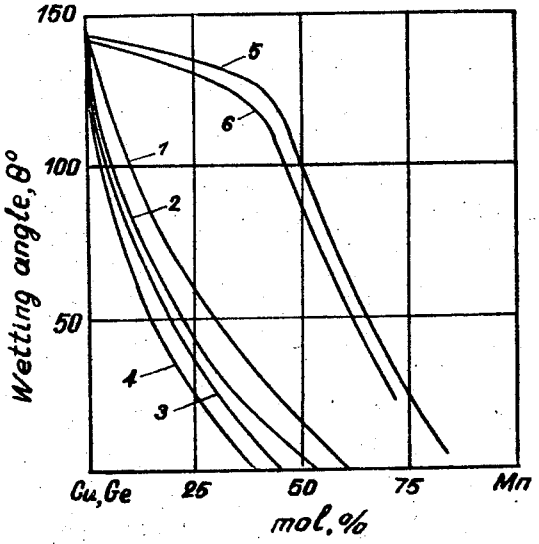

Fig. 1. The concentration dependencies of the wetting of graphite and diamond by the Cu-Mn alloy (I - vacuum, 2 - 4.5 GPa, 3 - 5.5 GPa, 4 - 6.5 GPa) and the Ge-Mn alloy (5- graphite, 6 - diamond).

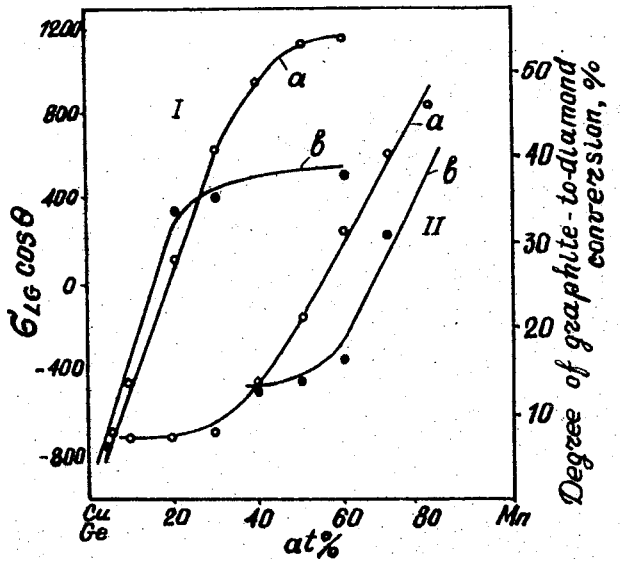

Fig. 2. The concentration dependencies of (1) the adhesion tension and (2) the degree of graphite-to-diamond conversion in the process of diamond synthesis in the presence of the Cu-Mn (1a,2a) and Ge-Mn (1b,2b) metal melts.

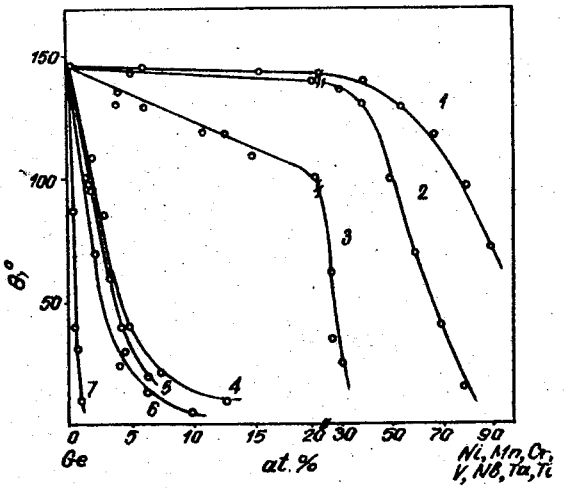

Fig. 3. The concentration dependencies of the wetting of graphite by the melts of germanium containing additives: Ni - 1; Mn - 2; Cr - 3; V - 4; Nb - 5; Ti - 6; Ta - 7.

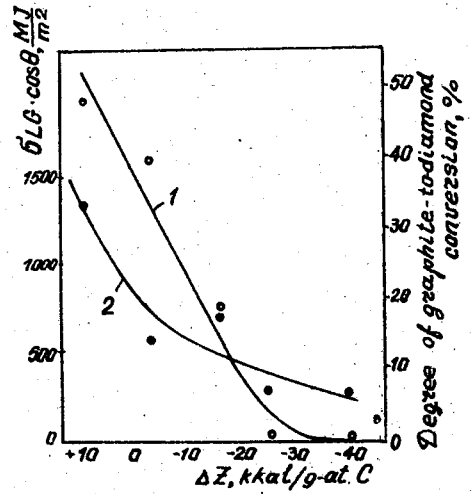

Fig. 4. The dependencies of a change in the adhesion tension of melts at the interface with diamond (1) and the degree of graphite-to-diamond conversion (2) on the value of Gibbs energy in the reaction of metal plus additives and carbon.

THE CHEMICAL COMPOSITION OF SYNTHETIC DIAMOND SURFACES AS A RESULT OF ACTION BY LIQUID-PHASE OXIDIZERS

V.G.Alyoshin, G.P.Bogatyreva, V.B.Kruk
Institute for Superhard Materials, Academy of Sciences of the UkrSSR, Kiev, USSR

The type and the kind of superficial impurities in diamond depend on numerous variable factors directly related to the technology of synthesis, concentration, recovery, sorting, classification and so on. On the other hand, the information on the surface chemistry of diamond obtained in each particular case can explain a number of peculiarities of the synthetic diamond behaviour in the processes of metal-coating, floatation, sedimentation, oxidation, in the sintering of diamond powders and in the study of the adsorption processes and the interaction between diamond and various media. The "pure" surface of diamond can exist only in theory.

The superficial chemical composition of natural diamond powders has been most comprehensively studied by J.Thomas [1] and E.Evans [2].

This work deals with the results obtained when studying the chemical composition of synthetic diamond surfaces by the XPS- and AES-methods.

The diamonds studied were synthetized in the Ni-Mn-C system and only those crystals that contained minimal inclusions were selected. The Auger-spectra were obtained by the technique described in our work [3].

The results of the quantitative analysis of the diamond surface composition related to the type of chemical treatment and the time of etching by a flux of argon ions are given in the Table.

The tabled results indicate higher oxygen content as compared to initial level after all types of chemical treatment. Considering the low retention of oxygen in molecular form on the diamond surfaces as was shown in [3] it is possible to suppose that the chemical interaction occurs between the diamond surface and the known oxidizers. As the AES-method is rather inefficient for defining a chemical interaction, a special study using XPS-method was carried out. The experiments were conducted on the electron spectrometer ЭСКАЛАБ-5. K_α - radiation of magnesium was used as the source of the X-ray quanta. The study was done on AC15 grade

345/250 diamond treated by strong liquid oxidizers such as those based on six-valency compounds of chrome and sulfuric acid; those based on seven-valency compounds of manganese and sulfuric acid; and concentrated sulfuric acid.

The influence of the chemical treatment on the surface composition of synthetic diamonds

Specimen No	Treatment	Time of etching by argon ions, s	Concentration of elements, % (atomic) C	O	S	N	Cr	Fe
1	None	-	100	-	-	-	-	-
		600	100	-	-	-	-	-
		600	100	-	-	-	-	-
2	Mixture of concentrated sulfuric and nitric acids (volume ratio 2:5)	-	88	8	1	3	-	-
		600	84	9	1	6	-	-
		600*						
3	Mohr's salt ($FeSO_4(NH_4)_2 \cdot SO_4$ (2.5 % solution in bidistillate)	-	57	12	3	-	-	28
		600	61	12	3	-	-	24
		600	60	12	3	-	-	25
		600	59	12	3	-	-	26
4	Mixture of 50 % chromic and concentrated sulfuric acids (volume ratio 1:1)	-	98	1.5	-	-	0.5	-
		600	94.4	3.3	0.9	-	1.4	-
		600*						
5	Mixture of 40%-solution of caustic soda and 30% solution of hydrogen peroxide (volume ratio 4:1)	-	96	4	-	-	-	-
		600	96	4	-	-	-	-
6	Solution of persulfuric ammonium acid ($(NH_4)_2S_2O_8$) saturated in cold	-	94	6	-	-	-	-
		600*						
7	Concentrated perchloric acid ($HClO_4$) (without steaming)	-	96	4	-	-	-	-
		600*						

* Specimen charging occurs

The treatment with the liquid oxidizer based on six-valency chrome compound in sulfuric acid medium cause an asymmetry in the line of carbon 1s-electrons (Fig., line 1), wich suggests the

existence of the products resulted from establishing carbon - oxygen links on the surface. The asymmetry of this line disapeared when the diamond surface was etched by argon for 60 s. Consequently, the products of the chemical interaction is retained in the thinnest surface layer what is confirmed by the diamond surface oxidation. The retention of sulfur (1.9 % at) in the form of SO_4^{2-} anions on the diamond crystal surface is suggested by the binding energy level equal 169.3 eV for the s2p-line.

The oxidation-reduction process was also observed when treated with a liquid oxidizer based on the seven-valency manganese ion at the presence of sulfuric acid. The asymmetry of C1s-electron line (Fig., line 2) is more marked than in the case of line 1. The etching with argon for 60 s does not result in this case in the disappearence of the line asymmetry. The presence of the sulfur ions in the form of SO_4^{2-} anions (6.4 % at) was also established on the diamond crystal surfaces.

The treatment of crystals with concentrated sulfuric acid at its boiling temperature also leads to the asymmetry of the C1s--electron line (Fig., line 3) and the retention of SO_4^{2-} anion by the surface (0.5 % at).

The comparison of amounts of retained SO_4^{2-} anions when chemically treated in the above-mentioned manner indicates that the levels of SO_4^{2-} anions differ, that is, it is evident that the amount of the retained SO_4^{2-} ions allows to estimate the generated defectiveness of the diamond surface.

The results obtained make it possible to affirm that the surface layer of the synthetic diamond crystal is chemically active, the diamond carbon acting as a reducer.

References

1. Thomas J.M. Adsorbility of diamond surfaces //The Properties of Diamond. - London; New York; San Fransisco: Academic Press, 1979. - P.211-214.

2. Evans E.L., Thomas J.M. Surface chemistry of diamond: Review. Diamond Research 1975, P.2-8.

3. Алешин В.Г., Богатырева Г.П., Крук В.Б., Смехнов А.А. Влияние химической обработки на состав поверхности синтетических алмазов //Докл. АН УССР. Сер.А. - 1985. - №3. - С.75-78.

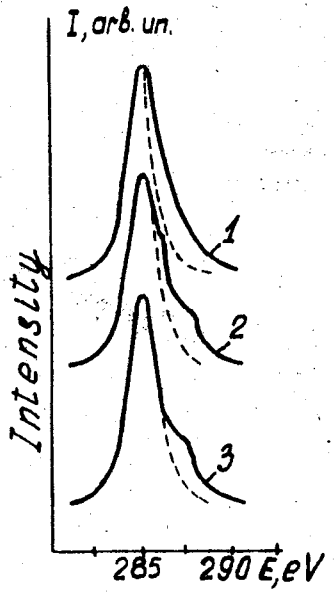

XPS-spectra of C1s-electrons after treating the surface with oxidizers based on the six-valency Cr ion (1), seven-valency manganese ion (2), and concentrated sulfuric acid (3), The pattern of XPS spectra of C1s-electrons in the high-energy region when the interaction between the surface and oxidizer does not occur is also shown (- - -).

THE GROWTH OF DIAMONDS ON SEED CRYSTALS IN THE HIGH-PRESSURE APPARATUS OF RECESSED-ANVIL TYPE

S.A.Ivakhnenko, V.I.Vityuk, I.S.Belousov
Institute for Superhard Materials, Academy of Sciences of the UkrSSR, Kiev, USSR

The growing of diamonds on seed crystals is a complicated methodical task. The reason lies in a rather small (in order of some cub. cms) reaction volume of the high pressure apparatus (HPA) and in related problems of performing pressure and temperature measurements and choosing materials for the cell isolation and the pressure transmission. The HPA of recessed-anvil type [1] has a number of advantages as compared with the "belt"-type apparatus[2] that is used in western countries of which main are the simplicity and the reliability. So far it was not known, however, whether there existed a possibility to maintain temperature and pressure necessary for growing diamonds on seeds in the recessed-anvil type HPA for periods of time amounting to tens of hours.

The diamond growth on seed crystals was performed in the HPA of recessed anvil type of 35 mm in diameter. As a pressure-transmitting media sodium chloride, pyrophyllite and lithographic stone were used which had been preliminary heat-treated to remove crystal and adsorbed water [3].

The temperature measurements in the cell at room temperature were done by defining the resistivity in the fixed phase transition points of bismuth, thallium and barium. At high temperatures the differential method for pressure measuring was used [4]. The method consists in that to measure pressure a temperature difference between two lines of phase transition sufficiently known in the T-P coordinates is used. The T-P diagrams for gold, silver and copper constructed to high pecision by applying the precision piston-cylinder apparatus [5], Fig.1, were used to this purpose. The temperature differences were defined by the DTA method. The thermoanalytical curves are given in Fig.2. The measurement of pressure by the above method permitted to choose cell materials in such a way that their phase transitions at temperatures up to 1450 ^{o}C were prevented. As a result, pressure as well as temperature of the diamond synthesis were kept constant during tens of houns.

To grow diamonds, the temperature gradient method was used, the gradient depth being the same as in [6]. Alloys of nickel-iron and nickel-manganese were used as solvents.

The recessed-anvil type HPA used permitted to readily develop pressures and temperatures necessary to grow diamonds by the temperature gradient method [6,7] and to hold them at levels necessary for growing high quality diamond crystals in the duration of 36 hours. The colour of the grown crystals was light yellow, their heat conductivity being 1800 W/m K.

Thus the recessed-anvil type HPA can be successfully applied for the diamond growth on seed crystals by the temperature gradient method.

References

1. Новиков Н.В., Герасимович А.В. Исследование деформируемых уплотнений АВД типа наковальни с углублениями. Сверхтвердые материалы, 1983, №4, стр.3-7.
2. Hall H.T., Ultra high-pressure, high-temperature apparatus - the "Belt". Rev.Sci.Instr., 31, 125, 1960, p.125-127.
3. Getting I.C., Kennedy G.C. Effect of pressure on the e.m.f. Chromel-Alumel and Platinum-Platinum 10% Rhodium Thermocouples. J.Appl.Phys., 41, N11, 1970, p.4552-4562.
4. Ивахненко С.А., Белоусов И.С., Витюк В.Н. Измерение давления дифференциальным методом по кривым плавления серебра и меди. Тезисы доклада IУ Всесоюзной конференции "Гидростатическая обработка материалов", Донецк, 1985, с.44.
5. Akella J., Kennedy G.C. Melting of copper (Cu), gold (Au) and silver (Ag) at high pressure up to 65 kbar in piston-cylinder apparatus .J. Geophys.Res., 1971, 76, N20, p.4969-4979.
6. Strong H.M., Chrenko R.M. Further studies in diamond growth rates and physical properties of laboratory-made diamond. J.Phys.Chem. 75 , 12., 1971, p.1838-1843.
7. Wentorf R.H. Some studies of diamond growth rates. J.Phys.C Chem., 75,12, 1971, p.1833-1837.

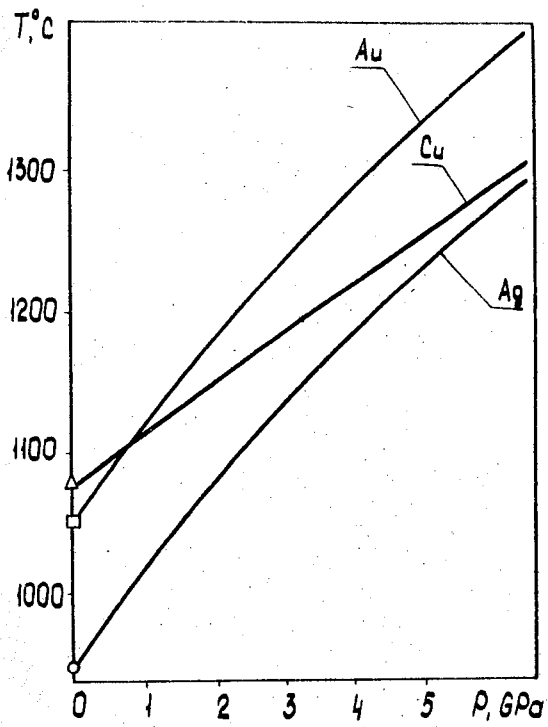

Fig. 1. The melting lines for copper, silver and gold.

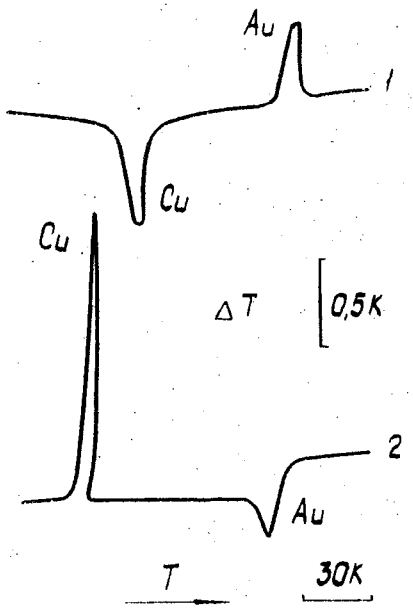

Fig. 2. The thermoanalytical curves: melting and crystallization of copper and gold:
1 - heating, 2 - cooling.

BIG ALCOHOLS FROM SMALLER ONES
HOMOLOGATION OF ALCOHOLS UNDER CO/H_2 PRESSURE

G. Jenner and P. Andrianary
Université Louis Pasteur, EHICS, Strasbourg, France

Introduction

Alcohols are valuable industrial products and are used as basic chemicals (for example they are the starting material for the synthesis of α-olefins). In the last ten years, new perspectives came to light due to the shortage of oil supplies. As a matter of fact, alcohols may be used as additives to gasoline, either as fuels or to ensure solubilization of methanol in gasoline-methanol mixtures [1] .

The synthesis of higher alcohols from lower ones is called the homologation reaction and is achieved via catalyzed hydrocarbonylation -

$$R\,CH_2OH \xrightarrow{CO/H_2} R\,CH_2CH_2OH$$

Two factors must be considered to make a CO/H_2 reaction a viable economical process: conversion and selectivity. Selectivity is not a problem, if the reaction products are used as additives. However, if the goal is to seek a basic product, it is obvious that highest selectivity to the specific compound must be attained.

1. Synthesis of ethanol from methanol

Methanol is a cheap material. It can easily and economically be produced in great quantities from CO and H_2 or from almost anything containing carbon and hydrogen. The conversion of methanol to ethanol via hydrocarbonylation is achieved catalytically and usually produces a wide spectrum of compounds in addition to the desired alcohol. The best catalytic systems combine cobalt compounds with free iodine or iodides (either ionic or covalent).

The homologation reaction does not proceed directly, but involves acetaldehyde as intermediate, which leads to ethanol via subsequent hydrogenation :

$$CH_3OH + CO + H_2 \longrightarrow CH_3CHO + H_2O$$
$$\downarrow H_2$$
$$CH_3CH_2OH$$

We have been, therefore, interested in the acetaldehyde synthesis and have found that one of the critical reaction parameter is pressure. The pressure effect was examined up to 260 MPa in following conditions : catalytic system (cobalt acetate / iodine = 1 : 10 -molar ratio-), T (165°C), CO : H_2 (1 : 2) (Table 1).

Visibly, high pressures are beneficial both for the production of acetaldehyde (very high turnover frequencies are achieved) and for the selectivity to acetaldehyde. There is an optimal pressure range between 130-160 MPa. Beyond 160 MPa, yields are strongly depressed, whereas the selectivity to ethanol is much less affected. The reason is still unclear though most probably in the higher pressure range, there should be a detrimental effect on the various equilibria of the mechanistic scheme which involves a complex catalytic cycle [2] whose discussion is out of context here. The many equilibria that are established during the activation process can be very sensitive to pressure changes. Condensed phases are promoted by pressure, while equilibria allowing ligand abstraction from the catalyst metal center are theoretically shifted in the opposite direction. The most critical step in the formation of acetaldehyde is a reductive elimination involving the acylcobalt carbonyl complex [3] :

$$CH_3CO\ Co(CO)_4 + HCo(CO)_4 \longrightarrow CH_3CHO + Co_2(CO)_4$$

This step is thought to be pressure accelerated.

2. Synthesis of higher C_{n+1} alcohols from the lower C_n alcohols

The homologation of the next higher alcohols via hydrocarbonylation is a difficult reaction [4] and could not be satisfactorily resolved until recently [5] . We could show that the reaction proceeded in the presence of a complex catalytic system comprising a cobalt and a ruthenium compound (in the adequate ratio) associated with free iodine [5,6] .

Pressure was shown to be a determining parameter as exemplified in Table 2. Reaction conditions must be strict : cobalt acetate : ruthenium acetylacetonate : iodine = 5 : 1 : 10 -molar ratio-), t (170-200°C), CO : H_2 (1 : 2), t (2 h).

Table 1.
Pressure effect in the homologation of methanol

Pressure (MPa)	Methanol conversion (%)	Acetaldehyde	
		Turnover frequency[a]	Selectivity\%
0.1	0	-	-
16	18	65	9
30	29	258	36
52	44	750	39
100	73	2530	70
143	94	3500	75
200	88	3015	67
260	51	1615	66

[a] mol CH_3CHO/mol cobalt/h

Table 2.
Pressure effect in the homologation of alcohols

Alcohol	Pressure (MPa)	Conversion and yields[a] (%)			
		45	60	100	200
Ethanol	Conversion	65	70	85	90
	Propanol yield	16	9	7	6
	Higher alcohols	0.5	0.8	1	2
1-Propanol	Conversion	59	66	75	-
	Butanols yield	19	16	13	-
	Higher alcohols	0.3	0.6	1	-
2-Propanol	Conversion	58	65	76	-
	Butanols yield	23	23	25	-
	Higher alcohols	0.7	2	3	-

[a] Yields based on substrate. The results are not optimized

For all the investigated alcohols, we found an optimal pressure range located approximately between 40 and 55 MPa (for temperatures of 170-200°C). That the optimal pressure does not depend on the alkyl rest of the alcohol is significant and refers probably to a very same hydrocarbonylation mechanism. Another point deserving interest may be pointed out as a pressure increase leads to a further homologation reaction.

Again, as emphasized in the methanol reaction, the large pressure dependance of the alcohol yield suggests the possibility of catalyst transformations as integral parts of the catalytic process. For example, complex catalytic species such as $HRu_3(CO)_{11}^-$ derived from the initial ruthenium compound were evidenced by spectroscopy. These species may undergo a fragmentation with CO to produce more reactive ruthenium hydrides. The reaction is known to occur only under sufficiently high CO pressure.

Conclusion

Cobalt or cobalt-ruthenium catalyzed hydrocarbonylation of methanol and other C_n alcohols allows the synthesis of the next higher homologs (ethanol and C_{n+1} alcohols). Though the mechanism is different according to substrate, in each case, pressure increases the homologation activity.

References

1. Chen N.Y., Making gasoline by fermentation, Chemtech, 1983, 13, 488-492.
2. Koermer G.S. and Slinkard W.E., Methanol homologation reaction catalyzed by cobalt carbonyl, Ind. Eng. Chem. Prod. Res. Dev., 1978, 17, 231-236.
3. Alemdaroglu N.H., Penninger J.M. and Oltoy E., Mechanism of Hydroformylation, Monatsh. Chem., 1976, 107, 1043-1053.
4. Bahrmann H. and Cornils B., New syntheses with carbon monoxide, J. Falbe Ed., Springer, Berlin, 1980, 226-242.
5. Jenner G. and Andrianary P., Reductive carbonylation of ethanol using homogeneous cobalt-ruthenium catalysts, J. Catal., 1987, 103, 37-45.
6. Jenner G., Bitsi G. and Andrianary P., Effect of homogeneous bimetallic catalysts in the hydrocarbonylation of alcohols, Appl. Catal. 1986, 24, 319-321.

THE REGULARITIES OF THE CHEMICAL REACTIONS OF SOLID ORGANIC COMPOUNDS UNDER SHEAR DEFORMATION AND HIGH PRESSURE UP TO IO GPa

Zharov A.A.
N.D.Zelinsky Institute of Organic Chemistry, Academy of Sciences of the USSR, Moscow, USSR

Until present about thirty chemical reactions of solid organic compounds under the combined effect of shear deformation and high pressure (SD + HP) have been discovered.

The chemical processes occurring in the single-component systems have been studied most thoroughly [*]. The regularities in the interaction of compounds in the two-component systems were studied much poorly, in particular due to the difficulties arising from the inhomogeneity of reaction mixtures.

The experiments were carried out under a pressures of I-IO GPa at temperatures 77 to 300 K.

The deformation and compression of substances can be accomplished by different methods: with Bridgman anvils (Fig.Ia), under extrusion through a die (Fig.Ib) and under extrusion through an annual gap with the simultaneous rotation of the dorn (Fig.Ic), and, finally, under a shock-wave compression accompanied by the plastic deformation of a substance (Fig.Id). Regardless of the method used for creating the SD+HP conditions just the same reactions occur in solid reagents (Table I). At the same time, these reactions do not occur at the usual compression up to high pressures.

The kinetic features of the process and their regularities have been studied mainly on an opposed anvils device[*]. Particular attention has been paid to the two-component systems. In these systems the yield of reaction products often depends on the method of preparation of the reaction mixture.

An effective method for the homogenization of the reaction components is to combine the reacting molecules or their fragments in a single molecule, either as a complex, or a salt, or any other chemical compound. In the general case the reproducibility of the observed results can be essentially improved by preparation of the samples by cooling the eutectic melts.

[*] Zharov A.A. The Polymerization Reactions of Solid Monomers under Deformation at High Pressure, Uspekhi khimii, 1984, v.53, No.2, p.236-250

Table I. Chemical reactions occurring under SD+HP conditions, effected by different methods

Reaction	Compression up to 8 GPa	Anvils	Shock-waves	Extrusion
Addition of NH_3 at the -C=C-bond (aminoacid synthesis)	-	+	+	+
Synthesis of amides from ammonium salts of saturated acids	-	+	+	+
Esterification reaction	-	+	+	
Polymerization of solid vinyl monomers	-	+	+	+
Peroxide decay	-	+		+
Synthesis of peptides from amino acids	-	+	+	

+ the reaction does occur

- the reaction was not detected

The study of heterogeneous systems under SD+HP conditions was also carried out with the reagents dispersed in a chemically indifferent compound (matrix). The concentration of reagents in the matrix varied from I to IO wt.%.

The experiments with a large number of organic compounds showed that the reactions in the presence of indifferent compounds chosen occasionally can be both accelerated and slown down, as compared with the interaction of pure reagents.

Adamantan (possessing high plasticity and shearing stress and being indifferent to many reagents) has found wide application as a matrix. Table 2 gives the threshold pressures P_{thres} (i.e. a pressure at which a chemical transformation of a substance is detected) for various organic compounds and for the same compounds in the adamantan matrix. The reactivity of the reagents is seen to increase very sharply in the case they are subjected to deformation as mixtures with adamantan.

On the examples of a large number of two-component systems, capable of entering various reactions under the SD+HP conditions, the following rule has been established: when the matrix possesses plasticity and its shearing stress is geater than that of the reagents,

Table 2. Threshold pressures (P_{thres}) for organic compounds under SD+HP conditions

Compound	P_{thres}(GPa), Anvils rotation angle 360°		Shearing stress of reagent at 5 GPa (GPa)
	Pure reagent	2 % mixture with adamantan	
Polymerization with aromatic ring opening			
Naphtalene	4.0	2.0	0.I75
o-Terphenyl	4.5	3.0	0.06
Diphenyl	7.0	4.0	0.I35
Benzene	7.0	4.0	-
Hexafluorobenzene	9.0	6.0	-
2,6-Dimethylnaphthalene	I0.0	3.5	0.I45
Hexamethylbenzene	> I0.0	7.0	0.055
Tetramethylbenzene	> I0.0	3.5	0.I40
Polymerization at -C≡N bonds			
Succinic acid dinitrile	I0.0	3.0	-
Decomposition reaction			
$Cr(CO)_6$	4.0	4.0	0.240
$Mo(CO)_6$	7.0	3.5	0.205
$W(CO)_6$	5.0	2.5	0.2I0

the reactivity of the latter in this matrix is higher as compared with the reactivity of the pure reagents.

The use of the plastic matrices with a high shearing stress proved to be a very effective way to increase the reactivity of substances under SD+HP conditions. In this case the pressure required to initiate the chemical reaction can be essentially lower (Table 2). In some cases the deformation in the matrix produced chemical transformations of even those compounds, which otherwise did not enter the reaction.

In series of experiments with the matrices, matching each other in nature and crystalline structure, a linear dependence has been established between the shearing stress of the matrix and the rate constant of the reaction under SD+HP conditions.

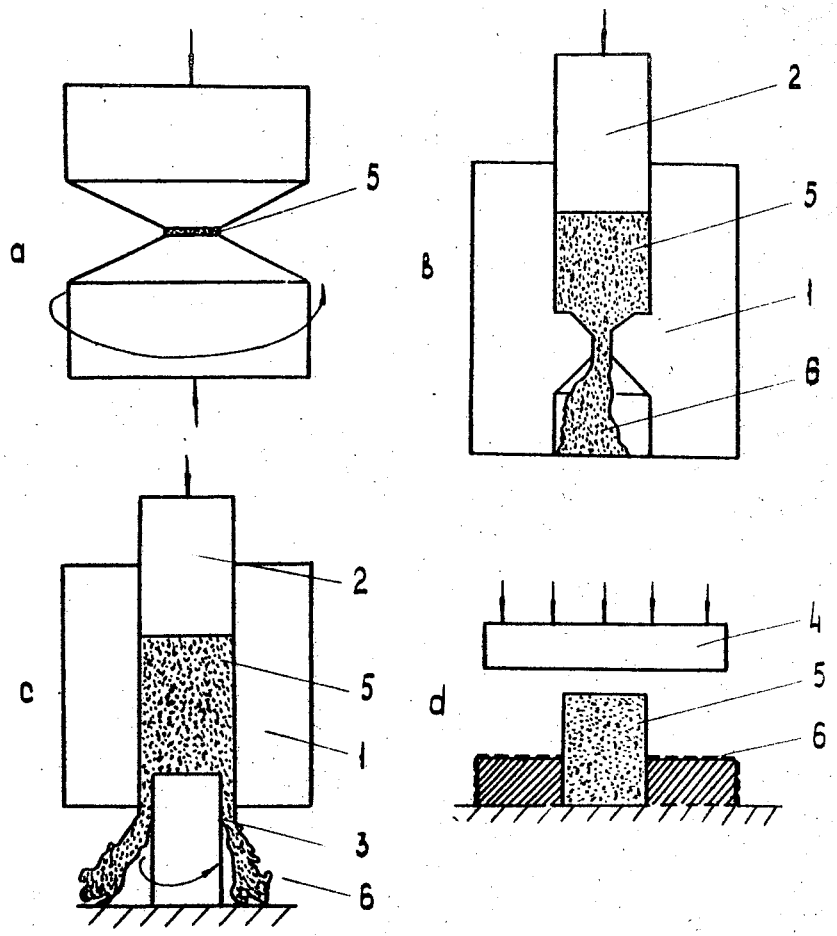

Methods for creation of high pressure and shear deformation in substances: a) Bridgman anvils; b) extrusion through a die; c) extrusion through an annual gap with simultaneous rotation of dorn; d) shock-wave compression with plastic deformation of a substance:
I-high pressure block; 2-high pressure rod; 3-rotating rod (dorn); 4-plate moving by explosion products; 5-substance; 6-substance after deformation under high pressure.

TRANSFORMATION MECHANISM OF CARBON CONTAINING SUBSTANCES TO DIAMOND

V.Shanov
High Institute of Chemical Technology
Department of Semiconductors
1156 Sofia, Bulgaria

INTRODUCTION

At present, the number of the reported successful methods for diamond synthesis is considerably increased. Most generally, the investigations along these lines can be divided in two main groups: synthesis in the thermodynamically stable region for diamond and metastable growth. The first one requires the use of high pressure (HP) and high temperature (HT) and covers the well known catalyst processes and the direct transformation of graphite to diamond at high static pressure or by shock compression, as well. Upon the metastable growth is realized the crystallization of diamond from carbonaceous gases (1-2) or by employing accelerated carbon ions (3). It was also reported for overgrowths of diamond in a dissolution medium in the presence of nickel at atmospheric pressure (4).

Due to the variety in the methods for growing of diamond crystals, it can hardly be proposed a uniform transformation mechanism of carbon containing substances to diamond. There exist a number of hypotheses treating the separate processes for diamond synthesis. A detailed discussion upon them is given in (5-6). The hypothesis presented in this paper, reflects some theoretical and experimental considerations regarding growing of diamond crystals, both at HP catalyst process and at metastable crystallization from carbonaceous gases.

DISCUSSION

From our point of view, in order to perform a successful transformation of carbon containing substances to diamond, two basic conditions are important to exist:

1. The carbon atoms or small groups of these atoms have to be brought to free atomic state.
2. Presence of seed crystals is necessary and it should organize the free atoms into crystal structure of diamond.

The truth of above conditions is obvious for the case of metastable growth of diamond seeds. We think that these considerations could be applied also for the catalyst solvent processes at HP and HT. In the latter case the graphite is dissolved in the metal-catalyst which provides disorganized atomic carbon.

Most of the metals, including those from group VIII upon melting do not undergo considerable structural changes (7-8). In the metal melt of the catalyst, certain regions keep the far order of the crystal state and remain in it as clusters. These micro-crystal clusters of the metal-catalyst in the metal-carbon solution could play the role of seed crystal nuclei on which growth of diamond in the conditions of liquid phase heteroepitaxy starts. The opposite process of gas-phase epitaxy of the popular catalyst nickel on diamond crystal (9) is known.

From these points of view, the surprisingly high similarity on the crystal structures and in the lettice parameters between the most frequently used catalyst and the diamond can be explaind - Table 1. In support of the supposition expressed are a number of X-Ray and neutron diffraction structure analysis (11-12) of the synthetic diamond which show the presence of metal clusters epitaxially connected with the lettice of the diamond crystals. Besides the above pointed out similarity in the crystal data, in order to perform successful transformation to diamond, the melt catalyst should be a good dissolver of carbon so that it could bring its atoms to free atomic state.

On the basis of the abovementioned considerations, Fig.1 shows the schematic energy level diagram for carbon when transformation to diamond in its thermodinamically stable region takes place. Let us assume, that the carbon atoms are dissolved and the dissolver does not have the same crystal structure as the diamon, i.e. it is not a catalyst. Although the thermodynamic driving force ΔG_v will be less for the growth of graphite as opposed to diamond nucleation, a small energy barrier ΔG_g^* may allow graphite growth without the spontaneous nucleation of diamond. In this case, the energy barrier of diamond ΔG_d^* is bigger than that of graphite ΔG_g^*, since the presence of clusters of graphite nuclei is allowed in the system. If a free carbon atom starts out with free energy G_{fc}, then it is easier for the atom to go over the smaller energy barrier ΔG_g^* for graphite. Thus, most of the free carbon atoms will form graphite under these conditions. In this way, heterogeneous nucleation of graphite on its own seeds will take place.

If a metal-catalyst with a suitable crystal data exists in the system, the energy barrier of the diamond ΔG_d^* can be lowered and to become lower than that of the graphite. The clusters of metal nuclei shall serve as seed crystals on which could start the growth in the conditions of liquid phase heteroepitaxy. In this case, most probably occurs the spontaneous heterogeneous nucleation of diamond in comparison with the graphite. Since the carbon atoms have a statistical energy distribution, some atoms will go over the large energy barrier ΔG_g^* to the graphite lettice, while most of them will go over the diamond lettice.

The proposed hypothesis is not applicable for the cases of direct transformation of graphite to diamond at high static pressure or by shock wave compression. Upon these processes, however, the possibility for contamination of the graphite charge with impurities of metal-catalyst, for example iron, is not excluded. The latter may occur from the sample holder or from the metal parts of the HP apparatus. In this case again an occurence of the catalytic mechanism can be expected, as part from the whole process of the carbon transformation.

In conclusion, it could be said, that the presented hypothesis could give some general considerations in the research of a new catalyst for diamond synthesis.

Table I. Comparison between the lattice parameters of metal-catalyst and diamond

Element	Lattice parameter (IO) ^{o} (A)	Lattice mismatch between the metal-catalyst and diamond (%)	Lattice type
Pt	3.9238	9.08	fcc (F)
Rh	3.8030	6.2I	fcc (F)
Pd	3.8902	8.3I	fcc (F)
Mn	3.8624	7.65	fcc (F)
Fe	3.6467	2.I9	fcc (F)
Co	3.5442	0.63	fcc (F)
Ni	3.5238	I.22	fcc (F)
Ta	3.3074	7.83	bcc (I)
Diamond	3.5667	0	fcc (F)

References

I. Poferl D.J., Gardner N.C., Angus J.C., "J.Appl.Phys." 44(I973) I428.

2. Deryaguin B.V., Fedoseev D.V., "Sci. Amer.", 233 (I975) I02.

3. Freeman J.H., Temple W., Gard G.A., "Nature", 275 (I978) 634.

4. Patel A.R., Cherian K.A., "J.Cryst. Growth.", 46 (I979) 706.

5. Shanov V., Dr.Thesis - High Institute of Chemical Technology - Sofia (I98I).

6. Vereshchagin L.F., Kalashnikov Ya.A., Shalimov M.D., "H.Temp. - H.Pr." 7 (I975) 4I.

7. Ubbelohde A.A., "Melting and Crystal Structure", Cl.Pr., Oxford (I965).

8. Arsentiev P.P., Koledov L.A., "Metal Melts and Their Properties", Moscow, "Metallurgy" (1976).
9. Pavlidis P., "Thin Solid Films", 42 (1977) 221.
10. Samsonova G.B., Handbook "Properties of the Elements", Part I, Moscow, "Metallurgy" (1976).
11. Lonsdale K., Milledge J., Nave E. "Mineral Mag." 32, (1959) 185.
12. Buzin V.I., Alichanov R.A., "FTT" (Solid St.Phys.) 13 (1971) 8.

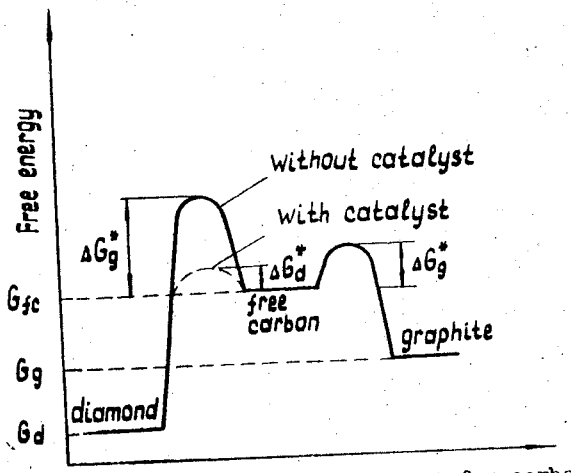

Schematic energy level diagram for carbon when transformation to diamond in its thermodynamically stable region takes place.

ON SOLID STATE DIAMOND NUCLEATION AT STATIC PRESSURE

U. Gerlach[1], G. Risse[1], H. Vollstädt[2]

[1]Central Institute of Solid State Physics and Materials Research, Academy of Sciences of the GDR, Dresden, GDR

[2]Central Institute for Physics of the Earth, Academy of Sciences of the GDR, Potsdam, GDR

Diamond synthesis is usually carried out in the region of 5 - 8 GPa, 1200 - 1800 °C in a metal catalyst system. Up to now the nucleation process is not fully explained, especially the question whether the nucleation is a homogeneous, heterogeneous or solid-state process and where a martensitic solid-state transition takes place, in the melt or in solid carbon phase.

Diamond formation under those conditions depends strongly on the structural perfection of the carbon source used, Fig. 1. Amorphous carbon, diamond-like carbon (i-c), glassy carbon or carbon black cannot transform into diamond, only the graphitization process takes place. A.A. Shul'zhenko [1] showed that this graphite resulting from the first step can be successfully used in obtaining diamond in a second step of resynthesis. In the case of coke it was showed by Kasatochkin et al. [2], that the extent of transformation into diamond goes with the degree of graphitization. Dissolved diamond (in metal catalyst) is not able to nucleate new diamond and only graphite can be found, even though diamond is thermodynamically stable [3]. Also during synthesis recrystallized or grown graphite cannot transform into diamond.

These experimental facts point out the preconditions for the diamond-nucleation process:

- a well crystalline graphitic structure
- mechanical or heat treatment of the graphitic source material.

We also investigated the effect of HP/HT-treatment on a carbon source from natural graphite at conditions to 6 GPa/1400 °C and considerable deformation of the source /Fig. 2/. The metastable 3R-polytype of graphite was produced and is stable under these conditions. Naka et al. /4/ also found a partial conversion of 2H- into 3R-graphite at 14 GPa and high temperatures. This 3R-formation is easily possible by mechanical sliding of the carbon layers in a well-crystalline graphite /Fig. 3/. On the other side many stacking faults and defects are produced by the HP/HT-treatment, the crystallinity of this graphite is lowered. In this time also the diffusion of metal-catalyst atoms into the graphitic structure takes place.

At normal pressures this 3R-graphite will be unstable at high temperatures about 1500 °C and the 3R-polytype changes slowly into the 2H-structure, but at high pressures there is a kinetic stabilization due to lower mobility of the carbon layers as a result of the decrease of the layer distance to about a_o 3.1 A. It means that the equilibrium adjustment

$$3\,R \underset{\text{mechanical}}{\overset{T}{\rightleftharpoons}} 2\,H$$

is kinetically hindered.

At a thermodynamically consideration of the different graphite polytypes we can state, that the 2H-structures are, as a rule, the thermodynamically form; e.g. 2H-graphite, -PbJ_2, - MoS_2, - $TaSe_2$, - GeS a.s.o. The 3R-polytypes should have higher

enthalpy and entropy values, as other higher polytypes. For the enthalpy difference of hexagonal and rhombohedral graphite Boehm and Coughlin have measured a value of 0,586 ± 0,17 KJ/g-atom /5/.

This higher energetic level of 3R-polytype has a consequence to the phase boundary line between graphite and diamond, because the usually used line is the 2H-graphite/diamond line. With the enthalpy value of 3R-graphite and a somenhat higher value of entropy at normal conditions we can estimate an equlibrium pressure of about 0,3 GPa lower than for 2H-graphite. Because the 3R-phase will not be stable at HP/HT-conditions the 3R/diamond line is established below the 2H/diamond line also at higher conditions (graphite grown during the synthesis is 2H-graphite). This 3R/diamond phase boundary line /Fig. 4/ is situated between the other calculated lines of different carbon-materials by Vereshchagin /6/. The lower equilibrium pressure of 3R/diamond means, that the transition 3R-graphite into 3C-diamond is thermodynamically preferred to 2H → 3C. The way 2H ⇌ 3R ⇌ 3C corresponds to Ostwald's step rule and at the HP/HT-graphitization of diamond also the kinetically stabilized 3R-graphite was found by Titova and Futergendler /7/.

TEM-investigations, carried out by means of a JEM-200 CX, show the transition of graphitic plates with uniform orientation, if natural graphite was used as a source as in Fig. 5 - 7*. These investigations also point to a solid-state transformation of graphite into diamond in the catalytic synthesis process.

Considering the structure dependence of diamond formation, the effect of HP/HT-treatment on the crystalline graphite and the thermodynamically position of a 3R/diamond equilibrium line we can conclude, that diamond nucleation process

*The Figures are given at the end of the book.

- is a martensitic, solid-state phase transition from 3R-graphite polytype into the dense 3C-diamond structure
- is only possible by use of well crystalline graphite crystallite (in or without another carbon matrix) under HP/HT-treatment by partial formation of 3R-graphite.

References

1. A.A. Shul'zhenko
   5th International symposium "High purity materials in science and technology"
   Dresden, GDR, 5. - 9. May 1980, part I, p. 122.

2. V.I. Kasatochkin, L.E. Shterenberg, V.N. Slesarev and N. Yu. Nedoshivin
   Dokl. Akad. Nauk SSSR 194, 801 (1970).

3. R.H. Wentorf, Jr.
   Ber. Bunsenges. phys. Chem. 70, 975 (1966).

4. S. Naka, K. Forii, Y. Takeda and T. Hanawa
   Nature 259, 38 (1976).

5. H.P. Boehm and R.W. Coughlin
   Carbon 2, 1 (1964).

6. L.F. Vereshchagin, E.N. Jakowlev, L.M. Butsnev and B.K. Dymov
   Teplophys. vys. Temp. 15, 316 (1977).

7. V.M. Titova and S.I. Futergendler
   Kristallografija 7, 926 (1962).

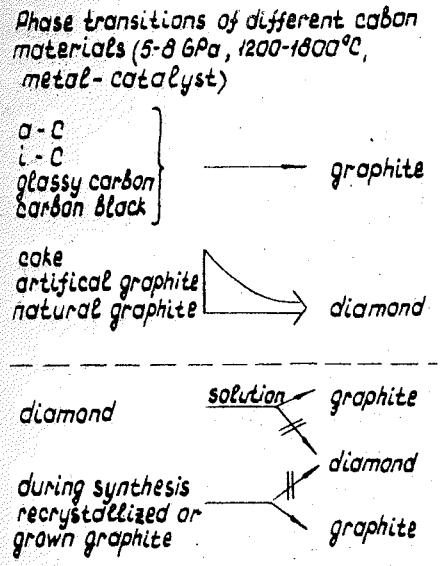

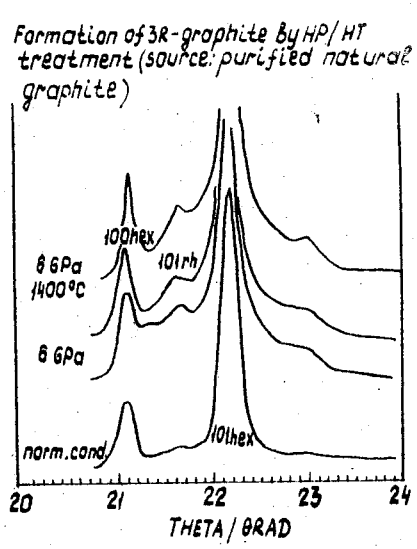

Fig. 1. Phase transitions of different carbon materials (5 - 8 GPa, 1200 - 1800 °C, metal-catalyst).

Fig. 2. HP/HT-treatment of natural graphite and partial formation of 3R-graphite polytype.

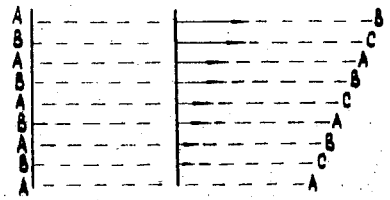

Fig. 3. Formation of 3R-graphite by sliding.

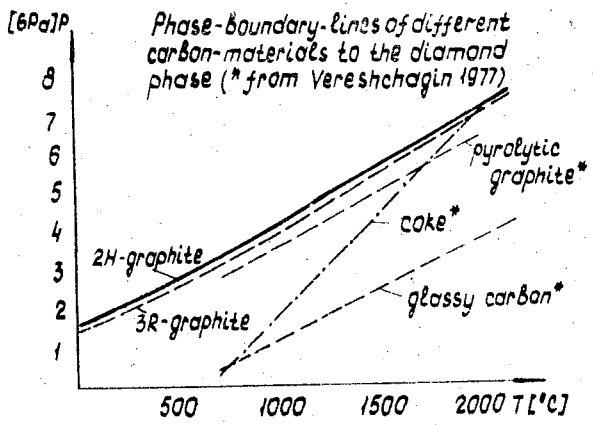

Fig. 4. Phase boundary line of 3R-graphite and different carbon materials to diamond.

THE GROWTH KINETICS OF SPONTANEOUSLY NUCLEATED DIAMOND CRYSTALS IN THE Mn-Ni-C SYSTEM

M.Ya. Katsay
Institute for Superhard Materials, Academy of Sciences of the UkrSSR, Kiev, USSR

To resolve the set problems it was necessary to define the character of the interrelation between the phase interface (R) movement in the process of the crystal growth and the duration (τ) of the synthesis cycle. This was achieved by the induced striation method. The zonal structure was produced by a periodical short-time raising of temperature during the crystal growth and subsequent going back to the basic synthesis temperature. The multiple temperature fluctuations allowed a set of light bands to form in crystals and delineate their contours at the moment of the peak temperature [1]. The above temperature fluctuations conducing to the activation of the growing surface of faces do not cause any distortion in the pattern of the growth kinetics in contrast to the techniques involving a temperature lowering accompanied by an entrapment of the crystallization medium.

The temperature within the reaction volume of the cell was controlled usingthe platinum/platinum-rhodium thermocouple (Pt/PtRh10).

The rate of the diamond crystals growth in the {100} direction was defined by the movement of the phase interface which was measured from the center of growth to the face along the normal during the intervals between the heating cycles.

The estimations of the initial and a current pressure in the synthesis process that were based on the evaluation of the copper melting point detected by the Pt/PtRh10 thermocouple and corrected according to Kennedy in [2,3] were achieved by the periodical raising (lowering) temperature in answer to the observed thermal effect ocurring concurrently with the melting of the reference metal. It was found that the drop of the initial pressure within the temperature range of 1523 to 1610 K amounts to 7 to 10% in the time span of 1200 s.

As a carbon source the graphite of МГ, ОСЧ7-3 type was used. The experiments were carried out in the interval of 1500 to 1580 K the deviation from the equilibrium line [4] within the cell being 0.98 to 0.18 GPa (ΔP) and the maximal temperature gradient within the reaction volume being 7 K.

It is established that the temperature perturbations induced during a period of 120 s from the beginning of the synthesis cycle were indiscernible in diamonds of any size to which they have grown in the synthesis cycle. When estimating the linear growth rates there was an uncertainty for the time interval related to the first occurrence of delineation which was stipulated by the lack of information about the moment of diamond nucleation.

Depending on the growth conditions the linear growth rate for the crystal studied measured up to 670 μm varied from $(5-4)\cdot10^{-5}$ $cm\cdot s^{-1}$ to $0.5\cdot10^{-5}$ $cm\cdot s^{-1}$.

The study on the interrelation between the movement of the front of growth (R) for the (100) face and the duration of growth (τ) has shown that the growth of diamond crystals at ΔP=0.98-0.18 GPa and temperatures of 1580 to 1500 K is limited by the kinetics of the surface processes because the linear dependence of R on τ has been discovered. The lowering of the pressure in the reaction volume of the cell does not affect the limiting stage whatsoever.

When increasing the initial pressure up to ΔP=0.92 GPa at 1523 K a deviation of the R (τ) function from the linearity was observed on diamond reaching a size of 400 μm. The similar tendency was observed in the case of raising the process temperature (Fig.1). Probably, the subsequent growth of the crystals would lead to the change of the limiting stage.

It is established that the maximal growth rates for the cubic faces of diamond of the same size growing without entrapping the crystallization medium go higher with the pressure lowering (Fig.2). The diamond growth activation energy for the (100) face was defined by the function $\ln V(^1/_T)$ and it equals to 130 kJ/mol at 1523 K and 1580 K.

The results presented make it evident that within the pressure-temperature range of interest the growth of spontaneously nucleated diamond crystals in the Mn-Ni-C system is limited by the kinetics of the surface processes.

References

1. Кощей М.Л., Влияние P, T, c-условий на кинетику роста кристаллов алмаза и захват азота//Оптическая спектроскопия и ЭПР примесей и дефектов в алмазе. - Киев:Ино-тут сверхтвердых материалов АН УССР, 1986. - с.89-95.

2. I.G. Getting, G.C. Kennedy. Effect of pressure on the emf chromel-alumel and platinum 10% rhodium thermocouples// J.of Appl.Physics.-1970.-V.41,N11.-P.4552-4562.

3. I.A. Akella, G.C. Kennedy. Melting of gold, silver and copper-proposal for a new high pressure calibration scale// J. of Geophysical Research. - 1971.-V.76, N20.-P.4969-4977.

4. C.S. Kennedy, G.C. Kennedy. Equilibrium line from graphite and diamond//J. of Geophysical Research. -1976.-V.81, N14.-P.2467-2470.

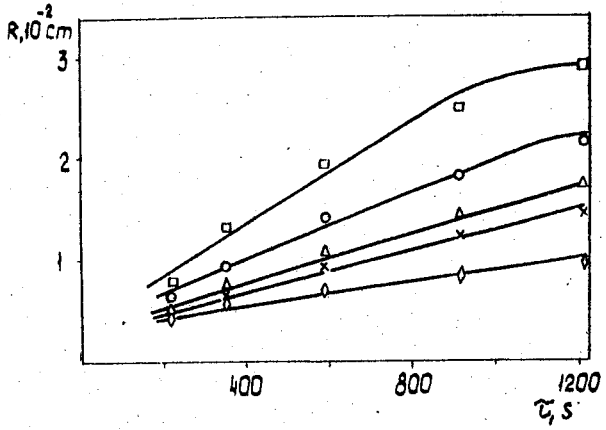

Fig. 1. The movement in time of the growth front (R) for the cubic faces of diamond crystals at ΔP=0.58 GPa and 1580 K.

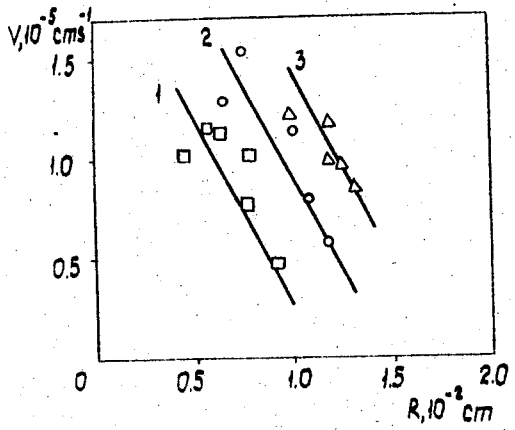

Fig. 2. The linear growth rate (V) and the size (R) of diamond crystals growing without entrapping any inclusions at 1523 K and ΔP 0.35 (1), 0.25 (2), 0.15 (3) GPa respectively.

THE SYNTHESIS OF DIAMONDS FROM CARBOHYDRATES

L.F.Kulikova, M.D.Shalimov, V.N.Slesarev
The Institute of High Pressure Physics, USSR Academy of Sciences, Troitsk, USSR

Wentorf[*] studied a number of different organic compounds which were heated to about 2275 K for about I5 min at a pressure of about I2 GPa.Most of compounds formed diamond but a few formed of graphite. The experiments with antracene, naphtalene, chrysene showed that the formation of diamond is not impossible.

In order to investigate the possibilities of diamond formation in C-H-O system we studied the behaviour of organic carbohydrates (sucrose, for example) in the preceding diamond formation. The pyrolysis products of carbohydrates at high pressure and temperature were hydrogen simple carbohydrogens and such oxygen compounds as carbon dioxide, carbon oxide, water, that differs from the pyrolysis products of carbohydrogens.

The pressure in the apparatus used to compress the sample was estimated with the reference to the resistance change in bismuth, barium at room temperature. The temperature of the sample was measured by chromel-alumel and platinum-platinum-I0 rhodium thermocouples situated near graphite heater, with following extrapolation to more high temperatures. The compounds under investigation were packed into graphite tubes which were heaters, and exposed to high pressure and temperature. After cooling and release of pressure the sample was examined by various methods, including X-ray diffraction, electron microscopy, IR-spectroscopy.

The results of thermobaric treatment in the region preceding diamond formation are summarized in Table. It was discovered that during the first stage of thermobaric treatment sucrose under investigation underwent thermal destruction giving rise to carbon material with only a (002) X-ray diffraction (IR-spectra of adsorption showed that sucrose pyrolyzed at 523 K). With the increase of temperature its structure becomes more ordered up to that of a well ordered graphite, comparable with a natural Ceylon graphite. A

[*] Wentorf R.H., The behavior of some carboneceous materials at very high pressure and high temperature, J.of Phys.Chemistry, I965, 69,No.9, 3063-3069

further increase of temperature results in appearance of the first diamond area.

The obtained diamonds actually represent polycrystalline aggregates formed from monocrystalline octahedra or plates of up to 80 /um size. The obtained diamonds are transparent and have light-green and yellow color. There are monocrystals of diamond of octahedral and plates form.

The stability to oxidation by air for these diamonds is almost the same as for the natural ones.

The structural changes of the pyrolysis products of sucrose in consequence thermobaric treatment

Temperature, K	550	703	I063	II23	I343	I623
Diffraction lines	(002) (I0)	(002) (I0) (004)	(002) (I0) (004)	(002) (I00) (I0I) (I02) (004) (I03) (II0)	(002) (I00) (I0I) (I02) (004) (I03) (II0) (II2)	(002) (I00) (I0I) (I02) (004) (I03) (II0) (II2)
Interatomic spacing d_{002} (nm)	-		0.3389	0.3382	0.3366	0.3363
Degree of graphitization $\frac{0.344-d_{002}}{0.344-0.3356}$	-	-	0.6I	0.69	0.88	0.98
Halfwidth line Δ_{002} (grad)	-	-	0.40	0.35	0.30	0.26

INFLUENCE OF METALS ON PHASE TRANSFORMATION OF DIAMOND INTO GRAPHITE

A.V.Nozhkina
NPO VNIIALMAZ, Moscow, USSR

Quality of diamond tools depends to a considerable extent on the interaction between diamond, bond components and workpiece material: dissolution of carbon of diamond with formation of intermediate phases, adhesion of diamond with metal, phase transformation of diamond into graphite at high temperatures. Studies of interaction between diamond and metals are devoted mainly to problems of wetting and adhesion [1-5]. Influence of metals on phase transformation of diamond into graphite has not been studied completely enough.

The aim of the work was obtaining complex information about processes of contact interaction between diamond and metals at high temperatures. Results of investigation of influence of metals on the process of phase transformation of diamond into graphite in the temperature range of 500-1900 °C were used in the process of the work.

It is known that equality of molar (g.at.) isobaric potentials corresponds to diamond-graphite equilibrium as in the general case $G_g = G_d$. Under usual conditions ($P = 9.8 \cdot 10^4$ Pa, T=298K) this equation is not fulfilled. In fact, applying the expression

$$G = H - TS \qquad (1)$$

to isothermal transformation of the system from state I to state II we can write down the difference

$$\Delta G_T = G_2 - G_1 = \Delta H_T - T \Delta S_T \qquad (2)$$

where ΔH_T - heat of transformation at constant pressure;
ΔS_T - corresponding change of entropy.

Heat of diamond-graphite transformation $H^\circ_{298} = -453.2$ cal./mole. Entropy of diamond $S^\circ_{298} = 0.5918$ e.u., entropy of graphite $S^\circ_{298} = 1.3737$ e.u.

Thus, $\Delta S_T = 0.7819$ cal./degree·mole for transformation of gram-atom of diamond into graphite and according to equation (2) $\Delta G^\circ_{298} = -685$ cal./mole. In other words, under these conditions transformation of diamond into graphite is connected with reduction of isobaric potential, and transformation of diamond into

graphite must proceed spontaneously from the point of view of thermodynamics. In practice this is not observed because of extremaly low speed of the process which can be accelerated by means of increasing temperature. According to Ormont calculations activation energy of diamond graphitization process is above 100 kcal/mole. Experimentally diamond graphitization was observed in vacuum or in the atmosphere of inert gases; diamond graphitization in vacuum takes place at low partial pressure of oxygen [6-9].

In calculating activation energy of the process of phase transformation of diamond into graphite under the action of metals, which are chemically active to carbon, it was supposed that graphitization energy $Q_{gr} = 0.7\ \lambda$ subl. (sublimation energy). The value of bond energy C-C of diamond in contact with a metal Q_{C-C} was evaluated by means of phase-boundary energy (σ_{s-l}). Evaluations have shown that transition and nontransition carbide forming metals are catalysts of phase transformation of diamond into graphite; in this case activation energy of the process is 95-110 kcal/mole.

Table gives losses of diamond mass in the process of sintering with metals in vacuum at T=1100 °C, τ =2 h.

Activation energy of phase transformation of diamond to graphite in sintering diamond with metals depends on metal nature and reduces considerably in contact with Mn, Ni and Cr and in smaller degree in contact with Si, Ti, W.

It is proved experimentally that if diamond sinteres with metals which do not form carbides in the studied temperature range phase transformation of diamond into graphite does not occur, diamond surface does not change, corrosion of diamond does not observed.

According to increasing catalytic action on the phase transformation of diamond to graphite during sintering metals may be arranged in the following order: Si, W, Ti, Ni, Cr, Mn. Activation energy of the process is maximum for Si (40 kcal/mole) and minimum for Mn (13 kcal/mole).

Rate of phase transformation of diamond to graphite in its metastable region depends on crystallographic orientation of diamond, inclusions and medium contacting with diamond. Rate of phase transformation of perfect crystals is very low in the medium inert to carbon at T < 1900 °C, because of extremely high energy of bond between carbon atoms in diamond, great values of

Metal coating	Losses of diamond mass															
	Total			In MeC			Graphite			Oxidation						
	m, g	$\frac{m}{s}\cdot10^4$, g/cm^2	h, μm	m, g	$\frac{m}{s}\cdot10^4$, g/cm^2	h, μm	m, g	$\frac{m}{s}\cdot10^4$, g/cm^2	h, μm	m, g	$\frac{m}{s}\cdot10^4$, g/cm^2	h, μm	m, g	$\frac{m}{s}\cdot10^4$, g/cm^2	h, μm
Ti	0.0230	3.38	0.96	0.0162	2.38	0.67	0.0068	1.0	0.28	-	-	-	-	-	-
Cr	0.0436	6.41	1.82	0.0169	2.48	0.68	0.0267	3.93	1.12	-	-	-	-	-	-
Ni	0.0217	3.19	0.91		0.17	0.05			0.86						
Si	0.0031	0.47	0.13	0.0019	0.28	0.079	0.0007	0.102	0.03	0.0006		0.09	0.025		
W	0.0205	2.98	0.86	0.0002	-	-	0.0122	1.79	0.508	0.1081		1.19	0.33		

free surface energy of diamond and activation energy of the process (above 100 kcal/mole).

Mechanism of phase transformation of diamond to graphite under the influence of temperature includes two stages: production of a layer of surface carbon on diamond with a disordered structure of carbon atoms and production of graphite stable structure as a result of rapid crystallization of amorphous carbon.

Influence of metals, reacting with diamond chemically, on the process of phase transformation of diamond into graphite comes mainly to sharp increasing the value of diamond free surface energy on the boundary with metal, decreasing activation energy of the process. Mechanism of phase transformation of diamond into graphite in presence of metals includes the following main studies: chemisorption of metals, producing of intermediate phase of amorphous carbon, catalytic crystallization of amorphous carbon, diffusion of carbon into metal and diffusion of metal through the layer of surface carbon to the surface of diamond.

In principle it is possible that mechanism of phase transformation of diamond into graphite includes solution of diamond in metal and subsequent separation of amorphous carbon and graphite from the solid supersaturated solution of carbon in metal or nonstable carbide because of temperature gradient or chemical potential gradient of carbon in diamond and graphite ($M_c^d - M_c^{gr} < 0$). However calculations, taking into account constitutional diagrams of Me - C for studied system and experimental conditions, show that phase transformation rate of diamond into graphite according to this mechanism as well as according to the mechanism based on Kirkendall effect may be one order less than those observed in the experiment.

Local graphitization of diamond powders takes place at pressures corresponding to the range of diamond stability at temperatures from 800 to 2000 °C; this graphitization is determined with the presence of zones of metastable state in diamond grains subjected to pressure. Graphitization rate increases in the presence of transition metals. In this case IV-VI group metals are also catalysts for graphitization. Kinetics of carbide production has been investigated in the system of carbide layer growth on diamond surface under conditions of diamond stability and metastability at high pressures.

Thus, it is found experimentally that transformation of di-

amond into graphite is not observed when diamond interacts with transition metals in its stable region. Interaction of diamond with transition metals of IV-VI groups of the periodic system runs through the stage of catalytic phase transformation of diamond into graphite at high pressures and temperatures, corresponding to metastable diamond region.

References

1. Nozhkina A.V., Kostikov V.I. Wetting of diamonds with transition metal alloys. - Theses of the All-Union Conference "News in theory and practice of production and application of synthetic superhard materials in the national economy". Kiev, ICM, 1977.
2. Kostikov V.I., Maurakh M.A., Nozhkina A.V. Wetting of diamond and graphite with ferrum titanium alloys. - "Powder Metallurgy". Kiev, Naukova Dumka, 1970, N1.
3. Kostikov V.I., Maurakh M.A., Nozhkina A.V. Wetting of graphite and diamond with ferrum vanadium alloys. - Proceedings of IV Conference on surface effects, Kiev, Naukova Dumka, 1970.
4. Kostikov V.I., Nozhkina A.V., Shesterin V.A. Interaction of diamond with highmelting metals. - Collected articles "Diamonds", M., NIIGraphite, 1971, N3.
5. Kostikov V.I., et al. Wetting of diamond with alloys. - Adhesion of melts. Kiev, Naukova Dumka, 1974.
6. Nozhkina A.V., Otopkov P.P. Wetting of diamond with manganese, germanium, stannum and plumbum. - Collected articles "Diamonds", M., NIIGraphite, 1971, N5.
7. Elutin V.P., Kostikov V.I., Maurakh M.A. Evaluation of velocity of titan spreading over graphite surface. - In collected articles "Surface effects in melts and solid phases resulted from them". Nalchik, Kabardino-Balkarsk Publishing House, 1965.
8. Zadumkin C.N. Modern theory of pure metal surface energy. - In book: Surface effects in melts and solid phases resulted from them. Nalchik, Kabardino-Balkarsk Publishing House, 1965.
9. Haltgen R. et al. Selected Values of Thermodynamic Properties of Metals and Alloys. London, 1976.

QUANTITATIVE ASPECTS OF HIGH PRESSURE EFFECTS ON THE RATE AND EQUILIBRIUM OF CHEMICAL REACTIONS

B.S. El'yanov, E.M. Gonikberg

N.D.Zelinsky Institute of Organic Chemistry, Academy of Sciences of the USSR, Moscow, USSR

The equations of linear free energy relationship (LFER) type have previously been proposed for the description of the influence of pressure on the rate and equilibrium constants of liquid-phase reactions:

$$\lg(k_p/k_0) = -\frac{\Delta V_0^{\neq}}{T}\varphi, \qquad (1)$$

where $\Delta V_0^{\neq}$ is the activation or reaction volume at atmospheric pressure and φ is a function of pressure, common to related reactions /1/. Analytical expressions have been proposed for φ as a function of pressure:

$$\varphi = p/(1+bp)R\ln 10 \qquad (2)$$

for ionization reactions, where $b = 9.20\cdot10^{-4}$ MPa $^{-1}$ in aqueous solutions. For the non-ionic organic reactions

$$\varphi = [(1+\alpha)p - (\alpha/\beta)(1+\beta p)\ln(1+\beta p)]/R\ln 10, \qquad (3)$$

where α is taken to be 0.170. The aim of the present study is to verify the general nature of Eqs.(1-3) on the basis of numerous experimental data, to refine the value of b , and to determine β for the reactions of different types.

For reactions of each type the values of b or β determined by the joint statistical treatment of a large number of observed dependencies of the equilibrium or reaction rate constants on pressure /1/. Next, the equation (2) or (3) with the parameter determined together with the Eq.(1) were examined using different tests of fit and accuracy indices [1,2].

The following tests were used:

I. Special tests (for each reaction):

1) the test of linearity for the dependence "lg k - φ";

2) the test of systematic error absence (Abbe test).

II. General tests:

1) the test of error randomness;

2) the Abbe test.

The reactions which did not satisfy the special tests were successively excluded from the consideration, and the parameter was recalculated. Next, the parameter values finally determined were examined by the general tests. The data given in Table show that the special test for the majority of the reactions were satisfied with a fair accuracy. The general tests for the reactions of all types, and also for the ionization reactions with b=9.20x x 10^{-4} MPa^{-1}, were also satisfied. Graphical checking showed good linearity for the reactions of all types in the coordinates lg k versus Φ.

An empirical equation describing the influence of pressure on the diffusion-controlled viscous flow was proposed:

$$\ln \eta_P V_P = \ln \eta_0 V_0 + \frac{\Delta V_D^{\neq}}{RT}\left[(1-\alpha')P + \frac{\alpha' P}{1+\beta' P}\right], \qquad (4)$$

where η is the viscosity, V is the molar volume, $\Delta V_D^{\neq}$ is the activation volume of viscous flow /3/. However, it was found that this process cannot be described by a common equation of the LFER type; in 24 from 58 cases the test of linearity for the dependence "lg k-Φ" was not satisfied.

Based on the values of δ and β, the values $\beta = [-(\partial \Delta V^{\neq}/\partial P)/\Delta V^{\neq}]_{P=0}$ can be calculated; there are equal to 2b for (2) and $\alpha\beta$ for (3). It is clear from the Table that these values can differ significantly. In our opinion this variation is connected with the different contribution of the free volume into $\Delta V_0^{\neq}$: the higher the fraction of free volume the greater the compressibility of $\Delta V_0^{\neq}$ and β value. The change in the free volume depends on the change of the mobility of molecules or their fragments during the transition state formation /4/. The contribution of the free volume into $\Delta V_0^{\neq}$ is minimal for the reaction of homolytic bond scission; it is larger in the case of the formation of new bonds, and is particularly large for the diffusion processes /3/. In the reactions of /3,3/-sigmatropic shift the changes in the proper volume for the bonds being formed and broken are of opposite sign and, hence, they partially compensate each other. There is no compensation for the increments of the free volume, and that is why the β value for these reactions is 1.5 times as great as that for Diels-Alder reactions. For Menshutkin reactions the contribution of free volume

Verification of applicability of Eqs. (1)-(3) and calculation of parameters β and B.

Reaction type	Number of reactions	Upper pressure limit, MPa	$\beta \cdot 10^2$, MPa^{-1}	$B \cdot 10^3$, MPa^{-1}	Fulfillment of special tests; Accuracy									
					Test of linearity			Abbe test			exc.	good	satis.	low
					+	-	+-	+	-	+-				
Ionization in water*	109	800	0.00925	1.85	94	6	9	93	1	-	98	7	4	-
Homolytic bond scission	11	600	0.36	0.61	11	-	-	11	-	-	7	4	-	-
Radical abstraction of H atom	29	800	4.15	7.06	29	-	-	29	-	-	14	7	6	2
Diels-Alder reactions	56	600	4.94	8.40	50	3	3	48	2	2	13	22	12	9
/3,3/-sigmatropic shift	13	1000	7.12	12.1	13	-	-	13	-	-	-	9	4	4
Menshutkin reactions														
a) in nitrobenzene	9	260	8.24	13.9	9	-	-	9	-	-	7	2	-	-
b) in acetone	21	800	19.4	33.0	21	-	-	21	-	-	6	5	4	6

* β value for Eq.(2)

** + Test is satisfied; - test is not satisfied; +- doubtful case.

into $\Delta V_0^{\neq}$ increases due to the "freezing" of the solvent molecules in the solvating sphere of the polar TS, and this leads to an increase of β values. As could be anticipated, the β value is larger for the reactions in acetone than in nitrobenzene.

The equation (1) has been used for precise calculations of $\Delta V_0^{\neq}$ and $\Delta\Delta V_0^{\neq}$, which allowed to reveal a number of delicate peculiarities of the TS structure and the mechanism of the processes.

References

1. El'yanov B.S., Vasylvitskaya E.M., Some Recent Approaches to the Quantitative Description of the Effect of High Pressure on the Thermodynamic and Kinetic Parameters of Chemical reactions, Rev.Phys.Chem.Japan, 1980, v.50, p.169-184.
2. El'yanov B.S., Vasylvitskaya E.M., On the Functional Dependence of Rate and Equilibrium Constants on Pressure, Zhurn. fiz.khimii, 1985, v.59, No.1, p.264-265.
3. El'yanov B.S., Vasylvitskaya E.M., Zhulin V.M., Botnikov M.Ya., Pressure Effect on the Rate Constants of Elementary Steps of Homolytic Decomposition Reactions of Organic Compounds, Izv. AN SSSR, Ser.khim., 1985, No.9, p.1973-1978.
4. El'yanov B.S., Klabunovsky E.I., Gonikberg M.G., Parfenova G.M. Godunova L.F., The Effect of Pressure on the Asymmetric Synthesis, Izv. AN SSSR, Ser.khim., 1971, No.8, p.1658-1663.

SOLID-STATE KINETICS OF ESTERIFICATION AND AMIDIZATION UNDER SHEAR DEFORMATION AND HIGH PRESSURES UP TO 8 GPa

V.M.Zhulin, N.P.Chistotina, I.I.Yakovleva, A.A.Zharov
N.D.Zelinsky Institute of Organic Chemistry, Academy of Sciences of the USSR, Moscow, USSR

The kinetics of the solid carboxylic acids esterification with solid alcohols and of their ammonium salts amidization under shear deformation and high pressure (SD+HP) was studied. The experiments were carried out on an apparatus of Bridgman anvils type* at 293 K, 2-8 GPa with anvils rotation angles up to 720°. Examples of the systems studied are given in Tables I-3.

Table I. Conditions of experiments under SD+HP and yields of esters in the reaction of solid acids with solid alcohols

Acid	Alcohol	Reagent ratio (w/w)	P (GPa)	θ (degree)	Yield of ester (% theor. value)
Mandelic	Borneol	3:1	4	180	6.0
Mandelic	Borneol	3:1	4	520	15.6
Mandelic	Borneol	6:1	3	360	5.3
Mandelic	Borneol	6:1	7	360	20.7
Mandelic	Menthol	3:1	4	520	6.4
Mandelic	Menthol	12:1	4	520	10.4
Mandelic	Adamantyl-carbinol	3:1	4	520	10.0
Benzoic	Borneol	1:1	4	520	2.3
Benzoic	Menthol	3:1	4	520	1.2
Benzoic	Adamantyl-carbinol	3:1	4	520	ester not detected
Picolinic	Borneol	3:1	4	360	1.2
Nicotinic	Borneol	3:1	4	360	2.4
Isonicotinic	Borneol	3:1	4	360	4.8
Adamantan-carboxylic	Adamantan-carbinol	3:1	4	520	8.6

It can be seen that the yield of the reaction products (esters and amides) increases with the growth of pressure and shear deformation. The reactivity of the reagents varies within wide depending on a particular acid-alcohol pair (Table I). Thus, benzoic and mandelic acids readily interact with borneol and menthol,

* Zharov A.A., Chistotina N.P. "An Apparatus for the Measurement of Shearing Stresses under High Pressure", PTE,1974,No.2, p.229-231

whereas only mandelic acid interacts with adamantylcarbinol. The isomeric pyridinic acids (picolinic, nicotinic, isonicotinic) interact under SD+HP conditions in different ways: isonicotinic acid is four times as active as picolinic one, and their reactivity does not correlate with their ionization constants.

Table 2. Yields of mono- and diamides of dihydric acids

Ammonium salt of acid	Yield (%), at 8 GPa, θ = 140°, 293 K	
	Monoamide	Diamide
Malonic	0.7	0.1
Succinic	2.4	0.2
Glutaric	9.0	1.0
Adipic	16.0	2.0
Pimelic	18.0	1.5
Suberic	20.0	2.6
Azelaic	21.0	2.0
Sebacic	24.0	3.0

Table 3. Yields of mono- and diesters on deformation of mixtures of dihydric acids and borneol

Acid	θ (degree)	Monoester yield (% theor.value, M_1)	Diester yield (% theor.value, M_2)	$\frac{M_2}{M_1}$	$\frac{K_2}{K_1}$
Succinic	360	0.93	0.30		
Glutaric	360	1.2	0.30		
Adipic	90	0.60	0.09	0.15	90
Adipic	180	1.2	0.25	0.21	50
Adipic	360	2.7	0.60	0.23	30
Adipic	720	6.2	1.5	0.24	20
Suberic	360	4.5	0.70		
Azelaic	360	7.6	1.0		
Sebacic	360	3.8	0.40		

The rate constants of the reactions under SD+HP conditions can change very essentially depending on the composition of the reaction mixture . This behaviour of rate constants can be related to some physical properties of the reaction mixture (plasticity, shearing stress). Thus, an increase in the plasticity of the medium and its shearing stress, resulting from the increase in the mandelic acid content in the mixture with borneol, leads to a growth of the esterification constant (Fig.1).

The rate constants for the reaction between mandelic acid and borneol under SD+HP conditions and in liquid phase were estimated. The rate constants in the first case were found to be more than 10^4 times as great as those for the liquid-phase processes.

Series of experiments with mixtures of dihydric acids and alcohols and with ammonium salts of organic acids revealed a peculiar feature, i.e. a comparatively high content of diesters and diamides at low conversion values (Tables 2 and 3). The solution of the system of differential equations, which describe the esterification of dihydric acids

$$\frac{dM_1}{dx} = 2K_1AB - K_2M_1B, \qquad \frac{dM_2}{dx} = K_2M_1B,$$

(where A, B, M_1, M_2 are the concentration of the acid, alcohol, monoester, and diester, respectively; x is a shearing stress), allowed to calculate the rate constants K_1(monoester formation) and K_2 (diester formation) for the model reaction between adipinic acid and borneol. It was found that K_2 is considerably greater than K_1, and the K_2/K_1 ratio decreases with increasing conversion. For the elucidation of these results it was suggested that the deformation of the sample was nonuniform, but rather occured within certain zones. In this case within the sliding zones the shearing stress value is greater than the mean value for the sample, and a greater value of deformation ensures higher conversions.

The calculations based on the assumption of nonuniform shear deformation, supplemented with a natural conjecture, $K_1 \simeq K_2$, showed that to reproduce the observed ratio of mono- and disubstituted products one should adopt that the yield of the monoester in the deformation zone is 50-60 % of the theoretical value.

Similar calculations were carried out for the amidization reactions to arrive at the same conclusion on the nonuniform deformation of the ammonium salts under SD+HP conditions.

Thus, it was shown that for the reactions of esterification and amidization under SD+HP conditions the reaction mixtures are subjected to the nonuniform deformation. The kinetic data obtained in the experiments show that the deformation of a substance within certain zones of the sample may be 10-100 times as great as the mean value for the sample.

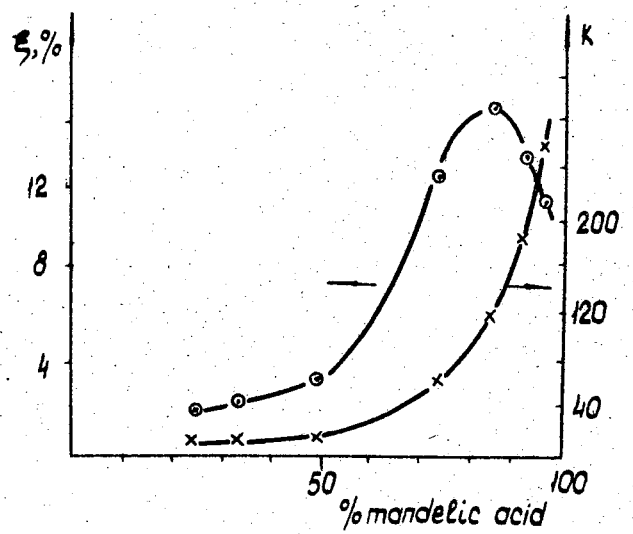

Dependence of the ester yield ξ and the esterification rate K on the composition of the mandelic acid/borneol mixture (4 GPa, 293 K, anvils rotation angle 360°).

GROWTH OF GaN SINGLE CRYSTALS FROM THE SOLUTION UNDER HIGH NITROGEN PRESSURE

I.Grzegory, J.Jun and St.Krukowski
High Pressure Research Center "Unipress" Polish Academy of Sciences, 01-142 Warsaw, Sokolowska 29/37, Poland.

Abstract

The high pressure - high temperature solution growth has been used to obtain GaN single crystals. High temperatures increase the solubility of nitrogen in liquid gallium ,high pressure is necessary to prevent thermal decomposition of GaN.In order to increase crystal growth rate temperatures up to 1700°C and pressures up to 18 kbar were used.

After each process a thin polycrystalline GaN layer was found on the gallium surface. Relatively large (several mm) GaN single crystals were grown on the internal side of the film. The plate-like or column-like crystals were grown in dependence on the temperature and pressure used. Crystal shape seems to be controlled by crystal growth kinetics. Microscopic observations of crystal surface structure suggest that several mechanisms of growth operate.

1.INTRODUCTION.

Gallium nitride is a wide direct band gap (3.5eV) semiconductor which has not yet been prepared in the form of large single crystals. There are serious technological difficulties in growing high quality large single crystals;

which could be used for measurements and applications. These difficulties are directly related to thermodynamical properties of GaN-Ga-N2 system. Gallium nitride has an extremely low solubility in the liquid gallium at temperatures normally used for crystal growth of GaN from the liquid phase [1,2]. Some attempts to grow GaN crystals from the solution by the use of ammonia as an active nitrogen source were reported by Elwell et al [3]. This method was most successful between 650-1000°C .

The solubility of GaN in gallium can be increased by rising temperature of the process. However, at higher temperatures GaN easily decomposes and in order to prevent this, high pressure has to be applied. High pressure solution growth of GaN was carried out by Madar et al [2]. They have succeded in preparing crystals with dimensions below 1 mm using nitrogen pressure 10 kbar and temperature 1200 °C. The growth rate at such conditions was several hundreds microns per day.

The description of crystal growth process at higher nitrogen pressure (12-18kbar) by temperature gradient solution method was the purpose of this study.

II.THERMODYNAMICS.

The synthesis of GaN from its constituent elements can be described by the reaction:

$$2Ga + N_2 = 2GaN \qquad (1)$$

Equilibrium conditions for coexistence of the three phases at high pressure (up to 60 kbar) and temperature (up to 2000 °C) were measured. The molar Gibbs free energies of all the components were analysed to estimate the influence of high

pressure on the change of standard Gibbs free energy of reaction (1) [4]. It was concluded that this influence is determined mainly by the pressure activity of compressed nitrogen and that one can neglect the corrections due to mechanical stress in liquid and solid phases. It was also shown that the solubility of nitrogen in gallium does not significantly change the chemical potential of the liquid gallium.

The p-T conditions for chemical equilibrium of the reaction (1) were determined experimentally [5] and the values of nitrogen activity corresponding to equilibrium temperature and pressure were calculated. Since compressed nitrogen deviates strongly from the ideal gas, its pressure activity reaches the values much higher than the applied pressure. For example at 1500 °C it suffices to apply 15 kbar to reach this activity value which for the ideal gas would require 200 kbar.

III.EXPERIMENTAL.

1. Fundamentals.

Karpinski et al. [5] estimated that nitrogen solubility is low and does not exceed 10^{-3} mole fraction at 1500 °C at 15 kbar. This leads to a very small crystal growth rate from the liquid gallium solution. On the other hand one of the well known features of the Ga-N_2-GaN system that liquid gallium reacts rapidly with nitrogen at high temperatures creating GaN polycrystalline crust on the gallium surface. This crust separates liquid gallium from gaseous and the rate of GaN synthesis rapidly falls.Then the growth of GaN crystals from the solution on the internal surface of the crust begins.

In order to increase the growth rate of GaN Logan et al.[1] proposed the use of the temperature gradient solution method with NH_3 as a nitrogen source. They concluded that the temperature gradient across the melt was synergetic with the the formation of large area of GaN epitaxial layers. However Elwell et al. observed that the temperature gradient transport has not a significant effect on crystal growth of GaN from the solution in the temperature range 900-1000 °C. We have concluded that the temperature gradient combined with the diffusion of the solute led to stationary conditions for crystal growth (see section 0).

One can also increase the crystallization rate by the use of higher temperatures. However this requires high nitrogen pressure to enforce the condition of GaN stability.

Our technical apparatus permits us to apply nitrogen under pressure up to 20 kbar and temperatures up to 1700 °C.

2. Experimental arrangement.

The horizontally arranged crucible, divided into three isolated compartments, was used to investigate the temperature influence on the growth process. The crucible, with the three gallium samples inside, was placed into the high temperature furnace. The experiments were carried out in the high pressure vessel. The nitrogen gas pressure apparatus was similar to that described in [5]. The thermocouples were used to measure the temperatures in the important zones of the system. Fig.1 shows the experimental arrangement used in this work. The temperature gradient along the crucible was about 50 °C/cm and the maximum temperature in the system did not exceed the equilibrium one for the reaction(1).

3.RESULTS.

The GaN crust was always observed on the gallium surface in our experiments.The crust preserved its shape after gallium etching.The general view of such crust is shown in Fig.3* and 4*. We observed that the crystals of various habits were grown on the internal surface of the crust. The crystal habits differs with temperature and pressure of the process. In Fig.2 we show the diagram indicating the crystal shape dependence on the temperatures and pressures used in our experiments.

Relatively large (1-2mm) column-like crystals were found for the pressure as high as 17 kbar and temperature 1360 °C. As mentioned above, the crystals grew on the crust in the cooler zone of each compartment. This type of crystals had well pronounced {1010} faces and topped with pyramidal form created by {0001} and {1012} faces. In addition we have also observed quite different quasi-columnar crystals. They had 6-arm star-like structure. The arms were comparatively long and they had pronounced layer structure on the top of each of them. The structure was surrounded by flat thin walls creating the regular hexagon. Fig.5* shows one of such crystals. Similar columnar patterns were observed for 16 kbar and 1380 °C as well as for 12 kbar and 1200 °C.

Growth of plate-like crystals occured for the higher temperatures at the same pressure. The general view of the plates grown on the GaN crust is presented in Fig.4*.

A rare example of intermediate region where both forms were grown is shown in Fig.6*.

Figs 7* and 8* show the mode of layer growth on {0001} and {1010} faces respectively. It indicates a presence of kink sites

*The Figure is given at the end of the book.

in the growing layers. Two-dimensional nucleation on (0001) face is illustrated in Fig.9* reflecting 6-fold symmetry of the crystals.

4.DISCUSSION.

As it was shown in the previous section, we have observed GaN crystals with quite different shapes. There are, however, some regularities of those crystal growth patterns. Since in all our experiments we have observed the presence of GaN polycrystalline crust on the gallium surface, we conclude that the formation of this crust is the first stage of crystallization process. We are convinced that the first stage is completed when rather thick GaN crust is created so that it effectively prevents free access of nitrogen and blocks the surface reaction.

After the crust formation two processes can occur:

i/ GaN crust dissolves in gallium to saturate the solution,

ii/ nitrogen from the gas phase penetrates, by the diffusion, through the crust, and reconstructs dissolved crust.

to thermal gradient across the solution the situation
cooler parts of the system is quite different.
different at different temperatures we
transport from the hotter to the
processes i/ and ii/ continue
cooler zone, where the
GaN crystallization occurs.
crust serves as a source of
sults in the dense wood of well
on this surface (Fig.10*). The
rmation is governed by the mechanism

Pl
ves
descri
temperat
the experi
gradient al
temperature i
the reaction(1).

of competetive growth. Indeed, larger crystallites grow faster and inhibit the growth of neighbouring small ones. As the outcome, growth of sparsely distributed large column-like crystals, perpendicular to crust surface, is observed. It seems that the mechanism leading to this transformation is analogous to the mechanism observed in constrained dendritic growth [6,7]. In both cases we observe the transition from the growth of large number column-like structures distributed very densely to the growth of relatively small number of elongated, sparsely distributed structures. As mentioned in the previous section this pattern is observed at temperatures much lower than the temperature of equilibrium for GaN synthesis.

For the temperature closer to the equilibrium one we observe a change of the shape of the crystals. The crystals become plate-like indicating that the growth rate in [10$\bar{1}$0] direction is greater than in direction [0001]. Observation revealed that the crystals become developed in [0001] direction (i.e. column-like) when the pressure is high or the temperature is low in respect to the P-T conditions when the plate-like crystals grow. The distribution of both column and plate-like crystals on the GaN crust indicates that the fast growth occurs in the direction perpendicular to the crust surface. This confirms the indication that the growth is mainly due to thermal gradient across the solution.

In most cases the crystals grew by the edge nucleated layer mechanism. The structure of the layers on the crystal faces (Fig.11*) suggests that there is a inflow of the solute from the hotter part of the solution. Also our observations revealed the presence of two-dimensional nucleation mechanism in the case of growth at lower temperature (Fig.9*).

The edge nucleation may lead, in the extreme, to the unstable growth that is frequently observed on the (10$\bar{1}$0) face. In the lower temperature region (column-like crystals) we observed special kind of unstable forms (Fig.5*). It seems that these star-like forms are created by the combination of edge nucleation and depletion zone formation. These observations suggest that in both cases the surfaces of polyhedral GaN crystals become morphologically unstable by preferred growth of edges of crystals. The possible connection between thermal conditions, crystal dimensions and the instabilities is still an open question.

6.CONCLUSIONS.

High pressure-high temperature th of GaN from the solution temperature consists of two stages: surface synthesis reaction leading to the creation of polycrystalline GaN crust and crystal growth from the solution precipitated on the internal surface of the crust. In the second stage the transition from the growth of the dense wood of small crystallites to the growth of sparsely distributed relatively large crystals occurs. In this way the crystals of mm size can be grown during several hour sition.s expoihe material for crystallization is provided by th olutiona dissin the hotter part of the compartment.

The habit of the crystals change from the columnar to the plate-like with the change of temperature and pressure.

The dominant growth mechanism is the edge nucleated layer growth but sometimes two-dimensional nucleation on (0001) crystal face is also observed.

Edge nucleation correlated with depleted zone formation leads to the growth of morphologically unstable forms.

7.Acknowledgement.

We are indebted to Prof. I.A.Iurski from the Institute for Theoretical Physics PAS for many stimulating discussions during performing this paper.

This work was supported by grant No. CPBP.01.04.

References

1. R.A.Logan & C.D.Thurmond, "Heteroepitaxial Thermal Gradient Solution Growth of GaN", J.Electrochem.Soc.(1972),119,1727-1735.
2. K.Madar, G.Jacob, J.Hallais and R.Fruchart, "High Pressure Solution Growth of GaN", J.Crystal Growth (1975),31,197-203.
3. D.Elwell, R.S.Feigelson, M.M.Simkins and W.A.Tiller, "Crystal Growth of GaN by the Reaction between Gallium and Ammonia", J.Crystal Growth (1977),66,45-54.
4. J.Karpinski and S.Porowski, "High Pressure Thermodynamics of GaN", J.Crystal Growth (1984),66,11-20.
5. J.Karpinski, J.Jun and S.Porowski, "Equilibrium Pressure of N_2 over GaN and High Pressure Solution Growth of GaN", J.Crystal Growth (1984),66,1-10.
6. D.I.Meiron, "Selection of Steady States in the Two-dimensional Symmetric Model of Dendritic Growth", Phys. Rev.(1986),A33,4,2704-2715.
7. R.Trivedi and K.Somboonsuk, "Constrained Dendritic Growth and Spacing", Mater.Sci.Eng. (1984),65,1,65-74.

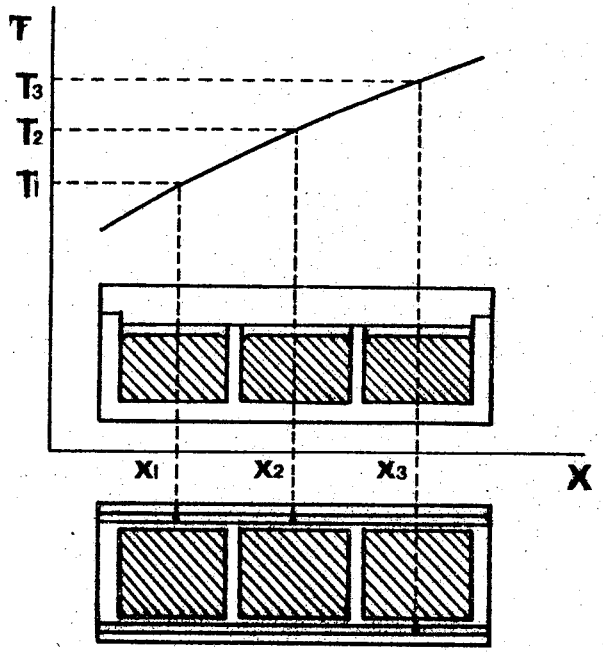

Fig. 1. The crucible arrangement and the temperature distribution in the GaN crustal growth experiments.

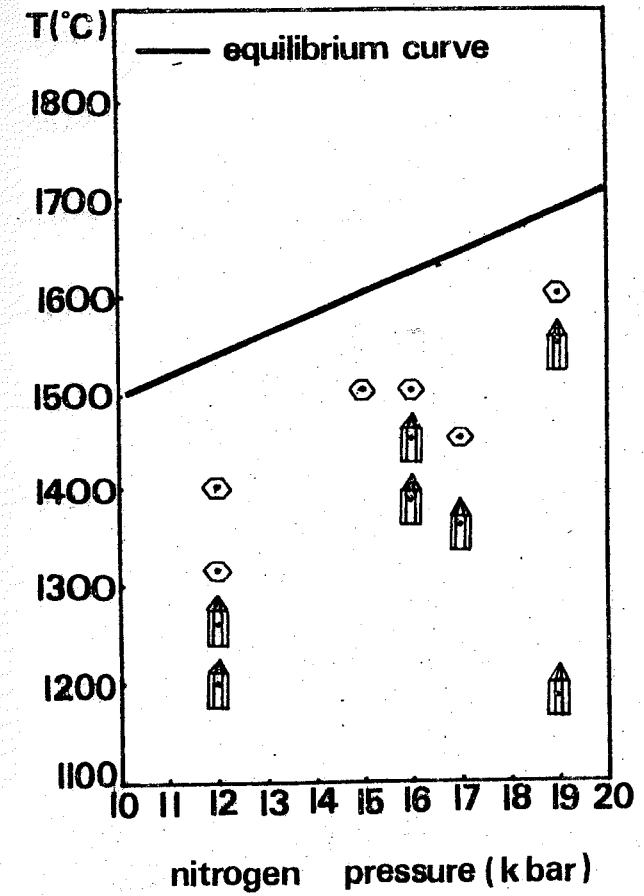

Fig. 2. The diagram illustrating change of the shape of crystals grown in various temperature and pressure.

MONO- AND POLYCRYSTALLINE DIAMONDS PRODUCED FROM HYDROCARBONS

O.A.Voronov, A.V.Rahmanina
Institute of High Pressure Physics, Troitsk, USSR

As shown in the paper [1], the fine crystalline diamond powders can be obtained by recrystallization of graphite at high pressures and temperatures in presence of metal catalyst. The polycrystalline diamonds can be produced in the same manner also [2,3].

Produced by this method synthetic diamonds have one common defect in comparison with natural diamonds. This defect is the presence of metal inclusions entered during the process of recrystallization. These inclusions result in destruction of synthetic diamonds during their heating to temperatures about 900-1000 °C without access of oxygen. The low thermal strength reduces competitive abilities of synthetic diamonds in comparison with natural ones.

We realized the method of decomposition of hydrocarbons at high pressures and temperatures [4] which allows to produce carbon in the forms of coke, graphite of diamond:

$$CH_{2x} \rightarrow C + xH_2$$

The carbon forms depend on condition of decomposition of the molecules. This decomposition does not require metal catalyst, therefore resulting diamond does not contain metal inclusions.

We have prepared the diamond powder consisting from crystals 1-200 μm in size (Fig.1*) using decomposition of hydrocarbons to carbon and hydrogen at pressures and temperatures corresponding to thermodynamically stable region for diamond.

The diamond crystals obtained from hydrocarbons tend to grow into octahedral shapes with good mirror smooth faces. Practically all crystals are colourless, optically transparent, natural-looking. There is certain amount of isometrical crystals, but many crystals are flat triangular and sixangular plates. There are double crystals, sometimes star double crystals and many crystal aggregates among them. The skeleton crystal forms are absent. The sample represent excellent diamond according to the X-ray diffraction pattern. The electrical resistivity of colourless crystals is more than 10^{11} Ohm·cm.

Using this method we also obtained the polycrystalline diamond aggregates. These aggregates are cylinders up to 12 mm in diamater [5]. The photograph of one type of the aggregates is shown in Fig.2*. These aggregates are white cylinders with black layer on the side surface, which has thickness up to 50 μm. The size of the aggregate crystallites varies from 1 to 100 μm. These crystallites have octahedral configuration. Produced aggregates contain less than 0.2 wt.% of incombustible impurities (ashes). These consist mainly of amorphous and crystalline silicone dioxide. The colour of ashes is white, with local spots of yellow. Pycnometer density of aggregates is 3.49 g/cm^3.

In appearance these aggregates most of all resemble to well known Brazilian natural polycrystalline aggregates.

* The Figure is given at the end of the book.

References

1. Bundy F.P., Hall H.T., Strong H.M., Wentorf R.H. Artificial diamonds. Usp.Phys.Nauk, 1955, 57, No.4, 691-699.
2. Vereshchagin L.F., Kalashnikov J.A., Feklichev E.M., Sukhushina I.S. Artificial production of ballas type diamond. Dokl. Akad.Nauk SSSR, 1967, 172, No.1, 76-77.
3. Vereshchagin L.F., Yakovlev E.N., Varfolomeeva T.D., Slesarev V.N., Shterenberg L.E. The synthesis of "carbonado" diamonds. Dokl.Akad.Nauk SSSR, 1969, 185, No.3, 355-356.
4. Yakovlev E.N., Voronov O.A., Rakhmanina A.V. The synthesis of diamond from hydrocarbons. Sverkhtvjordye materialy, 1984, No.4, 8-11.
5. Yakovlev E.N., Voronov O.A., Rakhmanina A.V. Polycrystalline diamond aggregates produced by means of hydrocarbons. Sverkhtvjordye materialy, 1987, No.2, 3-5.

SEEDED GROWTH OF DIAMOND CRYSTALS WITH δP METHOD

Yang Zongqing[1], M.Wakatsuki[2]

[1]Research Institute for Abrasives & Grinding, Ministry of Machine Building Industry, Zhenzhou, China

[2]Institute of Materials Science, the University of Tsukuba, Ibaraki, Japan

Introduction

It may be the best interest for a diamond-synthesis researcher to grow larger and more perfect diamond single crystals which are by no means inferior to the treasure of natural diamonds. Fifteen years after the first synthetic diamond was born in G.E.Company, U.S., the same company claimed they had got synthetic gem-sized diamond single crystal about 5 mm in size and about 1 carat in weight [1]. After that, Japanese researchers in NIRIM [2] and in Sumitomo Elec.Co.[3], and Chinese researchers in Shanghai Institute of Ceramics, Academia Sinica [4], also succeeded in making large diamond crystals by using ΔT method which is same as that in G.E. Co.

Creating a new method of δP, Wakatsuki [5] opened another road to growing large diamond crystals. He discovered that it usually occurs that a lot of tiny recrystallized graphite flakes cover around a well-grown diamond [6]. It seems as if they were competing with diamond on the interface between graphite and flux. He put forward his assumption that the recrystallized graphite could supress the nucleation of diamonds. According to this assumption, following equation is expressed:

$$\frac{dN}{dt} = K_d S = K_d \cdot S_0 \left\{1 - \alpha_g(t) - \alpha_d(t)\right\}, \qquad (1)$$

where N: nucleation number,

t: time,

S: the net area of graphite-flux interface, that is, the area which has not yet been covered either with diamond nuclei or recrystallized graphite flakes,

S_0: initial surface area of graphite disc,

$\alpha_g(t)$ and $\alpha_d(t)$: ratios of surface area of graphite disc already covered with recrystallized graphite and with diamond, respectively, to the initial area S_0, and

K_d: a kinetic coefficient, given by

$$K_d = \frac{3kT Z_d^* n}{\sigma_d} \left(\frac{\Pi^2}{\delta P}\right)^2 \exp\left\{-\left(\frac{\Pi}{\delta P}\right)^2\right\}, \qquad (2)$$

where $\Pi^2 = \frac{16\pi\sigma_d^3}{3kT\left(-\frac{\Delta U}{\delta_d}\right)^2}$,

k: Boltzmann's constant,

Z_d^*: number of solute atoms striking unit area of embryos surface in unit time,

n: number of solute atoms in unit volume of solution,

σ_d: interface energy between diamond and solution.

At least, at the initial stage of diamond nucleation, $\alpha_g(t) \gg \alpha_d(t)$, therefore

$$\frac{dN}{dT} = K_d \cdot S_0 \left\{1 - \alpha_g(t)\right\}. \qquad (3)$$

We can see from Eq.3 that the nucleation rate relates to the covering ratio of recrystallized graphite. Thus opened a new thinking road, that is, to control the diamond nucleation by controlling the formation of recrystallized graphite.

Experiments and Results

Based on the idea mentioned above, we can design the experiments as follows. In order to make it clear, it is necessary to refer to Fig.1. In Fig.1, P_e is the equilibrium pressure between diamond and graphite in presence of solvent, P_0 is the minimum pressure for fresh graphite to nucleate diamond spontaneously, and P^* is the minimum pressure for recrystallized graphite to nucleate diamond spontaneously. First we raise the pressure to P_1 which is somewhat lower than P_0, then raise the temperature up to the ultimate temperature T. Keep this T, P condition for a few minutes to let the graphite be recrystallized. After that, raise the pressure up to ultimate value $P_2 (P_e < P_2 < P^*)$. In the range between P_e and P^*, the diamond is thermodynamically stable, therefore the seed crystal could exist safely and would not re-transform to graphite, furthermore it could grow in condition that there exists plenty of graphite source. The driving force for diamond growth is the solubility difference between graphite and diamond in solution. For a particular solvent and at a par-

ticular temperature, it depends on the excess pressure δP only. Therefore as long as the pressure is higher than the equilibrium pressure at the related temperature, diamond crystals could grow even if the temperature within the reaction cell is uniform. On the other hand, because of the recrystallized graphite covering on the graphite-flux interface the spontaneous nucleation of diamond has no position to occur.

The press machine used is 3000 tons one with mono-pressure source, equiped with four-slides type apparatus. This type of high pressure apparatus is of good synchronism of less than 0.05 mm. Fig.2* shows the full view of the press and apparatus. The curve of pressure calibration at room temperature is shown as Fig.3. The control system for pressure and heating wattage was made in ASEA Co., Sweden, which precision is less than 0.5% both in pressure and in wattage. This system has two modes: automatic and manual. The automatic system is controlled by a micro process unit into which we can set the P, W program in advance.

It is very important to determine P_o, P^* and T. In our case, they are 4.9 GPa, 5.33 GPa and 1220 ^oC respectively.

The start material of carbon is spectrum-grade graphite made in Shanghai Carbon Factory, and the flux used is Ni-based alloy. The seed crystals were chosen from synthetic diamonds, they are well-shaped and almost no inclusions. The assembly of seeded growth with δP method is shown in Fig.4. The experiments were very successful, we got well-grown diamond crystals (as shown in Fig.5*) among which the largest is about 2.5 mm, the smallest is 1.5 mm.

Discussion

Based on the solution mechanism me would like to treat the diamond growth in dilute environmental phase.

After having worked out the thickness of the boundary layer for diamond growth is much larger than the coefficient concerning the dynamics of solvent molecules exchange between bulk phase and crystal surface, that is, $\delta \gg \Lambda$, Liu pointed out that the growth rate of diamond is controlled by bulk diffusion [4]. As we know, the crystal growth rate controlled by bulk diffusion is linearly related to the supersaturation.

Since the supersaturation for diamond growth

*The Figure is given at the end of the book.

$$\frac{\partial x}{x_d} = \left(\frac{\Delta V}{RT}\right) \delta P \qquad (4)$$

where ∂x: excess solubility,

x_d: diamond solubility in flux,

ΔV: molar volume decrease from graphite to diamond,

R: gas constant,

T: synthesis temperature,

δP: excess pressure, i.e., $P-P_e$.

From Eq.4, we know the supersaturation has a linear relation to δP, therefore, the growth rate depends linearly on δP logically. This was confirmed by our experiments which were performed at same temperature and within same synthesis duration, only by varied pressure. As shown in Fig.6, the slope of the growth rate line of the diamonds grown on bottom is 6.3 mm/GPa·hr which is very similar to Wakatsuki's result 6.5 mm/GPa·hr [5].

As for the smaller growth rate of top crystal, we can explain it as follows. Because of the smaller density of diamond seed than flux melt, the seed would float up during synthesis process, thus increases the distance from seed to carbon source, and the bulk diffusion of carbon becomes more difficult than that in the case of bottom crystals.

Acknowledgement

The authors are very grateful to Mr.Wu Zhaoqing, Mr.Wang Weidong and Mr.Zhang Youjung for their kindly cooperation in experiments.

References

1. New Scientist, 1970, 47(27), 407.
2. H.Kanda et al., in High-Pressure Research in Geophysics (Proc. U.S.-Japan Seminar on High Pressure Research in Geophysics, 1981, Hakone), Eds.S.Akimoto, Center for Academic Publications Japan/D.Reidel, Tokyo/Dordrecht, 525-535.
3. S.Yatsu. Heat Sinks from Synthetic Diamond Large Grains, New Diamonds, 1985, 1(1), 42-43.
4. G.Z.Liu et al., The Mechanism of Synthetic Diamond Growth from Solution,J.of the Chinese Silicate Society,1984, 12(1), 91-95.
5. M.Wakatsuki, Proc.U.S.-Japan Seminar on the Application of Ultrahigh Pressure to Geophysics & Geochemistry,1986,Hawaii, U.S.A.
6. M.Wakatsuki et al., in High-Pressure Research in Geophysics (Proc.U.S.-Japan Seminar on High Pressure Research in Geophysics, 1981,Hakone),Eds.S.Akimoto, Center for Academic Publications Japan/D.Reidel, Tokyo/Dordrecht, 13-45.

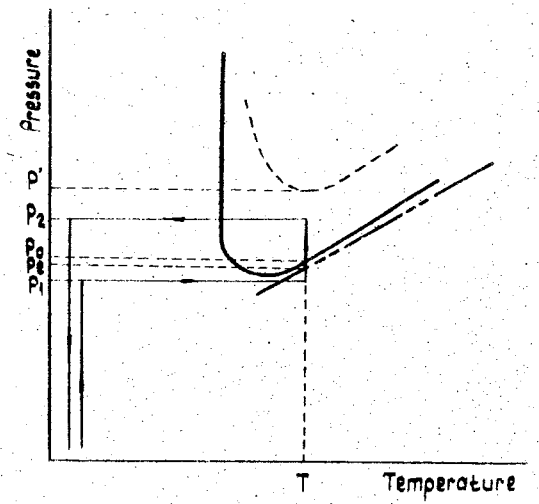

Fig.1. Pressure and temperature path in experiments.

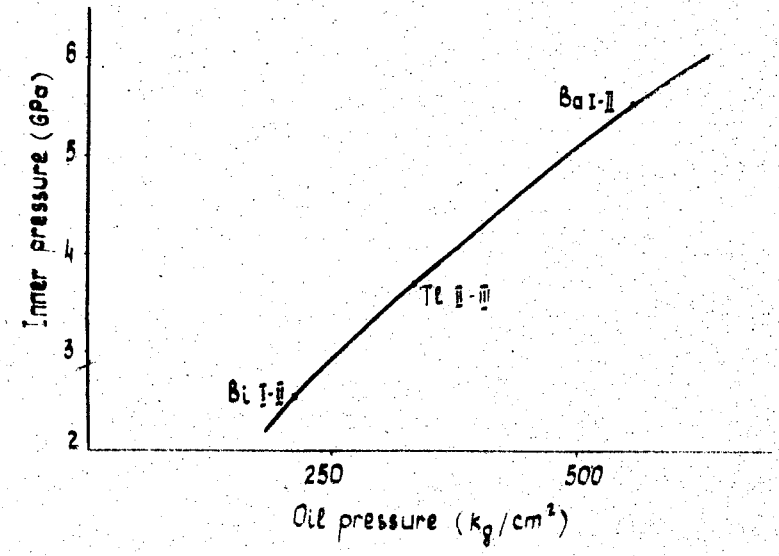

Fig.3. The pressure calibration curve.

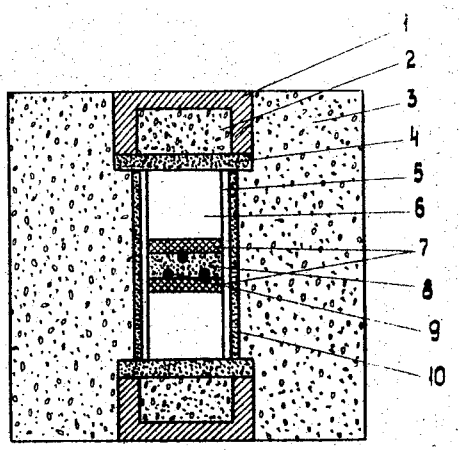

Fig.4. The sectional view of the assembly of seeded growth experiment using δP method:
1-current cap; 2-pyrophyllite disc; 3-pressure medium; 4-graphite disc; 5-pyrophyllite sleeve; 6-pyrophyllite plug; 7-flux discs; 8-carbon source; 9-seed crystals; 10-heater.

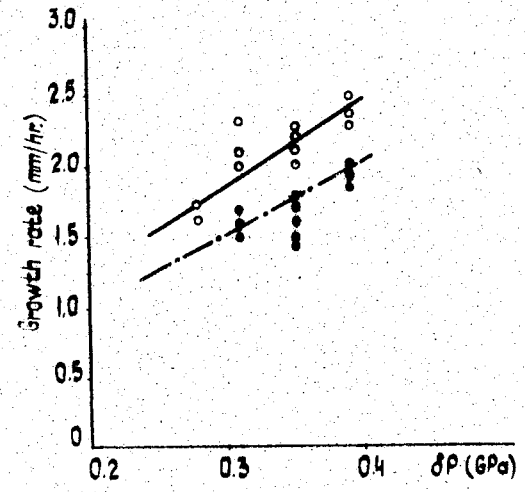

Fig.6. The relation between growth rate and excess pressure: ○ - bottom crystals; ● - top crystals.

THE PECULIARITIES OF THE DIAMOND GROWTH IN MAGNESIUM-BASE SOLUTION - MELT SYSTEMS

A.A.Shul'zhenko, N.V.Novikov, G.V.Chipenko
Institute for Superhard Materials, Academy of Sciences of the UkrSSR, Kiev, USSR

The Institute for Superhard Materials of the Ukrainian Academy of Sciences has developed a method [1] for synthetizing semiconducting diamonds in magnesium-base alloys. The mechanism of the semiconducting diamond formation in these systems was considered in [2]. In this work the properties and the growth peculiarities of the crystals were studied.

The crystals grown in the magnesium-base systems are overwhelmingly cubic, this habit persisting at all the synthesis temperatures. The major peculiarity found in the crystals lies in the presense of readily seen positive growth steps on faces of a cube, the steps forming concentric layers grown one over another and successively reduced in size. The steps are well-polygonized and their end faces are formed by a small number of rectilinear sections. An end face of a step that is more than 1 μm in height stands for a subface of octahedron. The steps extend in <110> directions, i.e. are parallel to the edges between cubic and octahedral faces. At low growth rates small sections of the steps are located in parallel to the edges of a cube and their end faces are subfaces of a cubic. On tiers formed by larger growth steps a substantial number of steps of less than 1 μm in height can be observed.

The steps formation occurs either at the center of a face or is shifted toward an edge or the vertex. At low growth rates the height of steps does not exceed 1 μm and several centers of their formation can be observed. Higher growth rates predominantly cause

the steps formation from one center and the height of the steps may reach tens of microns. When carbon black was added to the reaction mixture (20% against graphite) the diamond growth dropped substantially. In these condition numerous hillocks were formed on cubic faces and the height of the growth steps was less than 1 μm. The formation of growth layers in the middle of faces characterises the case when the source of the layers growth is represented by screw dislocations. Most probably, the growth of diamond cubic faces in the studied growth systems is governed by the dislocation mechanism of the growth layers formation.

To grow crystals in the magnesium-base system, seed crystals of natural and synthetic diamond of various habit were used what allowed to gather some in formation on the growth behaviour for faces of different types, viz. octahedral and tetragon-trioctahedral ones. At lower growth rates positive steps of about 1 μm in height are formed on octahedral faces. Unlike cubic faces the concentric arrangement is not observed in these steps. At higher growth rates the steps are formed developing from the vertices and the edges forming a depression in the center of a face. The tetragon-trioctahedral faces are rough due to the presense of steps of about 3 μm in height extending in parallel to the edges between cubic (octahedral) and tetragon-trioctahedral faces.

To define the growth rate (both the linear and the mass ones) [3], the method of thermal cycling was used, namely, the twofold short-time temperature lowering was (with time intervals of 3 minutes) resulting on the formation of three distinguished zones in a crystal. Fig.1 shows the location of a crystal in relation to the carbon source (graphite) in the solution. In the (001), (100) and $(0\bar{1}0)$ directions the linear growth rate was $2.3 \cdot 10^{-6}$ m/s, $2.1 \cdot 10^{-6}$ and $1.8 \cdot 10^{-6}$ m/s for the first, the second and the third zones

respectively. In the (00$\bar{1}$) and ($\bar{1}$00) directions these values are reduced by 1.6 to 1.8 times. The mass growth rates in the 1st, the 2nd and the 3rd zones amounted to $8 \cdot 10^{-7}$, $5 \cdot 10^{-5}$ and $1 \cdot 10^{-5}$ g/s respectively. The highest growth rate was observed in the direction of the graphite location. Notwithstanding the higher growth rate values the crysral is characterized by a small amount of inclusions. In this case the factor that limits the maximal growth rate allowing a single crystal to grow with a good quality is the twinning.

The stength and the heat-resistance are some of the basic physical and mechanical properties of diamond crystals. The heat-resistance is understood as the ability of a crystal to retain its strength while being heated up to 1200 ^{o}C which defines the diamond performance when used in a tool. For the crystals of 400/315 grown in our experiments (without sorting) the strength before and after the heat treatment was 66 and 34 N respectively. Being sorted into groups of "light" and "dark", the strength of the crystals of the first group before and after the heat treatment was 69 and 40 N and that for the "dark" group was 38 and 30 N respectively. Let us mention for the comparison that the strength of the AC65-type crystals of the same grit size synthetized in the presense of transient metals at the growth rate of 6 to 7 times lower than that for the crystals in question and produced using a special sorting method at that,is slightly higher (100N) but their thermal resistance (34N) proved to be even lower than that of crystals grown in the magnesium-base system.

It is known that the diamond crystals grown on seeds in transient metals-base systems (the so-called onion-like crystals) are of low strength. The strength of grown semiconducting crystals and that of the initial seed crystals of AC7-type were studied in this work.

To define the compression strength rate 8 well-formed seed crystals of cubic-octahedral habit and 4 grown crystals of cubic one were selected.

The strength rate was calculated as a ratio between the load causing the crystal fracture and the contact area between the crystal and the support. The average seed crystals strength (at average contact area of 0.31 mm^2) was 4500 N/mm^2 and that for the grown crystals (at average contact area of 0.68 mm^2) amounted to 5000 N/mm^2.

References

1. Патент № 2226550 ФРГ, Способ синтеза алмазов/ В.Н.Бакуль, А.А.Шульженко, А.Ф.Гетьман. - Опубл. 22.09.77.
2. А.А.Шульженко. Сверхтвердые синтетические материалы // Неорганическое материаловедение в СССР. - Киев: Наукова думка, 1983, с.445-457.
3. A.A.Šhulženko, G.V.Šipienko. Synteza i wlasnošci pólprzewodnikowych diamontow.//International conference on diamond crystallization under reduced pressure. - Warsaw, 1985: Archiwum nauki o materialach. - 1986. - t.7, z.2. - Str.207-211.

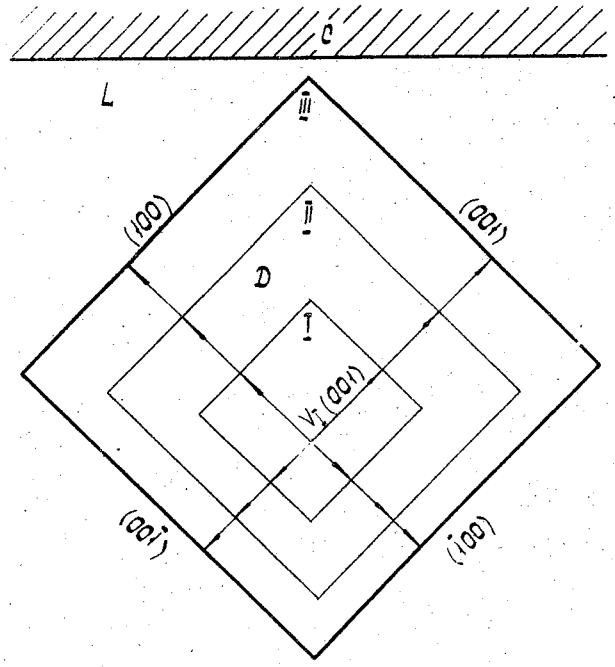

The definition of the diamond growth rates: I, II, III are numbers of zones ; C, D, L are carbon source, diamond and melt respectively ; $V_{I(00I)}$ is the growth rate for the (00I) face in the zone I.

HEAVY NITROGEN DOPING OF GaP CRYSTALS GROWN UNDER HIGH PRESSURE CONDITIONS

Bernard GIL
Groupe d'Etude des Semiconducteurs, Université des Sciences et Techniques du Languedoc, Place Eugène Bataillon, 34060-Montpellier-Cedex, France

Henri MARIETTE
Laboratoire de spectrométrie physique, Université Scientifique Médicale de Grenoble, BP.87, 38042-Saint Martin-d'Hères-France

Jan JUN and Izabella GRZEGORY
High Pressure Research Center Pol.Ac.of Sci., Sokolowska 29/37, OI I42 Warsaw, Poland

Abstract

We present a series of photoluminescence measurements performed at 2 K on GaP crystals grown from the melt under high nitrogen pressure. The luminescence spectra are characteristics of nitrogen doped GaP: both single nitrogen and nitrogen pairs bound excitons are observed. The nitrogen concentration has been obtained from absorption measurements performed at 77 K on sample slices of 207 μm thickness. It has been found to increase with the growth pressure. A value of 3.5×10^{19} cm^{-3} has been measured for a growth pressure of I9 kbar; such a concentration exceeds the limit of solubility of nitrogen in GaP when standard growing processes are used. At high nitrogen concentration, the near band edge luminescence disappears in favor of lower energy transitions NN_3 and NN_I. This is a direct proof of efficient exciton transfers via hopping processes which increase with the nitrogen concentration in the samples as predicted by statistical calculations.

I. Crystal growth and doping

GaP crystals highly doped with nitrogen were grown from the melt by the gradient-freeze method under nitrogen gas pressure up to I9 kbar. The application of N_2 pressure allow to obtain an active source of nitrogen dopant and prevents the decomposition of

GaP during the high temperature process of crystallization [1]. The nitrogen concentration ([N]) has been calibrated using the method proposed by Lightowlers et al. [2] and the correspondence between the predictions and experimental finding is given in Figure I. The N_2 pressure dependence of substitutionally incorporated nitrogen in GaP follows the solubility curve proposed by Grzegory et al.[1] and achieves the value of order $3.5 \times 10^{19} cm^{-3}$ for the highest N_2 pressure applied.

II. Optical properties

Transmission investigations have been performed at pumped liquid helium temperature in order to check the quality of our samples. Figure 2 displays some of the transmission spectra obtained in the wavelength region between 550 and 533 nm with [N] differing of one order of magnitude between the most doped sample and the less one. Clearly we observe a series of sharp transitions which energy correspond to the well known energy of lines related to NN_3, NN_4, NN_5, NN_7, NN_9 and NN_{oo} bound excitons [3,4]. The higher the nitrogen growth pressure, the stronger the absorption coefficients as expected from the calibration of optically active nitrogen incorporated during the growth process.

Please note that one can also observe the Stoke replicas of the NN_{oo} exciton involving longitudinal and transverse optic phonons, which lie at higher energy than the NN_3 bound exciton. This obviously is a criterion of high quality of our samples. From sample HPM-2 (High Pressure Melt - 2 kbar) up to HPM-I5 one observes a low energy shift of the absorption edge; it results from both influence of [N] (the NN_{oo} exciton strongly broadens to form an absorption band as soon as [N] exceeds $I.5 \times 10^{18}$ cm^3 [5] and of the influence of the intrinsic absorption larger for HPM-I5 than for HPM-2 due to sample thickness effects.

The luminescence spectra of such samples have been displayed for comparison on Figure 3. In that case we have extended the energy scale up to 590 nm in order to cover the whole scale of nitrogen related transitions. [N] is high in these samples and the pump power (5I4.5 nm line of Ar^+ laser) has been kept small enough to prevent an overlap of the nitrogen bound hole wave functions; as a consequence both transmission and luminescence spectra concern the same region of the phase diagram of the electron hole system [6] and can be fruitfully compared. The luminescence spectra present a series of sharp transitions which corresponds to the transmission features plus a lower energy shoulder. Such a shoulder can be resolved and is then found to correspond with the B state of the NN_I exciton. The fine structure of both A and B could not be always resolved in these samples, this is probably related to the high nitrogen concentration which produce some screenings.The most streaking feature on the luminescence patterns concern the exciton transfer via hopping processes from the high energy states towards the lower energy pairs when the nitrogen concentration increases. Consider for instance both the transmission and luminescence patterns NN_5 and NN_4 in sample HPM-5. The absorption coefficient is stronger for NN_5 than for NN_4; simple arguments enable us to say that the density of NN_5 traps is higher than the NN_4 one. On the other hand, the NN_4 luminescence is stronger than the one corresponding to NN_5; this is a direct proof of efficient exciton transfers in these samples as already observed in LPE and VPE growth ones [7]. One important point to outline concerns the luminescence spectrum of heavy doped samples; the band edge luminescence is totally in favor of NN_3 and NN_I as soon as the [N] reaches $3 \times 10^{19} cm^{-3}$. Such a point previously predicted by the stochastic transfer model [8] is now observed. The last point we want make concerns the change in the shape of the luminescence lines with [N]. Figure 4 displays the shape of the NN_3 related luminescence for four typical concentrations. One observes a broadening of the luminescence on the low energy side of the B multiplet [9]. Such a broadening forms a tail extending up to 5 mev below the energy of the B_I line, it has been predicted by the stochastic transfer model of Leroux-Hugon et al. [8]. The traps responsible of this luminescence are NN_3N_i triplets (NN_i being nitrogen pair configurations for which the excitons are weaker bound than NN_{IO}). The shape of the triplet tail reflects the density of triplet configuration and can be calculated as a function of the nitrogen concentration using the method detailed in Ref. [8].

To conclude we shall say that the gradient-freeze growth of GaP under high nitrogen pressure enables to obtain high quality samples and to control the concentration of nitrogen incorporated with a great accuracy.

References

I. I.GRZEGORY, J.JUN and J.KARPINSKI. Physica I39 & I40B,347,(I986).
2. E.C.LIGHTOWLERS, J.C.NORTH and O.G.LORIMOR.J.Appl.Phys. 45, 2I9I, (I974).
3. D.G.THOMAS and J.J.HOPFIELD. Phys.Rev. I50, 680, (I966).
4. B.GIL, J.CAMASSEL, P.MERLE and H.MATHIEU. Phys.Rev.B25, 3987, (I982).
5. H.MARIETTE. Physica B (I987) in press.
6. M.COMBESCOT and C.BENOIT a la GUILLAME. Phys.Rev.Lett.44, I82, (I980).
7. H.MARIETTE, J.KASH, D.J.WOLFORD and A.MARBEUF. Phys.Rev. B3I, 52I7, (I985).
8. P.LEROUX HUGON and H.MARIETTE. Phys.Rev. B30, I622, (I984).
9. B.GIL. Physica B (I987) in press.

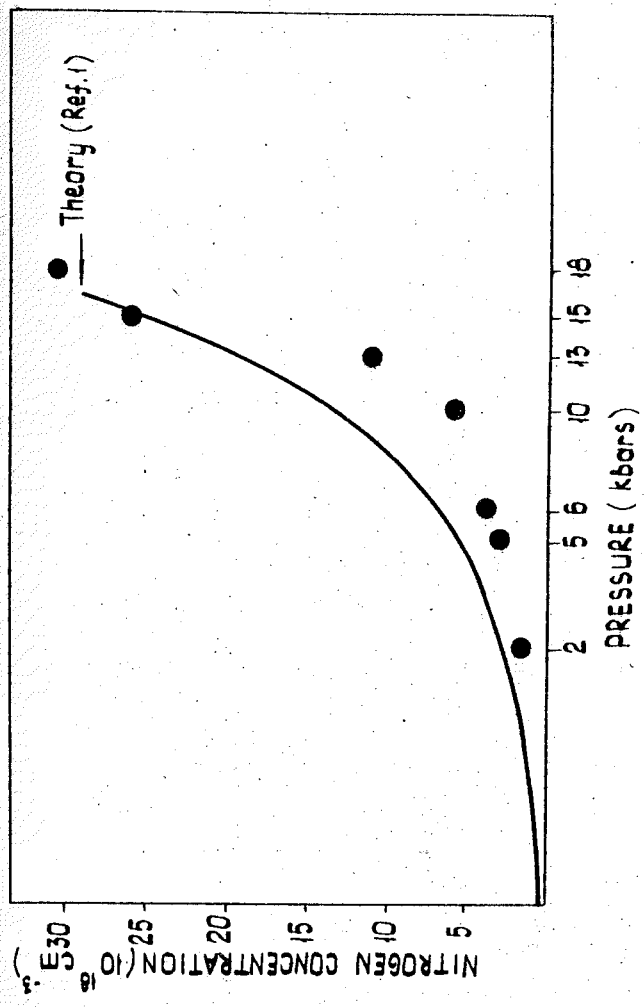

Fig. 1. Nitrogen concentration versus N_2 pressure for a melting temperature of 1730 K. Solid line: theory after Ref./1/ and experimental points (full circles).

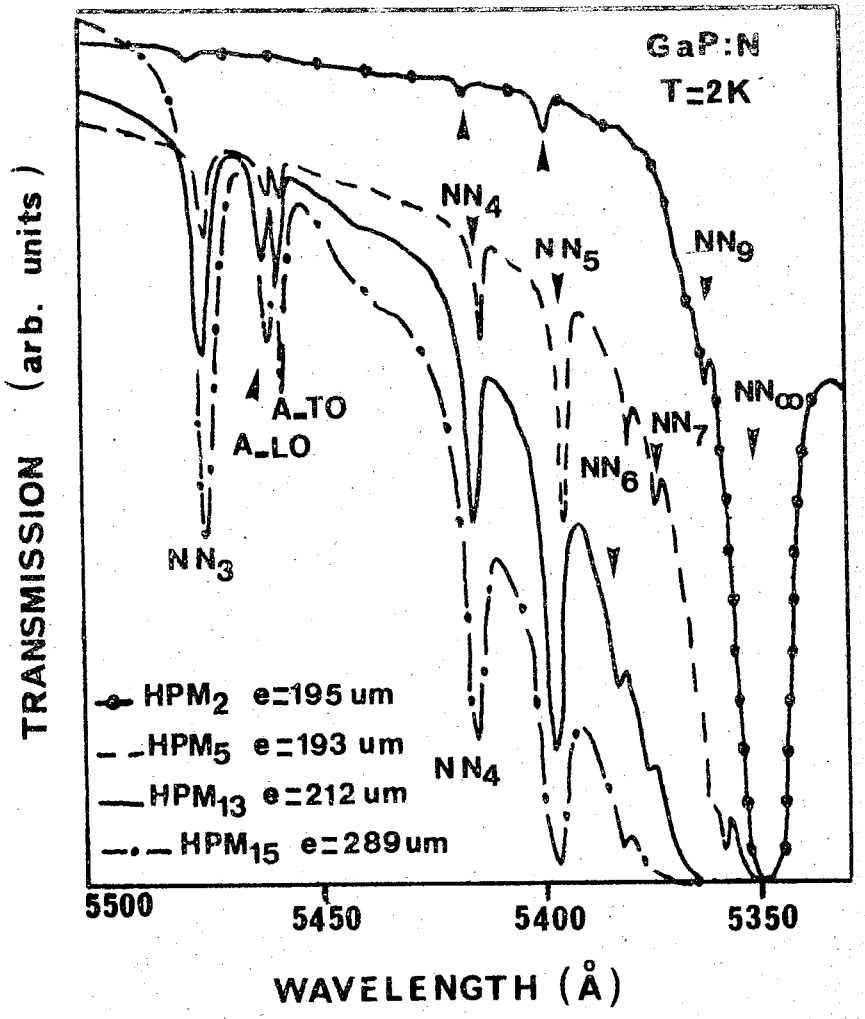

Fig. 2. Transmission spectra of the nitrogen doped sample at 2 K.

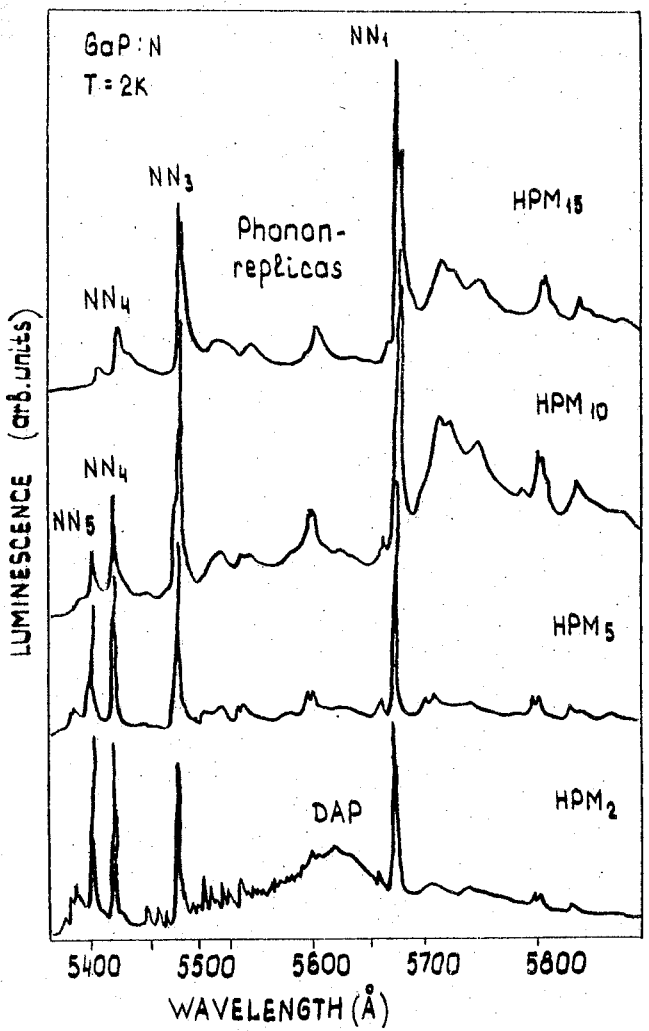

Fig. 3. Luminescence spectra at 2 K. Increasing the nitrogen concentration increases the probability of excitons transfers toward NN_I.

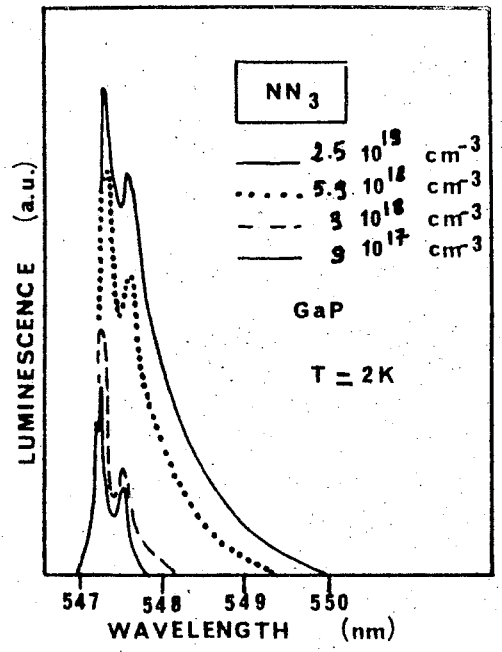

Fig. 4. Luminescence tail related to NN_3N_1 triplets as a function of the nitrogen concentration.

BRIDGMAN AWARD LECTURE

DIAMOND SYNTHESIS AND HIGH PRESSURE RESEARCH

F.P. Bundy, retired from General Electric Research and Development Center
Home Address: PO Box 29, Alplaus, New York 12008, USA

I. DIAMOND SYNTHESIS [1]

Since 1797 when Tennant first established that diamond is a crystalline form of pure carbon there have been many attempts to synthesize it in the laboratory. The claims of Hannay (1880), Moissan (1894), Parsons (1918), and many others have not been verifiable, or reproducible.

By 1938 improved thermodynamic data on graphite and diamond showed clearly that diamond is thermodynamically stable relative to graphite only at quite high pressures such as 1.6 GPa at room temperature and 3.1 GPa at 900K. Data were not available for higher temperatures and reasonable extrapolations had to be made to estimate the pressures that would be required at higher temperatures.

Attempts reported in 1943 by Gunther, et al. in Germany, and in 1947 by Bridgman in USA, to convert graphite to diamond by heating it to white hot temperatures and quickly subjecting it to pressures believed to be over 10 GPa were unsuccessful. This verified what was already known from high temperature experiments on graphitization of diamond; - namely, that the activation energy for the direct reaction of diamond to graphite, or graphite to diamond, is very high. Bridgman once wryly commented that "graphite is nature's best spring."

In 1951, when the ultra high pressure synthesis project was started at our laboratory with diamond synthesis as one of the prime objectives, the literature surveys indicated that reaction conditions in the area of 6 GPa and 2000K would have to be attainable for time periods of minutes or hours, and that chemical systems involving carbon would have to be found which could effectively reduce the activation energy of transformation of graphite to diamond. No apparatus was known at the time which was capable of the estimated pressure, temperature, time conditions. The first priority task was to develop adequate apparatus and heating techniques. We started with Bridgman opposed anvil apparatus and modified it to tolerate specimens heated electrically to high temperatures. Many gasketing arrangements were tried which would allow more compression stroke while confining the high pressure. Over a period of about two years adequate apparatus gradually evolved. The most successful one became known as the "belt" apparatus [2].

Even with apparatus of the P, T capability stated above nearly a year of exploratory experimentation was consumed trying to find a reaction system that would convert graphite, or some physical or chemical forms of carbon, to diamond. Many experiments involving direct transition from graphite, release of free carbon from carbides, electrolysis of alkaline earth carbides, various solvent media for carbon, etc., were carried out.

The first transient success was by Strong in mid-December 1954 using a small diamond seed wrapped in pure iron foil and surrounded by a commercial carburizing compound known as STEEL-O.

Only a few days after Strong's transient success, H.T. Hall with an early version of the "belt" apparatus, operating at substantially higher pressure, in which the "sample" consisted of a tube of graphite filled with iron-rich iron sulfide and capped at each end with Ta "current discs", yielded small black diamond at each end on the Ta discs. This system proved to be reproducible.

Naturally, all hands started experimenting night and day to find what the successful reactions were, and what alternate ones might work. Within a few weeks it was established that Ni, Fe, Co, and their alloys together, or with some other metals, would convert graphite to diamond, - providing the pressure was high enough and the temperature was high enough to melt the metal in the presence of graphite. The reaction took place at the interfaces between the metal and graphite.

Within a few weeks work was directed toward improving the diamond yields per run, and to the accumulation of enough synthesized diamond to make a small grinding wheel for performance tests. Fortunately the dirty-looking diamond material we synthesized had properties satisfactory for resin bonded grinding wheel use because it performed at least as well as similar wheels containing crushed natural diamond. It gave promise of being a useful viable product, and the next question was whether it could be produced at costs competitive with existing crushed natural diamond. It was at this time that Professor Bridgman was engaged to consult, Fig. 1*, with the hope that he might help find ways to increase the service life of the apparatus and increase its efficiency.

On the first visit we showed him the apparatuses and the process and asked if he would like to make a diamond run himself. He did, and with direction from us assembled a cell, put it in the press, and put it through the procedure. It was a successful run, and we gave him the diamonds.

The development of the high-pressure, catalyst-solvent diamond synthesis process to an economically feasible status took place jointly at our laboratory and at General Electric's Carboloy Department in Detroit, Michigan, which was to be the commercial producer of synthetic diamond abrasive if everything worked out satisfactorily. The commercial availability of synthesized diamond abrasive in quantities of thousands of carats, was announced in November 1957, very shortly after our Russian colleague scientists and engineers put the first Sputnik into orbit around the earth.

II. P, T PHASE DIAGRAMS FOR CARBON AND BN

After diamond synthesis had been accomplished and work aimed at making it a commercial enterprise was underway, more scientific work was needed to establish more accurately the diamond/graphite equilibrium line, and to learn more about the behavior of carbon at higher pressures and temperatures. There was the possibility that there were alternate ways to synthesize diamond, and they might be competitive. The first part of this work culminated in the now-classical scientific paper by me and my colleagues on the experimental determination of the graphite/diamond equilibrium line (1961) [3].

After modifying the design of the belt apparatus to make it capable of much higher pressures I extended the investigation of the phase diagram of carbon to include the melting line of graphite and the fast direct

*The Figure is given at the end of the book.

transition of graphite to diamond. This work involved attaining specimen transient temperatures of 3000 to 5500K, and required the development of transient heating and monitoring techniques. This work was successful and was reported in 1963 in a pair of papers, one on the melting line, heat of fusion, etc., of graphite [4], and the other on the direct transformation of graphite to diamond in static pressure apparatus [5].

III. GROWTH OF GEM-QUALITY SINGLE CRYSTAL DIAMONDS

There were many scientific questions about what foreign elements might be incorporated into a growing diamond, and what electrical, optical, thermal, and mechanical effects such substitutional elements might produce. For example, if one could made n- and p-type diamond there would be the possibility of making thermistors, transistors, and other solid state electronic devices that would be serviceable at much higher temperatures than silicon or germanium devices because of its higher DeBye temperature. Also there was the possibility of utilizing the unexcelled thermal conductivity of perfect diamond crystal for heat sink purpose, - and the wide-band light transmitting properties of perfect diamond for windows in special technological applications.

By the mid-1960's it was recognized that the graphite/thin metal film/diamond system was very difficult to control precisely, and furthermore the size of reasonably good single crystals that could be grown by that process seemed to be limited to about one millimeter. Wentorf proposed abandoning the thin film process in favor of a diamond/molten metal bath/diamond system in which the carbon concentration gradient in the bath would be established by a temperature gradient which could be controlled. His early experiments showed promise, but problems involving unwanted secondary nucleation of diamond and graphite, and of dissolution of the essential "seed diamond" during the start-up of the run, were impressive obstacles. Strong worked tenaciously on these problems and eventually solved them. By 1970 it was possible to grow single crystals of diamond of very high crystal quality, and with controlled doping, Fig. 2.* It was found that only B and N, - the neighbors of carbon in the periodic table, - would grow substitutionally into the diamond lattice. Boron doping, as expected, produced p-type semi-conducting properties, and blue coloration. Nitrogen doping produced yellow coloration, but the crystals remained good electric insulators. The lack of n-type diamond defeated the possibility of a diamond transistor.

Thermal conductivity measurements on some of our colorless single crystal diamond showed them to have the highest thermal conductivity of any known material at room temperature, - even slightly better than that of the best Type II natural diamond crystals. This result was corroborated when high energy atomic beam transmission and back-scattering tests made at Bell Labs showed our crystals to give results quite close to those predicted theoretically, whereas the best natural diamond crystals were not so good.

The most recent mechanical strength tests of our single diamond crystals were by Professor Ruoff at Cornell University. A pair of bluish, boron-doped crystals were shaped to the latest Mao/Bell tapered face geometry [6] and run in an experiment by steps up to about 120 GPa. Failure occurred during the next upstep loading step. This pressure generation performance is as good as that of most natural diamonds selected especially for diamond anvil cell use.

*The Figure is given at the end of the book.

IV. SINTERING DIAMOND AND CUBIC BN

Single crystal diamond cleaves relatively easily along the octahedral planes. For this reason single crystal diamond is not satisfactory for heavy cutting-tool work. A compact made of randomly oriented diamond particles sintered completely together, diamond to diamond, at near 100 percent packing density, would be just as hard, much tougher and stronger, and more resistant to wear than single crystal diamond.

Many years of experimental work at our laboratory were devoted to developing a high-pressure, high-temperature process for such sintering. Each of us would have a try at it when we had an idea that appeared to have merit. This is not the appropriate time or place to go into the details of the basic problems and solutions. These are discussed quite thoroughly by Wentorf, DeVries and Bundy in their 1980 review article in Science [7]. High-pressure, high-temperature methods with proper chemistry were developed which resulted in sintered compacts of diamond powder with over 95 percent bulk density of diamond, a large fraction of the particle interface area sintered diamond-to-diamond, and bulk hardness and strength comparable to single crystal diamond. Due to their randomly oriented polycrystallinity they were quite tough, relatively impact resistant, remarkably wear resistant, and held their strength and hardness to quite high temperatures. This wear resistance property made the sintered diamond material particularly useful for the cores of wire-drawing dies and it has become widely used in that application as well as for the cutters for hard metallic and non-metallic materials and for cutters in well drilling heads used in many different types of geologic rock layers. Sintered diamond has also been used effectively as the highly-stressed parts of static ultra-high pressure apparatus.

Ways were found to sinter cubic BN into strong, relatively tough, polycrystalline compacts also, and tools utilizing these materials have their unique applications in industry.

V. ULTRA-HIGH STATIC PRESSURES

Prior to the early 1970's the most useful static very-high pressure apparatuses used cemented tungsten carbide or single crystal diamond for the most highly stressed parts. The maximum pressure capability of cemented tungsten carbide apparatus is set by its limited shear strength of about 5.0 GPa. By careful tailoring of the total geometry of the apparatus, including the gasketing structures, it has been possible to generate static pressures in opposed piston apparatus which are 4 to 5 times greater than the shear strength of the piston material [8]. In the case of single crystal diamond anvil apparatus the sizing and shaping of the anvil faces and the gasketing are very critical for the prevention of catastrophic cleavage fracture [6,9].

In the mid-1970's with the new sintered diamond process available in our organization it became possible to make composite pistons of cemented tungsten carbide and sintered diamond powder in which the most highly stressed parts were comprised of sintered diamond. A Drickamer-like opposed anvil apparatus using this innovation was designed and made. With it we were able to extend the pressure range of resistance-monitored experiments from about 20 GPa up to over 60 GPa [10]. In this apparatus the pressurized zone was many times larger than that available in single crystal diamond apparatus, making it possible to do quantitative electrical resistance experiments on many substances. Among the substances investigated by K.J. Dunn and me were S, Se, Te, Fe, FeV alloys, I, Si, Ge, GaP, GaSe, $(SN)_x$, Eu, Ba, Sr, and Ca.

At room temperature we could achieve the $\alpha \rightarrow \varepsilon$ transition in Fe20V alloy, Fig. 3, which according to the shock compression people occurred at about 50 GPa. When sulfur was compressed at room temperature it acted as a semiconductor with band-gap decreasing with added pressure until at nearly 50 GPa the band-gap became zero and the behavior became like a semimetal.

At that period of time there was great interest and excitement about the possibility of producing metallic hydrogen, which in addition to being metallic might also be a high-temperature superconductor. As a move in the direction of investigating substances at pressures approaching 100 GPa at liquid helium temperatures a clamp press arrangement was designed and made for our sintered diamond tipped apparatus so that specimens could be pressurized, clamped at pressure, and cooled to cryogenic temperature [11]. We never did get to the point of experimenting with hydrogen in this apparatus, but we succeeded in determining the high-pressure, low-temperature, behavior of many relevant substances. We discovered some new phases and some new superconductors.

An example is Te, which in its first high pressure metallic form was reported to go superconducting at about 3.5K [12]. In our experiments at increasingly higher pressures it was found that new phases formed with higher critical temperatures, T_c, as illustrated in Fig. 4 [13].

Another very interesting example was the behavior exhibited by the Ba, Sr, Ca family of alkaline earth metals [14]. Ba was known to become a superconductor at pressures above about 4 GPa, with higher pressure phases having higher T_c's. Our work with Ba showed that the T_c reaches a maximum of about 5K at a pressure of about 16 GPa and for pressures above that there is a linear decrease, reaching about 4K at 50 GPa, Fig. 5. In our experiments Sr did not show any superconductivity at temperatures within our capability (>2.8K) until pressures of nearly 40 GPa were reached. Above 40 GPa the T_c increased slowly with pressure, but seemed to approach a maximum of about 4K at about 50 GPa. The work with Ca indicated several phase changes upon compression up to over 40 GPa. At 44 GPa, the Ca specimen showed the beginning of a small reproducible drop in resistance at the threshold of our lowest attainable temperature (~2K). This may be the threshold of the transition to superconductivity for Ca, but our experiment was not good enough to prove it. The point is shown with a question mark in Fig. 5.

VI. HIGH PRESSURE APPARATUS DESIGN

The design, construction and use of ultra-high pressure apparatus has been of great interest to me from the beginning of our work in the high pressure field. We started with Bridgman opposed anvil apparatus and modified it with thermal insulation features to allow the heating of specimens to high temperatures while holding them under pressure. The need for more compression and "follow-through" stroke led to the development of the deformable conical sandwich gaskets, and eventually to the "belt" concept of Hall's.

The need for higher pressure capability in the late 1950's for experimentation on melting of graphite and possible direct transformation of graphite to diamond called for extension of the general stress design of the belt type apparatus to what I called the "high compression belt".

To get to still higher pressures we had to go to the composite pistons with high strength sintered diamond in the most highly stressed regions. This worked out quite well in the Drickamer-type, enclosed, opposed-anvil geometry [10].

In the last plenary lecture of the last AIRAPT International Conference [Amsterdam (1985)] I went into the details of materials and designs to use to achieve the highest possible static pressures [9]. The piston material has to be diamond, the strongest and hardest known material, with precisely the optimum geometry and gasketing. At that time (1985), I suggested that 350 to 400 GPa should be attainable if all details of the design and construction of the apparatus were optimized. Such pressures, corresponding to that at the center of the earth, have already been nearly attained by Mao and Bell's group at the Geophysical Laboratory in Washington, D.C. *Professor Bridgman would be pleased to know that high pressure techniques have been advanced so much by his many followers.*

References

1. Bundy, F.P., "Behavior of Carbon at Very High Pressures and Temperatures", Koninkl. Nederl. Akademic van Wetenschappen-Amsterdam Proceedings, Series B, *72*, No. 5 (1969), pp. 302-316.

   Bundy, F.P., Strong, H.M., Wentorf, R.H. Jr., "Methods and Mechanisms of Synthetic Diamond Growth", Chem. and Phys. of Carbon, (1973), *10*, 213-263.

2. Hall, H.T., "Ultra-High-Pressure, High-Temperature Apparatus: The 'Belt'", Rev. Sci. Instr. (1960), *31*(2), 125-131.

3. Bundy, F.P., Bovenkerk, H.P., Strong, H.M., and Wentorf, R.H. Jr., "Diamond-Graphite Equilibrium Line from Growth and Graphitization of Diamond", J. Chem. Phys. (1961), *35*(2), 383-391.

4. Bundy, F.P., "Melting of Graphite at Very High Pressure", J. Chem. Phys. (1963), *38*(3), 618-630.

5. Bundy, F.P., "Direct Conversion of Graphite to Diamond in Static Pressure Apparatus", J. Chem. Phys. (1963), *38*(3), 631-643.

6. Goettel, K.A., Mao, H.K. and Bell, P.W., "Generation of Static Pressures above 2.5 Megabars in a Diamond Anvil Pressure Cell", Rev. Sci. Instr. (1985), *56*(7), 1420-1427.

7. Wentorf, R.H. Jr., DeVries, R.C., and Bundy, F.P., "Sintered Superhard Materials", Science (1980), *208*, 873-880.

8. Bundy, F.P., "Designing Tapered Anvil Apparatus for Achieving Higher Pressures", Rev. Sci. Instr. (1977), *48*(6), 591-596.

9. Bundy, F.P., "Design and Development of Apparatuses to Achieve the Highest Possible Static Pressures", Physica (1986), *139 & 140B*, 42-51.

10. Bundy, F.P., "Ultrahigh Pressure Apparatus Using Cemented Tungsten Carbide Pistons with Sintered Diamond Tips", Rev. Sci. Instr. (1975), *46*(10), 1318-1324.

11. Bundy, F.P. and Dunn, K.J., "Application of Sintered Diamond Tipped Ultra High Pressure Apparatus to Cryogenic Experiments", Rev. Sci. Instr. (1980), *51*(6), 753-758.

12. Berman, I.V., Binzarov, Zh. I., and Kurkin, P., "Superconducting Properties of Tellurium at Pressures up to 260 kbar", Sov. Phys. Solid State (1973), *14*(9), 2192-2194.

13. Bundy, F.P. and Dunn, K.J., "Pressure Dependence of Superconducting Transition Temperature of High-Pressure Metallic Te", Phys. Rev. Ltrs. (1980), *44*(24), 1623-1626.

14. Dunn, K.J. and Bundy, F.P., "Pressure-Induced Superconductivity in Strontium and Barium", Phys. Rev. (1982), *B25*(1), 194-197.

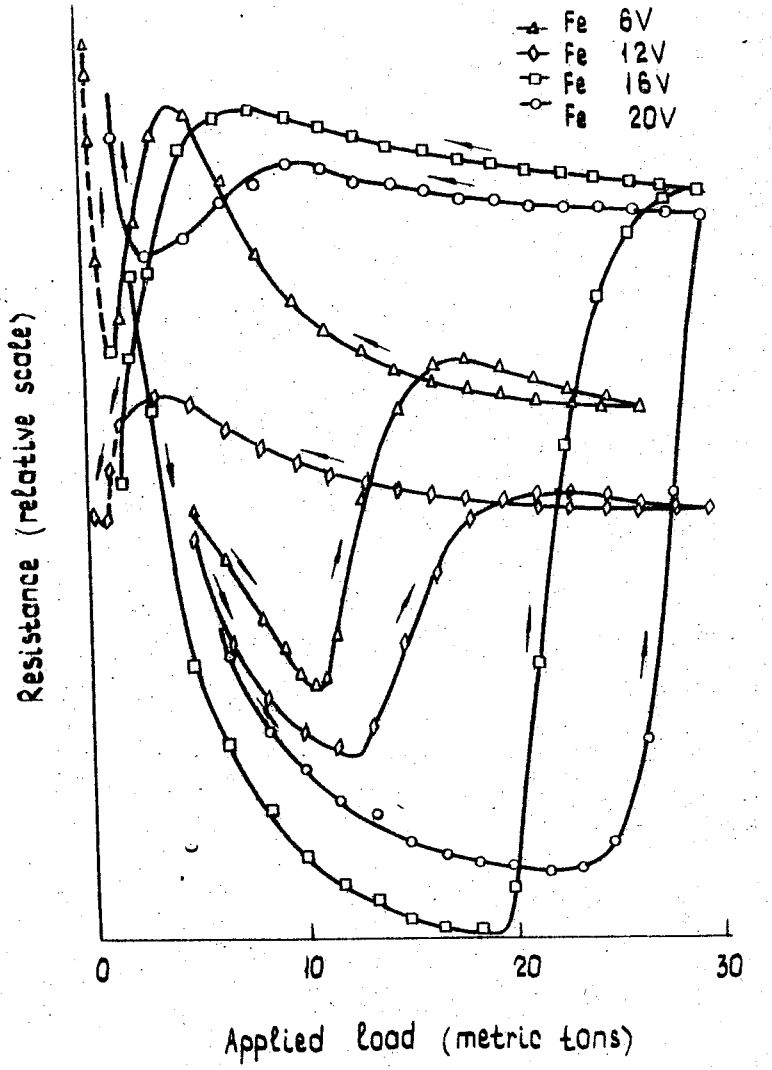

Fig. 3. Resistance vs loading of Fe-V alloys in sintered d .mond tipped opposed anvil apparatus. Up-jump of resistance occurs at the $\alpha \rightarrow \varepsilon$ phase transition.

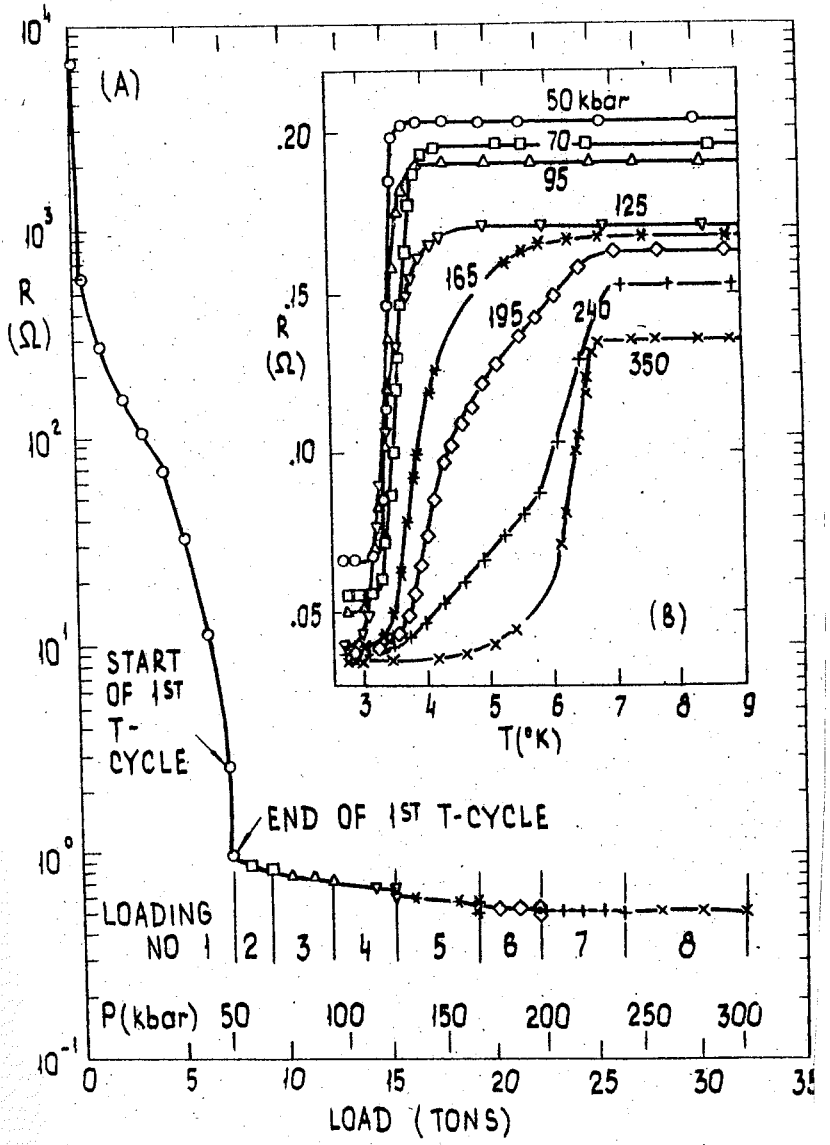

Fig. 4. Pressure dependence of the T_c of high-pressure "metallic" Te.

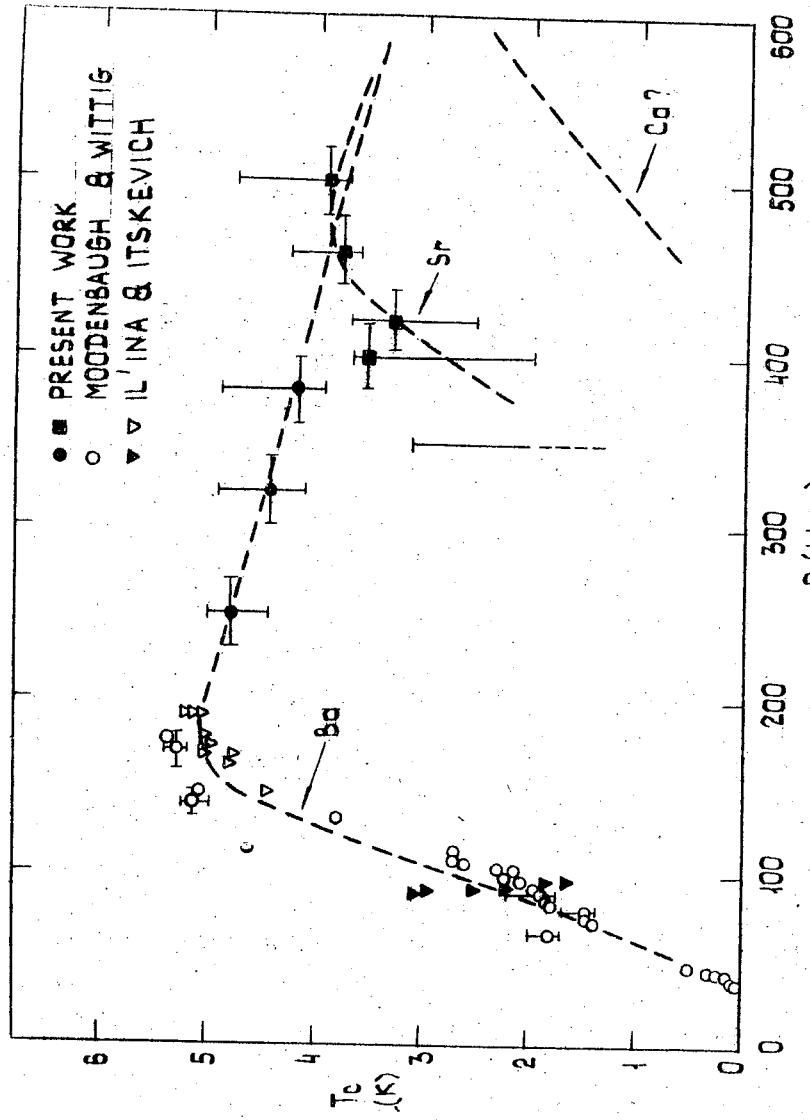

Fig. 5. Pressure dependence of the T_c for Ba, Sr, and Ca.

МЕЖДУНАРОДНАЯ АССОЦИАЦИЯ ПО РАЗВИТИЮ ИССЛЕДОВАНИЙ
В ОБЛАСТИ ВЫСОКИХ ДАВЛЕНИЙ

ВЫСОКИЕ ДАВЛЕНИЯ В НАУКЕ И ТЕХНИКЕ

ТРУДЫ
XI МЕЖДУНАРОДНОЙ КОНФЕРЕНЦИИ МАРИВД

в 4 томах

Том 1

Ответственный редактор Н.В.Новиков

На английском языке

Киев, издательство "Наукова думка"

Оформление художника В.С.Мельничук
Художественный редактор И.Е.Писарева
Технический редактор Т.К.Валицкая

Н/К

Подп. в печ. 23.02.88. Формат 60x84/16. Бум. офс. № 2. Офс. печ. Усл. печ. л. 26,97. Усл. кр.-отт. 27,20. Уч.-изд.л. 20,91 + вкл. 0,60 = 21,51. Тираж 720 экз. Заказ. 8-384. Цена 1 р. 20 к.

Издательство "Наукова думка". 252601 Киев 4, ул. Репина, 3.
Киевская книжная типография научной книги. 252004 Киев 4, ул. Репина, 4.

FOR NOTES

To the paper: Franck E. U. «Supercritical fluid mixtures at high pressures».

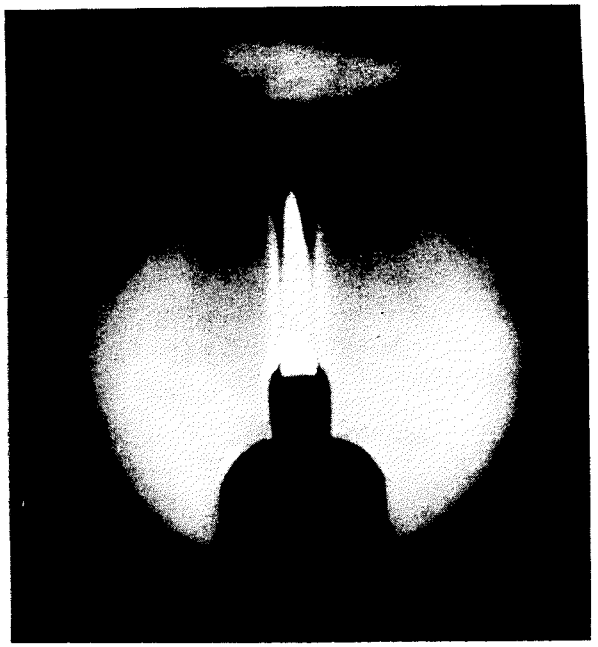

Fig. 9. «Hydrothermal» flame at 2000 bar. Oxygen is injected at about 2 mm^3 sec^{-1} into the supercritical homogeneous fluid (0.70 H_2O + 0.30 CH_4) at 450 °C. The spontaneous ignited flame is 4 mm high and 0.5 mm wide. Sapphire windows are used. (Observations by W. Schilling, Institute for Physical Chemistry, Karlsruhe University.)

To the paper: Dobromyslov A. V., Taluts N. I., Demchuk K. M,. Martemianov A. N. «The influence of pressure on the α — ω transformation in Zr and its alloys».

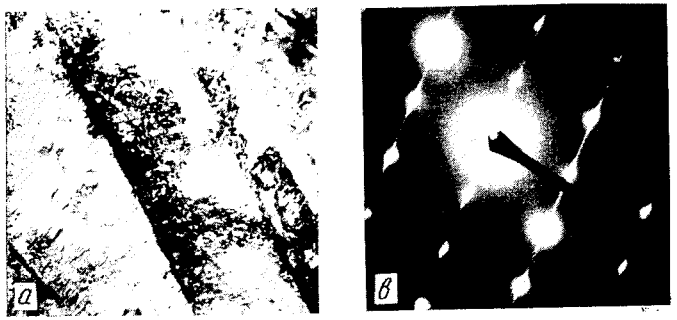

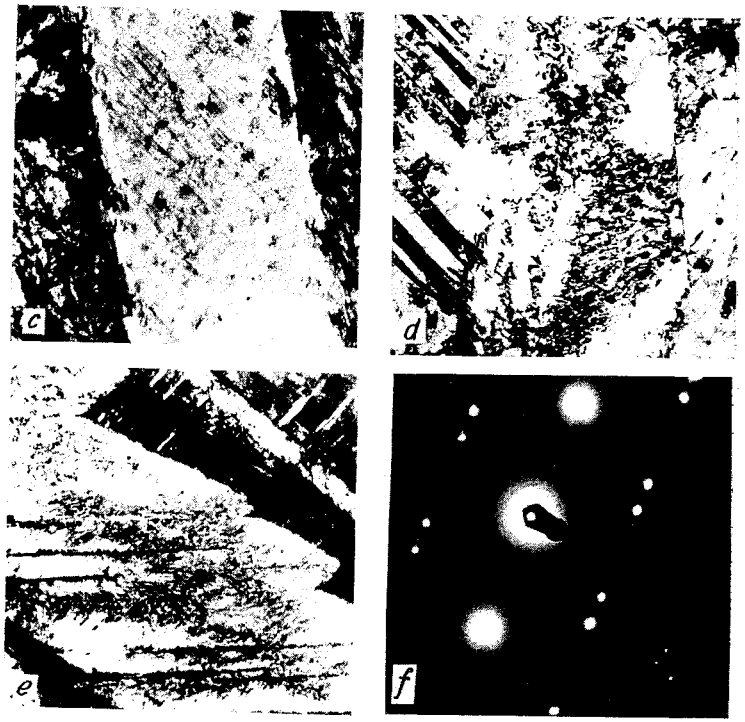

Fig. 1. Structure of Zr and Zr — 2,5 % Nb alloy after different treatment: *a* — Zr after quenching and holding at pressure 8 GPa, ×30000; *b* — electron diffraction pattern corresponding to (*a*), zone axis [100] ω-phase; *c* — Zr — 2,5 % Nb after quenching and holding at pressure 8 GPa, ×30000; *d* — Zr after holding at pressure and heat treatment at 400 °C for 1 hr, ×30000; *e* — Zr — 2,5 % Nb after holding at pressure and heat treatment at 400 °C for 1 hr, ×30000; *f* — electron diffraction pattern corresponding to (*e*), zone axis **[011]** of principal α-phase orientation.

To the paper: Yakovlev E. N. «Diamond formed of organic compounds».

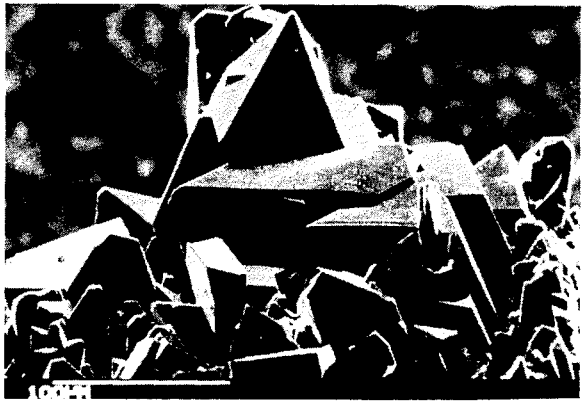

Typical diamonds formed from organic compounds.

To the paper: Kurdyumov A. V. «Martensitic transformations in carbon at hi pressures».

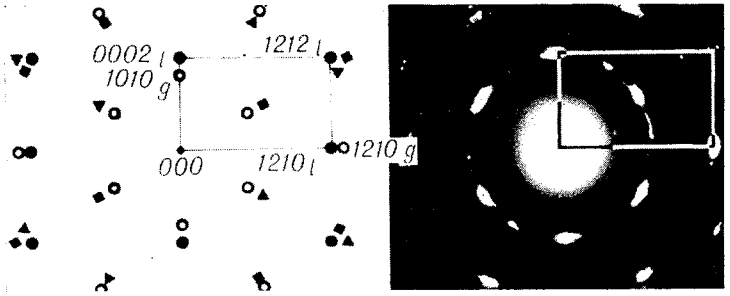

Fig. 1. Electron diffraction pattern from a lonsdaleitegraphite particle; C graphite reflections; ●, ▲, ■ — lonsdaleite reflections at three equivalent entations («three—fold texture»).

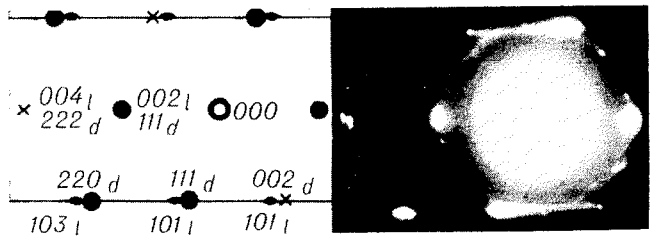

Fig. 3. Electron diffraction pattern from a lonsdaleite-diamond particle; × forbidden reflections.

To the paper: Gerlach U., Risse G., Vollstädt H. «On solid state diamond nucleation at static pressure».

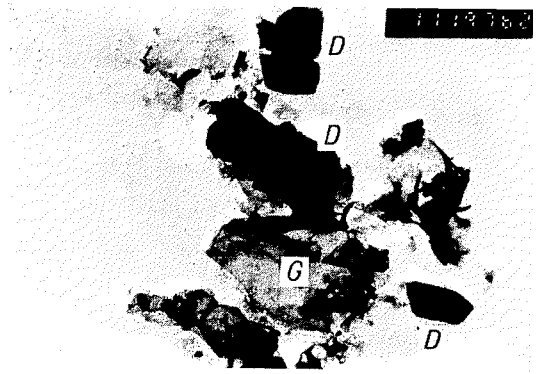

Fig. 5. TEM of carbon phases after synthesis (soure: natural graphite) (Magn. 10 000).

Fig. 6. TEM-dark field with 022-diamond reflex.

Fig. 7. REM of synthesis product after graphite oxidation.

To the paper: Grzegory I., Jun J., Krukowski St. «Growth of GaN single crystals from the solution under high nitrogen pressure».

Fig. 3. GaN crust with columnar crystals on its internal surface — general view — 17 kbar and 1360 °C.

Fig. 4. GaN crust with plate-like crystals on its internal surface — 12 kbar at 1400 °C.

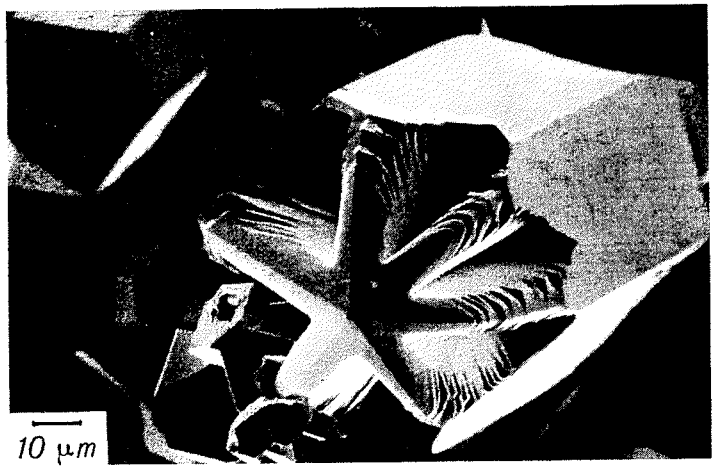

Fig. 5. The hollow star-like crystals showing morphological instability — 17 kbar and 1360 °C.

Fig. 6. Intermediate region between plates and columns — 12 kbar and 1300 °C.

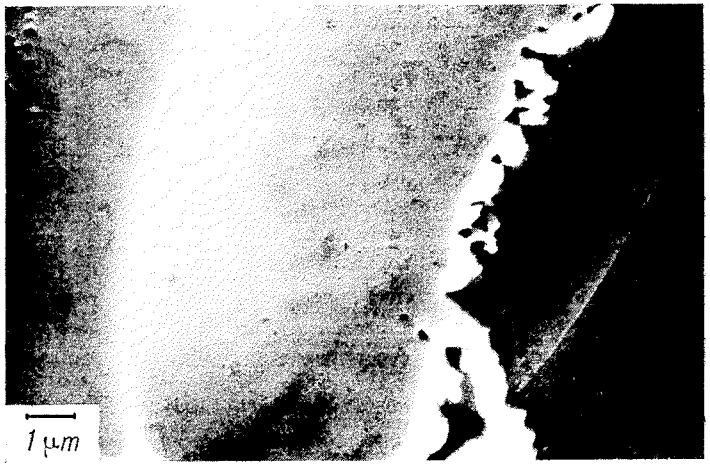

Fig. 7. Growth layers on the [0001] face.

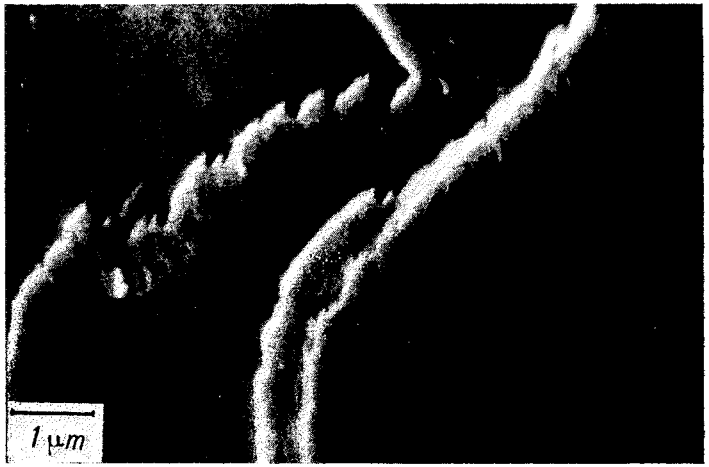

Fig. 8. Growth layers on the [1010] face.

Fig. 9. Two-dimensional nucleation on [0001] face.

Fig.
and

Fig. 10. First stage of growth of crystals on the internal side of the crust. The dense wood of small crystallites is growing.

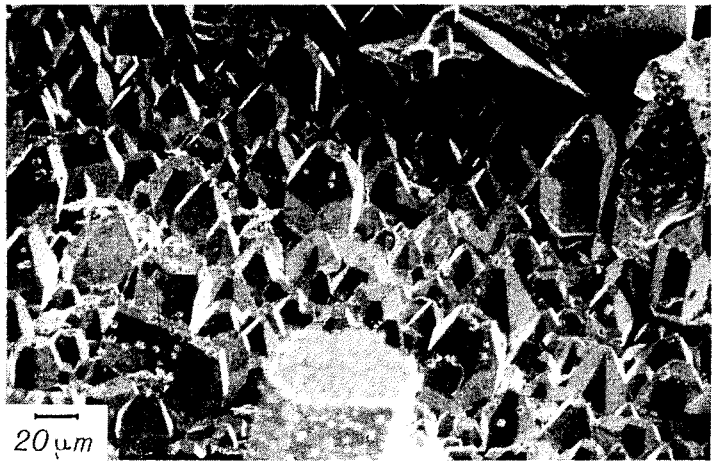

Fig.

Fig. 11. Structure of layers indicating the direction of solute current.

To the paper: Voronov O. A., Rahmanina A. V. «Mono- and polycrystalline diamonds produced from hydrocarbons».

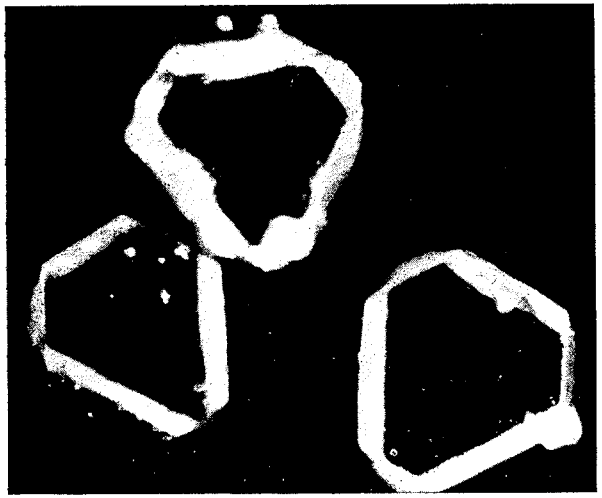

Fig. 1. Diamond crystals 200 μm in size, produced from hydrocarbons.

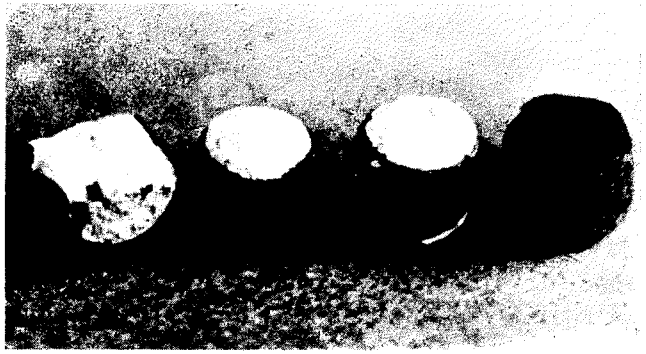

Fig. 2. Diamond polycrystalline aggregates, produced from hydrocarbons (left). The polycrystalline carbonado [3], produced from graphite using metal catalyst under the same conditions of experiment (right).

Fi
an

To the paper: Zongqing Y., Wakatsuki M. «Seeded growth of diamond with δP method».

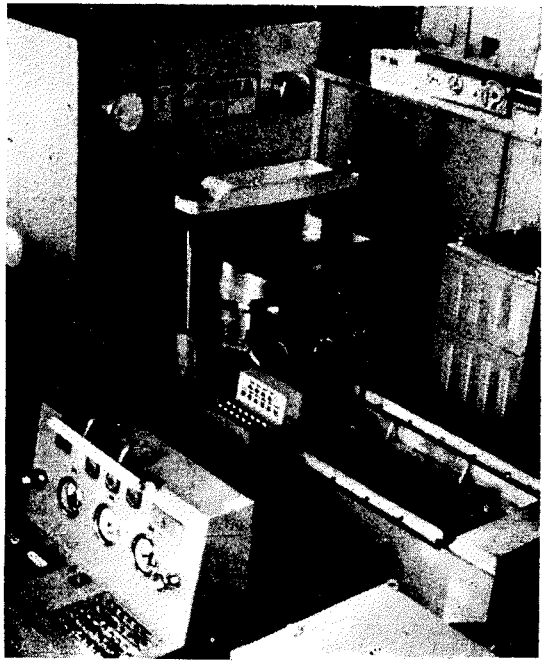

Fi

Fig. 2. The full view of the press and high-pressure apparatus used.

Fig. 5. The diamond single crystals grown using δP method.

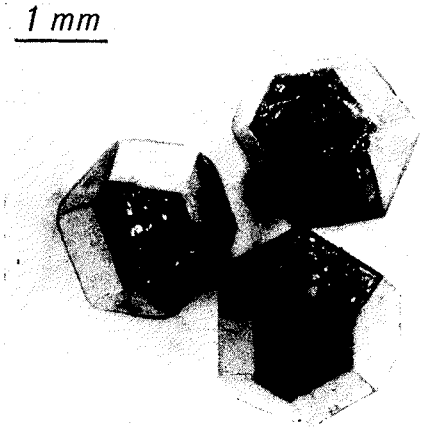

To the paper: Bundy F. P. «Bridgman Award lecture. Diamond synthesis a high pressure research».

Fig. 1. Group photo, including Bridgman and Langmuir (1955).

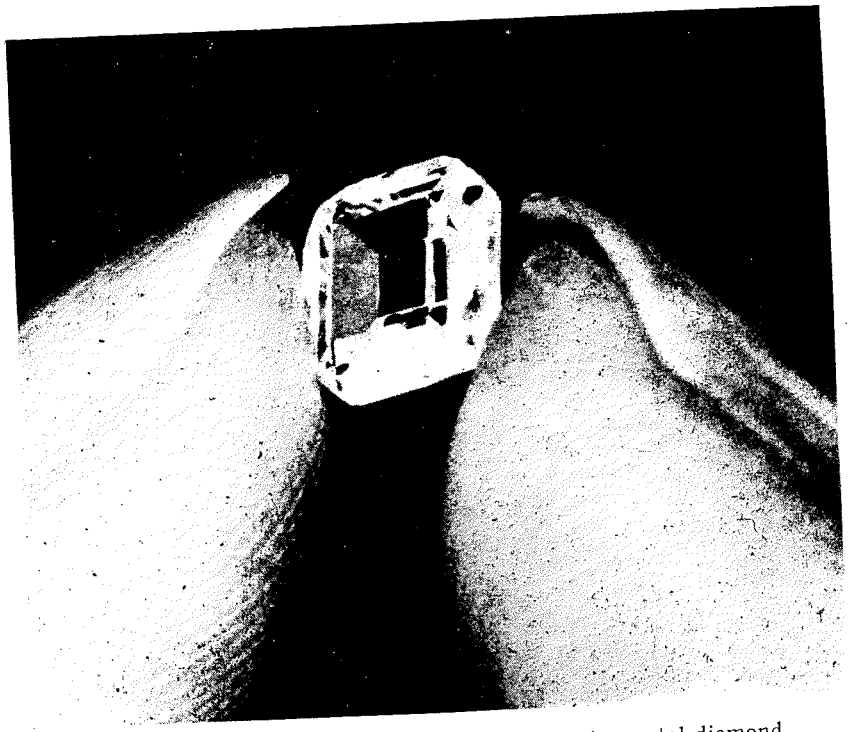

Fig. 2. Photo of high quality, laboratory-grown, single crystal diamond.

Fig
The
lysi

To
met